

Modulation of p53 signalling and response to MDM2-p53 binding antagonists

**Thesis submitted in partial fulfilment of the requirements of the degree
of Doctor of Philosophy**



Arman Esfandiari

University of Newcastle upon Tyne

Faculty of Medical Sciences

Molecular Oncology Research Group

Northern Institute for Cancer Research

09/2015

Abstract

Mutational inactivation of the p53 tumour suppressor protein, encoded by the *TP53* gene, occurs in $\approx 50\%$ of malignancies overall. Non-genotoxic activation of p53 signalling in the remaining *TP53* wild-type malignancies is a promising therapeutic strategy. MDM2 inhibitors, such as Nutlin-3 and RG7388, can activate p53 in a non-genotoxic manner, mobilising p53-dependent signalling; however, sensitivity to these compounds varies widely among *TP53* wild-type cell lines. In this study p53 signalling network components involved in the response to DNA damage and p53 homeostasis are investigated for their role as determinants of cellular sensitivity to MDM2 inhibitors. Deciphering determinants of sensitivity to this group of compounds will enable optimisation of their therapeutic potential.

Chemical inhibition of kinases, ATM and DNA-PKcs, which are critical for DNA double strand break repair and activation of p53 signalling in response to DNA damage, did not affect the cellular sensitivity to Nutlin-3 in the absence of DNA damage. However, inhibition of these kinases enhanced the cellular sensitivity of *TP53* wild-type cells to the combined effect of Nutlin-3 and DNA damage induced by ionising radiation, in a cell type dependent manner. In a neuroblastoma derived *TP53* wild-type and mutant, otherwise isogenic, cell line pair, ionising radiation increased the growth inhibitory effect of Nutlin-3 in a p53-dependent manner and this was enhanced significantly in the presence of the DNA-PKcs inhibitor NU7441. In contrast, in the osteosarcoma derived *TP53* wild-type and mutant, otherwise isogenic, cell line pair, exposure to ionising radiation decreased the growth inhibitory effect of Nutlin-3 in a p53-dependent manner and DNA-PKcs inhibition did not influence this protective effect.

Given that ATM and DNA-PKcs activate p53 through phosphorylation of key residues, inhibition of the WIP1 phosphatase (encoded by the *PPM1D* gene) that dephosphorylates one such residue, was tested for the effect on cellular sensitivity to MDM2 inhibitors. Cellular growth/proliferation was assessed in *TP53* wild-type and matched mutant/null cell line pairs, differing in their *PPM1D* genetic status, when treated with MDM2 inhibitors Nutlin-3/RG7388 \pm a highly selective WIP1 inhibitor GSK2830371 or transient siRNA knockdown of WIP1 expression. The effects of GSK2830371 and transient WIP1 siRNA knockdown on MDM2 inhibitor induced p53^{Ser15} phosphorylation, p53-mediated global transcriptional activity and apoptosis

were also investigated.

WIP1 transient siRNA knockdown increased p53^{Ser15} phosphorylation and sensitivity to MDM2 inhibitors in *TP53* wild-type parental cell lines. *TP53* wild-type and mutant cell line pairs were relatively insensitive to single agent GSK2830371 regardless of their *PPM1D* status. However, a non-growth inhibitory dose of GSK2830371 markedly potentiated the response to MDM2 inhibitors in *TP53* wild-type cell lines, most notably in those harbouring *PPM1D* activating mutations or copy number gain (up to 5.8-fold decrease in GI50). Potentiation also concurred with significant increase in MDM2 inhibitor induced cell death endpoints which were preceded by a marked increase in phosphorylated p53^{Ser15}, a WIP1 negatively regulated substrate, and known to increase p53 transcriptional activity. Microarray-based gene expression profiling showed that the combination treatment increases the subset of early RG7388 induced p53-transcriptional target genes involved in growth inhibition and apoptosis.

Increased mRNA and protein expression of WIP1 has been associated with poor clinical outcome in various malignancies in which MDM2 inhibitors are being considered as a potential therapeutic strategy. For neuroblastoma mining the Amsterdam microarray databank showed WIP1 mRNA expression to correlate with worse survival. Therefore, WIP1 protein expression was assessed by immunohistochemical (IHC) staining of neuroblastoma tissue microarrays. A wide range of WIP1 IHC staining was found, however there was no significant association between high WIP1 staining and clinical outcome.

Overall these findings show that manipulating p53 post-translational modification following its activation by MDM2 inhibitors or DNA damaging agents can increase cellular sensitivity to this class of compounds. Furthermore, these observations provide evidence to support the inhibition of WIP1 phosphatase activity as a strategy for enhancing the efficacy of MDM2 inhibitors, particularly in *TP53* wild-type, *PPM1D* overexpressing/overactive malignancies.

Declaration

I certify that this thesis is my own work, except where stated, and has not been previously submitted for a degree or any qualification at this or any other university.

Acknowledgments

I would like to thank my supervisor Professor John Lunec for his infinite patience, persistent support and guidance throughout my MRes/PhD degrees. My gratitude also goes to the other members of the molecular oncology research group for technical support and stimulating discussions.

I would also like to thank the following colleagues for providing tissue, cell lines, reagents and/or technical support: Professors Herbie Newell, Nicola J Curtin, Olaf Heidenreich and Craig N Robson, Dr Ximena Montano, Dr Sari Alhasan, Dr Ahmad Mahdi, Dr Laura Woodhouse, Dr Chiao-En Wu, Dr Ashleigh Herriot, Dr Gesa Junge, Dr Lindi Chen, Dr Clair Hutton, Dr Jennifer Jackson, Dr Steven Darby, Dr Olivier Binda, Dr Richard Heath and Mr Ricky Tirtakusuma.

I thank the Undergraduate and MRes students whom I supervised over the last 3 years, for their hard work and dedication to advancement of their projects.

I must also thank my parents Iraj Esfandiari and Fahimeh Alipour, and my siblings Ramin Esfandiari, Fardin Esfandiari and Elham Toussi (sibling-in-law), for their unrelenting support of my academic endeavours.

Finally, I would also like to acknowledge and thank all cancer patients and their families for donating valuable tissue samples to potentially lifesaving research.

Table of Contents

Abstract	I
Declaration	III
Acknowledgments	IV
List of Figures	XII
List of tables	XXV
List of abbreviations	XXVII
Chapter 1 Introduction	1
1.2 Genomic integrity	2
1.3 Cancer	2
1.4 Hallmarks of cancer	3
1.4.1 Proto-oncogenes	5
1.4.2 Tumour suppressor genes	5
1.5 A brief history of p53	6
1.5.1 Discovery	6
1.5.2 Oncogenic tendencies	6
1.5.3 A classic tumour suppressor	7
1.5.4 <i>Trp53</i> knockout transgenic mice	10
1.5.5 Human germline mutations in <i>TP53</i>	11
1.5.6 <i>TP53</i> gene and its isoforms	11
1.5.7 <i>TP53</i> mutations: Gain-of-function or dominant-negative?	12
1.6 p53 structure and function	14
1.6.1 Transactivation domain	14
1.6.2 Proline rich region	16
1.6.3 DNA binding domain	17
1.6.4 C-terminus	21
1.7 Cell cycle checkpoints	25
1.7.1 Regulation of cell cycle progression	25
1.7.1.1 CDK inhibitors	26
1.8 Cell cycle checkpoints and the role of p53	27
1.9 Cellular senescence and the role of p53	29
1.10 Apoptosis and the role of p53	31
1.11 MDM2 regulates p53 stability and function	34
1.11.1 Indirect regulation of p53 stability and function from the <i>CDKN2A</i> locus	34
1.12 An overview of MDM2	37
1.12.1 MDM2 gene and protein	37
1.12.2 MDM2: Inhibitor of p53 transactivation	37
1.12.3 MDM2 a transcriptional target of p53	39
1.12.4 MDM2 ubiquitinates p53	40
1.12.5 Nuclear Shuttling of MDM2	41
1.12.6 MDMX	42
1.13 DNA strand break repair mechanisms	43
1.13.1 Homologous recombination repair	43
1.13.2 Non-homologous end joining	44
1.14 Strand break repair machinery and p53 crosstalk	44
1.14.1 WIP1 phosphatase and homeostasis of p53 in response to stress and DNA damage	45
1.15 An overview of PPM1D/WIP1	48
1.15.1 PPM1D/WIP1 gene and proteins	48
1.15.2 <i>PPM1D/WIP1</i> C-terminal truncating mutations and other variants	49
1.15.3 <i>PPM1D</i> transcriptional regulation	50
1.15.4 WIP1 degradation	50

1.15.5	WIP1 substrates.....	51
1.15.6	<i>Ppm1d</i> knockout transgenic mice models.....	51
1.16	MDM2 inhibitors	52
1.16.1	Oligonucleotides and peptides	52
1.16.2	Small molecule MDM2 inhibitors	53
1.16.3	Further developments.....	55
1.16.4	Combination of MDM2-antagonists with DNA damaging agents	58
1.16.5	Range of sensitivity to MDM2 inhibitors	59
1.16.6	Determinants of cell fate after activation of wild-type p53 by MDM2 inhibitors	62
1.16.6.1	Screening for synergy with MDM2 inhibitors	66
1.16.6.2	Candidate target investigation.....	66
Aims.....		68
Chapter 2	Materials and methods.....	69
2.1	Tissue culture practice and cell line authentication	70
2.1.1	Cell line growth conditions and husbandry.....	70
2.1.1.1	Monitoring cell morphology using a phase contrast microscope.....	70
2.1.2	MDM2 inhibitor resistant <i>TP53</i> mutant sub-clones.....	71
2.1.3	U2OS cell line pairs	71
1.1.1	Culturing of glioblastoma cell lines stably transfected with Firefly and Renilla Luciferase enzymes	74
2.1.4	Cell count	76
2.1.4.1	Haemocytometer	76
2.1.4.2	Coulter counter	76
2.1.5	Cryogenic preservation and revival of cells.....	76
2.2	Sulforhodamine B assay.....	77
2.2.1	SRB staining protocol	77
2.3	Growth curves	77
2.3.1	Growth inhibition assay and calculation of 50% growth inhibitory concentration (GI50)	78
2.3.2	Measuring Potentiation, Synergy, additivity or antagonism.....	78
2.4	Clonogenic assay.....	81
2.4.1	Conventional method	81
2.4.2	Modified method.....	81
2.4.3	Clonogenic survival in response to ionising radiation	82
2.5	Drugs and specificities	82
2.5.1	MDM2 inhibitors	82
2.5.2	PPM1D/WIP1 inhibitor.....	82
2.5.3	Kinase inhibitors	83
2.6	Analysis of cell cycle distribution via fluorescence-activated cell sorting (FACS)	86
2.6.1	Sample preparation and FACS protocol	86
2.6.2	FACSCalibur instrument setting and gating	87
2.6.3	FACS data analysis	87
2.7	Targeted silencing of gene expression using RNA interference (RNAi).....	89
2.7.1	Design of synthetic siRNA molecules	89
2.7.2	Transfection protocol	91
2.8	Caspase-3/7 activity	92
2.9	Western blotting	92
2.9.1	Principles of western blotting.....	92
2.9.2	Lysate (Cellular protein mixture) preparation.....	92
2.9.3	Measuring total protein	93

2.9.4 SDS-PAGE and transfer stages	94
2.9.5 Protein visualisation using enhanced chemiluminescence.....	94
2.10 Primer-directed polymerase chain reaction (PCR)	97
2.10.1 Quantitative real-time PCR.....	97
2.11 Bacterial culture	99
2.11.1 Bacterial transformation.....	99
2.11.2 Plasmid DNA Extraction	99
2.11.3 Estimation of nucleic acid concentration via spectrophotometry	100
2.12 Immunocytochemistry.....	101
2.13 Protein detection by immunofluorescence	101
2.13.1 Immunofluorescence protocol.....	102
2.14 Confocal microscopy	102
Chapter 3 Exploring the combination treatment of Nutlin-3 and inhibitors of DNA repair enzymes in MDM2 inhibitor sensitive and resistant cell line pairs	104
3.1 Introduction	105
3.1.1 Use of MDM2 inhibitor resistant clones in investigating determinants of MDM2 inhibitor sensitivity	105
3.1.2 Exploring the role of DNA repair enzymes as determinants of response to MDM2 inhibitors	105
3.1.3 Use of small-molecular-weight inhibitors of DNA-repair enzymes in exploring determinants of MDM2 inhibitor sensitivity	106
3.2 Hypotheses	107
3.3 Specific materials and methods.....	107
3.3.1 MDM2 inhibitor resistant clones and their use.....	107
3.3.2 Assessing growth inhibition by SRB assay.....	108
3.3.3 Clonogenic assays	108
3.3.4 Detection of γ H2AX by immunofluorescence staining	108
3.3.4.1 Integrated density quantification	108
3.3.5 Statistical analysis	109
3.4 Results	109
3.4.1 Analysing the cellular and biological response of MDM2 inhibitor resistant cell lines to MDM2 inhibitors.....	109
3.4.2 Cellular response of the MDM2 inhibitor resistant cell lines to IR	109
3.4.3 Biochemical p53 activity in MDM2 inhibitor resistant cells in response to IR	110
3.4.4 Phosphorylation of histone H2AX ^{Ser139} (γ H2AX) following Nutlin-3 is a late event.....	115
3.4.5 Pharmacological inhibition of ATM by KU55933 does not sensitise cell lines to mechanistically relevant doses of MDM2 inhibitors.	118
3.4.6 DNA-PKcs is efficiently inhibited by 1 μ M NU7441	120
3.4.7 DNA-PKcs inhibition by NU7441 does not affect cellular response to MDM2 inhibitors in the absence of DNA damage	120
3.4.8 Biochemical Nutlin-3 mediated p53 response was not affected by 1 μ M NU7441	123
3.4.9 Inhibition of DNA-PKcs potentiates cellular sensitivity to Nutlin-3 in the presence of IR in a cell-type-dependent manner.....	126
3.4.11 NGP cells are sensitive to PARP-1 inhibition by Rucaparib	129
3.4.12 Non-growth inhibitory doses of Nutlin-3 potentiates the response to the combination of IR and NU7441	131
3.5 Discussion	133
3.5.1 MDM2 inhibitor resistant cell lines are not cross-resistant to IR	133
3.5.2 Doses of Nutlin-3 associated with on-target mechanism of action.....	133

3.5.3 Inhibition of DNA repair enzymes involved in double strand break repair in the absence of detectable DNA damage does not potentiate the response to MDM2 inhibitors	134
3.5.4 Inhibition of DNA-PKcs did not alter p53 transcriptional function following Nutlin-3	135
3.5.5 Sensitivity to DNA damage in the presence of Nutlin-3 is context-dependent.	135
3.5.6 Summary	136
Chapter 4 WIP1/PPM1D transient siRNA mediated knockdown enhances cellular sensitivity to Nutlin-3.....	137
4.1 Introduction	138
4.1.1 The WIP1/PPM1D phosphatase as a modulator of p53 crosstalk with DNA damage and stress response pathways.....	138
4.1.2 WIP1 as a determinant of response to MDM2 inhibitors	139
4.1.3 Summary	140
4.2 Hypothesis.....	140
4.3 Specific materials and methods.....	141
4.3.1 Cell lines	141
4.3.2 Monitoring cell morphology, growth and proliferation using IncuCyte Zoom®	141
4.3.2.1 Treatment schedule	142
4.3.3 WIP1/PPM1D siRNA mediated knockdown	143
4.3.3.1 The effect of transient knockdown and drug combination treatment on cell proliferation and morphology assessed by IncuCyte Zoom®	143
4.3.4 WIP1 targeting siRNA and antibody optimisation	143
4.3.5 Clonogenic survival in response to drug-siRNA combination treatments... ..	148
4.3.6 FACS analysis of cells treated with MDM2 inhibitor and WIP1 siRNA combinations	149
4.3.7 Statistical analysis	149
4.4 Results	150
4.4.1 WIP1 basal protein expression and induction by Nutlin-3 among selected cell line pairs with varying <i>PPM1D</i> genetic status	150
4.4.2 Biochemical response to MDM2 inhibition combined with WIP1 transient siRNA knockdown.....	153
4.4.3 WIP1 siRNA mediated knockdown increases sensitivity to Nutlin-3 in <i>TP53</i> wild-type cell lines	156
4.4.4 WIP1 siRNA transient knockdown decreases clonogenic survival in response to Nutlin-3 in a p53-dependent manner	162
4.4.5 WIP1 knockdown enhances Nutlin-3 mediated cell cycle distribution changes and increases Sub-G1 apoptotic signals.....	165
4.4.6 Caspase-independent cell death in HCT116 ^{+/+} cells in response to Nutlin-3	169
4.5 Discussion	171
4.5.1 WIP1 knockdown and antibody optimisation.....	171
4.5.2 WIP1 knockdown increases sensitivity to Nutlin-3.....	172
4.5.2.1 Transfection conditions results in vacuole formation and potential off-target effects in HCT116 and SJS-1.....	172
4.5.3 Summary	173
Chapter 5 Selective chemical inhibition of WIP1/PPM1D by GSK2830371 potentiates cellular response to MDM2-p53 binding antagonists	174
5.1 Introduction	175
5.1.1 Selective WIP1 inhibition by GSK2830371	175

5.1.2 Activity in cell culture and <i>in vivo</i>	176
5.1.3 Allosteric inhibition and WIP1 degradation	176
5.1.4 Summary	177
5.2 Hypothesis	177
5.3 Specific materials and methods.....	178
5.3.1 Cell lines	178
5.3.2 Assessing growth inhibition by SRB assay.....	178
5.3.3 Measuring synergy in drug combination treatments.....	179
5.3.4 Treatment of cells before FACS analysis	179
5.3.5 Quantification of Caspase-3/7 catalytic activity	179
5.3.6 Continuous exposure cloning efficiency experiments	179
5.3.7 Statistical analysis	180
5.4 Results	180
5.5 Sensitivity to single agent GSK2830371 in cell <i>TP53</i> wild-type and mutant cell line pairs differing in <i>PPM1D</i> genetic status	180
5.5.1 GSK2830371 potentiates the response to MDM2 inhibitors Nutlin-3 and RG7388 in a p53-dependent manner.....	182
5.5.2 Biochemical response to single agent GSK2830371 in MCF-7 cells.....	185
5.5.3 Biochemical response to single agent GSK2830371 treatment and its combination with Nutlin-3 in NGP cells.....	187
5.5.4 WIP1 inhibition by GSK2830371 potentiates caspase-3/7 activation by Nutlin-3 in NGP and SJSA-1 cell lines	189
5.5.5 Potentiation of MDM2 inhibitors by GSK2830371 in HCT116 ^{+/+} cells is due to increase in p53 mediated cell cycle arrest.....	193
5.5.6 Biochemical response of HCT116 ^{+/+} cells in response to GSK2830371 and its combination with MDM2 inhibitors	195
5.5.7 Analysis of cell cycle distribution by FACS following pharmacological inhibition of MDM2, WIP1 or their combination.....	196
5.5.8 GSK2830371 synergises with MDM2 inhibitors in <i>TP53</i> wild-type ovarian cancer cell lines	200
5.6 Discussion	203
5.6.1 WIP1 as a target for non-genotoxic activation of p53	203
5.6.2 The role of WIP1 in determining sensitivity to MDM2 inhibitors	204
5.6.3 Role of WIP1 in cell cycle regulation following MDM2 inhibition.....	205
5.6.4 Potential role for p53 ^{Ser15} phosphorylation in enhancing p53 activity.....	206
5.6.5 Summary	207
Chapter 6 Phosphorylation of p53 ^{S15} is of mechanistic importance in GSK2830371 mediated potentiation of response to MDM2 inhibitors	208
6.1 Introduction	209
6.1.1 Phosphorylation of p53 ^{Ser15} after MDM2 inhibition	209
6.1.2 The role of p53 ^{Ser15} phosphorylation in regulation of p53 transcriptional activity.....	211
6.1.2.1 The role of p53 N-terminal phosphorylation events as studied in transgenic mice	212
6.2 Hypothesis.....	213
6.3 Specific materials and methods.....	213
6.3.1 Cell lines	213
6.3.1.1 Treatment schedules and lysate collection before western blotting	214
6.3.2 Reporter gene analysis	214
6.3.3 RNA extraction for microarray gene expression profiling and qRT-PCR validation.....	214
6.3.4 RNA quality analysis	215

6.3.5 Global gene expression analysis by Illumina HumanHT-12 v4.0 Expression BeadChip array.....	217
6.3.5.1 Experimental design and sample preparation.....	217
6.3.5.2 . Uploading data and statistical analysis.....	221
6.3.5.3 Array quality control.....	221
6.3.5.4 Conclusion of array experimental controls.....	225
6.3.5.5 <i>Pathway analysis</i>	225
6.3.6 Site-directed mutagenesis of cDNA in plasmids.....	225
6.3.7 Transient overexpression of p53 in <i>TP53</i> null mammalian cells.....	226
6.4 Results.....	230
6.4.1 Comparison between Nutlin-3 and ionising radiation induced p53 ^{Ser15} phosphorylation.....	230
6.4.2 Phosphorylation of p53 ^{Ser15} after Nutlin-3 is not exclusive to class of MDM2 inhibitors or cell type.....	231
6.4.3 Phosphorylation of p53 following Nutlin-3 is due to the basal activity of PI3KK.....	233
6.4.4 Pharmacological elevation of p53 ^{Ser15} phosphorylation in the absence of DNA damage concurs with induction of a larger subset of genes regulated by p53-driven promoters.....	236
6.4.5 Pathway analysis of gene expression.....	243
6.4.5.1 qRT-PCR validation of the array data.....	246
6.4.6 p53-dependent reporter gene expression was induced by Nutlin-3 but showed no further change with the addition of GSK2830371 (WIP1i).....	248
6.4.7 Mutations of p53 ^{Ser15} modulate the levels of p53 induced transcriptional targets.....	250
6.5 Discussion.....	254
6.5.1 Phosphorylation of p53 ^{Ser15} in the absence of DNA damage.....	254
6.5.2 Increasing MDM2 inhibitor induced pp53 ^{Ser15} coincides with enhanced p53 transcriptional activity.....	255
6.5.2.1 Induction of p53 targets and kinetics of PTM's.....	256
6.5.2.2 Luciferase reporter gene expression in response to the combination of MDM2 and WIP1 inhibitors.....	256
6.5.3 Transient expression of p53 containing mutations in p53 ^{Ser15}	257
6.5.4 Summary.....	257
Chapter 7 The expression of <i>PPM1D</i> mRNA and WIP1 protein in neuroblastoma: relationship to pathology and survival.....	260
7.1 Introduction.....	261
7.1.1 PPM1D/WIP1 expression as a marker of prognosis in human malignancies.....	261
7.1.2 Summary.....	263
7.2 Hypothesis.....	263
7.3 Specific materials and methods.....	263
7.3.1 Online resources.....	263
7.3.2 Use immunocytochemistry to determine WIP1 antibody specificity.....	264
7.3.2.1 Confocal microscopy z-stack and WIP1 sub-cellular localisation.....	264
7.3.3 Immunohistochemistry.....	268
7.3.3.1 Sample preparation.....	268
7.3.3.2 Slide preparation from paraffin embedded formalin fixed blocks.....	268
7.3.3.3 Antigen retrieval.....	268
7.3.3.4 Antibody application and visualisation.....	268
7.3.4 Neuroblastoma tissue microarrays.....	270
7.3.5 WIP1 immunohistochemical staining and antibody optimisation.....	270

7.3.5.1 Slide scanning and H-score calculation	273
7.3.6 Statistical analysis	273
7.3.6.1 Receiver operating characteristic (ROC) curve	273
7.3.6.2 The log-rank test and Kaplan Meier survival curves	274
7.3.6.3 Contingency tables and Fisher's exact test	274
7.3.6.4 Normality test	274
7.4 Results	277
7.4.1 Data-mining shows that neuroblastoma cell lines have the highest average <i>PPM1D</i> mRNA expression	277
7.4.2 Increased <i>PPM1D</i> mRNA expression in Neuroblastoma is a marker of poor prognosis	277
7.4.3 The relationship between WIP1 IHC staining and patient survival in a panel of neuroblastoma tumour samples	285
7.5 Discussion	292
Chapter 8 General discussion	294
8.1 Mechanistically relevant dose range and scheduling of MDM2 inhibitors in pre-clinical evaluation	294
8.2 DNA repair enzymes as potential co-determinants of response to MDM2 inhibitors	295
8.3 WIP1 phosphatase activity as a determinant of cellular response to MDM2 inhibitors	298
8.4 Phosphorylation of p53 and altered p53-dependent transcription in the potentiation of MDM2-p53 binding antagonists by WIP1 inhibition	300
8.5 Assessing the role of WIP1 protein expression as a prognostic factor in neuroblastoma	305
8.6 MDM2 inhibitor resistant clones show the same sensitivity to IR	306
8.7 Achieving the full potential of MDM2-p53 binding antagonists in anti-cancer therapy	310
References	311
Appendix I: Publications	341

List of Figures

- Figure 1-1 Diagram outlines the six “hallmarks of cancer” as first described by Hanahan and Weinberg in 2000 (Hanahan and Weinberg 2000)..... 4
- Figure 1-2 Diagram obtained from “Hallmarks of Cancer: Next generation” depicts the four additional proposed archetypal tumour traits and outlines examples of targeted therapeutic agents, at different stages of pre-clinical and clinical development, designed to combat these ten traits (Hanahan and Weinberg 2011). 4
- Figure 1-3 Cross species alignment of the p53 amino acid sequence showing the most conserved regions of p53 amino acid sequence (I-V). Image taken from Soussi and May 1996 (Soussi and May 1996). 9
- Figure 1-4 Topological diagram of the core domain of p53 shows the loops and the LSH motif and the coordinated zinc atom within the secondary structure. The conserved regions are colour coded, Yellow; region II, Blue; Region II, Red; Region IV, and Purple; region V. The diagram was taken from Cho *et al.*, 1994 (Cho, Gorina *et al.* 1994) 20
- Figure 1-5 The five conserved regions of *TP53* with relation to its mutational hotspots detected in tumours. The bars show the approximate position and relative frequency of these mutations in human cancers. Figure from Cho *et al.*, 1994 (Cho, Gorina *et al.* 1994) 20
- Figure 1-6 Ribbon drawing of the p53 oligomerisation domain and important amino acid residues involved in its function. Figure taken from Clore *et al.*, 1994 (Clore, Omichinski *et al.* 1994)..... 24
- Figure 1-7 The cell cycle, and the regulation of its progression by different cyclin-CDK complexes and CDK inhibitors. Adapted from Vermeulen *et al.*, (2003)..... 27
- Figure 1-8 Alternate reading frame of the *CDKN2A* locus giving rise to p14^{ARF}. Exons 1 α and 3 are reportedly excluded during transcription to allow the p14^{ARF} mRNA. 36
- Figure 1-9 MDM2 is the most important regulator of p53. Transcriptional activity stability and nuclear localisation of p53 are all regulated primarily by MDM2. Cellular stress can result in disruption of this molecular interaction and lead to p53 stability MDM2 is also a direct downstream transcriptional target of p53 and hence these two molecules form an auto-regulatory feedback loop. Figure obtained and modified from (Tweddle, Pearson *et al.* 2003). 36
- Figure 1-10 Some of the mechanisms through which WIP1/PPM1D has been reported to directly and indirectly regulate the p53 network in response to oncogenic stress and DNA damage. Image adapted and modified from Lu *et al.*, 2008 (Lu, Nguyen *et al.* 2008)..... 47
- Figure 1-11 A) Figure obtained from Chuman *et al.*, (2009) shows the alternative splicing and inclusion of exon 5' between PPM1D exons 5 and 6. B) Sequence corresponding to intron exon boundaries of exon 5' in addition to the 10 amino acids and the stop codon encoded by the PPM1D430 transcript. C) The diagram shows the location of the stop codon in

PPM1D430 with respect to the WIP1 catalytic site.	48
Figure 1-12 This shows how Nutlins (Nutlin-2: carbon atoms drawn as white spheres, nitrogen in blue, oxygen in red, and bromine in brown) can mimic important p53 residues (F19, W23 & L26 carbon atoms drawn as green spheres) and therefore interfere with the interaction of p53 and MDM2. One bromophenyl moiety sits in the W pocket and the other in the L pocket. The ethyl ether moiety sits in the F pocket. The imidazoline ring plays the role of the peptide backbone of p53.....	55
Figure 1-13 A) Co-crystal structure of MDM2 and the pharmacophore used for the derivation of RG7388 shows the π - π interaction of the 2-chlorophenyl moiety with H96 in the eMDM2 hydrophobic binding pocket. B) Chemical structure of RG7388. The additional fluorine atoms on the chlorophenyl moieties and the m-methoxybenzoic acid (blue) increased MDM2 binding affinity, cellular potency, microsomal stability and PK properties of the pharmacophore. Images were obtained from (Zhao, Aguilar et al. 2015).	57
Figure 1-14 Volcano plot shows that although TP53 is the strongest determinant of response to Nutlin-3a, there are many other genes, which if altered, can influence sensitivity to Nutlin-3a. Y-axis: The p-value from multivariate ANOVA of drug gene interaction on an inverted \log_{10} scale. X-axis: Magnitude of the effect that genetic events have on the GI50 of the drug in cell lines. The size of the circle indicates the number of genetic events corresponding to the analysis for a given gene or a drug. Figure obtained from (http://www.cancerrxgene.org/).	61
Figure 1-15 Range of Nutlin-3a IC50/GI50 in TP53 mutant and wild-type panel of cell lines from the Wellcome Trust Sanger Institute drug sensitivity database.....	62
Figure 2-1 A & B) Schematic diagrams describing the derivation of MDM2 inhibitor resistant sub-clones including segments of the chromatograms generated by Sanger sequencing which show the sites of mutations in these clones. C) Fluorescent <i>in situ</i> hybridisation of the chromosome 17 centromer (Red foci) and 17p loci (Green foci) in parental and resistant cell lines. D) Mutant specific PCR amplification showing that the mutations could not be detected in the parental population.....	73
Figure 2-2 Cartoon of the process involved in generation of glioblastoma clones with stably transfected p53 response element (RE) driven Firefly reporter and minimal transactivating promoter (mTA) driven Renilla luciferase internal control. TA: Transactivation; bp: base pairs; R: Resistance; Wt: Wild-type; Mut: Mutant.....	75
Figure 2-3 SRB growth curve experiments were carried out in order to determine the doubling time and the optimal cell density (cells/well) for growth inhibition assay experiments	79
Figure 2-4 Manual gating of events based on FL2-A v FL2-W plots and FL2-A frequency distribution histogram.	88
Figure 2-5 An example of a standard curve for used for protein estimation.	93
Figure 2-6 Screen shot showing Nanodrop 1000 software presentation of absorbance spectra	

pertaining to a plasmid sample purified by a Miniprep kit.	101
Figure 3-1 A) SRB Nutlin-3 growth inhibition curves obtained for 72Hrs exposure of cell line pairs to Nutlin-3 (0.1-50 μ M). Bar charts show Nutlin-3 GI50 values calculated based on the growth inhibition curves and p-values represent paired t-tests for n=3 repeats. B) Nutlin-3 clonogenic survival curves after 48Hrs exposure to Nutlin-3 (1.25-10 μ M) for n=3 repeats. GI50: 50% growth inhibitory concentration. LC50: Concentration that causes 50% loss of clonogenic survival; LC10: Concentration at which there is 10% clonogenic survival.	112
Figure 3-2 A) SRB ionising radiation (IR) growth inhibition curves obtained 72Hrs following treatment show that there is little difference in sensitivity between the <i>TP53</i> wild-type parental cell lines and their <i>TP53</i> mutant otherwise isogenic clones. B) There was no difference clonogenic cell survival following IR between the <i>TP53</i> wild-type and mutant cell line pairs C) Colony formation in HCT116 cell line pair shows that sensitivity to IR is not dependent on the <i>TP53</i> genetic status.	113
Figure 3-3 A) Immunoblots showing the induction of early p53 transcriptional targets in <i>TP53</i> wild-type and mutant cell line pairs 4Hrs following IR. B) Immunoblot showing the extent of caspase-3 cleavage (marker of apoptosis) 48Hrs following IR treatment of the NGP cell line pair. C) Cleaved caspase-3 and PARP-1 cleavage could not be detected in SJSA-1 and HCT116 cell line pairs 48Hrs following IR.	114
Figure 3-4 5 μ M Nutlin-3 does not lead to γ H2AX staining in SJSA-1 and NGP cells until 24Hrs following treatment. Each cell line was also treated with 2Gy IR and stained for γ H2AX in parallel as positive control for staining.	116
Figure 3-5 A) Representative γ H2AX immunofluorescence staining of MCF-7 cells 30min after treatment with Nutlin-3 at different doses. IR induced γ H2AX staining was used as positive control. B) Mean + SEM integrated immunofluorescence signal for three independent experiments.	117
Figure 3-6 A) Immunoblot showing the inhibition of IR induced ATM ^{Ser1981} autophosphorylation in the presence of 10 μ M KU55933. B) KU55933 (0.1-50 μ M) SRB growth inhibition curves after 72Hrs of treatment shows that 10 μ M KU55933 causes ~10% growth inhibition in both cell lines regardless of their <i>TP53</i> genetic status.	119
Figure 3-7 Immunoblots on lysates from untreated and irradiated cell line pairs in the presence or absence of 1 μ M NU7441. Cells were pre-treated with 1 μ M NU7441 for 30min prior to irradiation. DNA-PKcs is functional in both cell lines pairs and its autocatalytic activity is inhibited by 1 μ M NU7441.	121
Figure 3-8 SRB growth inhibition curves obtained after 72Hrs of exposure of cell line pairs to NU7441 (0.1-10 μ M). Sensitivity to NU7441 is independent of the <i>TP53</i> genetic status and 1 μ M NU7441 is the highest non-growth inhibitory dose of DNA-PKcs inhibitor tested.	122
Figure 3-9 A) SRB growth inhibition curves after 72Hrs treatment with Nutlin-3 + 1 μ M	

NU7441. B) Bar charts showing Nutlin-3 GI50 values in the presence and absence of 1µM NU7441. P-values were derived from paired t-tests between the columns indicated.	124
Figure 3-10 Biochemical response of the <i>TP53</i> wild-type (Green) and mutant (Red) cell line pairs 4Hrs following treatment with Nutlin-3 + 1µM NU7441. Canonical transcriptional targets of p53 induced by Nutlin-3 such as, MDM2 and p21 ^{WAF1} are not affected in the presence of 1µM NU7441.....	125
Figure 3-11 A) SRB growth inhibition curves for NGP cells 72 hours after treatment with Nutlin-3 + IR + 1µM NU7441. % growth inhibition is calculated with respect to either DMSO + IR treated wells or 1µM NU7441 + IR treated wells, where NU7441 is present. B) Bar charts showing Nutlin-3 GI50 values calculated based on the curves in A.....	127
Figure 3-12 A) SRB growth inhibition curves of SJSA-1 cells 72 hours after treatment with Nutlin-3 + IR + 1µM NU7441. Growth inhibition is calculated as a % of to either DMSO + IR treated wells or 1µM NU7441 + IR treated wells, where NU7441 is present. B) Bar charts showing Nutlin-3 GI50 values calculated based on the curves in A.	128
Figure 3-13 A) Week long SRB Rucaparib growth inhibition curves show that NGP cell line pair are more sensitive to PARP-1 inhibition irrespective of their <i>TP53</i> genetic status compared to the SJSA-1 cell line pair and MCF-7 cells. B) Rucaparib GI50 values in each cell line. Mean + SEM represent three independent repeats. Rucaparib did not reach its GI50 in SJSA-1 and SN40R2 cells there fore the bars represent GI50>10µM.....	130
Figure 3-14 A) IR clonogenic survival curves for NGP and N20R1 cells pre-treated for four hours with 0.2µM Nutlin-3, 1µM NU7441 or their combination. Survival is presented as a % of untreated DMSO alone plating efficiency. B) Bar charts for NGP cells showing raw cloning efficiencies for each treatment condition. One-tailed paired t-tests were carried out to assess whether the differences between the treatments are statistically significant.	132
Figure 4-1 Positions and sequences of WIP1 siRNA constructs 1-4 are highlighted in yellow over the WIP1 reference sequence obtained from the UCSC genome browser. The sequence in dark blue encodes full length WIP1, pale blue letters indicate the exon-exon boundaries and the sequence in red outlines the retained alternatively spliced exon which leads to a premature stop codon in spite of a longer transcript.	145
Figure 4-2 An increment of WIP1.4 siRNA concentration (25nM-100nM), the sequence for which had previously been defined and used in the literature, was examined to optimise WIP1 protein knockdown conditions at different time-points post transfection. WIP1.4 did not result in a notable dose- or time-dependent knockdown of basal WIP1 protein levels in MCF-7 cells.....	146
Figure 4-3 A) Optimisation of WIP1 antibody and siRNA mediated knockdown in MCF-7 cells. Following 24 and 48Hrs of siRNA mediated knockdown conditions, MCF-7 cells were treated with 10Gy IR and lysates were collected 4Hrs later for western blot analysis. Two antibodies were used to probe for WIP1 (F-10 and H-300). B) The optical densities (OD)	

of bands detected by F-10 were measured to quantify the extent of WIP1 knockdown and select the most effective siRNA construct. C) WIP1 knockdown was expressed as a % of WIP1 OD in the control (Cont. siRNA) treated samples and was approximately 60% with the WIP1.2 construct. SE: Short Film Exposure; LE: Long film exposure; tfxn:

transfection..... 147

Figure 4-4 A) Basal WIP1 expression of *TP53* wild-type (green) and *mutnat/null* (Red) cell line pairs. B) Induction of p53 targets, such as WIP1, MDM2, p21^{WAF1} and BAX, after 4Hrs 5µM Nutlin-3 treatment (Nut-3). Different duration of exposure of the X-ray film to the nitrocellulose membrane corresponding to each protein are denoted either as SE: Short exposure or LE: Long exposure. Arrows point to the band at the expected molecular weight for that given protein. FL-WIP1: Full length WIP1; S-WIP1 shorter WIP1 isoform ; T-WIP1: Truncated WIP1 isoform. B was carried out by supervised M.Res student Mrs Liang Zhao. 151

Figure 4-5 Dose-dependent response to Nutlin-3 treatment in *TP53* wild-type cell lines with different *PPM1D* status. The anti-WIP1 antibody H-300 was used for these blots. SE: Short exposure; LE: Long exposure..... 152

Figure 4-6 The effect of WIP1 siRNA knockdown on p53 post-translational modification and its downstream targets over 8 hours in NGP cells. Cells were pre-treated for 24 hours with control siRNA or WIP1 siRNA and then treated with 5µM Nutlin-3. Lysates were collected in parallel at the stated time-points after drug treatment and immunoblots carried out simultaneously. Two identical controls were loaded onto the first two tracks on each blot as reference points for optical density (OD) comparison of bands between blots. WIP1.2 siRNA suppresses Nutlin-3 mediated WIP1 induction and increases pp53^{S15} without affecting total p53. LE: Long exposure: SE: Short exposure..... 154

Figure 4-7 Densitometry of blots shown in Figure 3-21 where the. OD of each band was measured relative to actin and then normalised to 0.5Hr DMSO control (lane 2) which represents the baseline protein expression on each blot. A) Nutlin-3 mediated WIP1 induction over time is suppressed in the presence of WIP1.2 siRNA compared to Cont. siRNA. B) Total p53 induction after 5µM Nutlin-3 in the presence of WIP1.2 siRNA was not affected compared to control. C) Phosphorylation of p53 on serine 15 (pp53^{S15}) after 5µM Nutlin-3 treatment increases in the presence WIP1.2 siRNA compared to control siRNA. Datapoints represent one experiment. 155

Figure 4-8 Monitoring of (A) NGP and (B) N20R1 cell confluence over time during treatment with WIP1.2 or control (Cont.) siRNA ± 5µM Nutlin-3 using IncuCyte. WIP1 siRNA alone reduces confluence over time and markedly increases NGP sensitivity to Nutlin-3 for the NGP wild-type *TP53* cells. Tfxn: Transfection; Nut-3/DMSO: 5µM Nutlin-3 or 1% (v/v) DMSO 157

Figure 4-9 Monitoring of (A) HCT116^{+/+} and (B) HCT116^{-/-} cell confluence over time using

IncuCyte as described in Figure 3-24. WIP1 siRNA alone reduces confluence over time of both cell lines and markedly increases HCT116 ^{+/+} sensitivity to Nutlin-3. Tfxn: Transfection; Nut-3/DMSO: 5μM Nutlin-3 or 1% (v/v) DMSO	158
Figure 4-10 Monitoring of (A) SJSA-1 and (B) SN40R2 cell confluence over time using IncuCyte as described in Figure 3-24. WIP1 siRNA alone reduces confluence over time of both cell lines and markedly increases SJSA-1 sensitivity to Nutlin-3. Tfxn: Transfection; Nut-3/DMSO: 5μM Nutlin-3 or 1% (v/v) DMSO.	159
Figure 4-11 WIP1 knockdown Immunoblots carried out in parallel with the IncuCyte experiment in NGP cell line pair shows that WIP1 knockdown and combination with Nutlin-3 results in an increase in p21 ^{WAF1} and MDM2 expression in <i>TP53</i> wild-type NGP cells but it does not affect pp53 ^{S20} in contrast to the <i>TP53</i> mutant N20R1 cells. Cells were transfected with siRNA 24 Hrs before treatment with DMSO/Nutlin-3 and lysates were then collected after 4Hrs of drug incubation.	160
Figure 4-12 Transfection conditions result in formation of numerous cytoplasmic vacuoles in HCT116 cells by 72 hours.....	161
Figure 4-13 A) Cytoplasmic vacuoles in response to transfection conditions in HCT116 cells. B) Loss of membrane integrity in the presence of Nutlin-3 and WIP1.2 siRNA.....	161
Figure 4-14 WIP1 siRNA mediated knockdown increases sensitivity to Nutlin-3 in clonogenic survival assays in a p53 dependent manner. A & B) NGP cell line pair were treated with Cont. siRNA/ WIP1 siRNA and after 24 hours exposed to Nutlin-3 (0.03-1.3μM) for 48 hours before being re-plated at different densities (500-10000). Cells were left to form colonies, fixed, stained and then colonies counted. C) Colony formation assay images of Cont. siRNA + Nutlin-3 and WIP1 siRNA + Nutlin-3 (0 means DMSO control). Images are representative of the biggest difference observed in three independent repeats. Supervised MRes student Mrs Liang Zhao assisted with this experimental procedure. ...	163
Figure 4-15 WIP1 knockdown combined with Nutlin-3 treatment carried out in parallel with the clonogenic survival assays showed a marked increase in pp53 ^{S15} compared to control (Cont.) siRNA in NGP cells and to a lesser extent in N20R1 cells. Cells were transfected with siRNA 24 Hrs before treatment with DMSO/Nutlin-3 and lysates were then collected after 4Hrs of drug incubation.	164
Figure 4-16 Analysis of cell cycle distribution in response to WIP1 knockdown. In NGP or N20R1 cells WIP1 targeting siRNA (WIP1.2) does not affect cell cycle distribution at 72 hours and does not cause an increase in Sub-G1 events compared to control siRNA (Cont. siRNA).	166
Figure 4-17 In NGP cells combination of WIP1 knockdown and Nutlin-3 treatment does not result in changes in cell cycle distribution (A) but it leads to a significant increase in Sub-G1 events (B). Paired t-test p-value. Cells were transfected with siRNA 24 Hrs before treatment with DMSO/Nutlin-3 and harvested after a further 48 hours of incubation.....	167

Figure 4-18 in N20R1 cells combination of Nutlin-3 and WIP1 knockdown does not affect either cell cycle distribution or % of sub-G1 events. Cells were transfected with siRNA 24 Hrs before treatment with DMSO/Nutlin-3 and harvested after a further 48 hours of incubation.....	168
Figure 4-19 Comparison of late cell death markers in NGP and HCT116 ^{+/+} cells after 48 hours treatment with 5µM Nutlin-3 ± Cont./WIP1.2 siRNA. Cleaved caspase-3 appears most notably in NGP cells in the presence of Nutlin-3 under transfection conditions which correlates with caspase-3 related cleaved PARP-1 fragment (C-PARP apoptosis = 85KDa). The cleaved caspase-3 signal was very low in HCT116 ^{+/+} cells and the pattern of PARP-1 cleavage indicated a mode of cell death associated with release Cathepsin B and G enzyme activity (C-PARP necrosis = 55KDa). Overall WIP1 knockdown appeared to lead to increased caspase-3 cleavage or necrosis related PARP-1 cleavage. Western blot carried out by supervised student Mrs Liang Zhao.	170
Figure 5-1 Chemical structure of the allosteric WIP1 inhibitor GSK2830371 as described by Gilmartin <i>et al.</i> , (2014). Image was obtained from http://www.selleckchem.com/	177
Figure 5-2 Week-long (168hrs) dose-dependent growth inhibition in response to the WIP1 inhibitor GSK2830371 in MCF-7 cells and the four <i>TP53</i> wild-type (Green) and mutant (Red) cell line pairs. MCF-7 cells are the most sensitive cell line to GSK2830371 as a single agent.....	181
Figure 5-3 Non-growth inhibitory doses of GSK2830371 (WIP1i) potentiated the response of <i>TP53</i> wild-type cell lines to MDM2 inhibitors. A-H) SRB growth inhibition assays were performed on cell lines described in 5.3.2 with stated doses of Nutlin-3/RG7388 in the presence or absence of 2.5µM GSK283037.....	183
Figure 5-4 Non-growth inhibitory dose of 2.5µM GSK2830371 (WIP1i) potentiated the response of HCT116 ^{+/+} cells to Nutlin-3 and RG7388 to a lesser extent over 72 hours. A & B) SRB growth inhibition assays performed on HCT116 ^{+/+} cells with the stated doses of Nutlin-3/RG7388 in the presence or absence of 2.5µM GSK283037.....	184
Figure 5-5 A & B) Biochemical response of MCF-7 cells to 2.5µM GSK2830371 (~GI50) and its impact on p53 transcriptional activity and post-translational modification over time. GSK2830371 results in time-dependent degradation of WIP1, stabilisation of p53, increased p53 ^{Ser15} and induction of p21 ^{WAF1}	186
Figure 5-6 A) Biochemical response of NGP cells to the stated doses of Nutlin-3, GSK2830371 and their combinations at 4Hrs and 24Hrs. In contrast to the single treatment with each agent, phosphorylated p53 ^{Ser15} (pp53 ^{Ser15}) is most prominently detected in response to the combination treatment and it is associated with p53 stabilisation over the time course and cleaved caspase-3 at 24Hrs. B) Immunoblot showing the biochemical response to single agent GSK2830371 and its combination with 3µM Nutlin-3 over time. Treatment with 2.5µM GSK2830371 alone results in degradation of WIP1 but does not induce p53	

transcriptional targets.	188
Figure 5-7 WIP1 inhibitor GSK2830371 (WIP1i) potentiates the Nutlin-3 mediated caspase-3/7 activity in <i>TP53</i> Wild-type parental cell lines and not their <i>TP53</i> mutant Nutlin-3 resistant daughter cells. A) NGP cells were treated with 0.5 × and 1 × their approximate Nutlin-3 GI50 (1.5μM and 3.0μM respectively) ± 2.5μM GSK2830371 for 24 hours and Caspase-3/7 catalytic activity was quantified. B) Caspase-3/7 activity in response to 48 hour treatment with Nutlin-3 GI50 (3.0μM) + 2.5μM GSK2830371 was measured in NGP cells showing that the combination treatment results in a significant increase in caspase-3/7 signal. SJSA-1 cells were treated with 0.5 × and 1 × their approximate Nutlin-3 GI50 (0.75μM and 1.5μM respectively) ± 2.5μM GSK2830371 for 48 hours and Caspase-3/7 catalytic activity was quantified. There was no caspase-3/7 catalytic activity in neither of the Nutlin-3 resistant cell lines (red bars) derived from NGP and SJSA-1 (green bars). P-values represent paired t-test. *: p<0.05; **: p<0.005.	191
Figure 5-8 Induction of caspase-3/7 activity was not detected in HCT116 ^{+/+} and MCF-7 cells 48 hours following treatment with Nutlin-3 ± 2.5μM GSK2830371 (WIP1i). A) HCT116 ^{+/+} cells treated with 0.5 × and 1 × their Nutlin-3 GI50 (4.5μM and 9.0μM respectively) ± 2.5μM GSK2830371 for 48 hours and Caspase-3/7 catalytic activity was quantified. B) MCF-7 cells were treated with 0.5 × and 1 × their approximate Nutlin-3 GI50 (1.5μM and 3.0μM respectively) ± 2.5μM GSK2830371 for 48 hours and Caspase-3/7 catalytic activity was quantified.	192
Figure 5-9 A) Continuous treatment clonogenic efficiency experiment in HCT116 ^{+/+} cell lines in response to 4.5μM Nutlin-3 (0.5 × GI50) ± 2.5μM GSK2830371 (WIP1i). B) Colony formation following 10 days of treatment. Images representative of the biggest difference observed between single and combination treatment among the three independent repeats. P-value t-test.....	194
Figure 5-10 Biochemical response of HCT116 ^{+/+} cells to 3μM Nutlin-3, 2.5μM GSK2830371, or their combination after 4Hrs treatment.	195
Figure 5-11 Analysis of cell cycle distribution of <i>TP53</i> wild-type cells treated with stated doses of Nutlin-3 (GI50 or 0.5 × GI50 dose), GSK2830371 (WIP1i), or combination over 72 hours. Sub-G1 events were gated out in this analysis.	197
Figure 5-12 Representative cell cycle distribution histograms for NGP and SJSA-1 cells indicating the increase in the proportion of Sub-G1 events in response to 72 hours of treatment with GSK2830371 (WIP1i), Nutlin-3 and their combination. P-values are from paired t-test.....	198
Figure 5-13 3D representation of analysis of cell cycle distribution histograms following treatment with multiples of Nutlin-3 GI50 dose ± 2.5μM GSK2830371 (WIP1i). Histograms correspond to one biological repeat representative of grouped bar charts in Figure 3-21.	199

Figure 5-14 A) 72Hrs GSK2830371 SRB growth inhibition in a panel of <i>TP53</i> wild-type (wt-green) and mutant (mut-red) ovarian cancer cell lines. B & C) Cellular sensitivity to MDM2 inhibitors Nutlin-3 and RG7388. D) Immunoblots showing the biochemical response to GSK2830371 after 4 hours. PA1 cells harbouring a <i>PPM1D</i> -truncating activating mutation (c.1370delC) show the most p53 activation following treatment with GSK2830371.....	201
Figure 5-15 A) Table in aid of interpretation of combination index (CI) values. B) CI values calculated based on 3 independent repeats of 72Hrs growth inhibition experiments combining MDM2 inhibitors Nutlin-3/RG7388 and GSK2830371 at 1:1 ratio of doses with known effects. MDM2 inhibitors are shown to synergise with GSK2830371 at lower doses.....	202
Figure 6-1 Growth curves of DD7 and DR4 cells stably transfected with p53 luciferase reporter and internal control.....	214
Figure 6-2 Aligent Bioanalyzer electropherogram trace and gel representation (on the right). RNA concentration and RIN value are calculated and presented. The ratio of 28S:18S rRNA molecules are calculated based on the area under each curve. Peaks associated with other rRNA or tRNA molecules has been arrowed in addition to the control molecule. .	216
Figure 6-3 A cartoon explaining the inner workings and specifications of Illumina-HumanHT-12-v4.0 BeadChip expression arrays.....	219
Figure 6-4 Experimental design and RNA extraction for use in microarray gene expression analysis. Total protein was also extracted as explained in (2.9.2) from replica samples in parallel.....	220
Figure 6-5 Ranked mean signal intensity per probe and standard deviation between samples show that standard deviation does not correlate positively with mean signal intensity ...	223
Figure 6-6 A) Boxplot of median signal intensities of arrays show that median signal intensity and the spread of the data are similar among arrays. B) Density plot of intensity of all arrays shows that the spread of signal intensity is the same among samples.....	223
Figure 6-7 A-E) Summary of controls from 12 arrays/samples as suggested by Illumina. Sample –dependent and independent controls (explained in 6.3.5.3) show no signs of experimental errors or inconsistencies. In D mm2: Mismatch; pm: Perfect match	224
Figure 6-8 The map of pcDNA3.1 plasmid as presented in its online user manual (Invitrogen #: V790-20 and V795-20). The full-length p53 cDNA sequence was cloned downstream of the Cytomegalovirus (CMV) promoter. This plasmid was used in site-directed mutagenesis studies of p53 and for overexpression of p53 in HCT116 ^{-/-} cells.....	227
Figure 6-9 Kinetics of p53 ^{Ser15} phosphorylation in NGP cells following either 10Gy IR (A) or 5µM Nutlin-3 (B). The first and the last lanes on each blot can be used as positive control for p53 ^{Ser15} and comparators for band intensity on each blot.	231
Figure 6-10 Phosphorylation of p53 ^{Ser15} 4Hrs following treatment with MDM2 inhibitors is	

neither class nor cell type specific. Different classes of MDM2 inhibitors all cause an increase in p53 ^{Ser15} phosphorylation in both NGP and SJSA-1 cell lines. Supervised undergraduate student Mr Alex Smith assisted with this experiment.	232
Figure 6-11 IR induced phosphorylation of p53 ^{Ser15} is dependent on ATM catalytic activity. NGP and their otherwise isogenic <i>TP53</i> mutant daughter cell line N20R1 were pre-treated for 30min with the stated doses of kinase inhibitors and then exposed to IR 30 min before lysate extraction. KU: ATM inhibitor KU55933; NU: DNA-PK inhibitor NU7441; WMN: Broad spectrum PI3K inhibitor Wortmannin.	234
Figure 6-12 Phosphorylation of p53 ^{Ser15} following MDM2 inhibitors is dependent on both ATM and DNA-PK kinase activity. Individual specific kinase inhibitors NU7441 (DNA-PK) and KU55933 (ATM) did not reduce p53 ^{Ser15} phosphorylation as effectively as their combination. Cells were treated simultaneously with doses of Nutlin-3 or stated kinase inhibitor(s) 4Hrs prior to lysate collection. KU: ATM inhibitor KU55933; NU: DNA-PK inhibitor NU7441; WMN: Broad spectrum PI3K inhibitor Wortmannin.	235
Figure 6-13 Volcano plot showing the top 50 differentially expressed genes between DMSO and the two treatment conditions. A larger subset of p53 target genes are differentially expressed in response to the combination of RG7388 and GSK2830371 at compared RG7388 single treatment at 4Hrs. Y-axis shows $-\log_{10}$ adjusted p-value (Benjamini-Hotchberg Corrected) and the x-axis shows \log_2 fold-change.	241
Figure 6-14 Immunoblot shows treatment with the combination of RG7388 and GSK2830371 compared to RG7388 alone results in an increase in p53 ^{Ser15} phosphorylation pp53 ^{Ser15} at 4Hrs which correlates with an increase in p53 transcriptional targets p21 ^{WAF1} and MDM2.	242
Figure 6-15 Canonical p53 transcriptional targets induced in response to treatment with 75nM RG7388 and their involvement in cellular processes ($p=3.19 \times 10^{-9}$). Nodes filled grey are not induced in response to RG7388 single treatment.	244
Figure 6-16 Canonical p53 transcriptional targets induced in response to treatment with 75nM RG7388 + 2.5 μ M GSK2830371 and their involvement in cellular processes as identified by IPA reference data set ($p=7.78 \times 10^{-10}$). PIDD1 and PUMA are induced in the presence of WIP1 inhibition.	245
Figure 6-17 Quantitative real-time PCR carried out to assess the validity of microarray data. Data represent mean \pm standard error of mean (SEM) relative quantities of four independent repeats where <i>GAPDH</i> was used as endogenous control and DMSO as the calibrator for each independent repeat with the formula $2^{-\Delta\Delta C_T}$. P-values calculated by paired t-test; *: $p<0.05$; **: $p<0.005$; ***: $p<0.0005$	247
Figure 6-18 A) Firefly luciferase reporter enzyme activity 24Hrs following $1 \times$ and $2 \times$ Nutlin-3 DD7 GI50. B) SRB Growth inhibition of stably transfected glioblastoma cell lines in the presence and absence of 2.5 μ M GSK2830371. Potentiation of the <i>TP53</i> wild-type cell	

lines is modest. Wt: Wild-type; Mut: Mutant.....	249
Figure 6-19 Chromatogram traces from the Sanger sequencing experiment before and after site-directed mutagenesis of full-length p53 plasmid.	251
Figure 6-20 Phosphorylation of p53 influences expression of p53 transcriptional targets MDM2 and p21 ^{WAF1} at the protein level. A) Immunoblot showing <i>TP53</i> Null HCT116 cells (HCT116 ^{-/-}) transfected with 4.0µg of either wild-type (Wtp53) or mutant p53 (p53 ^{S15A} or p53 ^{S15D}) expression plasmids 12Hrs before lysate extraction and western blotting. B) Immunoblot of HCT116 ^{-/-} cells transfected with lower amounts of p53 overexpressing plasmids with lysate collection at two different time-points. HCT116 ^{+/+} cells were used as a positive control in B. Tfxn: transfection; Conc.: Concentration	252
Figure 6-21 Apoptotic morphology of HCT116 ^{-/-} cells 24Hrs following overexpression of wild-type p53 (Wtp53) compared to p53 ^{S15A} or p53 ^{S15D} . Apoptotic/floating cells were more numerous in.....	253
Figure 6-22 The working model explaining the underlying mechanism of regulation of p53 ^{Ser15} phosphorylation status and its contribution to potentiation of MDM2 inhibitors by the WIP1 inhibitor GSK2830371.....	259
Figure 7-1 Confocal microscopy images of MCF-7 cells treated with DMSO, 5µM Nutlin-3, 2.5µM GSK2830371 or their combination for 4Hrs. GSK2830371 results in a dramatic reduction in both cytoplasmic and nuclear WIP1 signal intensity (AF-488 channel) which is restored modestly when it is combined with Nutlin-3. Nutlin-3 increases WIP1 signal intensity, most likely due to p53 dependent induction of WIP1.	266
Figure 7-2 Gain on both DAPI and AF488 channels was increased to assess the no primary control. There was no WIP1 staining detected at high detector gain in the absence the WIP1 primary antibody showing that the secondary antibody does not bind to other non-specific antigens	267
Figure 7-3 WIP1 IHC staining of xenografts arisen from NGP and N20R1 cell line pair. F-10 antibody dilution used here was 1:50 as recommended in the datasheet by the vendor. .	271
Figure 7-4 WIP1 IHC staining in ovarian TMA's at two different dilutions. 1:500 dilution is more specific at staining tumour tissue and nuclei compared to connective tissue.	272
Figure 7-5 Range of WIP1 IHC staining and their corresponding H-scores.	275
Figure 7-6 A) Overlapping distributions of hypothetical test results for a given continuous variable. B) Hypothetical representation of the ROC curve for an ideal test and the optimal cut off point (green point). TN: True Negative; TP: True Positive; FN: False Negative; FP: False Positive; AUC: Area Under the Curve.....	276
Figure 7-7 Relationship of <i>PPM1D</i> mRNA to DNA copy number in cell lines. R-Pearson = 0.474.....	279
Figure 7-8 Box and whiskers plot mine from the Broad Institute database for <i>PPM1D</i> mRNA expression among cancer cell lines of different tissue origin.....	280

Figure 7-9 Range of <i>PPM1D</i> mRNA expression in neuroblastoma tumours. Age at diagnosis: Red \leq 18 months old, Green \geq 18 months old; Alive: Green = alive Red = dead; Histology: Red = Neuroblastoma; INSS stage: Green = stages 1 or 2, Amber = stage 3, Red = stage 4, Blue = stage 4s.	281
Figure 7-10 Correlation between <i>MYCN</i> and <i>PPM1D</i> expression. Age at diagnosis: Red \leq 18 months old, Green \geq 18 months old; Alive: Green = alive Red = dead; Histology: Red = Neuroblastoma; INSS stage: Green = stages 1 or 2, Amber = stage 3, Red = stage 4, Blue = stage 4s.....	282
Figure 7-11 Above median <i>PPM1D</i> mRNA expression is associated with poorer overall survival in the Versteeg neuroblastoma dataset.	283
Figure 7-12 <i>PPM1D</i> mRNA prognostic significance is not independent of <i>MYCN</i> amplification.	284
Figure 7-13 Metastasis and advanced INSS stage disease are significantly associated with of poor survival in our cohort of neuroblastoma patients.....	287
Figure 7-14 Tumour <i>MYCN</i> -amplification and 11q deletion are significantly associated with poor survival in our neuroblastoma patient cohort. Log-rank test and patient survival according to tumour <i>MYCN</i> -amplification (A) and 11q deletion status (B).....	288
Figure 7-15 Tumour 17q gain and 1p deletion were not significantly predictive of overall survival in our neuroblastoma patient cohort. Log-rank test and patient survival according to tumour 17q gain (A) and 1p deletion status (B). C) There is no statistical difference between mean WIP1 H-score in tumours with and without 17q gain (Unpaired t-test $p = 0.239$).	289
Figure 7-16 The three normality tests used to assess whether H-scores belonging to each subgroup of follow a Gaussian distribution. H-scores associated with the 17q gain subgroup are not normally distributed.....	290
Figure 7-17 A) ROC curve of WIP1 H-scores as a prognostic test. B) Log-rank test and Kaplan Meier plot of WIP1 H-Scores < 7.5 and H-scores > 7.5 groups show that WIP1 protein expression was not significantly related to survival in our cohort of neuroblastoma patients.	291
Figure 8-1 The volcano plot shows that the <i>TP53</i> genetic status is a far better determinant of response to Nutlin-3a ($P\text{-value} = 1.26e^{-54}$) than it is for DNA damaging agents or other targeted agents. Y-axis: The p-value from multivariate ANOVA of drug gene interaction on an inverted \log_{10} scale. X-axis: Magnitude of the effect that genetic events have on the GI50 of the drug in cell lines. The size of the circle indicates the number of genetic events corresponding to the analysis for a given gene or a drug. Figure obtained from (http://www.cancerrxgene.org/).	308
Figure 8-2 The diagram outlines the proposed ideal model for the use of MDM2 inhibitors in combination with other non-genotoxic and genotoxic agents. The main underlying	

assumption is that *TP53* mutant MDM2 inhibitor resistant cells remain sensitive to DNA damaging agents. See chapter 3 for data in support of this assumption. This strategy has the potential to reduce healthy tissue toxicities and the likelihood of secondary cancers.³⁰⁹

List of tables

Table 2-1 <i>TP53</i> Wild-type (Wt) and mutant (Mt)/Null cell line pairs from different tumour origins and their <i>MDM2</i> , <i>MDMX</i> and <i>PPM1D</i> genetic status. Amp.: Amplified; OE: Overexpressing.....	72
Table 2-2 Selection conditions for glioblastoma cell lines stably transfected with a reporter and an internal control vector.....	74
Table 2-3 Seeding densities used for growth inhibition assays along with the approximate doubling time of each cell line during exponential growth.....	80
Table 2-4 Cellular and Cell free assay 50% inhibitory concentrations (IC ₅₀) values for the top three WIP1 inhibitors commercially available along with data on cellular activity in MCF-7 cells. *IC ₅₀ values in two different cell free assays with different substrates; **: Data obtained from the Sanger institute drug sensitivity database; N/A: Not analysed	83
Table 2-5 Published cell free assay IC ₅₀ values for GSK2830371 and SPI-001. * Yeast phosphatase; ** % Inhibition and 40µM. Table derived from data published in (Gilmartin, Faitg et al. 2014) & (Yagi, Chuman et al. 2012).....	84
Table 2-6 <i>In-vitro</i> IC ₅₀ values with respect to other kinases within the kinome are provided above to give a scope of the selectivity of these two kinase inhibitors. Final column data were obtained from (Sarkaria, Tibbetts et al. 1998).....	85
Table 2-7 <i>In-vitro</i> IC ₅₀ values for LY2228820 with respect to other kinases obtained from (Campbell, Anderson et al. 2014).	85
Table 2-8 Recipe for PI solution used for live cell FACS	88
Table 2-9 siRNA constructs and their respective sequence.	91
Table 2-10 SDS-loading buffer constituents and final concentration are stated above.	95
Table 2-11 10 × Running buffer was prepared as stated above and diluted 1:10 for each use... ..	95
Table 2-12 Transfer buffer was prepared as stated above.....	95
Table 2-13 TBS 0.1% Tween-20 was prepared as stated above and the pH was adjusted to 7.6.	95
Table 2-14 Information on antibodies and incubation times are been stated above. HRP: Horseradish peroxidase, Hr: Hour.....	96
Table 2-15 Primer sequences used in qRT-PCR. F: Forward; R: Reverse.	98
Table 3-1 Nutlin-3 (0.1-50µM) SRB growth inhibition in SJSA-1 and SN40R2 cells in the presence of 10µM KU55933. SEM and GI ₅₀ values are representative of three independent experiments (Data obtained from dissertation of Mrs Laura Kettlewell). ...	119
Table 4-1. <i>TP53</i> Wild-type (Wt) and mutant (Mt)/Null cell line pairs with different <i>PPM1D</i> status.....	141
Table 4-2 Seeding densities used in 24 well plates for the incucyte experiment.	142
Table 4-3 Doses of Nutlin-3 and seeding densities for NGP and N20R1 cell lines in 100mm	

dishes. NT: Non transfected.....	148
Table 5-1 Table outlining Ovarian cancer cell lines used by Mrs Rachael Mason and additional relevant information obtained from the literature and catalogue of Somatic Mutations in Cancer (COSMIC) database.....	178
Table 5-2 Number of cells seeded per 100mm dish for assessing cloning efficiency in response to the stated treatments.....	180
Table 6-1 Table shows sample names, their treatment and groups (Independent repeats). Sentrix positions are related to the position of each planar silica slide exposed to a sample.	222
Table 6-2 Primers used in site-directed mutagenesis experiments. Codons modified are denoted in red text.....	228
Table 6-3 Constituents of the PCR reaction for site-directed mutagenesis.....	228
Table 6-4 Thermal cycling during the site-directed mutagenesis PCR experiment.....	229
Table 6-5 Genes induced following treatment of NGP cells with 75nM RG7388 (GI50). OR: Odds Ratio; ROS: Reactive oxygen species.....	238
Table 6-6 A larger subset of p53 transcriptional targets are induced by a combination of 75nM RG7388 and 2.5µM GSK2830371. OR: Odds ratio; ROS: Reactive oxygen species. This table is a continuation of the table on the previous page.....	240
Table 7-1 Buffers ad their constituents	270
Table 7-2 Contingency tables generated to assess any association between other prognostic markers and above and below median WIP1 H-score. The p-values in the last column were determined by Fisher’s exact test.	292
Table 8-1 Differential Trp53 target gene expression between Trp53 wild-type and Trp53 ^{S18A} knock-in transgenic mouse thymocytes, 8Hrs following 5Gy IR, show that Trp53 induced transcription of its canonical targets are diminished in a promoter specific manner when Trp53 Ser18 is mutated to Ala and cannot be phosphorylated. The cells highlighted in amber showed greater than 2-fold reduction in mRNA expression as measured by a murine Affymetrix array. The table is reproduced in modified form from Chao <i>et al.</i> , (2003)...	303

List of abbreviations

53BP1	Tumour protein p53 binding protein 1
53BP2	Tumour protein p53 binding protein 2
APAF-1	Apoptotic peptidase activating factor-1
ATM	Ataxia telangiectasia mutated
ATR	ATM and Rad3-related
ATRIP	ATR interacting protein
AUC	Area under the curve
BAX	Bcl-associated X protein (gene)
BAX	Bcl-associated X protein
BR	Basic region
BRCA1	Breast and ovarian cancer susceptibility protein 1
BRCA2	Breast and ovarian cancer susceptibility protein 2
CCLC	Cancer Cell Line Encyclopaedia
CDC2	Cyclin dependent kinase 1
CDC25A	Cell division cycle 25A
CDC45	Cell division cycle 45
CDK2	Cyclin dependent kinase 2
CDK4	Cyclin dependent kinase 4
CDK6	Cyclin dependent kinase 6
CDKi	Cyclin dependent kinase inhibitor
CDKs	Cyclin dependent kinases
cDNA	Complementary DNA
<i>c-fos</i>	Cellular proto-oncogene fos
CHEK1	Checkpoint kinase 1
CHEK2	Checkpoint kinase 2
<i>c-jun</i>	Cellular proto-oncogene jun
<i>c-myc</i>	Cellular proto-oncogene myc
DAXX	Death associated protein 6
DBD	DNA binding domain
DDR	DNA damage response

DNA	Deoxyribonucleic acid
DNA-PKcs	DNA dependent protein kinase catalytic subunit
<i>DR5</i>	Death receptor 5 gene
DR5	Death receptor 5 protein
DSBs	Double strand breaks
E2F1	E2F transcription factor 1
ELISA	Enzyme linked immunosorbent assay
EMSA	Electrophoretic mobility shift assay
<i>ERCC2</i>	Excision Repair Cross-Complementing Rodent Repair Deficiency, Complementation Group 2
<i>ERCC3</i>	Excision Repair Cross-Complementing Rodent Repair Deficiency, Complementation Group 3
<i>ERCC6/CSB</i>	Excision Repair Cross-Complementing Rodent Repair Deficiency, Complementation Group 6
<i>FASR/APO-1/CD95</i>	FAS receptor gene
FASR/CD95/Apo-1	FAS receptor protein
FGF	Fibroblast growth factor
F-MuLV	Friend murine leukaemia virus
G0	Gap 0
G1	Gap 1
G2	Gap 2
<i>GADD45</i>	Growth arrest and DNA damage inducible
GFP	Green fluorescent protein
HAT	Histone acetyl transferase
HAUSP	Herpesvirus-associated ubiquitin-specific protease
HPV-E6	Human papilloma virus E6
HR	Homologous recombination
HRR	Homologous recombination repair
<i>hsc-70</i>	Heat shock cognate 71 KDa protein
IARC	International Agency for Research on Cancer
ICC	Immunocytochemistry
<i>ICE</i>	Mammalian Ced-3 homologue
<i>Ich-1L</i>	Ice/ced-3-related gene

IGF-1	Insulin like growth factor
IHC	Immunohistochemistry
<i>IL-6</i>	Interleukin 6
IR	Ionising radiation
KDa	Kilo Dalton
Ki67	Proliferation-related Ki-67 antigen
LOH	Loss of heterozygosity
LSH	Loop sheet helix
MAPK	Mitogen activated protein kinase
MCK	Muscle creatine kinase
<i>MDM2</i>	Mouse double minute gene (human homologue)
MDM2	Mouse double minute protein (human homologue)
<i>mdm2</i>	Mouse double minute gene mouse
MEK	MEK kinase (mitogen activated)
MRE11	Meiotic recombination 11 homolog
MRN	Mre11, Rad50 and Nbs1
mRNA	Messenger RNA
NBS1	Nijmegen breakage syndrome 1
NHEJ	Non-homologous end joining
NLS1	Nuclear localisation sequence 1
NLS2	Nuclear localisation sequence 2
NLS3	Nuclear localisation sequence 3
<i>NOXA</i>	Phorbol-12-myristate-13-acetate-induced gene 1 or PMAIP1
NOXA	Phorbol-12-myristate-13-acetate-induced protein 1 or PMAIP1
OD	Optical density
P1	MDM2 promoter 1
P2	MDM2 promoter 2
p21/WAF1/CIP1	Wild-type p53-activated fragment 1
P3	MDM2 promoter 3
p300/CBP	E1A-binding protein, 300kDa
PARP-1	Poly (ADP-ribose) polymerase 1

PCAF	p300/CBP associated factor
PCD	Programmed cell death
PDGF	Platelet derived growth factor
PIDD	p53 induced protein with death domain
PIKKs	Phosphatidylinositol 3-kinase like serine/threonine kinase
PPM1D/WIP1	Protein phosphatase, Mg²⁺/Mn²⁺ dependent, 1D
Praja1	Praja ring finger 1, E3 ubiquitin protein ligase
PRR	Proline rich region
PTEN	Phosphatase and tensin homologue
PUMA	p53 upregulated modulator of apoptosis (gene)
PUMA	p53 upregulated modulator of apoptosis (protein)
RAD50	Rad50 homologue (Human gene)
RAF	Proto-oncogene A-Raf
RB	Retinoblastoma protein
<i>RB1</i>	Retinoblastoma gene
ROS	Reactive oxygen species
RPA	Replication protein A
S	S-phase
SDS	Sodium dodecyl sulfate
SFFV	Spleen focus-forming virus
SH3	Src homology 3 domain
SNPs	Single nucleotide polymorphism
SSBs	Single strand breaks
SV40	Simian virus 40
TA	Transactivation domain
TAFII31	TATA Box Binding Protein (TBP)-Associated Factor 31
TAFII40	TATA Box Binding Protein (TBP)-Associated Factor 40
TAFII60	TATA Box Binding Protein (TBP)-Associated Factor 60
TBP	TATA binding protein
TFIID	Transcription factor IID
TFIIH	Transcription factor IIH

Topo 1	Topoisomerase I
TP53	Tumour protein p53
<i>TP53I3/PIG3</i>	TP53 inducible protein 3
TPEN	N,N,N',N'-tetrakis(2-pyridylmethyl)-ethylenediamine
<i>Trp53</i>	Transformation related protein 53 (Murine gene)
Trp53	Transformation related protein 53 (Murine protein)
TUNEL	terminal deoxynucleotidyl transferase dUTP nick end labelling
UCSC	University of California Santa Cruz
UV	Ultraviolet
VP16	Herpesvirus protein VP16
WEE1	Wee1 homologue (Human protein)
wt	Wild-Type
<i>WTAP</i>	Wilm's tumour gene
XLF	XRCC4-like factor
XP	Xeroderma pigmentosum
XPC	Xeroderma pigmentosum complementation group
<i>YWHA/14-3-3 sigma</i>	Tyrosine 3-Monooxygenase/Tryptophan 5-Monooxygenase Activation Protein, Sigma Polypeptide
γH2AX	H2A histone family member X phosphorylated at Ser139

Chapter 1 Introduction

1.2 Genomic integrity

The genomic integrity of cells is constantly threatened by exogenous and endogenous factors that can directly or indirectly result in DNA damage. However, cells have evolved a series of mechanisms that prevent the propagation of deleterious genetic alterations to their daughters. There is extensive crosstalk between the signalling networks involved in detection of DNA damage and those which orchestrate normal cell cycle progression, growth, differentiation, senescence and programmed cell death (e.g. apoptosis). DNA damage response (DDR) biochemical signalling pathways are triggered by cytotoxic DNA lesions, which then either promote arrest at specific cell cycle checkpoints to provide sufficient time for repair mechanisms to rectify the damage, or alternatively signal the initiation of programmed cell death to effector molecules if the damage incurred is irreparable. Defects or overwhelming of such safeguard mechanisms can lead to positive selection of non-lethal genetic alterations which favour autonomous cellular proliferation, disturbance of tissue homeostasis and the ultimate emergence of malignant cancer cells that are unfavourable for the survival of the organism (Fearon and Vogelstein 1990, Hanahan and Weinberg 2000, Hanahan and Weinberg 2011). A pivotal component of the mechanisms evolved to protect genomic integrity of the germline and somatic tissue is the *TP53* gene, encoding the tumour suppressor p53 protein, which has been aptly dubbed “guardian of the genome” (Lane 1992, Belyi, Ak et al. 2010). This chapter aims to introduce p53 signalling and discuss its potential utility in cancer therapy.

1.3 Cancer

Cancers are defined as a group of more than 100 distinct diseases that are characterised by autonomous cellular growth and their malignant invasion of other anatomical locations (metastasis), which can potentially result in the death of the organism. The aetiologies of human cancers are considered mostly environmental with only 5-10% of cancers considered to be associated with identifiable germline mutation which increase predisposition to development of particular cancers (Garber and Offit 2005). The correlation of cancer incidence with age and its stepwise pathological progression from premalignant (benign) to malignant tissue observed throughout tumourigenesis suggests that cancer development is a multistep process (Hanahan and Weinberg 2000). A clonal model of cancer development, first put forward in 1976 by Peter Nowell, postulates that stepwise acquisition of stochastic genetic changes in a progenitor somatic cell

ultimately, through Darwinian adaptive evolution, results in transformation from normal to malignant pathology (Nowell 1976). This model has consistently been supported by more advanced genetic and molecular examination of cancer development (Greaves and Maley 2012). The traits associated with these groups of stepwise and sequential genetic changes have been categorised into distinct groups and proposed to represent “Hallmarks of cancer” (Hanahan and Weinberg 2000, Hanahan and Weinberg 2011).

1.4 Hallmarks of cancer

In a seminal publication by Douglas Hanahan and Robert A. Weinberg (2000) it was proposed that the prerequisite genetic changes for malignant growth manifest themselves in six distinct traits depicted in Figure 1-1. The authors also emphasised the potential importance of “heterotypic signalling”, or the interaction of transformed cells with the tumour microenvironment, in studying disease progression and pursuing new treatment strategies (Hanahan and Weinberg 2000). This conceptual framework was built upon with the addition of new traits in a more recent publication (Hanahan and Weinberg 2011) (Figure 1-2).

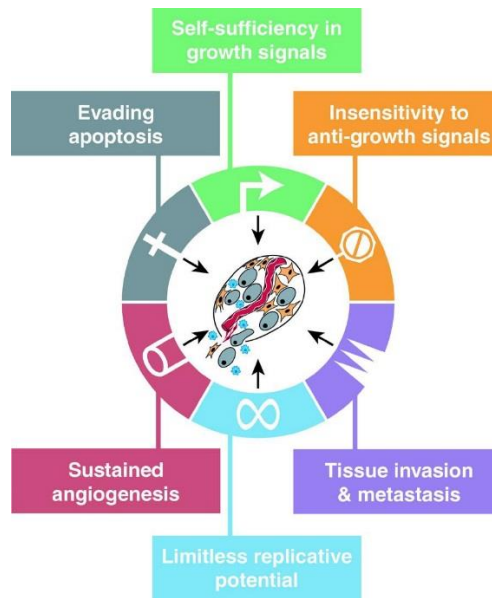


Figure 1-1 Diagram outlines the six “hallmarks of cancer” as first described by Hanahan and Weinberg in 2000 (Hanahan and Weinberg 2000).

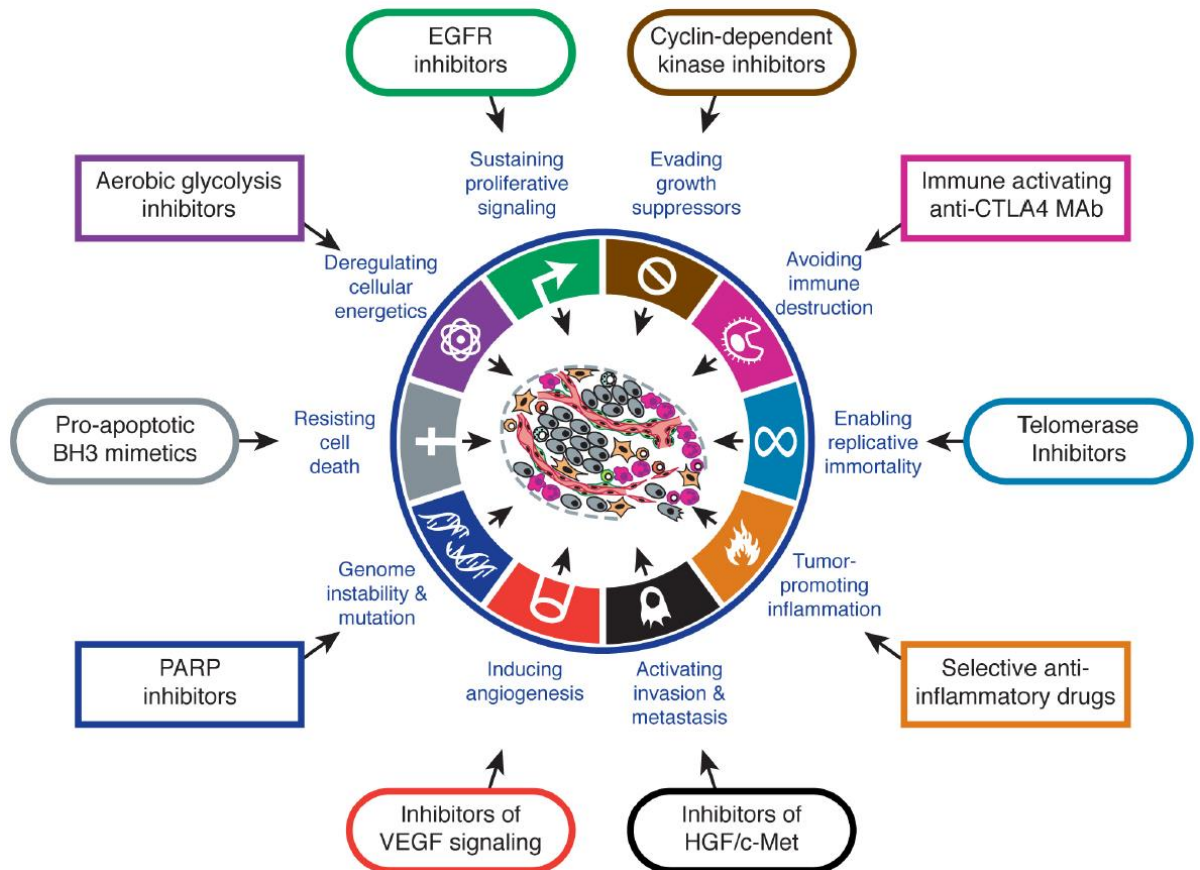


Figure 1-2 Diagram obtained from “Hallmarks of Cancer: Next generation” depicts the four additional proposed archetypal tumour traits and outlines examples of targeted therapeutic agents, at different stages of pre-clinical and clinical development, designed to combat these ten traits (Hanahan and Weinberg 2011).

1.4.1 Proto-oncogenes

Proto-oncogenes are a group of genes which when overexpressed or overactive have been shown to promote malignant transformation. The discovery of proto-oncogenes was initially through the study of acutely transforming RNA retroviruses (Pierotti MA, Sozzi G et al. 2003). These viruses reverse transcribed their own genome into DNA, which is then incorporated into the host's genomic DNA, promoting tumour formation (Varmus 1988). It was shown that these viruses carry hyperactive mutant versions (gain-of-function) of genes present within the host cell. These host genes were termed proto-oncogenes as it was shown that their gain-of-function mutation or increased expression could result in transformation and tumourigenesis in animal models and human cancer patients (Pierotti MA, Sozzi G et al. 2003). Changes in expression of proto-oncogenes can be due to changes in chromosomal structure such as amplification/copy number gain or juxtaposition of enhancer elements upstream, increasing their expression. Inhibition of activated or overexpressed proto-oncogenes (i.e. oncogenes) by small molecular weight compounds has been a successful strategy for targeted cancer therapy, which is consistent with the proposed addiction of cancer cells to oncogenic drivers (Vivanco 2014). This thesis explores the function of *MDM2* and *PPM1D* proto-oncogenes and their small molecular weight inhibitors in regulation of p53 signalling.

1.4.2 Tumour suppressor genes

Tumour suppressor genes (TSGs) are a group of genes the loss of which results in tumour formation. These genes were discovered through investigation of somatic hybrid cells by Henry Harris *et al.*, (1969) who showed that hybridisation of transformed cells with normal cells resulted in reversal of their ability to form tumours in compatible murine hosts (Harris, Miller et al. 1969). This suggested that genetic material from the normal cell was suppressing tumour formation by the transformed cells. The molecular identification of individual TSG's was achieved through different routes of investigation some of which are introduced in the context of the *TP53* tumour suppressor gene.

1.5 A brief history of p53

1.5.1 Discovery

The human tumour suppressor gene *TP53*, was discovered early on to be one of the most frequently mutated genes in cancers (Hollstein, Sidransky et al. 1991, Caron De Fromental and Soussi 1992, Lane 1992, Levine 1997) and remains so to date (mutated in >50% cancers overall) (Olivier, Hollstein et al. 2010). Transformation related protein 53 (Trp53/p53), the product of the *Trp53* gene (murine homologue of *TP53*), was first identified by immunoprecipitation (IP) experiments as a 54kDa protein bound to simian virus 40 (SV40) large T-antigen in SV40-transformed rodent fibroblasts (Chang, Simmons et al. 1979, Kress, May et al. 1979, Lane and Crawford 1979, Linzer and Levine 1979, Melero, Stitt et al. 1979). When Levin and Linzer showed that p53 was also overexpressed in SV40-uninfected embryonal carcinoma cell lines F9 and PCC-4aza-1, it was established that p53 was encoded by the host's genome and was not a viral protein (Linzer and Levine 1979). Antibody mediated responses towards p53 were also detected both in the serum of animal models with chemically/virally induced tumours and in human cancers (De Leo, Jay et al. 1979, Kress, May et al. 1979, Melero, Stitt et al. 1979, Rotter, Witte et al. 1980, Crawford, Pim et al. 1982). These findings brought to light the importance of p53 in the regulation of tissue homeostasis and ultimately cancer development.

1.5.2 Oncogenic tendencies

Early data on p53 behaviour suggested that this protein plays an oncogenic role in cell cycle regulation. When non-transformed murine 3T3 cells were serum deprived and serum was reintroduced, p53 mRNA and protein levels elevated immediately before the initiation of DNA synthesis commenced (Reich and Levine 1984). Another group showed that mitogenic stimulation of non-dividing murine T-lymphocytes, using concanavalin A, leads to increased expression of p53 right before the cells undergo DNA synthesis and mitotic division (Milner and McCormick 1980). Around the same time it was also shown that microinjection of quiescent *Trp53* wild-type (Wt) murine NIH3T3 cells with antibodies raised against p53; abolishes serum induced growth stimulation (Mercer, Nelson et al. 1982, Mercer, Avignolo et al. 1984). The case for oncogenic activity of p53 became stronger when it was shown, in independent studies, that ectopic co-expression of p53 with activated *ras* oncogene (encoded by *C-Ha-Ras* oncogene) could immortalise and transform cells as implied by loss of contact inhibition

measured by foci formation efficiency in culture (Eliyahu, Raz et al. 1984, Jenkins, Rudge et al. 1984, Parada, Land et al. 1984, Jenkins, Rudge et al. 1985). Because of the sub-cellular localisation of p53 and its short half-life (~6 min in splenocytes) it was suspected that p53 plays an important role in cell cycle progression (Reich, Oren et al. 1983, Rogel, Popliker et al. 1985). In the former study specific p53 cDNA was used in northern blots to measure p53 mRNA levels and then a pulse chase method was used to measure p53 protein half-life in four different cell lines in addition to a cell line transformed by SV40 (Reich, Oren et al. 1983). The authors showed that p53 turnover has biphasic kinetics, that p53 has a short half-life and that its half-life varies between cell lines of different origin (Reich, Oren et al. 1983). Importantly, unbeknown to the authors they had demonstrated that Wt p53 levels are regulated at the protein level rather than mRNA level because they were misled by the increase in F9 p53 mRNA levels, which expressed mutant p53 (explained later). Full-length p53 antisense RNA mediated downregulation of p53 protein was also shown to prevent DNA synthesis, as measured by tritiated thymidine incorporation, and cell cycle progression in transformed and non-transformed 3T3 fibroblasts (Shohat, Greenberg et al. 1987). In addition immunocytochemical (ICC) and immunohistochemical (IHC) evidence showed accumulation of p53 and until 1990 it was thought that this was accumulation of Wt p53 (Soussi 1994).

1.5.3 A classic tumour suppressor

The evidence for the tumour suppressor activity of p53 emerged from studying immunocompetent mice infected with the Friend leukaemia virus, which is a complex of two different viruses: a replication-defective spleen focus-forming virus (SFFV) and a replication-competent Friend murine leukaemia virus (F-MuLV) (Mowat, Cheng et al. 1985). These mice develop erythroleukaemia and foci of transformed cells in their spleen. Cell lines were established from the transformed cells and showed 40% of the infected mice had given rise to cell lines that either did not express p53 or expressed a truncated form. Genomic rearrangements resulting in aberrations of both alleles of *Trp53* were detected using cDNA clones corresponding to *Trp53* in southern blotting experiments (Mowat, Cheng et al. 1985). The regions of p53 that were removed were evolutionarily conserved and their absence, which was likely to be associated with loss of function, seemed to result in growth advantage implying strongly that p53 had a role in growth suppression. Most importantly it was shown that the transformation activity in combination with activated *ras* oncogene differed among p53 cDNA clones from

alternative sources (Finlay, Hinds et al. 1988). For example cDNA clone that was derived from the F9 embryonal carcinoma cells was incapable of transforming cells when co-expressed with activated *ras* oncogene (Finlay, Hinds et al. 1988). However by inserting certain mutations in F9 derived p53 cDNA it gained the ability to transform primary embryo fibroblast cells when co-expressed with *ras* oncogene (Finlay, Hinds et al. 1988). It was concluded in this paper that it was likely that the F9 cDNA encodes the Wt allele of p53 as its sequence was identical to pcD35 clone derived from the concanavalin A stimulated T cells (Milner and McCormick 1980, Finlay, Hinds et al. 1988). Sequence comparison of p53 between various species indicated that these deviations from the F9 sequence were not likely to be polymorphisms due to their frequent occurrence in highly conserved regions (I-V) of the p53 open reading frame (Figure 1-3) (Soussi, Defromental et al. 1987, Soussi and May 1996). This brought forward the notion that the p53 cDNA sequences used in the previous experiments, wherein the co-expression of p53 with *ras* had led to transformation of fibroblasts, harboured inactivating mutations (Soussi, Defromental et al. 1987, Soussi and May 1996). The role of p53 as a tumour suppressor was further validated when the ectopic co-expression of Wt *Trp53* and activated *ras* oncogene did not lead to transformation of murine fibroblasts. Importantly, the plasmid encoding Wt *Trp53* was also capable of preventing the transforming properties of other oncogene co-expressions such as E1A and *ras* which further supported the notion that Wt p53 is a universal tumour suppressor protein (Finlay, Hinds et al. 1989). Along with the animal data being consistent with tumour suppressor activity of p53, human data were also emerging which showed aberrant p53 in many different tumour types. In a key publication where the authors had mapped chromosome deletions in 172 colorectal cancer specimens, chromosome 17p loss (which includes the locus for *TP53*; 17p13) occurred in 75% of colorectal carcinomas cases (Vogelstein, Fearon et al. 1988). Recurrent loss of heterozygosity (LOH) at a given locus in tumour specimens was hypothesised to be associated with the location of a tumour suppressor gene; based on the loss of 13q corresponding to the loss of Retinoblastoma protein (*RBI* gene) and 11p13 Wilms' Tumour (*WTAP* Gene) (for Knudson's two hit hypothesis refer to (Knudson 1971)) (Ponder 1988) (Call, Glaser et al. 1990). Baker et al., 1989 subsequently showed by direct sequencing that where 17p is lost the remaining *TP53* allele is also mutated in colorectal cancer specimens (Baker, Fearon et al. 1989). In lung cancer cell lines LOH of 17p was also coupled with *TP53* mutation (Takahashi, Nau et al. 1989). Since these key early publications the evidence for the role of p53 in tumour suppression has accumulated and many of the upstream

and downstream signalling mechanisms leading to its activation and tumour suppression have been deciphered in detail and will be introduced in more in the following sections of this chapter (Meek 2015).

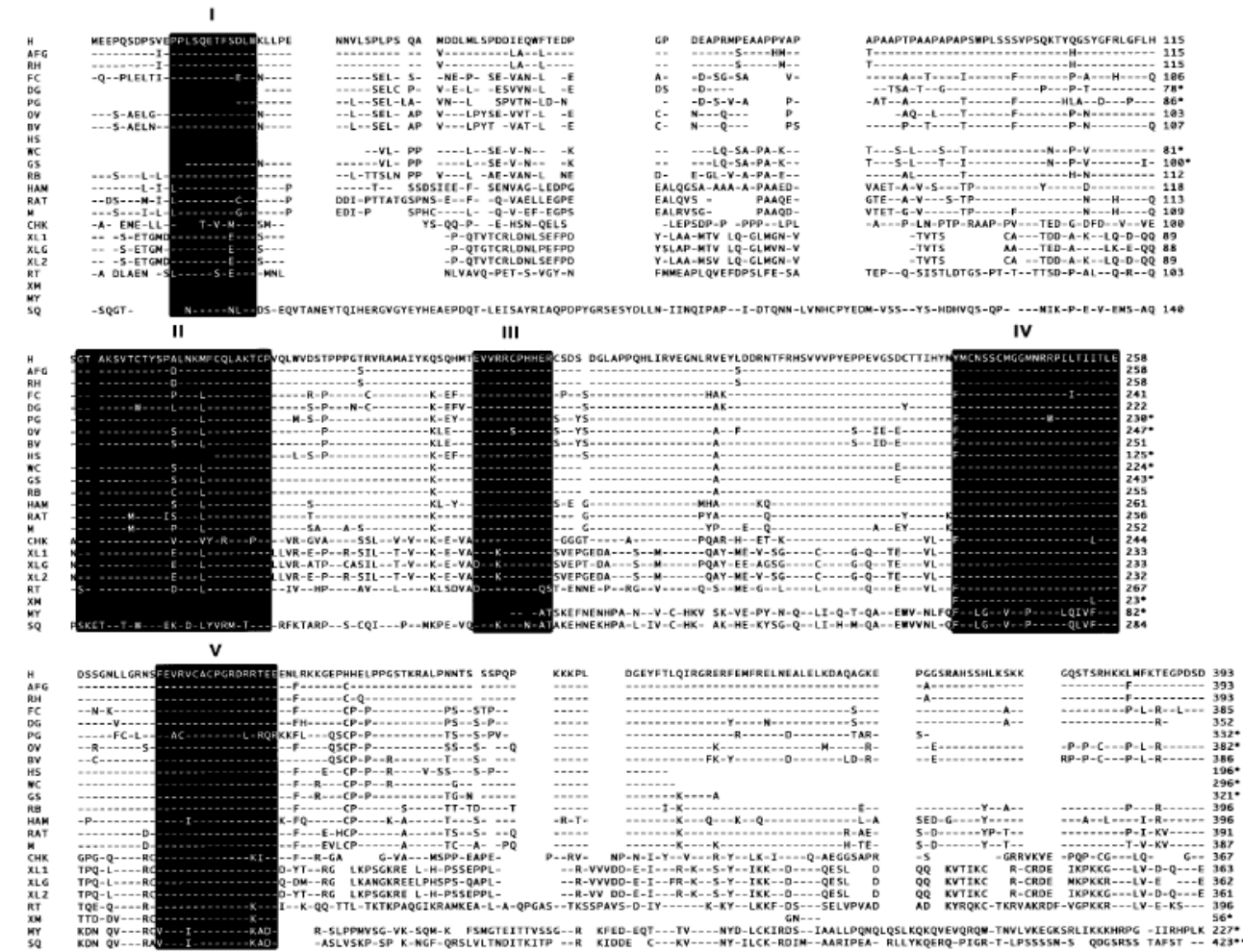


Figure 1-3 Cross species alignment of the p53 amino acid sequence showing the most conserved regions of p53 amino acid sequence (I-V). Image taken from Soussi and May 1996 (Soussi and May 1996).

1.5.4 *Trp53* knockout transgenic mice

Further evidence validating the role of p53 as a tumour suppressor was the increased incidence of tumour formation in *Trp53*^{-/-} transgenic mice (Donehower, Harvey et al. 1992). The birth rate of *Trp53* null mice was not affected and these mice appeared otherwise developmentally normal, however by the age of six months 74% had developed tumours and by ten months all of the mice had died. *Trp53*^{+/-} transgenic mice were also more susceptible to tumour development in comparison to *Trp53*^{+/+} mice, as by the age of 15 months 27% of them had developed tumours (For review see (Donehower and Bradley 1993)). Furthermore transgenic mice expressing the Friend erythroleukaemia mutant version of p53 (46kDa protein described earlier) showed an increased incidence of lung adenocarcinomas, osteosarcomas and lymphomas. It was later shown that the female *Trp53*^{-/-} mice had neural tube malformations resulting in craniofacial abnormalities and reduced frequency of females at birth (Sah, Attardi et al. 1995) (For further information of the developmental abnormalities of *Trp53*^{-/-} mice refer to (Armstrong, Kaufman et al. 1995)) (Rotter, Schwartz et al. 1993).

The role of p53 as the “guardian of the genome” was strongly supported by the protective effect of p53 against the formation of abnormal offspring after exposure to known teratogenic agents such as IR or Benzo[a]pyrene (Nicol, Harrison et al. 1995, Norimura, Nomoto et al. 1996). *Trp53*^{-/-} embryos showed much higher rates of malformation : embryonic lethality ratio (10:1) after IR exposure than their Wt counterparts (1:3) (Norimura, Nomoto et al. 1996). This was attributed to p53 mediated apoptosis of p53 Wt murine embryos, in response to IR induced DNA damage, thus protecting the integrity of the genome (Norimura, Nomoto et al. 1996). In other studies whole body exposure of adult mice to gamma radiation resulted in tissue specific accumulation of p53 (Midgley, Owens et al. 1995). Mouse splenocytes, thymocytes and osteocytes showed accumulation of p53 whereas no accumulation was observed in hepatocytes. This difference may be reflective of tissue proliferation and turnover. This meant that *in vivo* upstream signals resulting in accumulation of p53 after DNA damage work in a tissue specific manner (Midgley, Owens et al. 1995). Among tissues that showed p53 accumulation, osteocytes did not undergo apoptosis, which suggests that the consequences of p53 accumulation and its downstream signalling are also regulated in a tissue specific manner. Another study demonstrated that the tissue specific regulation of p53 in response to DNA damage observed in adult mice is not the same in murine embryos (MacCallum, Hupp et al. 1996). Using previously developed transgenic

mice in which there is a p53 dependent lacZ reporter, they showed that DNA damage induced accumulation of p53 is homogeneous (not tissue specific) in murine embryos in contrast to adult mice (MacCallum, Hupp et al. 1996). This may be because embryonic tissue are rapidly proliferating and undergoing differentiation.

1.5.5 Human germline mutations in *TP53*

The autosomal dominantly inherited Li-Fraumeni syndrome is characterised by high incidence of a group of diverse but well defined cancers particularly sarcomas (Malkin, Li et al. 1990). Other familial cancer predispositions had been associated with loss of a tumour suppressor gene, as it was discovered to be the case in Retinoblastoma (RB) and Wilms Tumour (Knudson 1971, Ponder 1988, Call, Glaser et al. 1990). The tumour suppressor role of p53 and the fact that p53 null/mutant transgenic mice also showed a high incidence of sarcomas was a strong indication that it may be involved in the Li-Fraumeni syndrome. Subsequently it was found that mutant *TP53* allele transmission was strongly correlated with cancer incident in Li-Fraumeni families (Malkin, Li et al. 1990, Srivastava, Zou et al. 1990). Non-cancerous skin fibroblasts from a Li-Fraumeni family with an inherited *TP53* germ-line mutation were found to be radio-resistant (Srivastava, Zou et al. 1990). Genomic DNA obtained from two generations of this family carried the same mutation of their p53 (D245G) (Srivastava, Zou et al. 1990). This data further validated the role of p53 in tumour development and DNA damage induced cell death.

1.5.6 *TP53* gene and its isoforms

TP53 is located on the minus strand of the short arm of chromosome 17 (17p13.1) with the genomic co-ordinates chr17:7571720-7590863 (UCSC genome browser). The p53 protein is encoded by 11 exons which can give rise to multiple isoforms and variants due to alternative splicing and multiple transcription start sites (Khoury and Bourdon 2010). *TP53* gene family also has two structurally related members *TP63* and *TP73* that encode for p63 and p73 respectively. They both share transcriptional targets with p53 and play distinct roles from p53 in murine development (Murray-Zmijewski, Lane et al. 2006). Details about single nucleotide polymorphisms (SNPs), variants and isoforms can be found on the International Agency for Research on Cancer (IARC) database and UCSC genome browser, which is regularly updated and curated.

1.5.7 *TP53* mutations: Gain-of-function or dominant-negative?

Within the last decade however, evidence has emerged that certain *TP53* mutations may incur a gain-of-function phenotype promoting tumourigenesis. This has been reviewed in detail by Muller and Vousden (2014) (Muller and Vousden 2014). The first publication suggesting p53 gain-of-function mutation relied on evidence from mutant p53 ectopic overexpression in p53 null cells which resulted in much higher expression of mutant p53 than is observed in physiological or pathophysiological settings (Dittmer, Pati et al. 1993). Since then many studies have shown that stable transfection or endogenous levels of gain-of-function mutant p53 in cell lines results in phenotypes conferred by well-characterised oncogenes such as increased migration, invasion, anchorage independent growth, colony formation, xenograft growth etc. (Listed in Muller and Vousden table 1). The most compelling data for p53 gain-of-function mutations comes from studies in knock-in transgenic mice. Knock-in mice harbouring heterozygous *Trp53*^{R172H} (Equivalent of human R175H) were shown to have more aggressive tumours, as measured by metastasis and survival, than the heterozygous wild-type mice missing the other copy of *Trp53* (Doyle, Morton et al. 2010, Morton, Timpson et al. 2010). It is worth mentioning that in both studies these mice also expressed a well-known oncogenic driver mutation such as *KRas*^{G12D}. Interestingly, in the Li Fraumeni mouse models harbouring *Trp53*^{R172H/+} only 3/13 tumours had p53 LOH strongly suggesting that the loss of the wild-type copy of *Trp53* is not necessary for the aggressive phenotype observed these mice (Lang, Iwakuma et al. 2004). Similar observations were made in another independent study of *Trp53*^{R172H/+} and *Trp53*^{R270H/+} (Equivalent of human R273H) (Olive, Tuveson et al. 2004). This suggests that certain p53 mutations may confer a selective advantage for tumour progression independent of the genetic status of the other *Trp53* allele. The human data for *TP53* gain-of-function mutations are also consistent with the transgenic mouse data. A proportion of Li Fraumeni patients ($\approx 70\%$, figures vary), a condition typified by predisposition to early tumour development (diverse but well characterised tumours), have been associated with heterozygous *TP53* mutations passed through the germline (Li and Fraumeni 1969, Li and Fraumeni 1969, Li, Fraumeni et al. 1988). Recent studies have compared Li Fraumeni patients with heterozygous *TP53* mutations that result in either loss of function or no expression of p53 from one allele. The data showed that the age of onset of tumours was significantly earlier (by approximately a decade) in patients with *TP53* missense heterozygous mutation compared to those with mutations that resulted in no

p53 expression from one allele (Bougeard, Sesboüé et al. 2008, Zerdoumi, Aury-Landas et al. 2013). Crucially, the second copy of *TP53* is frequently lost in malignancies with p53 mutations (described earlier to be due to chromosome 17p deletion). Although, the authors did not investigate whether loss of the second copy of *TP53* was necessary for tumourigenesis or not in these Li Fraumeni patients, the fact still remains that the age of onset of tumours was earlier in cases with *TP53* gain-of-function mutations. This suggests that certain *TP53* mutations may be playing a role accelerating tumour development. However, the homo-tetramerisation of p53, which is required for consensus sequence binding, is unaffected by these proposed gain-of-function mutations. This has been shown to result in p53 Wt and DNA binding defective mutant hetero-tetramer formation which results in the loss of p53 tetramer consensus sequence binding (Reviewed by (Sabapathy 2015)). This may mean that a gain-of-function phenotype observed may simply be due to a dominant-negative effect on the tumour suppressor function of the wild-type *TP53* allele. Although, other data support the gain-of-function hypothesis. Two main mechanisms have been proposed to explain the gain-of-function activity conferred by certain *TP53* mutations (Reviewed by Weisz et al., (2007)) (Weisz, Oren et al. 2007). First model is based on the observation that gain-of-function mutant p53 protein were shown to inhibit the transcriptional activity of other p53 family members, p63 and p73, thereby inhibiting their tumour suppressor function. The second model arises from the observations that the transactivation domain of gain-of-function mutant p53 is necessary for the expression of certain oncogenes and that mutant p53 retains some degree of specific DNA binding. Others more recent publications have reported mutants to activate well known oncogenic signalling pathways through transcription dependent and independent mechanisms (Muller and Vousden 2014).

Overall the main body of evidence suggests that most of the proposed gain-of-function mutations of *TP53* primarily result in the loss of DNA binding to p53 consensus sequence and thereby loss of p53 transcriptional regulation from promoters of genes important in tumour suppressor mechanisms. Therefore, it must be clearly stated here that *TP53* is still widely accepted as a clear tumour suppressor. However, other data also suggest that a given mutation can both inactivate the tumour suppressor function of a protein while resulting in its gain of oncogenic function.

1.6 p53 structure and function

The nuclear phosphoprotein p53 encoded by the *TP53* gene, is 393 amino acids long and has a theoretical non-post-translationally modified mass of 43653Da (GeneCards, Weizmann Institute). The name p53 was assigned to this protein because it migrates at approximately 53kDa in SDS-polyacrylamide gel electrophoresis. Interspecies comparison of p53 sequence show five domains in p53 that are strongly conserved and encode residues 13-23, 117-142, 171-181, 234-250 and 270-286 (Figure 1-3) (Soussi and May 1996, May and May 1999). These conserved regions correspond to functional domains of p53 as a transcription factor (Fields and Jang 1990, Farmer, Bargonetti et al. 1992, Cho, Gorina et al. 1994, May and May 1999).

1.6.1 Transactivation domain

The N-terminal domain contains an acidic region which behaves as a transcriptional transactivator (Fields and Jang 1990, Raycroft, Wu et al. 1990). This was demonstrated by using the yeast and mammalian two hybrid system utilising the fusion of the N-terminal fragment suspected of transactivation activity with GAL4 DNA binding domain (DBD) (Fields and Jang 1990). Residues 1-73 on the amino terminus of p53 form a very effective transactivation domain (TA) likened to the strongest known TA domain found on herpes virus protein VP16 (May and May 1999). It was later established that only residues 1-42 are essential for transactivation activity (Unger, Mietz et al. 1993). Using reporter gene analysis to study the structure function relationship of p53 in a *TP53* null background, the authors showed that the truncated forms of p53 and mutants commonly found in cancers differed in their transactivation efficiency (Unger, Mietz et al. 1993). This transactivation activity of p53 was found to be coupled to the nonspecific binding to the DNA and also 15 tumour derived murine transforming p53 mutations altered this non-specific binding ability (Steinmeyer and Deppert 1988, Kern, Kinzler et al. 1991). Immuno-precipitation of ³²P end-labelled random fragments (300-1000bp) of the human genome and cosmid and plasmid libraries with p53 showed that p53 binds to a specific DNA sequence. By further mutational analysis and assessing whether sub-fragments can be precipitated with p53 the authors characterised a 33-mer sequence that was precipitated with p53 which was also affected by cytosine methylation and particular base substitutions (Kern, Kinzler et al. 1991). These findings paved the way for identifying the consensus p53 DNA binding

site which consists of two repeats of the 10bp symmetrical motif 5'-PuPuPuC(A/T)(T/A)GPyPyPy-3' separated by 0-13 nucleotides where Pu and Py stand for purines (Adenine/Guanine) and pyrimidines (Thymine/Cytosine), respectively (Eldeiry, Kern et al. 1992). It was interestingly shown that mutations in the hotspots of p53 found most commonly in cancers (discussed later) abolished p53 binding to this consensus sequence (Eldeiry, Kern et al. 1992). It was also found that p53 must form a homo-tetramer in order to bind to the consensus p53 binding sequence, indicating that p53 must have an oligomerisation domain (Kraiss, Quaiser et al. 1988, Clore, Omichinski et al. 1994). The p53 homotetramer requires one Zinc ion per subunit (Bargonetti, Friedman et al. 1991, Rahman-Roblick, Johannes Roblick et al. 2007). Further identifications of an expanded version of this consensus sequence and alternative versions revealed new p53 transcriptional targets (for details see (Bargonetti, Friedman et al. 1991, Funk, Pak et al. 1992, Bourdon, DeguinChambon et al. 1997)). The consensus sequence was thought to be in the promoter/intronic regions of target genes and allows the p53 TA domain to interact with the basal transcription machinery such as TATA box binding factors, replication protein A (RPA) and p62 subunits of the TFIID holoenzyme (Wagner, Ma et al. 2005). Using reporter gene analysis it was found that p53 can also downregulate transcription from other important promoter sequences such as those associated with *c-fos*, *c-myc*, *c-jun*, *β -actin*, *hsc-70* and IL-6 (Ginsberg, Mechta et al. 1991, Lechner, Mack et al. 1992, Ko and Prives 1996). The interaction of p53 with TATA binding protein (TBP) which is also a subunit of the TFIID transcriptional machinery was discovered to be responsible for p53 mediated transrepression and that DNA binding was not required for this function of p53 (Seto, Usheva et al. 1992, Ragimov, Krauskopf et al. 1993, Truant, Xiao et al. 1993). More recent findings have shown that the N-terminus of p53 is subject to complex post-translational modification which fine tunes its transactivation/transrepression function in response to the type of stimulus and the genetic and epigenetic background of the cell. This will be introduced further in the following sections of the introduction and then in the context of the results in the following chapters.

The functional significance of specific residues in p53 transcriptional transactivation has been investigated using site-directed-mutagenesis both *in vivo* and *ex vivo*. Brady CA et al., (2011) generated Cre-Lox conditional p53 knock-in mice homozygous for *Trp53*^{L25Q} & W26S and/or *Trp53*^{F53Q & F54S} which only expressed these mutant p53 alleles when Cre was expressed (Brady, Jiang et al. 2011). Microarray gene expression analysis was

carried out on MEFs derived from these mice after they were transfected with Cre expressing vector. It was shown that *Trp53*^{L25Q & W26S} and *trp53*^{L25Q & W26S, F53Q & F54S} homozygous knock-in MEFs cannot induce some of the well-established p53 transcriptional pro-arrest and pro-apoptotic target genes (e.g. *p21*^{Waf1}, *Noxa* and *Puma*) whereas the induction of others (e.g. *Bax*) were unaffected by these mutations. MEFs derived from *p53*^{F53Q & F54S} homozygous knock-in mice induced p53 targets as efficiently as *p53*^{wt} homozygous cells suggesting that these residues are dispensable for induction of p53 downstream target. Chromatin immunoprecipitation assays investigating the binding of *p53*^{L25Q & W26S} showed that these residues are dispensable for binding to p53 response elements. Mutation in *p53*^{L25Q & W26S} also resulted in the loss of p53 apoptotic response in radiosensitive tissue (e.g. thymus and intestinal) 6 hours following 5Gy ionising radiation as measured by terminal deoxynucleotidyl transferase dUTP nick end labelling (TUNEL). However, 6 hours may be too early to observe p53 dependent apoptotic effects and the FACT that TUNEL staining has diminished at 6 hours may be related to the impact of these mutations on p53 dependent DNA double strand break repair processes. The authors generated mice that also had a Cre dependent conditional *Kras*^{G12D} mutant knock-in mice with the p53 variant alleles explained above. In these mice intranasal Ad-Cre instillation results in non-small cell lung cancer like tumours if p53 is null. The tumour suppressor activity of p53 remained the same in each of the *Trp53*^{L25Q & W26S} or *Trp53*^{F53Q & F54S} homozygous mutant mice expressing *Kras*^{G12D}, whereas the compound mutation resulted in a dramatic loss of p53-dependent tumour suppression albeit to a lesser extent than what was observed in a p53 null background. Other subsequent studies have confirmed that only a small subset of p53 transcriptional target genes such as *Bax* and the more recently described *Phlda3*, *Abhd4*, and *Sidt2* are likely to have crucial involvement in p53 mediated tumour suppression in mice (Johnson, Hammond et al. 2005, Jiang, Brady et al. 2011). This is because the rest of the transcriptional targets have been shown to be dispensable in p53 mediated suppression of most if not all malignancies.

1.6.2 Proline rich region

The N-terminus of p53 also possesses a proline rich region (PRR) that bears a striking peptide sequence similarity to the Src homology 3 (SH3) domain, containing 6 repeats of the PXXP motif (Walker and Levine 1996, Sakamuro, Sabbatini et al. 1997). When mutant p53 (*p53* Δ PP) missing residues 77-89 (in the proline rich region) in the N-terminus was transfected into p53 null SAOS-2 cells, p53 still retained its

transcriptional transactivation activity (Sakamuro, Sabbatini et al. 1997). The authors then queried whether this region is important for the induction of apoptosis by using an established system namely a BRK cell line which has been transformed by the action of adenovirus E1A and a temperature sensitive mutant p53^{V135} (Sakamuro, Sabbatini et al. 1997). At 38°C the non-permissive temperature the p53^{V135} can oligomerise but cannot bind DNA and therefore the cells have a transformed phenotype. However, in the non-permissive temperature (32°C) the cells undergo cell cycle arrest followed by apoptosis. The additional shuttling of p53 Δ PP cDNA to this system abolishes the p53-induced apoptosis following the shift into the permissive temperature, (32°C) but not the transcriptional transactivation and cell cycle arrest (Sakamuro, Sabbatini et al. 1997). PRR was found to promote apoptosis by promoting transcriptional transrepression of certain genes and inducing TP53 inducible protein 3 (*TP53I3/PIG3*) gene which encodes an oxidoreductase (Venot, Maratrat et al. 1998). Loss of PRR was shown to not affect the induction of key p53 transcriptional target genes however, it contributed to loss of transrepression activity (Venot, Maratrat et al. 1998). It is also known that the PRR is important for suppression of tumour growth and it is one of the two binding sites of p53 with the high risk human papilloma virus E6 (HPV-E6) protein which leads to p53 degradation (Li and Coffino 1996, Walker and Levine 1996). Interestingly, codon 72 in p53 is polymorphic (P72R) and individuals carrying two copies of the R72 allele are reportedly more susceptible to tumour development caused by HPV-E6 infection in some populations (Rosenthal, Ryan et al. 1998, Storey, Thomas et al. 1998). However, epidemiological studies regarding this polymorphism are controversial due to contradiction. In the light of these data, investigating the genes that are repressed by p53 which lead to apoptosis may prove useful in understanding apoptotic fate of the cell after non-genotoxic p53 activation (Venot, Maratrat et al. 1998).

1.6.3 DNA binding domain

80-90% of p53 mutations occur in the previously mentioned DBD, residues 102-292, which also encompasses the last four highly conserved regions of p53 (Regions II-V see Figure 1-3) (Eldeiry, Kern et al. 1992). The DNA binding domain of p53 was characterised by assessing the binding of a p53 thermolysin digested proteolytic fragment to the consensus p53 binding DNA sequence (Bargonetti, Manfredi et al. 1993). A thermolysin resistant fragment of p53 migrating at roughly 27kDa was detected to bind strongly with the p53 binding site murine muscle creatine kinase promoter (MCK) (known to bind strongly to p53) as determined by electrophoretic

mobility shift assay (EMSA) (Bargonetti, Manfredi et al. 1993). The specific DNA binding ability of this fragment increased as more thermolysin was used which corresponded to a reduction in larger fragments that may have diminished the DNA binding ability of this region (Bargonetti, Manfredi et al. 1993). It was also demonstrated that proteolytic digestion of common mutant p53 fragments showed no DNA binding activity (corresponding to DBD) (Bargonetti, Manfredi et al. 1993). This region was also resistant to proteolysis by subtilisin and zinc ion was found to be required for DNA binding activity (Pavletich, Chambers et al. 1993). It is noteworthy that this core domain is the region essential for the interaction of SV40 large T-antigen and tumour protein p53 binding protein 1 & 2 (53BP1 and 53BP2) (Jenkins, Chumakov et al. 1988, Ruppert and Stillman 1993, Iwabuchi, Bartel et al. 1994, Gorina and Pavletich 1996). 53BP1 & 2 are involved in p53 response to DNA damage and they reportedly increase the transcriptional transactivation activity of p53 (Iwabuchi, Li et al. 1998).

When the x-ray crystallography structure of p53 in a complex bound to its putative consensus DNA target was solved, it showed two β -sheets that provide structural support for two large loops and a loop sheet helix (LSH) motif which can accommodate a tetrahedrally coordinated zinc atom (Cho, Gorina et al. 1994). The loops and the LSH motifs in the structure were found to correspond to previously known conserved regions (Figure 1-4) (Cho, Gorina et al. 1994). Arginine 248 located in loop 3 sits within the minor groove whereas loop 1 (LSH) binds to the major groove. Loops 2 and 3 are held together by a tetrahedrally co-ordinated zinc atom. This zinc atom is essential for consensus specific DNA binding (Hainaut and Milner 1993, Hainaut and Milner 1993). Most mutations in other tumour suppressor genes result in complete absence or loss of function however >90% of *TP53* mutations found in cancers are point missense, resulting in intact protein expression (Soussi and Beroud 2001). This suggests that *TP53* mutations that lead to intact mutant protein formation may confer a selective advantage to transformed cells as discussed earlier (section 1.5.7) (Michalovitz, Halevy et al. 1991). *TP53* mutations generally affect the DNA binding domain of this protein with functional consequences dependent on location and the properties of the altered amino acid residue (Rainwater, Parks et al. 1995). The 6 most frequently affected mutational hotspots in p53 are R248 (9.6%), R273 (8.8%), R175 (6.1%), G245 (6.0%), R249 (5.6%), R282 (4%) (Figure 1-5) (Cho, Gorina et al. 1994). Two of the most frequently mutated arginine residues are R248 and R273, which directly contact the DNA

molecules (Cho, Gorina et al. 1994). Some p53 mutations can result in the formation of inactive hetero-tetramers of p53 wild-type and mutant p53, resulting in loss of p53 activity (Gannon, Greaves et al. 1990). These p53 hetero-tetramers have a unique epitope that can be detected with PAb240 antibody (Gannon, Greaves et al. 1990, Sabapathy 2015). These mutations are considered to be dominant-negative p53 mutations, as despite the Wt copy of *TP53* the mutant allele is capable of abolishing p53 activity in these cell lines (Gannon, Greaves et al. 1990, Sabapathy 2015). Although in cancers, *TP53* loss of function is often associated with loss of heterozygosity due to 17q deletion (Baker, Fearon et al. 1989, Nigro, Baker et al. 1989), which is evidence in contradiction to dominant-negative p53 mutations.

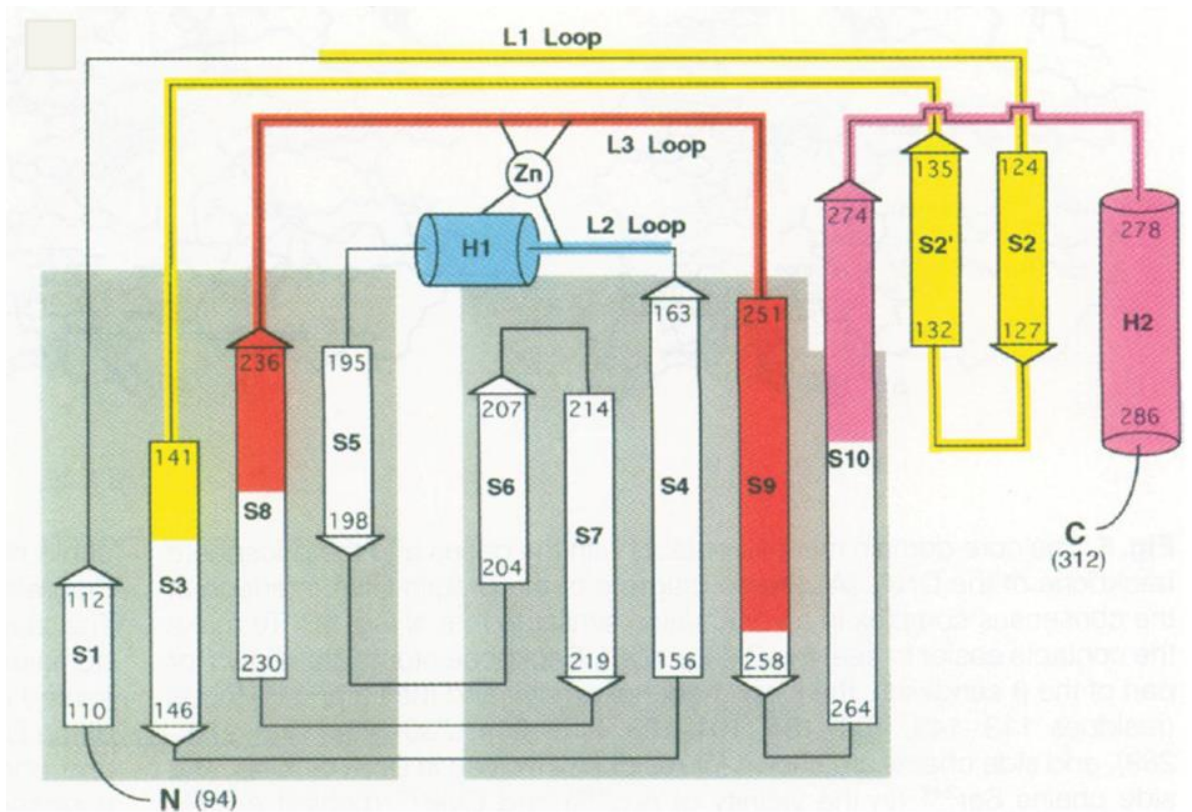


Figure 1-4 Topological diagram of the core domain of p53 shows the loops and the LSH motif and the coordinated zinc atom within the secondary structure. The conserved regions are colour coded, Yellow; region II, Blue; Region II, Red; Region IV, and Purple; region V. The diagram was taken from Cho *et al.*, 1994 (Cho, Gorina et al. 1994)

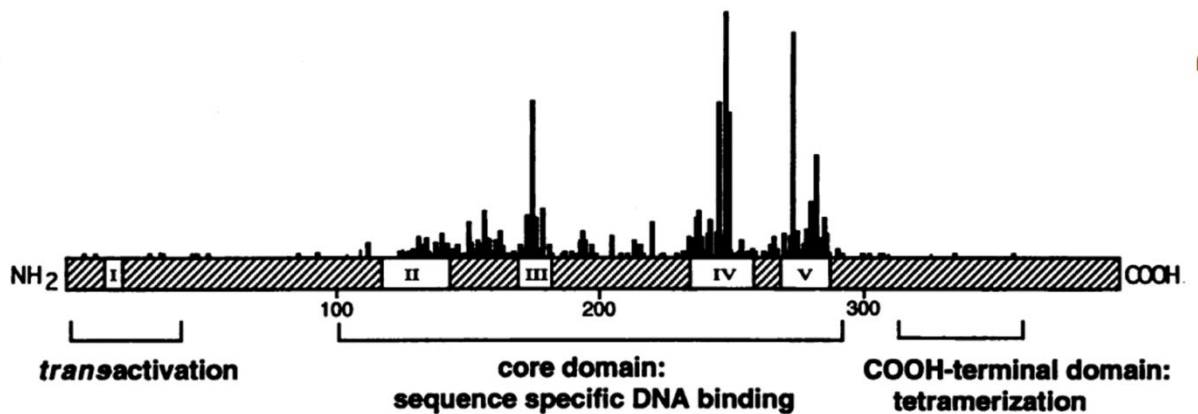


Figure 1-5 The five conserved regions of TP53 with relation to its mutational hotspots detected in tumours. The bars show the approximate position and relative frequency of these mutations in human cancers. Figure from Cho *et al.*, 1994 (Cho, Gorina et al. 1994)

1.6.4 C-terminus

It was discovered that truncated versions of p53 missing the C-terminal region were not capable of forming tetramers which implied that the oligomerisation domain of p53 may be located in this region (Milner and McCormick 1980, Kern, Pietenpol et al. 1992). In 1992 Shaulian and colleagues defined this hydrophobic oligomerisation domain of p53 to be at the C-terminal, and demonstrated that this region is important in explaining dominant-negative p53 mutations (Shaulian, Zauberman et al. 1992). Various truncated p53 mini-proteins representing the C-terminal hydrophobic regions of p53 which carried no mutations were nevertheless capable of transforming cells (Shaulian, Zauberman et al. 1992). Both X-ray crystallography and nuclear magnetic resonance (NMR) methods have shown the structure of the tetramerisation domain spanning from residues 323-356 (Jeffrey, Gorina et al. 1995) (Clore, Omichinski et al. 1994). The N-terminal of the oligomerisation domain monomer forms a beta-sheet which can interact with a beta sheet from a second monomer in an antiparallel fashion forming a dimer. The hydrophobic central and C-terminal residues of the oligomerisation domains form an alpha helical structure through which p53 dimers can form a homo-tetramer (Figure 1-6) (Clore, Omichinski et al. 1994). The transformation ability of dominant-negative p53 mutants is abolished when the oligomerisation domain is truncated. This suggested that if the tetramerisation domain is intact but the other critical domains such as transactivation domain/DBD are mutated, chimeric tetramers will form in spite of the presence of a wt copy of p53, giving rise to an array of complex phenotypes. Three nuclear localisation signals (NLS) are also located at the C-terminal region of p53, residues 316-325 (NLS1), 369-375 (NLS2), and 379-384 (NLS3). NLS1 mutation excludes p53 from the nucleus whereas mutations in NLS2 & 3 result in loss of signalling dependent localisation (Dang and Lee 1989, Shaulsky, Goldfinger et al. 1990). The basic region (BR) comprised of residues 363-393 is thought to also be involved in transcriptional regulation, DNA damage recognition and apoptosis (Reed, Woelker et al. 1995, Wang, Vermeulen et al. 1996). It was found that microinjection of a small modified peptide or an antibody which masks the BR in the C-terminus of p53 could lead to sequence specific binding in the absence of radiation induced DNA damage which meant that the BR was a negative regulator of p53 sequence specific binding (Hupp, Sparks et al. 1995, Abarzua, LoSardo et al. 1996). It was put forward that the C-terminal of p53 may be able to allosterically inhibit p53 tetramer's ability of sequence specific DNA binding (Halazonetis and Kandil 1993) (Hupp and Lane 1994,

Hupp, Sparks et al. 1995).

The C-terminal undergoes multiple forms of modification in response to different modes of p53 activation (Ko and Prives 1996, Shaw, Freeman et al. 1996, Sakaguchi, Herrera et al. 1998). Sakaguchi and colleagues showed that in response to DNA damage (by UV light or IR) histone acetyl transferases (HAT) p300 and PCAF are responsible for the acetylation of p53 K382 and K320 respectively (Sakaguchi, Herrera et al. 1998). Ser-33 and Ser-37 were also shown to be phosphorylated in response to these stressors using phosphorylation specific antibodies (Sakaguchi, Herrera et al. 1998). Small phosphopeptides corresponding to S33/S37 could inhibit the p300 and PCAF dependent acetylation of p53 on C-terminal residues in intact cells. The authors suggested that S33 and S37 phosphorylation events enhance the interaction of p300 and PCAF and promote the acetylation of the C-terminus of p53 by p300 and PCAF positively regulating p53 transcriptional activity (Sakaguchi, Herrera et al. 1998). The p53 tetramer was later found to be allosterically regulated by acetylation and phosphorylation events that modulate its interaction with transcriptional co-activators like p300/CBP and PCAF (Lill, Grossman et al. 1997, Scolnick, Chehab et al. 1997, Wadgaonkar and Collins 1999). There is also evidence of glycosylation-dependent proteolytic cleavage of the C-terminus in response to p53 activation (Shaw, Freeman et al. 1996, Okorokov, Ponchel et al. 1997). Okorokov and colleagues showed in 1997 that both p53 N-terminus and C-terminus undergo proteolytic cleavage after DNA damage and that this C-terminal cleavage is also induced by free ssDNA (Okorokov, Ponchel et al. 1997). It was shown that primary fibroblasts obtained from DNA repair deficient patients with Xeroderma pigmentosum (XP) were not sensitive to apoptosis induced by microinjection of Wt *TP53* expression vector (Wang, Vermeulen et al. 1996). Fibroblasts from these patients lacked Wt *XPD/ERCC2* or *XPB/ERCC3* helicase activity and are therefore defective in base excision repair (BER). The XP defective fibroblasts undergo apoptosis in response to other stimuli such as microinjection of human apoptosis inducing gene (*Ich-1L*) or mammalian *Ced-3* homologue (*ICE* gene). The authors showed that this lack of sensitivity can be reversed by microinjection of Wt *ERCC2* or *ERCC3* which encode helicases incorporated in the TFIIH complex, that also physically interact with the C-terminal region of p53 (Wang, Yeh et al. 1995, Wang, Vermeulen et al. 1996). A helicase *ERCC6/CSB* from the TFIIH complex involved in excision repair also interacts with p53 C-terminal domain *in vitro* (Wang, Yeh et al. 1995). Post-translational modifications of p53 C-terminus (particularly acetylation events) have also been shown

to impact the regulation of p53 stability which will be discussed in the context of p53 MDM2 interaction (Meek 2015).

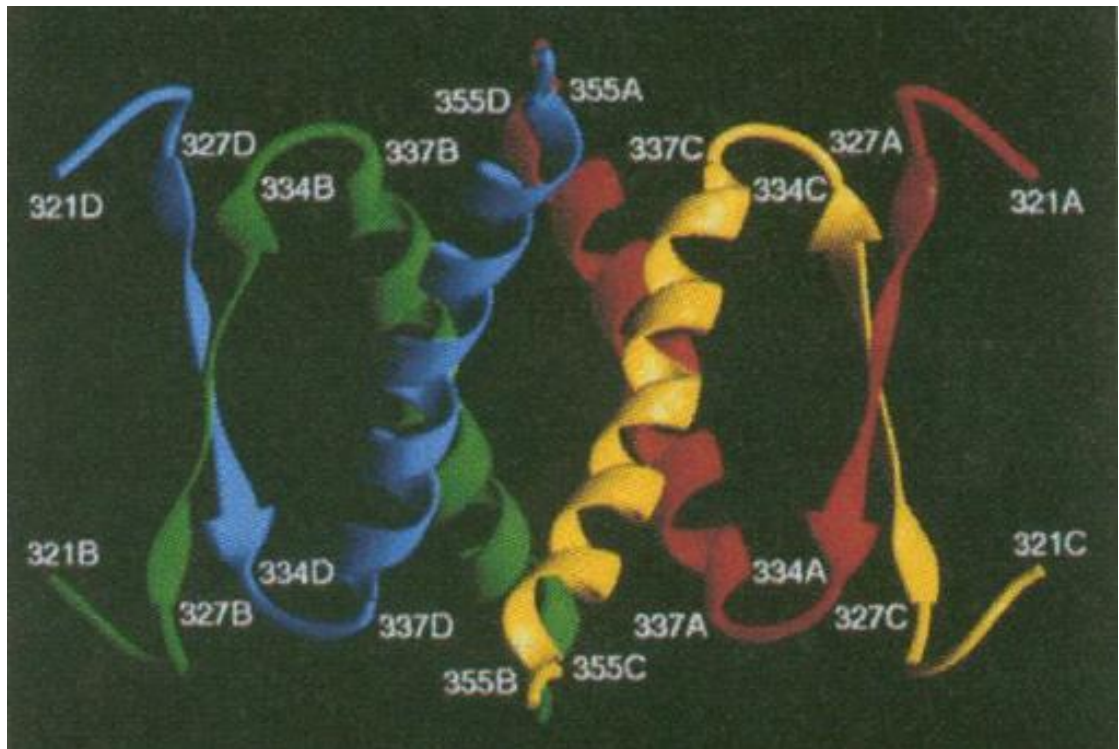


Figure 1-6 Ribbon drawing of the p53 oligomerisation domain and important amino acid residues involved in its function. Figure taken from Clore et al., 1994 (Clore, Omichinski et al. 1994).

1.7 Cell cycle checkpoints

Although the growth and proliferation of eukaryotic cells is a continuous process, phases have been characterised, that mark the beginning and completion of significant discontinuous events such as DNA synthesis (Hartwell and Weinert 1989). Eukaryotic cells appear to follow a cycle with respect to these discontinuous processes, and the initiation of each subsequent discontinuous phase in this cycle, is contingent on the accurate completion of the prior phase (Murray 1994). Cell cycle checkpoints safeguard that cell cycle events occur accurately and sequentially. Also in the face of errors or damage, checkpoints arrest progression to the next phase to provide sufficient time for repair or allow the initiation of programmed cell death. Defects in cell cycle checkpoints can lead to accumulation and propagation of changes conducive to the development of malignancies (Nyberg, Michelson et al. 2002).

1.7.1 Regulation of cell cycle progression

Four phases have been categorised for the life cycle of all eukaryotic cells namely Gap 1 (G1), DNA Synthesis (S), Gap 2 (G2) and Mitosis (M) with a quiescent stage G0 when the cells leave this cycle (Vermeulen, Van Bockstaele et al. 2003) (Figure 1-7). Cyclin-dependent kinases (CDKs) are a family of serine/threonine protein kinases involved in cell cycle progression and their activity is regulated by another family of proteins termed cyclins. CDK levels remain constant throughout the cell cycle however periodic expression of distinct cyclins at each stage of the cell cycle regulates cell cycle progression by activating specific kinases at each stage of the cell cycle. Cyclin expression is dependent on many intracellular and extracellular factors such as DNA integrity and availability of growth factors (mitogens). Different cyclin-CDK complexes phosphorylate and regulate specific target proteins that are critical for cell cycle progression at each stage. Unlike the periodic expression of other cyclins, D-type cyclins (Cyclins D1, D2 and D3) are expressed as long as mitogen signal is present. D cyclins couple with and activates CDK4/6 during G1 phase which phosphorylate downstream targets that promote progression into S-phase. A key phosphorylation substrate of Cyclin D-CDK4/6 complex is the product of the retinoblastoma tumour suppressor gene (RB). Hypophosphorylated RB negatively regulates E2F-1 and DP-1 transcription factors that are involved in the transcription of key genes for G1 to S-phase progression (Vermeulen, Van Bockstaele et al. 2003). Phosphorylation of RB

results in activation of E2F-1 and DP-1 which initiate cell cycle progression into S-phase by induction of Cyclin A, Cyclin E and CDC25. Cyclin E-CDK2 maintains RB phosphorylates throughout the cell cycle and is essential for G1 to S transition. Cyclin A-CDK2 complex is important throughout S-phase and Cyclin A-CDK1 promotes G2 to Mitosis transition. Cyclin B-CDK1 complex is also known to regulate mitosis by promoting chromosome condensation nuclear lamina resolution and mitotic spindle assembly (Vermeulen, Van Bockstaele et al. 2003).

1.7.1.1 CDK inhibitors

In response to a variety of stimuli such as cellular stress (e.g. DNA damage) or absence of mitogenic signal CDK activity can be inhibited by members of two distinct families of CDK inhibitor proteins INK4 and CIP/KIP (Sherr and Roberts 1995) (Figure 1-7). Members of the INK4 family include CDK inhibitor 2A (CDKN2A/INK4a/p16), CDK inhibitor 2B (CDKN2B/INK4b/p15), CDK inhibitor 2C (CDKN2C/INK4c/p18) and CDK inhibitor 2D (CDKN2D/INK4d/p19) which bind to CDK4/6 and prevent the interaction of D cyclins with these CDKs in G1 (Vermeulen, Van Bockstaele et al. 2003). CIP/KIP family of CDK inhibitors comprise of CDK inhibitor 1A (CDKN1A/WAF1/CIP1/p21), CDK inhibitor 3 (CDKN3/CIP2/p27) and CDK inhibitor 1C (CDKN1C//KIP2/p57) which are involved in inhibition of G1 cyclin-CDK complexes and to a lesser degree cyclin B-CDK1 (Vermeulen, Van Bockstaele et al. 2003). Inhibition of CDKs in this manner prevents cell cycle progression until either the stress is resolved or the cell undergoes programmed cell death.

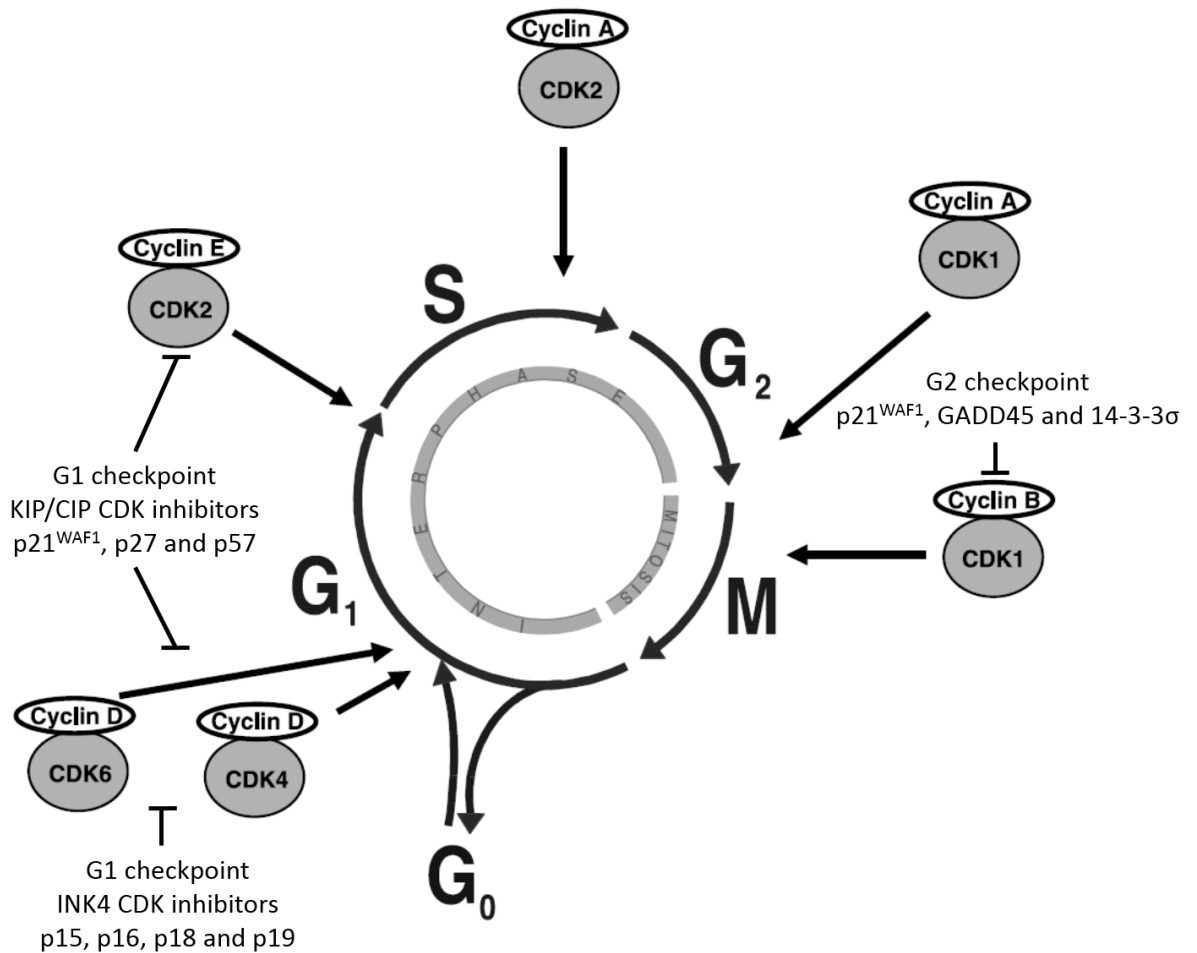


Figure 1-7 The cell cycle, and the regulation of its progression by different cyclin-CDK complexes and CDK inhibitors. Adapted from Vermeulen *et al.*, (2003).

1.8 Cell cycle checkpoints and the role of p53

Checkpoints and DNA repair mechanisms are very much intertwined, as the detection of DNA damage by surveillance mechanisms often leads to mobilisation of DNA repair proteins and signalling networks which are themselves involved in cell cycle regulation (For a comprehensive review refer to (Sancar, Lindsey-Boltz *et al.* 2004)). The inhibition of transition between these stages of the cell cycle, such as G₁ to S, due to cellular stress is what is referred to as cell cycle checkpoints (Sancar, Lindsey-Boltz *et al.* 2004). The checkpoint before DNA replication is termed the G₁/S checkpoint (a.k.a. restriction point) which regulates entry into/commencement of DNA synthesis and replication phase of the cell cycle. Cellular stressors or detection of DNA damage by the components of stress response machinery, lead to modulation of effector molecules that can inhibit critical downstream regulators of cell cycle progression. A critical transcription factor activated in response to cellular stress is the nuclear transcription factor transformation protein 53 (TP53/p53) encoded by the aforementioned *TP53* gene

(Meek 2004). Post-translational modifications of p53, and other molecules involved in its regulation, following stress and DNA damage can lead to its activation and subsequent transcriptional induction of its downstream target genes, the products of which are involved in cell cycle arrest and/or senescence (e.g. p21^{WAF1}, 14-3-3 σ , GADD45) (Figure 1-7) or apoptosis (e.g. BAX, NOXA, DR5 and PUMA). For example activation of ataxia telangiectasia mutated (ATM) or ATM and Rad3 related (ATR) protein kinases, in response to DNA damage, can directly and indirectly, phosphorylate p53 residue Ser15 which is considered a “nucleation event” for other activating post-translational modifications such as Thr18 and/or Ser20 phosphorylation or acetylation of p53 c-terminus (Saito, Yamaguchi et al. 2003, Meek 2004). These post-translational modifications culminate to free p53 from its negative regulatory binding partner MDM2, which leads to p53 stabilisation and activity (explained in more detail later). The most studied transcriptional target of p53 is *CDKN1A* which encodes the CDK inhibitor p21^{CIP1/WAF1} described earlier. In addition to inhibition of cell cycle progression at G1 and G2/M as described earlier, p21^{WAF1} also inhibits proliferating cell nuclear antigen (PCNA) which is critical for DNA synthesis hence causing S-phase arrest (Sherr and Roberts 1995, Waga, Li et al. 1997, Bartek and Lukas 2001). Cell cycle regulatory transcriptional target of p53, *14-3-3 σ /YWHAS*, encodes a scaffold protein 14-3-3 σ which removes cyclin B-CDK1 complex from the nucleus thus inhibiting G2/M progression (Hermeking, Lengauer et al. 1997). Another mechanism through which p53 negatively regulates G2/M progression is through direct induction of GADD45 which inhibits cyclin B-CDK1 interaction (Zhan, Antinore et al. 1999).

Induction of cell cycle arrest by p53 in response to DNA damage may at face value be considered a mechanism that protects genomic integrity by allowing sufficient time for DNA repair thus preventing propagation of genetic changes detrimental to the survival of the organism or the fitness of its offspring. However, because DNA repair mechanisms are error prone, it can also be postulated that p53-mediated reversible cell cycle arrest may allow the accumulation of oncogenic genetic alterations in successive generations of cells resulting in stepwise transformation of somatic tissue. This is indeed consistent with the observation that p53 is a relatively late mutational event in colorectal cancer development (Vogelstein, Fearon et al. 1988). This is also consistent with IR induced lymphomas being significantly delayed in *Cdkn1a* null mice, which develop normally but are deficient in G1 checkpoint, suggesting that p53 mediated G1 arrest may accelerate the selection of tumourigenic changes in certain contexts (Deng,

Zhang et al. 1995, Martín-Caballero, Flores et al. 2001). Furthermore, even though *Cdkn1a* null mice develop spontaneous tumours earlier than their wild-type counterparts, these tumours are observed later (after 7 months) than those in *Trp53* (murine homologue of *TP53*) null mice (74% of mice had tumours before 7 months). It may be that the reported roles of p53 mediated senescence and apoptosis are more important for tumour suppressor function of p53 (Symonds, Krall et al. 1994, Cosme-Blanco, Shen et al. 2007, Xue, Zender et al. 2007). In the following sections the role of p53 in induction of senescence and apoptosis in tumour suppression are introduced and discussed in more detail. Recently, transgenic mouse studies have shown that the role of p53 in regulation of cellular metabolism may also play an important role in tumour suppression (Explained in more detail later) (Jiang, Brady et al. 2011, Li, Kon et al. 2012, Valente, Gray et al. 2013). Due to such observations and the fact that the tumour suppressor function of p53 is the most frequent negatively selected process during tumourigenesis of somatic tissue reinstating the function of p53 is widely considered an effective cancer therapeutic strategy (Khoo, Verma et al. 2014).

1.9 Cellular senescence and the role of p53

Cells are considered senescent when they have exited the cell cycle and no longer divide in the presence of growth factors or mitogens. The role of p53 in senescence has been reviewed in detail by Rufini et al., (2013) therefore it will only be discussed briefly here. Senescent cells have an enlarged flat morphology and they express distinct biochemical markers as increased expression of β -galactosidase, p53, p21^{WAF1} and other CDK inhibitors along with senescence associated heterochromatic foci (Rufini, Tucci et al. 2013). There are three main proposed underlying causes for senescence: 1) shortening of telomeres referred to as replicative senescence, 2) sustained oncogenic drive and 3) Oxidative damage caused by reactive oxygen species (ROS). These stimuli activate stress response effector molecules that crosstalk with and modulate the role of p53 in inducing or inhibiting senescence.

Mouse embryonic fibroblasts (MEFs) derived from transgenic knock-in mice homozygous for *Trp53*^{R172P}, do not undergo senescence in response to ectopic expression of TRF2 (Telomere repeat binding factor 2) compared to their *Trp53* wild-type counterparts (Cosme-Blanco, Shen et al. 2007). Given that telomere dysfunction results in DNA damage (Double strand breaks at telomeres), it has been proposed that the activation of p53 in response to telomere dysfunction is through the activity of DNA

damage response kinases of the phosphatidylinositol 3-kinase like serine/threonine kinase (PI3KK) family such as ATM (Artandi and Attardi 2005, Rufini, Tucci et al. 2013). This suggests that post-translational modifications of p53 by stress response effector molecules may be important in inducing p53-dependent senescence following telomere shortening. Furthermore, sustained oncogenic drive from Ras in human fibroblasts results in the activation of DNA double strand break repair mechanisms followed by activation of p53 and oncogene induced senescence. Stable knockdown of p53 or DNA damage response protein ATM resulted in reversal of oncogene induced senescence suggesting that oncogene induced senescence is dependent on the ATM-p53 signalling pathway (Di Micco, Fumagalli et al. 2006). The role of p53 in response to ROS however is considered as a double edged sword. Although p53 activation is followed by induction of its anti-oxidant downstream transcriptional targets such as superoxide dismutase 1 (SOD1), glutathione peroxidase 1 (GPX1) and sestrin 1 and 2 (SESN1 & SESN2), ectopic p53 expression has been reported to induce an early increase in ROS in cells that undergo apoptosis in that context (Rufini, Tucci et al. 2013).

Other reports suggest that p53 may play an anti-senescent role in certain contexts. Senescence has classically been considered as an irreversible state. However, relatively recent evidence suggests that activation of p53 through the nutrient sensor mammalian target of rapamycin (mTOR) may play an anti-senescent role (Demidenko, Korotchkina et al. 2010). The authors initially showed that induction of p21^{WAF1} from an IPTG inducible promoter results in cellular senescence in culture. They then showed that non-genotoxic activation of p53 by an MDM2 inhibitor Nutlin-3 (discussed later), which also leads to induction of p21^{WAF1}, resulted in reversible cell cycle arrest (a.k.a quiescence). The phosphorylation of a substrate of mTOR and a surrogate marker of its activity (S6 ribosomal protein) was inhibited in response to Nutlin-3 or ectopic expression of p53 as compared to when p21^{WAF1} was induced by IPTG suggesting that p53 activation inhibits mTOR pro-senescent activity. Interestingly, transgenic knock-in mice homozygous for mutant p53 serine 18 to non-phosphorylatable alanine (p53^{S18A} equivalent of p53^{S15A} in human), show reduced induction of some p53 transcriptional targets (e.g. Puma), premature aging consistent with the anti-senescent role of p53. Homozygous *Trp53*^{S18A} knock-in mice are more likely to develop late-onset tumours compared to their homozygous wild-type or heterozygous littermates. Furthermore, B cells derived from p53^{S18A/S18A} mice show defects in DNA damage induced apoptosis

suggesting that modification of single residues on p53 in response to a particular stressor may be the determinant of the decision between cell cycle arrest senescence and cell death. Importantly, S18 is a key substrate for activity of stress response kinases such as ATM. Conversely, studying other hypermorphic mutant p53 knock-in mouse models (hyperactive p44 and p53^{T21D & S23D}) have indicated that increased p53 transcriptional activity can also promote premature ageing (Liu, Ou et al. 2010). These observations suggest that p53-mediated senescence is highly stimuli/context-dependent and the precise mechanism through which p53 transcriptional activity regulate cellular commitment to senescence is yet to be determined. Overall, post-translational modifications appear to play an important role in fate determination following p53 activity. The next section will introduce the role of p53 in programmed cell death or apoptosis.

1.10 Apoptosis and the role of p53

Apoptosis was first described in 1972 as an active cell death mechanism with distinct, active and controlled morphological steps which was in contrast to cell lysis or necrosis observed in response to noxious stimuli (Kerr, Wyllie et al. 1972). Apoptosis occurs in various physiological (e.g. during ontogenesis) or pathophysiological (e.g. in untreated malignant neoplasms) contexts and is considered both a mechanism of healthy tissue renewal and tumour suppression. During apoptosis chromatin is condensed and then the membrane forms apoptotic bodies (known as membrane budding) which are then phagocytosed by the surrounding cells. This is different in necrosis during which plasma membrane swells and ruptures releasing the contents of the cell in the surrounding tissue often leading to inflammation.

Apoptosis signalling can be generally perceived as extrinsic or intrinsic in that the mechanism initiating this process can be initiated by external or internal cellular signalling events (Reviewed in detail by (Reed 2000)). Extrinsic apoptosis is stimulated by ligand binding to a family of death receptors and their stimulation which is followed by recruitment of adaptor molecules that can activate an initiator member of the cysteine-aspartate protease (caspase) family. Initiator caspases then activate executioner caspases (caspase-3, -6 & -7) which then results in global proteolysis and cell death by apoptosis. The intrinsic apoptotic pathway on the other hand is initiated by stressors from within the cell and mediated through the release of apoptogenic molecules (e.g. cytochrome c) from mitochondria resulting in caspase-dependent and/or -independent

cell death (Dashzeveg and Yoshida 2015). It has been suggested that p53 exerts its pro-apoptotic effect primarily through the transcription of pro-apoptotic targets that promote the intrinsic apoptotic pathway (e.g. pro-apoptotic members of the BCL-2 family) and that other p53 transcriptional targets which are components of the extrinsic apoptotic pathway (e.g. Death receptor family) augment the intrinsic apoptotic signal (Fridman and Lowe 2003). Over 100 pro-apoptotic genes have been reported as p53 transcriptional target genes, based on chromatin immunoprecipitation, reporter gene analysis and/or analysis of global differential gene expression profiles after p53 activation (Mirza, Wu et al. 2003, Yu and Zhang 2005). Roles of a few key p53 transcriptional targets important in the extrinsic and the intrinsic pathway will be described here.

Key transcriptional targets of p53 that promote the extrinsic apoptotic pathway include tumour necrosis factor receptor superfamily, member 6 (TNFRSF6/FAS), 10A (TNFRSF10A/DR4) and 10B (TNFRSF10B/DR5) (Yu and Zhang 2005). These cell surface receptors contain intracellular death domains and are activated by ligands such as Fas ligand (TNFSF6), tumour necrosis factor-related apoptosis inducing ligand (TNFSF10/TRAIL) or tumour necrosis factor (TNF) (Duprez, Wirawan et al. 2009). For example TNFSF6 or TRAIL binding to their respective receptors result in the formation of an intracellular death inducing signalling complex (DISC) which can recruit and activate initiator caspase-8 and/or -10 through Fas-associated death domain (FADD). Caspase-8 and -10 can then activate executioner caspases downstream. For more detailed description regarding the interaction of other ligands that promote extrinsic apoptosis and their internal complexes the reader is directed to reviews by Duprez et al., (2009) and Siddiqui et al., (2015) (Siddiqui, Ahad et al. 2015).

The main pro-apoptotic mechanisms through which p53 induces intrinsic apoptosis are through altering mitochondrial outer membrane permeability (MOMP) and mitochondrial permeability transition pore (PTP). These mechanisms have been reviewed in detail by Dashzeveg and Yoshida (2015) and will therefore only be briefly introduced here (Dashzeveg and Yoshida 2015). Anti-apoptotic BCL-2 is thought to sequester pro-apoptotic BCL-2 family members such as BCL2-Antagonist/Killer 1 (BAK1), BCL2-Associated X Protein (BAX). Transcriptional induction of BAK and BAX by p53 overwhelms BCL-2 while p53 pro-apoptotic transcriptional targets such as p53-upregulated mediator of apoptosis (PUMA), Phorbol-12-Myristate-13-Acetate-Induced Protein 1 (NOXA) and Tumour protein p53-regulated apoptosis inducing

protein 1 (p53AIP1) are known to interact and inhibit the anti-apoptotic BCL-2 family members. It has also been reported that p53 can promote apoptosis through a transcription-independent mechanism by physically interacting and inhibiting the function of anti-apoptotic members of the BCL-2 family, BCL-XL and BCL-2, at the mitochondrial membrane. These overall enable BAK and BAX forming complexes that traverse the outer membrane of mitochondria and form pores its outer membrane allowing apoptogenic molecules such as cytochrome c to be released into the cytoplasm (Dashzeveg and Yoshida 2015). Cytochrome c then activates apoptotic peptidase activating factor 1 (APAF-1) which can then recruit and activate initiator caspase-9 as part of the apoptosome. Caspase-9 cleaves pro-caspase-3 and the activation of executioner caspase-3 leads to global proteolysis (Siddiqui, Ahad et al. 2015).

The importance of the role of p53 in induction of apoptosis was first brought to light when it was shown that thymocytes and intestinal stem cells derived from *Trp53* knockout mice are resistant to ionising radiation induced apoptosis while MEFs from the same mice were also shown to be resistant to oncogene or chemotherapy induced apoptosis compared to their wild-type counterparts (Clarke, Purdie et al. 1993, Lowe, Ruley et al. 1993, Lowe, Schmitt et al. 1993). Study of whole body radiation in *Trp53* null mice showed that DNA damage induced pro-apoptotic role of p53 is tissue-type dependent as gamma radiation induced apoptosis was notably deficient in radiosensitive tissue (e.g. thymus and spleen) of the *Trp53* null mice compared to the wild-type littermates; whereas there was no difference in apoptosis in other radio-resistant tissue types (e.g. osteocytes or hepatocytes) (Midgley, Owens et al. 1995). Transient ectopic expression of mutant variant of *Trp53*^{L25Q, W26S}, which is incapable MDM2 binding and of transactivation of p53 induced target genes, resulted in contradictory findings when investigated in different contexts, until it was shown that MEFs and embryonic stem cells derived from homozygous *Trp53*^{L25Q, W26S} knock-in mice were deficient in apoptosis induced by DNA damage compared to their wild-type counterparts (Chao, Saito et al. 2000, Jimenez, Nister et al. 2000). Also as mentioned earlier homozygous *Trp53*^{S18A} knock-in mice have defects in induction of p53 regulated apoptotic transcriptional target genes and DNA damage induced apoptosis (Chao, Hergenhahn et al. 2003, Chao, Herr et al. 2006, Armata, Garlick et al. 2007). These reports overall strongly suggested that p53 induced transactivation of pro-apoptotic genes is essential for apoptosis in these contexts.

1.11 MDM2 regulates p53 stability and function

In an unstressed cell, p53 remains mostly bound by mouse double minute 2 (MDM2/HDM2 in humans), an E3 ubiquitin ligase, which targets p53 for proteasome mediated degradation through the 26S proteasome complex (Böttger, Böttger et al. 1997, Kubbutat, Jones et al. 1997). MDM2 also regulates p53 function by inhibiting its transcriptional transactivation domain and localising p53 to the cytoplasmic compartment of the cell (Li, Brooks et al. 2003). However, in response to cellular stress, such as DNA damage, unbound p53 and MDM2 both undergo post-translational modifications which prevent their dimerization (Meek and Anderson 2009, Meek and Hupp 2010, Meek 2015). This leads to the stabilisation and accumulation of p53 in the nucleus where it can exert its effects as a transcription factor by binding a consensus sequence adjacent to its target genes and promoting their transcription (Dumaz and Meek 1999). The canonical transcriptional target genes up-regulated by p53 include *CDKN1A*, *BAX*, *PUMA* and growth arrest and DNA-damage-inducible (*GADD45*), all of which play a either growth inhibitory or pro-apoptotic role (Levine, Momand et al. 1991, Harper, Adami et al. 1993, Levine 1997). The *MDM2* gene is also transcriptionally up-regulated by p53, resulting in an autoregulatory feedback loop (Wu, Bayle et al. 1993).

1.11.1 Indirect regulation of p53 stability and function from the *CDKN2A* locus

Another important indirect regulator of p53 activity is encoded by the cyclin-dependent kinase inhibitor 2A (*CDKN2/INK4a/MTS1*) locus (Quelle, Zindy et al. 1995). Mice lacking this gene are embryonically viable but are prone to early spontaneous tumourigenesis and hypersensitive to genotoxic agents (Serrano, Lee et al. 1996). This locus is a tumour suppressor lost or silenced by methylation in many types of cancers and it encodes multiple transcripts one of which is p16^{INK4a} a cyclin D-dependent kinase CDK4 and CDK6 inhibitor preventing their phosphorylation of RB protein and hence cell cycle progression from G1 to S-phase. However, interestingly the same locus encodes another protein from an alternate reading frame (ARF), p14^{ARF} (p19^{ARF} in mice), which is also involved in the regulation of G1/S transition. Figure 1-8 depicts how p14^{ARF} is reportedly transcribed from the alternative reading frame of *CDKN2A* locus. There is strong evidence that the oncogenic induced activation of p53 happens through p14^{ARF}/p19^{ARF} mediated negative regulation of MDM2/Mdm-2 activity (Bates, Phillips et al. 1998, de Stanchina, McCurrach et al. 1998, Palmero, Pantoja et al. 1998, Zindy, Eischen et al. 1998). This p19^{ARF}/MDM2/p53 pathway is also activated in

response to oncogenic stress through the p38(Akt) mitogen activated kinase (MAPK) pathway and inhibits the interaction of p53 and MDM2 (Bulavin, Phillips et al. 2004). A diagram describing p53 activation by DNA damage response or oncogenic stress is shown in Figure 1-9.

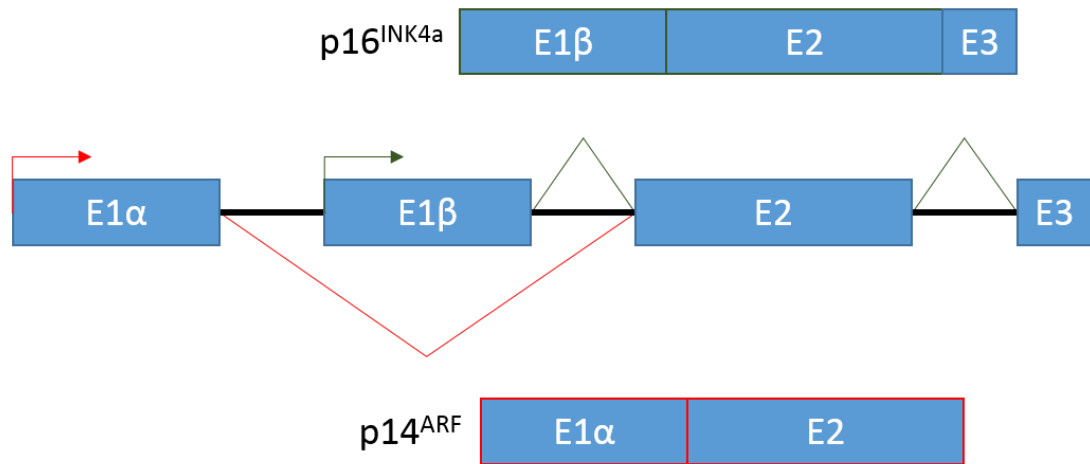


Figure 1-8 Alternate reading frame of the *CDKN2A* locus giving rise to *p14^{ARF}*. Exons 1 α and 3 are reportedly excluded during transcription to allow the *p14^{ARF}* mRNA.

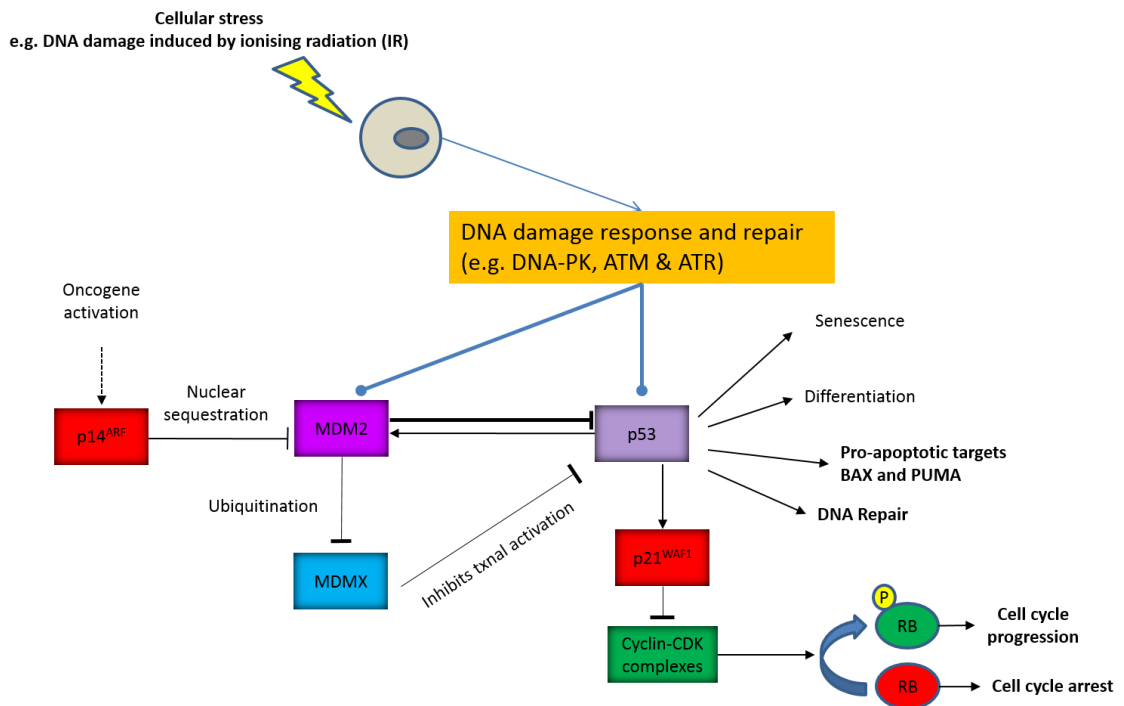


Figure 1-9 MDM2 is the most important regulator of p53. Transcriptional stability and nuclear localisation of p53 are all regulated primarily by MDM2. Cellular stress can result in disruption of this molecular interaction and lead to p53 stability. MDM2 is also a direct downstream transcriptional target of p53 and hence these two molecules form an auto-regulatory feedback loop. Figure obtained and modified from (Tweddle, Pearson et al. 2003).

1.12 An overview of MDM2

1.12.1 MDM2 gene and protein

MDM2/HDM2 is located on chromosome 12q15 with the genomic co-ordinates chr12:69,201,971-69,239,320 (UCSC genome browser). This gene comprises 11 exons, with more than 40 splice variants reported, in both normal and tumour tissue (Bartel, Taubert et al. 2002) (GeneCards, Weizmann Institute) some of which retain transforming ability despite loss of N-terminal p53-binding domain exons (Sigalas, Calvert et al. 1996). *MDM2* encodes a 491 amino acids long 55233Da protein which migrates at 90kDa and is known to behave as an E3 ubiquitin ligase most likely due to post-translational modifications. Characterised MDM2 functional domains include: p53 binding domain (residues 19–102), acidic domain (residues 223–274), a central zinc-finger (residues 305–332) and a RING-finger at its C-terminal end (residues 438–478) (Chen, Marechal et al. 1993, Boddy, Freemont et al. 1994).

1.12.2 MDM2: Inhibitor of p53 transactivation

The *Mdm2* (Murine homologue of *MDM2*) gene is a potent oncogene which was originally found in a spontaneously transformed murine 3T3 cell line that had double minute chromosomes (Double minutes are cytogenetically identified paired acentric chromatin bodies harbouring amplified genes) (Cahilly-Snyder, Yang-Feng et al. 1987). The overexpression of *Mdm2* was shown to increase the tumorigenicity of murine cell lines (Fakharzadeh, Trusko et al. 1991). The earliest evidence of p53-Mdm2 interaction was reported in 1992 when Momand and colleagues demonstrated a protein migrating at 90kDa which immunoprecipitated with both mutant and Wt p53. The authors then demonstrated with a reporter gene assay that MDM2 inhibited transcriptional activity induced by p53 (Momand, Zambetti et al. 1992). *MDM2*-amplification was detected in one third of human sarcomas and the association between this event and loss of p53-dependent cell cycle regulation was made (Oliner, Kinzler et al. 1992). Others have confirmed the prevalence of *MDM2*-amplification or overexpression (e.g. due to *SNP309* (Bond and Levine 2007)) in sarcomas and other cancers (Buesoramos, Yang et al. 1993, Ladanyi, Cha et al. 1993, Leach, Tokino et al. 1993, Cordoncardo, Latres et al. 1994). During the mid-1990s multiple groups showed that the physical interaction of the Mdm2 N-terminus and the N-terminal acidic TA domain of p53 was necessary for inhibition of p53 transactivation activity (Chen, Marechal et al. 1993, Oliner, Pietenpol et al. 1993, Haines, Landers et al. 1994, Lin,

Chen et al. 1994). This physical interaction between p53 and Mdm2 was later confirmed and detailed insight into the binding mode gained by determination of the X-ray crystal structure of the p53 and MDM2 N-terminal complex (See (Kussie, Gorina et al. 1996)). Chen and colleagues showed that p53 mediated G1 arrest and apoptosis is inhibited by Mdm2-dependent mechanisms (Chen, Wu et al. 1996). Two independent studies developed Mdm2 knockout transgenic mice and showed that these mice underwent early embryonic lethality, which was only rescued by concomitant deletion of *Trp53* (Jones, Roe et al. 1995, Luna, Wagner et al. 1995). This suggested that the most important role of Mdm2 in early development is negative regulation of the pro-apoptotic and cell cycle regulatory effects of p53.

After it was established that MDM2 interacts with the N-terminus of p53 (Picksley, Vojtesek et al. 1994), site specific mutagenesis of the key amino acids involved in transactivation function of p53, namely L22 and W23, were identified to interact with Mdm2 (Lin, Chen et al. 1994). L14 and F19 were also shown to be needed for the binding of p53 to MDM2 (Lin, Chen et al. 1994). As expected, none of these mutations affected p53 sequence specific DNA binding (Lin, Chen et al. 1994). To map the MDM2 binding site for p53 Böttger, A., et al., (1997) used pre-defined short peptides from a phage library to inhibit the interaction between MDM2 and p53 and assessed which peptide had the lowest inhibitory concentration 50 (IC₅₀) *in vitro* as measured by an enzyme-linked immunosorbent assay (ELISA) (Böttger, Böttger et al. 1997). This study also confirmed the earlier findings that the N-terminal domain of p53, especially F19, W23 and L26, were critical residues for the p53-MDM2 interaction (Böttger, Böttger et al. 1997). This was subsequently demonstrated by the X-Ray diffraction determined atomic resolution crystal structure of the MDM2-p53 dimer, which showed that p53 forms an N-terminal amphipathic alpha-helix with three critical side chains projecting from F19, W23 and L26 all of which sit in a small N-terminal hydrophobic binding pocket formed by MDM2 (Kussie, Gorina et al. 1996). Importantly MDM2-p53 association was identified to cause a steric hindrance to p53 interaction with TAFII40, TAFII60 and TAFII31 which thus inhibits transcriptional transactivation (Lu and Levine 1995, Thut, Chen et al. 1995). Böttger and colleagues also used electrophoretic mobility shift assays to assess whether the MDM2-p53 interaction inhibits p53 sequence specific DNA binding and observed that the p53-DNA complex was supershifted by MDM2 indicating that MDM2 does not inhibit the p53-DNA interaction (Böttger, Böttger et al. 1997). Despite the important role of MDM2 in p53 regulation it is also

known that MDM2 can directly interact with DNA, RNA, L5 ribosomal protein (Marechal, Elenbaas et al. 1994), RB (Xiao, Chen et al. 1995), E2F (Martin, Trouche et al. 1995) and NBS1 (Carrillo, Hicks et al. 2015). More recent findings suggest that p53 is active and ready for transcriptional induction at the promoter sites of some target genes and is only inhibited by MDM2 and another closely related protein MDMX. This is termed the “anti-repression model” which is consistent with p53 transcriptional activity observed after non-genotoxic decoupling of MDM2 and p53 by small molecular weight inhibitors or peptides (Kruse and Gu 2009).

1.12.3 MDM2 a transcriptional target of p53

It was shown that UV light-induced DNA damage promotes the expression of MDM2 in a p53-dependent manner and that this expression is delayed at higher doses of UV light in spite of the sharp rise in p53 (Perry, Piette et al. 1993). MDM2 has three promoter sequences in the *MDM2* gene however only the second one is responsive to p53 (Saucedo, Myers et al. 1999, Liang and Lunec 2005). The first promoter (P1) is located upstream of exon 1 and is regulated by the tumour suppressor phosphatase and tensin homologue (PTEN) (Chang, Freeman et al. 2004). The second promoter (P2) is regulated by p53 pertaining to four p53 response elements (*p53RE*) in intron 1 (Barak, Juven et al. 1993, Zauberman, Flusberg et al. 1995). The third promoter (P3) is in intron 3 and contains a p53 consensus DNA binding sequence, which in contrast to the P2 promoter acts as a repressor, negatively regulating MDM2 transcription at higher levels of p53 (Liang and Lunec 2005). The transcripts from P1 and P2 have the same transcriptional start site (exon 3) and they both possess two alternative translational start sites. This can give rise to two different size proteins, p90, is translated from the ATG in exon 3 and p76 is translated from ATG in exon 4 (Olson, Marechal et al. 1993, Iwakuma and Lozano 2003). The shorter alternate protein, p76, is thought to be involved in negative regulation of p90 as it is missing parts of the p53 binding domain. The transcripts from P1 and P2 are known to differ in their 5'-untranslated regions resulting in different translation efficiency (Jin, Turcott et al. 2003). The Ras-driven Raf/MEK/MAP kinase pathway also positively regulates MDM2 at the P2 promoter. Activated Raf in response to fibroblast growth factor (FGF), insulin like growth factor 1 (IGF-1) and platelet-derived growth factor (PDGF) upregulates *MDM2* mRNA and protein (Ries, Biederer et al. 2000). In the absence of p19^{ARF} (a physiological Mdm2 inhibitor protein) this Mdm2 upregulation leads to Mdm2 mediated degradation of p53 (Ries, Biederer et al. 2000). MDM2 has also been reported to be a downstream

transcriptional target of MYCN (Slack, Chen et al. 2005), although this requires further validation.

1.12.4 MDM2 ubiquitinates p53

The levels of p53 increase in response to DNA damage or oncogenic stress due to post-transcriptional events. This is due to an increase in p53 post-translational stabilisation of p53 while p53 mRNA remains more or less constant (Reich, Oren et al. 1983, Prives and Hall 1999). In 1997 Haupt and colleagues showed that Mdm2 is responsible for rapid degradation of p53 (Haupt, Maya et al. 1997). A construct encoding a truncated form of Mdm2 (ΔX), defective in binding to p53, was used to show that p53 degradation is dependent on interaction with Mdm2. A wild-type p53 construct was co-transfected with Wt *mdm2* or ΔX *mdm2* into a p53 null background (H1299 cells) and p53 protein levels were measured after 24 hours by immunoblotting. The p53 level was markedly reduced when Wt p53 and Wt *mdm2* were co-transfected into H1299 cells in comparison to co-transfection of ΔX *Mdm2* and Wt p53 (Haupt, Maya et al. 1997). Mutated p53, deficient in Mdm2 binding, was refractory to Mdm2 mediated degradation indicating that Mdm2-p53 binding is critical for p53 degradation (Haupt, Maya et al. 1997). Fusion of the first 42 N-terminal residues of p53 to a Gal4 DBD also resulted in rapid degradation of the fusion protein. Most importantly the Mdm2 dependent downregulation of p53 was shown to be independent of mRNA levels (Haupt, Maya et al. 1997).

Transactivation repression of p53 was only dependent on the N-terminus of Mdm2 leaving room for speculation as to what the rest of this protein does (Chen, Wu et al. 1996, Kubbutat, Jones et al. 1997). Previous knowledge of interaction of HPV E6 and its ability to target p53 for ubiquitin mediated degradation was also suggestive that p53 degradation was proteasomal (Scheffner, Werness et al. 1990). Using specific proteasome inhibitors it was shown that p53 ubiquitin mediated degradation is dependent on the 26S proteasome and subsequently that MDM2 is the E3 ubiquitin ligase primarily responsible for p53 ubiquitination (Maki, Huibregtse et al. 1996, Honda, Tanaka et al. 1997). Lactacystin (another proteasome inhibitor) was also able to abolish Mdm2 mediated degradation of p53, which supported degradation by a proteasomal dependent system (Kubbutat, Jones et al. 1997). It is important to note that both non-treated cells and cells pre-treated with IR accumulate ubiquitinated p53 when proteasomal degradation is inhibited, indicating that ubiquitination is involved in basal

p53 turnover (Maki, Huibregtse et al. 1996). The ubiquitination reaction is carried out in a three step biochemical reaction, starting from ubiquitin activating enzyme (E1), followed by ubiquitin conjugating enzyme (E2), and finally ubiquitin ligase (E3) (Honda, Tanaka et al. 1997). E1 attaches ubiquitin to a 76 residues long protein, E2 accepts this activated ubiquitin and passes it on to E3 ubiquitin ligase which catalyses the covalent attachment of ubiquitin to the target substrate (Iwakuma and Lozano 2003). MDM2 was found to carry out the final step with respect to p53 *in vitro* and also its amino acid sequence showed sequence similarity to other ubiquitin ligase enzymes (Honda, Tanaka et al. 1997). Multiple target lysine residues, namely K370, K372, K373, K381, K382 and K386, at the C-terminus of p53 were found to be ubiquitinated by MDM2 and site directed substitution mutations of these residues were found to interfere with ubiquitination (Nakamura, Roth et al. 2000, Rodriguez, Desterro et al. 2000). Although, later *in vivo* mouse knock-in data emerged showing that the equivalent of these residues are dispensable MDM2 mediated p53 degradation (see section 8.4) (Feng, Lin et al. 2005, Krummel, Lee et al. 2005). The ubiquitylating activity of MDM2 was reported to be dependent on its RING finger domain, which is also responsible for its self-ubiquitination (Fang, Jensen et al. 2000, Honda and Yasuda 2000). This autoubiquitination was shown to only require E1 and E2 enzymes *in vitro* (Fang, Jensen et al. 2000). When Zn was chelated using N,N,N',N'-tetrakis(2-pyridylmethyl)-ethylenediamine (TPEN) or MDM2 residues involved in coordination of Zn were mutated, the ubiquitination did not occur, indicating that MDM2-dependent ubiquitination and autoubiquitination require a Zn atom, consistent with the involvement of the RING finger domain. Interestingly when the RING domain of MDM2 was replaced with that of another E3 enzyme (Praj1), MDM2 failed to ubiquitinate p53 suggesting that the RING domain on MDM2 targets p53 in a substrate specific manner (Fang, Jensen et al. 2000). The Herpes virus-associated ubiquitin-specific protease (HAUSP; a deubiquitinase) and death domain associated protein (DAXX) are also involved in p53 turnover through MDM2. In unstressed conditions DAXX stabilises MDM2 and HAUSP complex also increases MDM2 stability and intrinsic enzymatic activity, thereby promoting degradation of p53 by MDM2 (Tang, Qu et al. 2006).

1.12.5 Nuclear Shuttling of MDM2

It was known that when MDM2 is transiently expressed it localises to the nucleus due to it possessing a nuclear localisation signal (Chen, Lin et al. 1995). Heterokaryon assay

was used to show the shuttling of ectopically expressed MDM2 between the nucleus and cytoplasm. Point mutations, G58A, D68A and V75A, which affected the interaction of p53 and MDM2 did not result in the abolition of MDM2 shuttling. This indicated that MDM2 nuclear export is independent of the interaction with p53. Sequence similarity between the nuclear export signal of lentiviruses and a domain on MDM2 highlighted the potential of a nuclear shuttling sequence on MDM2 (Roth, Dobbelstein et al. 1998). Loss of the nuclear export sequence meant nuclear localisation of MDM2.

1.12.6 MDMX

Another protein involved in the stability and negative regulation of p53 function is the closely related MDM2 paralogue, mouse double minute 4 (MDM4/MDMX), but unlike MDM2 it is not a transcriptional target of p53 (Finch, Donoviel et al. 2002, Wade and Wahl 2009). Despite very close sequence and structural similarities between MDMX and MDM2 these two proteins cannot compensate for one another *in vivo* in early development (Wade and Wahl 2009). Absence of MDM2 or MDMX results in embryonic lethality in mice, and in both cases the murine embryos can be rescued by concomitant loss of *Trp53* (de Oca Luna, Wagner et al. 1995, Jones, Roe et al. 1995, de Rozieres, Maya et al. 2000, Wade and Wahl 2009) (de Oca Luna, Wagner et al. 1995, Jones, Roe et al. 1995, de Rozieres, Maya et al. 2000, Wade and Wahl 2009). Temporal and tissue specific expression of both proteins may account for their lack of ability to compensate for one another in early development (Wade and Wahl 2009, Pant, Xiong et al. 2011). MDMX physically interacts with the RING domain on MDM2 and the transactivation domain of p53, preventing its transactivation activity (Tanimura, Ohtsuka et al. 1999, Popowicz, Czarna et al. 2007). Although MDM2/MDMX heterodimerisation regulates p53-MDM2 interaction and stability, this dimer is thought to be dispensable in later development and it is thought to not target p53 for degradation (Tanimura, Ohtsuka et al. 1999, Badciong and Haas 2002, Popowicz, Czarna et al. 2007). Increased expression of MDMX has been reported to reduce sensitivity to Nutlin-3 (an MDM2-p53 binding antagonist) which is known not to inhibit MDMX binding to p53 (Hu, Gilkes et al. 2006). *MDMX*-amplification or overexpression may be a causative reason for p53 pathway inactivation in retinoblastoma and other cancers, consistent with an oncogenic role for MDMX (Laurie, Donovan et al. 2006). Therefore considering the role of MDMX amplification as a determinant of response to MDM2 antagonists may be needed in cell lines that show reduced sensitivity.

1.13 DNA strand break repair mechanisms

The multitude of sources of DNA damage induce distinct yet diverse DNA damage lesions however DNA double strand breaks (DSB's) or single strand breaks (SSB's) that can lead to DSBs at the replication fork are considered the most lethal (Polo and Jackson 2011). Therefore in this section repair mechanisms of DNA DSB's are briefly introduced and their crosstalk with p53 signalling is discussed.

1.13.1 Homologous recombination repair

In homologous recombination DNA repair (HRR) DNA DSB's are detected by the MRN protein complex, comprised of MRE11, Rad50 and NBS1, which then directly stimulates ataxia telangiectasia mutated (ATM) enzymatic activity to target its downstream effectors including: histone H2AX^{S139}, CHEK2^{T68}, MDM2^{S407, S419, S425, S429 & S395}, MDMX^{S403}, Cdc25C (through CHEK2) and p53^{S15, S46} (Lee and Paull 2004, Meek 2009, Meek 2015). Phosphorylated H2AX (termed γ H2AX) results in nucleosome remodelling and increases DNA accessibility to other repair proteins such as breast and ovarian cancer susceptibility protein 1 (BRCA1) and 53BP1 (Celeste, Fernandez-Capetillo et al. 2003). CHEK2 however further modifies downstream targets including p53, MDM2 and MDMX (Meek 2009). Transgenic mice with Mdm2^{S394A} or Mdmx^{S342A, S367A & S403A} homozygous substitutions are radio-resistant and MEFs derived from Mdm2^{S394A} mice do not undergo apoptosis in response to ionising radiation (Maya, Balass et al. 2001, Gannon, Woda et al. 2012). Interestingly, responses to Nutlin-3 are unaffected in Mdm2^{S394A} mice suggesting that this residue is not pertinent in determining the response to MDM2 inhibitors. Although the affinity of Nutlin-3 to murine Mdm2 may not be the same as human MDM2. Another protein involved in HRR is poly (ADP-ribose) polymerase 1 (PARP-1). PARP-1 inactivation was discovered to have a synthetic lethal effect in BRCA1 and BRCA2 homozygously mutated cancer cells found in sporadic and familial types of breast and ovarian cancers (McCabe, Turner et al. 2006). PARP-1 is responsible for detecting DNA strand breaks and catalyses the poly ADP-ribosylation of proteins associated with chromatin structure, allowing chromatin remodelling and access of repair proteins to the site of damage (Shall and de Murcia 2000, Hochegger, Dejsuphong et al. 2006). SSBs as defined by discontinuities in one strand of the double stranded DNA molecule, are more prevalent than DSBs, and are cytotoxic to the cell if not repaired efficiently. SSBs can occur as a result of oxidative damage caused by endogenous ROS, aberrant topoisomerase 1 activity (or Topo 1 inhibitors), base excision repair (BER) of damaged bases/abasic sites

or direct disintegration of oxidised sugar (Caldecott 2008). Replication protein A (RPA) binds to and stabilizes SSBs present as part of the normal DNA replication process in between Okazaki fragments on the lagging DNA strand. RPA coated DNA can also recruit ATR-interacting protein (ATRIP) complex to the site of damage (Cortez, Guntuku et al. 2001, Caldecott 2008). ATM- and Rad3-related (ATR) is then activated and phosphorylates downstream proteins like CHEK1, p53 and MDM2 (Cortez, Guntuku et al. 2001). ATR is thought to mainly respond to replication stress and strand crosslinking, however the overlap between the role of ATR and ATM are not completely defined yet (Cortez, Guntuku et al. 2001). In contrast to *Atm* and *Trp53*, *Atr* null mice and human somatic cells are not viable (Brown and Baltimore 2000, Cortez, Guntuku et al. 2001). Interestingly loss of CHEK1, the well-established substrate of ATR, is also embryonically lethal in mice (Liu, Guntuku et al. 2000). ATR autophosphorylation and phosphorylation of CHEK1 are essential for the G₂/M cell cycle checkpoint response to DNA damage (Liu, Guntuku et al. 2000).

1.13.2 Non-homologous end joining

Non-homologous end joining (NHEJ) DNA repair begins by sequence independent recognition of DSB's (both blunt ended and 3'- or 5'-overhang) through a heterodimer protein called Ku which is composed of Ku80 and Ku70 (Yannone, Khan et al. 2008, Mahaney, Meek et al. 2009). Ku subsequently holds the two broken ends of DSBs together by self-association and then recruits other proteins involved in NHEJ such as DNA dependent protein kinase catalytic subunit (DNA-PKcs), XRCC4-Ligase IV complex, XLF, DNA polymerases μ and λ (Cary, Peterson et al. 1997, Mahaney, Meek et al. 2009). Recruitment of DNA-PKcs to either sides of the DNA DSB by Ku enables "synaptic complex" formation and allows both the catalytic subunits to trans-phosphorylate and thus activate one another (DeFazio, Stansel et al. 2002). Non-ligateable DNA ends are then processed to 5'-phosphate and 3'-hydroxyl ends so that they can be ligated in a sequence non-specific manner (Yannone, Khan et al. 2008, Serrano, Li et al. 2012).

1.14 Strand break repair machinery and p53 crosstalk

Integral to the function of the repair processes described above, are three members of the aforementioned PI3KK family of protein kinases; ATM, ATR and DNA-PKcs. Germline defects in genes encoding these kinases have been shown to cause syndromes typified by acute sensitivity to DNA damaging agents and predisposition to various

cancers, as well as immunodeficiency disorders (Savitsky, Bar-Shira et al. 1995, O'Driscoll, Ruiz-Perez et al. 2003, van der Burg, Ijspeert et al. 2009). Somatic mutations of these genes are also found in many different tumour types (Lempiaainen and Halazonetis 2009). As described above, recruitment and activation of each kinase to specific DNA damage lesions requires a complex of sensor proteins which first recognise the lesion and then provide a docking site for the specific kinases. In NHEJ DNA DSBs are first bound by Ku70/Ku80 heterodimer which then recruit and activate DNA-PKcs to the site of damage allowing for initiation of this process (Gottlieb and Jackson 1993). In HRR DNA DSBs are first bound by the MRN sensor complex (MRE11–RAD50–NBS1) which then recruits and activates ATM (Polo and Jackson 2011). Single strand breaks in the DNA are sensed by replication protein A (RPA) which recruits ATR to the site of the damage with the help of ATR interacting partner (ATRIP) (Polo and Jackson 2011). These three PI3KKs are then activated to directly and indirectly phosphorylate p53 on different and overlapping residues resulting in its dissociation from MDM2 and stabilisation (See Figure 1-9) (Meek 2009, Meek and Anderson 2009). Once p53 is stabilised it can induce the transcription of its pro-arrest transcriptional targets, to allow time for repair of the damage, or promotes cell suicide through a PCD mechanism (e.g. apoptosis) if the damage is irreparable, or the consequences of misrepair are unfavourable for the survival of the cell. ATM, ATR and DNA-PKcs can thus induce p53 tumour suppressor activity in response to different types and severities of DNA strand breaks (Meek and Anderson 2009).

1.14.1 WIP1 phosphatase and homeostasis of p53 in response to stress and DNA damage

Reversible p53 induced cell cycle arrest in the event of sub-lethal damage is made possible through multiple p53 negative autoregulatory mechanisms (Harris and Levine 2005). As described earlier, the p53-MDM2 negative autoregulatory feedback loop plays the most crucial role in homeostatic regulation of p53 stability and function. However, there are many more subtle feedback mechanisms to help keep the p53 growth inhibitory and lethal function at bay. One such mechanism involves p53 mediated induction of protein phosphatase, Mg²⁺/Mn²⁺ dependent, 1D (PPM1D/WIP1). Henceforth, *PPM1D* (*Ppm1d* in mice) will be used to denote the gene and WIP1 (Wip1 for the mouse homologue) to denote the protein. WIP1 directly dephosphorylates phospho-p53^{Ser15}, which is the product of PI3KKs, and indirectly affects the phosphorylation of other residues (Thr18 & Ser20) that are important for

dissociation of p53 from MDM2. Furthermore, WIP1 reportedly dampens down DNA damage response and stress signalling to p53 by dephosphorylation-mediated deactivation of ATM^{Ser1981}, CHEK1^{Ser345} & CHEK2^{Thr68}, γ H2AX, p38 α ^{Thr180} (MAPK-pathway), nuclear factor kappa B Ser536 (NF- κ B^{Ser536}), UNG2^{Thr6}, XPC^{Ser196} and XPA^{Ser892}. WIP1 also reportedly dephosphorylates MDM2^{Ser395} and MDMX^{Ser403} increasing their stability resulting in negative regulation of p53. The diagram highlights some of the mechanisms through which WIP1 dampens stress signalling to p53 as reviewed extensively by (Figure 1-10) (Lu, Nguyen et al. 2008, Lowe, Cha et al. 2012). In the chapters 4 and 5 of this thesis the role of WIP1 transient knockdown and chemical inhibition in regulation of p53 signalling will be explored and discussed in more detail.

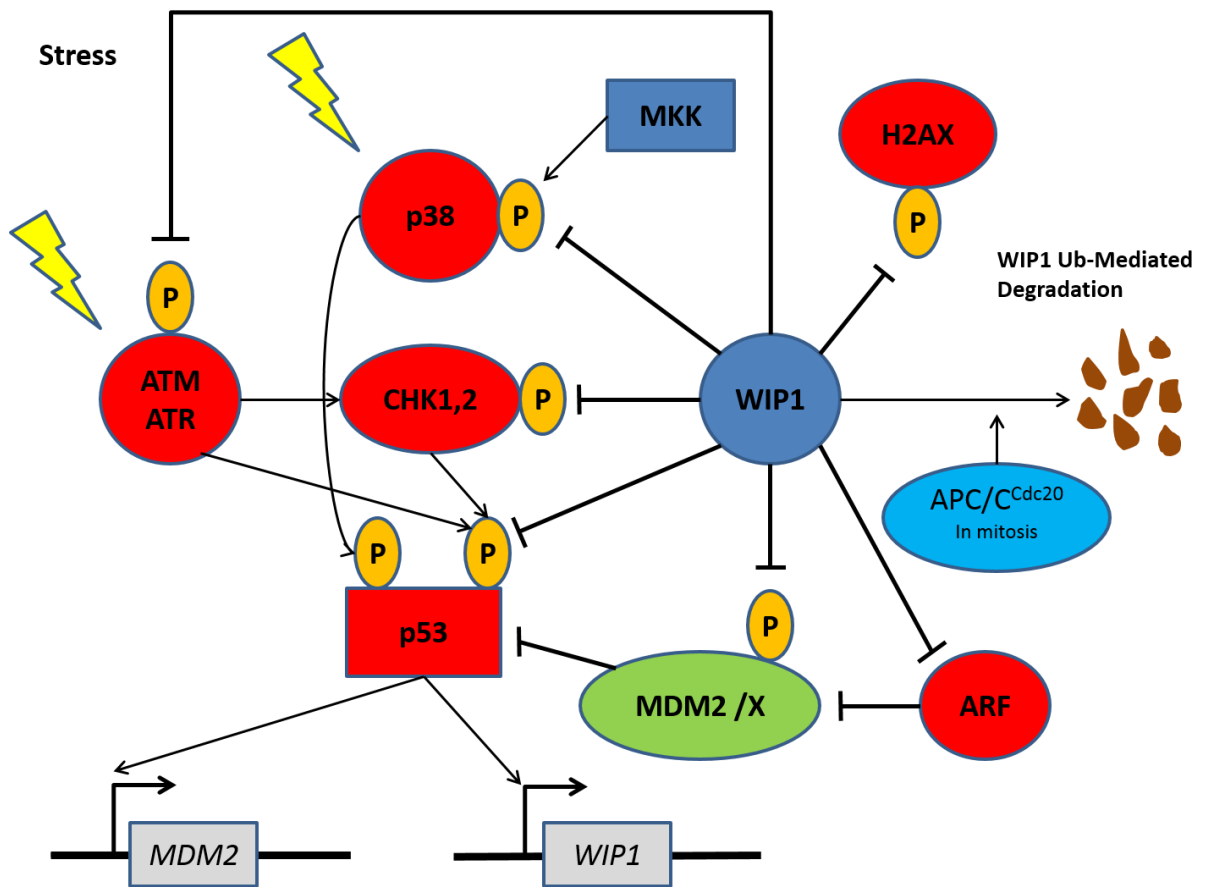
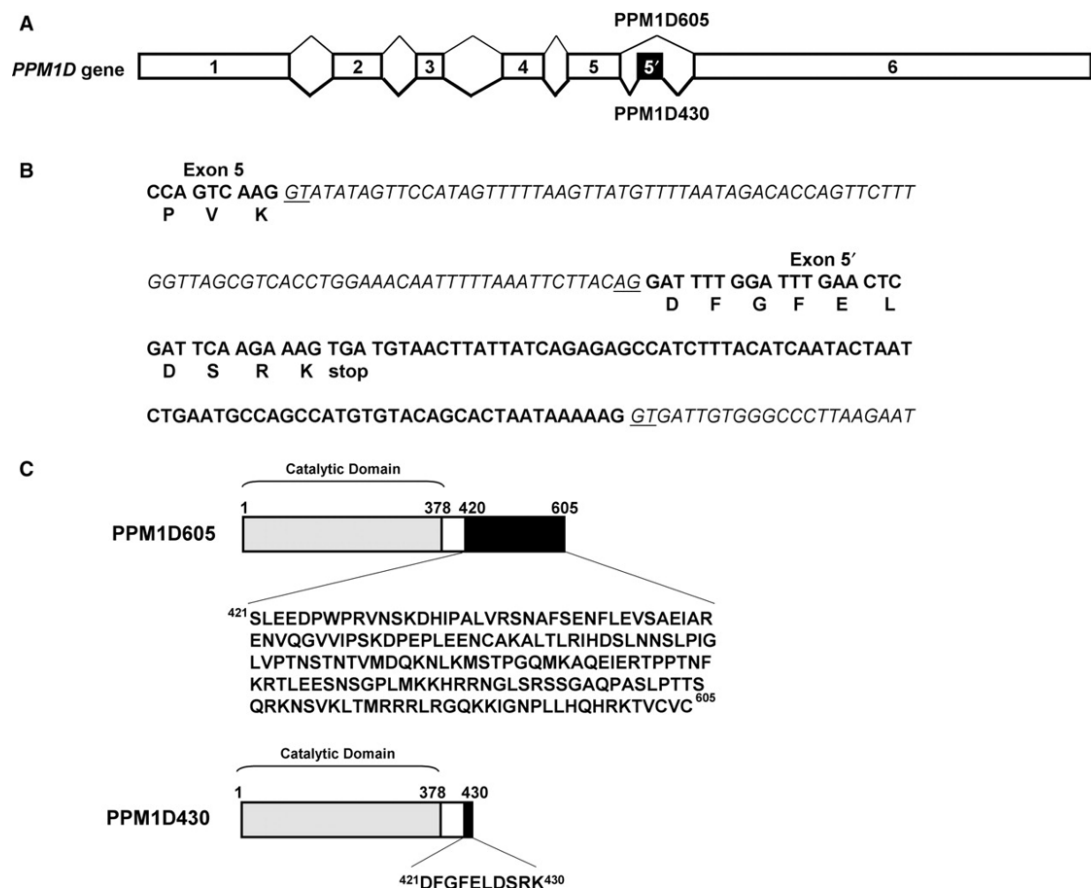


Figure 1-10 Some of the mechanisms through which WIP1/PPM1D has been reported to directly and indirectly regulate the p53 network in response to oncogenic stress and DNA damage. Image adapted and modified from Lu et al., 2008 (Lu, Nguyen et al. 2008)

1.15 An overview of PPM1D/WIP1

1.15.1 PPM1D/WIP1 gene and proteins

PPM1D is located on the positive strand of the long arm of chromosome 17 (17q23.2) with the genomic co-ordinates chr17: 60590183-60676280 (UCSC genome browser). Alternative splicing of the mRNA of this gene results in two transcripts producing two different sized proteins both of which retain their phosphatase activities (Chuman, Kurihashi et al. 2009). The short transcript produces a 605 amino acid long WIP1 protein (PPM1D605) whereas the longer transcript due to exon inclusion, and a premature stop codon within that exon, results in a 430 amino acid long WIP1 protein (PPM1D430) (Figure 1-11). While PPM1D605 is ubiquitous across human tissue types, WIP1430 is exclusive to testes and leucocytes.



Yoshiro Chuman et al. J Biochem 2009;145:1-12

Figure 1-11 A) Figure obtained from Chuman *et al.*, (2009) shows the alternative splicing and inclusion of exon 5' between PPM1D exons 5 and 6. **B)** Sequence corresponding to intron exon boundaries of exon 5' in addition to the 10 amino acids and the stop codon encoded by the PPM1D430 transcript. **C)** The diagram shows the location of the stop codon in PPM1D430 with respect to the WIP1 catalytic site.

1.15.2 *PPMID/WIP1* C-terminal truncating mutations and other variants

Similar to the truncated WIP1 isoform there have been reports of *PPMID* mutations in human cancer cell lines and primary tissue that confer a C-terminus truncated protein with gain-of-function phenotype. Kleiblova *et al.*, (2013) were the first to report the *PPMID* gain-of-function mutations in a colorectal cancer cell line, HCT116, and an osteosarcoma cell line, U2OS (Kleiblova, Shaltiel *et al.* 2013). The authors then went on to show that the truncated WIP1 was enzymatically more active *in vitro* and more stable than the full-length wild-type WIP1. Mutation of Asp314Ala abolishes the phosphatase activity of WIP1 (Takekawa, Adachi *et al.* 2000) hence it was used as a negative control in their *in vitro* phosphatase assay (Kleiblova, Shaltiel *et al.* 2013). The authors also showed that both these cell lines had impaired IR induced G1 arrest and that silencing of WIP1 by RNA interference (RNAi) resulted in G1 arrest in response to IR.

Importantly it was shown that this G1 arrest was p53-dependent as co-silencing of WIP1 and p53 prevented these cell lines to undergo G1 arrest in response to IR.

Germline mosaic mutation in the same region of *PPMID* were reported to predispose individuals to breast and ovarian cancers (Ruark, Snape *et al.* 2013). Also interestingly *PPMID* truncating gain-of-function activating mutations and *TP53* mutations were reported to be mutually exclusive in brainstem gliomas (Zhang, Chen *et al.* 2014).

Single nucleotide polymorphisms of WIP1 (A82S, L120F, P322Q and I496V) reported on the National Institute for Biotechnology Information have also been investigated to assess their potential impact on WIP1 function (Dudgeon, Shreeram *et al.* 2013). The phosphatase activity of these variants against Phospho-ATM^{Ser1981} was investigated *in vitro* showing that L120F and P223Q variants of WIP1 had lost their WIP1 phosphatase activity while A82S did not change WIP1 activity. It is noteworthy that in these experiments only truncated WIP1 was used as full-length WIP1 is poorly soluble. This meant that the impact of the I496V was not investigated *in vitro*. However when expressed in cell lines I496V was shown to reduce WIP1 phosphatase activity. When the authors investigated WIP1 mutations reported in cbiportal.org they found that two thirds of WIP1 mutations occur in the C-terminus. Interestingly, a unique WIP1 C-terminal truncating mutation, R552X, was found to not impact WIP1 stability or function in contrast to all other C-terminal truncating mutations of WIP1 which have been reported to increase WIP1 stability and phosphatase function (Dudgeon, Shreeram *et al.* 2013).

1.15.3 *PPM1D* transcriptional regulation

The *PPM1D* transcript was first discovered to be induced in response to ionising radiation (IR) in a p53-dependent manner (Fiscella, Zhang et al. 1997). It was discovered in subsequent studies that the *PPM1D* promoter region also contains response elements for cyclic AMP response element binding protein (CREB), NF- κ B, oestrogen receptor α (ER α), c-jun and E2F1 (Reviewed extensively in (Lowe, Cha et al. 2012)). Basal levels of WIP1 protein were reported to be regulated from the CREB response element (CRE) 283 bases upstream of the *PPM1D* translational start site. However, the p53 response element was discovered to be 168 bases to the upstream of the *PPM1D* translational start (Rossi, Demidov et al. 2008). This was consistent with the abundance of a transcript with a shorter 5'-untranslated region (UTR) in response to IR or UV light in *TP53* wild-type cells, suggesting that in response to DNA damage *PPM1D* transcription is regulated from the further downstream p53 response element rather than the CRE. It was reported that the longer *PPM1D* transcript has a very complex 5'-UTR structure which may make its export from the nucleus more difficult. Furthermore, it has been shown that the 3'-UTR region of the *PPM1D* transcript is also important in determining its stability and WIP1 protein expression following DNA damage by the radiation mimicking agent neocarzinostatin (NCS) (Zhang, Wan et al. 2010). MicroRNA-16 (miR-16), which undergoes processing and maturation in a p53 dependent manner, was found to be complementary to the 3'-UTR region of the *PPM1D* transcript. Antagonising miR-16 with oligonucleotides increased *PPM1D* mRNA stability and the rate and intensity of WIP1 protein induction suggesting that miR-16 negatively regulates WIP1 expression at an early time-point after DNA damage by binding to its 3'-UTR. Interestingly, the authors also showed that miR-16 inhibits the proliferation of mammary tumour stem cells from MMTV-*ErbB2* mice

1.15.4 WIP1 degradation

Investigations into the mechanism of degradation of WIP1 began by investigating the levels of WIP1 protein throughout the cell cycle (Macurek, Benada et al. 2013). A double thymidine block was used to synchronise the HeLa cells at the point of G1/S transition and then the medium was changed to one containing the anti-microtubule agent, nocodazol, to arrest cells in mitosis. It was shown that WIP1 protein expression was markedly diminished specifically at mitosis. The same was reported about U2OS cells however, the data were not shown. This could possibly be because the authors could not explain the faster migrating WIP1 band detected in U2OS cells. Interestingly

the levels of WIP1 mRNA were reported to remain constant throughout the double thymidine block and release experiment which suggested that WIP1 degradation during mitosis is at the protein level. Fluorescent, ubiquitination-based cell cycle indicator (FUCCI) was used on synchronous cells to assess whether the thymidine block influenced the cell cycle dependent degradation of WIP1. In this technique the cell cycle stage of each cell within an asynchronous population can be determined using fluorescent markers that are expressed and degraded at different stages of the cell cycle. Using FUCCI the authors confirmed that WIP1 is degraded during mitosis. The authors then showed that proteasome inhibitor MG132 inhibits WIP1 degradation during mitosis showing that WIP1 degradation relies on the function of the proteasome. It was then shown that ubiquitination of WIP1 relies on the E3 ubiquitin ligase activity of the anaphase promoting complex APC/C^{CDC20}. Depletion of APC/C activator CDC20 by siRNA resulted in stabilisation of WIP1 during mitosis. Furthermore, mass spectrometry of WIP1 in nocodazol arrested cells showed that 7 residues on the catalytic subunit of WIP1 (Thr34, Ser40, Ser44, Ser46, Ser54, Ser85 and Ser97) are heavily phosphorylated during mitosis. Site directed mutagenesis was used to show that the phosphorylation of these residues are important for WIP1 phosphatase activity following DNA damage. Interestingly the C-terminus of WIP1 was also shown to be phosphorylated during mitosis, however the impact of these phosphorylation events was not investigated further (Macurek, Benada et al. 2013).

1.15.5 WIP1 substrates

In a quest to develop a peptide inhibitor for WIP1 Yamaguchi *et al.*, (2006) were the first to define, in detail, the ideal substrate motifs for dephosphorylation by WIP1. The one letter code of amino acids are used here to define these motifs. The two optimal motifs dephosphorylated by WIP1 are X₋₁pTX₊₁pYX₊₃ where X₋₁ can be any amino acid, X₊₁ is an aliphatic amino acid and X₊₃ is any amino acid but proline (Yamaguchi, Durell et al. 2006) and (D/E)(D/E)X₋₁p(S/T)QX₊₄ where X₊₄ is any amino acid but proline or basic amino acids. The former is found on p38 α MAPK and UNG2, and the latter on the phosphorylation targets of PI3KK's which are involved in the DNA damage response and p53 signalling (Yamaguchi, Durell et al. 2007). The dephosphorylation of these motifs on proteins of the DNA damage response may result in homeostasis of DNA damage response in cases of reversible damage.

1.15.6 *Ppm1d* knockout transgenic mice models

Ppm1d null transgenic mice are viable however they present with sporadic male runting, male reproductive organ atrophy, reduced male fertility, reduced male longevity and immune defects (Choi, Nannenga et al. 2002). MEF's from *Ppm1d* knockout embryos do not grow well in culture and are resistant to transformation by combination overexpression of the following oncogenes *E1A + Hras1*, *Hras + Myc* or *Hras + ErbB2* in mouse xenografts experiments (Bulavin, Phillips et al. 2004). Interestingly, although xenografts of *Ppm1d* null MEF's overexpressing *Hras*, *Myc* or *ErbB2* did not result in the formation of tumours in mice, simultaneous loss of *Trp53* in these MEF's resulted in tumour formation, which implies that *Ppm1d* is important for holding back the tumour suppressor effect of p53. Importantly this protection against transformation was proposed to be due to p38 MAPK mediated activation of p16^{Ink4a} and p19^{ARF} expression in the absence of *Ppm1d*. Inhibition of p38 (by SB203580) in *Ppm1d* null MEFS overexpressing two oncogenes resulted in tumour formation in xenograft studies in mice.

1.16 MDM2 inhibitors

1.16.1 Oligonucleotides and peptides

Early findings that disruption of the MDM2 inhibitory activity on p53 can promote p53 stability and increase sensitivity to damage induced by IR came about in the late 1990s. Chen and colleagues screened nine 20-mer antisense oligonucleotides and identified one, namely HDMAS5, which could inhibit MDM2 expression in *MDM2*-amplified SJSA-1 (osteosarcoma) and JAR (Choriocarcinoma) cell line (Chen, Agrawal et al. 1998). They subsequently showed that antisense inhibition of MDM2 expression using this complementary phosphorothioate oligodeoxynucleotide can lead to stabilisation of p53, induction of its downstream transcriptional targets and increase sensitivity of the cell lines to Topo I inhibitor induced DNA damage in a synergistic manner (Chen, Agrawal et al. 1998). Following these findings it was demonstrated that inhibition of the MDM2-p53 interaction using a small peptide (IP3), homologous to the MDM2 interaction domain of p53, can result in p53 stabilisation transcriptional transactivation reduced colony formation, cell cycle arrest and cell death (Wasylyk, Salvi et al. 1999). The authors also demonstrated p53-dependent reduced E2F 1/DP1 activity in the presence of the IP3 peptide. A similar study in the following year assessed the ability of a synthetic peptide to inhibit the MDM2-p53 interaction, resulting in non-genotoxic activation of p53 as determined by the relative absence of p53^{Ser15} phosphorylation

(Chene, Fuchs et al. 2000). The phosphorylation of p53^{Ser15} induced by the peptide was very modest (at 24 hours) in comparison to that observed by cisplatin in the same cell line (Chene, Fuchs et al. 2000). Tortora and colleagues (Tortora, Caputo et al. 2000) showed that antisense inhibition of MDM2 expression using an oligonucleotide can also potentiate the effect of cytotoxic drugs such as topoisomerase inhibitors, taxanes and platinum-derived drugs as measured by colony formation assay *in vitro*. In this study nude mice were also injected with the GEO human colorectal carcinoma cell line and tumours were challenged by the *MDM2* antisense molecule in combination with different cytotoxic regimens (Tortora, Caputo et al. 2000). Relative increase in apoptosis was shown to be enhanced by combination of *MDM2* antisense with topotecan, taxotere and cisplatin *in vitro*. Apoptosis was determined by quantification of cytosolic DNA bound histone fragments by ELISA (Tortora, Caputo et al. 2000). Intraperitoneal injection of the same antisense molecule in combination with cytotoxic drugs resulted in reduced tumour growth as measured by tumour volume and improved percentage survival (Tortora, Caputo et al. 2000). For a review of *MDM2* antisense oligonucleotides refer to (Zhang and Wang 2003).

1.16.2 Small molecule MDM2 inhibitors

By high throughput screening of a library of synthetic chemicals Vassilev and colleagues were the first to identify a group of cis-imidazoline compounds (nicknamed Nutlins) which bound and masked the p53 binding pocket on MDM2 (Vassilev, Vu et al. 2004). Nutlins could inhibit the MDM2-p53 interaction in cell-free assays with IC₅₀ values of 100-300nM. Both enantiomers of a Nutlin-3 racemic mixture were isolated using a chiral column and the isomers were named Nutlin-3a and Nutlin-3b. It was shown that Nutlin-3a is a 150-fold more potent at inhibition of the MDM2-p53 interaction *in vitro* than the inactive enantiomer (Nutlin-3a IC₅₀=0.09µM and Nutlin-3b IC₅₀= 13.6µM). The atomic resolution X-Ray diffraction crystal structure of Nutlin-2 (another cis-imidazoline analogue) bound to MDM2 was derived, which verified that Nutlins mimic the three main amino acid residues on p53 involved in its interaction with MDM2 (Figure 1-12).

Nutlin treatment of various cell lines resulted in a dose dependent increase in p53 downstream transcriptional targets such as p21 and MDM2 contingent on a wild-type *TP53* status. This resulted in cell cycle arrest, apoptosis and growth inhibition of SJS-1 osteosarcoma cell lines *ex vivo*. SJS-1 tumour xenografts in nude mice treated with

200 mg/kg twice daily over a 20-day period showed inhibition of tumour growth with no apparent systemic toxicity to the mice. Inhibition of MDM2-p53 interaction was therefore shown to mirror earlier findings with antisense oligonucleotides and synthetic peptides. This was proof of concept that selective small-molecule inhibitors of the MDM2-p53 interaction could provide non-genotoxic therapeutic options for activating p53. The cellular inhibitory activity of MDM2 inhibitors and their biochemical effect on p53 signalling has since been extensively investigated with Nutlin-3 and other novel MDM2 inhibitors; reviewed in (Zhao, Aguilar et al. 2015). These studies have consistently shown that *TP53* wild-type cell lines respond by growth inhibition following treatment with MDM2 inhibitors and canonical p53 transcriptional targets are induced in a class independent manner.

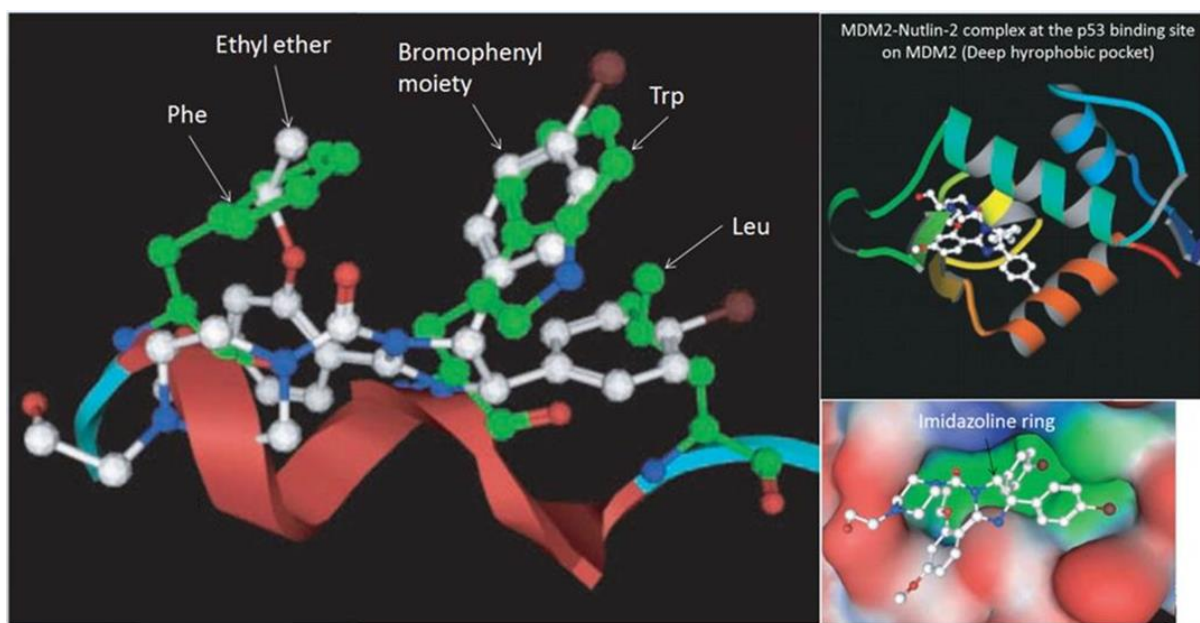


Figure 1-12 This shows how Nutlins (Nutlin-2: carbon atoms drawn as white spheres, nitrogen in blue, oxygen in red, and bromine in brown) can mimic important p53 residues (F19, W23 & L26 carbon atoms drawn as green spheres) and therefore interfere with the interaction of p53 and MDM2. One bromophenyl moiety sits in the W pocket and the other in the L pocket. The ethyl ether moiety sits in the F pocket. The imidazoline ring plays the role of the peptide backbone of p53.

1.16.3 Further developments

Since the discovery of Nutlins, multiple chemical classes of MDM2 antagonists, and indeed more potent compounds developed from Nutlins, have been identified and progressed through preclinical and early phase clinical studies (Zhao, Aguilar et al. 2015). Presently at least seven compounds have reached phase I clinical trials, namely RG7112/RO5045337, RG7388/RO5503781, MI77301/SAR405838, AMG232, CGM097, DS-3032b and MK8242. Nutlin-3a derived, RG7112 (IC₅₀ = 18nM), was the first MDM2 antagonist to reach phase 1 clinical trials (Ray-Coquard, Blay et al. 2012). This compound was orally administered to patients with advanced well-differentiated/poorly differentiated liposarcomas and haematological malignancies. Patients were administered three cycles of 20-1920mg/m²/day over a 10 day period with 18 days rest between each cycle. RG7112 was overall well-tolerated with the most prominent adverse effects being neutropenia and thrombocytopenia, which is in keeping with the mechanism of action of MDM2 antagonists and is considered an on-target effect, although this has not been unequivocally established. Immunohistochemistry and analysis by quantitative real time polymerase chain reaction (qRT-PCR) of tumour samples obtained from patients after 8 days of treatment indicated signs of activation of

p53 downstream targets (e.g. p21 and MDM2) and inhibition of proliferation (as measured by proliferative marker Ki67). However macrophage inhibitory cytokine-1 (MIC-1), which is a direct transcriptional target of p53, was the only marker of p53 activity that was shown to correlate with the area under the curve of (AUC) measurements of RG7112 in plasma. Thus the authors suggested that MIC-1 plasma levels could play the role of a surrogate pharmacodynamics marker for RG7112 activation of p53 (Ray-Coquard, Blay et al. 2012). Overall 14/20 patients showed stable disease for the duration of the treatment and one had confirmed partial response which is promising however it was concluded that in future trials the potential for haematological toxicities has to be considered carefully. In late 2011 RG7338 (IC₅₀ = 6nM), which was designed based on the structure of RG7112 and MI-219 (an mdm2 inhibitor of the spiro-oxindole family) entered into phase I clinical trials in solid tumour patients. In addition to mimicking structure of the three key amino acids at the N terminus of p53 (F19, W23 and L26) the 2-Chlorophenyl group also makes π - π interactions with p53 H96 (Figure 1-13) (Zhao, Aguilar et al. 2015). Maximum tolerated doses of RG7388 were dependent on scheduling and this compound had similar dose limiting haematological toxicities as observed in RG7112 (Siu, Italiano et al. 2014). This compound is being taken forward to phase II trials with the recommended dose of 500mg/m² with daily, 5 day scheduling. Clinical data for other classes of MDM2 inhibitors were not available at the time of drafting of this thesis however an extensive review of the list of reported MDM2 inhibitors at different stages of development has been carried out by Zhao *et al.*, (2015). This includes Newcastle University's in-house Isoindolinone derived series which are at an advanced stage of pre-clinical development.

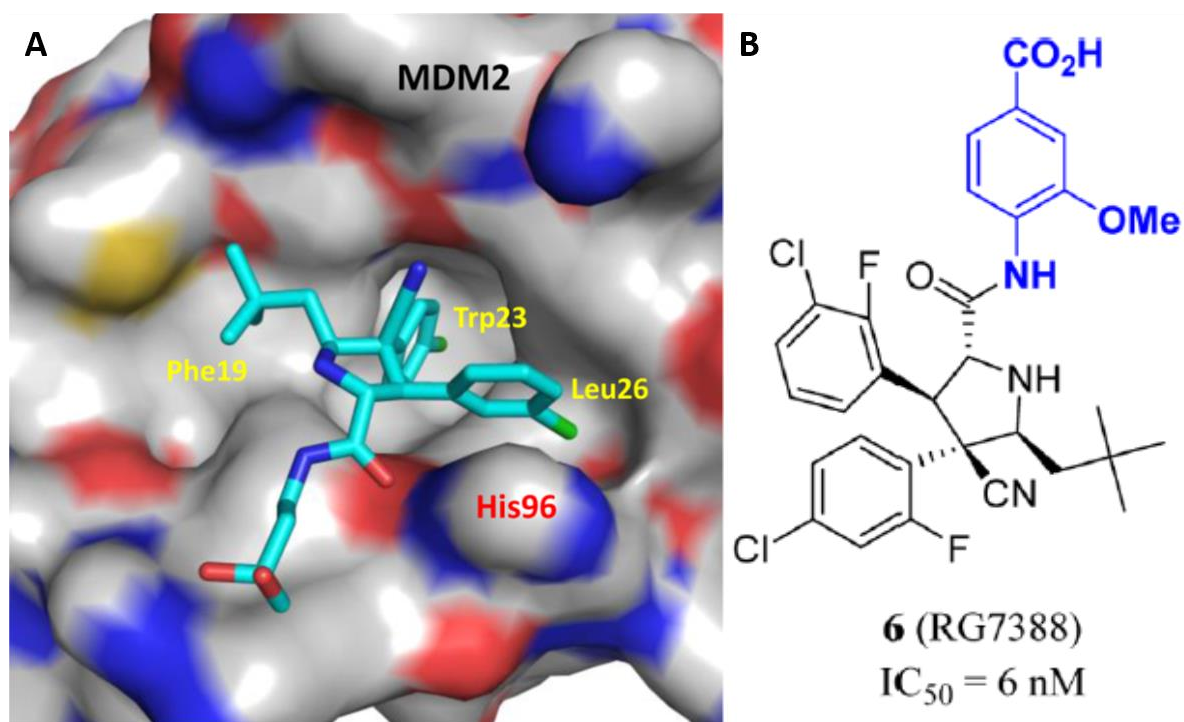


Figure 1-13 A) Co-crystal structure of MDM2 and the pharmacophore used for the derivation of RG7388 shows the π - π interaction of the 2-chlorophenyl moiety with H96 in the eMDM2 hydrophobic binding pocket. B) Chemical structure of RG7388. The additional fluorine atoms on the chlorophenyl moieties and the m-methoxybenzoic acid (blue) increased MDM2 binding affinity, cellular potency, microsomal stability and PK properties of the pharmacophore. Images were obtained from (Zhao, Aguilar et al. 2015).

1.16.4 Combination of MDM2-antagonists with DNA damaging agents

Since the discovery of MDM2 inhibitors their interaction with various DNA damaging agents have been assessed in a preclinical setting and early clinical combination trials have begun with more potent cis-imidazoline analogues (RO5045337/RG7112). Although the clinical results are still not published, the preclinical data are so far suggestive of potential benefits of combining MDM2 antagonists with DNA damaging agents. As discussed earlier, the antisense inhibition of the MDM2-p53 interaction had been shown to synergise and potentiate response to various DNA damaging agents using both *ex vivo* and *in vivo* models (Chen, Agrawal et al. 1998, Tortora, Caputo et al. 2000, Grunbaum, Meye et al. 2001). Since the discovery of Nutlins they have been shown to be radio-sensitisers of lung cancer cell lines and augment both cell cycle arrest and apoptosis *ex vivo* (Cao, Shinohara et al. 2006). Conradt and colleagues also showed recently with cell lines derived from murine KrasG12D-driven pancreatic ductal adenocarcinoma models that Topo II inhibitors and the MDM2 antagonist Nutlin-3a synergise (Conradt, Henrich et al. 2013). They also showed that MDM2 interacts with the MRN DNA repair complex and that it slows the rate of homologous recombination repair by comparing the γ H2AX staining 3 hours after the co-administration of etoposide (5 μ g/ml) \pm Nutlin-3a (5 μ M) (Conradt, Henrich et al. 2013). This increase in γ H2AX at an early time point was also observed with another MDM2 antagonist namely PXN822 (Priaxon AG) in combination with etoposide (Conradt, Henrich et al. 2013). Although genotoxicity data on this drug was not available, its mechanism of action mirrored that of the cis-imidazoline compounds (Conradt, Henrich et al. 2013). An earlier study had also shown an increase in γ H2AX staining in response to MDM2 antagonists Nutlin-3a and Caylin-1 (Nutlin-3 analogue) in combination with etoposide (Verma, Rigatti et al. 2010). Nutlin-3 treatment (at 10 μ M) of cancer cell lines was shown to induce activating phosphorylations of DNA damage response proteins including ATM and CHEK1 and increased γ H2AX staining in a p53-independent manner (Valentine, Kumar et al. 2011). The high doses of MDM2 antagonist used and the time points in the last two studies mentioned may have resulted in off-target effects or may have been a consequence of later apoptotic related events due to MDM2 antagonist treatment. This is in contrast to the study by Conradt et al., 2013 where, much lower doses of MDM2 antagonists were used in combination with etoposide. In the light of these data inhibition of DSB repair pathways may augment/synergise with the response to MDM2 antagonists in the presence of DNA damage.

1.16.5 Range of sensitivity to MDM2 inhibitors

The pharmacological inhibition of the MDM2-p53 interaction with small molecular weight MDM2 inhibitors has been a very successful approach of non-genotoxic activation of p53 in preclinical and clinical settings with encouraging anti-tumour activity (Vassilev, Vu et al. 2004, Ray-Coquard, Blay et al. 2012, Ding, Zhang et al. 2013, Zhao, Liu et al. 2013, Zhao, Aguilar et al. 2015) (For a comprehensive review of compounds see (Zhao, Aguilar et al. 2015)). Drug sensitivity data generated by the Sanger Institute using cell viability assays on a large panel of cancer cell lines, with known genetic status of cancer related genes, suggest that the strongest determinant of response to the MDM2 inhibitor, Nutlin-3a, is the genetic status of *TP53* (P-value = $1.26e^{-54}$; Figure 1-14) (Barretina, Caponigro et al. 2012, Garnett, Edelman et al. 2012). However, within the group of *TP53* wild-type cell lines there is nevertheless a range of sensitivity to the MDM2 inhibitor, Nutlin-3a, as measured by GI50/IC50 (50% growth inhibitory concentration) (Figure 1-15). It has been suggested that this approximate 3500-fold range in sensitivity to MDM2 inhibitors may be an exaggeration due to misclassification of cell lines with respect to their *TP53* genetic status. However, Amgen have also recently reported a wide range of sensitivity to their MDM2 inhibitor AMGDS3 among their carefully curated panel of *TP53* wild-type and functional cell lines (500-fold IC50 difference from the least to the most sensitive cell lines) (Saiki, Caenepeel et al. 2015). Interestingly, other cancer causing genetic events highlighted on the Sanger database to correlate with increased MDM2 inhibitor sensitivity have been independently verified. Examples of findings that are consistent with the overall Sanger Database predictions include *MYCN*-amplification which has been reported to increase sensitivity to MDM2 inhibitors (Gamble, Kees et al. 2012). Contradictory evidence also exists in the literature for example with regards to the *CDKN2A* (*p14^{ARF}*) the transient knockdown of which has been reported to decrease sensitivity to MDM2 inhibitors (Van Maerken, Rihani et al. 2011), whereas mutations in this gene are predicted to increase sensitivity to MDM2 inhibitors on the Sanger database. A more detailed approach for identifying such genetic variables was recently taken by Zhong *et al.*, (2015) (Roche pharmaceuticals), who compared RNASeq-derived transcript levels of 287 human cancer cell lines to their *in vitro* sensitivity to the MDM2 inhibitor RG7112 currently in clinical trials (Zhong, Chen et al. 2015). This showed that combined increase in basal mRNA expression of *MDM2*, *XPC* and *BBC3* and reduction in expression of *CDKN2A* were predictors of sensitivity to RG7112. Signature scores

($G_{MDM2} + G_{XPC} + G_{BBC3} - G_{CDKN2A}$ at baseline) obtained from pre-treated acute lymphoblastic leukaemia (ALL) patients corresponded with better clinical outcome in response to RG7112 and RG7388 (Zhong, Chen et al. 2015). Importantly, the signature score remained significant when adjusted for *TP53* genetic status which meant that changes in expression of other genes can also be predictors of MDM2 inhibitor sensitivity between *TP53* wild-type cell lines (Zhong, Chen et al. 2015). These data highlight the gap in knowledge of the underlying mechanistic determinants of MDM2 inhibitor sensitivity in *TP53* wild-type cells.

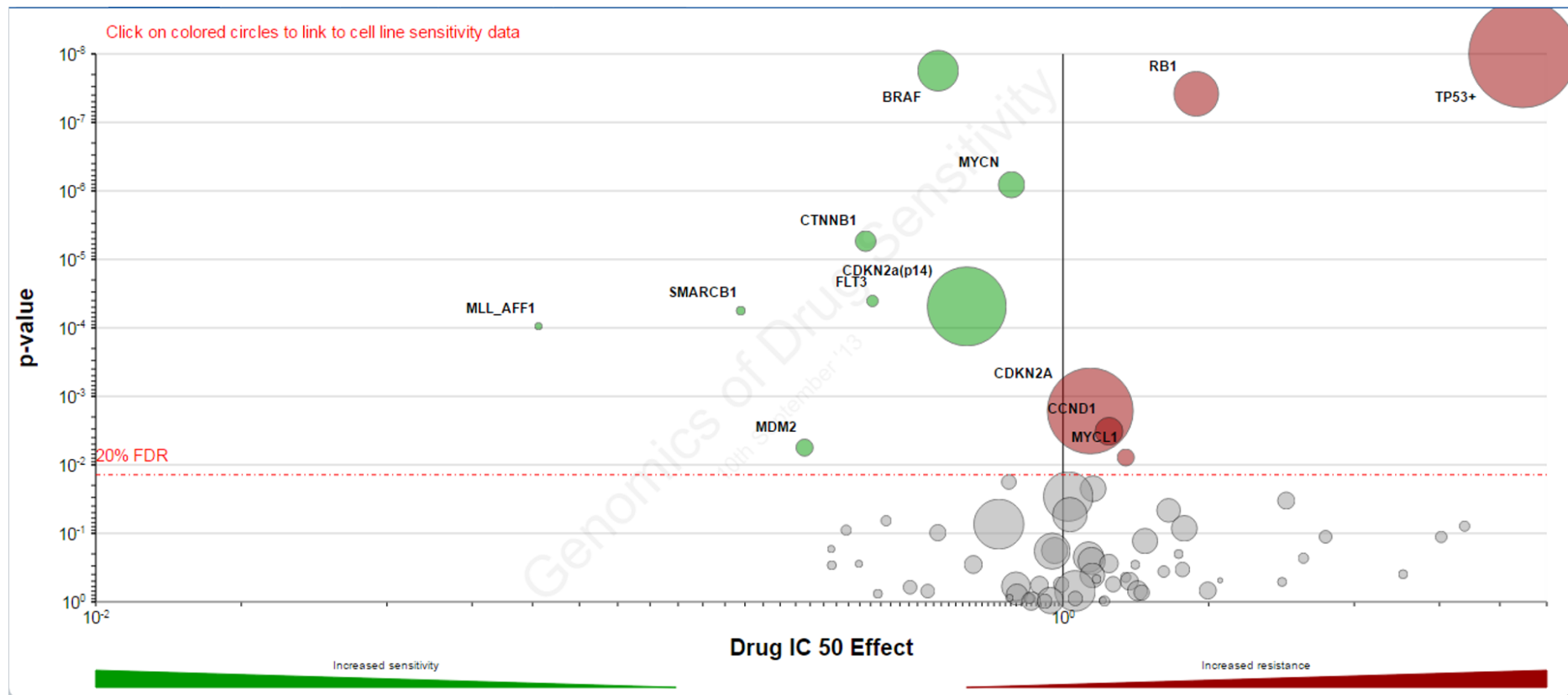


Figure 1-14 Volcano plot shows that although TP53 is the strongest determinant of response to Nutlin-3a, there are many other genes, which if altered, can influence sensitivity to Nutlin-3a. Y-axis: The p-value from multivariate ANOVA of drug gene interaction on an inverted log₁₀ scale. X-axis: Magnitude of the effect that genetic events have on the GI50 of the drug in cell lines. The size of the circle indicates the number of genetic events corresponding to the analysis for a given gene or a drug. Figure obtained from (<http://www.cancerrxgene.org/>).

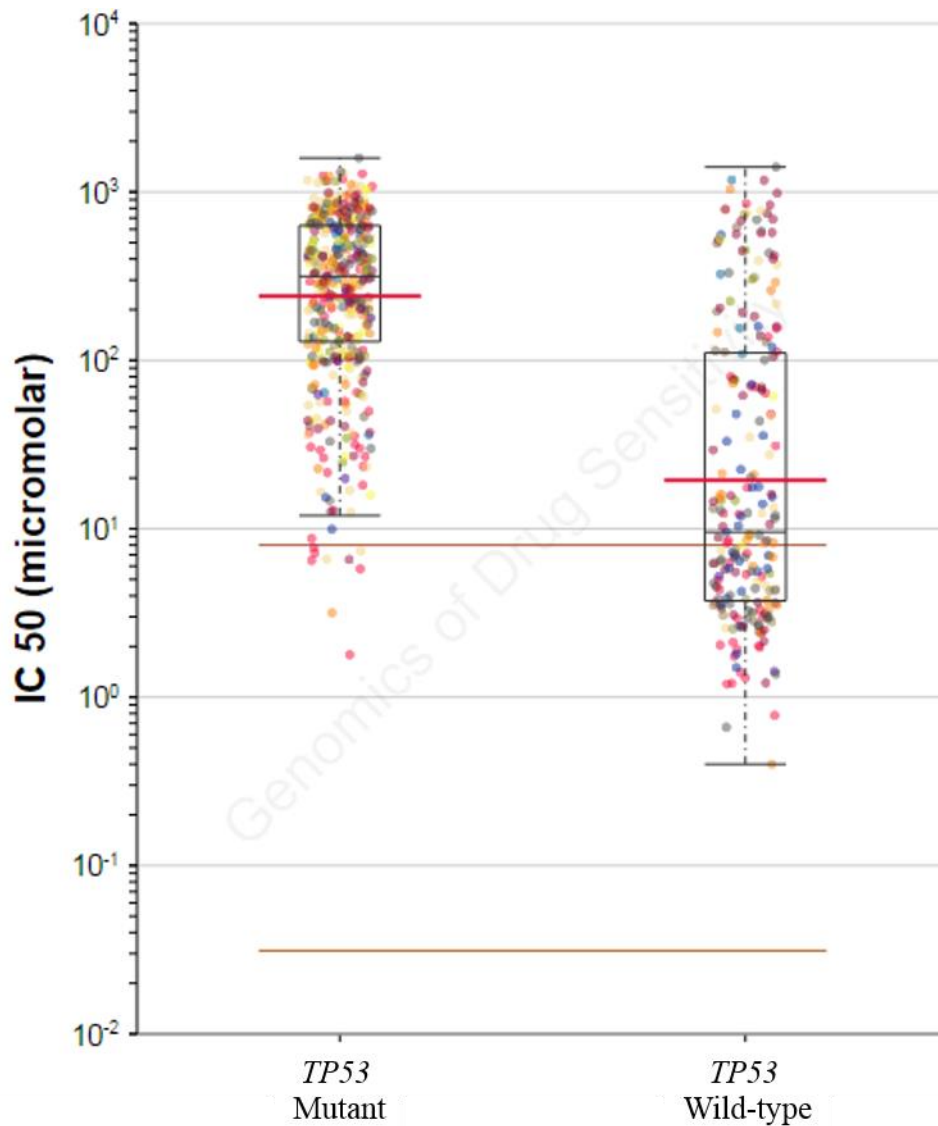


Figure 1-15 Range of Nutlin-3a IC₅₀/GI₅₀ in *TP53* mutant and wild-type panel of cell lines from the Wellcome Trust Sanger Institute drug sensitivity database.

1.16.6 Determinants of cell fate after activation of wild-type p53 by MDM2 inhibitors

Expectedly, the wide range in sensitivity of *TP53* wild-type cell lines translate into the clinic as it is implied by the interpatient variability in response to MDM2 inhibitors among patients with *TP53* wild-type tumours (Ray-Coquard, Blay et al. 2012). It has been suggested that the extent of sensitivity to MDM2 inhibitors in *TP53* wild-type cell lines is contingent on cell fate following p53 activation (Tovar, Rosinski et al. 2006, París, Henry et al. 2008, Sullivan, Padilla-Just et al. 2012). This can range from continual growth and division, reversible cell cycle arrest, senescence or programmed cell death. These alternative outcomes may be dependent on the type, duration and intensity of p53 activating stimuli, genetic and epigenetic background of the cell, and

cell growth stage at the time of p53 activation (Espinosa 2008, Murray-Zmijewski, Slee et al. 2008). Given the large numbers of variables that need to be considered large scale genetic knockdown or chemical inhibition screens have been carried out to identify optimal combination strategies. Alternatively single candidate targets based on our current knowledge of p53 signalling have also been investigated within the literature. An example of chemical inhibition screen (Saiki, Caenepeel et al. 2014) and single candidate gene investigation (Marine, Dyer et al. 2007) will be discussed in this chapter and an example of the shRNA library screen combined with Nutlin-3 will be described in the introduction of chapter 3 of this thesis (Sullivan, Padilla-Just et al. 2012). The tumour suppressor role of p53 relies heavily on its modular ability to regulate the transcription of different sets of genes in response to a diverse set of stimuli which are involved in cell fate decision making. Therefore understanding the underlying mechanisms that modulate p53 transcriptional function in favour of reversible arrest as opposed to irreversible arrest or apoptosis is important in understanding the determinants of cell fate after p53 activation.

The key concepts pertaining cell fate decision making following p53 activation has been reviewed in detail by Carvajal and Manfredi (2013) they will only be briefly introduced in this section (Carvajal and Manfredi 2013). One school of thought about cell fate decision after p53 activation (e.g. dissociation from MDM2) proposes that total level of active p53 is the main determinant of whether a cell undergoes cell cycle arrest senescence or apoptosis (Chen, Ko et al. 1996). In this model it is proposed that pro-arrest p53 transcriptional target genes have higher affinity p53 response elements compared to p53 pro-apoptotic transcriptional target genes, hence the likelihood of induction of apoptosis is proportional to the concentration of active p53. Consistent with this promoter affinity model; it has been shown that p53 pro-arrest target genes are induced at an earlier time-point than pro-apoptotic target genes (Zhao, Gish et al. 2000). However, *in vitro* binding assays comparing promoters for different p53 target genes have shown that although the majority of p53 pro-arrest target gene promoters have a higher affinity p53 response elements; there are still some key p53 pro-apoptotic targets such as *BBC3/PUMA*, *TP53AIP1* and *NOXA* which also have equally high affinity p53 response elements (Weinberg, Veprintsev et al. 2005). This suggests that there are other layers of regulation for p53 promoter binding and transcription than promoter affinity alone. One other factor proposed to influence the observed differences in the kinetics of p53 target induction is the variation in RNA Polymerase II occupancy

in the core promoters of p53 target genes in unstressed conditions (Espinosa, Verdun et al. 2003, Morachis, Murawsky et al. 2010). Using chromatin immunoprecipitation it had been shown that RNA polymerase II binding to endogenous *CDKN1A* (*p21^{WAF1}*, pro-arrest p53 transcriptional target) promoter was significantly greater than binding to the *FAS/APO1* (Pro-apoptotic p53 transcriptional target) promoters in unstressed cells (Espinosa, Verdun et al. 2003). To further investigate the role of core promoter structures in determining the kinetics of induction of these two p53 targets; Morachis et al., 2010 assessed the speed and frequency preinitiation complex formation on each promoter during *in vitro* transcription. The authors showed that *CDKN1A* core promoters support quicker TATA box-dependent assembly of RNA Polymerase II pre initiation complex relative to that of the *FAS* core promoter. However, the *FAS* core promoter was shown to support more rounds of preinitiation complex formation better suited for sustained induction of this gene (Morachis, Murawsky et al. 2010). This is consistent with *in silico* predictions suggesting that transient pulses of p53 activation promote pro-arrest gene expression and sustained pulses of p53 in the same context promote pro-senescent or pro-apoptotic gene expression (Zhang, Liu et al. 2009, Purvis, Karhohs et al. 2012).

Central to the data which will be presented in this thesis post-translational modifications of p53 have also been shown to influence p53 promoter selectivity following its activation. The complex set of p53 post-translational modifications and their potential roles in regulation of p53 function, stability and cell fate determination has been reviewed extensively to date (Murray-Zmijewski, Slee et al. 2008, Meek and Anderson 2009, Meek 2015). The complexity and heterogeneity of the set of post-translational modifications p53, which happen in a highly context dependent manner, make investigating roles of individual post-translational modifications in cell fate determination challenging. For example there are contradictory findings when it comes to the role of p53^{Ser15} phosphorylation in stability, transcriptional activity and cell fate determination (Fiscella, Ullrich et al. 1993, Huang, Clarkin et al. 1996, Rathmell, Kaufmann et al. 1997, Shieh, Ikeda et al. 1997, Banin, Moyal et al. 1998, Canman, Lim et al. 1998, Lambert, Kashanchi et al. 1998, Dumaz and Meek 1999). In spite of this challenging complexity more recent efforts by studies carried out in cell line models and knock-in transgenic mice have implicated this phosphorylation event in regulation of p53 transcriptional activity and tumour suppressor function (Introduced earlier and will be discussed in more detail in results and general discussion chapters) (Saito,

Yamaguchi et al. 2003, Armata, Garlick et al. 2007, Teufel, Bycroft et al. 2009, Loughery, Cox et al. 2014). Another N-terminal post-translational modification of p53 has also been implicated in promoter selectivity and induction of p53 pro-apoptotic target *TP53AIP1* which has been shown to localise to the mitochondria and promote the release of cytochrome c from the mitochondria (Oda, Arakawa et al. 2000). Consistent with this observation phosphorylation of p53^{Ser46} by p38 MAPK in response to UV has been reported to play a role in induction of apoptosis in response to UV mediated DNA damage (Bulavin, Saito et al. 1999). Embryonic stem cells, MEFs and thymocytes derived from homozygous *p53^{HupKIS46A}* Knock-in mice expressing a chimeric p53 including human p53 exons 4-6, with the mutated S46A, were partially defective in DNA damage and oncogene induced apoptosis (Feng, Hollstein et al. 2006). UV mediated induction of p53 pro-apoptotic targets *Noxa* and *Perp* was significantly reduced in the homozygous *p53^{HupKIS46A}* Knock-in mice. These observations are consistent with the previously reported role of this p53^{S46} in promoting the induction of p53 pro-apoptotic transcriptional targets and cell fate determination.

Cell fate determination after activation of p53 may also depend on the function of other proteins that can function as co-factors in p53-mediated transcription. The Apoptosis-Stimulating of p53 Protein (ASPP) family of proteins for example include ASPP1 & 2 (pro-apoptotic) and inhibitor of ASPP (iASPP, anti-apoptotic) which can interact with p53 to either promote or inhibit the transcription of its apoptotic target genes (Samuels-Lev, O'Connor et al. 2001, Bergamaschi, Samuels et al. 2006). The interaction of iASPP with the PRR of p53 has been shown to inhibit transcription from the p53 regulated BAX promoter. This is also consistent with earlier observations regarding the importance of the PRR in inducing apoptosis. Interestingly, it has also been shown that a propyl isomerase Pin1 binds to phosphorylated p53^{Ser46} and prevents iASPP binding therefore promoting apoptosis (Zheng, You et al. 2002). Other cofactors such as Haematopoietic Zinc Finger (Hzf) which is itself a p53 transcriptional target has been shown to promote cell cycle arrest after p53 activation promoting selective transcription of p53 pro-arrest target genes (Das, Raj et al. 2007). In contrast to *Hzf^{+/+}* MEFs, those MEFs derived from *Hzf^{-/-}* transgenic mice undergo p53 mediated apoptosis instead of cell cycle arrest following ionising radiation.

Mechanisms described above can potentially be targeted genetically and pharmacologically to assess how they would impact cell fate determination following treatment with MDM2 inhibitors. This thesis focuses on the role of WIP1 phosphatase

(described earlier) as a potential determinant of response to MDM2 inhibitors.

1.16.6.1 Screening for synergy with MDM2 inhibitors

Other pharmacological agents can also be used to screen for targets that synergise with MDM2 inhibitors. This is provided that the compounds used have little or no off-target effects at the doses used in the screen. Amgen and their academic partners recently screened a combination of 1169 compounds with MDM2 inhibitors in 10 cell lines (seven *TP53* wild-type and three mutant) (Saiki, Caenepeel et al. 2014). The screen identified thirteen targets the inhibition of which synergised with their MDM2 inhibitors. Three of the thirteen synergistic compounds targeted the MEK and PI3K pathways. Loewe's additivity model was used to measure synergy which requires dose effect curves for each individual drug including the dose effect slope together with the minima and maxima. Synergy was further validated in a panel of 40 cell lines (thirty-six *TP53* wild-type and four mutant) with MTT assay. Apoptotic endpoints Sub-G1 events and Caspase 3/7 activity were shown to be enhanced in a selected group of *TP53* wild-type cell lines. Multiple selective targeted agents such as the MEK inhibitor Trametinib, BRAF inhibitor Vemurafinib, PI3K inhibitor GDC-0941 and an mTOR kinase inhibitor AZD8055 were then used for inhibiting different nodes within the two pathways, which all resulted in synergy in combination with MDM2 inhibitors (Saiki, Caenepeel et al. 2014). Furthermore, these results are consistent with other independent reports in the literature using different classes of MDM2 inhibitors in combination with inhibition of these pathways (Lunghi, Mazzera et al. 2007, Zhang, Konopleva et al. 2007, Ji, Kumar et al. 2013, Wang, Zubrowski et al. 2014). However these combinations would likely be efficacious in a context-dependent manner such as *TP53* wild-type tumours that rely on MEK and PI3K signalling (i.e. *TP53* wild-type cases of melanoma) and not all malignancies. Therefore identifying other oncogenic pathways the inhibition of which synergise with MDM2 inhibitors remain a strategy to be explored.

1.16.6.2 Candidate target investigation

An alternative strategy for identification of determinants of cell fate following non-genotoxic activation of p53 by MDM2 inhibitors is a candidate target approach. Individual candidate targets can be selected based on their well established and validated present mechanistic understanding of their roles in the p53 network or cell survival in general. This allows for the identification of novel targets and can take into consideration the druggability of the targets, potential tissue tumour type stratification strategies and a more robust validation of mechanistic combinatorial effects.

The role of the MDM2 homologue, MDMX, in regulation of p53 transcriptional transactivation is well established (Marine, Dyer et al. 2007). Although mice null for MDM2 or MDMX are both embryonic lethal in a p53-dependent manner, ablation of MDMX *ex-vivo* does not result in the same extent of p53 activation as MDM2 inhibition (Jones, Roe et al. 1995, Parant, Chavez-Reyes et al. 2001, Hu, Gilkes et al. 2006). Conditional inactivation of *Mdmx* with a LoxP-Cre system in cardiomyocytes, smooth muscle cells and the gastrointestinal tract in mice also results in only modest defective phenotypes in those tissues (Boesten, Zadelaar et al. 2006, Grier, Xiong et al. 2006). This has been put down to compensation by the p53-MDM2 autoregulatory feedback mechanism (Barak, Juven et al. 1993, Wu, Bayle et al. 1993, Marine, Dyer et al. 2007). However, overexpression of MDMX at physiologically relevant levels by stable transfection has been reported to result in a decrease in MDM2 inhibitor sensitivity (Hu, Gilkes et al. 2006). MDMX knockdown was also reported to result in increased apoptosis in response to Nutlin-3 as measured by flow cytometry (Sub-G1 events) and MTT cell viability assay (Hu, Gilkes et al. 2006). Importantly MDMX is amplified or overexpressed in mostly *TP53* wild-type malignancies which would benefit from the dual inhibition of these two targets (Oliner, Kinzler et al. 1992, Shvarts, Steegenga et al. 1996, Gembarska, Luciani et al. 2012). Hence, MDMX inhibitors and/or MDM2-MDMX co-inhibitors are also being investigated pre-clinically (Pazgier, Liu et al. 2009, Bernal, Wade et al. 2010, Reed, Shen et al. 2010, Graves, Thompson et al. 2012).

Aims

The primary mechanism of action of MDM2 inhibitors is through no-genotoxic activation of p53 signalling. However, there is a wide range of sensitivity to MDM2 inhibitors among *TP53* wild-type cell lines and tumours. This suggests that there are other determinants of sensitivity to MDM2 inhibitors, and that combination regimens or tumour stratification strategies are necessary to harness the full potential of MDM2-p53 binding antagonists in the clinic.

There is extensive crosstalk between DNA repair and p53 signalling. This is mostly through post-translational modifications of components of p53 signalling by the machinery that sense and repair DNA damage. Therefore manipulating the activity of the components of DNA damage response which regulate post-translational modification of p53 may influence cellular sensitivity to MDM2-p53 binding antagonists.

- Investigate the role of DNA repair machinery and its crosstalk with p53 in determining the sensitivity to MDM2-p53 binding antagonists in the presence and absence of DNA damage.
- Determine whether the transient knockdown or chemical inhibition of WIP1 influences cellular sensitivity to MDM2 inhibitors.
- Determine the role of WIP1 phosphatase activity in regulation of p53 signalling following MDM2 inhibitors.

Chapter 2 Materials and methods

2.1 Tissue culture practice and cell line authentication

Tissue culture work on all cell lines listed in was carried out in the sterile environment of a class II biological safety cabinet (Biomat, Medair Technologies, MA, USA) at all times. Good cell culture practice was observed at all times to minimise the risk of cross contamination of cultures (For more details see Nims *et al*) (Nims, Sykes et al. 2010). All cell lines were authenticated using short tandem repeat (STR) DNA profiling (LGC Standards) and early post-authentication passages were cryogenically preserved in liquid nitrogen until the working stock reached post-authentication passage 30, after-which a lower passage number reserve batch was revived and used in subsequent experiments. STR DNA profiling uses hypervariable DNA microsatellite regions, which are 1-6bp long repeated DNA motifs, to assign unique molecular fingerprints to cell lines of interest which can then be monitored for potential cross contamination and/or genomic instability before and during experimental use of the cell lines (Reid and Storts 2013).

2.1.1 Cell line growth conditions and husbandry

All cell lines were grown in RPMI-1640 supplemented with L-glutamine (2mM) and sodium bicarbonate (Sigma Aldrich #R8758), 1% Pen/Strep (Sigma # P4333) and 10% heat-inactivated FBS (Gibco #10082147) in a humidified 37°C incubator containing 5% CO₂ in air unless otherwise specified (Table 2-1). When cells reached 70-90% confluence, growth media was removed, the monolayer of cells was washed with phosphate buffer saline (PBS, devoid of divalent cations and pH 7.2) and then the cells were incubated with 1 × trypsin EDTA (Sigma) for 1-5 mins to allow them to detach from the surface of the plate/flask. Ethylenediaminetetraacetic acid (EDTA) forms chelates with divalent cations which would otherwise inhibit the peptidase activity of trypsin. Following trypsinisations the cells were observed under the microscope to ensure that they had all detached then re-suspended in fresh media and split 1:10 or 1:20 into 25cm², 75cm² or 175cm² flasks (Corning, Amsterdam, Netherlands). Cell lines were tested every 3-6 months for mycoplasma infection through PCR based method (Work carried out by Mrs. Liz Matheson).

2.1.1.1 Monitoring cell morphology using a phase contrast microscope

Cell morphology was examined regularly with phase contrast microscopy to check for signs of infections, the integrity of cell membranes and cellular compartments. When light traverses through a specimen with a different refractive index (e.g. plasma

membrane) the velocities of light wave is reduced resulting in a phase shift with respect to the background light. A phase contrast microscope dims the background light by passing it through a grey filter then shifts the phase by passing it through a phase shift ring which causes destructive interference thus reducing its amplitude. This results in an overall higher amplitude of the light that has passed through the specimen which leads to a halo effect around intact cell membranes (Lab 2011).

2.1.2 MDM2 inhibitor resistant *TP53* mutant sub-clones

TP53 wild-type, *MDM2*-amplified SJSA-1 osteosarcoma cell line and *TP53* wild-type *MYCN*- and *MDM2*-amplified NGP neuroblastoma cell line, along with their Nutlin-3 resistant *TP53* mutant daughter clones S_N40R2 and N_N20R1 respectively were used to investigate MDM2 inhibitor mediated p53-dependent biochemical and cellular endpoints (Table 2-1). From this point onward in this thesis the underscore will be removed from these clone names (i.e. S_N40R2 will be referred to as SN40R2). MDM2 inhibitor resistant daughter cell lines were derived by continually growing the parental cell lines in escalating concentrations of Nutlin-3 and isolating the resistant clones and expanding them. Sanger sequencing later determined that these cell lines harbour *TP53* mutations and show loss of p53 transcriptional function. Derivation of these clones along with more detailed *TP53* genetic and functional characterisation along with fluorescent *in situ* hybridisation (FISH) were carried out by Dr Junfeng Liu, Dr Xiaohong Lu and Dr Catherine J. Drummond prior to the start of this project and a manuscript of this work is in progress for submission with additional data supplied by the author of this thesis (Figure 2-1). FISH data showed that SN40R2 cells have *TP53* loss of heterozygosity (17q loss) whereas N20R1 cells retained both copies of *TP53* with a possible mutation on each. STR DNA profiling described earlier was not able to differentiate parental *TP53* wild-type from their MDM2 inhibitor resistant daughter cell lines. These data lead to the assumption that in spite of their *TP53* mutations, the daughter cell lines are otherwise isogenic or very closely related to their parental cell lines. Furthermore the isogenic cell line pairs have been used routinely in preclinical development of MDM2 inhibitors by the Northern Institute for Cancer Research Drug Discovery team and other groups within the institute (Chen, Rousseau et al. 2015).

2.1.3 U2OS cell line pairs

U2OS cell line pair were grown in McCoy's 5A modified medium supplemented with 1% Pen/Strep and 10% heat-inactivated FCS and split as above.

Cell lines	Tumour of origin	<i>TP53</i> Status	<i>MDM2</i> status	<i>MDMX</i> status	<i>PPM1D</i> Status
SJSA-1	Osteosarcoma	Wt	Amp.	Wt	Wt
SN40R2	Osteosarcoma	Mut			
NGP	Nuroblastoma	Wt	Amp.	OE	OE
N20R1	Neuroblastoma	Mut			
HCT116+/+	Colorectal carcinoma	Wt	Wt	Wt	c.1344delT/Wt (L450X) Gain-of-function (Kleiblova, Shaltiel et al. 2013)
HCT116-/-	Colorectal carcinoma	Null			
U2OS	Osteosarcoma	Wt	Wt	Wt	c.1372C>T/Wt (R458X) Gain-of-function (Kleiblova, Shaltiel et al. 2013)
U2OS-DN	Osteosarcoma	Mut			
MCF-7	Breast adenocarcinoma	Wt	Wt	OE	Amp.

Table 2-1 *TP53* Wild-type (Wt) and mutant (Mt)/Null cell line pairs from different tumour origins and their *MDM2*, *MDMX* and *PPM1D* genetic status. Amp.: Amplified; OE: Overexpressing.

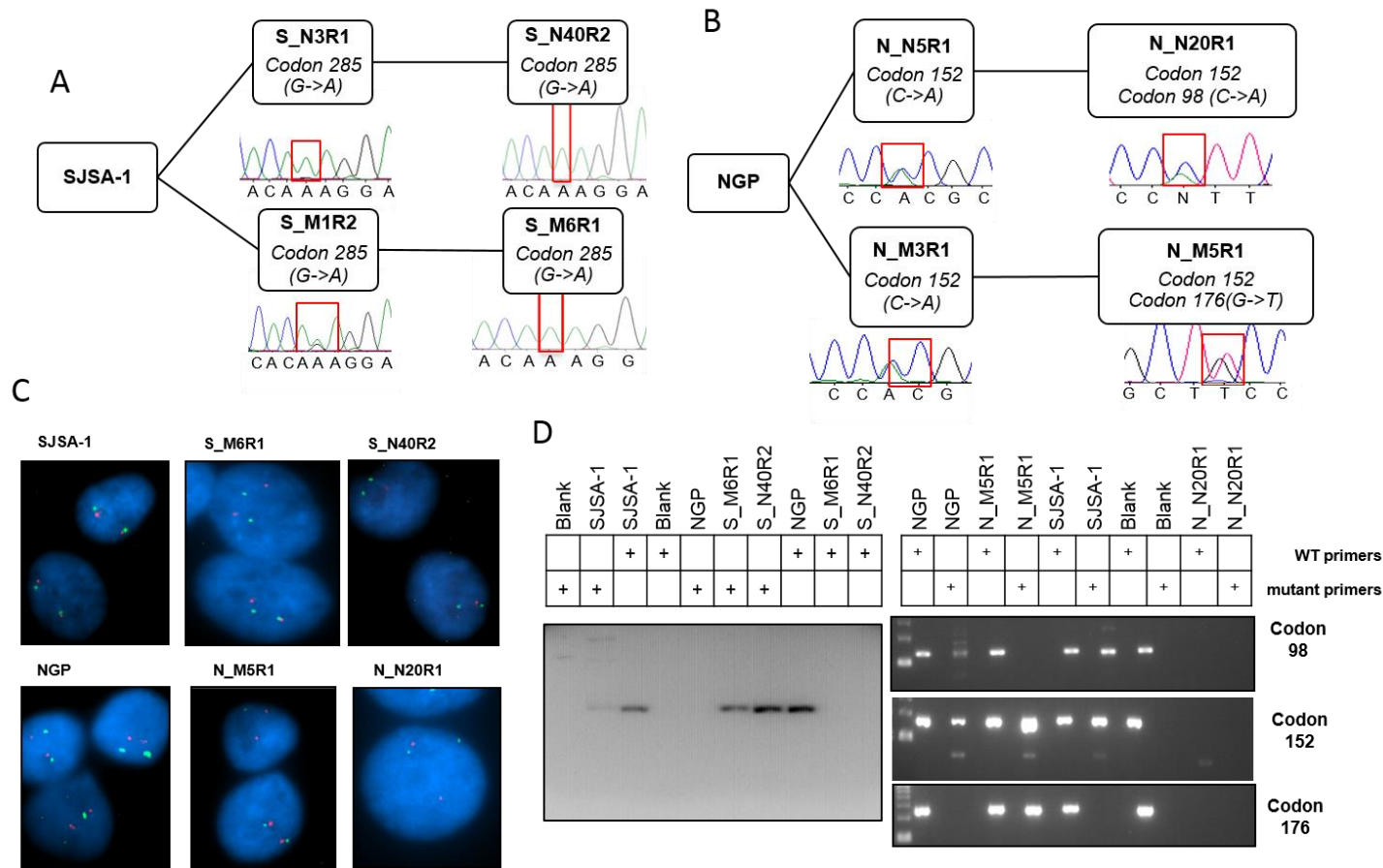


Figure 2-1 A & B) Schematic diagrams describing the derivation of MDM2 inhibitor resistant sub-clones including segments of the chromatograms generated by Sanger sequencing which show the sites of mutations in these clones. **C)** Fluorescent *in situ* hybridisation of the chromosome 17 centromere (Red foci) and 17p loci (Green foci) in parental and resistant cell lines. **D)** Mutant specific PCR amplification showing that the mutations could not be detected in the parental population.

1.1.1 Culturing of glioblastoma cell lines stably transfected with Firefly and Renilla Luciferase enzymes

DBTRG (*TP53* Wild-type) and T98G (*TP53* mutant) glioblastoma cell lines stably transfected with a reporter genes encoding Firefly (*Photinus pyralis*) and in internal control Renilla (*Renilla reniformis*) luciferase enzymes regulated by a p53-driven promoter and a minimal transactivation promoter respectively were provided to us by Sienna Biotech (Figure 2-2). DBTRG derived Dp53/R-DD7 cells were cultured in RPMI-1640 as above and T98G derived Tp53/R-DR4 cells grown in Eagle's Minimum Essential Medium (EMEM) with the same supplements as above. Both cell lines were kept under positive selection by Hygromycin B and Puromycin with doses outlined in Table 2-2 and sub-cultured as described above.

Cell line name	Hygromycin B ($\mu\text{g/ml}$ of media)	Puromycin (ng/ml of media)	<i>TP53</i> status
Dp53/R-DD7	30	250	Wt
Tp53/R-DR4	175	400	Mut

Table 2-2 Selection conditions for glioblastoma cell lines stably transfected with a reporter and an internal control vector

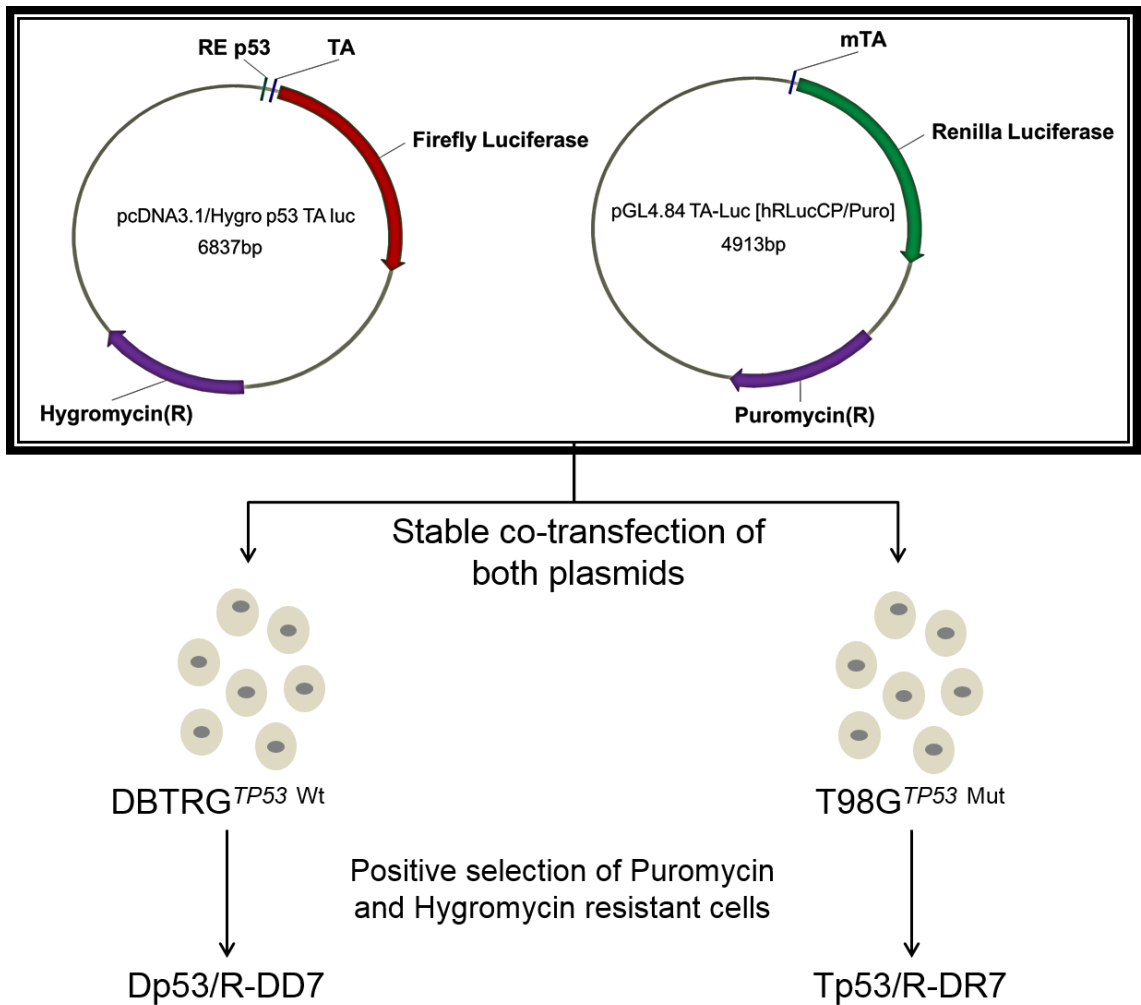


Figure 2-2 Cartoon of the process involved in generation of glioblastoma clones with stably transfected p53 response element (RE) driven Firefly reporter and minimal transactivating promoter (mTA) driven Renilla luciferase internal control. TA: Transactivation; bp: base pairs; R: Resistance; Wt: Wild-type; Mut: Mutant.

2.1.4 Cell count

Cell densities were estimated using either a Neubauer haemocytometer (Hawksley, Sussex, UK) or a Coulter counter (Beckman Coulter) depending on the number of samples that had to be counted in an experiment. The same technique was always used between repeats of an experiment.

2.1.4.1 Haemocytometer

The haemocytometer was prepared as per the manufacturer's instructions before 10 μ l of cell suspension or a 1:2 dilution of the suspension in 0.4% trypan blue dye (Biorad, #145-0021) were added to each side of the cover-slip. Each grid has a volume of 0.1mm³ and therefore counts/grid represent 1 \times 10⁴ cells/ml. A minimum of two grids on each side of the haemocytometer were counted and the average cell count/grid was then either multiplied by 10⁴, or 2 \times 10⁴ if the suspension had been diluted with the 0.4% trypan blue prior to loading. Dead/dying cells, with compromised membrane integrity, will be stained blue upon exposure to trypan blue while viable cells with intact plasma membrane will remain clear. Therefore absolute or % viability can be calculated however this count must be carried out within 5 min following the addition of the dye mixture otherwise viable cells will also be stained blue.

2.1.4.2 Coulter counter

The cell suspension was syringed with a 21G needle in order to remove any agglomerates of cells then 0.5ml of the cell suspension was diluted in 0.5ml Carnoy's fixative before being further diluted in 1:10 in BD FACSTFlow™ Sheath Fluid (#342003). This diluted suspension was then run through a particle counter (Coulter) where in cells/particles are suspended in a conductive fluid such as FACSTFlow will be sucked through a small hole to another compartment with conductive fluid disrupting the electrical current across the hole. Because the impedance caused by the cell/particle is proportional to its volume, parameters on the counter can be set so that only particles of a volume corresponding to an average mammalian cell (8-24 microns in diameter) will be counted. Coulter counter will count the number of particles per 0.5ml therefore the final average count of three was multiplied by 40 to obtain the number of cells/ml of the original cell suspension.

2.1.5 Cryogenic preservation and revival of cells

Exponentially growing cells were trypsinised and re-suspended in freezing media so that they are >10⁶ cells/ml. Freezing media consisted of each cell line's appropriate

growth media plus an additional 10% FBS (v/v) and Dimethyl sulfoxide anhydrous (DMSO) at 10% (v/v) (Sigma #276855). This cell suspension was then divided into 1ml aliquots in cryogenic vials (NUNC™, Rochester, NY, USA) and stored in -80°C freezer before being transferred to liquid nitrogen cryostore (Biosystem, Cryostor). Passage number and the date of harvest were recorded on the cryovials. When needed the vials were removed from liquid nitrogen and thawed rapidly in a water bath at 37°C before being diluted 1:10 in 37° growth media. This cell suspension was then centrifuged at 1000rcf, the supernatant was disposed and fresh media devoid of any DMSO was added to the pellet. The cells were then transferred to a tissue culture flask and placed in the incubator described above.

2.2 Sulforhodamine B assay

The use of Sulforhodamine B (SRB) in estimating cell numbers in multi-well plates for drug screening was developed by Skehan *et al* (Skehan, Storeng et al. 1990). SRB is an anionic protein dye, the sulphonic group of which electrostatically binds basic amino acids of proteins in cells under mild acidic conditions. Optical density of this dye is measured at 564 nm and it shows linearity with cell number. SRB has a signal to noise ratio of 1.5 with 1000 cells/well at this wavelength (Skehan, Storeng et al. 1990).

2.2.1 SRB staining protocol

Cells in 96-well plates were fixed with Carnoy's fixative at appropriate time-points and stored in 4°C up to 2 weeks. They were then washed 5 times with distilled H₂O (dH₂O) and allowed to dry overnight before staining with 0.4% SRB dissolved in 1% acetic acid (w/v) for 30 min. Unbound stain in wells was then washed off by washing the plate 5 times in 1% acetic acid. A fresh batch of 1% acetic acid was used for each plate as re-using the same batch between plates increases background SRB signal. Bound SRB was then solubilised in 100µl/well of 10mM Tris-HCL (pH10.5) and optical density at 564nm was quantified using a multi-well spectrophotometer, BioRad (Model 680).

2.3 Growth curves

Cells were seeded in 96-well plates (Corning, UK) at different densities in 6 inter-experimental repeats. The same plate was replicated 7 times to monitor the growth of cells over a week. Each plate was then fixed every 24 hours with Carnoy's fixative (3 parts methanol in 1 part acetic acid) and kept at 4 °C until SRB stain can be used as a surrogate for cell density in each well (See 2.2.1). Doubling time for each cell line was

then calculated by fitting the SRB growth curve data for the most rapidly growing density to an exponential function, $Y = Y_0 \cdot \exp(k \cdot X)$ where $Y_0 = y$ value when X time is 0, $k =$ the rate constant, and doubling time was calculated as $\ln(2)/k$ (See Prism user guide for more detail).

2.3.1 Growth inhibition assay and calculation of 50% growth inhibitory concentration (GI50)

Cells were seeded in 96-well plates at the densities stated in Table 2-3 and treated as detailed in specific materials and methods section of the relevant chapters. After treatment the cells were fixed and stained with SRB as described above. Mean, standard deviation (Std. Dev.) and standard error of mean (SEM) of optical density for each data point was calculated using the optical densities for 3-5 intra-experimental repeats. Mean optical densities were either expressed as a percentage of 1% DMSO treated control unless otherwise stated in specific materials and methods in each chapter. Concentration was Log_{10} transformed and a non-linear regression curve was fitted to the data (Lowess/spline fit, Chapters 5 and 6) using Graph Pad Prism 6 software and 50% growth inhibitory concentration (GI50) of a given drug in individual experiment was interpolated from the curve. Data from ≥ 3 independent experiments were compiled in order to generate overall GI50 values \pm Standard Error of Mean (SEM).

2.3.2 Measuring Potentiation, Synergy, additivity or antagonism

Potentiation, synergy, additivity or antagonism in this thesis were measured using data from SRB growth inhibition experiments. A drug was considered to potentiate the growth inhibition of another only when its administration at a non-growth inhibitory dose resulted in enhancement of the growth inhibitory effect of another drug.

Combination index (CI) values calculated based on median dose-effect analysis by CalcuSyn V2 (Biosoft, Cambridge, UK) were taken as a measure of synergy, additivity or antagonism as described by Chou and Talalay (Chou and Talalay 1984, Chou 2010). $CI < 1$ was considered synergistic, $CI = 1$ additive and $CI > 1$ antagonistic. Interpretation of combination index values are discussed more within the chapters where relevant.

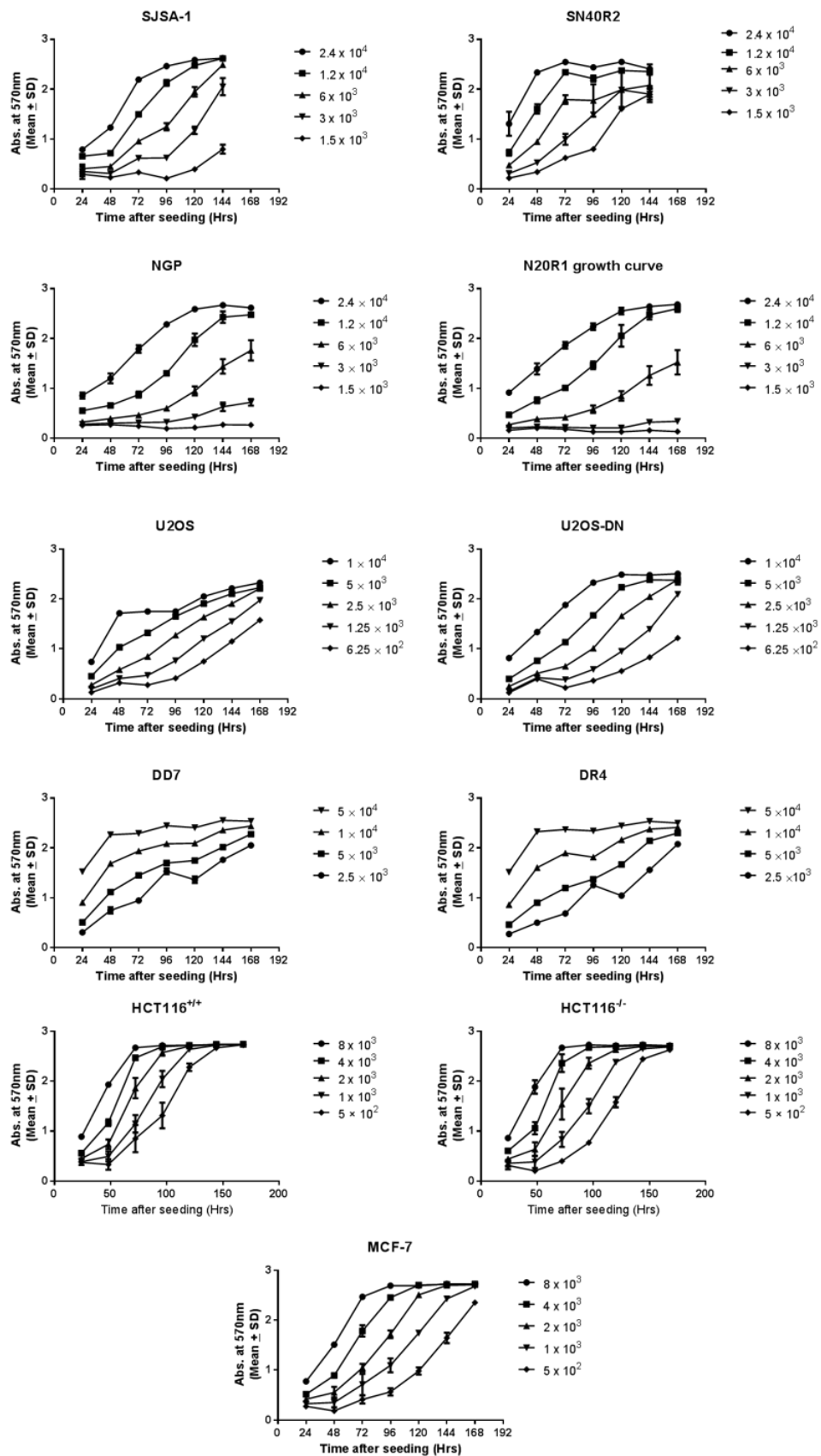


Figure 2-3 SRB growth curve experiments were carried out in order to determine the doubling time and the optimal cell density (cells/well) for growth inhibition assay experiments

Cell line name	Density seeded for growth inhibition (Cells/well)	Population doubling time (approximate Hrs)
SJSA-1	4×10^3	33-46
SN40R2	4×10^3	33-49
NGP	1.2×10^4	43
N20R1	1.2×10^4	49
HCT116 ^{TP53+/+}	4×10^3	24
HCT116 ^{TP53-/-}	4×10^3	24
U2OS	1.25×10^3	40
U2OS-DN	1.25×10^3	38
DD7	2.5×10^3	80
DR4	2.5×10^3	61
MCF-7	4×10^3	35

Table 2-3 Seeding densities used for growth inhibition assays along with the approximate doubling time of each cell line during exponential growth.

2.4 Clonogenic assay

Clonogenic assays were carried out to assess whether any of the treatment regimens resulted in reduced of colony formation ability of cells which is thought to be a superior measure of the cytotoxicity. Concentration which resulted in 50% loss of clonogenic survival (LC50) was determined by fitting a Lowess/Spline curve to the data-points and interpolating the X-coordinate from Y at 50% on the curve.

2.4.1 Conventional method

Exponentially growing cells were seeded at 6×10^5 cells/well of a 6-well plate (corning) and allowed to adhere for 24 hours before being treated with solvent or drug of interest for 48 hours. In the case of siRNA mediated knockdown and Nutlin-3 combination treatment, the drug treatment was delayed by a further 24 hours to allow efficient knockdown. Following treatment the adhered cells were trypsinised and pooled with floating cells from the same well, and counted using a coulter counter as described above. The cells were then re-seeded, at empirically determined densities for each dose, in triplicates into 100mm dishes (Corning, USA) containing their growth medium and placed back in the incubator 10-14 days (cell-type dependent) to form colonies. Media was then aspirated and the colonies fixed with Carnoy's fixative. Subsequently they were stained with 0.4% (w/v) crystal violet dissolved in dH₂O for 5 min, washed with slow running cold water and allowed to dry over-night. Visible colonies (>50 cells) were counted and cloning efficiency in control samples (i.e. DMSO treated) was calculated using the following formula: (Counted colonies/colonies seeded) \times 100. Percentage survival at each data-point was derived by normalising the colony counts/dish to the estimated expected number of surviving colonies based on the cloning efficiency of that cell line. An assumption was made that cloning efficiency remains constant across different seeding densities. These data were plotted against dose and fitted to a Fit spline/Lowess curve in GraphPad prism 6 software. The dose of drug which lead to 50% loss of colony efficiency or lethal dose 50 (LD50) was calculated by interpolating the x-coordinate based on the clonogenic survival curve.

2.4.2 Modified method

Empirically determined cell densities were seeded in triplicates in each well of a 6-well plate 24 hours before drug treatment. Following 48 hours of drug exposure media containing solvent/drug was replaced by normal growth media and the plates were left in the incubator to form colonies for 10-14 days. Colonies were fixed and stained as

described above and the same data processing was carried out.

2.4.3 Clonogenic survival in response to ionising radiation

Cells were seeded at empirically determined densities in 100mm dishes and allowed to adhere for 24 hours prior to being treated with increasing doses of ionising radiation (0-10Gy). The cells were then allowed to form colonies for 10-14 days. Fixing, staining and data processing was carried out as described in 2.4.1.

2.5 Drugs and specificities

2.5.1 MDM2 inhibitors

Racemic mixture of Nutlin-3 ($C_{30}H_{30}Cl_2N_4O_4$), an MDM2 antagonist with the molecular weight (MW) of 581.5 g/mol was purchased from NewChem Technologies Limited (#548472-68-0) in solid form. The powder was solubilised in DMSO (Sigma #276855) to a final concentration of 10mM, and then smaller aliquot were stored at -20 °C from which more dilute stocks were prepared each time when it was required. (+/-) Nutlin-3 racemic mixture is a combination of Nutlin-3a, the active enantiomer, and Nutlin-3b, the inactive enantiomer. (+/-) Nutlin-3 (Referred to as Nutlin-3 henceforth) inhibits MDM2-p53 interaction with cell free assay IC₅₀ value of 0.09 μ M *in vitro*.

Idasanutlin; also known as (a.k.a.) RG7388 or RO5503781 ($C_{31}H_{29}Cl_2F_2N_3O_4$, MW = 615.15) is the most potent MDM2 inhibitor (Cell free assay IC₅₀ = 6nM) by Roche currently in clinical trials. This compound was synthesised in-house by Newcastle University's medicinal chemistry group and prepared in 1mM stocks and stored as described above.

2.5.2 PPM1D/WIP1 inhibitor

After a comprehensive review of the literature for commercially available WIP1 inhibitors, the most selective and potent WIP1 inhibitor GSK2830371 ($C_{23}H_{29}ClN_4O_2S$, MW = 461.02) was purchased from Tocris (#5140) and prepared as explained above in 10mM stocks dissolved in DMSO. This WIP1 inhibitor binds to the unique flap-subdomain of WIP1, inhibits its catalytic activity and reduces WIP1 protein stability from this allosteric site which is proximal to a known WIP1 ubiquitination site (K238). Cell free assay IC₅₀ values of GSK2830371 for WIP1 and 21 other phosphatases were published to highlight the selectivity of this tool compound (Gilmartin, Faitg et al. 2014) (Table 2-4 & Table 2-5). This can be compared to SPI-001 and CCT007093

selectivities (Rayter, Elliott et al. 2007, Yagi, Chuman et al. 2012).

2.5.3 Kinase inhibitors

NU7441 a.k.a. KU57788 (C₂₅H₁₉NO₃S, MW = 413.49) is a DNA-PKcs inhibitor with an IC₅₀ of 14nM *in vitro* and was provided to us by Professor Herbie Newell (Newcastle University). The drug was already dissolved in 100% DMSO to a final concentration of 2mM, then smaller aliquots were stored in -20°C from which less concentrated stocks were prepared each time for use.

KU55933 (C₂₁H₁₇NO₃S₂, Mr = 395.49) is an ATM inhibitor is with an IC₅₀ of 13nM *in vitro* and was purchased from Tocris Bioscience in solid form. The powder was solubilised, stored, and used as explained above for Nutlin-3. A comparison of the cell free assay IC₅₀ values of NU7441 and KU55933 between different members of the PI3KK family can be made to assess the selectivity and specificity of these kinase inhibitors *in vitro* (Table 2-6).

Wortmannin (C₂₃H₂₄O₈, MW = 428.43) is fungal metabolite which is a potent but not specific PI3-K inhibitor with inhibitory function against members of the PI3KKs (Table 2-6).

Ralimetinib/LY2228820 (C₂₄H₂₉FN₆, MW = 420.52) is an ATP analogue selective MAPK p38 α and p38 β inhibitor with *in vitro* IC₅₀ of 5.3nM and 3.2nM respectively (Campbell, Anderson et al. 2014).

WIP1 inhibitor	IC ₅₀ (nM)	Cellular activity in PPMID-amplified cells
GSK2830371*	6 & 13	MCF-7 clonogenic sensitivity (IC ₅₀ = 0.5 μ M)
SPI-001	480 \pm 40	N/A
CCT007093	8400	MCF-7 cellular IC ₅₀ = 1.35 μ M**

Table 2-4 Cellular and Cell free assay 50% inhibitory concentrations (IC₅₀) values for the top three WIP1 inhibitors commercially available along with data on cellular activity in MCF-7 cells. *IC₅₀ values in two different cell free assays with different substrates; **: Data obtained from the Sanger institute drug sensitivity database; N/A: Not analysed

GSK2830371	
PPM1D/WIP1 and closely related Phosphatases	Cell free assay IC50
PPM1D	6 & 13
CD45	>30'000
DUSP22	>30'000
HePTP	>30'000
LMPTP-A	>30'000
LMPTP-B	>30'000
MKP5	>30'000
PP1α	>30'000
PP2A	>30'000
PP5	>30'000
PTP MEG1	>30'000
PTP MEG2	>30'000
PTP-1B	>30'000
PTPN22	>30'000
PTPβ	>30'000
RPTPμ	>30'000
SHP-1	>30'000
SHP-2	>30'000
TCPTP	>30'000
TMDP	>30'000
VHR	>30'000
YopH*	>30'000
SPI-001	
PPM1D	480
PPM1A	(68% at 40 μ M)**
PP2A	(11% at 40 μ M)**

Table 2-5 Published cell free assay IC50 values for GSK2830371 and SPI-001. * Yeast phosphatase; ** % Inhibition and 40 μ M. Table derived from data published in (Gilmartin, Fajt et al. 2014) & (Yagi, Chuman et al. 2012).

Closely related kinases	Cell free assay IC50		
	<i>In vitro</i> IC50 with NU7441 (nM)	<i>In vitro</i> IC50 with KU55933 (nM)	<i>In vitro</i> IC50 with Wortmannin (nM)
DNA-PK	14	2500nM	16
ATM	>100000	13nM	150
ATR	>100000	>100000nM	1800
mTOR	1700	9300nM	200
PI3-K	5000	16600nM	2

Table 2-6 *In-vitro* IC50 values with respect to other kinases within the kinome are provided above to give a scope of the selectivity of these two kinase inhibitors. Final column data were obtained from (Sarkaria, Tibbetts et al. 1998).

Kinase enzyme	IC ₅₀ (nmol/l) ± SEM
p38α MAPK	5.3 ± 1.6
p38β MAPK	3.2 ± 0.3
p38δ MAPK	>20,000
p38γ MAPK	>20,000
ERK1	>20,000
ERK2	>20,000
JNK1	894 ± 43
JNK2	80 ± 11
JNK3	158 ± 21

Table 2-7 *In-vitro* IC50 values for LY2228820 with respect to other kinases obtained from (Campbell, Anderson et al. 2014).

2.6 Analysis of cell cycle distribution via fluorescence-activated cell sorting (FACS)

As described in the introduction a population of dividing cells fall into three distinct phases of the cell cycle based on their DNA content. In G1/G0 phases cells harbour one copy of the genome ($n=2$) and in G2/M the DNA content has been doubled ($n=4$) following an intermediate DNA synthesis phase (S-phase) ($2 > n < 4$). Distribution of a population of cells into each phase of the cell cycle can be estimated by quantifying the DNA content of individual cells within a large sample derived from that population and plotting a frequency distribution histogram. Importantly, changes to cell cycle distribution in response to treatment can provide clues as to the underlying mechanism of drug action.

2.6.1 Sample preparation and FACS protocol

Cells were seeded at 3×10^5 cells/well (double this in transient knockdown) of a 6-well plate (Corning) and treated as outlined in specific materials and methods of the relevant chapters. After treatment floating and adherent cells in each well were harvested and pooled before being syringed 3 times to remove any clumps of cells. An aggregate of two G1/G0 cells (each $n=2$) can be counted as a G2/M ($n=4$) which will confound the results therefore syringing the cell suspension is critical. The cells were then washed and re-suspended in PBS before being diluted 1:1 in a propidium iodide (PI) solution (Table 2-8) and incubated at RT for 20 min before FACS. PI is a fluorescent nucleotide dye that intercalates between the bases in double stranded DNA and RNA. DNase free Ribonuclease A (RNase A) cleaves the P-O^{5'} bond in cellular RNA molecules that would otherwise be stained by PI and confound the results. When bound to DNA, PI has excitation/emission maxima of 535/617nm and the fluorescence intensity is proportional to the DNA concentration. After PI staining, the cell suspension was put through the FACSCalibur (Becton Dickinson, BD Biosciences) where a vacuum is used to suck the cells through a narrow sample injection tube that hydrodynamically focused a stream of fluid of single cells past a 488-nm argon ion laser beam. The cell and its PI stained nucleus intercepts the light which causes transmission and scattering of the light. The light that transmits through the cell is detected by a forward scatter (FSC) diode and the scatter by a side scattered (SSC) diode which provide measures of cell volume and granularity respectively. Also the fluorescence collection lens focuses the beams of scattered light toward dichroic mirrors positioned at a 90° angle to the laser and they specifically reflect the fluorescent light emitted from PI towards the FL-2 585/42 detector while transmitting other wavelengths of light through them for other detectors

to pick up (Omerod 2000). Detectors are photomultiplier tubes that can amplify signals from single photons so that they can be quantified and recorded electronically.

2.6.2 FACSCalibur instrument setting and gating

In order to record and analyse events attributed to cells rather than unrelated particles intercepting the light, instrument settings have to be optimised to detect objects with size and complexity characteristic of mammalian cells. Therefore CellQuest software (Beckton Dickinson), which enables simultaneous modification of instrument settings and data acquisition from FACSCalibur was used to optimise instrument settings based on FSC and SSC dot plots of untreated samples of each cell line. Also events attributed to aggregates of cells were identified and gated-out using FL2-A vs. FL2-W plots as shown in (Figure 2-4). FL2-A was set so that G1 peak frequency distribution histogram of control samples falls above 200 signal intensity so that events that have an FL2-A intensity just below $n=2$ DNA (Namely Sub-G1 events) can be detected. Data acquisition was capped at 10000 events/sample.

2.6.3 FACS data analysis

FCS files acquired were analysed using CellQuest software to generate representative 2D and 3D histograms of control and treated sample cell cycle distribution. In order to analyse the percentage (%) of events attributed to each stage of the cell cycle, Cyflogic v 1.2.1 software was used to manually gate-out sub-G1 events on the FL2-A histogram plots calculating the percentage of events in each of the peaks corresponding to G1/G0 and G2/M plus events in S-phase. Percentages were then plotted on grouped bar charts using GraphPad Prism 6 software. Sub-G1 events were also calculated as a percentage of total events in the same manner and expressed as bar charts. G1:S and G2:S ratios were calculated as measures of G1 and G2 arrest respectively in response to various treatment conditions and SubG-1 events were attributed to cell death.

Constituent	Mass or volume/ volume of PBS	Final concentration
Propidium iodide (Sigma)	1g/l	0.15mM
DNase free RNase A (Sigma)	2g/l	3.88mM
Triton-X 100 (Sigma)	3ml/l	0.3% (v/v)

Table 2-8 Recipe for PI solution used for live cell FACS

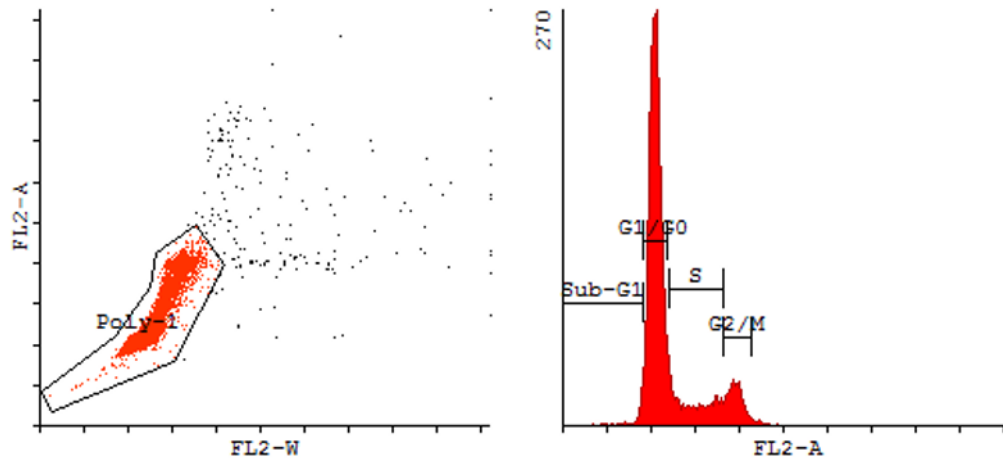


Figure 2-4 Manual gating of events based on FL2-A v FL2-W plots and FL2-A frequency distribution histogram.

2.7 Targeted silencing of gene expression using RNA interference (RNAi)

Napoli, *et al.*, reported in 1990 that ectopic overexpression of the chalcone synthase gene in petunia can somehow co-suppress the expression of the endogenous gene (Napoli, Lemieux et al. 1990). Multiple other findings during the early 1990's showed that viral RNA replicons homologous to endogenous genes can also suppress the expression of specific genes (Hannon 2002). However, targeted post-transcriptional silencing of specific genes with antisense double stranded RNA termed RNA interference (RNAi) was first reported in 1998 when Fire, *et al.*, (Fire, Xu et al. 1998) showed that double stranded RNA (dsRNA) was more efficient at knocking down gene expression in *Caenorhabditis elegans* compared to sense or antisense strands alone and that there was likely an underlying enzymatic reaction involved. It is now well-understood that this process is dependent on machinery that are conserved in many eukaryotic species both as a part of endogenous processing of endogenous non-coding RNA molecules into microRNA and as a mechanisms of protection against pathogenic and parasitic nucleic acids (Hannon 2002, Sen and Blau 2006, Rana 2007).

Entry of long RNA molecules into mammalian cells is followed by their enzymatic cleavage by Dicer, a member of the RNase III family, into 20-25 small interfering RNA (siRNA) molecules. These double stranded siRNA molecules then form a complex with RNA-induced silencing complex (RISC) which recognises and cleaves target RNA molecules through the catalytic activity of ribonucleases Argonaut and Dicer (Elbashir, Martinez et al. 2001). RNAi mediated knockdown using synthetic siRNA molecules delivered either by electroporation or transfection reagents is now routine for knockdown of specific genes in mammalian cell lines in culture.

2.7.1 Design of synthetic siRNA molecules

Targeted WIP1 siRNA molecule along with a universal control siRNA was selected from a comprehensive comparison of siRNA mediated knockdown reported in the literature selecting the construct that resulted in the most efficient WIP1 protein knockdown (Fujimoto, Onishi et al. 2005). These were modified and synthesised by Eurofins MWG Operon based on previously published methods with symmetrical 2-nucleotide 3' TT overhang which leads to approximately equal ratio of sense and antisense siRNA molecules in the formation of small interfering ribonucleoprotein complexes (siRNPs) and it does not influence the silencing of the target (Elbashir, Harborth et al. 2001, Elbashir, Martinez et al. 2001). Additional WIP1 targeting siRNA

molecules were also designed and synthesised by Eurogentec (SR-NP001-004). See for siRNA construct identifiers and their respective sequence.

siRNA	Sequence (5'-3') RNA [TT] DNA
WIP1.1	Sense: GUGCCAUAGUAAUCUGCAU
	Antisense: AUGCAGAUUACUAUGGCAC
WIP1.2	Sense: GGUGUAGUCAUACCCUCA
	Antisense: UUGAGGGUAUGACUACACC
WIP1.3	Sense: GCCCUUCCUAUAAUAGUCA
	Antisense: UGACUAUUAUAGGAAGGGC
WIP1.4 (Fujimoto, Onishi et al. 2005)	Sense: UUGGCCUUGUGCCUACUAA
	Antisense: UUAGUAGGCACAAGGCCAA
Universal control	Sense: GCGCGCUUUGUAGGAUUCG
	Antisense: CGAAUCCUACAAAGCGCGC

Table 2-9 siRNA constructs and their respective sequence.

2.7.2 Transfection protocol

Cells were seeded at 6×10^5 cells/well of a 6-well plate and allowed to adhere for 24 hours before transfection. Constructs of siRNA were stored as 20 μ M stocks and a fixed ratio of 1:1.25 (v:v) siRNA stock and Lipofectamine 2000 (Invitrogen) were mixed in order to allow the formation of optimal complexes for siRNA delivery (Method optimised by Dr Laura Gamble). Lipofectamine 2000 is composed of a propriety formula of cationic and neutral lipids that have undergone microfluidisation resulting in unilamellar liposomal structures with a positive surface which can form complexes with negatively charged siRNA molecules. These complexes cannot penetrate through the negatively charged surface of the phospholipid bilayer but they are taken up by endocytosis and are released in the cell. Lipofectamine and siRNA were added to separate vessels containing 400 μ l of OptiMEM-glutamax (Optimem) serum free media (Invitrogen) so that their mixture would observe the 1:1.25 (v:v) ratio and incubated at room temperature for 10 min before being mixed and allowed to form complexes for an additional 30-45min. Meanwhile growth media was aspirated from each well and replaced with 1.6ml of Optimem before the 800 μ l of additional Optimem containing siRNA-Lipofectamine complexes prepared earlier was added to appropriate wells in a dropwise manner. Cells were then left in a tissue culture incubator overnight before each well was supplemented with 10% FBS for collection or treatment at a later time-point.

2.8 Caspase-3/7 activity

The Caspase-Glo® 3/7 Assay (Promega, Southampton, UK) uses a pro-luminescent substrate which contains the substrate motif of executioner caspase-3 and -7 a DEVD. Presence of active caspase-3/7 results in cleavage and luminescence of this substrate. A Luminometer can then be used to measure luminescence as a surrogate for caspase-3/7 activity. Cells were seeded at 2×10^4 cells/well in white-well 96-well plates 24 hours before drug treatment then the Caspase-3/7 reagent was prepared as per manufacturer's protocol and added at a 1:1 ratio to the media containing cells. After 1 hour of incubation luminescence was measured using Fluostar Omega Plate Reader (BMG LABTECH).

2.9 Western blotting

2.9.1 Principles of western blotting

“Western blotting” was a term first coined by Neil Burnette in 1981 after he had optimised on a previously described technique by Towbin *et al.*, (1979) which allowed the electrophoretic transfer of proteins from a sodium dodecyl sulfate (SDS) polyacrylamide gel onto a nitrocellulose membrane (Towbin, Staehelin et al. 1979, Burnette 1981) This technique allowed the detection and semi-quantitative analysis of specific proteins and their post-translational modifications in a complex mixture of proteins by using specific antibodies. Proteins in a mixture are initially separated based on their mass (kDa) through SDS-polyacrylamide gel electrophoresis (SDS-PAGE) and are then transferred onto a nitrocellulose membrane across an electric field where they are adsorbed and immobilised most likely through electrostatic and hydrophobic interactions (Low, Shaimi et al. 2013). Specific antibodies conjugated to horseradish peroxidase (HRP) can then be used to detect proteins of interest and visualise them through detection of chemiluminescence.

2.9.2 Lysate (Cellular protein mixture) preparation

Cells were seeded at 6×10^5 cells/well of a 6-well plate 24 hours before being treated as described in specified materials and methods in each chapter. At the end of each treatment the cells were washed with 4°C PBS and 40µl of lysis buffer (0.0625M Tris-HCl pH 6.8, 2% w/v SDS (Sigma), 10% v/v Glycerol (Sigma)) was added to each well before cells were then scraped and the lysate was transferred into microfuge tubes (Eppendorfs). The lysates were kept on ice from this point onwards unless otherwise

stated. Lysates were heated at 95°C for 10 min before being sonicated at 23KHZ using Soniprep 150 plus (MSE) for 10 sec (Amplitude set at 6.0). Lysates were then centrifuged at 16000rpm at 4°C (Eppendorf Centrifuge 5417R) and the supernatant was preserved for measuring total protein and SDS-PAGE.

2.9.3 Measuring total protein

For measuring total protein concentration in lysates Pierce BCA Protein Assay Kit (Thermo Scientific; Prod. No: 23227) was used. This kit contains a detergent compatible formulation based on biocinchoninic acid (BCA) for the colourimetric detection and quantitation of total protein. This assay combines the reduction of Cu^{2+} to Cu^{1+} by protein in an alkaline medium with the colourimetric detection of Cu^{1+} . Firstly the Cu^{1+} is chelated to peptides >3 amino acids long (Biuret reaction) to form a coloured complex. Subsequently BCA can interact with the already chelated Cu^{1+} ion (2:1 ratio) to form a purple water soluble complex that has a linear absorbance at 570nm. The assay was carried out in a 96-well plate as per the manufacturer's protocol. Standard curves (0.2-2.0mg/ml) were obtained from 2mg/ml bovine serum albumin (BSA) stock each time and were quantified in parallel to lysates. The standard curve was then used to interpolate the lysate concentration estimate (Figure 2-5).

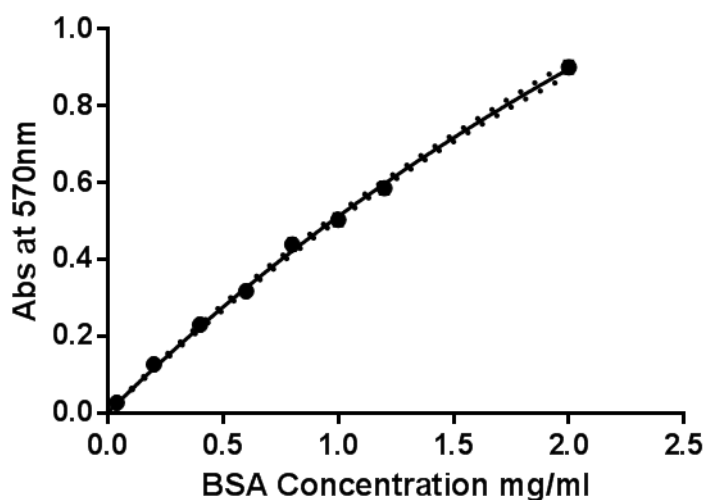


Figure 2-5 An example of a standard curve for used for protein estimation.

2.9.4 SDS-PAGE and transfer stages

20-30µg of each lysate was diluted in SDS-loading (Table 2-10) buffer and made up to a volume of 15µl before being incubated at 100°C on a heating block for 10 min. For analysis of low molecular weight proteins (<100kDa) the samples were loaded into wells of a Mini-protean TGX 4-20% gradient pre-cast gel (Bio-Rad) set up in the tank with running buffer (Table 2-11) along with SeeBlue Pre-stained molecular weight protein standard 1× (Life Technologies, #LC5625). The proteins were then transferred onto 0.45 micron nitrocellulose membrane (Hybond-C Ammersham, #RPN203C) (100V for 30 min). Transfer buffer constituents are listed in table (Table 2-12). Once transferred, the membrane was then blocked in 5% milk dissolved in 1 × TBS, 0.1% Tween-20 (Fisher BioReagents) pH 7.6 (TBS/T) (Table 2-13) at room temperature for an hour. In case of specified manufacturer guidelines or probing for phospho-epitopes the membrane was blocked in 5% bovine serum albumin (BSA) (Sigma) dissolved in TBS/T. The membrane was then cut and strips were probed with the appropriate 1° antibodies in blocking reagent of previously stated composition. Antibody specifications and incubation times are stated below (Table 2-14). The membranes were then washed briefly with TBS/T and exposed to the appropriate HRP-conjugated 2° for an hour in the stated blocking reagent.

For high molecular weight proteins (> 100 kDa), the same processes were carried out however a different gel and running buffer were used to get better separation. 3-8% Criterion XT Pre-cast gels (Bio-rad, #345-0129) and the 20× XT Tricine running buffer (Bio-Rad, #161-0790) diluted to 1× in dH₂O were used at the polyacrylamide gel electrophoresis stage.

2.9.5 Protein visualisation using enhanced chemiluminescence

After the incubation with the 2° antibody and the membranes were washed 7 × 4 min in TBST before being incubated for a 1 min at room temperature with enhanced chemiluminescent (ECL) substrate mixture. This mixture provides the chemiluminescent substrate and an oxidising agent (e.g. H₂O₂). HRP conjugated to the 2° antibody then converts the substrate to triplet carbonyl and its decay to singlet carbonyl results in emission of light. An X-ray film (Kodak) was then used to detect the emission from the product decay and autoradiographs were generated showing the relative amounts of proteins detected by the antibodies. The autoradiographs were then scanned and analysed.

Amount of constituent	Final Molarity in solution
2.5ml of 0.5M Tris/HCl pH 6.8	62.5mM
0.4g SDS	69.4mM
1ml β -mercaptoethanol (stock of 14.3M)	715.0mM
2ml Glycerol (density 1.261g/cm ³ , M _r = 92.09)	2.7mM
1ml 0.1% bromophenol blue (density 2.2g/ml, M _r = 669.96g/mol)	0.2 μ M
Note: make up to a final volume of 20ml in distilled water	

Table 2-10 SDS-loading buffer constituents and final concentration are stated above.

Amount of constituent	Final molarity in solution
144g Glycine (Sigma G8898)	1.9M
30g Tris base (Fisher 10667243)	247.6mM
10g SDS (Sigma L3771)	34.7mM
Note: dissolve and make up to a liter with distilled water	

Table 2-11 10 \times Running buffer was prepared as stated above and diluted 1:10 for each use.

Amount of constituent	Final molarity in solution
70.7 Glycine (Sigma G8898)	188.4mM
15.15 Tris base	25.0mM
1L 99.9% methanol (Fisher BioReagents)	
Note: dissolve and make up to a 5 liters with distilled water	

Table 2-12 Transfer buffer was prepared as stated above.

Amount of constituent	Final molarity in solution
80.0g NaCl (Sigma S7653)	1.4M
24.2 Tris base (Fisher 10667243)	199.8mM
Note: dissolve and make up to a 1 liters with distilled water	

Table 2-13 TBS 0.1% Tween-20 was prepared as stated above and the pH was adjusted to 7.6.

Antibody name/clone	Migrates at \approx kDa	Cat No. (Company)	Raised in	Dilution	Blocked/ Incubation in
Cleaved caspase-3	17, 19	9661S (Cell signaling)	Rabbit	1:1000	5% Milk 12-18Hrs
p21	18	OP64 (Calbiochem)	Mouse	1:100	5% Milk 1Hr
PUMA	21	PC686 (Calbiochem)	Rabbit	1:500	5% Milk 12-18Hrs
BAX	21	2772 (Cell signalling)	Rabbit	1;1000	5% BSA12-18Hrs
Actin	42	A4700 (Sigma)	Mouse	1:3000	5% Milk 1Hr
p53 (DO-7)	53	NCL-L-p53-DO7 (Novocastra)	Mouse	1:500	5% Milk 1Hr
pp53^{Ser15}	53	9284 (Cell signalling)	Rabbit	1:1000	5% BSA12-18Hrs
WIP1 (H-300)	85 & 67	sc-20712 (Santa Cruz)	Rabbit	1:200	5% Milk 12-18Hrs
WIP1 (F-10)	85 & 67	sc-376257 (Santa Cruz)	Mouse	1:200	5% Milk 12-18Hrs
MDMX	72	A300287A-2 (Bethyl laboratories)	Rabbit	1:1000	5% Milk 1Hr
MDM2	90	OP40 (Calbiochem)	Mouse	1:300	5% Milk 1Hr
ATM	350	Ab78 (Abcam)	Mouse	1:500	5% milk + 5% BSA 12-18Hrs
P-ATM^{Ser1981}	350	AF1655 (R & D Systems)	Rabbit	1:1000	5% milk + 5% BSA 12-18Hrs
DNA-PK (H163)	460	sc-9051 (Santa Cruz)	Rabbit	1:1000	5% milk + 5% BSA 12-18Hrs
P-DNA-PK^{Ser2056}	460	Ab18192 (Abcam)	Rabbit	1:500	5% milk + 5% BSA
PARP-1 (C2-10)	114 (85 for apoptosis)	4338-MC-50 (Trevigen)	Mouse	1:1000	5% Milk 12-18Hrs
2° goat anti mouse HRP	N/A	PO447 (Dako)	Goat	1:1000	Same as in 1°
2° goat anti rabbit HRP	N/A	PO448 (Dako)	Goat	1:1000	Same as in 1°

Note: All the solutions in the last column on the right were made up in TBS, 0.1% Tween 20 (pH 7.6) and if the incubation time was 12-18Hrs it was carried out at 4 °C.

Table 2-14 Information on antibodies and incubation times are been stated above. HRP: Horseradish peroxidase, Hr: Hour.

2.10 Primer-directed polymerase chain reaction (PCR)

Primer-directed polymerase chain reaction (PCR) is an *in vitro* biochemical procedure whereby low copies of specific sequences of nucleic acids can be amplified rapidly and accurately. The development and optimisation of this procedure spans over decades since the discovery of the structure of DNA in 1953 (Watson and Crick 1953).

However, PCR was finally optimised in its present form by Saiki *et al.*, in 1988 (Saiki, Gelfand *et al.* 1988). Small complementary oligonucleotides (~20mer primers) are designed to flank the region of interest on the target DNA molecule from which point they will prime the *in vitro* DNA polymerisation reaction carried out by thermostable DNA polymerase (From *Thermus aquaticus* or *Pyrococcus furiosus*) that can synthesise the remainder of the sequence in the presence of deoxyribonucleic acids (dNTPs) dATP, dTTP, dCTP and dGTP and appropriate co-factor. Thermal cycling allows template denaturation (95°C) and primer annealing (~62°C) which before an elongation step during which the polymerase synthesises the new strand (5'-3' direction). Because the molarity of reaction constituents are in excess of the target DNA molecule the number of copies of the DNA molecule of interest is increases exponentially.

2.10.1 Quantitative real-time PCR

Quantitative real-time PCR (qRT-PCR) is a technique used for amplification and simultaneous quantification of nucleic acids. Total messenger RNA was converted to cDNA using the Promega Reverse Transcription System (A3500, Promega) as described by the manufacturer. To assess quantity of transcripts of interest primers are designed to flank regions of a given gene's mRNA transcript including all known splice variants for that gene (Table 2-15). qRT-PCR was carried out using SYBR® green RT-PCR master mix (Life technologies) as per the manufacturer's guidelines. SYBR green is a double stranded DNA (dsDNA) binding (and intercalating) fluorescent dye with an excitation wavelength of ~ 485nm and an emission wavelength of ~ 524nm. Fluorescent signal from SYBR green directly correlates with dsDNA quantity and therefore PCR dsDNA products can be quantified after every elongation step in real time. 50ng/μl of the cDNA samples per 10μl final reaction volume, with the standard cycling parameters (Stage 1: 50°C for 2min, Stage 2: 95°C for 10min then 40 cycles of 95°C for 15 Sec and 60°C for 1 min), were set and carried out on an ABI 7900HT sequence detection system. Data were presented as mean ± standard error of mean (SEM) relative quantities (RQ) of four independent repeats where *GAPDH* was used as endogenous control and DMSO used as the calibrator for each independent repeat with the formula $2^{-\Delta\Delta C_T}$.

Analysis was carried out using SDS 2.2 software (Applied Biosystems).

Target Gene	Primer sequence 5'-3'
<i>AEN</i>	F-CTTCCAGGCGCTCAAGTATGT
	R-GGGCCAGGTCCTTTAGAGAGA
<i>BTG2</i>	F-CCTGTGGGTGGACCCCTAT
	R-GGCCTCCTCGTACAAGACG
<i>CDKN1A</i>	F-TGTCCGTCAGAACCCATGC
	R-AAAGTCGAAGTTCCATCGCTC
<i>GAPDH</i>	F-CAATGACCCCTTCATTGACC
	R-GATCTCGCTCCTGGAAGAT
<i>MDM2</i>	F-CAGTAGCAGTGAATCTACAGGGA
	R-CTGATCCAACCAATCACCTGAAT
<i>PHLDA3</i>	F-GCCTCTGCCAGATGCCTCC
	R-GGCACATCCCGCGAGCTGCC
<i>TNFSRF10B</i>	F-ATGGAACAACGGGGACAGAAC
	R-CTGCTGGGGAGCTAGGTCT
<i>TP53INP1</i>	F-TCTTGAGTGCTTGGCTGATACA
	R-GGTGGGGTGATAAACCAGCTC
<i>XPC</i>	F-CATCGTGGGAGCCATCGTAAG
	R-CTCACCATCGCTGCACATTTT

Table 2-15 Primer sequences used in qRT-PCR. F: Forward; R: Reverse.

2.11 Bacterial culture

Aseptic techniques were observed throughout working with bacterial cultures. Bacterial cells were grown in nutrient rich lysogeny broth (LB) medium (Bertani 1951) or on LB agar plates (1.5% agar w/v) containing 100µg/ml ampicillin (Sigma, # A0166) for selection of bacteria carrying vector of interest that harboured a copy of the β-lactamase TEM-1(*blaTEM-1*) gene which confers resistant to β-lactam antibiotics (i.e. ampicillin) by hydrolysing the β-lactam ring in their structure (Bush 1988).

2.11.1 Bacterial transformation

Bacterial transformation is a naturally occurring process whereby bacteria in certain environmental conditions become competent to acquire external naked DNA molecules (i.e. accessory DNA such as plasmids) which contributes to horizontal gene transfer (Lorenz and Wackernagel 1994). Bacterial cells (i.e. *Escherichia coli* (*E.coli*)) can also be made competent in the laboratory through their incubation with CaCl₂ (50mM) which affects the porosity of their membranes, allowing the uptake of hydrophilic molecules, such as DNA, during a heat shock procedure (Mandel and Higa 1970). Concentrated plasmid stocks (50-250ng/µl) were diluted 1:20 (v/v) in a 50µl aliquot of commercially available NEB 5-α transformation competent *E. coli* (Transforming efficiency: 1 - 3 x 10⁹ cfu/µg pUC19 DNA) cells (New England Biolabs Inc., C2987H) and incubated on ice for 30min, placed on a heating block at 42°C for 30sec (heat shock) and then put back on ice for a further 5min. The cells were then transferred to 0.5ml of SOC Outgrowth Media (New England Biolabs Inc., B9020S), incubated at 37°C while being shaken for 45min-1Hr. An aliquot of the cell suspension (50µl) was streaked on LB Agar plates containing Ampicillin (Sigma) at 100µg/ml final concentration and incubated overnight at 37°C in order to positively select for clonal populations of *E. Coli* carrying a plasmid with a selectable marker. Individual colonies were then picked using sterile pipette tips, inoculated in 5ml of LB broth containing Ampicillin (100µg/ml), and placed on a shaker in a 37°C incubator to grow overnight (12-16Hrs) at which point the culture would be in the transition between the logarithmic to stationary phase. Cell suspension was then centrifuged at 3000rpm, supernatant was disposed of and the pellet was used to extract the plasmid as described below.

2.11.2 Plasmid DNA Extraction

Plasmid DNA was extracted using a QIAGEN Plasmid Mini Kit (QIAGEN, 12123) which employs modified alkaline cell lysis method followed by the use of columns with

silica-gel stationary phase and high salt concentration mobile phase to allow adsorption of plasmid DNA. Ribonuclease A (RNase A) is present during the lysis process to degrade RNA and unbound molecules are removed and disposed of in wash steps before the plasmid DNA is eluted in low salt concentration (Please refer to QIAprep® Miniprep Handbook 05/2004).

Larger amounts of Plasmid DNA were extracted using QIAGEN Plasmid Maxi Kit (QIAGEN, 12162) as per the manufacturer's protocol. Anion-exchange columns/tips were used to In order to purify large quantities of plasmid from a pellet containing approximately $9 \times 10^9 - 1.2 \times 10^{10}$ total cell number (3ml of a culture at $3-4 \times 10^9$ cells/ml). The underlying principle behind his anion-exchange procedure kit is that there is a unique stationary phase or resin which is composed of hydrophobic silica beads, 100µm in particle size, large pore size, coated with diethylaminoethanol (DEAE) which is positively charged a the neutral pH of the mobile phase and can therefore retain negatively charged macromolecule that pass through (i.e. DNA at pH 7.0). The plasmid DNA can then be eluted by stepwise increment of the salt concentration of the mobile phase and nucleic acid concentration was quantified using a Nanodrop as described below.

2.11.3 Estimation of nucleic acid concentration via spectrophotometry

After nucleic acid purification the concentration of each stock was determined using a Nanodrop 1000 Spectrophotometer V3.7. Nanodrop sample loading platform has a receiving fibre optic cable onto which 1µl of the sample is loaded and a second source fibre optic that folds with the sampling arm onto the sample and the receiving fibre. The surface tension of the solvent containing the sample (e.g. H₂O) is used to hold he sample between the small gap generated by the higher and lower measurement platforms allowing the light from the xenon flash lamp source to traverse through the sample so that a linear charge coupled device (CCD) array on the other side can analyse the light that has passed through the sample. The Nanodrop covers a spectrum of 220nm-750nm which can be used for spectrophotometric measurement of concentrated samples containing molecules that show absorbance in this spectral range. Sample type DNA-50 was used for DNA quantification and RNA-40 for RNA quantification. A blank measurement was taken before sample measurements using the appropriate solvent devoid of sample and the pedestals were cleaned with distilled water between each measurement. The absorbance spectra were then presented as in Figure 2-6 with

readouts for 260:280 and 260:230 ratios. Nucleic acids absorb at 260nm and protein or phenol contaminants absorb at 280 therefore this ratio can be used as a measure of sample purity. The 260:280 ratio of ~1.8 was considered as pure DNA and ~2.0 as pure RNA. A 260:230 ratio is another measure of nucleic acid purity which is normally higher than the 260:280 ratio for a given sample (normally 1.8-2.2). Considerably lower 260:230 ratio suggests carbohydrate or solvent contamination as they both absorb strongly at 230nm.

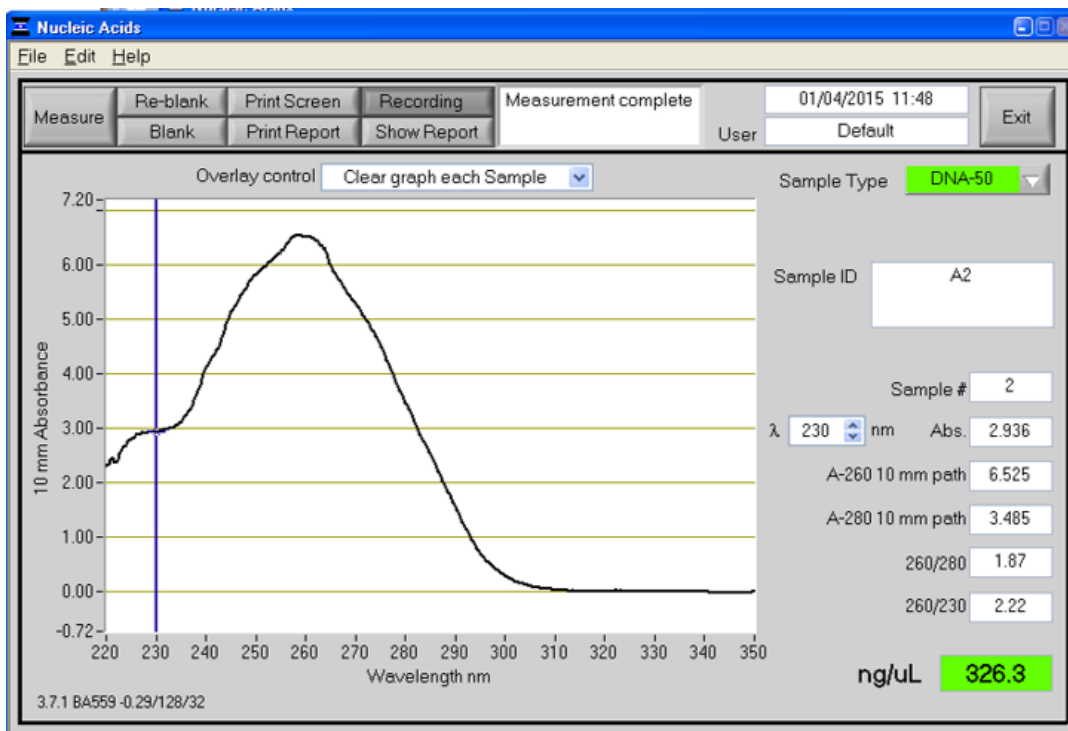


Figure 2-6 Screen shot showing Nanodrop 1000 software presentation of absorbance spectra pertaining to a plasmid sample purified by a Miniprep kit.

2.12 Immunocytochemistry

Immunocytochemistry can be used to localise antigen of interest with a specific primary antibody which is then visualised directly if it is already conjugated to a fluorophore or indirectly by a secondary antibody conjugated to a fluorophore. The nucleus is often stained with a nucleic acid fluorescent intercalating dye 4',6-Diamidino-2-Phenylindole, Dihydrochloride (DAPI). The samples can then be visualised and assessed by fluorescent microscopy. Alternatively confocal microscopy can be used for more high resolution imaging and generation of 3 dimensional (3D) images of single cells in high resolution for assessing subcellular localisation of antigens.

2.13 Protein detection by immunofluorescence

Fluorescent microscopy relies on the physical phenomenon of fluorescence to localise molecules within the cell *in situ*. Fluorophores or, fluorescent dyes, are molecules that can absorb the energy of light (photons) at a particular wavelength and emit a lower amount back to their environment at a different wavelength.

2.13.1 Immunofluorescence protocol

Cells were grown on glass coverslips in 6-well plates so that they are 50-70% confluent before treatment. At time points of interest following treatment media was aspirated and cells were washed with 4°C PBS before being fixed with 100% methanol (slides can be stored at -20°C for up to a week). Ethanol was removed and the slides were washed with 4°C PBS twice and transfer slides with forceps onto Parafilm M® in a 15cm petri dish surrounded by rolled up damp paper towels on the sides. 200µl of blocking reagent (2% BSA v/v, 1.5% Triton-X v/v in PBS) was then added to each cover slip and incubated for 1 hour before it was aspirated by a micro pipette (Gilson) from the corner and 200µl of the primary antibody of interest diluted in blocking reagent also containing milk and goat serum (2% BSA v/v, 10% milk w/v, 10% goat serum v/v, 1.5% Triton-X v/v in PBS) was added onto the coverslip. WIP1 (F-10) primary antibody was diluted at 1:500 and the γ H2AX (Mouse, 05-636, MERK Millipore) antibody at 1:1000 in blocking reagent. Coverslips were incubated at room temperature for 1Hr or at 4°C overnight before dipping the coverslip 3 times in 1.5% triton-X-100 v/v in PBS. They were then transferred into 6-well plates and wash with 1.5% triton-X-100 v/v in PBS another 3×15 min on a platform shaker. Coverslips were then removed and blocking buffer containing goat anti-mouse AlexaFluor-488 conjugated antibody (A11001, Thermo Fisher scientific) was added and incubated for a further 1 hour incubation, at room temperature, in the dark. Alexafluor-488 is a fluorophore that is excited by light at 495nm and emits 519 which can be detected by the optics in the microscope.

Immunofluorescence is a technique where antibodies are used to detect specific proteins in their anatomical locations. This technique either primary or secondary antibodies that are conjugated to fluorophores to detect specific epitopes *in situ* then a fluorescent or confocal microscope is used to examine the localisation of the epitopes within the cell. Antibody was removed then the coverslip was washed as above before adding a drop of VECTASHIELD® HardSet™ Mounting Medium with DAPI onto the cells and mounting the coverslip on a slide approximately 20min before confocal microscopy.

2.14 Confocal microscopy

In a confocal microscope out of focus rays from the fluorophore are filtered out by a set of pinholes positioned in the same confocal plane in front of the excitation source and the photomultiplier tube. This generates sharper images which allow z-stacking, the capture of images at different heights from the base of the sample, which in turn allows a 3D reconstruction of the images using the appropriate software.

Zeiss LSM 700 confocal microscopy system was used to capture images and the z-stack. The microscope was prepared for imaging using the Zen 2009 software as described by the manufacturer. A drop of Immersol (Zeiss, #ISO 8036-1/2) oil was placed on the coverslip and the slide was placed into its allocated slot on the microscope platform. Laser intensity, master gain, resolution and averaging were kept the same within the same experiment. 40× and for z-stacking 63× magnifications were used for γ H2AX staining and z-stacking respectively. Z-stacking was carried out according to the manufacturer's protocol (with the averaging set at 1). The number of slices taken for different z-stack experiment ranged from 30-50. Images taken from different slices were presented as a video rather than a 3D image.

Chapter 3 Exploring the combination treatment of Nutlin-3 and inhibitors of DNA repair enzymes in MDM2 inhibitor sensitive and resistant cell line pairs

3.1 Introduction

This chapter describes experiments to explore the role of DNA repair and stress response enzymes in determining the sensitivity to MDM2 inhibitors. The strongest predictor of response to MDM2 inhibitors is the genetic status of *TP53*. However, *TP53* wild-type cell lines show a wide range of sensitivity to MDM2 inhibitors suggesting that there are more complex mechanisms underlying p53 regulation following its activation by MDM2 inhibitors (Saiki, Caenepeel et al. 2015). Deciphering mechanistic determinants of sensitivity to MDM2 inhibitors may allow us to stratify tumour types more effectively and use optimal combination regimens in *TP53* wild-type malignancies.

3.1.1 Use of MDM2 inhibitor resistant clones in investigating determinants of MDM2 inhibitor sensitivity

Mechanisms of drug chemotherapy resistance often involve mutations in the target protein or upregulation of pumps such as p-glycoprotein (P-gp) and multi-drug resistance protein (MRP-1) that can actively export the drug from the cytoplasm (Gottesman, Fojo et al. 2002). However, work carried out by our own group and published data show that the primary mechanism of resistance to MDM2 inhibitors is through mutational inactivation of *TP53* (Aziz, Shen et al. 2011, Michaelis, Rothweiler et al. 2011, Jones, Bjorklund et al. 2012). Repeat exposure to MDM2 inhibitors results in the selection of *TP53* mutant, and otherwise isogenic, MDM2 inhibitor resistant clones. However, the origin of these *TP53* mutations is unclear. Interestingly, these clones have also been reported to show cross-resistance to other genotoxic chemotherapeutic agents (Michaelis, Rothweiler et al. 2011, Jones, Bjorklund et al. 2012). Unique MDM2 inhibitor resistant clones generated in our laboratory are used throughout this thesis to investigate the determinants of sensitivity/response to MDM2 inhibitors and other functional aspects of p53-dependent biological processes.

3.1.2 Exploring the role of DNA repair enzymes as determinants of response to MDM2 inhibitors

The roles of components of the DNA repair and stress response machinery in determining MDM2 inhibitor sensitivity are poorly understood. Sullivan *et al.*, (2012) introduced the concept of “synthetic lethality with Nutlin-3 (SLN)”. This was based on a genome wide shRNA screen in which a panel of genes was identified, the transient knockdown of which, on their own, had little or no effect on cell growth and

proliferation while increasing sensitivity of *TP53* wild-type cells to Nutlin-3 (Sullivan, Padilla-Just et al. 2012). The authors then validated synthetic lethality of two of their panel of targets, ATM and MET kinases, by showing that combination of specific ATM or MET kinase inhibitors with Nutlin-3 had a synergistic effect in six *TP53* wild-type cancer cell lines albeit to varying degrees. Given the established role of ATM in post-translational modification and activation of p53 in response to DNA damage, synergism observed by combining an ATM inhibitor and an MDM2 inhibitor raised questions about the underlying mechanism. This was proposed initially to be through the role of ATM in the pro-survival NFκB signalling cascade (Sullivan, Padilla-Just et al. 2012). Later the authors also claimed that the synergy observed was independent of p53 transcriptional regulation and dependent on ATM's role in regulation of autophagy (Sullivan, Palaniappan et al. 2014). Interestingly the doses of Nutlin-3 used in both studies were beyond doses associated with on target non-genotoxic activation of p53 in culture ($\geq 10\mu\text{M}$) (Sullivan, Padilla-Just et al. 2012, Sullivan, Palaniappan et al. 2014). ATM is a member of the PI3KK family and is involved in homologous recombination repair (HRR) of double strand breaks (DSB's). It is well-established that inhibition of ATM potentiates the response to DNA damaging agents such as ionising radiation (IR) as it results in persistence of lethal DNA DSB lesions (Hickson, Zhao et al. 2004). Using high doses of Nutlin-3 in combination with an ATM inhibitor may be potentiating the response to Nutlin-3 induced DNA damage rather than an intricate non-genotoxic mechanism as described by Sullivan et al., (2012 & 2014). Indeed phosphorylation of histone H2AX^{Ser139} (γH2AX), a marker of DNA DSB's, in response to $\geq 10\mu\text{M}$ Nutlin-3, has been reported independently (Verma, Rigatti et al. 2010, Valentine, Kumar et al. 2011, Rigatti, Verma et al. 2012). These studies assessed γH2AX immunofluorescence staining at later time-points following treatment which may correspond with DNA-fragmentation due to p53 mediated apoptosis. This suggests that the DNA damage observed may be due to off-target effects of Nutlin-3 or a later consequences of on-target non-genotoxic activation of p53 through MDM2 inhibition as γH2AX staining is also observed during apoptosis (Rogakou, Nieves-Neira et al. 2000). Therefore, mechanistic understanding of novel targets involved in sensitising cells to non-genotoxic activation of p53 by MDM2 inhibitors requires careful consideration of dosage and scheduling.

3.1.3 Use of small-molecular-weight inhibitors of DNA-repair enzymes in exploring determinants of MDM2 inhibitor sensitivity

In addition to HRR, repair of DSBs is also achieved through non-homologous end-joining (NHEJ) which relies on DNA-PKcs another kinase from the PI3KK family. Selective inhibition of DNA-PKcs by NU7441, similar to ATM inhibition, also potentiates the response to DSB inducing genotoxic agents (Hickson, Zhao et al. 2004, Leahy, Golding et al. 2004, Zhao, Thomas et al. 2006). Sullivan *et al.*, (2012) reported that pharmacological inhibition of ATM by KU55933 increases sensitivity to Nutlin-3 in a p53-dependent manner ($>10\mu\text{M}$). As discussed above this reported increase in cellular sensitivity is likely caused by off-target Nutlin-3 induced DNA damage due to high doses of this compound reported by Verma *et al.*, (2010), Valentine *et al.*, (2011) and Rigatti *et al.*, (2012) rather than through the intricate mechanisms explained by Sullivan *et al.*, (2012 & 2014).

Given the overlapping roles of ATM and DNA-PKcs in repairing DSBs, it would be pertinent to assess whether the selective pharmacological inhibition of ATM or DNA-PKcs can sensitise cells to mechanistically relevant doses of Nutlin-3 ($<10\mu\text{M}$). Furthermore, inhibition of DNA-PKcs may influence the sensitivity of cells to Nutlin-3 in the backdrop of DNA damage.

3.2 Hypotheses

- Pharmacological inhibition of ATM by KU55933 and DNA-PKcs by NU7441 sensitises cells to Nutlin-3 in the absence of DNA damage.
- Inhibition of DNA-PKcs by NU7441 increases cellular sensitivity to MDM2 inhibitors in the backdrop of DNA damage

3.3 Specific materials and methods

3.3.1 MDM2 inhibitor resistant clones and their use

SJSA-1 and NGP *TP53* wild-type parental cell lines and their MDM2 inhibitor resistant daughter cell lines SN40R2 and N20R1 respectively had previously been derived in our laboratory as described in materials and methods (2.1.2). These resistant cell lines lack p53 function due to *TP53* mutational inactivation (See 2.1.2) and are routinely used in pre-clinical development of in-house MDM2 inhibitors. In this chapter these cell line pairs were used to investigate the sensitivity to Nutlin-3 in combination with NU7441, a widely used potent selective DNA-PKcs inhibitor, or KU55933, a widely used ATM inhibitor.

3.3.2 Assessing growth inhibition by SRB assay

Appropriate densities of cells were seeded in 96-well plates (Corning, UK) 24 hours before treatment with 0-50 μ M Nutlin-3 + 1 μ M NU7441 or 0-10 μ M NU7441 alone. Where IR was added to the treatment a growth inhibition assay 72 hours after 0-6Gy dose of IR alone was also carried out in conjunction. Plates where Nutlin-3 + 1 μ M NU7441 were combined, a 1 μ M NU7441 control was present to enable measurement of the effect of NU7441 on the growth inhibition curve of Nutlin-3 + IR. The undergraduates' focus was on combination of 0-50 μ M Nutlin-3 + 10 μ M KU55933 and 0-50 μ M KU55933 alone no IR was added to the treatment. The final concentration of DMSO was kept at 1% in all wells except the media control well. At the end of the treatment the cells were fixed stained and analysed as described in materials and methods (2.2). GI50 values were calculated as described in (2.3.1). Drug-drug combination schedules in this chapter were simultaneous unless otherwise stated. Exposure to IR was always 4Hrs following commencement of treatment with solvent/drugs unless it is otherwise stated in figure captions. In growth inhibition assays with the PARP-1 inhibitor the cells were treated with 0.08-10 μ M Rucaparib for 1 week before SRB assay was carried out.

3.3.3 Clonogenic assays

Clonogenic assays for assessing drug sensitivity were carried out as described in 2.4.1. Drug-drug combinations were simultaneous and exposure was 48 hours before re-plating. Cells were always exposed to IR 4Hrs following commencement of Nutlin-3 treatment in the presence or absence of 1 μ M NU7441 unless otherwise stated in figure captions. Clonogenic assays for assessing IR sensitivity alone were carried out as described in 2.4.3. Lethal concentrations at given % survival (e.g. LC50) were calculated as described in (2.4).

3.3.4 Detection of γ H2AX by immunofluorescence staining

Cells were seeded at 3×10^5 cells/well of a 6-well plate onto glass coverslips 24Hrs before treatment with Media/DMSO, Nutlin-3 or 2Gy IR. 100% chilled (4°C) methanol was used to fix the cells at the time-points stated and in the coverslips stored at -20°C. All antibodies, staining protocol and microscopy techniques are explained in general materials and methods.

3.3.4.1 Integrated density quantification

The immunofluorescent staining for γ H2AX foci in MCF-7 cells was quantified by calculating the integrated density (IntD) using Image-Pro Plus software. Areas of >100 DAPI stained nuclei were measured per treatment. The mean density of pixels corresponding to γ H2AX (Secondary antibody Alexa Fluor-488) signals within the area of each nucleus were also quantified. IntD was then calculated through multiplying the area of each DAPI stained nucleus by the total mean density of γ H2AX pixels detected within. IntD was then normalised to mean density of the background before further analysis.

3.3.5 Statistical analysis

Three or more independent experiments were carried out to assess statistical significance of paired data using paired t-tests on GraphPad Prism 6 Software.

3.4 Results

3.4.1 Analysing the cellular and biological response of MDM2 inhibitor resistant cell lines to MDM2 inhibitors

SRB growth inhibition experiments were carried out on NGP and SJSA-1 cells along with their resistant daughter cell lines N20R1 and SN40R2 respectively for 72Hrs exposure to Nutlin-3 (0.1-50 μ M). The Nutlin-3 GI50 was ~9-fold higher in N20R1 cells compared to the *TP53* wild-type parental NGP cells ($p = 0.0003$). Similarly, Nutlin-3 GI50 was ~21-fold higher in SN40R2 cells compared to its parental SJSA-1 cell line ($p=0.0005$) (Figure 3-1A). The growth inhibition observed in *TP53* mutant daughter cell lines at >10 μ M does not require functional p53 and may therefore be either an off-target effect or an MDM2 effect independent of p53 activation. . Clonogenic survival following 48Hrs of treatment with Nutlin-3 (1.25-10 μ M) was then investigated in both cell line pairs. SJSA-1 cells were very sensitive to MDM2 inhibitors with an LC50 1.69 ± 0.11 (Mean \pm SEM) a marked contrast to their resistant SN40R2 daughter clone with an LC50 >10 μ M (Figure 3-1B). NGP cells were also sensitive to Nutlin-3 with an LC50 of 3.21 ± 0.21 (Mean \pm SEM) in contrast to their *TP53* mutant daughter clone N20R1. Interestingly, there was a 2.8-fold ($p = 0.04$) difference between LC25 of NGP and SJSA-1 cell lines and NGP cells did not reach LC10 within the dose range tested. This suggests that a sub-population of NGP cells may undergo reversible cell cycle arrest in response to MDM2 inhibitors which does not result in clonogenic cell death.

3.4.2 Cellular response of the MDM2 inhibitor resistant cell lines to IR

Previous work carried out by our group had shown that Nutlin-3 resistant clones used here are also cross-resistant to other classes of MDM2 inhibitors such as spiroindoles and isoindolinones (Data not shown but available upon request). It was of interest to assess whether the MDM2 inhibitor resistant sub-clones are also equally resistant to growth inhibition and loss of clonogenic survival after exposure to IR. NGP cells were slightly more sensitive to IR in SRB growth inhibition assays compared to N20R1 cells (Figure 3-2A). There was no notable difference in sensitivity to IR treatment between SJSA-1 and SN40R2 cells. SRB IR growth inhibition curves appeared to plateau after ~4Gy IR in both cell line pairs. These observations suggested that SRB growth inhibition may not be suitable for detection of dose-dependent cellular response to IR, as cells may undergo reversible cell cycle arrest or senescence within the first 72Hrs following treatment.

Interestingly, clonogenic survival assays for both the parental and daughter cell lines showed very similar sensitivity to IR (Figure 3-2B). Clonogenic assays were also carried out on HCT116^{+/+} *TP53* wild-type and its otherwise isogenic HCT116^{-/-} null cell line pairs and these also showed no difference in their sensitivity to IR between the two matched isogenic cell lines (Figure 3-2B and C). These data show that clonogenic cell death following IR in these cell lines is independent of *TP53* genetic status.

3.4.3 Biochemical p53 activity in MDM2 inhibitor resistant cells in response to IR

TP53 wild-type parental cell lines and their MDM2 inhibitor resistant *TP53* mutant and otherwise isogenic sub-clones showed the same sensitivity in response to IR. Therefore, the p53 functional status was assessed after exposure to IR in these cell lines. Canonical p53 transcriptional target, MDM2, was markedly induced 4Hrs following IR in *TP53* wild-type parental cell lines and not in their *TP53* mutant daughter clones (Figure 3-3A). The p53 induced early apoptotic marker, PUMA, was only detected in NGP cell line pair in a p53-dependent manner following IR. This correlated with a marked increase in cleaved-caspase-3 48Hrs following IR treatment in NGP cells compared to N20R1 cells (Figure 3-3B). Cleaved caspase-3 was not detected in either SJSA-1 or HCT116 cell line pairs (Figure 3-3C). Different patterns of PARP-1 cleavage reportedly can be markers of different types of cell death (Reviewed in (Chaitanya, Alexander et al. 2010)). The Anti-PARP-1 antibody (C2-10) used here showed that PARP-1 is cleaved in a caspase-dependent manner in NGP cells following Nutlin-3 producing an 85kDa fragment (Figure 3-3C). This fragment was not detected in the other cell line

pairs. Caspase-independent forms of cell death produce different size fragments and a 62kDa fragment, which is associated with necrotic cell death, was modestly increased in response to IR. Interestingly this fragment was also detected in NGP cells that undergo caspase-dependent apoptosis.

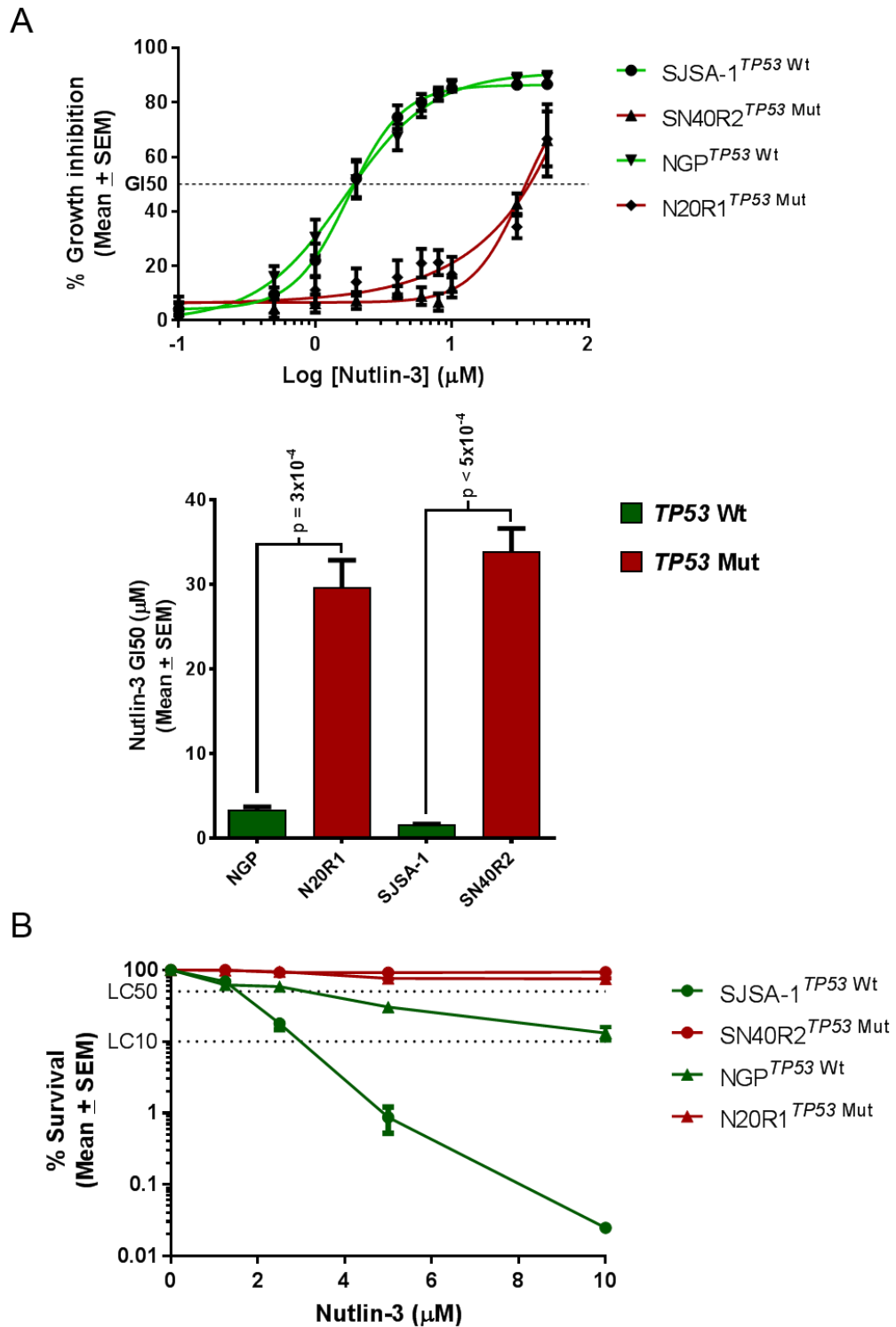


Figure 3-1 A) SRB Nutlin-3 growth inhibition curves obtained for 72Hrs exposure of cell line pairs to Nutlin-3 (0.1-50 μ M). Bar charts show Nutlin-3 GI50 values calculated based on the growth inhibition curves and p-values represent paired t-tests for n=3 repeats. B) Nutlin-3 clonogenic survival curves after 48Hrs exposure to Nutlin-3 (1.25-10 μ M) for n=3 repeats. GI50: 50% growth inhibitory concentration. LC50: Concentration that causes 50% loss of clonogenic survival; LC10: Concentration at which there is 10% clonogenic survival.

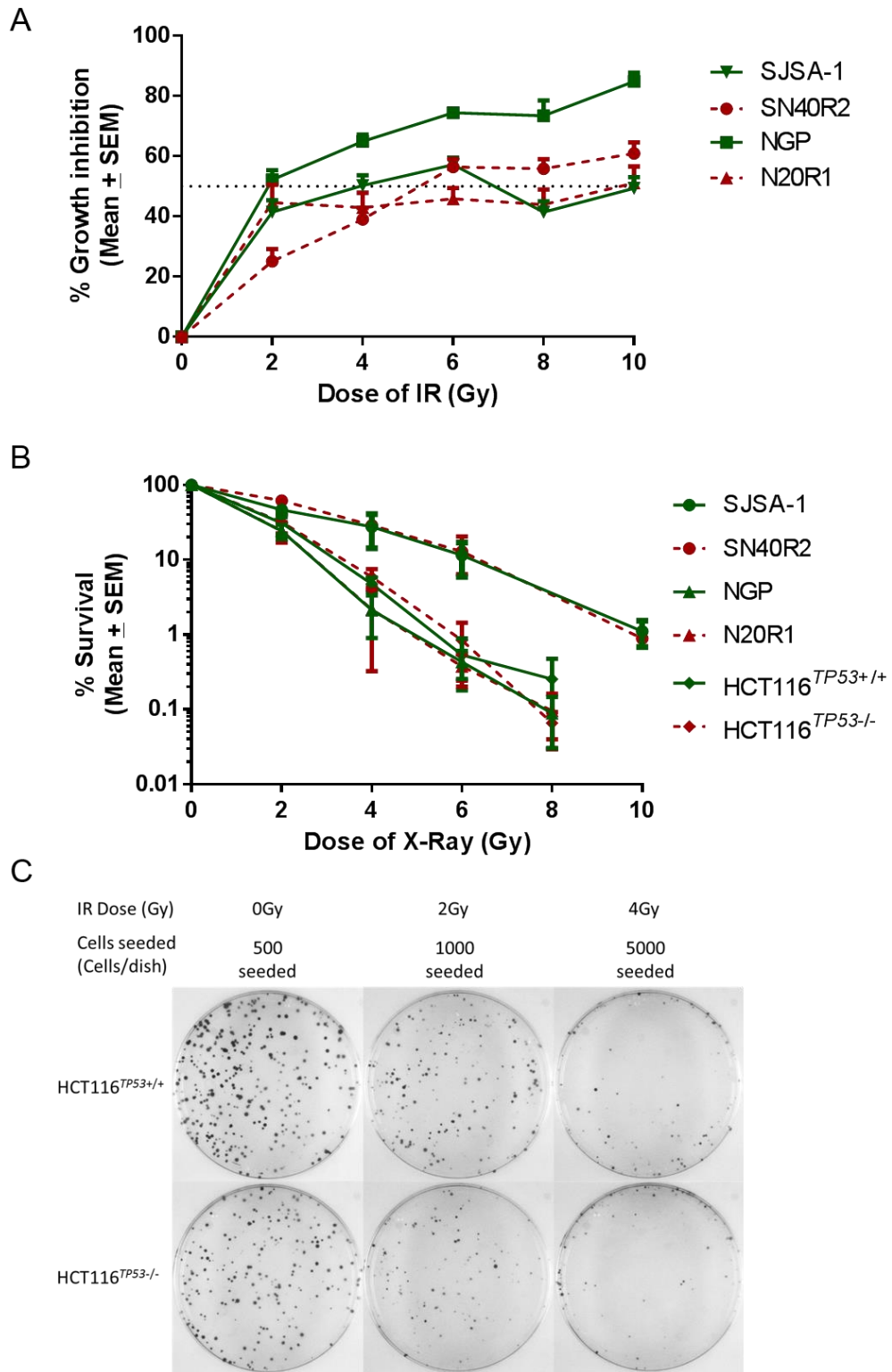


Figure 3-2 A) SRB ionising radiation (IR) growth inhibition curves obtained 72Hrs following treatment show that there is little difference in sensitivity between the *TP53* wild-type parental cell lines and their *TP53* mutant otherwise isogenic clones. **B)** There was no difference clonogenic cell survival following IR between the *TP53* wild-type and mutant cell line pairs **C)** Colony formation in HCT116 cell line pair shows that sensitivity to IR is not dependent on the *TP53* genetic status.

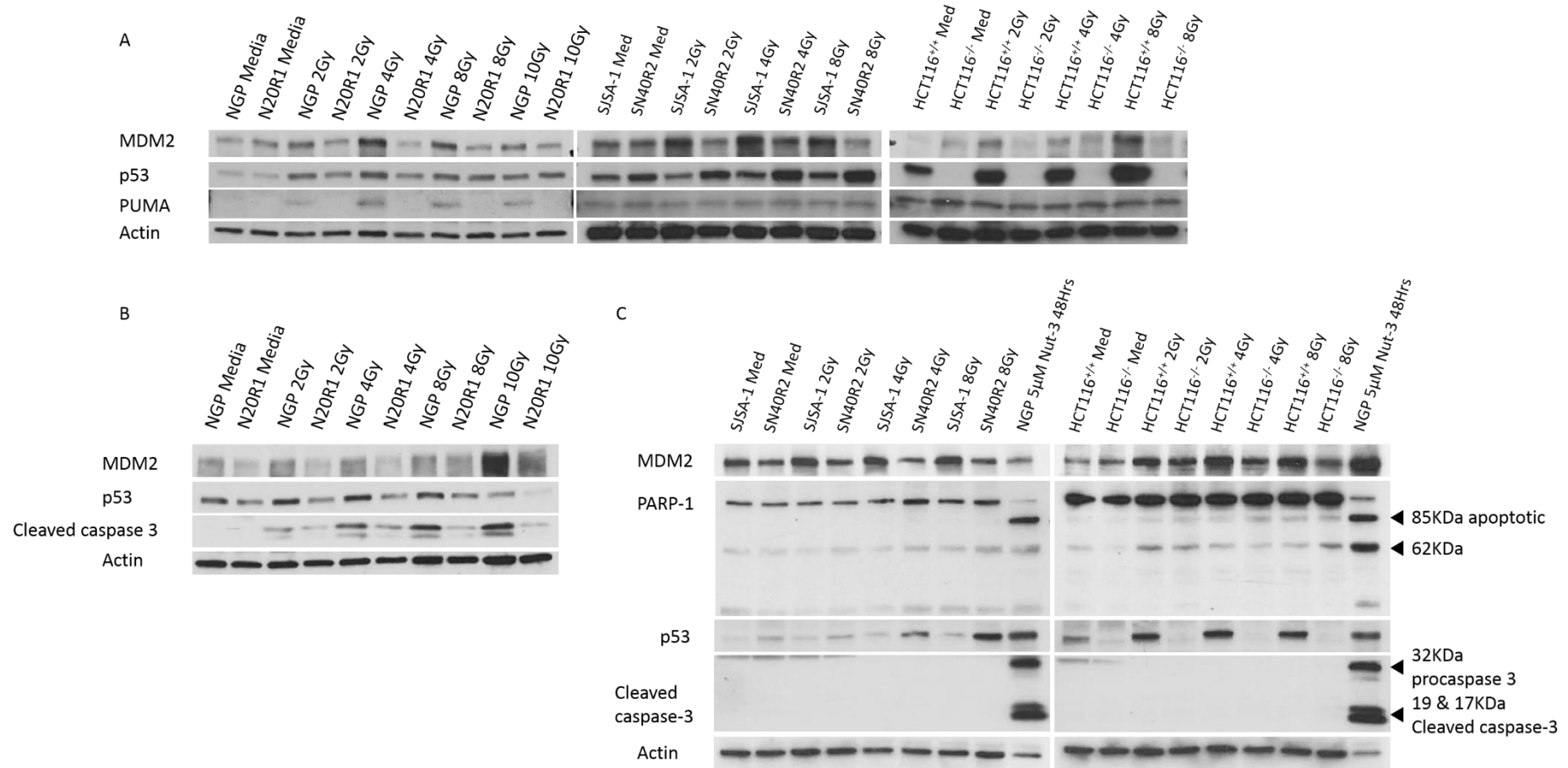


Figure 3-3 A) Immunoblots showing the induction of early p53 transcriptional targets in *TP53* wild-type and mutant cell line pairs 4Hrs following IR. B) Immunoblot showing the extent of caspase-3 cleavage (marker of apoptosis) 48Hrs following IR treatment of the NGP cell line pair. C) Cleaved caspase-3 and PARP-1 cleavage could not be detected in SJS-1 and HCT116 cell line pairs 48Hrs following IR.

3.4.4 Phosphorylation of histone H2AX^{Ser139} (γ H2AX) following Nutlin-3 is a late event

As discussed earlier, three publications had reported γ H2AX immunofluorescent staining (foci) in the nucleus, a marker of DNA double strand breaks, following treatment with Nutlin-3 (Verma, Rigatti et al. 2010, Valentine, Kumar et al. 2011, Rigatti, Verma et al. 2012). In all cases the dosage and/or timing had not been considered in relation to the mechanism of action of MDM2 inhibitors. We sought to investigate the kinetics of the mechanistically relevant doses of Nutlin-3 (0.2-5.0 μ M) in inducing γ H2AX staining. Gamma (γ)-H2AX can be detected within the first 30mins following IR therefore this was used as a positive control for the immunofluorescent staining for this marker (Figure 3-4/See electronic copy for better contrast). Treatment of SJS-1 cells with 5 μ M Nutlin-3 ($\sim 3 \times$ GI50 dose) resulted in no detectable levels of γ H2AX staining until 24Hrs following treatment, while in contrast distinct γ H2AX foci were detected 30min following 2Gy IR (Figure 3-4). Pan-nuclear staining was also observed in SJS-1 cells at 24Hrs. Treatment of NGP cells with 5 μ M Nutlin-3 ($\sim 1.7 \times$ GI50) also resulted in no γ H2AX staining until 24Hrs post-treatment when pan-nuclear staining was also observed in fragmented nuclei (Figure 3-4). Higher background is observed in NGP cell images due to a higher gain settings on the Alexa Fluor-488 channel before capturing images in order to increase the sensitivity of the photomultiplier tube. Similarly an increment of Nutlin-3 doses (0.2-5.0 μ M) resulted in no increase in γ H2AX signal in MCF-7 cells (Nutlin-3 GI50 = 1.8 μ M, Data not shown). Integrated density of pixels was calculated in three independent experiments and paired t-tests showed that while IR at 30mins resulted in a statistically significant increase in γ H2AX staining ($p = 0.03$) Nutlin-3 does not at any of the mechanistically relevant doses used (Figure 3-5). These findings suggest that Nutlin-3 is not damaging DNA at doses that are sufficient for activation of p53 followed by apoptosis/growth arrest. Therefore, dosage and timing must be considered carefully when investigating markers of DNA damage in response to treatment with MDM2 inhibitors.

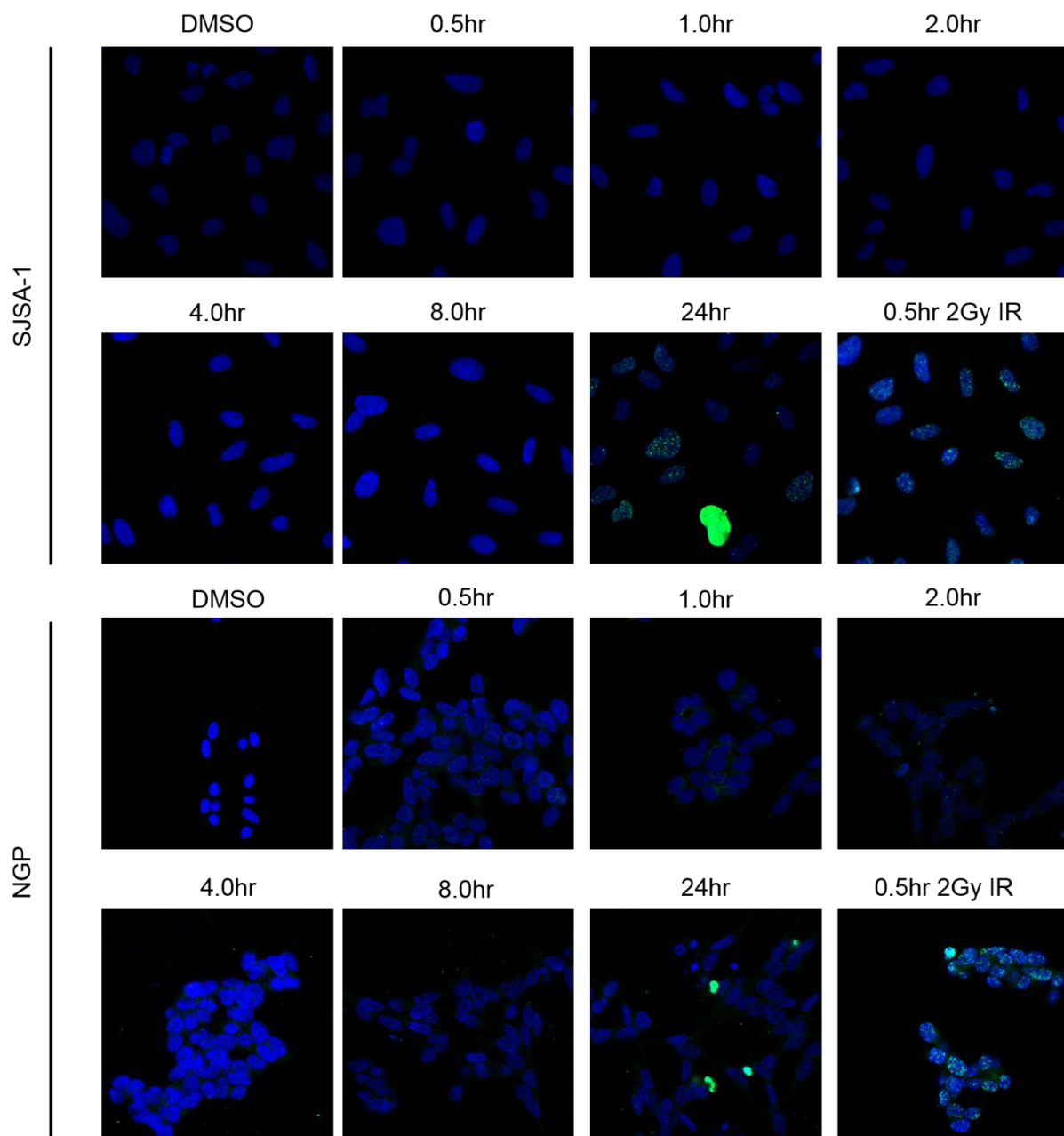


Figure 3-4 5 μ M Nutlin-3 does not lead to γ H2AX staining in SJSA-1 and NGP cells until 24Hrs following treatment. Each cell line was also treated with 2Gy IR and stained for γ H2AX in parallel as positive control for staining.

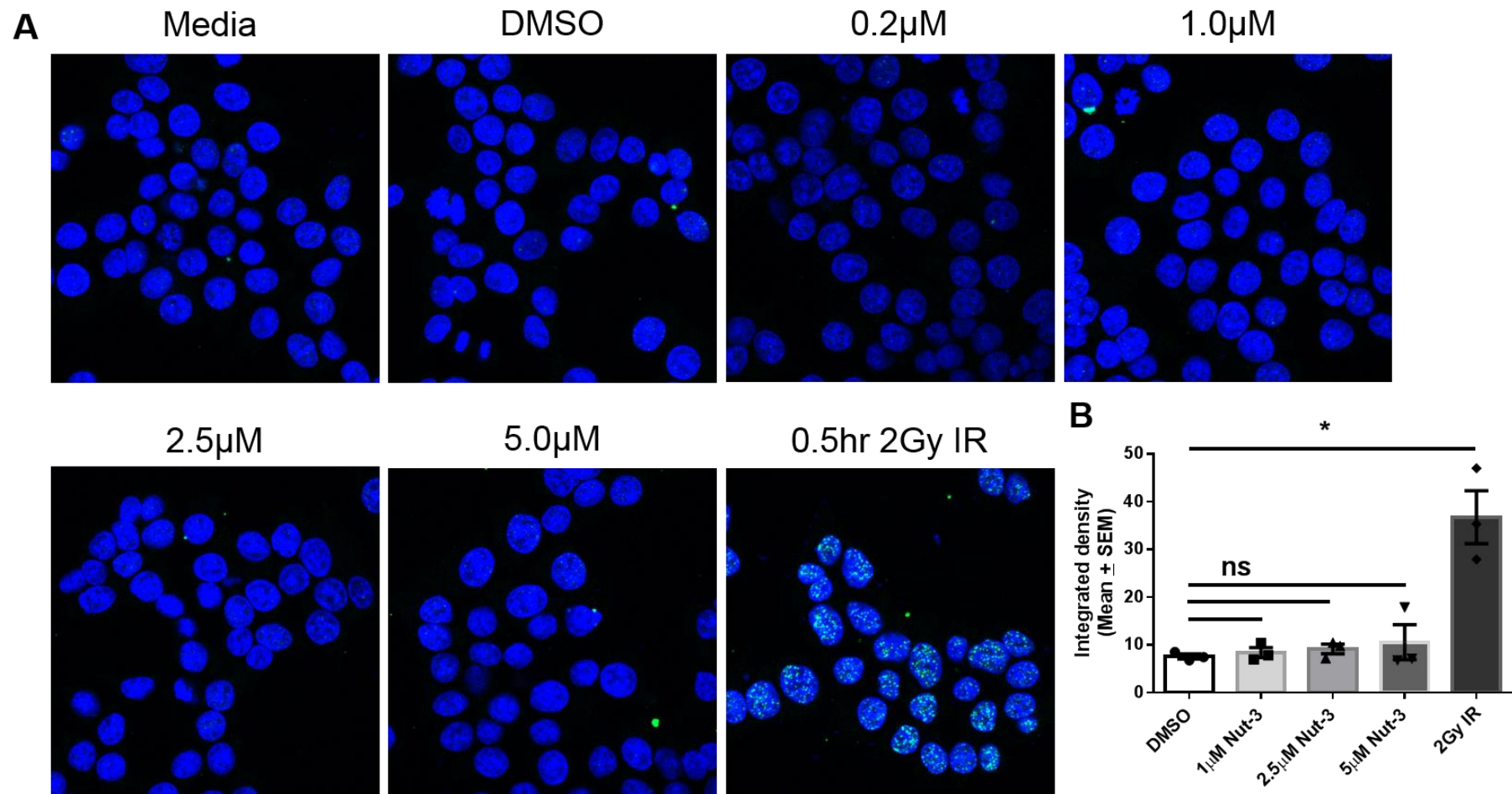


Figure 3-5 A) Representative γ H2AX immunofluorescence staining of MCF-7 cells 30min after treatment with Nutlin-3 at different doses. IR induced γ H2AX staining was used as positive control. B) Mean \pm SEM integrated immunofluorescence signal for three independent experiments.

3.4.5 Pharmacological inhibition of ATM by KU55933 does not sensitise cell lines to mechanistically relevant doses of MDM2 inhibitors.

Work summarised in this section was carried out by supervised undergraduate student Mrs Laura Kettlewell. Auto-phosphorylation of ATM^{Ser1981} can be used as a marker of ATM activity in cell lines following IR. SJSA-1 cell line pair were pre-treated with solvent/10 μ M KU55933 30min before exposure to 6.3Gy IR. Immunoblots showed that ATM^{Ser1981} was phosphorylated 30min following exposure to IR, whereas this phosphorylation event was not detected when cells had been pre-treated with 10 μ M KU55933 (Figure 3-6A). This shows that ATM catalytic activity is intact in these cells and that it is efficiently inhibited by 10 μ M KU55933. Single treatment with KU55933 resulted in similar GI50 values for both cell lines and only slight growth inhibition (~10%) was observed at 10 μ M KU55933 (Figure 2B). The SJSA-1 cell line pair was then treated with an increment of Nutlin-3 (0.1-50 μ M) in the presence or absence (\pm) 10 μ M KU55933 for 72Hrs. Nutlin-3 GI50 for SJSA-1 cells remained unchanged in the presence of 10 μ M KU55933 (Table 3-1). Interestingly, in contrast to the parental cell line, the SN40R2 cells were made more sensitive to higher doses of MDM2 inhibitors by ATM inhibition as predicted. The Nutlin-3 GI50 was approximately halved in SN40R2 cells.

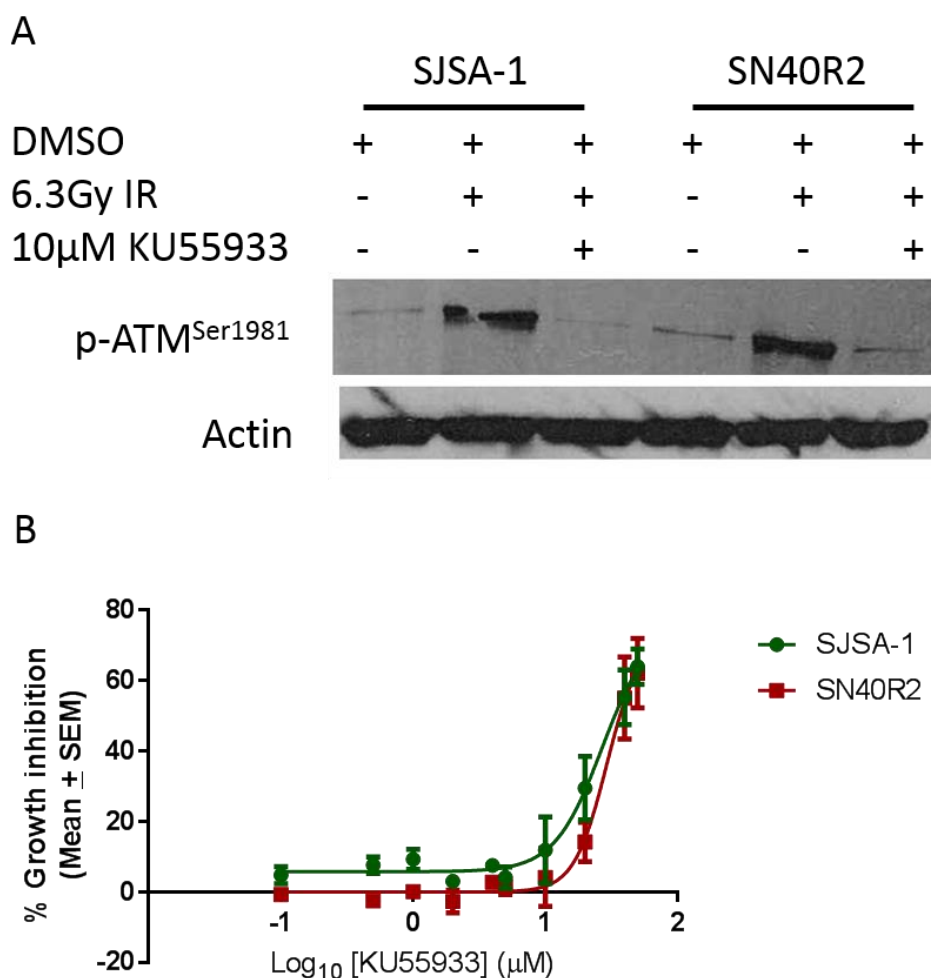


Figure 3-6 A) Immunoblot showing the inhibition of IR induced ATM^{Ser1981} autophosphorylation in the presence of 10 μ M KU55933. **B)** KU55933 (0.1-50 μ M) SRB growth inhibition curves after 72Hrs of treatment shows that 10 μ M KU55933 causes ~10% growth inhibition in both cell lines regardless of their *TP53* genetic status.

	KU55933 (Mean \pm SEM)	Nutlin-3 (Mean \pm SEM)	Nutlin-3 & 10 μ M KU55933 (Mean \pm SEM)
SJSA-1	43.08 \pm 0.86	2.21 \pm 0.59	2.26 \pm 0.52
SN40R2	32.51 \pm 0.63	34.86 \pm 2.37	17.43 \pm 0.68

Table 3-1 Nutlin-3 (0.1-50 μ M) SRB growth inhibition in SJSA-1 and SN40R2 cells in the presence of 10 μ M KU55933. SEM and GI50 values are representative of three independent experiments (Data obtained from dissertation of Mrs Laura Kettlewell).

3.4.6 DNA-PKcs is efficiently inhibited by 1 μ M NU7441

Extensive previous studies had established that 1 μ M NU7441 leads to optimal DNA-PKcs enzymatic inhibition and hence it is the dose used in preclinical studies for potentiation of DSB inducing DNA damaging agents (Zhao, Thomas et al. 2006). Auto-phosphorylation of DNA-PKcs^{Ser2056} (p-DNA-PK^{Ser2056}) can be detected following exposure to IR and is used as a surrogate marker of DNA-PKcs kinase activity and is required for NHEJ (Chen, Chan et al. 2005). Phospho-DNA-PK^{Ser2056} was detected by immunoblotting in both *TP53* wild-type and mutant cell lines 30mins following treatment with 6.3Gy of IR. Importantly, p-DNA-PK^{Ser2056} was markedly diminished when cells were pre-treated with 1 μ M NU7441 30min before irradiation (Figure 3-7). These data show that DNA-PKcs is functional in both cell line pairs and that 1 μ M NU7441 can inhibit its catalytic activity efficiently.

3.4.7 DNA-PKcs inhibition by NU7441 does not affect cellular response to MDM2 inhibitors in the absence of DNA damage

It was pertinent to first determine whether 1 μ M NU7441 results in growth inhibition in our cell lines before assessing whether Nutlin-3 sensitivity was altered in its presence. NU7441 SRB growth inhibition curves showed that 1 μ M NU7441 is approximately the highest non-growth inhibitory dose of this compound tested (Figure 3-8A and B). Interestingly, NU7441 had the same GI50 in our cell line pairs regardless of their *TP53* status. Then in order to assess the role of DNA-PKcs catalytic function in determining sensitivity to MDM2 inhibitors we carried out Nutlin-3 growth inhibition assays in the presence and absence (\pm) of 1 μ M NU7441. Nutlin-3 growth inhibitory curves were not affected \pm 1 μ M NU7441 (Figure 3-9).

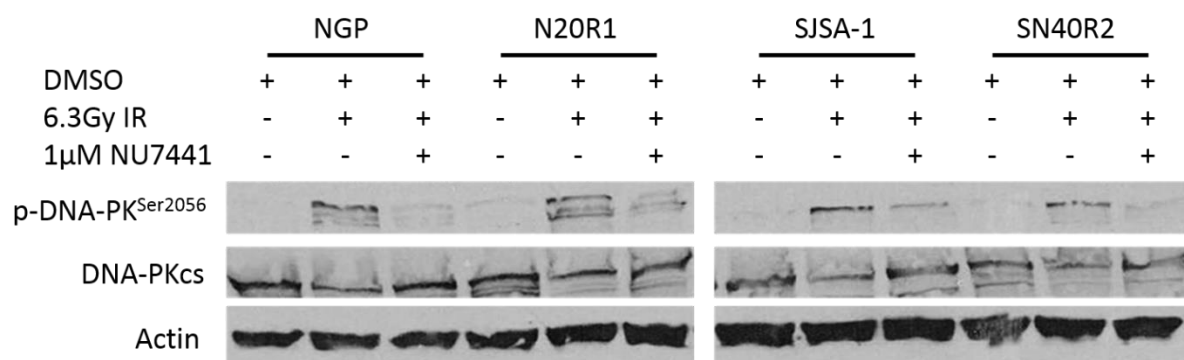


Figure 3-7 Immunoblots on lysates from untreated and irradiated cell line pairs in the presence or absence of 1 μ M NU7441. Cells were pre-treated with 1 μ M NU7441 for 30min prior to irradiation. DNA-PKcs is functional in both cell lines pairs and its autocatalytic activity is inhibited by 1 μ M NU7441.

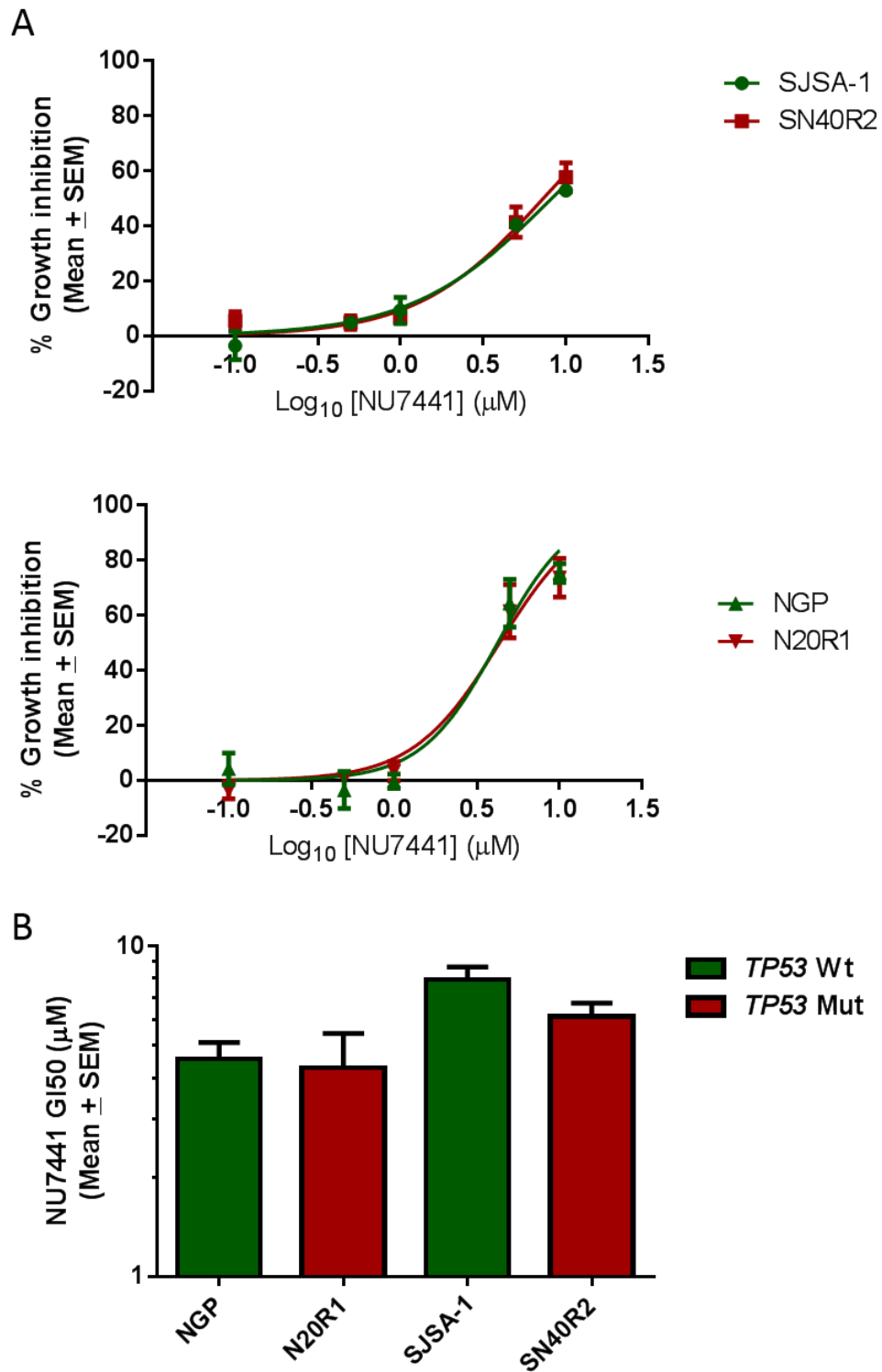
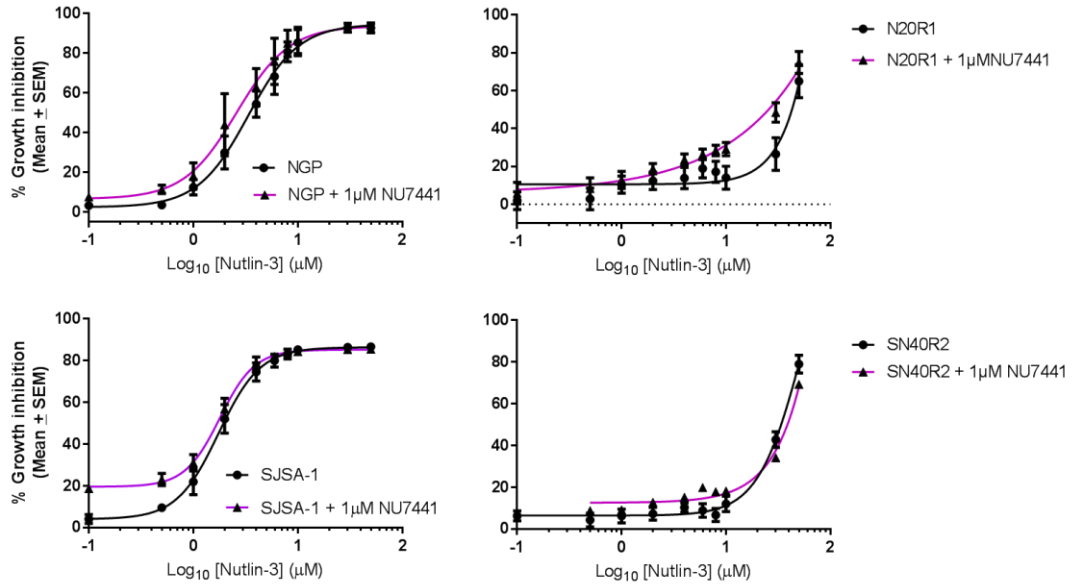


Figure 3-8 SRB growth inhibition curves obtained after 72Hrs of exposure of cell line pairs to NU7441 (0.1-10µM). Sensitivity to NU7441 is independent of the *TP53* genetic status and 1µM NU7441 is the highest non-growth inhibitory dose of DNA-PKcs inhibitor tested.

3.4.8 Biochemical Nutlin-3 mediated p53 response was not affected by 1 μ M NU7441

Immunoblotting showed that canonical transcriptional targets of p53, p21^{WAF1} and MDM2, were markedly induced at 4Hrs in a Nutlin-3 dose-dependent manner in *TP53* wild-type parental cell lines (Figure 3-10). The induction of these targets were much lower or absent in their *TP53* mutant and otherwise isogenic clones. Importantly, the presence of 1 μ M NU7441 did not affect their induction notably. Interestingly, there was a modest reduction in p53^{Ser15} phosphorylation which is a known substrate for DNA-PKcs suggesting that this enzyme may be involved in the phosphorylation of this residue following Nutlin-3 treatment.

A



B

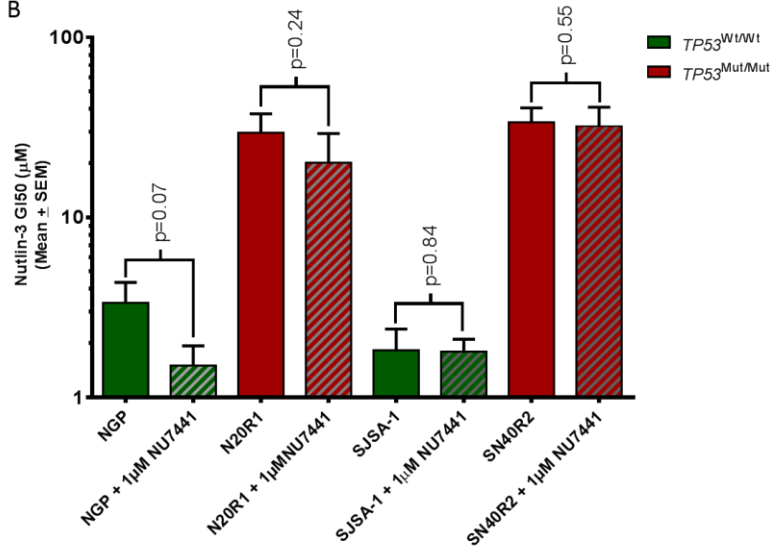


Figure 3-9 A) SRB growth inhibition curves after 72Hrs treatment with Nutlin-3 ± 1µM NU7441. B) Bar charts showing Nutlin-3 GI50 values in the presence and absence of 1µM NU7441. P-values were derived from paired t-tests between the columns indicated.

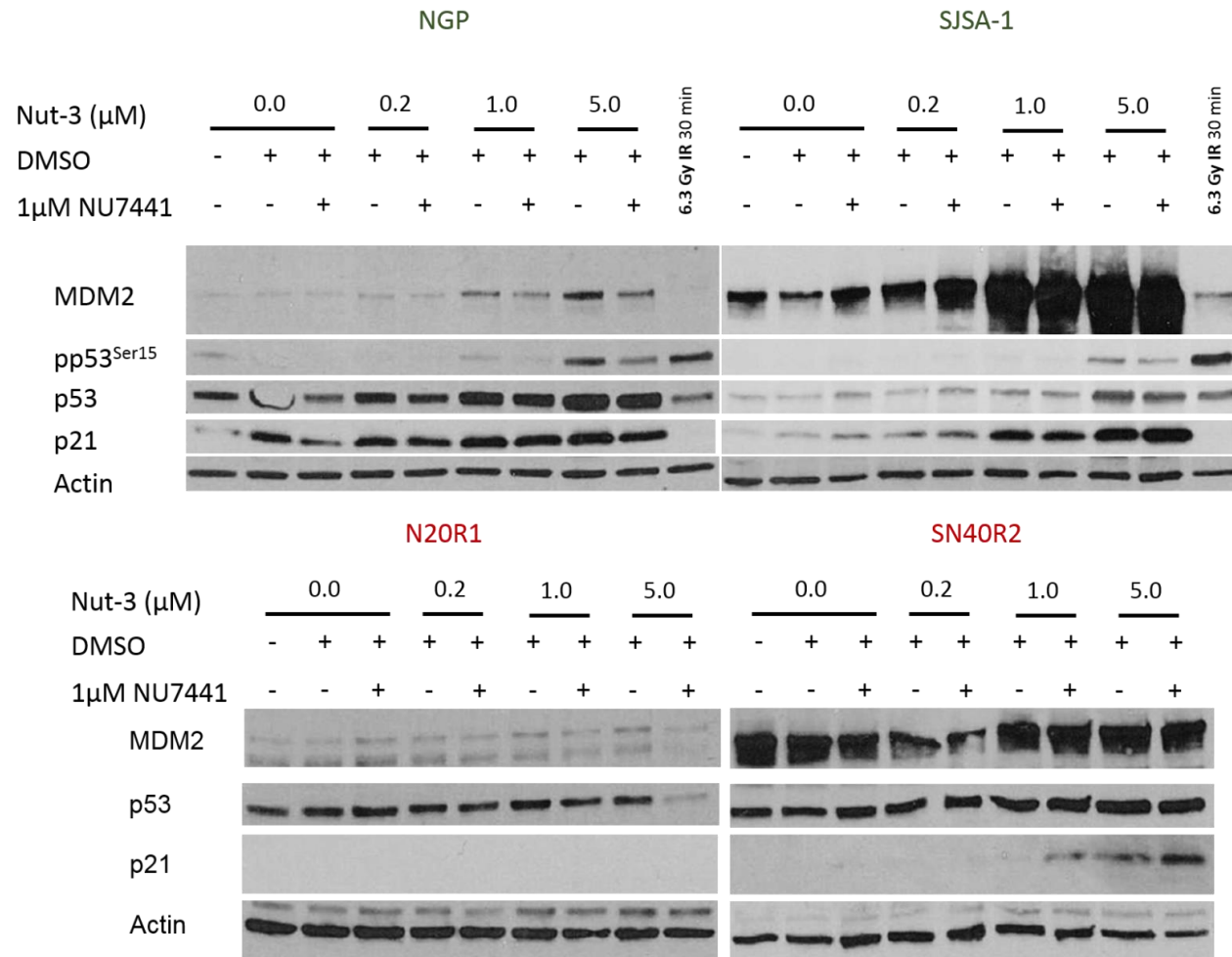


Figure 3-10 Biochemical response of the *TP53* wild-type (Green) and mutant (Red) cell line pairs 4Hrs following treatment with Nutlin-3 \pm 1 μM NU7441. Canonical transcriptional targets of p53 induced by Nutlin-3 such as, MDM2 and p21^{WAF1} are not affected in the presence of 1 μM NU7441.

3.4.9 Inhibition of DNA-PKcs potentiates cellular sensitivity to Nutlin-3 in the presence of IR in a cell-type-dependent manner

Cellular sensitivity to Nutlin-3 and its combination with multiples of IR GI50 were examined in the presence and absence of 1 μ M NU7441. The cells were irradiated at 4Hrs following treatment with Nutlin-3 \pm 1 μ M NU7441 so that it coincides with the time of maximal Nutlin-3 induced p53 stabilisation. Nutlin-3 growth inhibitory curves were generated by normalising out the growth inhibitory effect of DMSO/1 μ M NU7441 + IR for each curve exposed to either 2Gy or 4Gy of IR \pm NU7441 in order to assess the additional growth inhibitory response due to Nutlin-3. The Nutlin-3 growth inhibitory curves for NGP cells shifted to the left in the presence of NU7441 in an IR dose-dependent manner (Figure 3-11A). Moreover, the sigmoidal shape of the growth inhibition curve remained the same, indicating that Nutlin-3 dose-dependent growth inhibitory effect and change in GI50 values could be determined in spite of normalising out the growth inhibitory effect of IR + DMSO or IR + 1 μ M NU7441 on their respective plates. Exposure to IR shifts Nutlin-3 GI50 lower which is enhanced significantly in the presence of 1 μ M NU7441 (4.2-fold at 2Gy and 8.4-fold at 4Gy). These observations show that exposure to IR sensitises the cells to the growth inhibitory effect of Nutlin-3 and that this is potentiated by DNA-PK inhibition with NU7441.

For SJS-1 cells, not only was a shift to the left for Nutlin-3 growth inhibitory curves not observed with either IR or IR+NU7441 exposure, but also the Nutlin-3 mean GI50 increased significantly (~3.5-fold) (Figure 3-12). This suggests that exposure to IR may only sensitise cells to Nutlin-3 in a context dependent manner and in some circumstances may protect cells from growth inhibition by Nutlin-3.

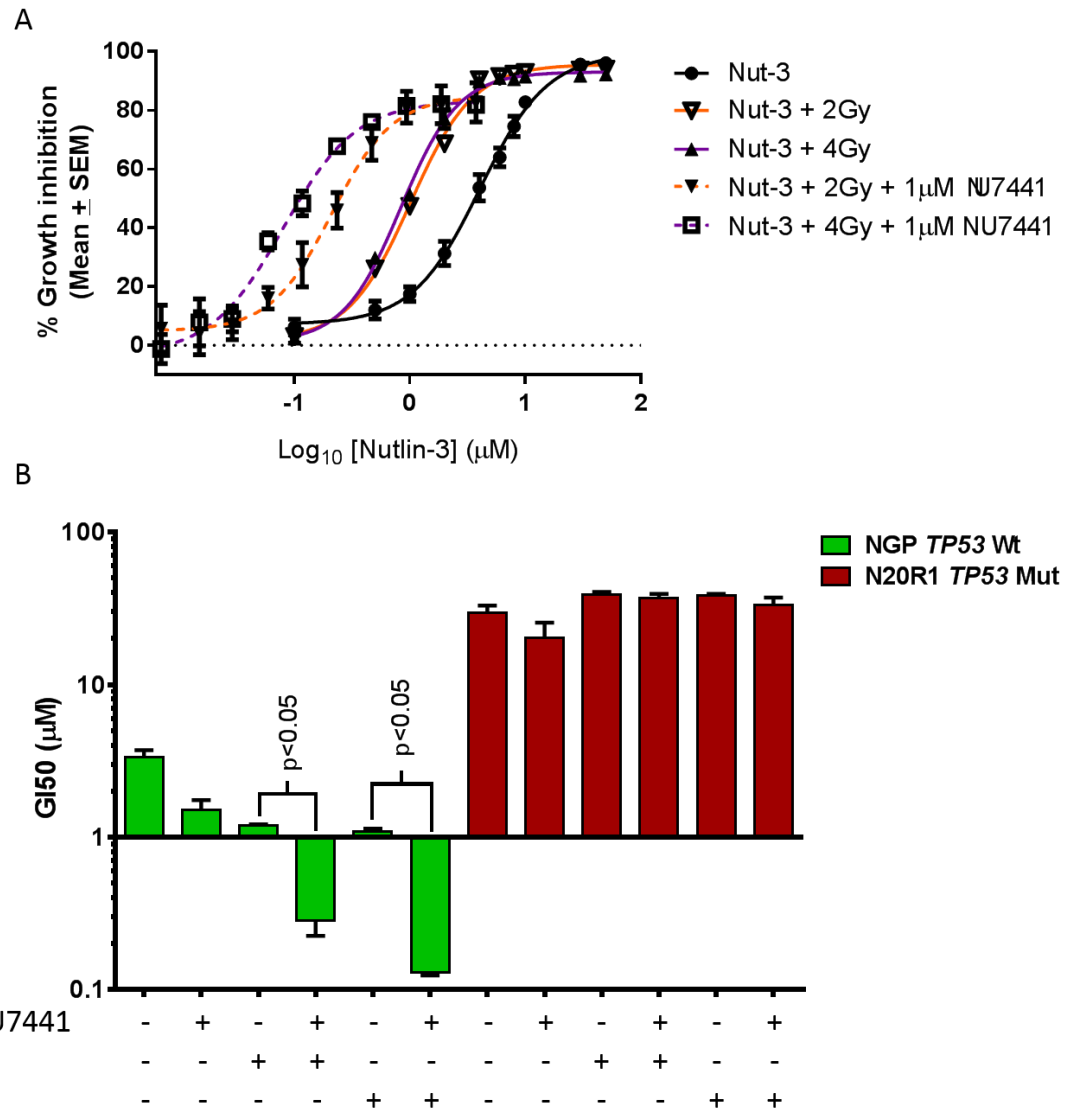


Figure 3-11 A) SRB growth inhibition curves for NGP cells 72 hours after treatment with Nutlin-3 \pm IR \pm 1µM NU7441. % growth inhibition is calculated with respect to either DMSO + IR treated wells or 1µM NU7441 + IR treated wells, where NU7441 is present. B) Bar charts showing Nutlin-3 GI50 values calculated based on the curves in A.

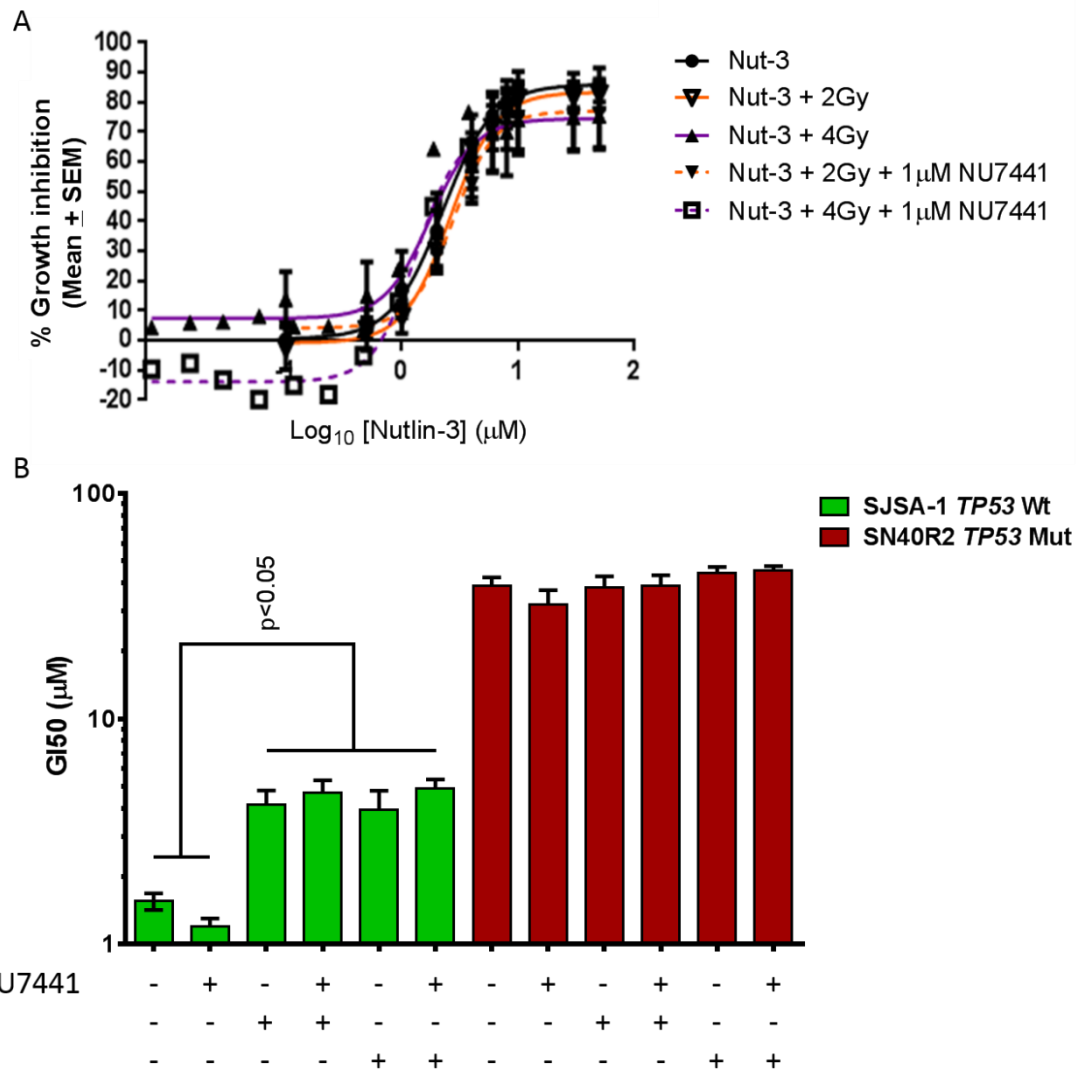


Figure 3-12 A) SRB growth inhibition curves of SJSA-1 cells 72 hours after treatment with Nutlin-3 \pm IR \pm 1 μ M NU7441. Growth inhibition is calculated as a % of to either DMSO + IR treated wells or 1 μ M NU7441 + IR treated wells, where NU7441 is present. B) Bar charts showing Nutlin-3 GI50 values calculated based on the curves in A.

3.4.11 NGP cells are sensitive to PARP-1 inhibition by Rucaparib

As the difference between NGP and SJSA-1 cells may be due to inherent differences in DNA repair integrity. We decided to assess whether treatment with the PARP-1 inhibitor Rucaparib (0.08-10 μ M), impacts cell growth in any of the cell lines tested. Inhibition of PARP-1 is known to be synthetically lethal with defects in homologous recombination repair (Helleday 2011). Interestingly, NGP cells were more sensitive to growth inhibition by Rucaparib. This may be due to mutations in DNA repair components involved in homologous recombination repair, such as the *BRCA1/2* genes, however this was not investigated further as it was beyond the scope of this project.

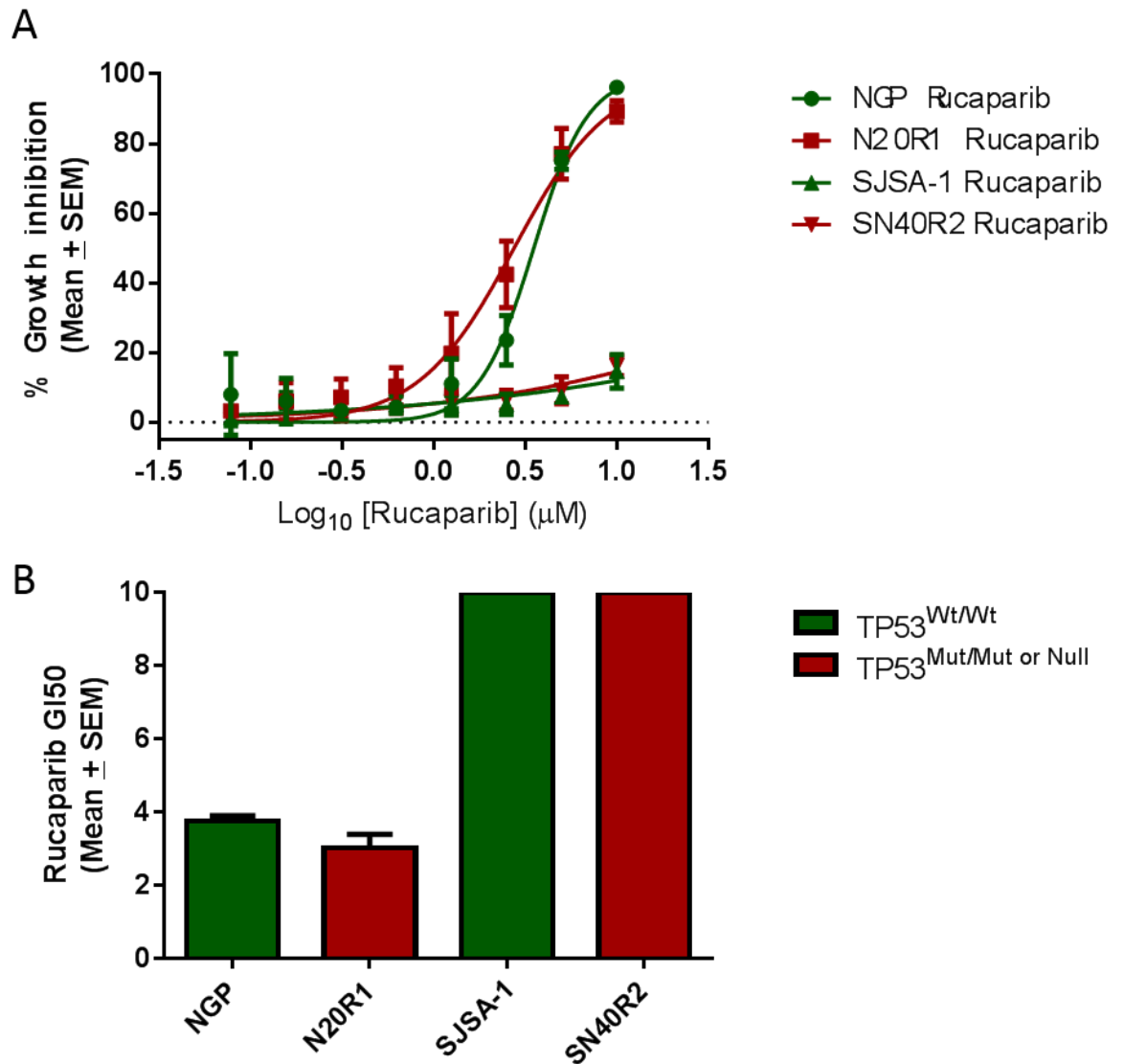


Figure 3-13 A) Week long SRB Rucaparib growth inhibition curves show that NGP cell line pair are more sensitive to PARP-1 inhibition irrespective of their *TP53* genetic status compared to the SJSA-1 cell line pair and MCF-7 cells. B) Rucaparib GI50 values in each cell line. Mean \pm SEM represent three independent repeats. Rucaparib did not reach its GI50 in SJSA-1 and SN40R2 cells there fore the bars represent GI50>10µM.

3.4.12 Non-growth inhibitory doses of Nutlin-3 potentiates the response to the combination of IR and NU7441

The maximal non-growth inhibitory dose of 1 μ M NU7441 inhibits DNA-PKcs proficiently and potentiates the response to IR in clonogenic assays (Zhao, Thomas et al. 2006). It was of interest to assess whether the highest non-growth inhibitory dose of Nutlin-3 (0.2 μ M) sensitised cells further in response to IR + 1 μ M NU7441. Cells were treated with 0.2 μ M Nutlin-3 \pm 1 μ M NU7441 4Hrs before treatment with either 2Gy or 4Gy of IR as above. Clonogenic assays were then set up after 48Hrs of exposure, which showed that combinations of 0.2 μ M Nutlin-3 and 1 μ M NU7441 significantly lowers cloning efficiency for NGP but not N20R1 cells (Figure 3-14A). When 0.2 μ M Nutlin-3 was present cloning efficiency was 3.1-fold lower ($p = 0.03$) at 2Gy and 4-fold lower ($p = 0.02$) at 4Gy following treatment with IR + NU7441 (Figure 3-14B). This suggests that when DSB repair is compromised Nutlin-3 can further sensitise NGP cell lines to a DSB inducing DNA damaging agent.

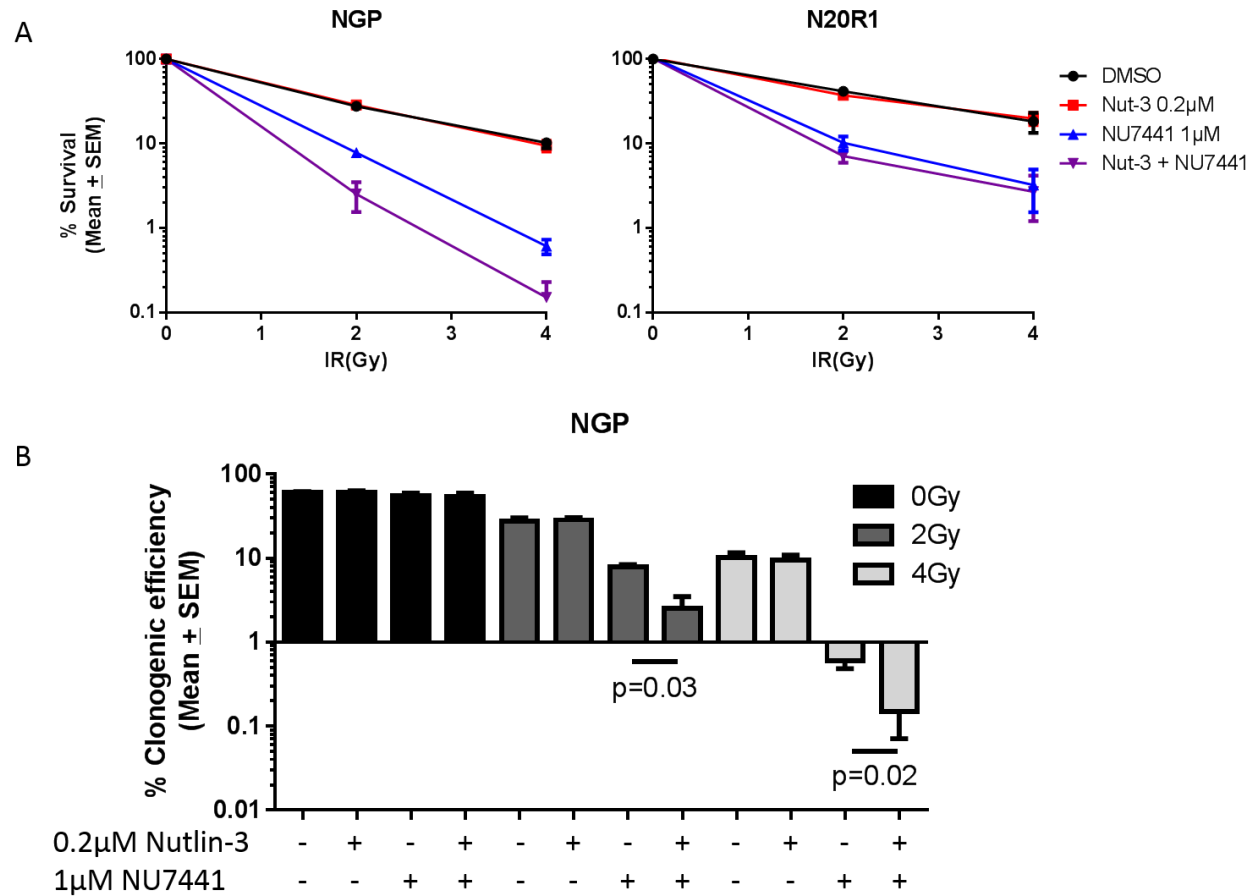


Figure 3-14 A) IR clonogenic survival curves for NGP and N20R1 cells pre-treated for four hours with 0.2µM Nutlin-3, 1µM NU7441 or their combination. Survival is presented as a % of untreated DMSO alone plating efficiency. B) Bar charts for NGP cells showing raw cloning efficiencies for each treatment condition. One-tailed paired t-tests were carried out to assess whether the differences between the treatments are statistically significant.

3.5 Discussion

3.5.1 MDM2 inhibitor resistant cell lines are not cross-resistant to IR

Our findings are consistent with wild-type *TP53* genetic status being the most important determinant of response to MDM2 inhibitors. Nutlin-3 sensitivity was markedly different in the *TP53* mutant and otherwise isogenic MDM2 inhibitor resistant clones in both growth inhibition and clonogenic survival assays. Based on growth inhibition assays there was no notable difference between NGP and SJSA-1 cells in their sensitivity to Nutlin-3. However, SJSA-1 cells were much more sensitive to clonogenic cell killing by Nutlin-3 treatment compared to NGP cells. Given that clonogenic survival assays are more suitable for distinguishing cell death from reversible cell cycle arrest, this suggests that a sub-population of NGP cells undergo reversible cell cycle arrest in response to Nutlin-3. Interestingly, there was no difference between parental cell lines and their MDM2 inhibitor resistant paired cell lines in their sensitivity to IR in both growth inhibition and clonogenic assays. In the three cell line pairs tested wild-type *TP53* genetic status was not necessary for loss of clonogenic survival following IR induced DNA damage. Induction of caspase-3 cleavage by IR observed in NGP cells was shown to be p53-dependent as cleaved caspase-3 induction following IR was markedly lower in N20R1 cells in which p53 was shown to be mutant and non-functional. In SJSA-1 and HCT116 cell line pairs however, the cell death mechanism did not appear to be caspase-dependent, as not only cleaved caspase-3 could not be detected 48Hrs following IR but also there was no evidence of a PARP-1 85kDa apoptotic fragment which is cleaved from PARP-1 by other executioner caspases (e.g. caspase-7) during apoptosis (Reviewed in (Chaitanya, Alexander et al. 2010)). However a Cathepsin dependent PARP-1 fragment associated with necrosis was detected, but it was not a strong signal and therefore its biological relevance would require further investigation. These data overall show that MDM2 inhibitor resistant *TP53* mutant clones may still be sensitive to DNA damage. Furthermore our observations emphasise the important of assessing multiple cellular and biochemical endpoints for investigation of the efficacy of treatment regimens and their mechanisms in a preclinical setting.

3.5.2 Doses of Nutlin-3 associated with on-target mechanism of action

TP53 mutant and otherwise isogenic MDM2 inhibitor resistant cell lines allow the pre-clinical determination of doses of MDM2 inhibitors associated with their on target activity. Canonical p53 transcriptional targets were not detectably induced at the protein

level 4Hrs following either IR or MDM2 inhibitor treatment in the MDM2 inhibitor resistant clonal cell lines, in contrast to their *TP53* wild-type parental cell lines. This shows that the *TP53* mutations detected in the resistant clones (SN40R2: Homozygous Glu285Lys, N20R1: Heterozygous Pro152Thr and Pro98His) have led to the loss of p53 transcriptional function following DNA damage. Although Nutlin-3 (0.2-5 μ M) did not detectably induce MDM2 in the resistant cell lines however there was a modest induction of p21^{WAF1} in SN40R2 cells which may be due to p53-independent mechanisms (Macleod, Sherry et al. 1995). These findings call into question reports of γ H2AX immunofluorescence staining following treatment with Nutlin-3 at doses >10 μ M and leads one to suspect that such observations are also due to off-target activity of MDM2 inhibitors. This would be consistent with the absence of DNA reactive groups in the chemical structure of Nutlin-3. Here we have shown that the on-target mechanism of growth inhibition and/or cell death following MDM2 inhibition relies solely on the biochemical function of wild-type p53 protein rather than DNA damage. We have also showed that γ H2AX staining was not detected following mechanistically relevant doses of Nutlin-3 within which effective growth inhibition is observed in *TP53* wild-type cell lines. In both parental *TP53* wild-type cell lines γ H2AX staining was undetected until 24Hrs following treatment. Staining at 24 hours was pan-nuclear which coincides with the timing of apoptosis during which γ H2AX immunofluorescent staining has been reported. Gamma-H2AX immunofluorescent staining was not assessed in *TP53* mutant cell lines. Furthermore reported γ H2AX staining in response to >10 μ M doses of Nutlin-3 (Verma, Rigatti et al. 2010, Valentine, Kumar et al. 2011, Rigatti, Verma et al. 2012) was not investigated. Data presented here overall emphasises the importance of appropriate dosing and scheduling when investigating and interpreting combination treatments with targeted agents, particularly MDM2 inhibitors.

3.5.3 Inhibition of DNA repair enzymes involved in double strand break repair in the absence of detectable DNA damage does not potentiate the response to MDM2 inhibitors

Pharmacological inhibition of ATM or DNA-PKcs catalytic activity did not potentiate the response to mechanistically relevant doses of single agent Nutlin-3. This is a testament to the non-genotoxic mechanism of action of MDM2 inhibitors in inhibiting the growth and survival of *TP53* wild-type cell lines. Inhibition of these enzymes is established to result in potentiation of DSB inducing DNA damaging agents (Hickson, Zhao et al. 2004, Leahy, Golding et al. 2004, Zhao, Thomas et al. 2006). Interestingly,

the inhibition of ATM or DNA-PKcs combined with Nutlin-3 >10 μ M appeared to result in a slight increase in growth inhibition in *TP53* mutant MDM2 inhibitor resistant cell lines, although this was not quantified. The data presented in this chapter overall strongly suggests that the synthetic lethality with Nutlin-3 observed by Sullivan *et al.*, (2012 & 2014) in response to ATM inhibition is likely due to off-target secondary DNA damage induced by Nutlin-3 rather than the non-genotoxic mechanisms proposed by the authors.

3.5.4 Inhibition of DNA-PKcs did not alter p53 transcriptional function following Nutlin-3

When cells were treated simultaneously with Nutlin-3 and NU7441 there was no difference in the induction of p53 transcriptional targets at 4Hrs. This was consistent with DNA-PKcs inhibition not affecting cellular sensitivity to Nutlin-3. However, there was a notable reduction in p53^{Ser15} phosphorylation in NGP cells when DNA-PK was inhibited showing that DNA-PKcs may be involved in this phosphorylation event. Phosphorylation of p53 at this residue is widely deemed a marker of DNA damage and it was reportedly not detected following Nutlin-1, which was used by the authors to claim a non-genotoxic mechanism of action for these compounds (Vassilev, Vu *et al.* 2004). Phosphorylation of p53^{Ser15} following MDM2 inhibitors has been reported since, suggesting the possibility that there may be a secondary genotoxic element to the mechanism of action of MDM2 inhibitors. However, given the evidence presented above, this observation is more likely to be explained by the basal activity of kinases and phosphatases targeting this residue following the non-genotoxic unmasking of the p53 N-terminus from MDM2 by the MDM2 inhibitor. Overwhelming evidence in the literature suggests that this phosphorylation activates p53 (Meek and Anderson 2009). Therefore it would be of interest to assess whether non-genotoxic manipulation of the p53 phosphorylation status following MDM2 inhibitor treatment affects p53 biochemical function and consequently cellular sensitivity to MDM2 inhibitors.

3.5.5 Sensitivity to DNA damage in the presence of Nutlin-3 is context-dependent.

The Nutlin-3 SRB growth inhibition experiments showed that NGP cells were made more sensitive to the effect of Nutlin-3 in the presence of IR in a p53-dependent manner which was then enhanced in the presence of NU7441. IR had a small p53-dependent protective effect on SJSA-1 cells from growth inhibition by Nutlin-3 \pm 1 μ M NU7441. These findings suggest that the effect of a DNA damage signal on the sensitivity to

Nutlin-3 is context-dependent. NGP cells had a larger sub-population of cells that appeared to undergo reversible cell cycle arrest following Nutlin-3 treatment in clonogenic assays compared to SJSA-1 cells. The additional growth inhibition observed with the NGP cells using SRB assays were then mirrored in NGP cells by clonogenic assays. Interestingly, the presence of a non-growth inhibitory dose of Nutlin-3 (0.2 μ M) significantly reduced clonogenic survival following IR only in the presence of the DNA-PKcs inhibitor NU7441. This was not observed with *TP53* mutant N20R1 cells. This shows that MDM2 inhibition increases the sensitivity of NGP cells to IR only when DNA-PKcs is functional.

3.5.6 Summary

The data presented in this chapter is consistent with wild-type genetic status of *TP53* being the strongest determinant of response to MDM2 inhibitors. There is a difference sensitivity to MDM2 inhibitors when comparing matched *TP53* wild-type and mutant cell lines, however substantial differences in response can also be seen between wild-type *TP53* cell lines, such as when comparing the clonogenic response of SJSA-1 and NGP cells. This indicates that there are other determinants of response to MDM2 inhibitors that although secondary to wild-type *TP53* status are nevertheless likely to be important in a therapeutic context.

Given that mutations in the MDM2 inhibitor resistant clones result in loss of transcriptional activity of p53, this functional aspect of p53, must also be important in determining MDM2 inhibitor sensitivity in *TP53* wild-type cell lines. Therefore, modulating p53 transcriptional function by influencing its post-translational modification through combination treatments should be considered for harnessing the full potential of MDM2 inhibitors. Genotoxic agents can be used to activate kinases involved in DNA repair such as ATM and DNA-PKcs to increase activating post-translational signalling to p53, however a non-genotoxic targeted approach would be ideal. Indeed p53^{Ser15} phosphorylation which is important for p53 transcriptional transactivation is detectable following non-genotoxic activation of p53 by relevant doses of Nutlin-3, albeit to a lesser extent compared to that induced by IR. Therefore, non-genotoxic inhibition of phosphatases that lead to an increase in the active phosphorylation status of p53 may result in increased sensitivity to MDM2 inhibitors. This strategy will be explored in Chapters 4-6.

**Chapter 4 WIP1/PPM1D transient siRNA mediated knockdown
enhances cellular sensitivity to Nutlin-3**

4.1 Introduction

The human kinome and its role in the regulation of p53 stability and function has been extensively investigated in contrast to the phosphatome (Meek and Anderson 2009, Donehower 2014). Kinases directly involved in phosphorylation of p53 in response to DNA damage promote p53 stability and activity (Appella and Anderson 2001, Meek and Anderson 2009). Therefore, inhibiting phosphatases that dephosphorylate the same residues might enhance p53 activity following treatment with MDM2 inhibitors. Given the importance of *PPM1D* oncogene product WIP1 phosphatase in homeostatic regulation of the p53 network and its cross-talk with stress response pathways (Lowe, Cha et al. 2012), the role of this phosphatase in determining sensitivity to MDM2 inhibitors was investigated.

4.1.1 The WIP1/PPM1D phosphatase as a modulator of p53 crosstalk with DNA damage and stress response pathways

Wild-type p53-inducible phosphatase-1 or protein phosphatase Mg²⁺/Mn²⁺ dependent 1δ (WIP1/PPM1D) is a member of the PP2C (PPM) family of phosphatases and it has been reported to be involved in homeostatic regulation of p53 and its crosstalk with stress response (Fuku, Semba et al. 2007, Lu, Ma et al. 2007, Castellino, De Bortoli et al. 2008, Lowe, Cha et al. 2012). Italicised '*PPM1D*' will be used to denote the gene and 'WIP1' will be used to denote the protein product hereafter. *PPM1D* is a *bona fide* oncogene which is gained/amplified or overexpressed mostly in *TP53* wild-type malignancies (Bulavin, Demidov et al. 2002, Ruark, Snape et al. 2013, Zhang, Chen et al. 2014). *PPM1D*-amplification occurs in approximately 11% of primary breast tumours, among which *TP53* mutations are rare events (Bulavin, Demidov et al. 2002, Rauta, Alarmo et al. 2006). Interestingly, *PPM1D* gain-of-function mutations and *TP53* inactivating mutations are mutually exclusive in brainstem gliomas, which is consistent with the role of WIP1 as a negative regulator of p53 tumour suppressor activity (Zhang, Chen et al. 2014). Multiple studies have shown that WIP1 knockdown result in growth inhibition and loss of survival in cell lines that rely on this phosphatase for negative regulation of their wild-type p53 activity (Tan, Lambros et al. 2009, Buss, Read et al. 2012, Choi, Shi et al. 2012, Zhang, Chen et al. 2014, Zhang, Sun et al. 2014).

WIP1 is induced in a p53-dependent manner, forming a negative auto-modulatory loop by dephosphorylating p53 and other DNA damage and stress signalling components involved in activating the p53 network (Figure 1-10) (Fiscella, Zhang et al. 1997, Lu,

Ma et al. 2007, Lu, Nguyen et al. 2008, Donehower 2014). Direct and indirect WIP1 phosphatase activity results in hypophosphorylation of p53, which reduces its stability and transcriptional activity, allowing the reversal of cell cycle arrest (Donehower 2014). Phosphorylation of p53^{Ser15} is considered a key event in the sequence of post-translational modifications of p53 following DNA damage that results in enhanced p53 stability and activity. Phosphorylated p53^{Ser15} detected following Nutlin-3 is weaker and takes longer to appear compared to that observed after exposure to DNA damaging agents (Loughery, Cox et al. 2014). It has been suggested that this low level phosphorylation following MDM2 inhibitor treatment is due to the basal activity of ATM and ATR, which target that residue on p53 decoupling from MDM2 (Loughery, Cox et al. 2014). Since phosphorylated p53^{Ser15} is also a WIP1 phosphatase substrate, it is of interest to investigate whether knockdown of WIP1 expression enhances the response to MDM2 inhibitors.

4.1.2 WIP1 as a determinant of response to MDM2 inhibitors

In silico modelling of the p53 network and its negative autoregulatory loops has highlighted WIP1 as a critical component determining cell fate following p53 activation and predicted that a combination of WIP1 inhibition and Nutlin-3 would be synergistic by promoting apoptosis (Choi, Shi et al. 2012). In another study combination of WIP1 inhibition by CCT007093 and MDM2 by Nutlin-3a was shown to be more effective at inhibiting growth in a stably transfected *PPM1D*-overexpressing *TP53* wild-type medulloblastoma clone of D556 cells (D556-WIP1) and not a *TP53* mutant *PPM1D*-overexpressing clone of Daoy cells (Buss, Read et al. 2012). However, the Daoy and D556-WIP1 cell lines are not an isogenic or closely related *TP53* mutant pair in which Nutlin-3 mediated p53-dependent cellular endpoints can be compared with confidence. The response of D556-WIP1 to Nutlin-3a was also compared to D556 with an empty vector (D556-pcDNA3) or the vector overexpressing a phosphatase dead variant of WIP1 protein (D556-D314A). Although these clones were deemed to be otherwise isogenic to D556-WIP1, the authors did not note that they were insensitive to single agent treatment with Nutlin-3a (8µM) (See (Buss, Read et al. 2012) Figure 5D). This suggests that these clones are likely *TP53* mutant and therefore not appropriate for comparing with the on-target activity of Nutlin-3a in the parental cell line (Buss, Read et al. 2012). Therefore, more thorough investigation into the role of WIP1 as a determinant of response to MDM2 inhibitors is needed. In this chapter *TP53* wild-type and mutant isogenic pairs that differ in their *PPM1D* status, including the gain-of-

function mutation of *PPM1D* (Kleiblova, Shaltiel et al. 2013) have been used to further investigate this question.

4.1.3 Summary

Consistent with prior findings, in the previous chapter it was shown that pp53^{Ser15} is detected following treatment with Nutlin-3. Furthermore, this phosphorylation was observed over a non-genotoxic dose range of Nutlin-3 which could activate p53 efficiently and lead to growth inhibition and reduced clonogenic survival. The phosphorylation of p53^{Ser15} reportedly increases p53 transcriptional activity and it is considered a “nucleation event” for other activating p53 post-translational modifications (Meek and Anderson 2009, Loughery, Cox et al. 2014). Therefore, the modulation of this particular post-translational modification event is of particular interest. WIP1 has been shown to dephosphorylate p53^{Ser15} directly and it is also likely to be involved in the homeostatic regulation of the p53 network following MDM2 inhibition and re-entry from reversible cell cycle arrest (Lu, Nannenga et al. 2005, Donehower 2014). The role of WIP1 in homeostatic regulation of Nutlin-3 induced p53 signalling and cell fate determination has not been adequately investigated in *TP53* wild-type and mutant isogenic cell lines pairs with different *PPM1D* genetic status. In this chapter experiments with a panel of *TP53* wild-type and mutant cell line pairs with different *PPM1D* genetic status are presented, which critically assess the role of WIP1 in determining the cellular and functional response to MDM2 inhibitors.

4.2 Hypothesis

- WIP1/PPM1D siRNA mediated knockdown sensitises cells to Nutlin-3 in a p53-dependent manner.

4.3 Specific materials and methods

4.3.1 Cell lines

TP53 wild-type and mutant/null otherwise isogenic cell line pairs, differing in their *PPM1D* genetic status, were used in this study to investigate p53-dependent and independent processes in differing *PPM1D* genetic and functional backgrounds (Table 4-1). The HCT116 and U2OS cell line pairs harboured *PPM1D* truncating activating mutations (Kleiblova, Shaltiel et al. 2013). The U2OS-DN cells constitutively overexpress a transfected dominant-negative mutant of p53 (R175H) and have no p53 functional activity.

<i>TP53</i> Wild-type parental cell lines	<i>TP53</i> mutant/Null pair	Tumour of origin	<i>PPM1D</i> genetic alteration
SJSA-1	SN40R2	Osteosarcoma	Wild-type (COSMIC (Forbes, Beare et al. 2015))
HCT116+/+	HCT116-/-	Colorectal carcinoma	c.1344delT/Wt (L450X) Gain-of-function (Kleiblova, Shaltiel et al. 2013)
U2OS	U2OS-DN	Osteosarcoma	c.1372C>T/Wt (R458X) Gain-of-function (Kleiblova, Shaltiel et al. 2013)
NGP	N20R1	Neuroblastoma	Copy number gain (Richter, Dayaram et al. 2015)
MCF-7	–	Breast adenocarcinoma	Amplified (Castellino, De Bortoli et al. 2008)

Table 4-1. *TP53* Wild-type (Wt) and mutant (Mt)/Null cell line pairs with different *PPM1D* status.

4.3.2 Monitoring cell morphology, growth and proliferation using IncuCyte

Zoom®

IncuCyte Zoom® consists of a microscope gantry which can be placed in a cell incubator. With the use of robotics phase contrast images of cells are captured from fixed coordinates on the flask, without perturbing the culture, and the data are recorded on a networked external controller hard drive for further analysis. Images were

presented as time-lapse videos for qualitative assessment or in the graphical format by analysing cell confluence in all individual images captured over time, using IncuCyte Zoom® software package. Data presented in this chapter were acquired by 10 × phase contrast microscope time lapse images acquired automatically every 6 hours using IncuCyte Zoom® throughout the experiment. Image processing parameters were optimised for each cell line before use to account for shape and size (see IncuCyte™ ZOOM User Manual) to enable the calculation of percentage confluence over time in response to treatment. Each data-point corresponds to an average % confluence calculated from 9 images/well of a 24-well plate.

4.3.2.1 Treatment schedule

Cell line pairs were seeded in 24-well plates, at the densities stated in Table 4-2, and placed on the microscope gantry of IncuCyte Zoom® 16-24 hours before the plates were removed again and a scaled down version of the siRNA transfection protocol as described in section 2.7.2 was carried out in the appropriate wells. Plates were then immediately placed back in IncuCyte 24 hours before addition of either DMSO (1%) or 5µM Nutlin-3. Nutlin-3/DMSO were added directly to the media in each well so that the cells are not perturbed. The plates were placed back in IncuCyte immediately for another 120 hours image capture. High definition images allowed closer observation of changes such as those associated with differentiation, cell division, nuclear fragmentation and large cellular compartments.

Cell line pair	Densities (Cells/well)
NGP	6×10^4
HCT116	1×10^4
SJSA-1	4×10^4

Table 4-2 Seeding densities used in 24 well plates for the incucyte experiment.

4.3.3 WIP1/PPM1D siRNA mediated knockdown

For lysate collection and flow cytometry, cells were seeded at 6×10^5 cells/well of a 6-well plate (Corning) and allowed to adhere for 24hrs (60-70% confluence) before they underwent transfection with WIP1/PPM1D siRNA constructs and Lipofectamine 2000™ transfection reagent (Invitrogen) complex as described in materials and methods (2.7). Transfection conditions resulted in marked reduction in confluence and adherence of the cells if the media was aspirated to add fresh media containing drug. During assessment of cell cycle distribution by flow cytometry, or for lysate preparation, solvent/drug was added directly to the media and any floating cells were pooled with attached cells before the next step.

4.3.3.1 The effect of transient knockdown and drug combination treatment on cell proliferation and morphology assessed by IncuCyte Zoom®

For the IncuCyte experiments, siRNA mediated knockdown of WIP1/PPM1D was performed in 24-well plates (Corning) for monitoring of cell confluence using different starting cell plating densities and WIP1 expression was assessed in parallel to ensure a successful WIP1 knockdown. HCT116, SJSA-1 and NGP cell lines and their respective *TP53* mutant/null pairs were seeded at, 10^4 , 4×10^4 and 6×10^4 cells/well, and allowed to adhere for 16-24Hrs and then underwent transfection with WIP1.2 siRNA as described earlier (2.7). 24 hours following the transfection, DMSO or stated doses of Nutlin-3 were added directly to the media in order not to disturb the cells and then the cells were monitored by IncuCyte® for the remainder of the experiment.

4.3.4 WIP1 targeting siRNA and antibody optimisation

PPM1D-amplified MCF-7 cells were used to optimise WIP1 antibodies and siRNA constructs. Initially two WIP1 antibodies, namely the rabbit polyclonal antibody (H-300) and the mouse monoclonal WIP1 antibody (F-10) purchased from Santa Cruz Biotechnology, were evaluated for western blotting. Both antibodies resulted in up to 4 distinct bands in MCF-7 cell lysates derived from untreated or irradiated (10Gy, 4Hrs time-point) cells. To determine the band corresponding to WIP1 four siRNA constructs (WIP1.1-4) were designed to target full-length WIP1 transcript and the alternatively spliced but functional shorter isoform (1.15.1) (Figure 4-1). WIP1.1-3 were designed by Eurogentec and the sequence for WIP1.4 was obtained from the literature (Fujimoto, Onishi et al. 2005). Knockdown of basal WIP1 protein expression was small regardless of siRNA dose or time of exposure (Figure 4-2) therefore we decided to assess the

ability of our siRNA constructs to suppress WIP1 induction and hence WIP1 phosphatase activity in response to 10Gy ionising radiation (IR) (Figure 4-3). This resulted in 3 out of 4 constructs (WIP1.1, WIP1.2 and WIP1.4) leading to a suppression of band intensity detected by the WIP1 antibody at the anticipated molecular weight and reduced phosphatase activity as measured by increased pp53^{Ser15} band intensity 4Hrs post 10Gy IR. The bands that were commonly detected by both antibodies and those that were consistently diminished in intensity in response to the siRNA were deemed to correspond to full length WIP1/PPM1D605 (\approx 85-90KD) and its shorter isoform (WIP1/PPM1D430 \approx 65-70KDa) (1.15.1) or other unknown isoforms/potential WIP1 breakdown products (<60KDa). Bands that were detected by only one antibody and/or those that did not change in response to any of the siRNA constructs were considered to be non-specific. For example the band detected by WIP1 H-300 at \approx 50KDa was assumed to be nonspecific. A 25nM concentration of WIP1 siRNA construct 1.2 (WIP1.2) was chosen for all subsequent knockdown experiments as it lead to the longest duration of WIP1 knockdown and reduction in phosphatase activity as measured by increased p53^{Ser15} phosphorylation (Figure 4-3). Also F-10 was chosen as the optimal antibody for detection of WIP1.

ATGGCGGGGCTGTACTCGCTGGGAGTGAGCGTCTTCTCCGACCAGGGCGGGAGGAAGTACATGGAGGACGTTACT
 CAAATCGTTGTGGAGCCCGAACCGACGGCTGAAGAAAAGCCCTCGCCGCGGGCGGTTCGTGTCTCAGCCGTTGCCT
 CCGCGGCGGTTCGCGGGCCCGCCTTCCCGGGCGGGAAGTCTCGGGGAAAGGCCAGCGGTGGCAGCCCCGAGAGGCT
 CGCGACCCTCTCCCGGACGCCGGGGCCTCGCCGGCACCTAGCCGCTGCTGCCGCCGCCGTTCTCCGTGGCCTTT
 TTCGCCGTGTGCGACGGGCACGGCGGGCGGGAGGCGGCACAGTTTGCCCGGAGCATTGTGGGGTTTCATCAAG
 AAGCAGAAGGGTTTACCTCGTCCGAGCCGGCTAAGGTTTGGCGTGCCATCCGCAAAGGCTTTCGCTTGTGCAC
 CTTGCCATGTGGAAGAACTGGCGGAATGGCCAAAGACTATGACGGGTCTTCTAGCACATCAGGGACAAGTCC
 AGTGTGGTCATCATTCGGGGCATGAAGATGTATGTAGCTCACGTAGGTGACTCAGGGGTGGTTCTTGGAAATTCAG
 GATGACCCGAAGGATGACTTTGTGAGAGCTGTGGAGGTGACACAGGACCATAAGCCAGAAGTCCCAAGGAAAGA
 GAACGAATCGAAGGACTTGGTGGGAGTGAATGAACAAGTCTGGGGTGAATCGTGTAGTTTGGAAACGACCTCGA
 CTCACTCACAATGGACCTGTTAGAAGGAGCACAGTTATTGACCAGATTCTTTTTCTGGCAGTAGCAAGAGCACTT
 GGTGATTTGTGGAGCTATGATTTCTTCAGTGGTGAATTTGTGGTGTACCTGAACCAGACACAAGTCCACACT
 CTTGACCCCTCAGAAGCACAAGTATATTATATTGGGGAGTGTGGACTTTGGAATATGATTCACCACAAGATGCC
 ATCTCAATGTGCCAGGACCAAGAGGAGAAAAAATACCTGATGGGTGAGCATGGACAATCTTGTGCCAAAAATGCTT
 GTGAATCGAGCATTGGGCCGCTGGAGGCAGCGTATGCTCCGAGCAGATAAACACTA (1) GTGCCATAGTAATCTG
 CATCTCTCCAGAAGTGGACAAACCAATGAAGATGAGTTATACCTGAACCTGACTGACA (3)
 GCCCTTCCTATAATAGTCAAGAACTGGTGTGATGACTCCTTCCCATGTTCTACACCACCAGTCAAGgattttg
 gatttgaactcgattcaagaaagtgatgtaacttattatcagagagccatctttacatcaataactaatctgaatg
 ccagccatgtgtacagcactaataaaaagTCACTGGAGGAGGATCCATGGCCAAGGGTGAATTCTAAGGACCATA
 TACCTGCCCTGGTTTCGTAGCAATGCCTTCTCAGAGAATTTTTTAGAGGTTTCAGCTGAGATAGCTCGAGAGAATG
 TCCAA (2) GGTGTAGTCATACCCTCAAAGATCCAGAACCCTTGAAGAAAATTGCGCTAAAGCCCTGACTTTA
 AGGATACATGATTCTTTGAATAATAGCCTTCCAA (4) TTGGCCTTGTGCCTACTAAATTCACAAACACTGTGCAT
 GGACCAAAAAAATTTGAAGATGTCAACTCCTGGCCAAATGAAAGCCCAAGAAATTGAAAGAACCCTCCAAACAAA
 CTTTAAAAGGACATTAGAAGAGTCCAATTCGGCCCCCTGATGAAGAAGCATAGACGAAATGGCTTAAGTCGAAG
 TAGTGGTGTCTCAGCCTGCAAGTCTCCCCACAACCTCACAGCGAAAGAACTCTGTTAAACTCACCATGCGACGCAG
 ACTTAGGGGCCAGAAGAAAATTGGAAATCCTTTACTTCATCAACACAGGAAAAGTGTGTGTTTGTCTGA

Stop codon

Figure 4-1 Positions and sequences of WIP1 siRNA constructs 1-4 are highlighted in yellow over the WIP1 reference sequence obtained from the UCSC genome browser. The sequence in dark blue encodes full length WIP1, pale blue letters indicate the exon-exon boundaries and the sequence in red outlines the retained alternatively spliced exon which leads to a premature stop codon in spite of a longer transcript.

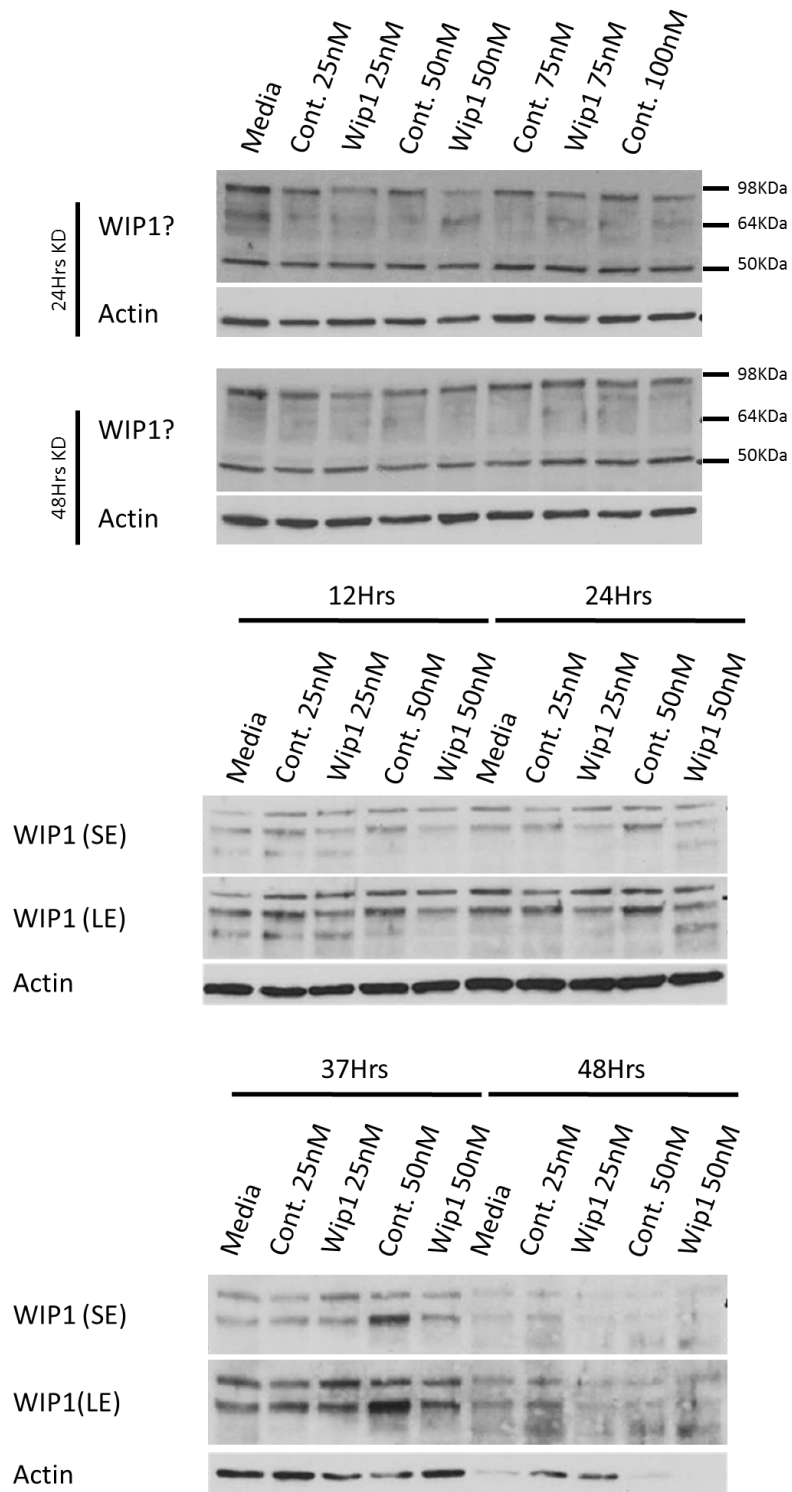


Figure 4-2 An increment of WIP1.4 siRNA concentration (25nM-100nM), the sequence for which had previously been defined and used in the literature, was examined to optimise WIP1 protein knockdown conditions at different time-points post transfection. WIP1.4 did not result in a notable dose- or time-dependent knockdown of basal WIP1 protein levels in MCF-7 cells.

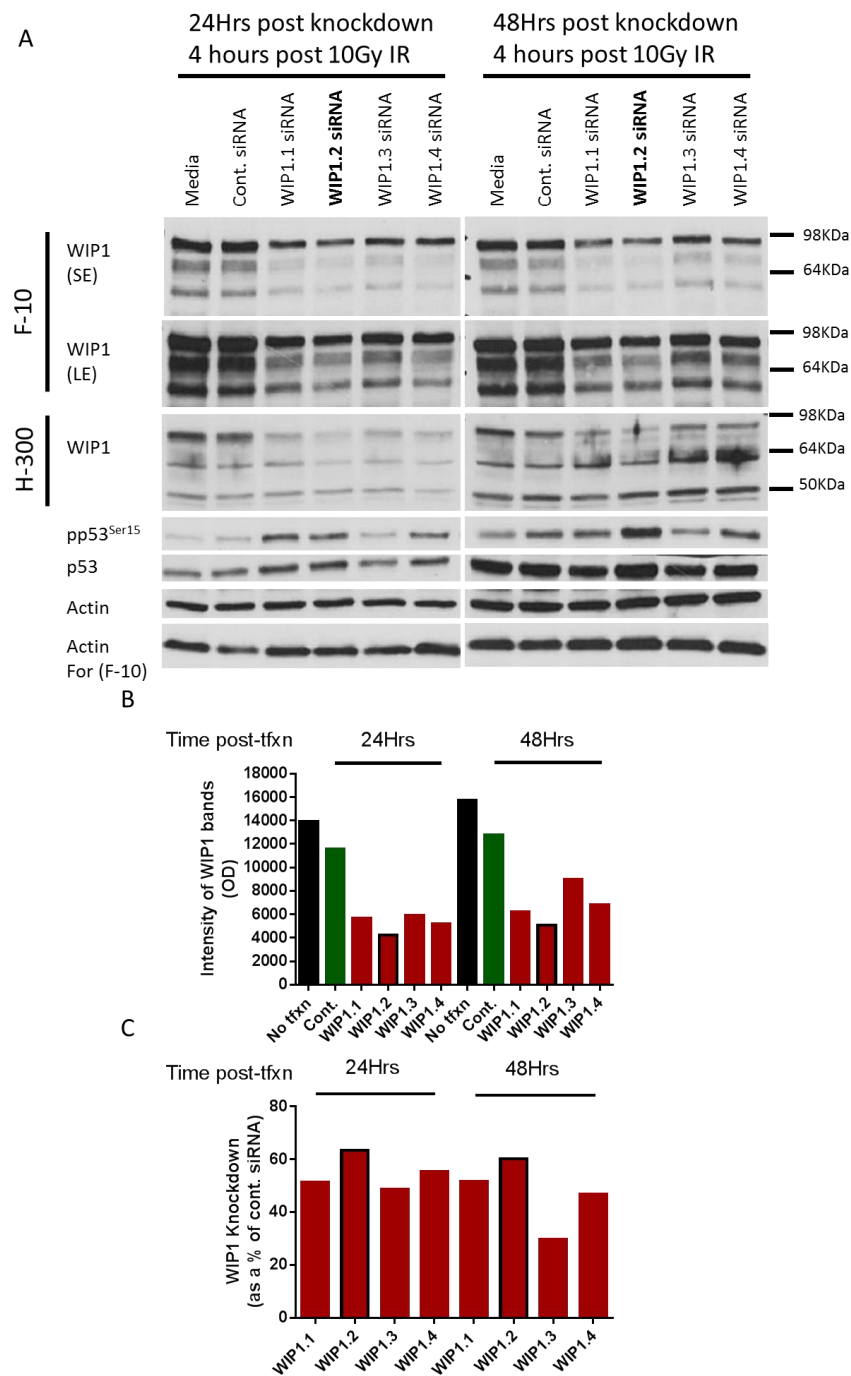


Figure 4-3 A) Optimisation of WIP1 antibody and siRNA mediated knockdown in MCF-7 cells. Following 24 and 48Hrs of siRNA mediated knockdown conditions, MCF-7 cells were treated with 10Gy IR and lysates were collected 4Hrs later for western blot analysis. Two antibodies were used to probe for WIP1 (F-10 and H-300). B) The optical densities (OD) of bands detected by F-10 were measured to quantify the extent of WIP1 knockdown and select the most effective siRNA construct. C) WIP1 knockdown was expressed as a % of WIP1 OD in the control (Cont. siRNA) treated samples and was approximately 60% with the WIP1.2 construct. SE: Short Film Exposure; LE: Long film exposure; tfxn: transfection

4.3.5 Clonogenic survival in response to drug-siRNA combination treatments

Clonogenic cell survival was investigated in NGP and its daughter cell line N20R1 cells. The NGP cell line pair were seeded in 6-well plates at 6×10^5 cells/well and treated with Control or WIP1.2 siRNA constructs for 24 hours, as described earlier, then incubated with multiples of Nutlin-3 LC50 doses for the NGP parental cell line (previously calculated to be $1.3\mu\text{M}$) for a further 48 hours (See table 6.5) After Nutlin-3 treatment cells were harvested, counted with a coulter counter and diluted to two densities (1×10^4 cells/ml & 1×10^3 cells/ml) in order to seed the appropriate cell numbers in 100mm tissue culture dishes (Corning) containing 7.5ml growth media. The cell seeding number and Nutlin-3 doses for each well are listed in (Table 4-3). The cells were then allowed to form colonies over 2 weeks, after which they were fixed with Carnoy's fixative and stained with 0.4% crystal violate. Visible colonies (>50 cells) were counted and expressed as a percentage of colony survival relative to DMSO control.

	DMSO	0.026 μM	0.13μM	0.65μM	1.3μM
NT	500	1000	1000	1000	1000
Control siRNA	5000	5000	5000	5000	5000/10000
WIP1.2 siRNA	5000	5000	5000	5000	5000/10000

Table 4-3 Doses of Nutlin-3 and seeding densities for NGP and N20R1 cell lines in 100mm dishes. NT: Non transfected

4.3.6 FACS analysis of cells treated with MDM2 inhibitor and WIP1 siRNA combinations

FACS analysis was carried out as described in general materials and methods (2.6) to analyse cell cycle distribution changes and apoptosis associated with drug induced growth arrest and cell death over 72 hours following drug exposure. Cells were seeded 24 hours before transfection and allowed to adhere. DMSO/Nutlin-3 were added to the wells 24 hours following initiation of siRNA transfection in the NGP cell line pair and cells were harvested after 48 hours of drug treatment. Drug treatment in siRNA knockdown experiments was carried out without aspirating or disturbing the culture in order not to lose the floating cell population. Western blots were carried out at least once in parallel with the FACS experiment to ensure efficient knockdown of WIP1 and silencing of its phosphatase activity had been achieved. Suspension and adherent cells in all wells were pooled before being prepared for FACS analysis.

4.3.7 Statistical analysis

The significance of differences between mean values was calculated by comparing the mean of 3 or more paired biological repeats using a paired t-test and p-values <0.05 were considered statistically significant.

4.4 Results

4.4.1 WIP1 basal protein expression and induction by Nutlin-3 among selected cell line pairs with varying *PPM1D* genetic status

TP53 wild-type and mutant cell line pairs with different *PPM1D* genetic status (outlined in Table 4-1) were assessed for basal WIP1 expression and induction following treatment with Nutlin-3. Lysates were obtained from exponentially growing cell lines (60-70% confluent cultures) and analysed by western blotting to assess basal WIP1 and p53 expression. Basal WIP1 expression was independent of *TP53* genetic status as there was no difference between the *TP53* wild-type cell lines and their respective mutant/null daughter lines (Figure 4-4A & B). Both isoforms of WIP1 showed the greatest basal protein expression as previously reported for the *PPM1D*-amplified MCF-7 cells (Li, Yang et al. 2002). The NGP cell line pair expressed the second highest level of full-length WIP1 which was consistent with their *PPM1D* copy number gain (Richter, Dayaram et al. 2015). Also consistent with previous reports HCT116 and U2OS cell line pairs harbouring *PPM1D/WIP1 L450X* and *PPM1D/WIP1 R458X* variants showed intense bands at a lower molecular weight assumed to be associated with lower molecular weight WIP1 isoforms (Kleiblova, Shaltiel et al. 2013). The SJSA-1 pair showed the lowest expression of full-length WIP1, as expected for the only *PPM1D* wild-type cell line pair (cancer.sanger.ac.uk and (Forbes, Beare et al. 2015)).

The protein products of well-established transcriptional targets of p53 namely WIP1, MDM2, p21^{WAF1} and BAX were analysed by western blotting 4Hrs following treatment with DMSO or 5.0µM Nutlin-3 (Figure 4-4). *PPM1D*-amplified MCF-7 cells showed the greatest Nutlin-3 mediated dose-dependent induction of WIP1 compared to NGP and SJSA-1 cells (Figure 4-4B to Figure 4-6). WIP1 induction appeared to be very weak in response to Nutlin-3 in all cell lines other than MCF-7. Slight WIP1 induction was also observed in *TP53* mutant/null daughter cell lines, which is consistent with *PPM1D* also showing some degree of transcriptional regulation through p53-independent mechanisms (Lowe, Cha et al. 2012) (Figure 4-4B). Nutlin-3 mediated MDM2 and p21^{WAF1} induction were greater in *TP53* wild-type cell lines out of each cell line pair, apart from NGP and N20R1 cell lines where MDM2 and p21^{WAF1} induction were not detected at this time-point and dose of Nutlin-3 in neither cell line (Figure 4-4B). BAX induction was also not detected at this time-point or Nutlin-3 dose in any of the cell lines other than MCF-7 cells (Figure 4-4B).

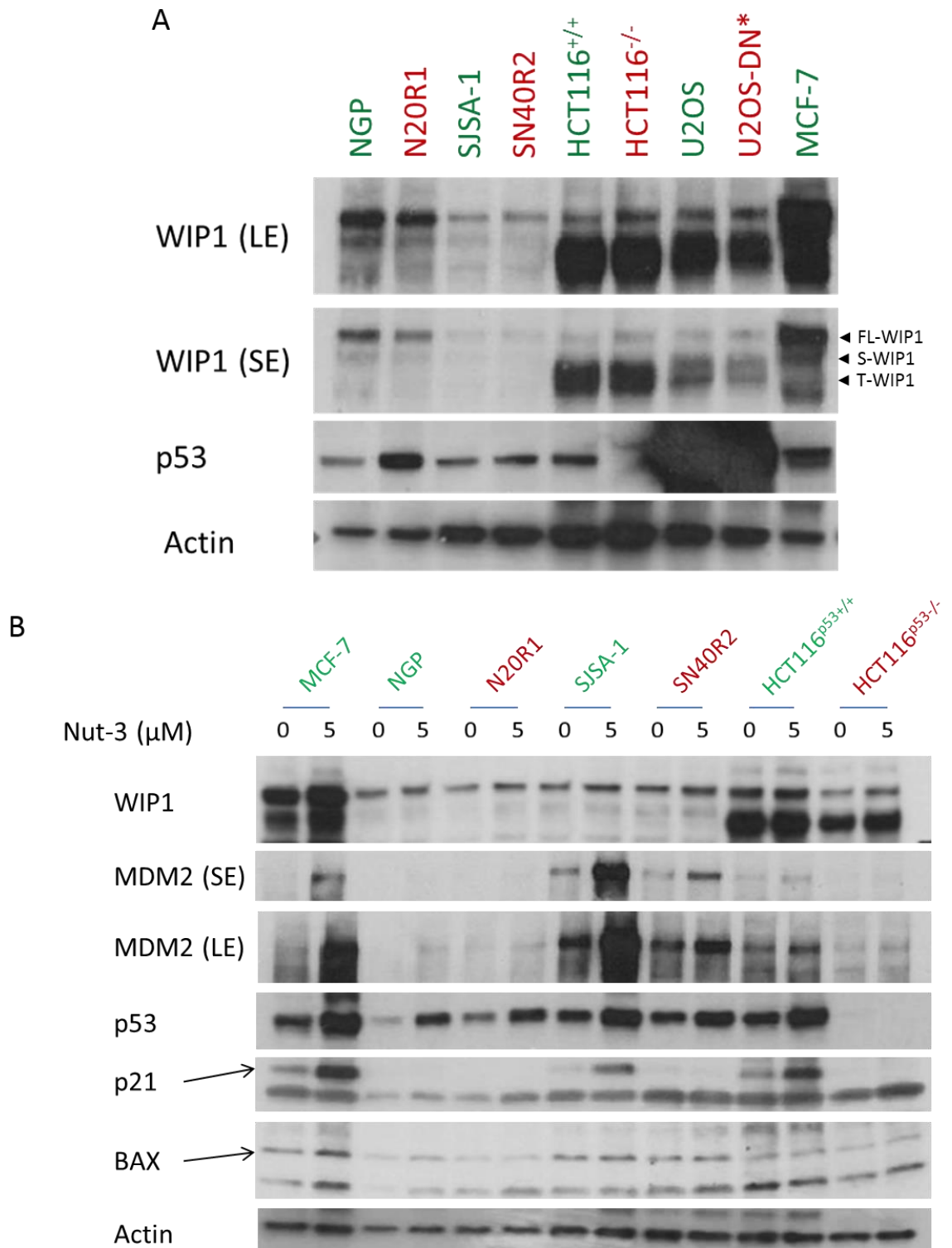


Figure 4-4 A) Basal WIP1 expression of *TP53* wild-type (green) and mutnat/null (Red) cell line pairs. B) Induction of p53 targets, such as WIP1, MDM2, p21^{WAF1} and BAX, after 4Hrs 5μM Nutlin-3 treatment (Nut-3). Different duration of exposure of the X-ray film to the nitrocellulose membrane corresponding to each protein are denoted either as SE: Short exposure or LE: Long exposure. Arrows point to the band at the expected molecular weight for that given protein. FL-WIP1: Full length WIP1; S-WIP1 shorter WIP1 isoform ; T-WIP1: Truncated WIP1 isoform. B was carried out by supervised M.Res student Mrs Liang Zhao.

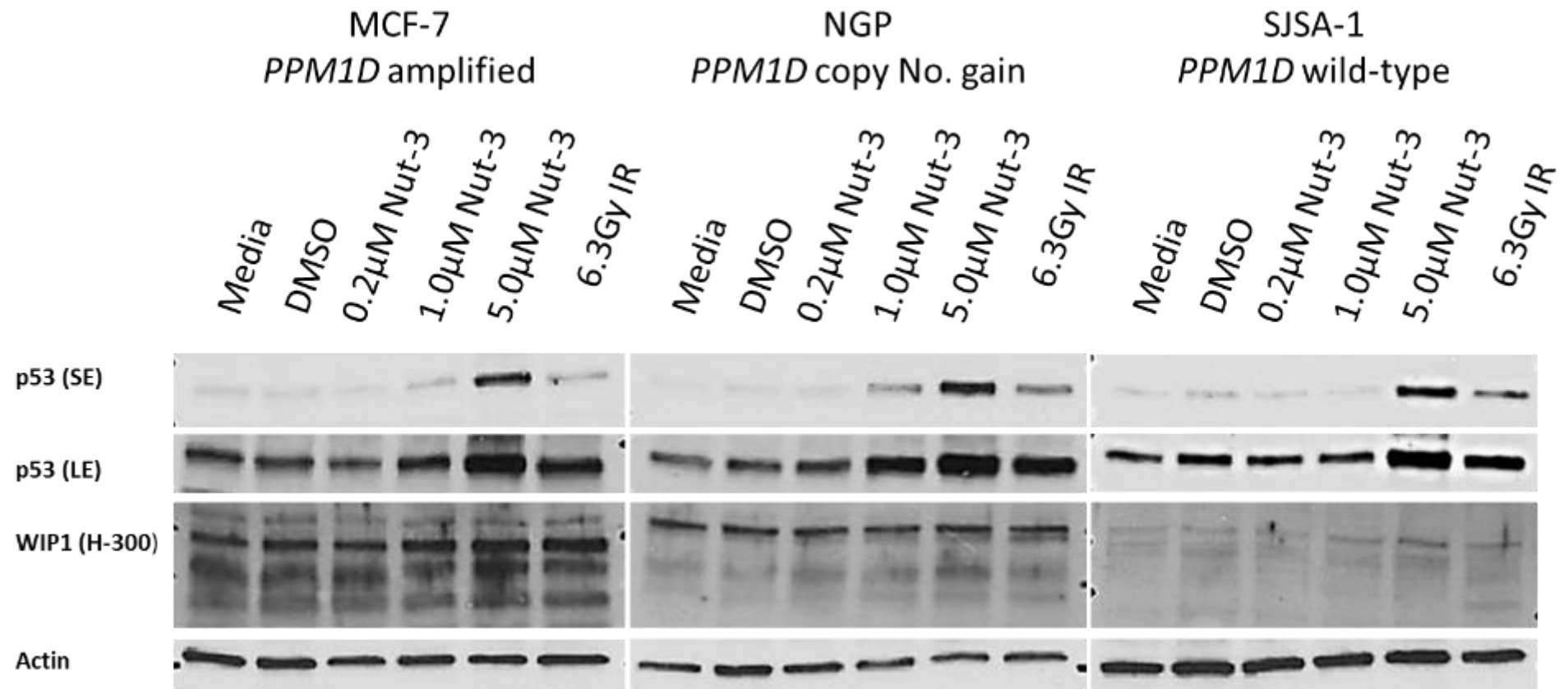


Figure 4-5 Dose-dependent response to Nutlin-3 treatment in *TP53* wild-type cell lines with different *PPM1D* status. The anti-WIP1 antibody H-300 was used for these blots. SE: Short exposure; LE: Long exposure

4.4.2 Biochemical response to MDM2 inhibition combined with WIP1 transient siRNA knockdown

To assess whether siRNA mediated transient knockdown of *PPM1D* sensitises *TP53* wild-type cell lines to MDM2 inhibitors, 4 siRNA constructs (WIP1.1-4) were designed and optimised to target WIP1 and its shorter isoform as described in 4.3.4. WIP1.2 siRNA construct was chosen for all subsequent experiments as it resulted in the most robust WIP1 knockdown (~50-60%) and increase in pp53^{Ser15} compared to Cont. siRNA (Figure 4-3).

Nutlin-3 mediated WIP1 induction was decreased in the presence of WIP1.2 siRNA compared to non-targeting control (Cont.) siRNA (Figure 4-6). Lanes 1 and 2 are the same on both immunoblots presented in Figure 4-6 which allowed for densitometry and graphic comparison of relative protein expression in other lanes on the same blot (See Figure 4-7). Knockdown of WIP1 resulted in strong enhancement and persistence of pp53^{Ser15} phosphorylation (Figure 4-6 & Figure 4-7). Increased p53^{Ser15} was concurrent with slightly higher intensity p21^{WAF1} and MDM2 bands but not BAX and PUMA (Figure 4-6).

Phosphorylation of p53^{Ser46} (pp53^{Ser46}) has previously been reported to be a pro-apoptotic p53 modification in response to DNA damage (Mayo, Seo et al. 2005) and phosphorylation of p53^{Ser20} (pp53^{Ser20}) is known to be necessary for p53 and MDM2 dissociation in response to DNA damage (Chehab, Malikzay et al. 1999). Therefore we attempted to assess whether these two post-translational modifications are affected by Nutlin-3 or WIP1 transient knockdown in the presence of Nutlin-3. Although these antibodies were not optimal, comparing lanes 9 and 10 to lanes 3-8 on the blot on the left, it appears that transfection conditions result in increased pp53^{Ser46} and pp53^{Ser20} and that Nutlin-3 and WIP1 do not appear to play a significant role in these phosphorylation events (Figure 4-6). Surprisingly, MDMX was stabilised in response to the combination of Nutlin-3 and control siRNA, given that MDMX is not a direct p53 transcriptional target. MDMX stabilisation in response to Nutlin-3 was not observed in the presence of WIP1 siRNA. This is in line with the previously reported role of WIP1 phosphatase in positively influencing MDMX stability by dephosphorylating Ser403 on MDMX (Zhang, Lin et al. 2009). Nutlin-3 mediated p53-dependent induction of MDM2 was affected modestly in spite of the reported role of WIP1 in regulating MDM2 stability (Lu, Ma et al. 2007). However, in this context the reduced stability of MDM2, is most

likely masked by its p53-dependent induction by Nutlin-3.

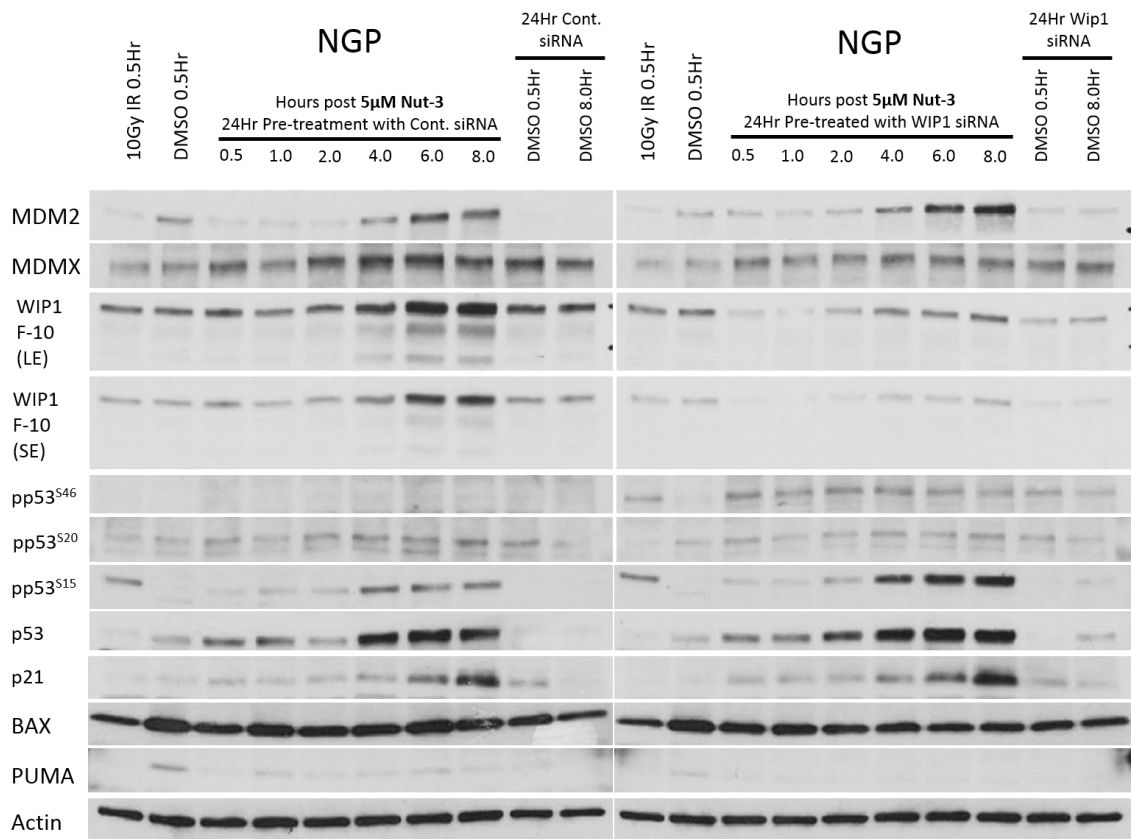


Figure 4-6 The effect of WIP1 siRNA knockdown on p53 post-translational modification and its downstream targets over 8 hours in NGP cells. Cells were pre-treated for 24 hours with control siRNA or WIP1 siRNA and then treated with 5µM Nutlin-3. Lysates were collected in parallel at the stated time-points after drug treatment and immunoblots carried out simultaneously. Two identical controls were loaded onto the first two tracks on each blot as reference points for optical density (OD) comparison of bands between blots. WIP1.2 siRNA suppresses Nutlin-3 mediated WIP1 induction and increases pp53^{S15} without affecting total p53. LE: Long exposure: SE: Short exposure.

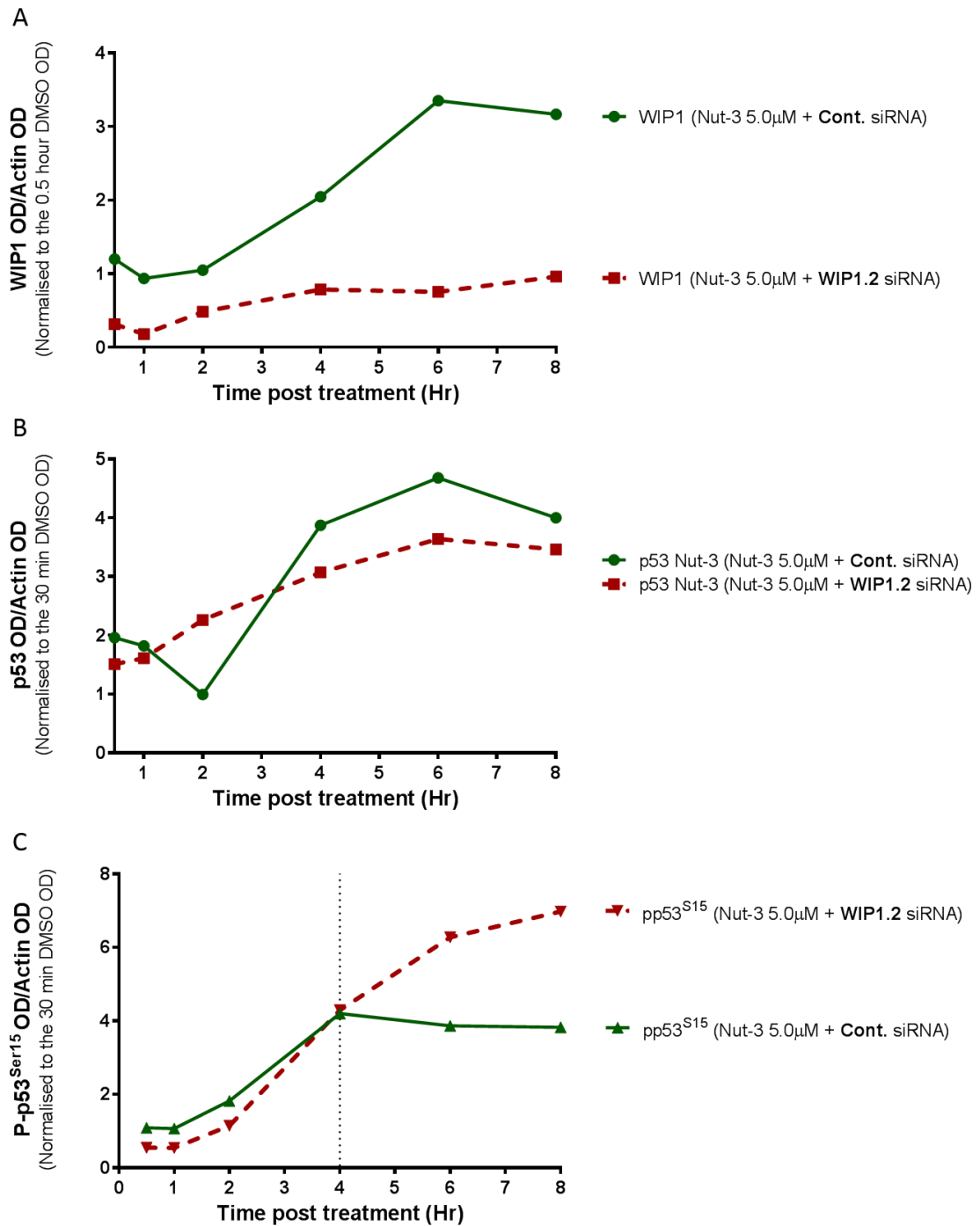


Figure 4-7 Densitometry of blots shown in Figure 3-21 where the OD of each band was measured relative to actin and then normalised to 0.5Hr DMSO control (lane 2) which represents the baseline protein expression on each blot. A) Nutlin-3 mediated WIP1 induction over time is suppressed in the presence of WIP1.2 siRNA compared to Cont. siRNA. B) Total p53 induction after 5 μ M Nutlin-3 in the presence of WIP1.2 siRNA was not affected compared to control. C) Phosphorylation of p53 on serine 15 (pp53^{S15}) after 5 μ M Nutlin-3 treatment increases in the presence WIP1.2 siRNA compared to control siRNA. Datapoints represent one experiment.

4.4.3 **WIP1 siRNA mediated knockdown increases sensitivity to Nutlin-3 in *TP53* wild-type cell lines**

Monitoring cell morphology and proliferation in response to Nutlin-3 ± Cont./WIP1.2 siRNA using IncuCyte showed that WIP1 knockdown increases sensitivity to growth inhibition by Nutlin-3 in *TP53* wild-type cell lines (Figure 4-8 to Figure 4-10) (See time-lapse images presentation in enclosed CD). In contrast, none of the *TP53* mutant null cell lines were made significantly more sensitive to growth inhibition by Nutlin-3 with WIP1.2 siRNA compared to the control. WIP1 targeting siRNA resulted in slightly slower rate of growth for the *TP53* wild-type cells NGP, HCT116^{+/+} and SJSA-1 compared to control siRNA. Interestingly numerous vacuoles were observed in HCT116 (Figure 4-12) and SJSA-1 cells (data not shown) under transfection conditions compared to non-transfected controls, regardless of their *TP53* genetic status. Reduction in growth rate was also observed in HCT116^{-/-} and SN40R2 *TP53* null and mutant cells respectively (Figure 4-8 to Figure 4-10). This suggests that WIP1 knockdown may sensitise these cell lines to transfection conditions in a p53-independent manner. Nutlin-3 resulted in necrotic morphology in HCT116^{+/+} cells, with compromised membranes and fragmented nuclei observed (Figure 4-13).

Immunoblots carried out on the NGP cell line pair in parallel with the IncuCyte experiments showed efficient WIP1 knockdown and an increase in Nutlin-3 mediated induction of p53 transcriptional targets p21^{WAF1} and MDM2 compared to control siRNA in the wild-type *TP53* NGP cells (Figure 4-11). In spite of p53 stabilisation in the *TP53* mutant N20R1 cells 4Hrs following 5µM Nutlin-3 treatment, MDM2 and p21^{WAF1} were not induced in the *TP53* mutant N20R1 cells. Interestingly, p53 Serine 20 phosphorylation (pp53^{S20}), reported to be indirectly affected by WIP1 through its role in deactivating ATM, CHEK1 & 2 dephosphorylation (Shreeram, Demidov et al. , Fujimoto, Onishi et al. 2005, Lu, Nannenga et al. 2005, Yoda, Xu et al. 2006, Oliva-Trastoy, Berthonaud et al. 2007), only increased in *TP53* mutant N20R1 cells after WIP1 knockdown and Nutlin-3 treatment. Furthermore, in N20R1 cells MDM2 was stabilised by the combination of Nutlin-3 + WIP1.2 siRNA compared to Nutlin-3 + Cont. siRNA in N20R1 cells (Figure 4-11) although this may be due to the differences in loading in the last two lanes.

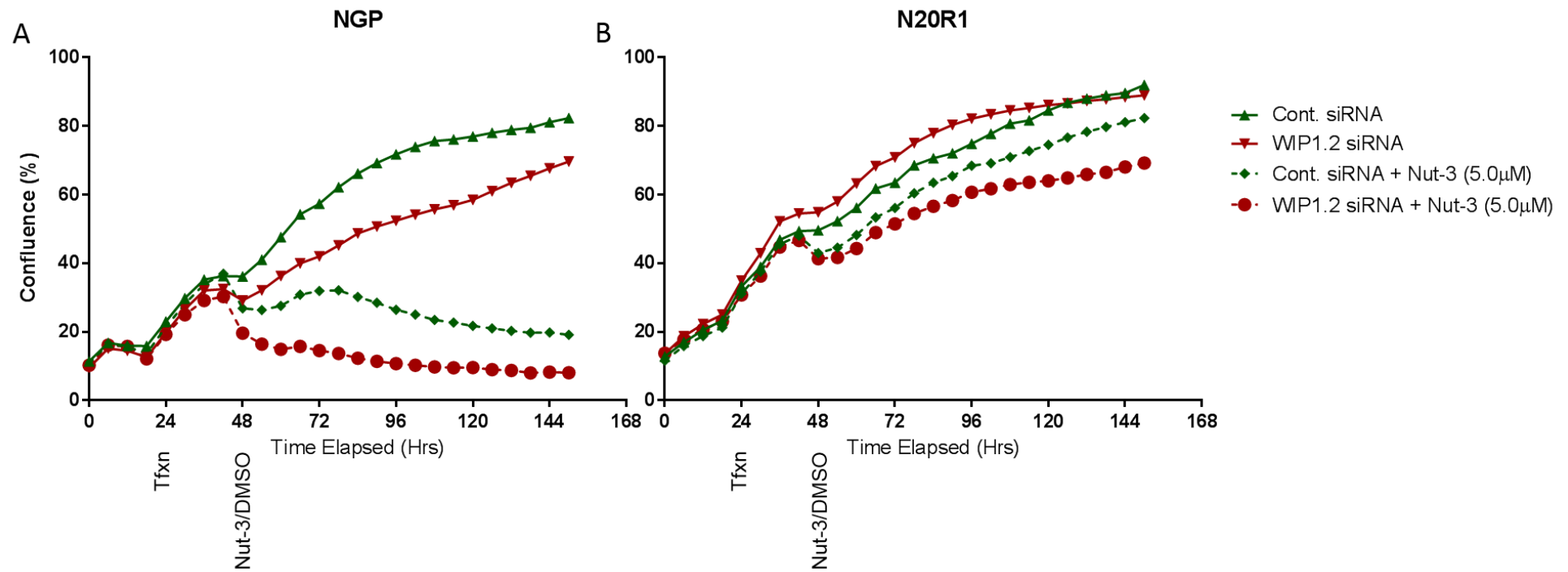


Figure 4-8 Monitoring of (A) NGP and (B) N20R1 cell confluence over time during treatment with WIP1.2 or control (Cont.) siRNA \pm 5µM Nutlin-3 using IncuCyte. WIP1 siRNA alone reduces confluence over time and markedly increases NGP sensitivity to Nutlin-3 for the NGP wild-type *TP53* cells. Tfxn: Transfection; Nut-3/DMSO: 5µM Nutlin-3 or 1% (v/v) DMSO

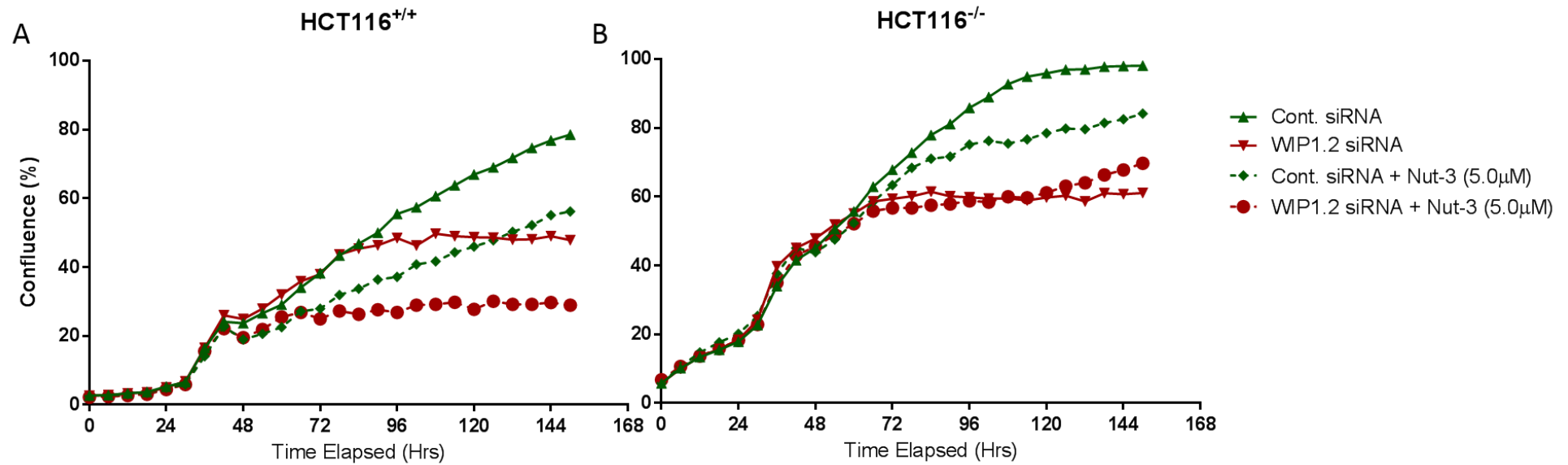


Figure 4-9 Monitoring of (A) HCT116^{+/+} and (B) HCT116^{-/-} cell confluence over time using IncuCyte as described in Figure 3-24. WIP1 siRNA alone reduces confluence over time of both cell lines and markedly increases HCT116^{+/+} sensitivity to Nutlin-3. Tfxn: Transfection; Nut-3/DMSO: 5μM Nutlin-3 or 1% (v/v) DMSO

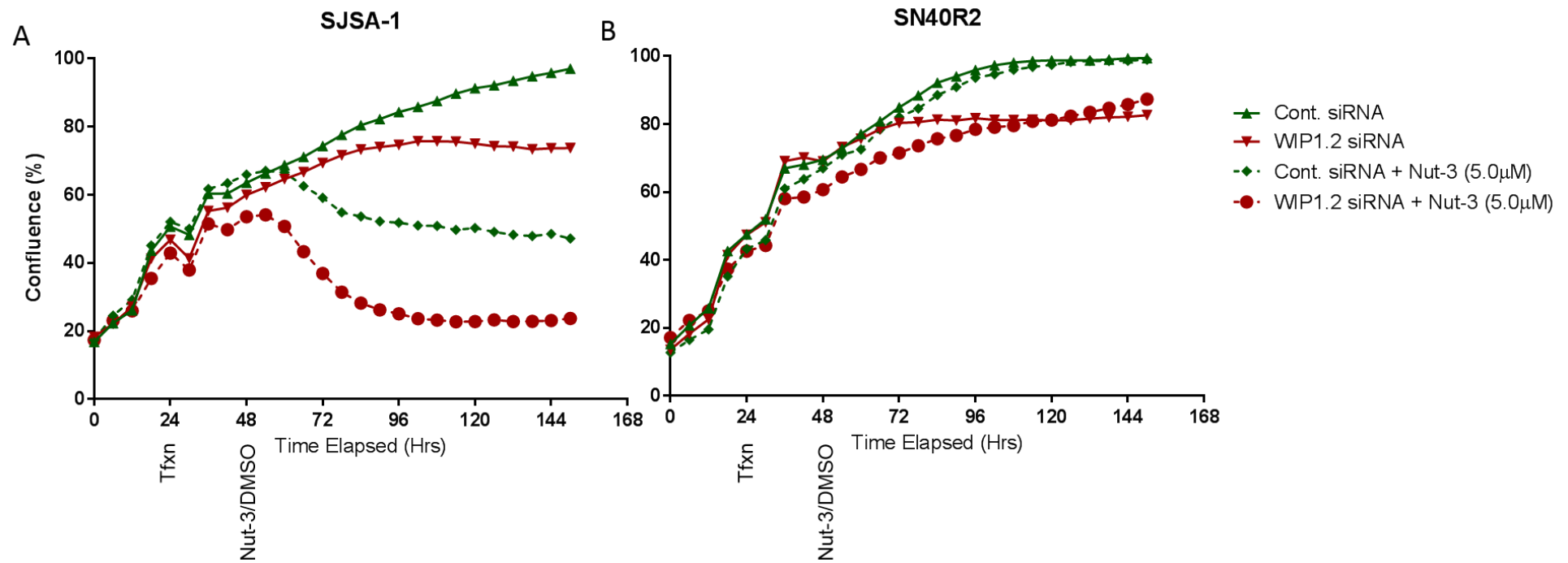


Figure 4-10 Monitoring of (A) SJSA-1 and (B) SN40R2 cell confluence over time using IncuCyte as described in Figure 3-24. WIP1 siRNA alone reduces confluence over time of both cell lines and markedly increases SJSA-1 sensitivity to Nutlin-3. Tfxn: Transfection; Nut-3/DMSO: 5µM Nutlin-3 or 1% (v/v) DMSO.

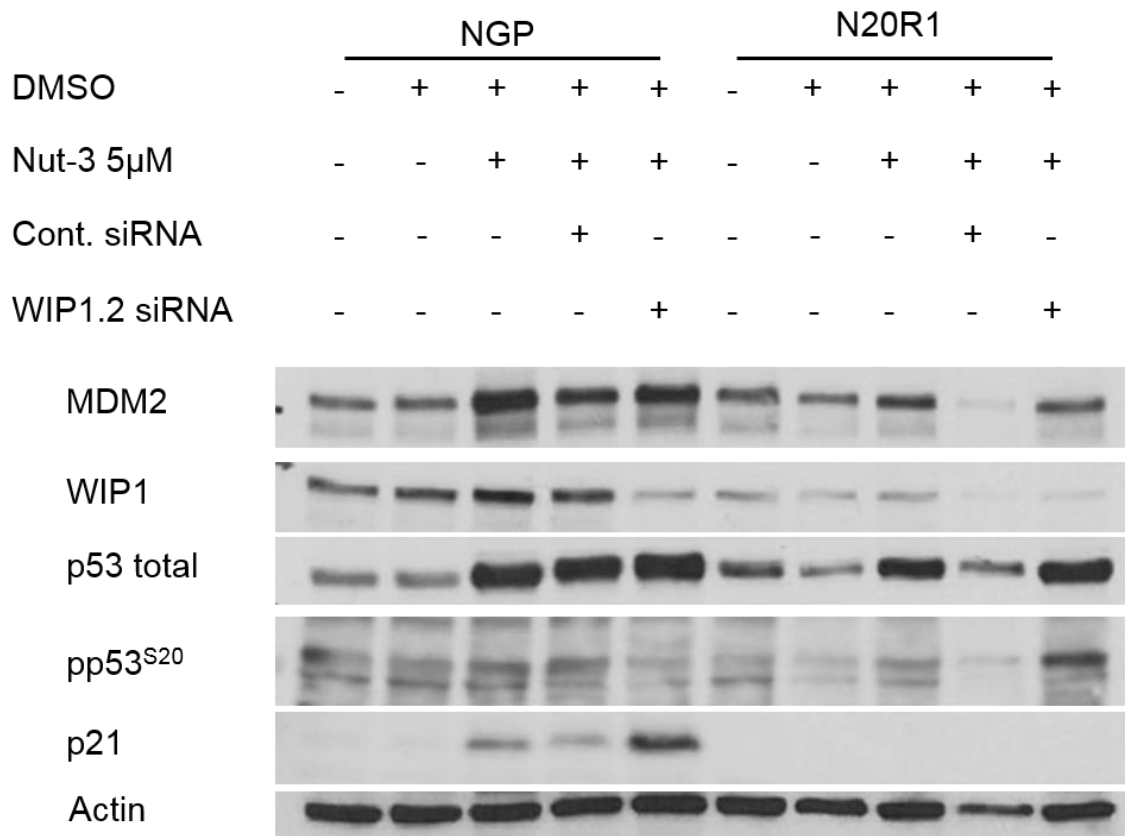


Figure 4-11 WIP1 knockdown Immunoblots carried out in parallel with the InCuCyte experiment in NGP cell line pair shows that WIP1 knockdown and combination with Nutlin-3 results in an increase in p21^{WAF1} and MDM2 expression in *TP53* wild-type NGP cells but it does not affect pp53^{S20} in contrast to the *TP53* mutant N20R1 cells. Cells were transfected with siRNA 24 Hrs before treatment with DMSO/Nutlin-3 and lysates were then collected after 4Hrs of drug incubation.

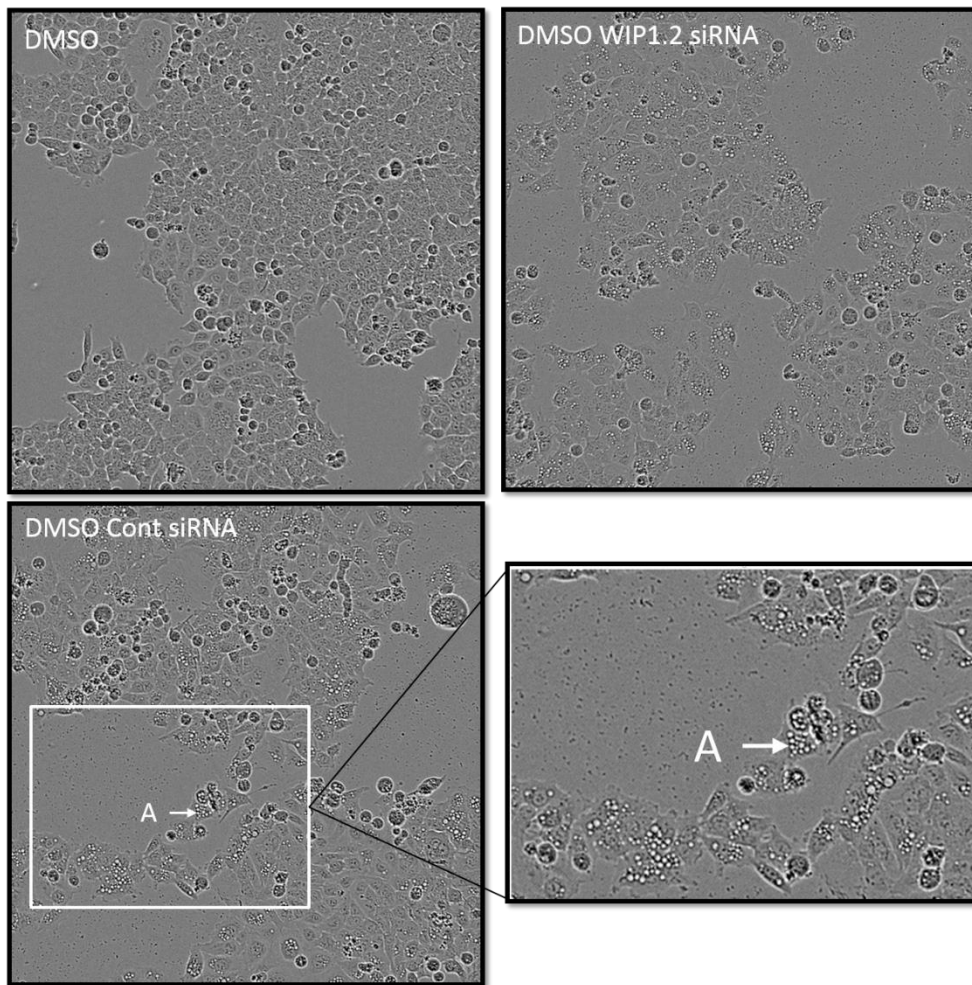


Figure 4-12 Transfection conditions result in formation of numerous cytoplasmic vacuoles in HCT116 cells by 72 hours.

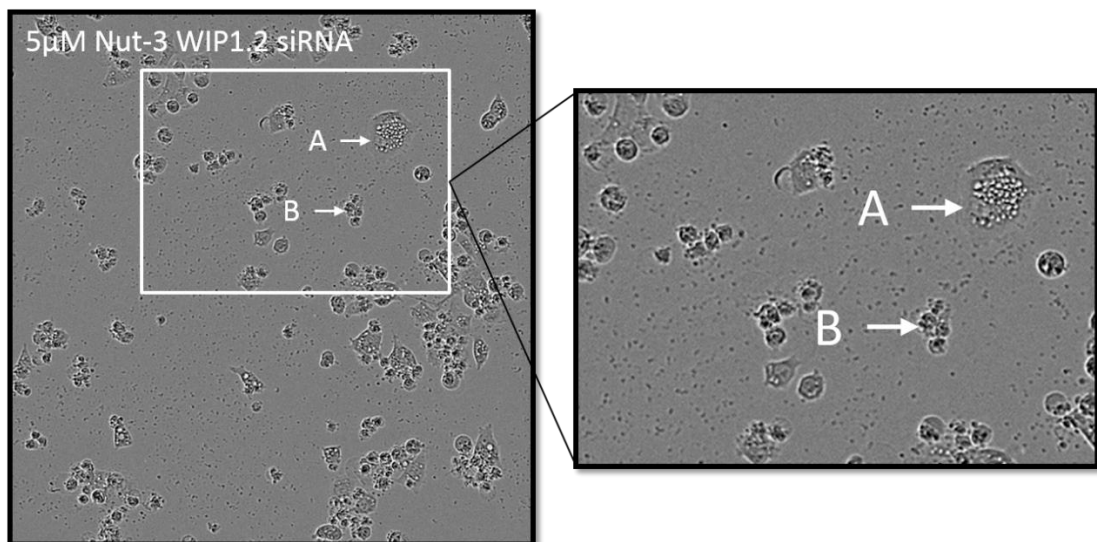


Figure 4-13 A) Cytoplasmic vacuoles in response to transfection conditions in HCT116 cells. B) Loss of membrane integrity in the presence of Nutlin-3 and WIP1.2 siRNA.

4.4.4 WIP1 siRNA transient knockdown decreases clonogenic survival in response to Nutlin-3 in a p53-dependent manner

The NGP and N20R1 cell line pair was transfected with control or WIP1.2 siRNA and then treated with multiples of 50% lethal concentration (LC50) of Nutlin-3 (Previously obtained LC50=1.3 μ M) for 48 hours, following which they were re-seeded and allowed to form colonies. WIP1.2 siRNA increased the sensitivity of *TP53* wild-type NGP cells to Nutlin-3 but not the *TP53* mutant N20R1 cells. WIP1 knockdown resulted in a 2.7-fold ($p=0.0004$) decrease in the clonogenic survival of NGP cells in response to Nutlin-3 + WIP1.2 siRNA compared to Nutlin-3 + Cont. siRNA (Figure 4-14). Immunoblotting carried out in parallel with the first repeat of the clonogenic assay showed an increase in Nutlin-3 induced pp53^{S15} in the presence of WIP1.2 siRNA compared to control siRNA in NGP and to a lesser extent in N20R1 cells (Figure 4-15). In NGP cells this correlated with a notable increase in well-established p53 transcriptional target gene products, MDM2 and WIP1 but not the pro-apoptotic p53 transcriptional target BAX. In spite of similar p53 stabilisation N20R1 cells did not induce WIP1 or BAX in any of the treatment conditions but there was a modest induction of MDM2.

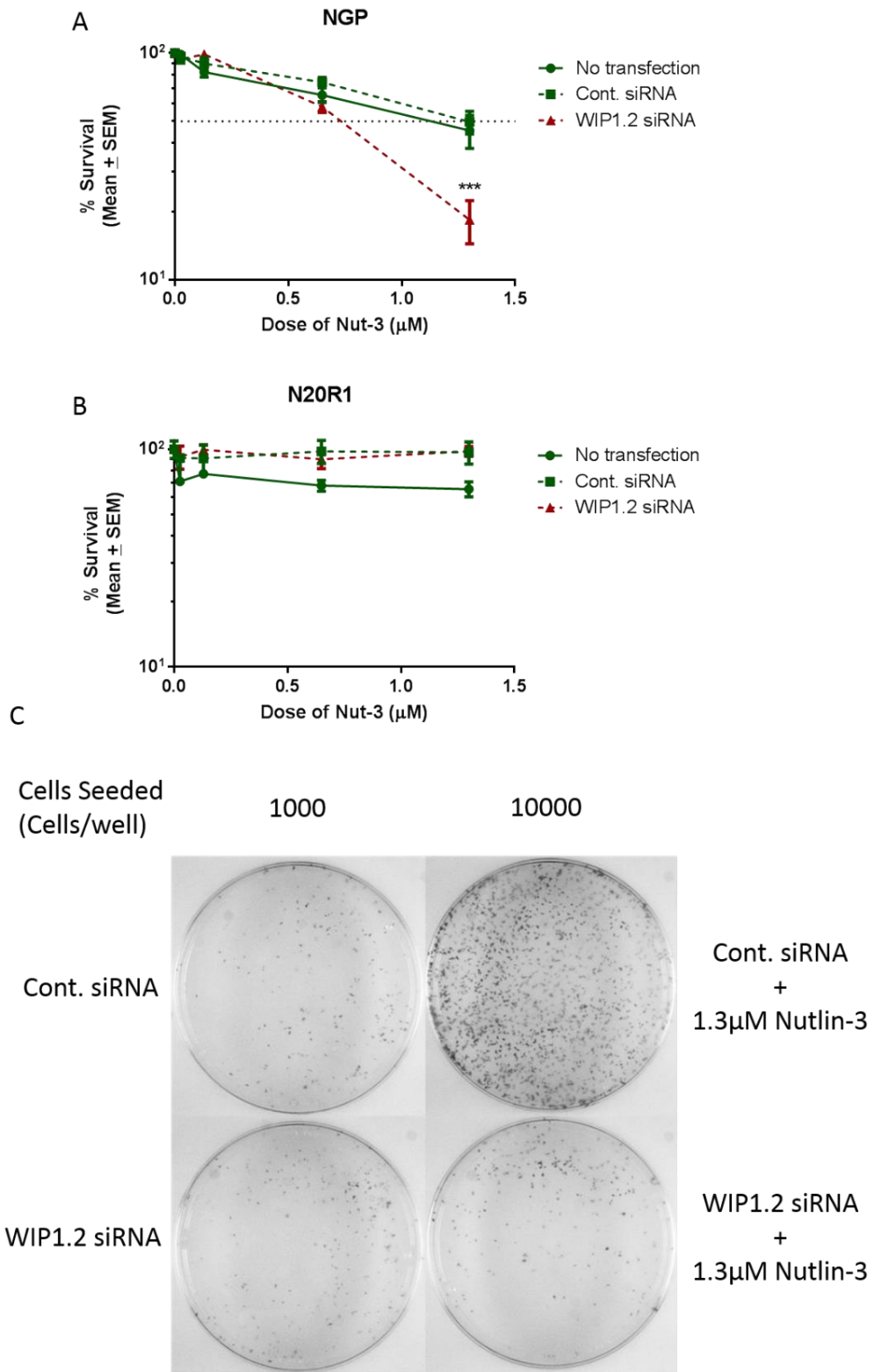


Figure 4-14 WIP1 siRNA mediated knockdown increases sensitivity to Nutlin-3 in clonogenic survival assays in a p53 dependent manner. **A & B**) NGP cell line pair were treated with Cont. siRNA/ WIP1 siRNA and after 24 hours exposed to Nutlin-3 (0.03-1.3µM) for 48 hours before being re-plated at different densities (500-10000). Cells were left to form colonies, fixed, stained and then colonies counted. **C**) Colony formation assay images of Cont. siRNA + Nutlin-3 and WIP1 siRNA + Nutlin-3 (0 means DMSO control). Images are representative of the biggest difference observed in three independent repeats. Supervised MRes student Mrs Liang Zhao assisted with this experimental procedure.

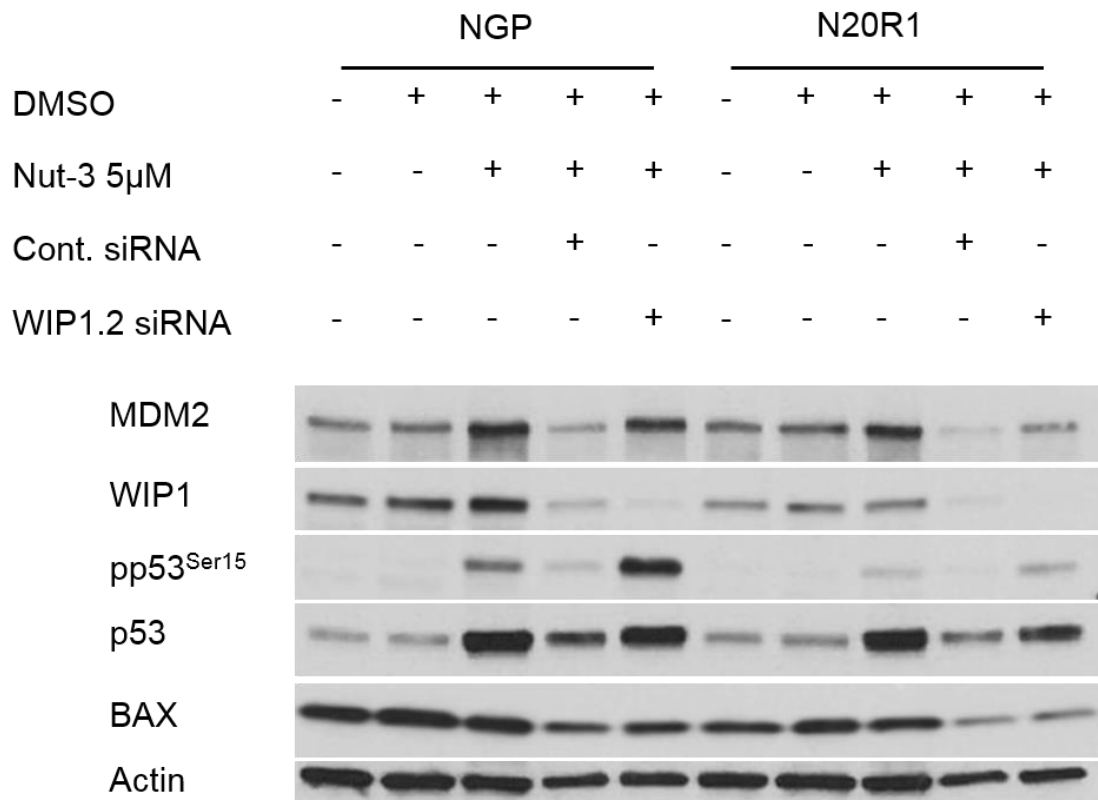


Figure 4-15 WIP1 knockdown combined with Nutlin-3 treatment carried out in parallel with the clonogenic survival assays showed a marked increase in pp53^{S15} compared to control (Cont.) siRNA in NGP cells and to a lesser extent in N20R1 cells. Cells were transfected with siRNA 24 Hrs before treatment with DMSO/Nutlin-3 and lysates were then collected after 4Hrs of drug incubation.

4.4.5 WIP1 knockdown enhances Nutlin-3 mediated cell cycle distribution changes and increases Sub-G1 apoptotic signals

The NGP and N20R1 cell line pair was transfected with control siRNA or WIP1.2 siRNA 24 hours before being treated with 0.5 × and 1 × NGP GI50 doses of Nutlin-3 and then cell cycle distribution was analysed by flow cytometry. WIP1 siRNA mediated knockdown alone (Also treated with 1% DMSO) resulted in no change in cell cycle distribution of the NGP cell line pair at 48 hours (Figure 4-16). In spite of the observations by IncuCyte and the clonogenic data, WIP1 siRNA results in only a slight but statistically significant (paired t-test, $p=0.009$) increase in Nutlin-3 induced Sub-G1 apoptotic events in the *TP53* wild-type NGP cells and had no effect on the *TP53* mutant N20R1 daughter cell line (Figure 4-17). Cell cycle distribution was unaffected by Nutlin-3 in the presence or absence of Cont./WIP1.2 siRNA constructs.

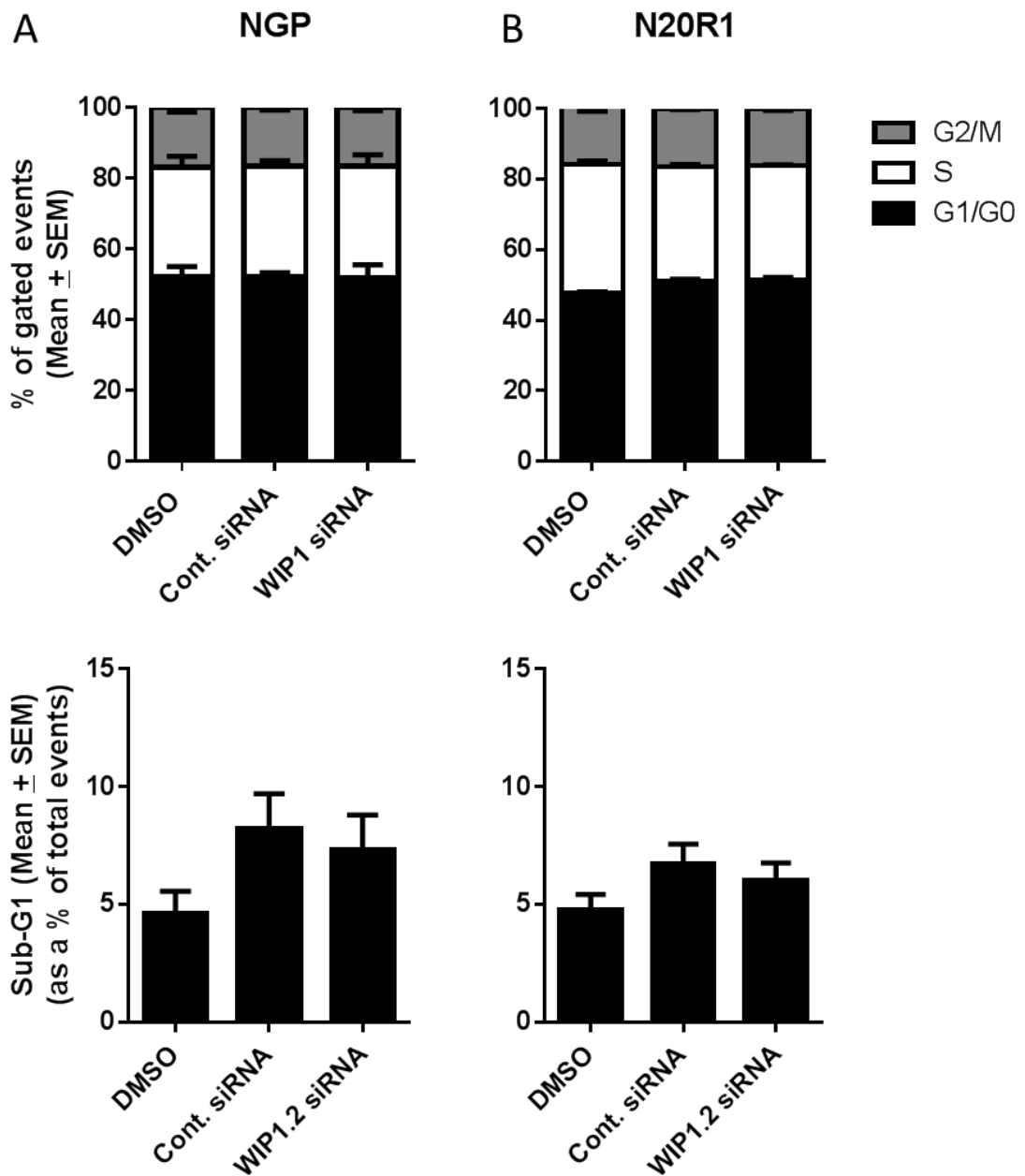


Figure 4-16 Analysis of cell cycle distribution in response to WIP1 knockdown. In NGP or N20R1 cells WIP1 targeting siRNA (WIP1.2) does not affect cell cycle distribution at 72 hours and does not cause an increase in Sub-G1 events compared to control siRNA (Cont. siRNA).

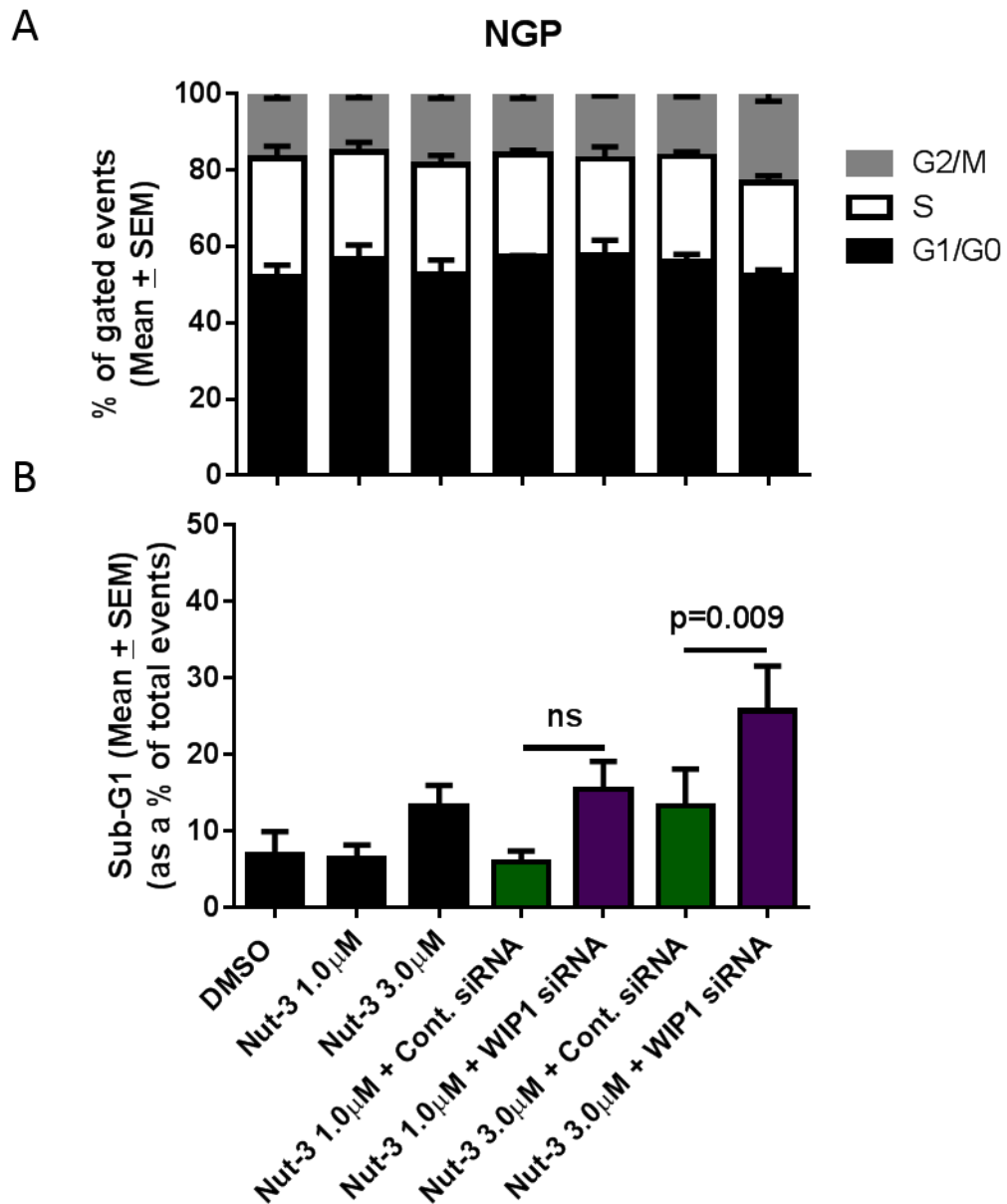


Figure 4-17 In NGP cells combination of WIP1 knockdown and Nutlin-3 treatment does not result in changes in cell cycle distribution (A) but it leads to a significant increase in Sub-G1 events (B). Paired t-test p-value. Cells were transfected with siRNA 24 Hrs before treatment with DMSO/Nutlin-3 and harvested after a further 48 hours of incubation.

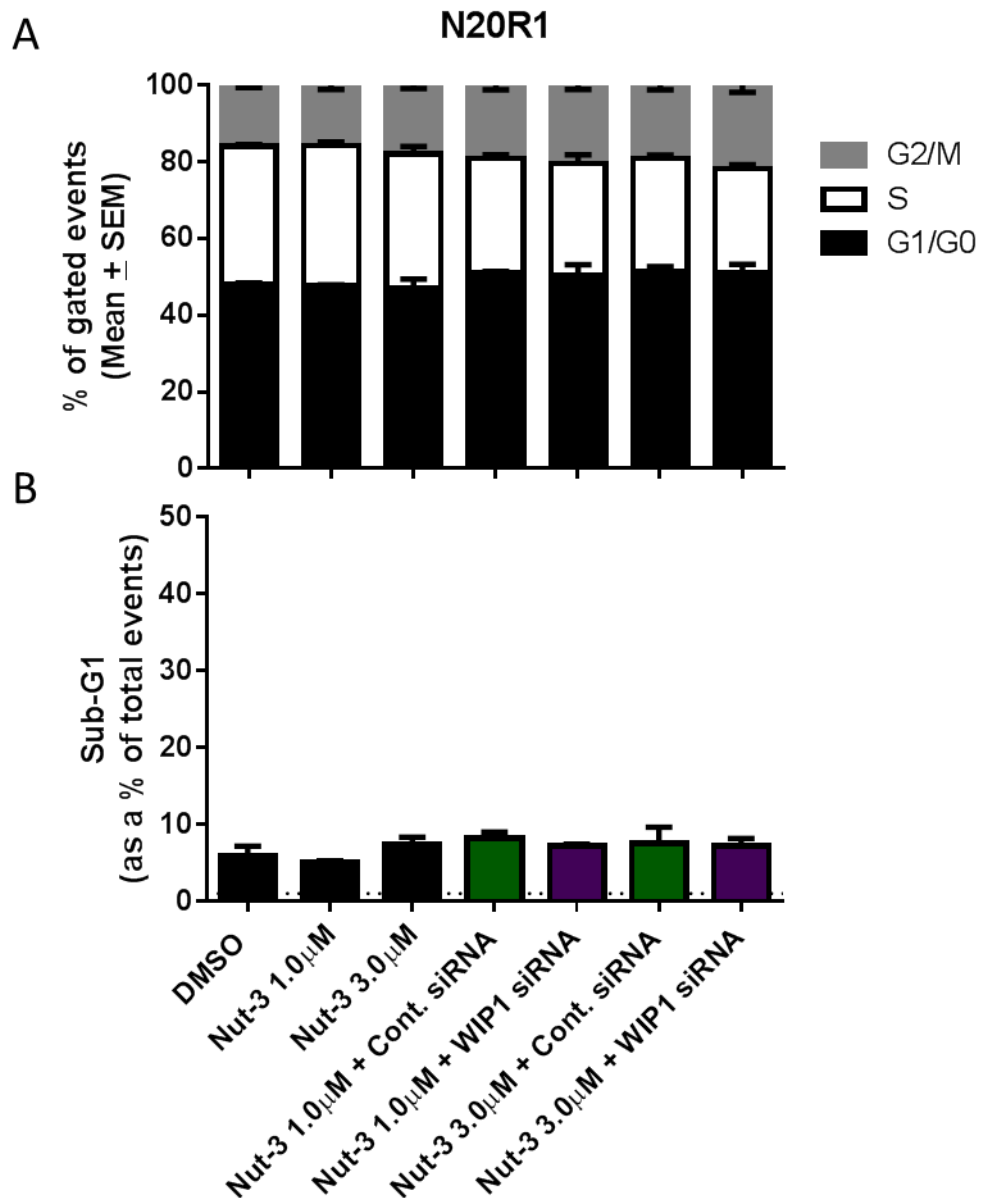


Figure 4-18 in N20R1 cells combination of Nutlin-3 and WIP1 knockdown does not affect either cell cycle distribution or % of sub-G1 events. Cells were transfected with siRNA 24 Hrs before treatment with DMSO/Nutlin-3 and harvested after a further 48 hours of incubation.

4.4.6 Caspase-independent cell death in HCT116^{+/+} cells in response to Nutlin-3

The observation of numerous vacuoles in HCT116^{+/+} cells under transfection conditions (Figure 4-12 and Figure 4-13) and their increase in response to Nutlin-3 and its combination with WIP1 knockdown prompted an investigation into the underlying mechanism of cell death in this cell line. The pattern of PARP-1 cleavage can be a marker of caspase-dependent or independent cell death (Reviewed in (Chaitanya, Alexander et al. 2010)). While cleavage of PARP-1 holoenzyme from 114KDa to 85KDa and 24KDa fragments is associated with caspase-mediated apoptosis, an alternative cleavage pattern caused by lysosomal enzymes (e.g. cathepsins), which results in a 55KDa PARP-1 fragment, has been associated with necrotic cell death (Gobeil, Boucher et al. 2001). PARP-1 cleavage was therefore compared between NGP and HCT116^{+/+} cells to assess whether WIP1 siRNA mediated knockdown affects PARP-1 cleavage.

Although WIP1 knockdown had not persisted through 72Hrs following the transfection, pp53^{Ser15} was higher in HCT116^{+/+} cells treated with Nutlin-3 + WIP1.2 siRNA compared to Nutlin-3 + Cont. siRNA; however, it was not detected in NGP cells (Figure 4-19). Interestingly, pp53^{Ser15} was associated with higher MDM2 levels in HCT116^{+/+} cells. This is inconsistent with reported role of WIP1 in stabilising MDM2 as knocking down WIP1 would destabilise MDM2 (Lu, Ma et al. 2007). However, increased transcriptional activity of p53 due to increased pp53^{Ser15} may be masking this effect. The p53 induced pro-apoptotic marker PUMA was induced in response to Nutlin-3, although WIP1.2 siRNA did not influence its expression at 48Hrs. A band was detected by the PARP-1 C2-10 antibody at ~55KDa in HCT116^{+/+} Nutlin-3 treated siRNA transfected and non-transfected cells (Figure 4-19). The combination of Nutlin-3 and WIP1 knockdown resulted in an increase in the 55KDa PARP-1 fragment compared to Nutlin-3 + Cont. siRNA. The 55KDa fragment was weak or absent in NGP cells. This suggests that the mechanism of Nutlin-3 induced cell death is different between NGP and HCT116^{+/+} cells and that the caspase-3 independent mode of cell death observed in HCT116^{+/+} cells in response to Nutlin-3 is enhanced in the presence of WIP1.2 siRNA.

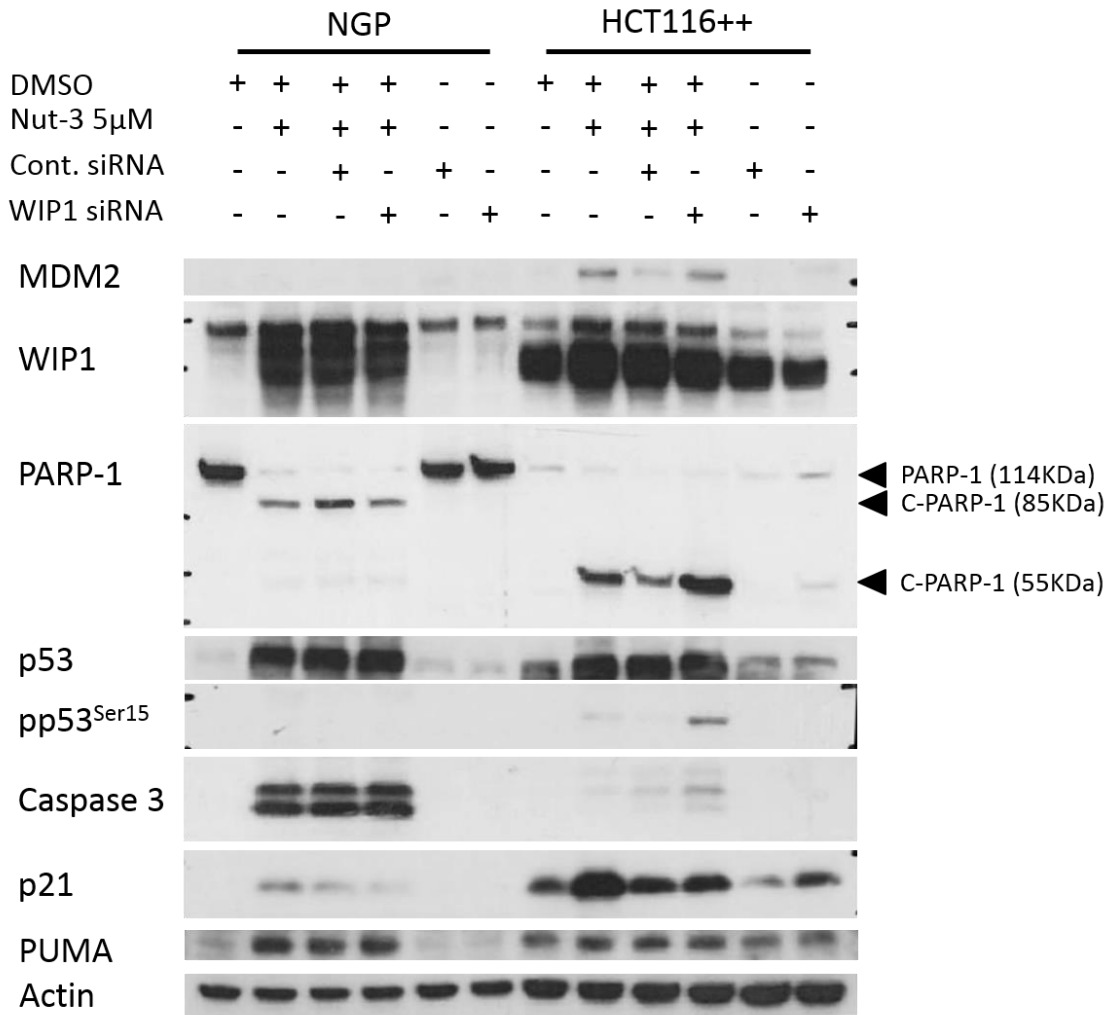


Figure 4-19 Comparison of late cell death markers in NGP and HCT116^{+/+} cells after 48 hours treatment with 5 μ M Nutlin-3 \pm Cont./WIP1.2 siRNA. Cleaved caspase-3 appears most notably in NGP cells in the presence of Nutlin-3 under transfection conditions which correlates with caspase-3 related cleaved PARP-1 fragment (C-PARP apoptosis = 85KDa). The cleaved caspase-3 signal was very low in HCT116^{+/+} cells and the pattern of PARP-1 cleavage indicated a mode of cell death associated with release Cathepsin B and G enzyme activity (C-PARP necrosis = 55KDa). Overall WIP1 knockdown appeared to lead to increased caspase-3 cleavage or necrosis related PARP-1 cleavage. Western blot carried out by supervised student Mrs Liang Zhao.

4.5 Discussion

The range of sensitivity in response to MDM2 inhibitors among *TP53* wild-type cell lines suggests that factors secondary to the *TP53* genetic status may contribute to this variability in response. In the previous chapter it was shown that inhibition of members of the PI3KK family which are involved in DNA DSB repair did not enhance sensitivity to MDM2 inhibitors. The activation of PI3KKs, in response to DNA damage, are known to stabilise and activate p53 to promote cell cycle arrest/cell death (Appella and Anderson 2001). Phosphatases that target the same residues are also known to negatively regulate p53 stability and function to allow recovery from p53 induced cell cycle arrest (Donehower 2014). WIP1 is one such phosphatase that negatively regulates p53 by dephosphorylating pp53^{Ser15} and other p53 activating components of the stress response which renders them less active (Lu, Ma et al. 2007, Lu, Nguyen et al. 2008). Therefore, it was hypothesised that WIP1/PPM1D siRNA mediated knockdown would sensitise cells to Nutlin-3 in a p53-dependent manner.

4.5.1 WIP1 knockdown and antibody optimisation

With the use of two different anti-WIP1 antibodies and four different WIP1 targeting siRNA molecules it was reliably shown which bands correspond to WIP1 in immunoblotting experiments. This enabled the assessment of basal WIP1 expression and its induction following p53 activation. This also allowed the smaller WIP1 isoform to be distinguished from the truncated mutated forms of WIP1 in the HCT116 cell line pair and U2OS cell line pair. Basal WIP1 expression and its induction in response to Nutlin-3 corresponded to WIP1 copy number, with *PPM1D*-amplified MCF-7 cells showing the highest level of WIP1 induction. Importantly, it was shown that WIP1 knockdown results in a robust increase in pp53^{Ser15} following Nutlin-3 treatment in NGP cells. Phosphorylated p53^{Ser15} is a substrate for WIP1 phosphatase activity (Lu, Nannenga et al. 2005) which means that pp53^{Ser15} can be used as a marker of WIP1 phosphatase activity following Nutlin-3 treatment. Interestingly, WIP1 knockdown and corresponding increase in pp53^{Ser15} correlated with a slight increase in the induction of well-established p53 targets, MDM2, p21^{WAF1} and BAX, by 4Hrs of Nutlin-3 treatment. This is consistent with the previously reported role of p53^{Ser15} phosphorylation in enhancing p53^{Ser15} transcriptional activity (Meek and Anderson 2009, Loughery, Cox et al. 2014).

4.5.2 WIP1 knockdown increases sensitivity to Nutlin-3

Consistent with *TP53* wild-type genetic status being the strongest predictor of response to MDM2 inhibitors, none of the *TP53* mutant cells were notably growth inhibited by 5 μ M Nutlin-3 when cell proliferation was monitored by IncuCyte. Cellular sensitivity was enhanced in all *TP53* wild-type parental cell lines as hypothesised. With the NGP and N20R1 cell line pair, WIP1 knockdown alone only resulted in notable growth inhibition in NGP and not N20R1 cells. WIP1 knockdown when compared to control also resulted in increased sensitivity to loss of clonogenic survival in response to Nutlin-3 in NGP cells and not the *TP53* mutant N20R1 cells. This was consistent with the significant increase in Sub-G1 (apoptotic) cell cycle events observed in NGP parental cells only following the combination of WIP1 knockdown and Nutlin-3 treatment. This in turn is consistent with a significant role in the negative regulation p53 by WIP1 in NGP cells following activation of p53 with MDM2 inhibitors. Indeed the reported *PPM1D* copy number gain (Richter, Dayaram et al. 2015) in this cell line may be a contributory factor in the observed lower sensitivity to Nutlin-3 in clonogenic assays compared to SJSA-1 cells in the previous chapter.

4.5.2.1 Transfection conditions results in vacuole formation and potential off-target effects in HCT116 and SJSA-1

In the SJSA-1 and HCT116 and their otherwise isogenic *TP53* mutant and null respective pairs, the growth inhibitory effect of WIP1 knockdown did not appear p53-dependent. Closer assessment of cell morphology, using the time-lapse phase contrast images, showed that large vacuoles formed following the initiation of transfection regardless of the siRNA molecules. These vacuoles were not observed in NGP cells. These may be lipid vacuoles which would normally be catabolised through autophagy. WIP1 has been shown to negatively regulate the degradation of these vacuoles by autophagy through its inhibition of ATM in macrophages from *Ppm1d* null mice (Le Guezennec, Brichkina et al. 2012). Therefore WIP1 knockdown may increase the autophagic degradation of vacuoles while promoting release of lysosomal enzymes such as cathepsins followed by autophagic cell death (Uchiyama 2001). Investigation of the pattern of PARP-1 cleavage showed that in HCT116^{+/+} cells the mode of cell death likely involved lysosomal proteases of the cathepsin family. Moreover, the smaller fragment of PARP-1 associated with necrosis was increased when Nutlin-3 and WIP1 silencing siRNA were combined compared to Nutlin-3 and cont. siRNA.

4.5.3 Summary

It was shown in this chapter that WIP1 siRNA mediated knockdown robustly influences the post-translational modification of p53 and increases sensitivity to Nutlin-3 in *TP53* wild-type cell lines. This increased sensitivity to Nutlin-3 was further examined and confirmed using clonogenic assays and flow cytometry in one cell line pair.

Importantly, closer examination of cell line morphology, using IncuCyte time-lapse images, brought to light a potential caveat in the use of transfection reagents (cationic liposome formulations) for siRNA delivery in target validation or combination treatment studies. Large vacuoles were observed in two of the cell line pairs (HCT116 and SJSA-1 cells) independent of the siRNA sequence or treatment with Nutlin-3.

Therefore, the effect of WIP1 knockdown on sensitivity to Nutlin-3 in these cell lines must be interpreted with these potential off-target effects in mind. Despite these potential caveats the data overall suggest that reduced WIP1 phosphatase activity increases sensitivity to MDM2 inhibitors. In the following chapter the role of WIP1 in determining the sensitivity to MDM2 inhibitors is further assessed using a recently developed highly selective allosteric WIP1 inhibitor, GSK2830371 (Gilmartin, Faitg et al. 2014).

**Chapter 5 Selective chemical inhibition of WIP1/PPM1D by
GSK2830371 potentiates cellular response to MDM2-p53 binding
antagonists**

5.1 Introduction

In the previous chapter WIP1 transient siRNA knockdown was used to investigate the role of this phosphatase in the response to Nutlin-3. WIP1 transient siRNA knockdown was shown to enhance sensitivity to Nutlin-3 in a p53-dependent manner. In this chapter the investigation of this hypothesis was extended to simultaneous selective pharmacological inhibition of WIP1 and MDM2. Recently a potent and highly selective allosteric inhibitor of WIP1 phosphatase has been developed (Gilmartin, Faitg et al. 2014), which is used throughout this chapter to investigate the role of WIP1 in p53 signalling and determining the response to MDM2 inhibitors.

5.1.1 Selective WIP1 inhibition by GSK2830371

Despite the importance of phosphatases in key cellular processes their selective inhibition has proven challenging. This may be due to the structural similarities between catalytic sites of phosphatases of different families and their complex relationship with multiple regulatory subunits (McConnell and Wadzinski 2009). Interestingly, WIP1 is a member of the PPM family of Ser/Thr phosphatases, which function as monomers (McConnell and Wadzinski 2009), and may theoretically be less complex to target and investigate biochemically. Given the identification of the role of *PPM1D* as an oncogene multiple approaches have been used to discover and develop selective and potent WIP1 inhibitors with varying degrees of success (Rayter, Elliott et al. 2007, Hayashi, Tanoue et al. 2011, Yagi, Chuman et al. 2012, Gilmartin, Faitg et al. 2014). Recently, a highly selective allosteric WIP1 inhibitor, namely GSK2830371, has been reported to both degrade WIP1 protein and potently inhibit its catalytic activity by binding to a structurally unique flap-subdomain on WIP1, proximal to its catalytic site (Gilmartin, Faitg et al. 2014). Two different high throughput screens were carried out to identify the ideal pharmacophore for selective WIP1 inhibition, 1) a high throughput biochemical screen measuring the hydrolysis of fluorescent diphosphate (FDP) by truncated WIP1 (amino acids 2-420); and 2) a high affinity binding assay based on DNA-encoded small-molecule library (DEL) to full length WIP1. In DEL a library of compounds are each labelled with a unique DNA sequence and are incubated in a one pot reaction with the target as the stationary phase. The unbound compounds are washed off and the bound compounds are identified by high throughput DNA sequencing. Both screens identified a group of structurally similar compounds, termed capped amino acids due to their amino acid-like cores, which inhibited WIP1 biochemical activity and bound to it with great affinity *in vitro* (Gilmartin, Faitg et al.

2014). These candidate compounds were shown to have cell free assay inhibitory activity against established WIP1 substrates, phospho-p38-MAPK14 (T180) and pp53^{Ser15} with half maximal inhibitory concentrations (IC50) of ≤ 20 nM. The optimal compound, GSK2830371 (WIP1 IC50 = 6nM), was tested for its ability to inhibit 20 other human phosphatases, showing that none of the other phosphatases could be inhibited by up to 30,000nM concentration *in vitro*.

5.1.2 Activity in cell culture and *in vivo*

GSK2830371 was reported to show growth inhibitory activity against *TP53* wild-type cell lines, out of a large panel, using metabolic activity as an end-point for growth (CellTiter-Glo, measuring ATP levels) (Gilmartin, Faitg et al. 2014). No growth inhibitory activity was observed in *TP53* mutant cell lines regardless of *PPM1D* status. However, there was a range of sensitivity to GSK2830371 (~270-fold range in GI50) within the *TP53* wild-type cell lines, with cell lines of haematological lineage showing the greatest sensitivity. This suggests that *TP53* wild-type is necessary but not sufficient for response to GSK2830371. This compound also showed *in vivo* inhibitory activity against DoHH2 (B-cell lymphoma) xenograft tumours in mice at 150mg/kg (thrice daily).

5.1.3 Allosteric inhibition and WIP1 degradation

Competition assays showed that these compounds do not bind to the active site of WIP1 (Gilmartin, Faitg et al. 2014). Photoaffinity labelling and ESI-LC/MS/MS sequencing techniques were then used to show that these series of compounds bind between P219-P295 which is characterised as a flap-subdomain unique to WIP1. Interestingly, the authors showed that treatment with GSK2830371 (Figure 5-1) resulted in marked degradation of WIP1 protein in cultured cell lines. The combination of GSK2830371 and MG132 was reported to result in reversal of this effect suggesting that this process is dependent on proteasomal mediated degradation. Interestingly, site-directed mutagenesis of a well-established WIP1 ubiquitination residue, K238A, also diminished the degradation of WIP1 in response to GSK2830371 compared to wild-type WIP1 suggesting that this process is ubiquitin-mediated.

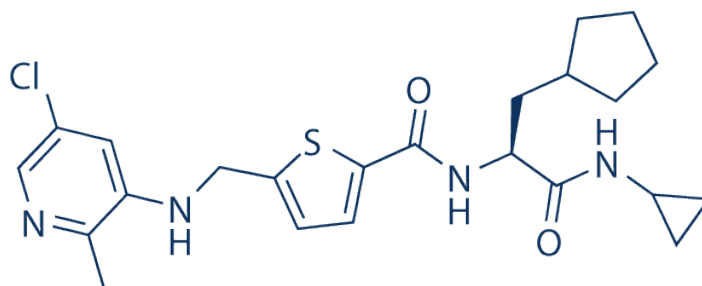


Figure 5-1 Chemical structure of the allosteric WIP1 inhibitor GSK2830371 as described by Gilmartin *et al.*, (2014). Image was obtained from <http://www.selleckchem.com/>

5.1.4 Summary

GSK2830371 is a highly selective low molecular weight inhibitor of WIP1 with promising cellular and *in vivo* activity. This compound also reportedly promotes ubiquitin mediated degradation of WIP1. In the only other study to date published on GSK2830371, which was carried out by the same group, it was shown that this compound is effective against *TP53* wild-type neuroblastoma cell lines with a wide range of sensitivity between them (Richter, Dayaram et al. 2015). Beyond its potential for clinical use as a single agent, GSK2830371 is a useful tool compound for investigating the role of WIP1, including potential modulation of the response to MDM2 inhibitors. Therefore *TP53* wild-type and mutant cell line pairs differing in their *PPM1D* genetic status are used in investigations described in this chapter to assess whether chemical inhibition of WIP1 affects cellular sensitivity to MDM2 inhibitors. Furthermore, the impact of GSK2830371 on p53 biochemical signalling, cell cycle regulation and cell killing are described to provide mechanistic insight.

5.2 Hypothesis

Pharmacological inhibition of WIP1 by GSK2830371 can sensitise cells to MDM2 inhibitors in a p53-dependent manner.

5.3 Specific materials and methods

5.3.1 Cell lines

Cell lines used and their relevant information are outlined in 4.3.1. Additionally ovarian cancer cell lines used by supervised MRes student, Mrs Rachael Mason and relevant information are outlined in (Table 5-1).

Cell line	<i>TP53</i> status	<i>PPM1D</i> status and additional information
A2780	Wild-type	<i>PPM1D</i> Wild-type
CP70	Mutant	<i>PPM1D</i> Wild-type, Cisplatin resistant sub-clone of A2780
CP70-MLH1 c.	Mutant	<i>PPM1D</i> status unknown CP70 with <i>MLH1</i> corrected
IGROV1	Wild-type	<i>PPM1D</i> Wild-type
OAW42	Wild-type	<i>PPM1D</i> Wild-type
PA-1	Wild-type (Polymorphic/silent p.P316P)	<i>PPM1D</i> truncating mutation (p.A457fs*8) (Forbes, Beare et al. 2015)

Table 5-1 Table outlining Ovarian cancer cell lines used by Mrs Rachael Mason and additional relevant information obtained from the literature and catalogue of Somatic Mutations in Cancer (COSMIC) database.

5.3.2 Assessing growth inhibition by SRB assay

Cell lines were seeded at densities ensuring approximately $\geq 3 \times$ population doubling times over the 7 day DMSO/drug exposure and that they were in their exponential growth phase before treatment initiation. Due to the rapid population doubling of the HCT116 cell line pair, 72Hrs drug exposure was also carried out using the same density. At the end of the treatment the cells were fixed stained and analysed as described in materials and methods (2.2). The drug combination schedule in this chapter was simultaneous unless otherwise stated. Solvent concentration was kept at 1% DMSO

which is a non-growth inhibitory concentration in these cell lines. GI50 values were determined by fitting a Lowess/Spline curve to the data-points and interpolating the X-coordinate from Y at 50% on the curve.

5.3.3 Measuring synergy in drug combination treatments

Synergy experiments summarised in 5.5.8 were carried out by Ms Rachael Mason, an MRes student under the supervision of Ms Maryam Zanjirband and the author of this thesis. Ovarian cancer cells lines described in Table 5-1 were seeded in 96-well plates 24Hrs before being treated with 1:1 ratio combinations of doses for each compound and fixed and stained as above after 72Hrs. Mean SRB optical density of cells fixed 24Hrs post-seeding (Day 0) was subtracted from SRB optical density from all wells prior to all calculations. The combination index (CI) values were produced by median dose-effect analysis using CalcuSyn v2 (Biosoft, Cambridge, UK) software as described in 2.3.2.

5.3.4 Treatment of cells before FACS analysis

FACS analysis was carried out as described in general materials and methods (2.6) to analyse cell cycle distribution changes and apoptosis associated with drug induced growth arrest and cell death over 72 hours following drug exposure. Cells were seeded 24Hrs before treatment with media/solvent/drug(s) and were harvested every 24 hours for analysis of cell cycle distribution by propidium iodide (PI) staining and FACS analysis. Suspension and adherent cells in all wells were pooled before being prepared for FACS analysis as described in (2.6).

5.3.5 Quantification of Caspase-3/7 catalytic activity

The Caspase-Glo® 3/7 assay system from Promega was used as described in Materials and Methods (2.8). Cells were seeded at densities stated in materials and methods and allowed to adhere for 24 hours before being treated with 1% DMSO, 2.5µM GSK2830371 and multiples of Nutlin-3 GI50 ± 2.5µM GSK2830371. Caspase-3/7 activity mediated luminescence was then measured 24 and 48 hours following drug treatment and absolute luminescence values of the DMSO/drug treated samples were normalised to media control values in order to assess their effect on Caspase-3/7 catalytic activity at that given time-point.

5.3.6 Continuous exposure cloning efficiency experiments

Continuous exposure cloning efficiency experiments were carried out in HCT116^{+/+}

cells as caspase 3/7 activity could not be detected in this cell line. Cells were seeded in 100mm dishes (corning) and left for 24 hours to adhere. They were then treated as outlined in the table and left to form colonies over 12 days. Visible colonies (>50 cells) were counted and plotted as absolute cloning efficiency values.

Treatment	Media	DMSO	GSK2830371 (2.5µM)	Nutlin-3 (4.5µM)	Combination
Cells/dish	250	250	250	4000	4000

Table 5-2 Number of cells seeded per 100mm dish for assessing cloning efficiency in response to the stated treatments.

5.3.7 Statistical analysis

The significance of differences between mean values was obtained by comparing the mean of 3 or more paired biological repeats using a paired t-test and p-values <0.05 were considered statistically significant.

5.4 Results

5.5 Sensitivity to single agent GSK2830371 in cell *TP53* wild-type and mutant cell line pairs differing in *PPM1D* genetic status

The novel and selective WIP1 inhibitor GSK2830371 was used to assess the role of WIP1 in the growth and proliferation of *TP53* wild-type and mutant/null cell line pairs differing in their *PPM1D* genetic status. SRB Growth inhibition assays were performed with 0.08-10µM GSK2830371 (WIP1i) as described in paragraph 3.3.2. MCF-7 cells were the only cell line sensitive to treatment with single agent GSK2830371, with a mean GI50 value of 2.65µM ± 0.54 (Mean ± SEM) (Figure 5-2). All the other cell lines had GSK2830371 GI50 values >10µM irrespective of their *PPM1D* or *TP53* genetic status and basal protein expression. Interestingly, the SRB growth inhibition curve for GSK2830371 in MCF-7 cells plateaued at doses in the range 2.5µM-10µM suggesting that a subpopulation of MCF-7 cells is resistant to growth inhibition following maximal inhibition of WIP1 catalytic activity.

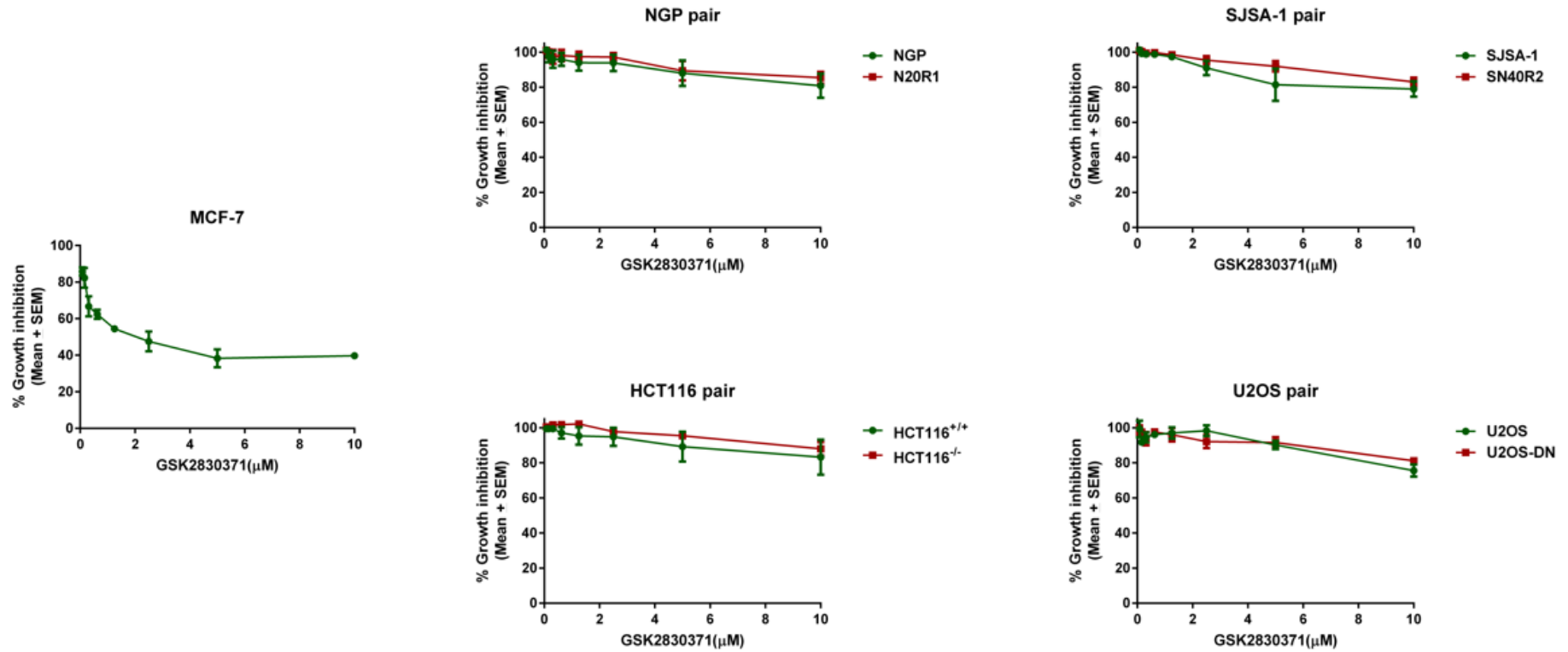


Figure 5-2 Week-long (168hrs) dose-dependent growth inhibition in response to the WIP1 inhibitor GSK2830371 in MCF-7 cells and the four *TP53* wild-type (Green) and mutant (Red) cell line pairs. MCF-7 cells are the most sensitive cell line to GSK2830371 as a single agent.

5.5.1 GSK2830371 potentiates the response to MDM2 inhibitors Nutlin-3 and RG7388 in a p53-dependent manner

The highest non-growth inhibitory dose of GSK2830371 (2.5 μ M), which corresponded approximately to the MCF-7 GI50, was combined with Nutlin-3/RG7388 to assess the effect of WIP1 inhibition on the response to MDM2 inhibitors. GSK2830371 at 2.5 μ M concentration potentiated the response to Nutlin-3 and RG7388 in a p53-dependent manner in cell lines that are not sensitive to growth inhibition by that dose of GSK2830371 alone (Figure 5-3). *TP53* wild-type parental cell lines HCT116, NGP and SJSA-1 showed a 2.4-fold (p=0.007), 2.1-fold (p=0.039) and 1.3-fold (p =0.017) decrease in their Nutlin-3 GI50 values respectively in the presence of GSK2830371 at 2.5 μ M. In contrast the Nutlin-3 GI50 did not change in their *TP53* null/mutant matched pairs: HCT116^{p53^{-/-}}, N20R1 and SN40R2. Interestingly, pertinent to the possibility of gaining a potential improvement in the MDM2 inhibitor therapeutic index in the clinic, the same dose of GSK2830371 resulted in a much greater potentiation of RG7388 in *TP53* wild-type cell lines with either *PPM1D* gain-of-function or copy number gain. NGP 5.8-fold (p=0.049), U2OS 5.3-fold (p=0.039) and HCT116^{+/+} 4.8-fold (p=0.018) compared to *PPM1D* wild-type SJSA-1 cells 1.4-fold (p=0.020). None of the *TP53* mutant/null isogenic daughter cell lines were growth inhibited by RG7388 \pm 2.5 μ M GSK2830371.

Despite the significant potentiation of RG7388, U2OS *TP53* Wt cells showed a trend towards potentiation of Nutlin-3 in combination with GSK2830371 at 2.5 μ M as the Nutlin-3 GI50 was reduced by 3.2-fold, however this was borderline not statistically significant (p=0.08). U2OS-DN cells were not sensitive to either treatment. Interestingly the growth inhibition curve for HCT116^{+/+} cells in response to Nutlin-3/RG7388 \pm GSK2830371 plateaued at approximately 30-45%. This was most likely caused by the combination of a resistant sub-population and relatively rapid doubling time (\approx 24Hrs) for this cell line, which meant that the resistant subpopulation would have grown back considerably by the end of the experiment. When the same seeding density of HCT116^{+/+} cell was used in a 72 hour growth inhibition, a 2.4-fold (p=0.01) and 2.7-fold (p=0.008) reduction in Nutlin-3 and RG7388 GI50 was observed respectively (Figure 5-4); moreover the subpopulation of resistant cells was reduced. This suggests that there is a resistant subpopulation of HCT116^{+/+} cells which may recover if in response to this combination treatment.

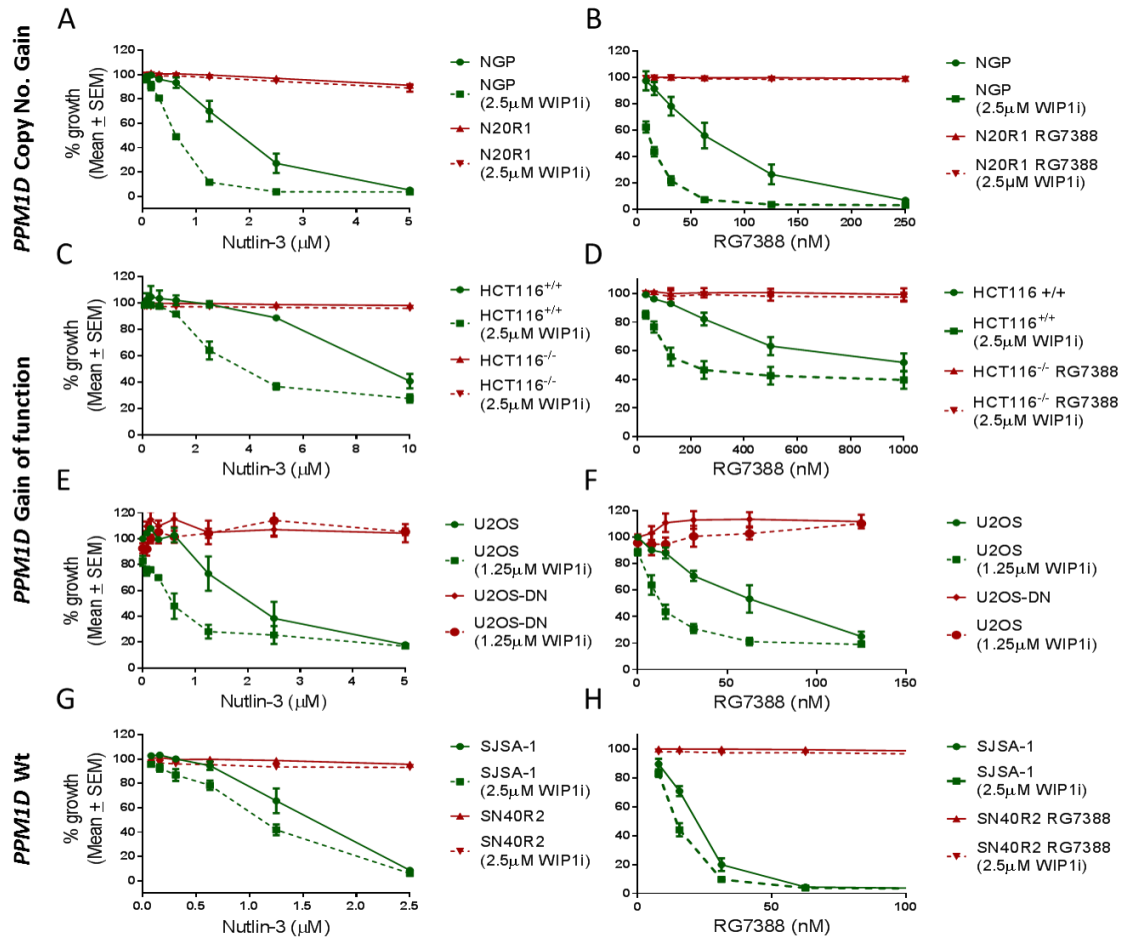


Figure 5-3 Non-growth inhibitory doses of GSK2830371 (WIP1i) potentiated the response of *TP53* wild-type cell lines to MDM2 inhibitors. A-H) SRB growth inhibition assays were performed on cell lines described in 5.3.2 with stated doses of Nutlin-3/RG7388 in the presence or absence of 2.5μM GSK283037.

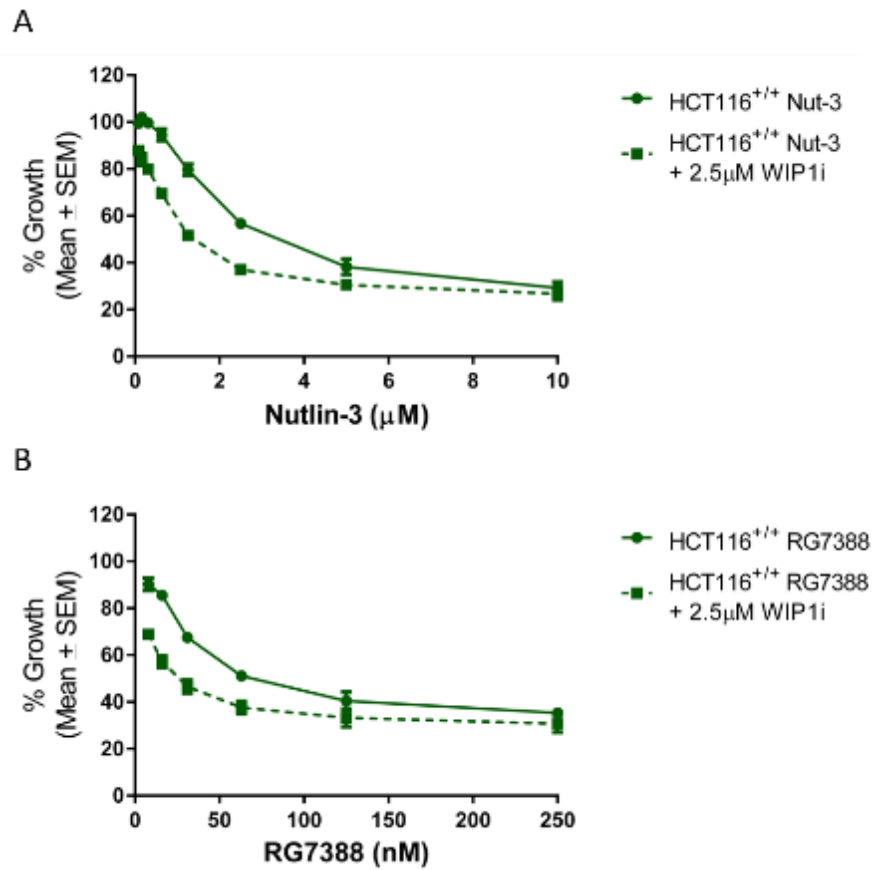


Figure 5-4 Non-growth inhibitory dose of 2.5µM GSK2830371 (WIP1i) potentiated the response of HCT116^{+/+} cells to Nutlin-3 and RG7388 to a lesser extent over 72 hours. A & B) SRB growth inhibition assays performed on HCT116^{+/+} cells with the stated doses of Nutlin-3/RG7388 in the presence or absence of 2.5µM GSK283037.

5.5.2 Biochemical response to single agent GSK2830371 in MCF-7 cells

Single agent growth inhibitory activity of the WIP1 inhibitor GSK2830371 in MCF-7 cells was associated with its ability to stabilise p53, increase p53 phosphorylation on Ser15 (pp53^{Ser15}), and induce p21^{WAF1} as a single agent at approximately the MCF-7 GI50 dose (2.5µM) of GSK2830371 (Figure 5-5 A & B). In Figure 5-5B p38 inhibitor did not appear to notably impact response to GSK2830371 so it was not further investigated but the p21^{WAF1} signal is more obvious in this blot. This suggests that growth inhibition in MCF-7 cells is likely through p53 stabilisation and its induction of p21^{WAF1}. There was a marked reduction in total WIP1 expression following 2.5µM GSK2830371 which is consistent with the reports that this compound promotes the degradation of WIP1 (Gilmartin, Faitg et al. 2014). There was an accompanying notable reduction in MDM2 expression in MCF-7 cells following GSK2830371 treatment, which is consistent with the reported role of WIP1 in increasing MDM2 stability (Lee, Kim et al. 2007).

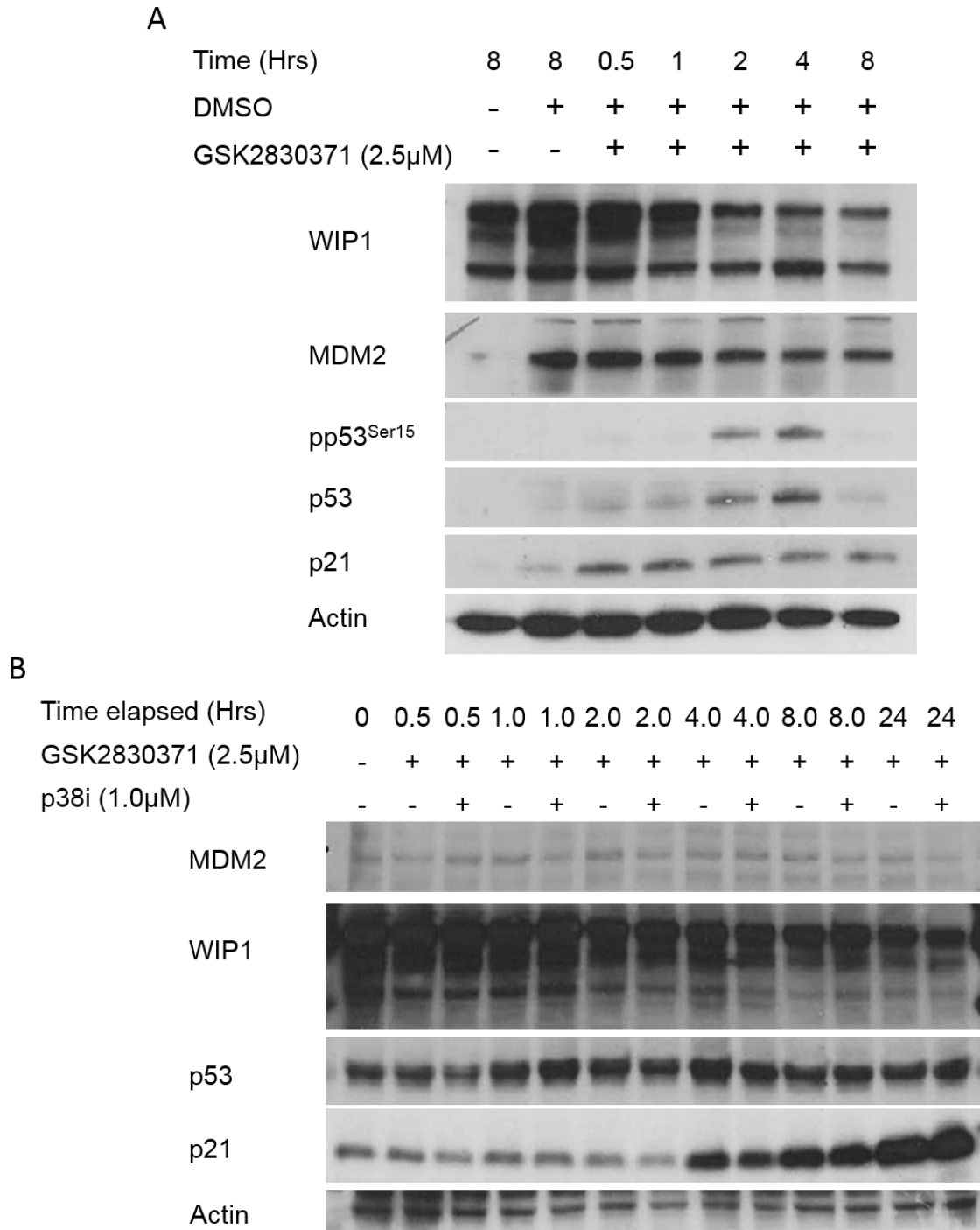


Figure 5-5 A & B) Biochemical response of MCF-7 cells to 2.5 μ M GSK2830371 (~GI50) and its impact on p53 transcriptional activity and post-translational modification over time. GSK2830371 results in time-dependent degradation of WIP1, stabilisation of p53, increased p53^{Ser15} and induction of p21^{WAF1}.

5.5.3 Biochemical response to single agent GSK2830371 treatment and its combination with Nutlin-3 in NGP cells

WIP1 inhibition by 2.5 μ M GSK2830371 resulted in a marked reduction in WIP1 protein expression in NGP cells which persisted through to 24Hrs following treatment (Figure 5-6A). However, stabilisation of p53, its phosphorylation at Ser15 and induction of p53 transcriptional targets such as MDM2, p21^{WAF1} and BAX was not detected in response to single treatment with GSK2830371 (Figure 5-6A & B). Well-established p53 transcriptional targets, notably MDM2 and WIP1, were induced following treatment with 3 μ M Nutlin-3 (Figure 5-6A & B). Where Nutlin-3 and GSK2830371 were combined, Nutlin-3 mediated WIP1 induction appeared to be offset by GSK2830371 mediated degradation. Phosphorylated p53^{Ser15} was observed most strongly in the combined presence of the WIP1 inhibitor with Nutlin-3 and was associated with the detection of cleaved caspase-3 at 24hrs.

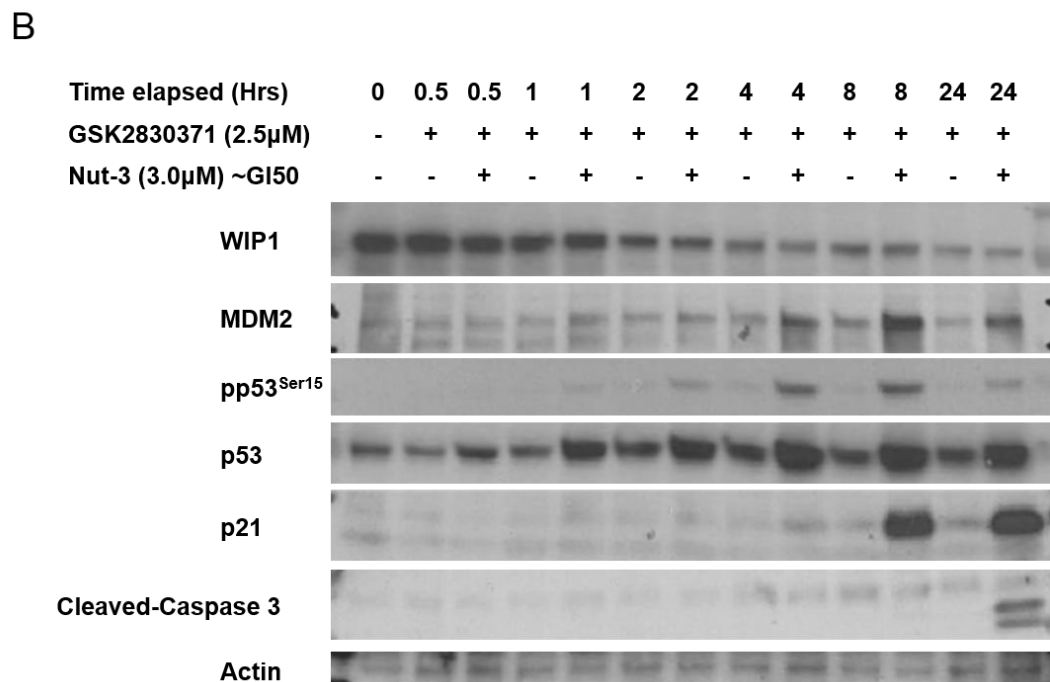
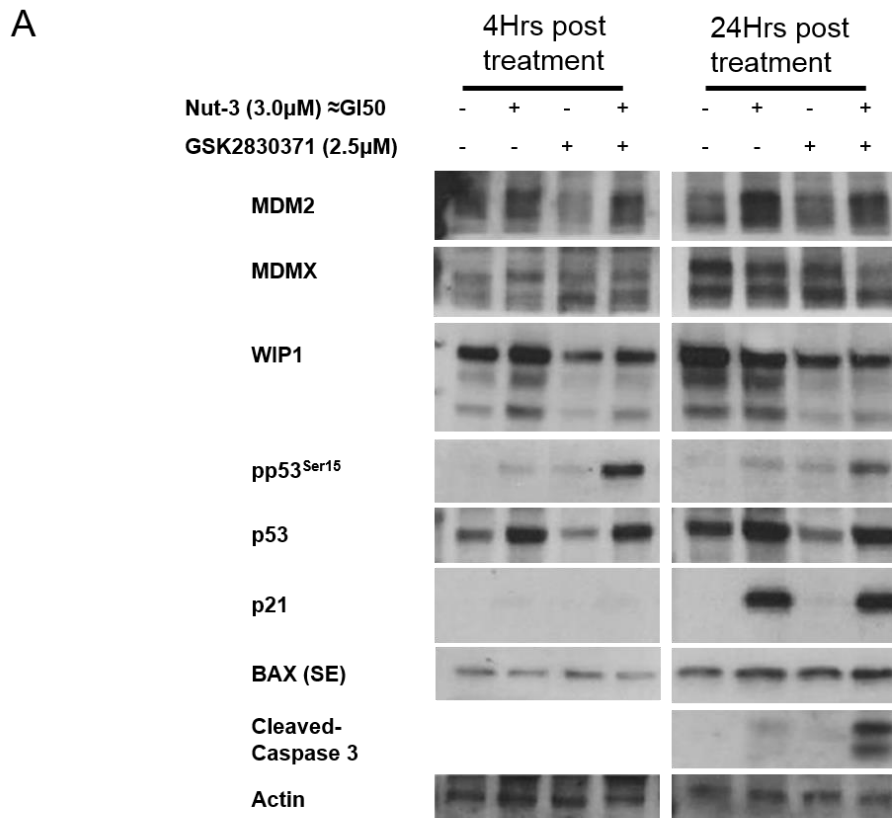


Figure 5-6 A) Biochemical response of NGP cells to the stated doses of Nutlin-3, GSK2830371 and their combinations at 4Hrs and 24Hrs. In contrast to the single treatment with each agent, phosphorylated p53^{Ser15} (pp53^{Ser15}) is most prominently detected in response to the combination treatment and it is associated with p53 stabilisation over the time course and cleaved caspase-3 at 24Hrs. B) Immunoblot showing the biochemical response to single agent GSK2830371 and its combination with 3 μ M Nutlin-3 over time. Treatment with 2.5 μ M GSK2830371 alone results in degradation of WIP1 but does not induce p53 transcriptional targets.

5.5.4 WIP1 inhibition by GSK2830371 potentiates caspase-3/7 activation by Nutlin-3 in NGP and SJSA-1 cell lines

Caspase 3/7 catalytic activity was measured following treatment with multiples of Nutlin-3 GI50 \pm GSK2830371 (2.5 μ M) in order to quantify and compare the amount of caspase-3/7 activation as a measure of apoptosis between these regimens.

NGP cells and SJSA-1 cells showed a dose-dependent increase in their caspase-3/7 activity in response to multiples of their Nutlin-3 GI50 values (0.5 \times and 1 \times GI50) at 24 and 48 hours respectively (Figure 5-7). However, caspase 3/7 activity could not be detected in these cell lines following 2.5 μ M GSK2830371 alone. In NGP cells, 24 hour combination treatment with 0.5 \times and 1 \times Nutlin-3 GI50 + 2.5 μ M GSK2830371 resulted in a 3.2-fold (p=0.005) and 4.1-fold (p=0.02) increase in caspase-3/7 activity respectively compared to Nutlin-3 alone at either dose (Figure 5-7A). In NGP cells 48 hour treatment with Nutlin-3 GI50 resulted in a 1.8-fold increase (p=0.002) in caspase-3/7 catalytic activity which was then increased by 3.1-fold (p=0.01) in the presence of 2.5 μ M GSK2830371. Treatment of the NGP derived Nutlin-3 resistant, *TP53* mutant daughter cell line (N20R1 cells), with Nutlin-3 alone or in combination with WIP1 inhibitor treatment for 48 hours, did not result in detectable increase in caspase-3/7 catalytic activity.

In SJSA-1 cells caspase-3/7 activity response was not detected until 48 hours after treatment with 0.5 \times and 1 \times Nutlin-3 GI50 (Figure 5-7B). The presence of 2.5 μ M GSK2830371 resulted in a 2-fold (p=0.04) increase in caspase-3/7 activity compared to the effect of the GI50 dose of Nutlin-3 alone in SJSA-1 cells (Figure 5-7B). Treatment of the SJSA-1 derived Nutlin-3 resistant, *TP53* mutant daughter cell line (SN40R2 cells), with Nutlin-3 alone or in combination with WIP1 inhibitor treatment for 48 hours, did not result in detectable increase in caspase-3/7 catalytic activity.

An increase in caspase-3/7 catalytic activity was not detected in MCF-7 and HCT116^{+/+} cell lines following treatment with multiples of Nutlin-3 GI50 and/or 2.5 μ M GSK2830371 at 24 and 48 hours (Data shown in the methods section). These results were consistent with previous reports that MCF-7 cells do not express caspase-3 and that they undergo apoptosis through caspase-3 independent mechanisms (Oberhammer, Wilson et al. 1993, Jänicke, Sprengart et al. 1998, Eck-Enriquez, Kiefer et al. 2000). Also HCT116^{+/+} cells reportedly do not undergo apoptosis in response to MDM2

inhibitors (Huang, Deo et al. 2009).

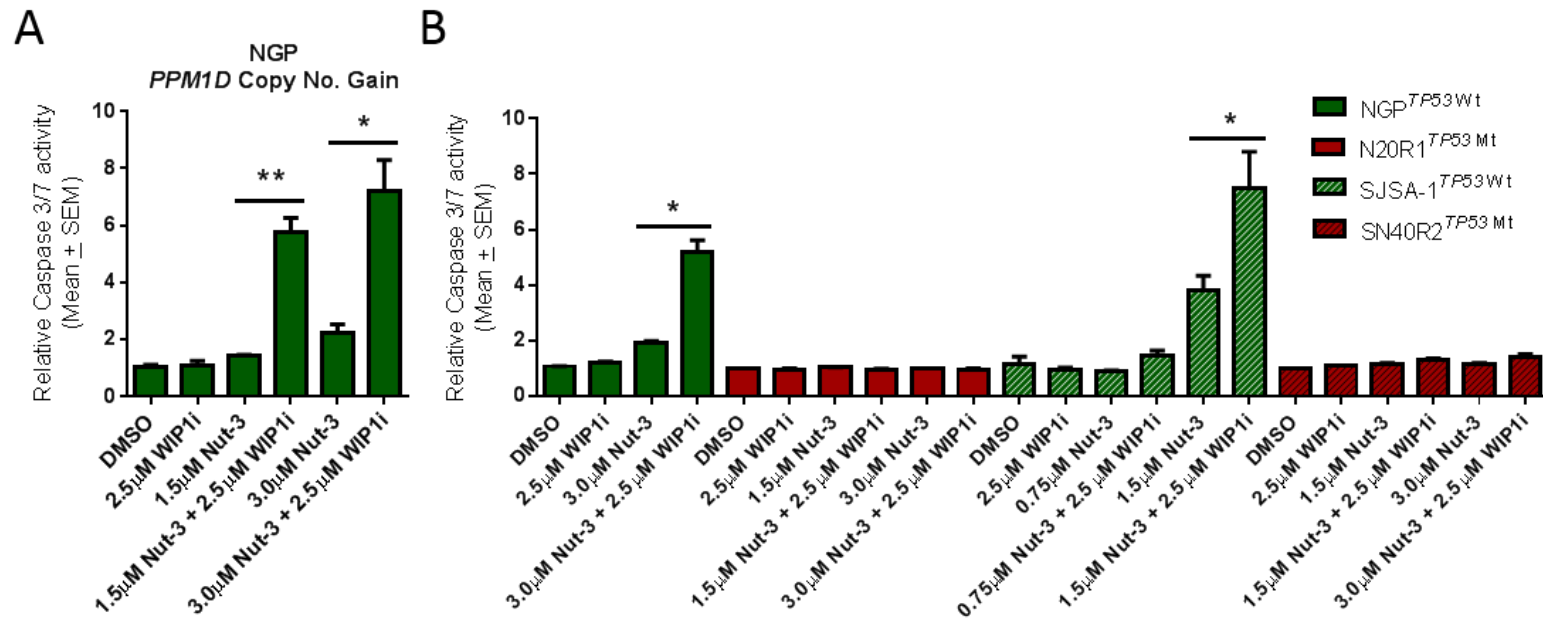


Figure 5-7 WIP1 inhibitor GSK2830371 (WIP1i) potentiates the Nutlin-3 mediated caspase-3/7 activity in *TP53* Wild-type parental cell lines and not their *TP53* mutant Nutlin-3 resistant daughter cells. **A)** NGP cells were treated with 0.5 \times and 1 \times their approximate Nutlin-3 GI50 (1.5 μ M and 3.0 μ M respectively) \pm 2.5 μ M GSK2830371 for 24 hours and Caspase-3/7 catalytic activity was quantified. **B)** Caspase-3/7 activity in response to 48 hour treatment with Nutlin-3 GI50 (3.0 μ M) \pm 2.5 μ M GSK2830371 was measured in NGP cells showing that the combination treatment results in a significant increase in caspase-3/7 signal. SJSA-1 cells were treated with 0.5 \times and 1 \times their approximate Nutlin-3 GI50 (0.75 μ M and 1.5 μ M respectively) \pm 2.5 μ M GSK2830371 for 48 hours and Caspase-3/7 catalytic activity was quantified. There was no caspase-3/7 catalytic activity in neither of the Nutlin-3 resistant cell lines (red bars) derived from NGP and SJSA-1 (green bars). P-values represent paired t-test. *: $p < 0.05$; **: $p < 0.005$.

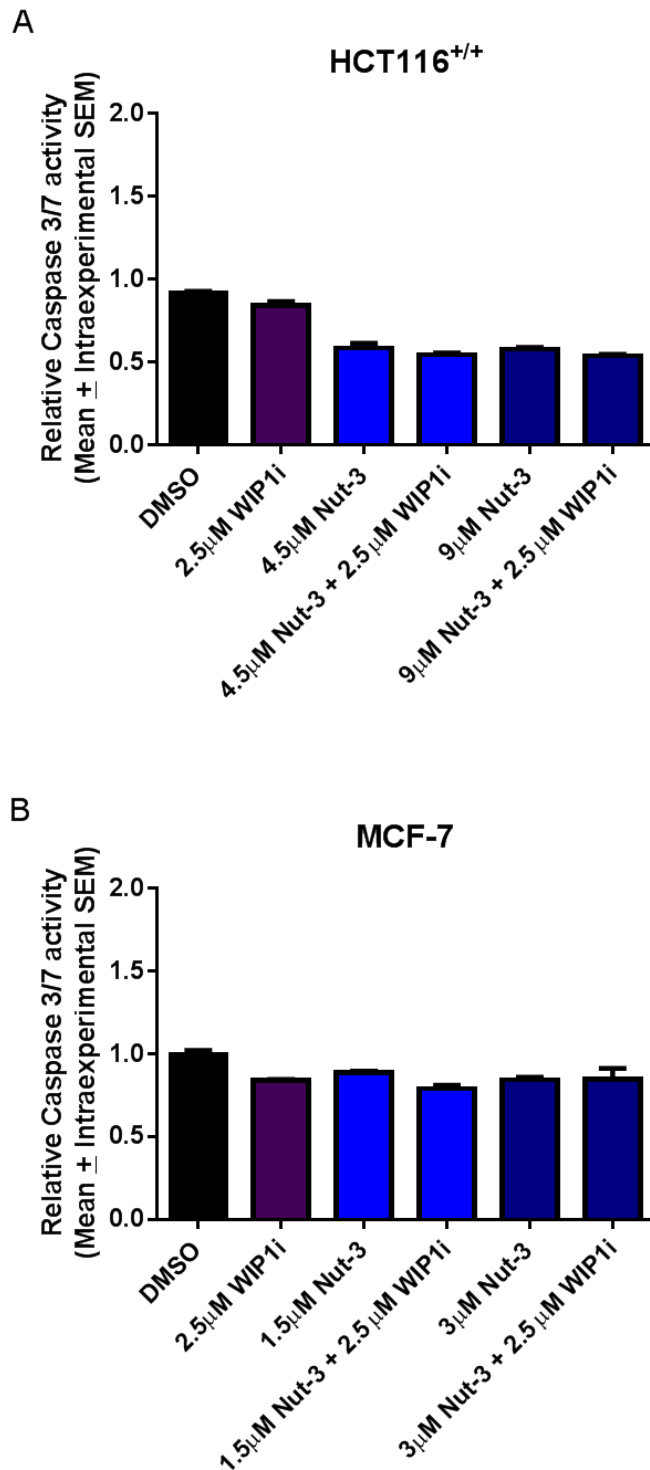


Figure 5-8 Induction of caspase-3/7 activity was not detected in HCT116^{+/+} and MCF-7 cells 48 hours following treatment with Nutlin-3 ± 2.5 μM GSK2830371 (WIP1i). A) HCT116^{+/+} cells treated with 0.5 × and 1 × their Nutlin-3 GI50 (4.5 μM and 9.0 μM respectively) ± 2.5 μM GSK2830371 for 48 hours and Caspase-3/7 catalytic activity was quantified. B) MCF-7 cells were treated with 0.5 × and 1 × their approximate Nutlin-3 GI50 (1.5 μM and 3.0 μM respectively) ± 2.5 μM GSK2830371 for 48 hours and Caspase-3/7 catalytic activity was quantified.

5.5.5 Potentiation of MDM2 inhibitors by GSK2830371 in HCT116^{+/+} cells is due to increase in p53 mediated cell cycle arrest.

Because neither caspase-3/7 activity nor cleaved caspase-3 were detected in HCT116^{+/+} cells in response to any of the treatments, continuous exposure cloning efficiency experiments were carried out to assess any potential reduction in survival by other mechanisms. There was no reduction in the cloning efficiency of HCT116^{+/+} cells in response to 2.5 μ M GSK2830371 alone in spite of the activating *PPM1DL450X* mutation (Figure 5-9A). However, there was a significant decrease in clonogenic survival of this cell line following Nutlin-3 at 0.5 \times GI50 dose compared to DMSO or WIP1 inhibitor treatment alone (p=0.02). Remarkably the combination of Nutlin-3 and GSK2830371 resulted in 89-fold reduction in cloning efficiency of HCT116^{+/+} cells (p=0.008).

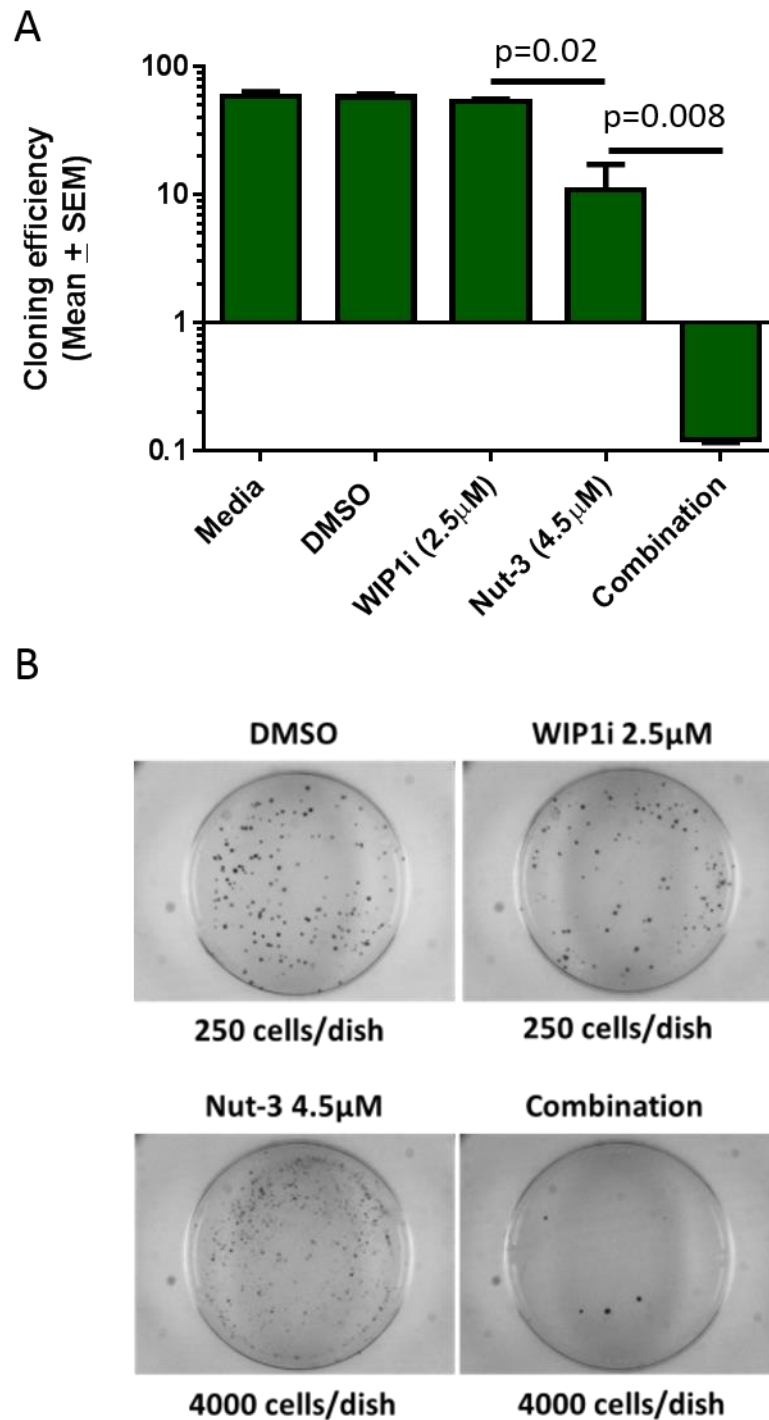


Figure 5-9 A) Continuous treatment clonogenic efficiency experiment in HCT116^{+/+} cell lines in response to 4.5µM Nutlin-3 (0.5 × GI50) ± 2.5µM GSK2830371 (WIP1i). B) Colony formation following 10 days of treatment. Images representative of the biggest difference observed between single and combination treatment among the three independent repeats. P-value t-test.

5.5.6 Biochemical response of HCT116^{+/+} cells in response to GSK2830371 and its combination with MDM2 inhibitors

Interestingly, the combination of 3.0 μ M Nutlin-3 and 2.5 μ M GSK2830371 resulted in a marked increase in p21^{WAF1} induction compared to each drug alone 4Hrs following treatment (Figure 5-10). Of additional interest, the truncated gain-of-function (*PPM1DL450X* gene product) protein was also degraded following GSK2830371.

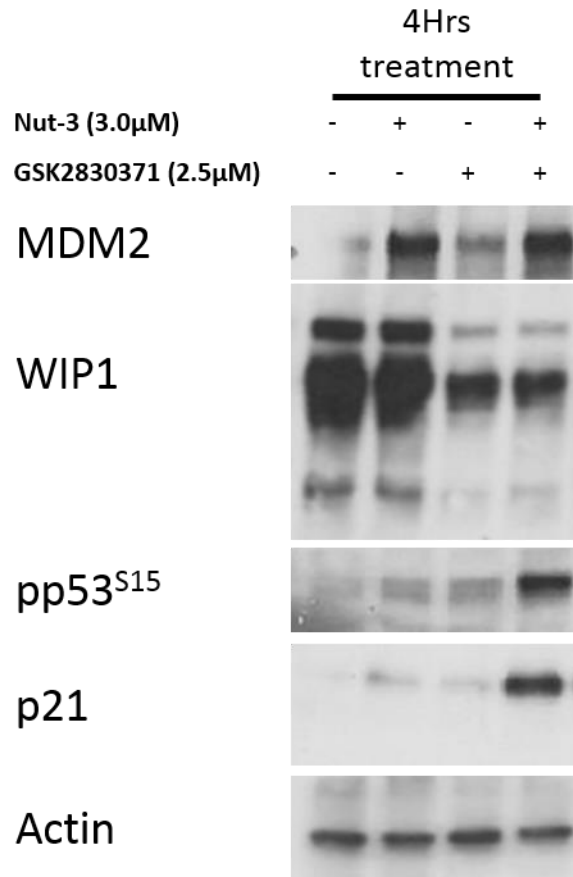


Figure 5-10 Biochemical response of HCT116^{+/+} cells to 3 μ M Nutlin-3, 2.5 μ M GSK2830371, or their combination after 4Hrs treatment.

5.5.7 Analysis of cell cycle distribution by FACS following pharmacological inhibition of MDM2, WIP1 or their combination

In all cell lines, 2.5 μ M GSK2830371 alone did not significantly affect cell cycle distribution throughout 72 hours of treatment (Figure 5-11). Changes in cell cycle distribution after exposure to Nutlin-3 + 2.5 μ M GSK2830371 were cell line-dependent. In SJSA-1 and NGP cell lines, 24 hours exposure to Nutlin-3 resulted in an increase in the proportion of cells in G1/G0 phases of the cell cycle. In SJSA-1 cells this effect of Nutlin-3 remained unchanged in the following 48 hours treatment with Nutlin-3 + GSK2830371. However, in NGP cells the relative proportion of cells in G2/M and S-phase increased over the following 48 hours when Nutlin-3 and the WIP1 inhibitor were combined compared to Nutlin-3 alone. In HCT116^{+/+} cells Nutlin-3 resulted in an increase in the proportion of cells in G1/G0 and G2/M phases at 24 hours, which persisted to the 72 hours treatment time point (Figure 5-11) Cell cycle distribution was not affected in HCT116^{-/-} cells regardless of the treatment condition, suggesting that the changes in cell cycle distribution observed in HCT116^{+/+} cells are p53-dependent (Figure 5-11).

In response to the combination treatment compared to Nutlin-3 alone, the increase in SubG1 FACS signal after exposure to Nutlin-3 was significantly augmented in the presence of 2.5 μ M GSK2830371 (WIP1i) in both SJSA-1 and NGP cell lines (Figure 5B and Supplementary figure S4B). This is in keeping with the increased cleaved caspase-3/7 activity in NGP and SJSA-1 cells (Figure 5-12). Sub-G1 signals were not significantly changed in HCT116^{+/+} cells throughout the 72 hours of Nutlin-3 \pm GSK2830371 treatment (Figure 5-12).

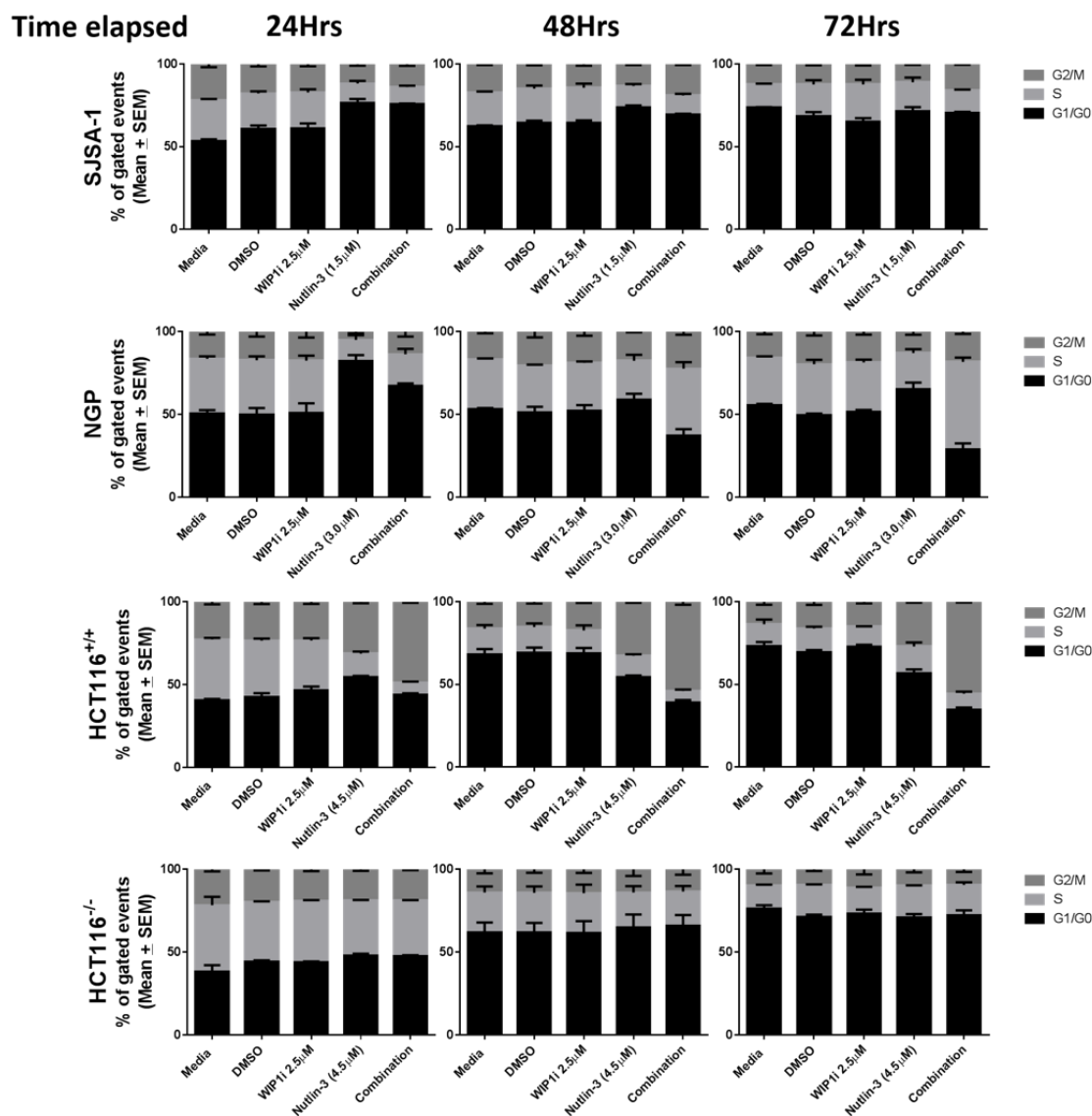


Figure 5-11 Analysis of cell cycle distribution of *TP53* wild-type cells treated with stated doses of Nutlin-3 (GI50 or 0.5 × GI50 dose), GSK2830371 (WIP1i), or combination over 72 hours. Sub-G1 events were gated out in this analysis.

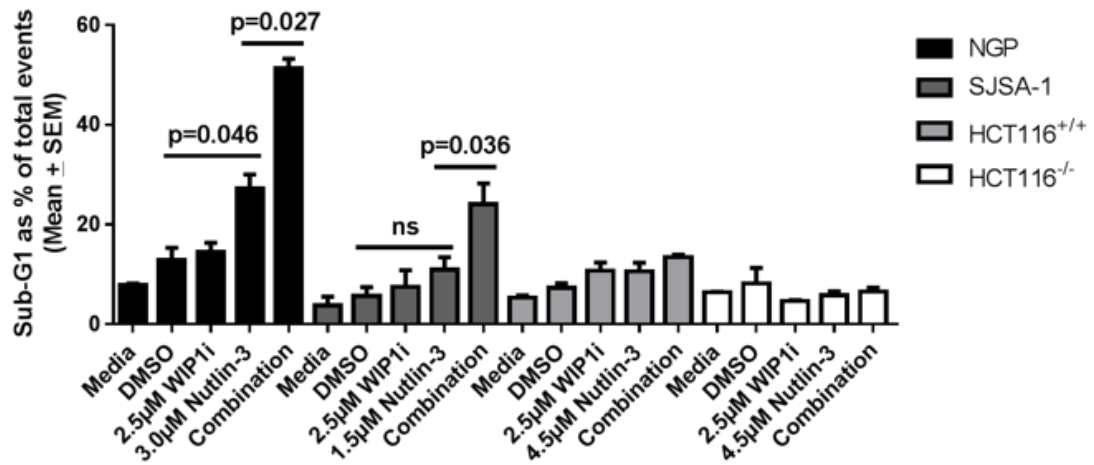


Figure 5-12 Representative cell cycle distribution histograms for NGP and SJSA-1 cells indicating the increase in the proportion of Sub-G1 events in response to 72 hours of treatment with GSK2830371 (WIP1i), Nutlin-3 and their combination. P-values are from paired t-test.

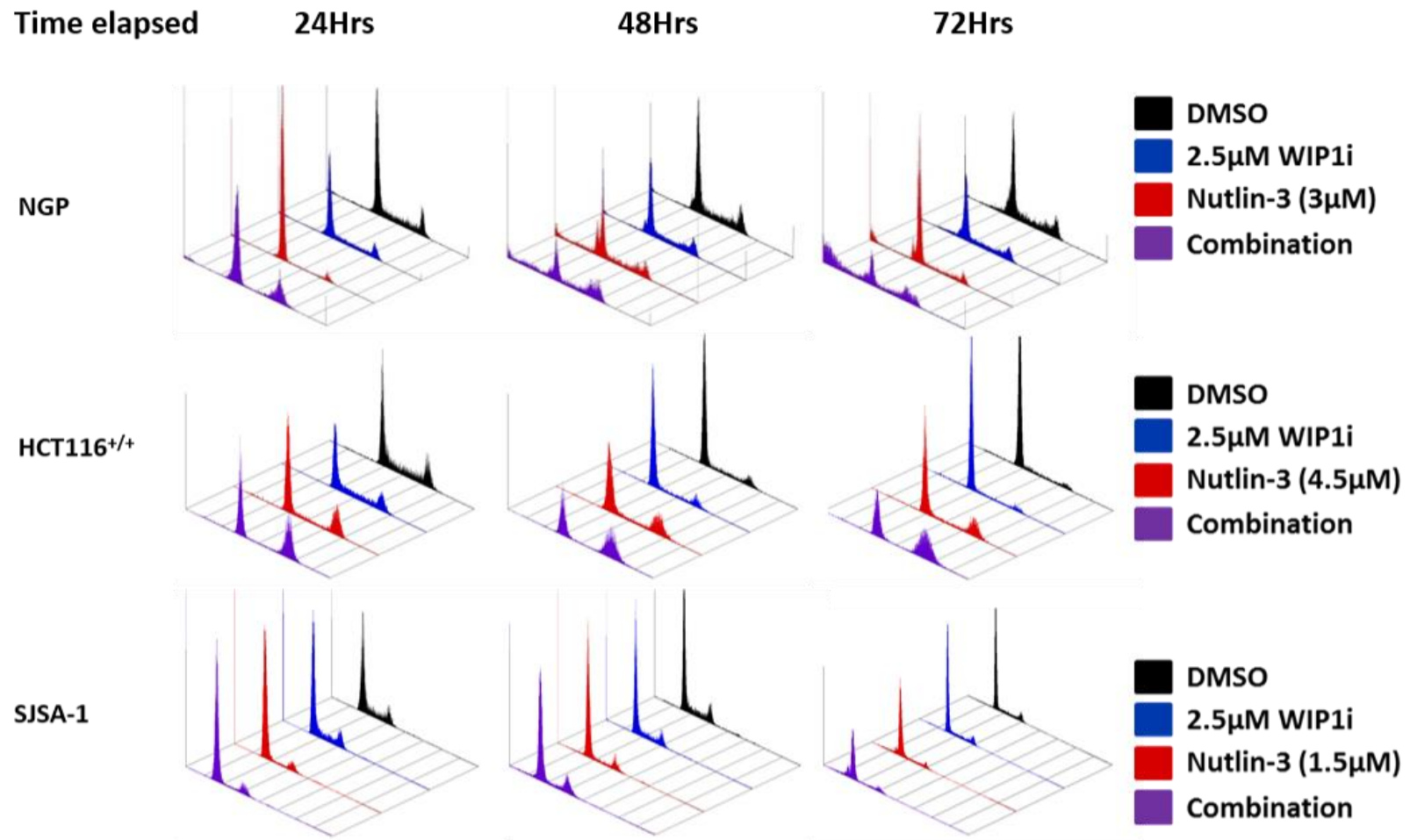


Figure 5-13 3D representation of analysis of cell cycle distribution histograms following treatment with multiples of Nutlin-3 GI50 dose \pm 2.5µM GSK2830371 (WIP1i). Histograms correspond to one biological repeat representative of grouped bar charts in [Figure 3-21](#).

5.5.8 GSK2830371 synergises with MDM2 inhibitors in *TP53* wild-type ovarian cancer cell lines

Mosaic *PPM1D*-truncating activating mutations have been reported to predispose individuals to breast and ovarian carcinoma (Ruark, Snape et al. 2013). *PPM1D* copy number gain is also associated with poor overall survival in ovarian carcinoma and has been shown to be a potential therapeutic target (Tan, Lambros et al. 2009). A panel of ovarian cell lines differing in their *TP53* genetic status was used to assess their functional and cellular response to GSK2830371 and its combination with MDM2 inhibitors. Relevant results summarised here were produced by Ms Rachael Mason, under the co-supervision of Mrs Maryam Zanjirband and the author of this thesis. Mono-treatment with GSK2830371 resulted in different degrees of growth inhibition in *TP53* wild-type ovarian cancer cell lines with a 50% growth inhibitory concentration (1.88 ± 0.67) only being achieved in PA-1 cells within the dose range tested (0.09-12 μ M) (Figure 5-14A). Interestingly this was the only cell line with a *PPM1D*-truncating activating mutation (c.1370delC, p.A457fs*8). All *TP53* wild-type cell lines were responsive to both Nutlin-3 and RG7388 in contrast to the two *TP53* mutant cell lines (Figure 5-14B and C). 4 hour treatment with incremental GSK2830371 doses resulted in marked p53 stabilisation and increased p53^{Ser15} phosphorylation in PA-1 cells (Figure 5-14D). This occurred to a lesser extent in the other *TP53* wild-type cell lines which were less sensitive to GSK2830371 (Figure 5-14D). Moreover, in all cell lines WIP1 protein was degraded at 4 hours after GSK2830371 exposure.

Combination of multiples of different growth inhibitory doses of GSK2830371 with multiples of MDM2 inhibitor GI50 doses resulted in more than additive or synergistic response in all *TP53* wild-type cell lines as measured by combination index (CI) values (Figure 5-15A & B) (Chou and Talalay 1984). Synergism was more pronounced at lower doses (Figure 5-15B).

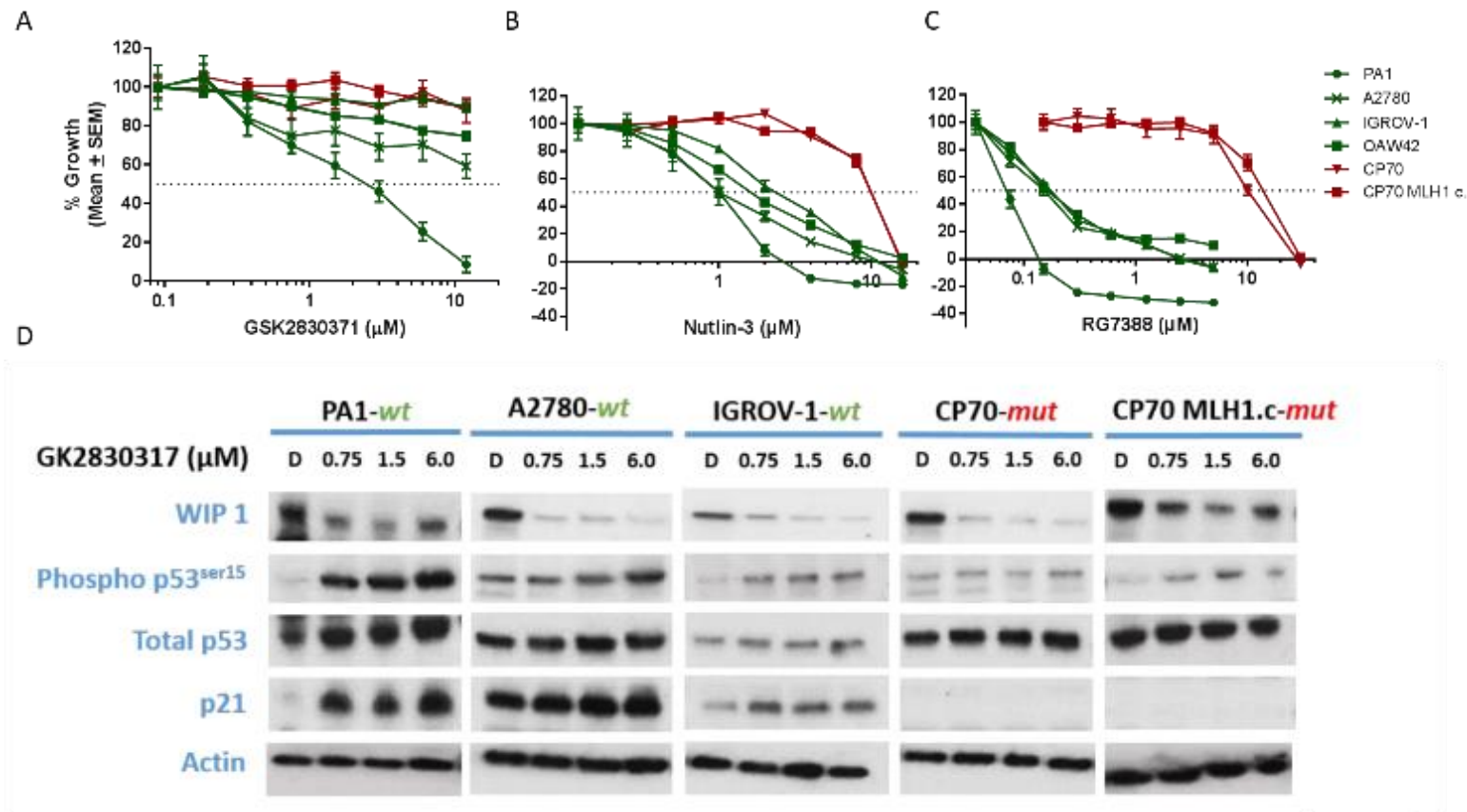


Figure 5-14 A) 72Hrs GSK2830371 SRB growth inhibition in a panel of *TP53* wild-type (wt-green) and mutant (mut-red) ovarian cancer cell lines. B & C) Cellular sensitivity to MDM2 inhibitors Nutlin-3 and RG7388. D) Immunoblots showing the biochemical response to GSK2830371 after 4 hours. PA1 cells harbouring a *PPM1D*-truncating activating mutation (c.1370delC) show the most p53 activation following treatment with GSK2830371.

A

CI Range	Description
<0.1	Very strong synergism
0.1-0.3	Strong synergism
0.3-0.7	Synergism
0.7-0.85	Moderate synergism
0.85-0.9	Slight synergism
0.9-1.1	Nearly additive
1.1-1.2	Slight antagonism
1.2-1.45	Moderate antagonism
1.45-3.3	Antagonism
3.3-10	Strong antagonism
>10	Very strong antagonism

B

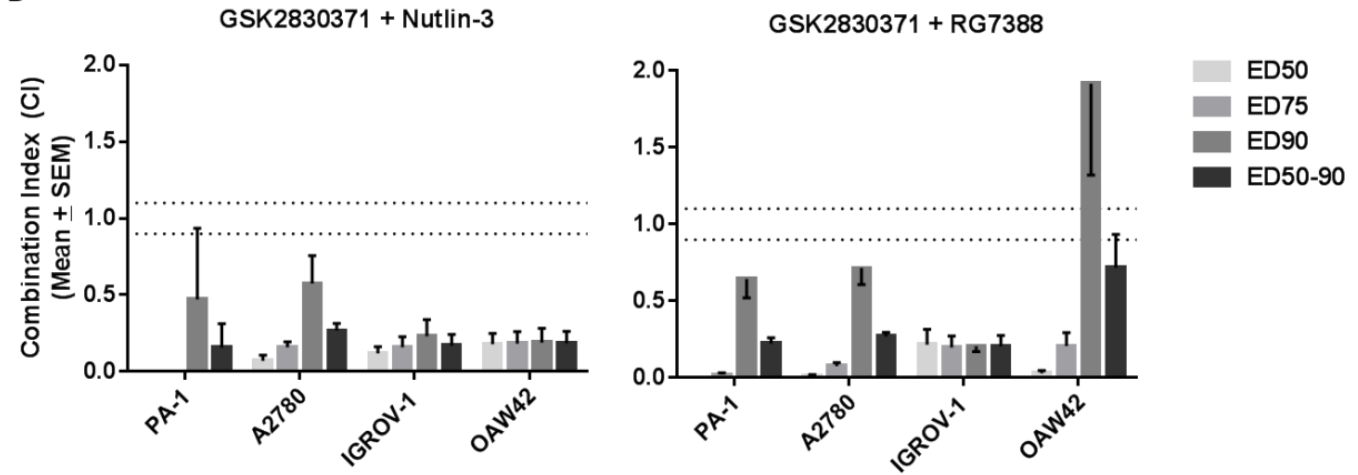


Figure 5-15 A) Table in aid of interpretation of combination index (CI) values. B) CI values calculated based on 3 independent repeats if 72Hrs growth inhibition experiments combining MDM2 inhibitors Nutlin-3/RG7388 and GSK2830371 at 1:1 ratio of doses with known effects. MDM2 inhibitors are shown to synergise with GSK2830371 at lower doses.

5.6 Discussion

MDM2 inhibitors are small targeted anti-tumour agents in pre-clinical and clinical development. Multiple pharmaceutical companies have compounds in late stage development and early phase clinical trials, hoping to establish the best in class clinical candidate, with Roche Pharmaceuticals presently leading the race (Ray-Coquard, Blay et al. 2012, Ding, Zhang et al. 2013, Zhao, Liu et al. 2013, Zhao, Aguilar et al. 2015). Preclinical and clinical data show that there is a heterogeneity in sensitivity to MDM2 inhibitors, even within and between, cell lines and tumours with a *TP53* wild-type genetic background (Ray-Coquard, Blay et al. 2012, Saiki, Caenepeel et al. 2015). Addressing this heterogeneity is in part also limited by on-target MDM2 inhibitor dose-limiting toxicity in a subpopulation of patients causing neutropenia and thrombocytopenia (Ray-Coquard, Blay et al. 2012, Iancu-Rubin, Mosoyan et al. 2014). Therefore research into determinants of sensitivity to MDM2 inhibitors is an important step in optimising their clinical use to provide a non-genotoxic alternative for wild-type *TP53* cancers or tumours with mixed population of *TP53* wild-type and mutant cells. This would allow for the design of effective combination treatment regimens which involve non-genotoxic agents capable of synergy with or potentiation of MDM2 inhibitors in a tumour-specific manner. This is provided that the second target is important for the survival of the tumour cells when p53 is activated by an MDM2 inhibitor and not important for the survival of the healthy cells in response to the same treatment. A lower dose of a chemotherapeutic agent might then be used to eliminate any remaining subpopulations of *TP53* mutant cells minimising unpleasant and sometimes irreversible off-target toxicities, particularly with genotoxic agents, while improving survival and quality of life.

5.6.1 WIP1 as a target for non-genotoxic activation of p53

The prevalence of *PPM1D* oncogenic activation, copy number gain or amplification in *TP53* wild-type malignancies is indicative of its role in negative regulation of p53 function (Saito-Ohara, Imoto et al. 2003, Rauta, Alarmo et al. 2006, Zhang, Chen et al. 2014, Richter, Dayaram et al. 2015). Multiple studies have now shown that silencing of WIP1 mRNA expression or pharmacological inhibition of its phosphatase activity can be anti-proliferative in cell lines that are dependent on WIP1 for negative regulation of wild-type *TP53* (Parssinen, Alarmo et al. 2008, Tan, Lambros et al. 2009, Gilmartin, Faitg et al. 2014, Richter, Dayaram et al. 2015). However, these data suggest *TP53*

wild-type status is necessary but not sufficient for *ex-vivo* growth inhibitory or apoptotic response to WIP1 inhibition (Gilmartin, Faitg et al. 2014). The same premise likely holds true *in-vivo* (Gilmartin, Faitg et al. 2014). Importantly, among responding cell lines there is a wide range of sensitivity to WIP1 inhibition by the most selective commercially available WIP1 inhibitor GSK2830371 (Gilmartin, Faitg et al. 2014, Richter, Dayaram et al. 2015). The exceptional selectivity of GSK2830371, owed to its targeting of a distinct allosteric site on WIP1, makes this compound a unique pharmacological tool for studying WIP1 chemical biology.

In our selected panel of *TP53* wild-type and mutant isogenic cell line pairs, with different *PPM1D* genetic status, GSK2830371 did not have single agent growth inhibitory activity within the mechanistically relevant dose range. However, MCF-7 cells treated in parallel with these isogenic pairs were responsive and therefore acted as a positive control for single agent activity of GSK2830371 in culture. Importantly, the response to single agent GSK2830371 correlated with WIP1 degradation, p53 stabilisation and Ser15 phosphorylation, followed by p21^{WAF1} induction. This was also consistent with single agent sensitivity to GSK2830371 in the ovarian panel of cell lines where the extent of growth inhibition concurred with WIP1 degradation, p53 stability and phosphorylation at Ser15 and p21^{WAF1} induction. Notably, the most GSK2830371 sensitive ovarian cancer cell line, PA-1, harboured a truncating mutation in WIP1 which is consistent with the role of activated WIP1 in regulation of p53 function. While WIP1 was also degraded by GSK2830371 in *TP53* wild-type HCT116^{+/+} and NGP cell lines, p53 stabilisation, p53^{Ser15} phosphorylation and p21^{WAF1} induction were not observed in response to GSK2830371. This correlated with no single agent GSK2830371 growth inhibitory activity in these cell lines. Therefore WIP1 inhibition/degradation by GSK2830371 does not impact the growth of the cell unless that cell relies on WIP1 for negative regulation of p53 function. Furthermore, the absence of p53 activation following GSK2830371 treatment shows that p53 dissociation from MDM2 is not dependent on WIP1 phosphatase activity in HCT116^{+/+} and NGP cell lines. This strongly supports the notion that p53 activation is necessary for *ex-vivo* growth inhibitory response to WIP1 inhibition by GSK2830371.

5.6.2 The role of WIP1 in determining sensitivity to MDM2 inhibitors

WIP1 chemical inhibition or transient knockdown consistently resulted in increased sensitivity to MDM2 inhibitors in all the *TP53* wild-type parental cell lines of the pairs

tested, while not affecting the sensitivity of their *TP53* mutant daughter cells. Potentiation/synergy occurred most notably in cell lines with *PPM1D* activating mutations or increased expression. This correlated with an increase in apoptotic endpoints as measured by caspase-3/7 activity, reduced clonogenic survival and increased Sub-G1 cell cycle signals. Interestingly, combination of MDM2 inhibitors in ovarian cancer cell lines that were sensitive to single agent GSK2830371 also resulted in synergy. An alternative form of PARP-1 cleavage associated with cathepsin mediated cell death (which was not seen with the chemical inhibitor) was also observed in response to transfection conditions and Nutlin-3 and was intensified by WIP1 siRNA knockdown (Chapter 4.4.6). The potentiation/synergy and increased apoptotic endpoints were also associated with an increased p53^{Ser15} phosphorylation.

5.6.3 Role of WIP1 in cell cycle regulation following MDM2 inhibition

Nutlin-3 mediated changes in cell cycle distribution were all enhanced in the presence of a dose of GSK2830371 which on its own did not affect cell cycle distribution. The observed increase in Sub-G1 FACS analysis signals following combination treatment of NGP and SJSA-1 cell lines with WIP1 and MDM2 inhibitors is consistent with potentiation of apoptosis and growth inhibition in these cell line. In NGP cells transient knockdown of WIP1 also resulted in an increased sensitivity to MDM2 inhibitors as measured by Sub-G1 signal in FACS analysis (See 4.4.5). This was not observed in N20R1 cells suggesting that the change in cell cycle distribution in response to the combination treatment is p53dependent.

Chemical inhibition by GSK2830371 or WIP1 knockdown did not influence Nutlin-3 mediated changes in cell cycle distribution in NGP cells However, in HCT116^{+/+} cells WIP1 inhibition enhanced the Nutlin-3 mediated increase in the proportion of cells in G2/M phase of the cell cycle whereas in HCT116^{-/-} cells no changes to cell cycle distribution were observed. This success that the additional cell cycle changes observed in response to the combination treatment are p53-dependent. A notable increase in p21^{WAF1} protein induction, as detected by western blotting, 4 hours after treatment the combination of Nutlin-3 and GSK2830371, preceded the increased proportion of cells in G2/M in HCT116^{+/+} cells. This is consistent with the importance of p21^{WAF1} negative regulation of cell cycle progression (Eldeiry, Harper et al. 1994, Deng, Zhang et al. 1995, Bunz, Dutriaux et al. 1998). Kleiblova *et al.*, (Kleiblova, Shaltiel et al. 2013) had previously shown that transient knockdown of truncated *PPM1D* increases G1

checkpoint arrest in response to ionising radiation (IR). Interestingly, in our study, WIP1 inhibition and depletion by GSK2830371 in HCT116^{+/+} cells harbouring a PPM1D/WIP1 L450X truncation mutation resulted in an increase in the proportion of cells in G2/M in a p53-dependent manner following p53 activation by Nutlin-3, while this did not occur in NGP and SJSA-1 cell lines that do not have gain-of-function mutations. Lindqvist A. *et al.*, 2009 (Lindqvist, de Bruijn et al. 2009) also reported that WIP1 knockdown ablates the competence of cellular p53-dependent G2 checkpoint recovery following cellular stress, although the authors were not aware of the gain-of-function PPM1D/WIP1 R458X mutation in U2OS cells used in their study, as it had not yet been reported. These findings suggest that the increase in the proportion of cells in G2 observed in HCT116^{+/+} cells treated with the combination of MDM2 and WIP1 inhibitor is likely due to inhibition of PPM1D/WIP1 L450X which would otherwise be negatively regulating p53 transcriptional activity in these cell lines.

5.6.4 Potential role for p53^{Ser15} phosphorylation in enhancing p53 activity

The phosphorylation status of p53^{Ser15} following treatment with MDM2 inhibitors has been reported to be due to basal activity of kinases, like ATM and ATR (and most likely other members of the PI3KK family), that are normally involved in phosphorylation of this residue in response to cellular stress such as DNA damage (Meek and Anderson 2009, Loughery, Cox et al. 2014). Phosphorylated p53^{Ser15} is also directly dephosphorylated by WIP1 and protein phosphatase 1 α (PP1A) (Haneda, Kojima et al. 2004, Lu, Nannenga et al. 2005). Phosphorylation of this residue has been implicated in increased p53 transcriptional activity and recruitment of key transcriptional co-factors, such as p300/CBP, which are required for chromatin remodelling at the sites of p53 regulated promoters and acetylation of p53 C-terminus on residues that would otherwise be ubiquitylated by MDM2 (Loughery, Cox et al. 2014, Meek 2015). We showed that although MDM2 or WIP1 inhibition alone do not result in strong p53^{Ser15} phosphorylation in HCT116^{+/+} and NGP cell lines, p53^{Ser15} is markedly increased when these agents are combined. Therefore, in these cell lines, the level of p53^{Ser15} phosphorylation can be used as a marker of WIP1 activity only if p53^{Ser15} is not masked by MDM2. Also consistent with this model was the observation that WIP1 knockdown alone does not impact pp53^{Ser15} phosphorylation in NGP cells at 8 hours, whereas in the presence of Nutlin-3, pp53^{Ser15} significantly increases. It is likely that the phosphorylation status of p53^{Ser15} is in a dynamic equilibrium that is catalysed by kinases and phosphatases for which this residue is a substrate. This is the

likely reason for an increase in Ser15 phosphorylation following increased kinase activity (e.g. in response to DNA damage) or decreased phosphatase activity (e.g. in response to WIP1 inhibition).

5.6.5 Summary

Wild-type *TP53* genetic status is the most important determinant of response to MDM2 inhibitors, while being necessary but not sufficient for growth inhibitory response to WIP1 inhibition by GSK2830371. Following their promising clinical outcomes so far in early phase clinical trials, MDM2 inhibitors will be explored in combination with other anticancer agents to optimise their therapeutic potential. Combination regimens of non-genotoxic agents which could minimise genotoxic stress to healthy tissue are a much preferred strategy. Here we have shown that specific pharmacological inhibition of WIP1 combined with MDM2 inhibitors is a promising therapeutic strategy in *TP53* wild-type tumours that show increased WIP1 function, and that phosphorylated p53^{Ser15} and *PPM1D* genotype are of potential mechanistic importance and can be predictive biomarkers for response to this combination treatment. In the next chapter global gene expression is following treatment with RG7388 in the presence or absence of GSK2830371 is analysed and the mechanistic role of p53^{Ser15} in transcriptional transactivation of p53 is explored.

**Chapter 6 Phosphorylation of p53^{S15} is of mechanistic importance in
GSK2830371 mediated potentiation of response to MDM2
inhibitors**

6.1 Introduction

Hotspot *TP53* mutations found in malignancies overall, affect residues functionally necessary for p53 DNA binding to its consensus sequence (Raycroft, Wu et al. 1990, Cho, Gorina et al. 1994, Hainaut and Hollstein 2000). This strongly suggests that p53 transcription factor function is very important for its role as a tumour suppressor (Levine, Momand et al. 1991). In order for wild-type p53 to become transcriptionally active it must dissociate from its key negative regulators MDM2 and MDMX that mask the p53 transcriptional transactivation domain (Chen, Marechal et al. 1993, Oliner, Pietenpol et al. 1993, Haines, Landers et al. 1994, Lin, Chen et al. 1994, Marine, Dyer et al. 2007). In response to many types of stress, such as DNA damage or oncogenic stress, p53 and its regulatory binding partners undergo a complex array of post-translational modifications (PTM's) which prevent their interaction (Appella and Anderson 2001, Kruse and Gu 2009, Meek and Anderson 2009, Meek and Hupp 2010). MDM2 inhibitors can potentially bypass these PTM's and activate p53 transcriptional function in the absence of DNA damage. Phosphorylation of p53^{Ser15} which is arguably "a critical focal point" for p53 function following cellular stress (Meek and Anderson 2009), has different intensity and kinetics in response to MDM2 inhibitors compared with response to DNA damage (Loughery, Cox et al. 2014). In the previous chapter we showed that p53^{Ser15} phosphorylation increased markedly in response to the combination of MDM2 inhibitors and GSK2830371 in contrast to the same dose of each drug alone. This correlated with potentiation of growth inhibition and an increase in apoptotic response in *TP53* wild-type cell lines, but not in their *TP53* mutant daughter cells which lack p53 transcriptional activity. These observations suggest that the potentiation of MDM2 inhibitors is likely through p53-dependent transcriptional mechanisms. Therefore we aimed to assess whether the difference in apoptotic response correlated with a difference in gene expression between single MDM2 inhibitor treatment and its combination with WIP1 inhibition.

6.1.1 Phosphorylation of p53^{Ser15} after MDM2 inhibition

Regulation of p53 stability, subcellular localisation and transcription factor function is primarily post-translational through modification by enzymes involved in cellular stress response. The complex array of p53 PTM's has been reviewed extensively by multiple authors (Meek 1999, Appella and Anderson 2001, Kruse and Gu 2009, Meek and Anderson 2009). Phosphorylation of p53^{Ser15} is broadly considered a marker of genotoxic stress as it is catalysed by the PI3KK family of kinases, such as ATM, ATR

and DNA-PK, which are activated in response to DNA damage. However, this phosphorylation also occurs in response to oncogenic stress and depleted energy levels by AMPK (AMP-activated kinase) (Jones, Plas et al. 2005). Absence of p53^{Ser15} phosphorylation, 20 hours following 6 μ M Nutlin-1, in comparison to genotoxic agents such as etoposide (1 μ M) and doxorubicin (10 μ M), was presented as evidence of the non-genotoxic mechanism of p53 activation by MDM2 inhibitors (Vassilev, Vu et al. 2004). However, since then many other groups have reported phosphorylation of p53^{Ser15} (pp53^{Ser15}) following treatment with Nutlin-3 the most potent MDM2 inhibitor reported in the original publication by Vassilev *et al.*, (2004). Treatment with Nutlin-3 racemic mixture (or Nutlin-3a the purified active enantiomer) has been shown to result in pp53^{Ser15} and in some publications this was reported to correlate with an increase in markers of DNA damage marker γ H2AX (Phosphorylation of Histone H2AX^{Ser139})(Verma, Rigatti et al. 2010, Valentine, Kumar et al. 2011, Rigatti, Verma et al. 2012). Although in chapter 3 it was discussed that this may be due to off-target effects of MDM2 inhibitors.

In a recent publication by Loughery et al., however pp53^{Ser15} was assessed at a mechanistically relevant time-point (6 hours post-treatment) with a range of doses of Nutlin-3a compared to other genotoxic activators of p53 such as IR, UV and etoposide in HCT116 and U2OS cell lines (Loughery, Cox et al. 2014). It was shown that phosphorylation of p53^{Ser15} is more intense in response to DNA damaging agents and that this PTM did not correlate with levels of total p53 stabilisation. Interestingly, it was also shown that the basal activities of ATM and ATR may be in part responsible for phosphorylation of this residue in response to Nutlin-3a. Inhibitors of ATM KU55933 (10 μ M) and ATR by VE821 (10 μ M) alone did not change 10 μ M Nutlin-3a mediated pp53^{Ser15}, whereas their combination decreased this phosphorylation notably. The effect of single treatment or combination treatment with each of the kinase inhibitors on inhibition of pp53^{Ser15} was much more marked in response to 50 μ M etoposide than in response to Nutlin-3a (Loughery, Cox et al. 2014). These observations were consistent with the hypotheses outlined in Chapter 5 (5.6.4) of a dynamic equilibrium of kinases and phosphatases regulating p53^{Ser15} phosphorylation status. It is important to note that the abundance of the common substrate of both groups of enzymes (unmasked p53^{Ser15}) appears to also be a factor in the amount of the product (pp53^{Ser15}) observed. The substrate is made more available by inhibition of MDM2 from masking p53 N-terminus and therefore the product gradually accumulates in the absence of DNA damaging

agents. This is likely the reason for observed p53^{Ser15} phosphorylation in response to MDM2 inhibitors in the absence of any credible evidence for DNA damage (Loughery, Cox et al. 2014). Importantly, our results in chapter 5 showed that this balance can be tilted in favour of p53 activating kinases by inhibition of WIP1. Loughery *et al.*, (2014) also showed that pp53^{Ser15} was associated with increased transcriptional transactivation from p53 regulated promoters. Therefore, the correlation of pp53^{Ser15} with increased apoptotic end-points may be due to an increase in transcriptional transactivation.

6.1.2 The role of p53^{Ser15} phosphorylation in regulation of p53 transcriptional activity

Initial studies to identify the function of various conserved domains of p53 were carried out during the early 1990's which distinguished an acidic N-terminus transactivation, DNA binding, and an oligomerisation domains (Reviewed in chapter 1). Hybrid studies in yeast showed that there are two sub-domains within the N-terminal transactivation domain (TAD) of p53 which span across amino acids 1-40 (TAD1) and 40-83 (TAD2) (Candau, Scolnick et al. 1997). By that time, it had already been shown that MDM2 inhibits p53 TAD interaction with components of the basal transcription machinery like TATA box binding protein (Truant, Xiao et al. 1993) and key transcriptional coactivators CBP/p300, TAFII60, TAFII40 and TAFII31 (Lu and Levine 1995, Thut, Chen et al. 1995, Lambert, Kashanchi et al. 1998, Dumaz and Meek 1999, Meek and Anderson 2009). Therefore it was important to find out which PTM's are key to the decoupling of p53 from its principal negative regulator MDM2. Due to the proximity of p53 residues Ser15, Thr18 and Ser20 to the three key p53 amino acids (Phe19, Try23 and Leu26) essential for MDM2 binding (Böttger, Böttger et al. 1997), it was suspected that phosphorylation of one or more of these residues would result in p53 dissociation from MDM2. Initially it was suggested that DNA damage induced p53^{Ser15} phosphorylation was critical for dissociation of p53 from MDM2 (Shieh, Ikeda et al. 1997). Independent publications in 1999 however, found that phosphorylation of p53^{Ser15} was dispensable for dissociation from MDM2 (Dumaz and Meek 1999) in contrast to phosphorylation of Ser20 and Thr18 (Chehab, Malikzay et al. 1999, Ferreon, Lee et al. 2009, Teufel, Bycroft et al. 2009). The functional significance of phosphorylation of individual p53 serine residues was investigated by their individual or combined site-directed mutagenesis to alanine residues which could no longer be phosphorylated. Alternatively mimicking a phosphorylation by mutating that same residue to aspartate which is negatively charged. Dumaz and Meek (1999) generated a

hybrid reporter system by fusing the DNA binding domain of the yeast GAL4 transcription factor with either wild-type p53 residues 1-42 (TAD1) or TAD1 with single or double mutations in putative phosphorylation sites (Dumaz and Meek 1999). Plasmids carrying the fusion constructs were then co-transfected with a GAL4 regulated reporter construct either into *Trp53* null MEFs or COS-7 cells which have no p53 activity due to SV40 large T antigen expression. Only p53^{S15A} and p53^{S15A/S37A} resulted in significant reductions of the reporter signal which suggests that p53^{Ser15} is important for transcriptional transactivation function carried out by this domain of p53. Moreover, p53^{S15D} rescued the transactivation function of the fusion protein. Importantly, reporter signal was diminished in a dose-dependent manner when constructs expressing wild-type and mutant p53 were co-transfected with different doses of a plasmid that expressed MDM2 suggesting that the mutations in these residues did not impact the MDM2-p53 interaction. Full-length p53^{S15A} or p53^{S15D} co-transfection with a reporter under the regulation of MDM2 or *CDKN1A* (p21^{WAF1}) promoters in MEF^{*Trp53*^{-/-}} also resulted in decreased expression in p53^{S15A} compared to wild-type p53 which was reversed by p53^{S15D} (Dumaz and Meek 1999). These data strongly suggests that p53^{Ser15} phosphorylation enhances p53 transcriptional activity. Subsequent studies published by the same group and others have supported this notion and suggested potential mechanisms for this enhanced p53 activity (Lambert, Kashanchi et al. 1998, Teufel, Bycroft et al. 2009, Loughery, Cox et al. 2014).

6.1.2.1 The role of p53 N-terminal phosphorylation events as studied in transgenic mice

In line with these findings, knock-in mice homozygous for *Trp53*^{S18A} (equivalent of human *TP53*^{S15A}) did not show impairment in IR induced stabilisation of p53 in their thymocytes (Chao, Hergenbahn et al. 2003). This suggests that dissociation from MDM2 is not solely regulated by p53^{S18} phosphorylation in mice. However, there was a difference between wild-type and mutant *Trp53* knock-in mice in their IR induced *Trp53*-mediated transcription and apoptosis in certain physiological contexts (Borges, Chao et al. 2004). Using murine Affymetrix gene chip system the authors showed that *Trp53*^{S18A} homozygous thymocytes had reduced *Trp53* target gene expression 8 hours after exposure to IR (5Gy) compared to *Trp53* wild-type mice. This reduced expression was promoter specific and correlated with histone acetylation consistent with earlier findings that p53^{Ser15} phosphorylation is important for recruitment of co-activators (Such as CBP/p300) to certain promoters (Lambert, Kashanchi et al. 1998). Crucially, a

more recent study has shown that *Trp53*^{S18A} knock-in mice are prone to late-onset malignancies such as lymphomas and that B cells derived from these mice show deficiencies in induction of Puma protein and apoptosis following 8Gy ionising radiation and in turn apoptosis compared to *Trp53* wild-type cells (Armata, Garlick et al. 2007). Surprisingly knock-in mice with *Trp53*^{Ser23} (equivalent of human *TP53*^{Ser20}) showed no difference in Trp53 induced transcription, apoptosis or Trp53 stabilisation following UV induced DNA damage (Wu, Earle et al. 2002). However, knock-in mice with *Trp53*^{S18A/S23A} double mutation, showed significant aberrations in p53 stabilisation and apoptotic response following DNA damage (Chao, Herr et al. 2006).

It has therefore been shown that p53^{Ser15} is functionally significant in cell fate determination in a context-dependent manner and that it most likely exerts its effect through modulating p53 transcriptional transactivation from p53-regulated promoters. Given that WIP1 and MDM2 inhibitor combination markedly increases p53^{Ser15} phosphorylation in the absence of any detectable DNA damage, it is important to assess whether this also impacts p53 transcriptional activity.

6.2 Hypothesis

- Potentiation of MDM2 inhibitors is due to increased transcription from p53 regulated promoters because of the non-genotoxic phosphorylation of p53^{Ser15} following MDM2 and WIP1 inhibition

6.3 Specific materials and methods

6.3.1 Cell lines

Cell lines used and their growth conditions are outlined in general materials and methods in 2.1.1. DD7 and DR4 cells were seeded at 1×10^4 cells/well and SRB growth inhibition assays were carried out as described in 2.2 and 5.3.2. Growth curves for DD7 and DR4 cell lines can be seen Figure 6-1.

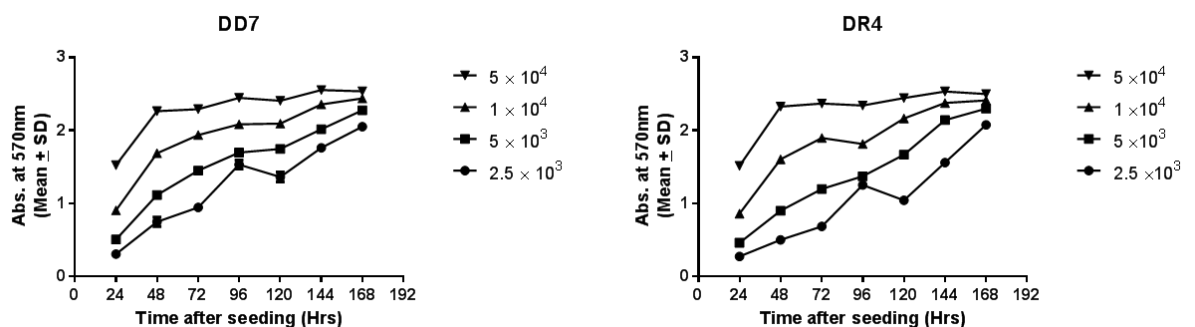


Figure 6-1 Growth curves of DD7 and DR4 cells stably transfected with p53 luciferase reporter and internal control.

6.3.1.1 Treatment schedules and lysate collection before western blotting

Kinase inhibitors were always added 30min before treatment with IR. All other drug combinations were administered simultaneously unless otherwise stated. Lysates were collected at time-points stated in captions and western blotting carried out as described in 2.9.

6.3.2 Reporter gene analysis

TP53 wild-type and mutant glioblastoma cell lines stably transfected with p53 responsive reporter are described in 2.1.1. Cells were also seeded at 1×10^4 cells/well of a white-well 96-well plates (Greiner Bio-one, #GN-VW-655083) 48Hrs before treatment with multiples of DD7 Nutlin-3 GI50 ($\sim 1.5\mu\text{M}$) in the presence or absence of $2.5\mu\text{M}$ GSK2830371. The dual-Glo luciferase assay system (Promega, #: E2920) was used to quantify Firefly and Renilla luciferase enzymatic activity in sequence as described in the manufacturer's protocol. The final volume of media containing drug however was kept at $50\mu\text{l}$ and the ratios of reagents were kept the same to reduce costs. The incubation time after the addition of each Luciferase reagent was 30min. A micro-well luminometer (FLUOstar Omega Reader, BMG Labtech) was used to measure luminescence/well. Raw Firefly luciferase activity value/well was then normalised to Renilla activity in that well before further data analysis.

6.3.3 RNA extraction for microarray gene expression profiling and qRT-PCR validation

NGP cells were seeded at 6×10^6 cells/well of a 6-well plate 24 hours before treatment and RNA was harvested 4 hours following treatment with either DMSO (0.5%), 75nM RG7388 \pm $2.5\mu\text{M}$ GSK280371. In order to isolate high quality RNA molecules for individual or global gene expression analysis QIAGEN RNeasy Plus Mini Kit was used, which comprises two different silica columns per sample processed. The first column allows the isolation and disposal of genomic double stranded DNA and the second the isolation $>200\text{mer}$ RNA molecules excluding irrelevant ubiquitous RNA molecules such as 5.8S rRNA, 5S rRNA, and tRNAs which together comprise 15-20% of cellular RNA content. Prior to RNA extraction, highly denaturing guanidine–thiocyanatecontaining lysis buffer is used to lyse the cells which prevents RNA degradation by RNases and then the genomic DNA is isolated using a gDNA column

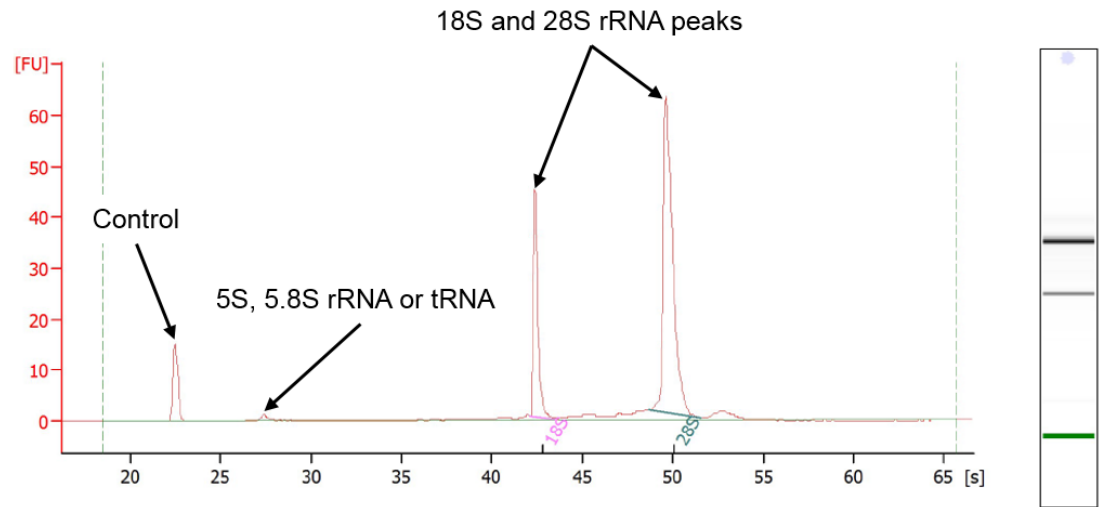
which allows the retention of genomic DNA in a high salt concentration buffer in the stationary phase and the column is then disposed of. RNA is isolated from the eluent by passing it through a specialised silica-gel column at high salinity and gradual decrement of salinity and centrifugation steps elute the RNA while disposing of other contaminants like proteins and solvents. RNA concentration was quantified using the Nanodrop as described in materials and methods.

6.3.4 RNA quality analysis

Concentration and quality (RNA integrity numbers) of mRNA were determined using Agilent RNA 6000 nano kit on an Agilent 2100 Bioanalyser ensuring RNA integrity number (RIN) >9 in all samples before gene expression analysis. A 16-well chip interconnected with microcapillaries was loaded with a sieving polymer and a fluorescent intercalating nucleotide dye and then the 12 RNA samples (diluted 1:3) along with a RNA 6000 ladder (a size reference point) were loaded in separate wells. 16-independent electrodes then enter the wells (1/well) and an electric current is applied throughout the polymer filled capillaries interconnecting the wells with charged molecules migrating through the capillaries at a rate proportional to their size. The smaller molecules migrate faster through the polymer and cross the path of a laser which excites the dye molecules intercalated with RNA molecules resulting in their fluorescence. An electropherogram is then digitally generated (y-axis: fluorescent units (FU) v x-axis: size relative to ladder fragments) by the 2100 Expert software (Figure 6-2). Fluorescence units are proportional to the amount of dye intercalated in RNA molecules. A smaller marker is also run with each sample to use as a control for potential shifts between the different samples run on each chip. When RNA has not been degraded ubiquitously expressed and stable 28S and 18S ribosomal RNA (rRNA) components that are normally detected as two distinct peaks have a ~2:1 ratio in FU peak intensity. Human 28S rRNA is 5034 bases long as compared to 18S rRNA which is 1870 bases long producing a theoretical ratio of 2.69. RNA integrity was traditionally calculated based on 28S:18S ratio with optical densities obtained running samples on a denaturing agarose gel (alkaline conditions) followed by densitometry. Aligent expert software uses an algorithm that uses the whole of the electropherogram trace generated to calculate an RIN value from a smaller amount of initial RNA and it offers standardisation of the equipment and reagents. It is also important to note that this procedure is not under denaturing conditions. RIN values range from 1-10 with values above 7-8 being acceptable for most applications (Schroeder, Mueller et al. 2006).

Assay Class: Eukaryote Total RNA Nano
 Data Path: C:\...Eukaryote Total RNA Nano_DE54704359_2015-04-15_15-21-47.xad
 Created: 15/04/2015 15:21:47
 Modified: 15/04/2015 15:45:39

Electropherogram Summary



Overall Results for sample 1 : Sample 1

RNA Area:	140.9	RNA Integrity Number (RIN):	10 (B.02.08)
RNA Concentration:	79 ng/μl	Result Flagging Color:	
rRNA Ratio [28s / 18s]:	2.3	Result Flagging Label:	RIN:10

Fragment table for sample 1 : Sample 1

Name	Start Time [s]	End Time [s]	Area	% of total Area
18S	42.10	43.62	33.2	23.6
28S	48.62	51.61	76.5	54.3

Figure 6-2 Aligent Bioanalyzer electropherogram trace and gel representation (on the right). RNA concentration and RIN value are calculated and presented. The ratio of 28S:18S rRNA molecules are calculated based on the area under each curve. Peaks associated with other rRNA or tRNA molecules has been arrowed in addition to the control molecule.

6.3.5 Global gene expression analysis by Illumina HumanHT-12 v4.0 Expression BeadChip array

Expression levels of multiple genes can be simultaneously quantified through the use of DNA microarray technology. Early experiments involved spot fixing fragments of cDNA, genomic DNA or plasmid libraries, often with known sequences, onto porous material such as nylon, and then hybridising radioactive labelled cDNA from sample of interest onto the membrane (Lockhart and Winzeler 2000). Bound material could then be detected by radiography allowing the identification and quantification by densitometry of genes that are expressed in that sample. In 1995 however, it was shown the nucleic acid probes can be secured on glass 96-well plates and that the hybridising material can be fluorescently labelled instead (Schena, Shalon et al. 1995). It was also suggested that robotic printing can be used to fix a high density of nucleic acid probes onto solid substrates and enable simultaneous measurement of thousands of genes. This led to a revolution in gene expression analysis which continues to date resulting in generation of various platforms enabling the analysis of global gene expression (Bumgarner 2013). Illumina BeadChip expression arrays are a variation of DNA microarray technology developed in 2004 (Kuhn, Baker et al. 2004). Messenger RNA is first converted to cDNA by *in vitro* reverse transcription using oligo-dT primers that will only bind to messenger RNA poly-A tails and synthesise cDNA from mRNA. Complementary RNA (cRNA) is then generated from cDNA by *in vitro* transcription and biotin is incorporated to the cRNA. Labelled cRNA from each sample is then directly hybridised to each BeadChip array on the planar silica slides which house 3µm silica beads with protruding 50mer DNA probes complementary to specific cRNA molecules (Figure 6-3 A cartoon explaining the inner workings and specifications of Illumina-HumanHT-12-v4.0 BeadChip expression arrays.). 47'000 transcripts can be detected with high degree of redundancy per probe (30/probe). Unbound cRNA molecules are washed-off and Streptavidin-Cy3 is then used to detect those bound to specific probes. The BeadChip arrays can then be scanned using a HiScan, iScan or Bead Array Reader to quantify and record the fluorescence signal intensity from each position on the array.

6.3.5.1 Experimental design and sample preparation

Details of the experimental design are outlined in Figure 6-4. Good quality total cellular RNA (RIN~10) was adjusted to 25ng/µl by dilution in distilled water and packaged with dry ice before being sent to AROS Applied Biotechnology for gene expression analysis.

Illimina-HumanHT-12-v4.0 BeadChip arrays were used for gene expression analysis as described above.

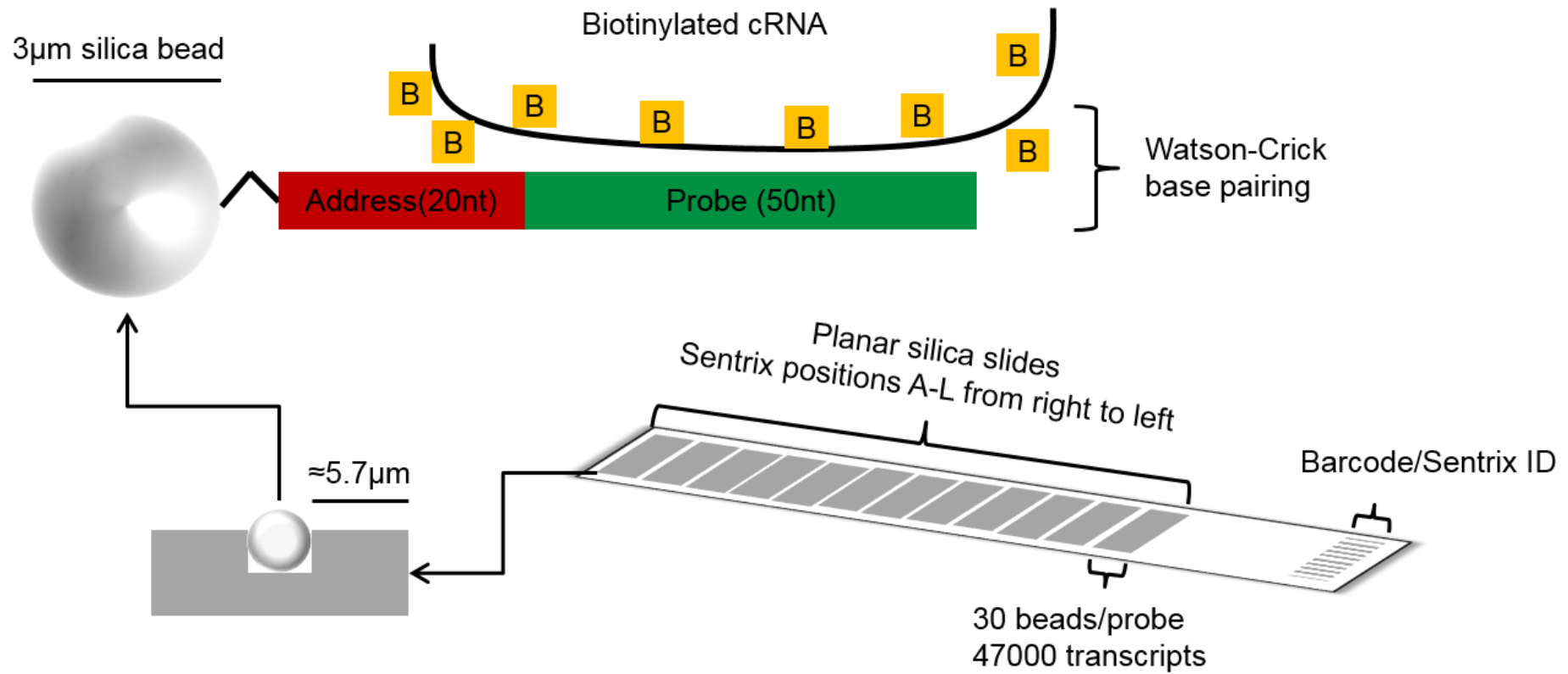


Figure 6-3 A cartoon explaining the inner workings and specifications of Illumina-HumanHT-12-v4.0 BeadChip expression arrays.

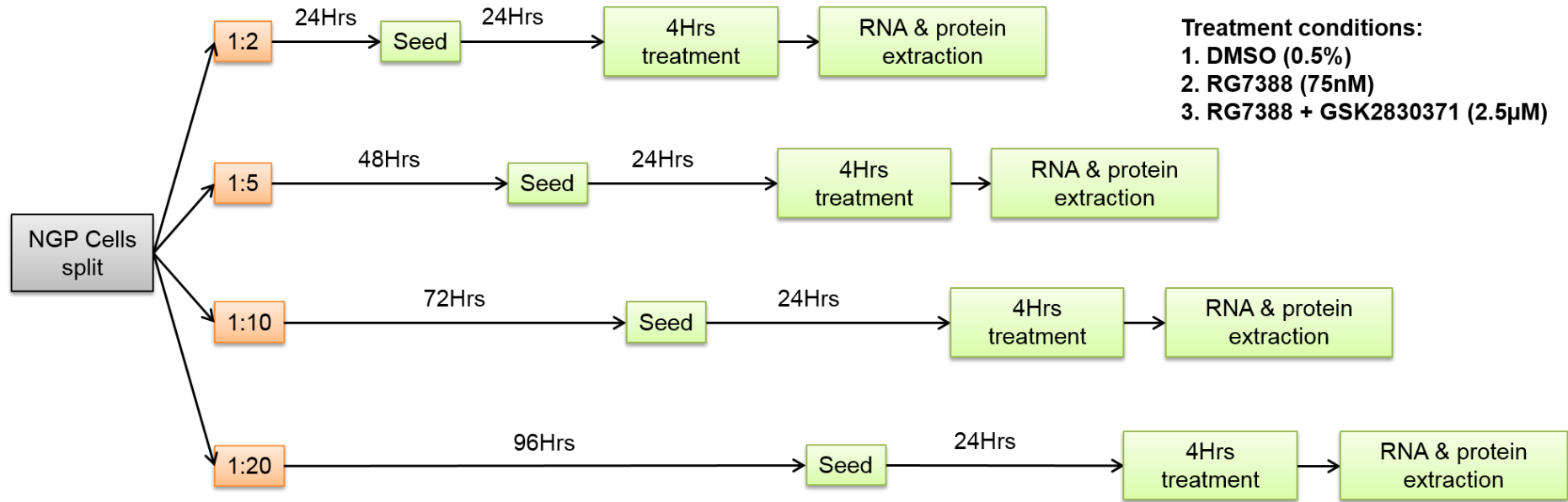


Figure 6-4 Experimental design and RNA extraction for use in microarray gene expression analysis. Total protein was also extracted as explained in (2.9.2) from replica samples in parallel.

6.3.5.2 . Uploading data and statistical analysis

Each treated sample was given a sample name before statistical analysis was carried out by Dr Sirintra Nakjang in our bioinformatics support group. A copy of the sample sheet containing grouping and Sentrix positions are shown in (Table 6-1). Microarray data was processed using an R Bioconductor package *lumi* (Du, Kibbe et al. 2008). For sample names and their respective treatments see Table 6-1. Probe intensity values were transformed using variance stabilising transformation implemented in the *lumi* package before data normalisation. The robust spline normalization method was used as a normalization method. Poor quality probes (detection threshold < 0.01), and probes that are not detected at all in the remaining arrays were removed. Differential expression analysis was performed using R Bioconductor package *limma* (Ritchie, Phipson et al. 2015). Benjamini-Hotchberg method was applied when correcting for multiple hypothesis testing.

6.3.5.3 Array quality control

The following controls were also carried out by Dr Sirintra Nakjang. The spread of the standard deviation of ranked mean signal intensities detected for each probe across the 12 arrays showed that the higher the mean signal intensity the greater the standard deviation (Figure 6-5). This modest increase in standard deviation observed with some probes with mean signal intensity >35000 was deemed acceptable as most probes fell <35000 mean signal intensity. Signal intensity box plots for each sample showed that all samples have around the same median signal intensity and the spread of the sample signal intensities are the same (Figure 6-6A). Density plot of sample intensities showed that the spread of signal intensity is the same between all 12 samples (Figure 6-6B). The raw average signal intensity data can be used to assess sample-dependent and -independent built in controls via the Illumina Genome Studio Software (Figure 6-7). Sample-dependent controls include 1) Negative controls: Negative control are probes with random sequence that should not detect any of the labelled cRNA molecules, 2) Noise controls: Shows the standard deviation of the negative control probes (Figure 6-7A), 3) Housekeeping controls: Shows the average signal caused by the expression of housekeeping genes that can be detected by the array, 4) All genes controls: Shows the average signal of all genes on the array (Figure 6-7B). Sample-independent controls include 1) Hybridisation controls: This control assesses whether the signal from Cy3 labelled oligonucleotides spiked into the hybridisation reaction correlates with their concentration (Figure 6-7C), 2) Low stringency control: The signal comparison between

two Cy3 labelled controls spiked into the hybridisation reaction that have 2 mismatches to their respective probes (Figure 6-7D), 3) Biotin controls: These are biotin labelled oligonucleotides that spiked into the hybridisation reaction that bind to specific probes and their successful secondary staining with Streptavidin-Cy3 conjugate demonstrates successful secondary staining (Figure 6-7E).

Sample Name	Treatment	Group	Sentrix positions
K1.1	DMSO	a	3999538022_A
K2.1	75nM RG7388	a	3999538022_B
K3.1	75nM RG7388 + 2.5µM GSK2830371	a	3999538022_C
K1.2	DMSO	b	3999538022_D
K2.2	75nM RG7388	b	3999538022_E
K3.2	75nM RG7388 + 2.5µM GSK2830371	b	3999538022_F
K1.3	DMSO	c	3999538022_G
K2.3	75nM RG7388	c	3999538022_H
K3.3	75nM RG7388 + 2.5µM GSK2830371	c	3999538022_I
K1.4	DMSO	d	3999538022_J
K2.4	75nM RG7388	d	3999538022_K
K3.4	75nM RG7388 + 2.5µM GSK2830371	d	3999538022_L

Table 6-1 Table shows sample names, their treatment and groups (Independent repeats). Sentrix positions are related to the position of each planar silica slide exposed to a sample.

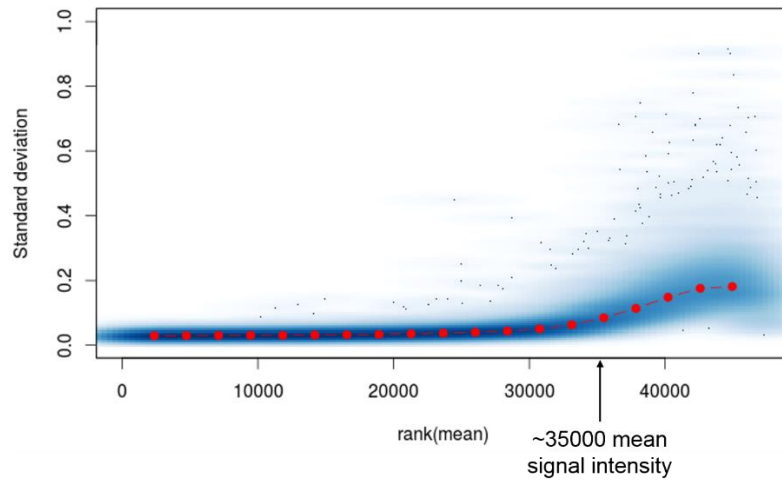


Figure 6-5 Ranked mean signal intensity per probe and standard deviation between samples show that standard deviation does not correlate positively with mean signal intensity

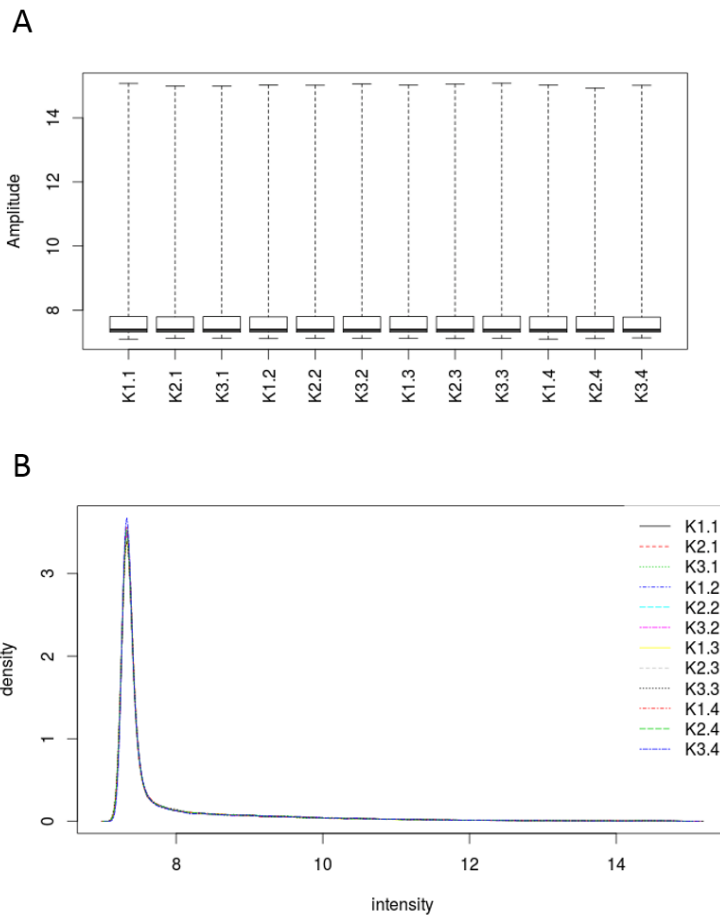


Figure 6-6 A) Boxplot of median signal intensities of arrays show that median signal intensity and the spread of the data are similar among arrays. B) Density plot of intensity of all arrays shows that the spread of signal intensity is the same among samples.

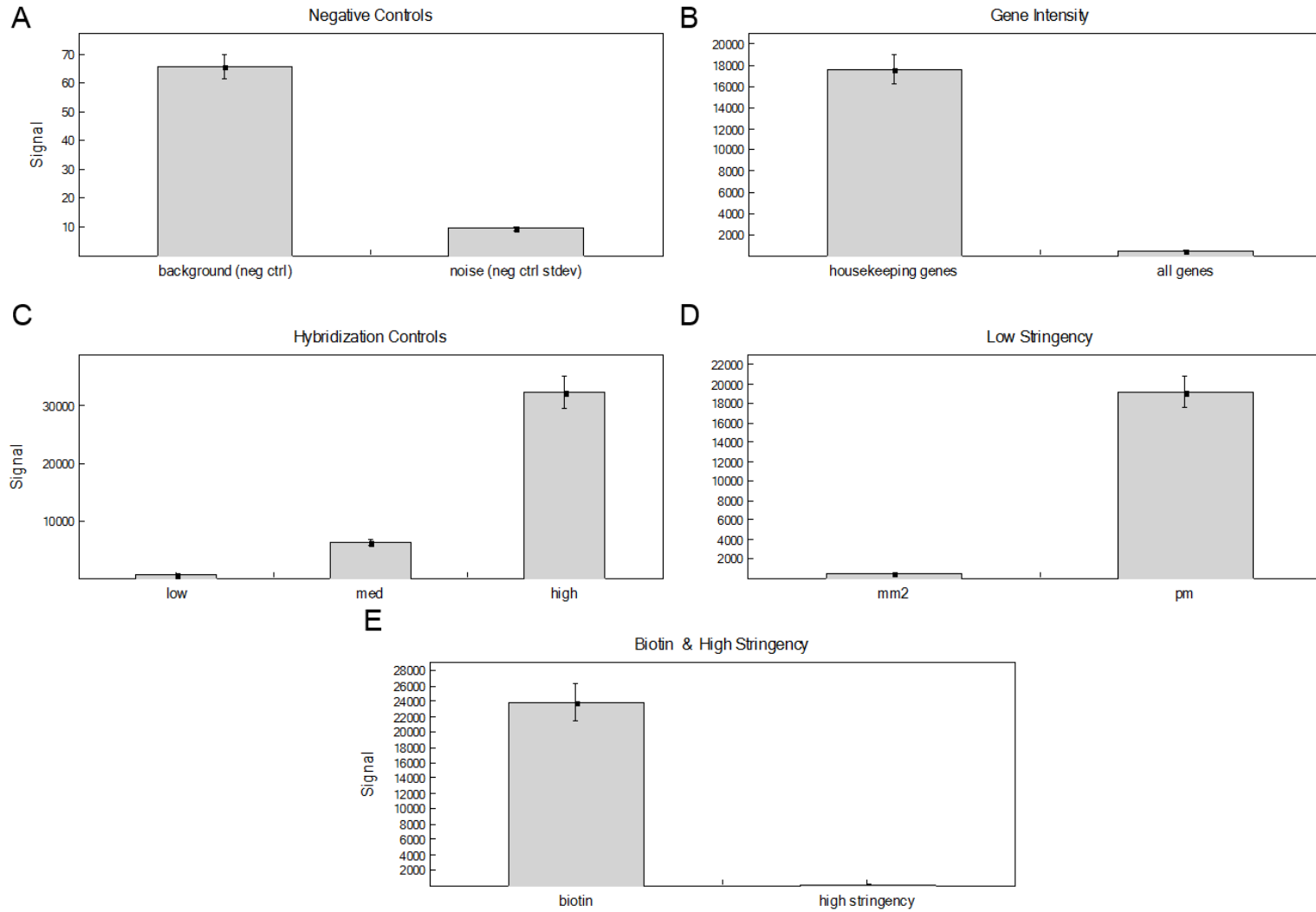


Figure 6-7 A-E) Summary of controls from 12 arrays/samples as suggested by Illumina. Sample –dependent and independent controls (explained in 6.3.5.3) show no signs of experimental errors or inconsistencies. In D mm2: Mismatch; pm: Perfect match

6.3.5.4 Conclusion of array experimental controls

There were no indications of failed samples and excessive background. Hybridisation and stringency controls were also satisfactory.

6.3.5.5 Pathway analysis

Because differentially expressed genes just below the statistical significance cut-off after Benjamini-Hotchberg correction for multiple testing were mostly p53 target genes we decided to upload the data of the top genes with the lowest p-values (cut-off $\alpha = 0.001$) into the Ingenuity Pathway Analysis (IPA) software package (Ingenuity Systems). The IPA calculates P-values based on the number of significantly differentially expressed genes that map to a specific biological function or pathway in comparison to the IPA knowledge base (Reference set). Fisher's exact test is then used to assess the following null hypothesis: The proportion of genes mapping to a function or pathway in our set of significant genes is similar to the proportion that map in the reference set. If the proportions were similar, then no biological effect was presumed.

6.3.6 Site-directed mutagenesis of cDNA in plasmids

Plasmid vector used in this study, pcDNA3.1 (+/-) 5428/5427bp, had been purchased from Invitrogen (# V790-20 and V795-20) and full-length human *TP53* complementary DNA (cDNA) was cloned into this backbone by Dr Xiaohong Lu prior to my arrival (Figure 6-8). This vector will be referred to as Wtp53 henceforth. Wtp53 was subsequently used in a site-directed mutagenesis procedure to generate full-length *TP53* cDNA sequences with two different mutations in codon 15 encoding p53 Serine15Alanine (S15A) and p53 Serine15Aspartate (S15D) mutants. Site-directed mutagenesis is a procedure through which a target DNA molecule can be mutated on specific sites so that the role of those sites in manifesting the phenotype associated with the target DNA can be investigated. Forward and reverse primers were designed so that they form Watson-Crick pairing with 5 codons upstream and downstream of the codon of interest which was modified with the mismatch that would encode either Alanine or aspartate. Primer sequences are provided in Table 6-2 were used to PCR amplify the Wtp53 vector under the conditions stated in (Table 6-3 and Table 6-4). *PfuTurbo* DNA polymerase (Aligent technologies, # 600254) is a proprietary enhanced recombinant version of *Pfu* DNA polymerase which shows higher replication fidelity and it is more thermostable. *PfuTurbo* shows an error rate 6-fold lower than that of *Taq* DNA polymerase (1.3×10^{-6} V 8×10^{-6}). A 30 μ l aliquot of each PCR reaction was then

incubated for 1 hour at 37°C with 1µl of the restriction endonuclease enzyme Dpn1 (Life Technologies, ER1702) which will degrade the methylated Wtp53 vector replicated by the host bacterium. The unmethylated PCR products were then used in transformation experiments as described above and DNA was extracted from 4 transformed bacterial colonies followed by Sanger sequencing (DBS genomics, Durham university) allowing the identification of mutant vectors. Mutation of Serine 15 to Alanine prevents the phosphorylation of this residue. A mutation to the negatively charged amino acid Aspartate at the same site had been reported to mimic a phosphorylated residue (pp53^{S15}). This site directed mutagenesis protocol was obtained and adapted from Gozani lab protocols (Gozani).

6.3.7 Transient overexpression of p53 in *TP53* null mammalian cells

HCT116^{-/-} cells were seeded at 6×10^5 cells/well of a 6-well plate 24Hrs before transient transfection with plasmid-lipofectamine complex. Transient transfection was carried out as explained in 2.7.2 with the minor modification so that the ratio of vector (µg):lipofectamine used for complex formation was 1:2.5. Lysates were collected at different time-points following transfection and immunoblotting was carried out to assess the biochemical effects of overexpression of different doses of both wild-type and mutant p53.

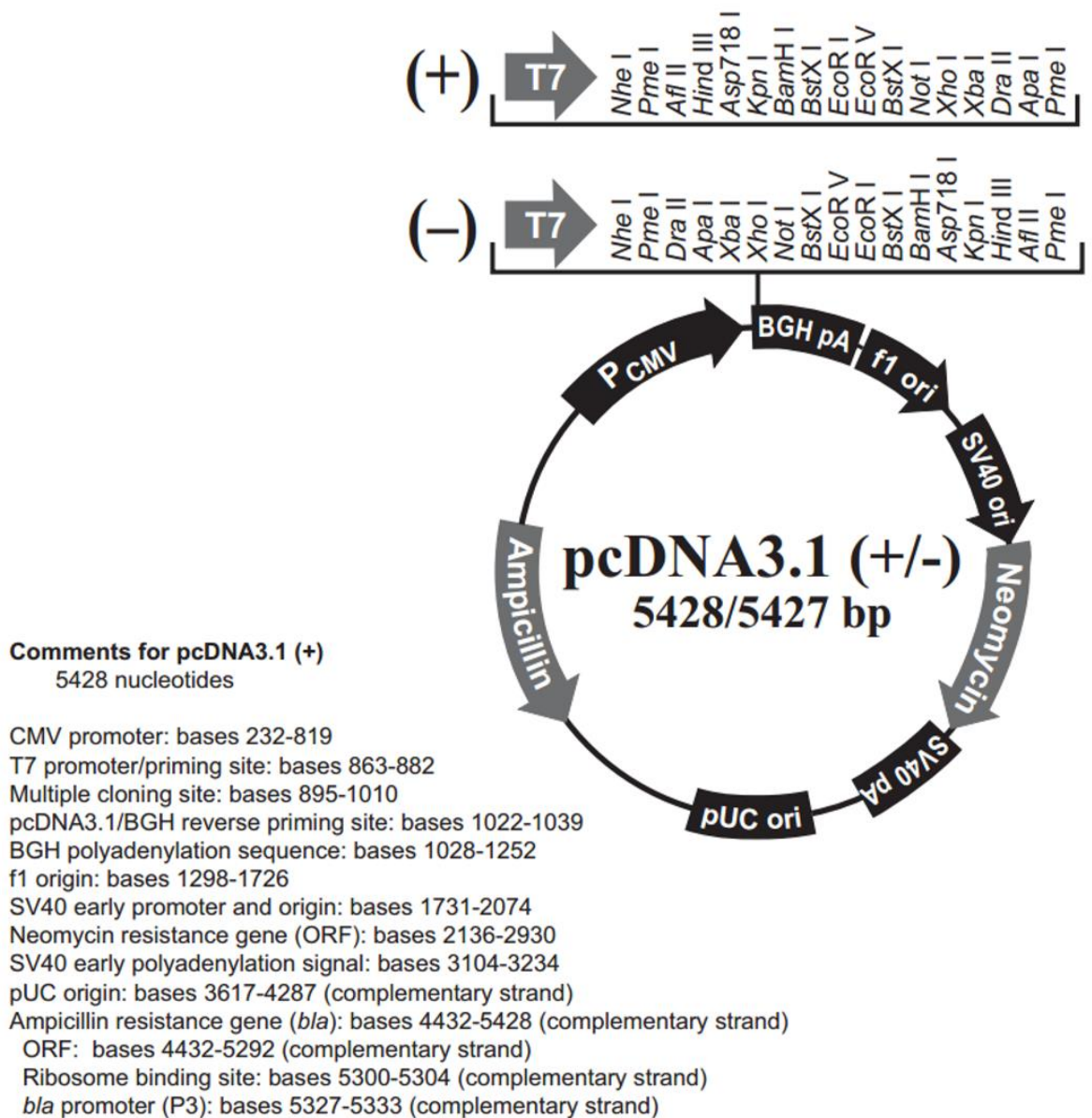


Figure 6-8 The map of pcDNA3.1 plasmid as presented in its online user manual (Invitrogen #: V790-20 and V795-20). The full-length p53 cDNA sequence was cloned downstream of the Cytomegalovirus (CMV) promoter. This plasmid was used in site-directed mutagenesis studies of p53 and for overexpression of p53 in HCT116^{-/-} cells.

Primer name	Primer sequence 5'-3'
Forward-p53 ^{S15A}	GTCGAGCCCCCTCTG GCT CAGGAAACATTTTCA
Reverse-p53 ^{S15A}	TGAAAATGTTTCCTG AGC CAGAGGGGGCTCGAC
Forward-p53 ^{S15D}	GTCGAGCCCCCTCTG GACC CAGGAAACATTTTCA
Reverse-p53 ^{S15D}	TGAAAATGTTTCCTG GTCC CAGAGGGGGCTCGAC

Table 6-2 Primers used in site-directed mutagenesis experiments. Codons modified are denoted in red text.

Constituent	Volume/amount
ddH ₂ O	33.5µl
10X <i>PfuTurbo</i> Reaction mix	5µl
2.5mM dNTP	2µl
DMSO	2.5µl
Forward Primer (10µM stock)	2µl
Reverse Primer (10µM stock)	2µl
Template DNA (2pg-200ng)	2µl
<i>PfuTurbo</i> DNA Polymerase (final concentration 1U/50µl reaction)	1µl
Total volume	50µl

Table 6-3 Constituents of the PCR reaction for site-directed mutagenesis.

Steps	Name	Temperature (°C)	Duration (Sec)
1	Template melting	95	120
2	Template melting	95	20
3	Primer annealing	55	30
4	Elongation	68	600* <i>PfuTurbo</i> (1min/kb)
5	Repeated cycles	Repeat steps 2-4 for 19 cycles	
6	Elongation	68	600
7	Storage	4	∞

Table 6-4 Thermal cycling during the site-directed mutagenesis PCR experiment.

6.4 Results

6.4.1 Comparison between Nutlin-3 and ionising radiation induced p53^{Ser15} phosphorylation

The absence of p53^{Ser15} phosphorylation was used as evidence for the non-genotoxic mechanism of action of MDM2 inhibitors in the initial publication by Vassilev *et al.*, where the Nutlin class of small molecular weight inhibitors of MDM2 were first reported (Vassilev, Vu *et al.* 2004). However, since then there have been multiple independent reports of p53^{Ser15} phosphorylation including consistent observations in our own laboratory. Given that Nutlin-3 does not possess any obvious chemical properties that are associated with genotoxic compounds we investigated the differences between ionising radiation (IR) and Nutlin-3 induced p53^{Ser15} phosphorylation. NGP cells treated with 10Gy IR showed rapid and maximal p53^{Ser15} phosphorylation which was disproportional in signal intensity to p53 stabilisation following IR exposure (Compare lane 1 to lanes 3-8 on Figure 6-9A) whereas in response to 5 μ M Nutlin-3 this phosphorylation event was more gradual and proportional to total p53 stabilisation (Compare lane 1 to lanes 3-8 on Figure 6-9B). The direct p53 transcriptional target MDM2 was induced in response to Nutlin-3 and IR. It is important to note that while in this experiment the dose of IR is $\sim 5 \times$ GI50 compared to the dose of Nutlin-3 which is $\sim 1.7 \times$ GI50, 4Gy IR which is around $\sim 2 \times$ GI50 also result in a very intense and more immediate p53^{Ser15} phosphorylation (Figure 6-11).

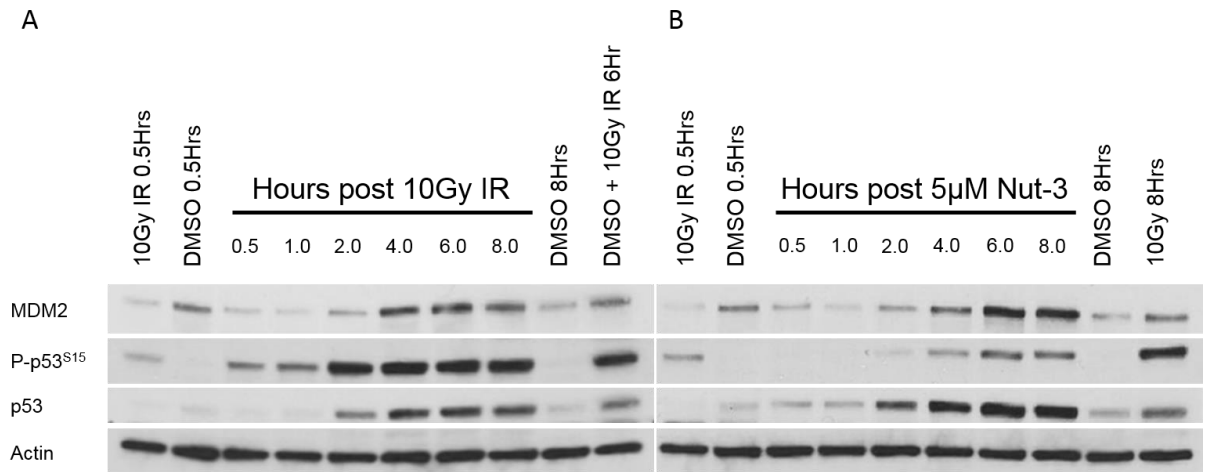


Figure 6-9 Kinetics of p53^{Ser15} phosphorylation in NGP cells following either 10Gy IR (A) or 5µM Nutlin-3 (B). The first and the last lanes on each blot can be used as positive control for p53^{Ser15} and comparators for band intensity on each blot.

6.4.2 Phosphorylation of p53^{Ser15} after Nutlin-3 is not exclusive to class of MDM2 inhibitors or cell type

We sought to assess whether p53^{Ser15} phosphorylation in response to MDM2 inhibitors is cell type or drug class specific. Immunoblots were used to investigate pp53^{Ser15} levels in NGP and SJSA-1 cell lines 4Hrs following MDM2 inhibitors of spiroxindole (MI63) and isoindolinone classes (NCL-20135, structure unpublished) along with another more potent cis-imidazoline clinical compound RG7112. All classes of MDM2 inhibitors showed increased pp53^{Ser15} in both cell lines suggesting that there is no class or cell line specific effect with regards to this PTM. Moreover, all MDM2 inhibitors increased the transcription of p53 targets MDM2 and p21^{WAF1}.

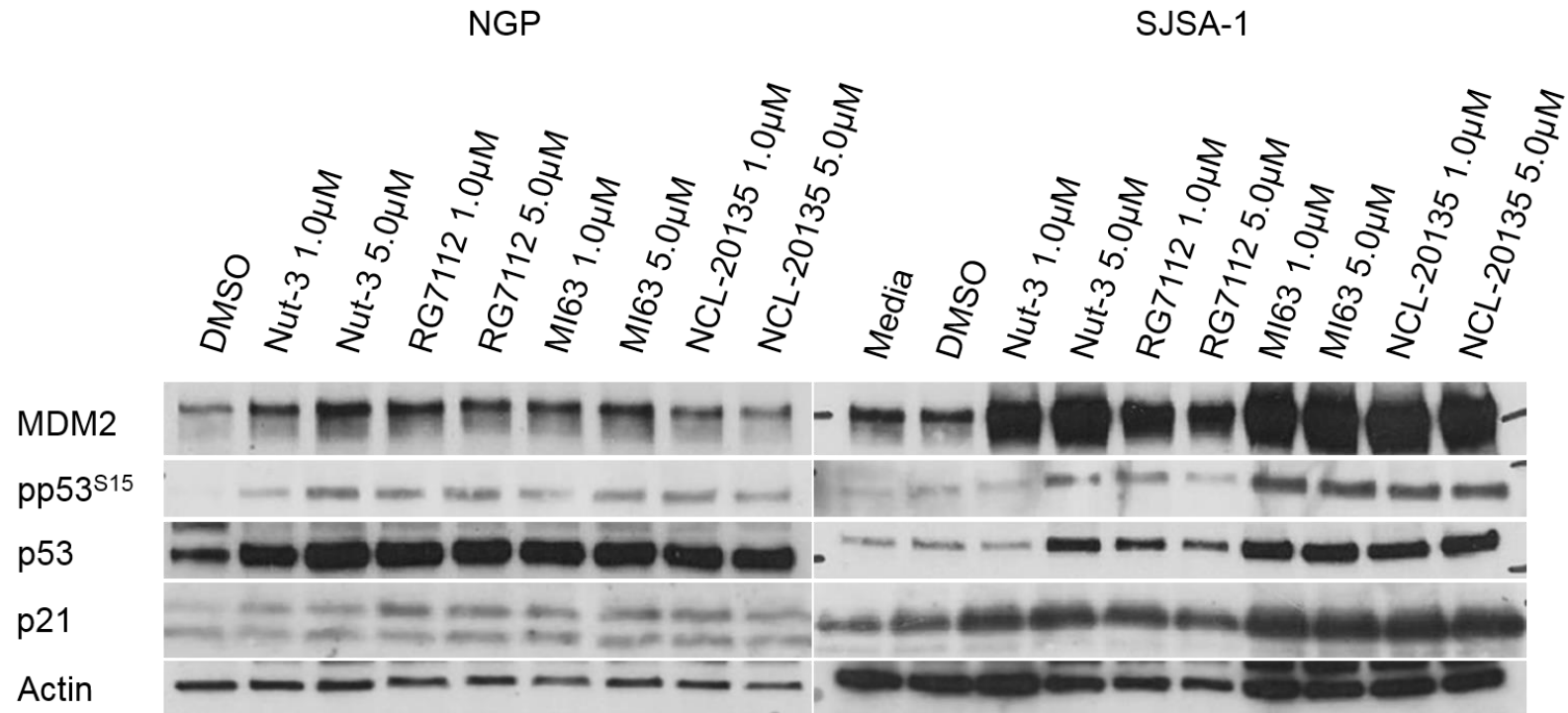


Figure 6-10 Phosphorylation of p53^{Ser15} 4Hrs following treatment with MDM2 inhibitors is neither class nor cell type specific. Different classes of MDM2 inhibitors all cause an increase in p53^{Ser15} phosphorylation in both NGP and SJSA-1 cell lines. Supervised undergraduate student Mr Alex Smith assisted with this experiment.

6.4.3 Phosphorylation of p53 following Nutlin-3 is due to the basal activity of PI3KK

In order to assess whether the p53^{Ser15} phosphorylation is due to the activity of the same kinases that phosphorylate p53 in response to DNA damage (PI3KKs) we tested the effect of specific and broad spectrum kinase inhibitors on pp53^{Ser15} levels 4Hrs following 5µM Nutlin-3 and 30min post 4Gy IR in the *TP53* Wild-type NGP cell line and its otherwise isogenic *TP53* mutant daughter cell line N20R1. NU7441 at 1µM resulted in no change in IR induced p53^{Ser15} phosphorylation while Wortmannin at 1µM inhibited this phosphorylation modestly. 10µM KU55933 however resulted in marked inhibition of p53^{Ser15} phosphorylation as predicted by the reported importance of ATM in targeting this residue in response to IR. The combination of ATM and DNA-PK inhibition also resulted in the same outcome although NU7441 likely did not contribute to the inhibition of this phosphorylation event. In stark contrast the most robust inhibition of p53^{Ser15} phosphorylation in response to 5µM Nutlin-3 was achieved by the combination of NU7441 and KU55933 followed by the broad spectrum PI3K inhibitor Wortmannin. Single treatment with either NU7441 or KU55933 did not affect Nutlin-3 mediated p53^{Ser15} phosphorylation. Not long following this observation; Loughery *et al.*, (2014) (Loughery, Cox et al. 2014) reported that the combination of ATR and ATM inhibition have a similar effect on p53^{Ser15} phosphorylation following Nutlin-3. This is consistent with the model that the basal activities of multiple kinases targeting this residue are likely responsible for this phosphorylation event (Loughery, Cox et al. 2014). Interestingly reduced p53^{Ser15} phosphorylation in the presence of the relevant kinase inhibitors coincided with diminished p53 mediated MDM2 induction (Figure 6-12). All these processes were independent of *TP53* genetic status with both wild-type and mutant cell lines undergoing phosphorylation which could be inhibited by ATM inhibition alone in the case of IR and modestly by the combination of ATM and DNA-PKcs inhibition.

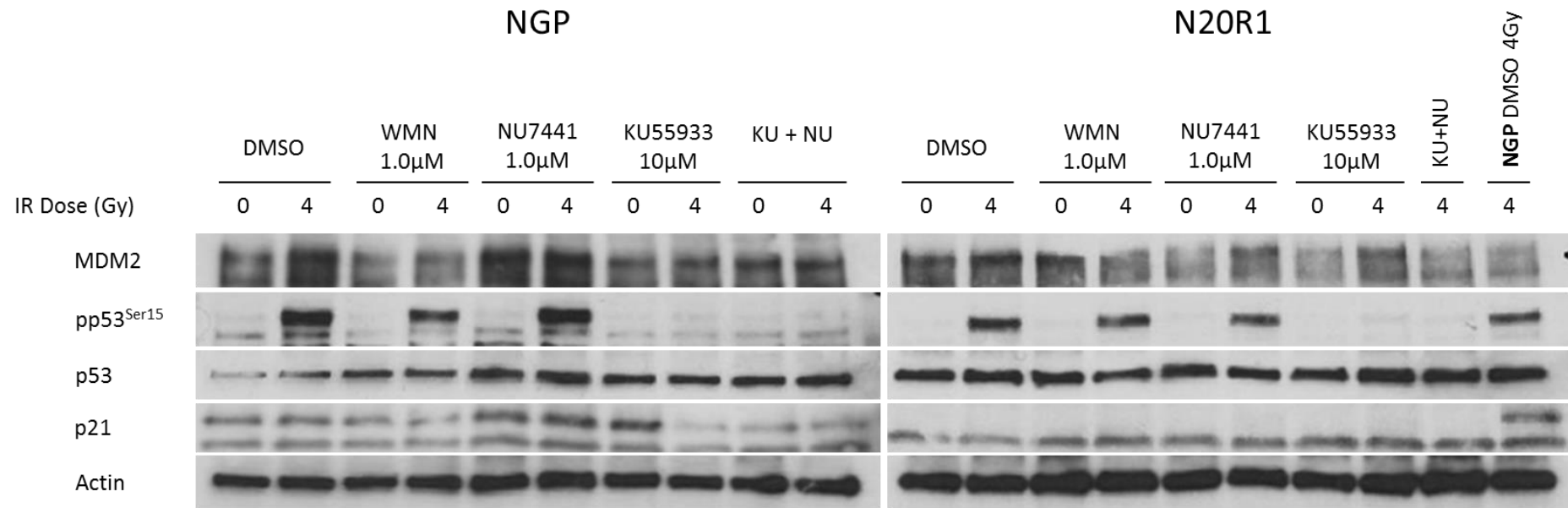


Figure 6-11 IR induced phosphorylation of p53^{Ser15} is dependent on ATM catalytic activity. NGP and their otherwise isogenic *TP53* mutant daughter cell line N20R1 were pre-treated for 30min with the stated doses of kinase inhibitors and then exposed to IR 30 min before lysate extraction. KU: ATM inhibitor KU55933; NU: DNA-PK inhibitor NU7441; WMN: Broad spectrum PI3K inhibitor Wortmannin.

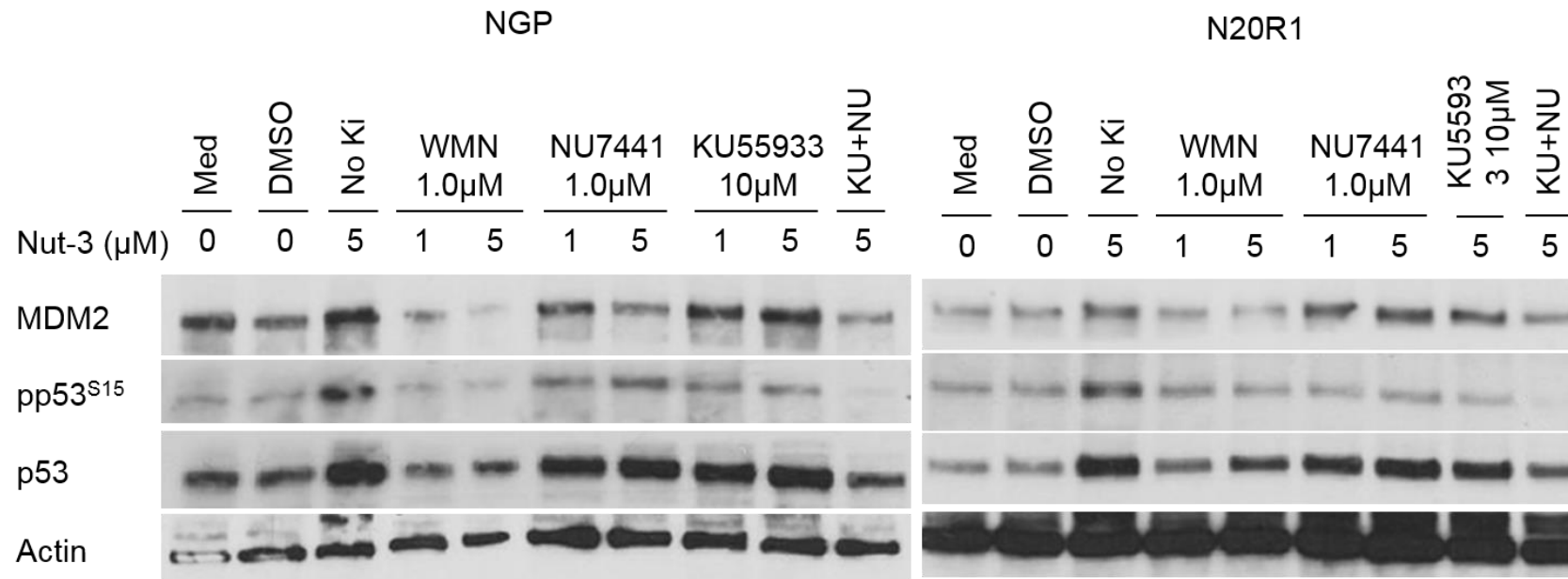


Figure 6-12 Phosphorylation of p53^{Ser15} following MDM2 inhibitors is dependent on both ATM and DNA-PK kinase activity. Individual specific kinase inhibitors NU7441 (DNA-PK) and KU55933 (ATM) did not reduce p53^{Ser15} phosphorylation as effectively as their combination. Cells were treated simultaneously with doses of Nutlin-3 or stated kinase inhibitor(s) 4Hrs prior to lysate collection. KU: ATM inhibitor KU55933; NU: DNA-PK inhibitor NU7441; WMN: Broad spectrum PI3K inhibitor Wortmannin.

6.4.4 Pharmacological elevation of p53^{Ser15} phosphorylation in the absence of DNA damage concurs with induction of a larger subset of genes regulated by p53-driven promoters

As was shown in Chapter 5, the combination of non-genotoxic doses of MDM2 inhibitors and GSK2830371 increases p53^{Ser15} phosphorylation markedly in cell lines where neither drug on their own detectably influence this residue. This phosphorylation event coincided with increased growth inhibition and cell death endpoints only when p53 was transcriptionally functional. Given the reported role of p53^{Ser15} phosphorylation in enhancing p53 interaction with transcriptional coactivator such as p300/CBP (Jenkins, Durell et al. 2012), it was of interest to assess whether the subset of early genes activated by p53 differed in response to the combination regimen compared to RG7388 treatment alone. This may be an important underlying mechanism for the observed potentiation in response to the combination treatment

Maximal p53 target protein induction in NGP cells by treatment with MDM2 inhibitors was reached at 6-8Hrs (Figure 6-9) so we predicted that transcripts would precede this by at least 2Hrs. Therefore we assessed global changes in gene expression at 4Hrs treatment in NGP cells which showed the greatest potentiation in response to the combination treatment (5.8-fold, Section 5.5.1). Induction of early p53 target genes were of particular interest given that the appearance of transcripts at later time-points may not be directly regulated by p53.

NGP cells were treated with 0.5% DMSO, 75nM RG7388 (~GI50) \pm 2.5 μ M GSK2830371 for 4Hrs before RNA and protein extraction in parallel. The number of statistically significant transcripts induced 4Hrs after 75nM RG7388 were 9 (after Benjamini-Hotchberg correction for multiple testing), all of which were known p53 transcriptional targets (Table 6-5, Table 6-6 and Figure 6-13). The subset of statistically significant p53 transcriptional target genes induced by RG7388 however increased from 9 to 24 when WIP1 was inhibited. There was an increase in both pro-apoptotic and pro-arrest genes in the combination treatment. Western blotting on lysates isolated from cells treated in parallel to the samples used for expression array analysis showed that this increase in differential expression correlates with p53^{Ser15} phosphorylation in the absence of any changes to total p53 levels (Figure 6-14). Furthermore all the statistically significant changes in p53 transcriptional targets show positive increase in transcript level and transcription suppression was not detected. This is also translated to

the protein level as p21^{WAF1} induction was subtly increased in two out of three repeats analysed by western blotting and MDM2 in one out of three repeats.

(A) RG7388 V DMSO

Gene Symbol	log ₂ (Fold-change)	Adjusted p-value	OR	Function summary
<i>CDKN1A</i>	2.07	0.002	3.95	Pro-arrest
<i>PHLDA3</i>	1.58	0.002	3.94	Pro-apoptotic
<i>SESNI</i>	1.12	0.018	2.57	↓ROS
<i>BTG2</i>	0.84	0.002	3.80	Pro-arrest
<i>AEN</i>	0.83	0.026	2.31	Pro-apoptotic/Exonuclease activity
<i>TP53INP1</i>	0.77	0.001	4.42	Pro-apoptotic
<i>RGMA</i>	0.66	0.018	2.63	Inhibitor of neurite outgrowth
<i>C12orf5</i>	0.59	0.016	2.85	↓ROS
<i>FAM212B</i>	0.52	0.017	2.74	Poorly understood

Table 6-5 Genes induced following treatment of NGP cells with 75nM RG7388 (GI50). OR: Odds Ratio; ROS: Reactive oxygen species

(B) RG7388 + WIP1i V DMSO

Gene Symbol	log₂ (Fold-change)	Adjusted p-value	OR	Function summary
<i>BTG2</i>	1.31	0.0001	6.77	Pro-arrest
<i>TP53INP1</i>	0.95	0.0001	6.76	Pro-apoptotic
<i>CDKN1A</i>	2.67	0.0002	6.35	Pro-arrest
<i>PHLDA3</i>	1.93	0.0002	6.15	Pro-apoptotic
<i>FAM212B</i>	0.88	0.0002	6.09	Poorly understood
<i>RGMA</i>	0.96	0.0009	5.38	Inhibitor of neurite outgrowth
<i>C12orf5</i>	0.77	0.0012	5.17	↓ROS
<i>SESN1</i>	1.46	0.0019	4.84	↓ROS
<i>SESN2</i>	0.58	0.0027	4.58	↓ROS
<i>ACTA2</i>	0.71	0.0028	4.51	Structural/Motility
<i>XPC</i>	0.66	0.0041	4.22	DNA Repair
				Nucleotide excision repair
<i>ZNF79</i>	0.43	0.0062	3.91	Poorly understood
<i>AEN</i>	0.85	0.0147	3.27	Pro-apoptotic/Exonuclease activity
<i>LOC101927383</i>	0.63	0.0151	3.21	Long non-coding RNA
<i>FAM212B</i>	0.32	0.0178	3.04	Poorly understood
<i>TNFRSF10B</i>	0.52	0.0210	2.87	Pro-apoptotic
<i>PIDD1</i>	0.37	0.0368	2.41	Pro-apoptotic
<i>TRIAP1</i>	0.66	0.0389	2.33	Anti-apoptotic
<i>ARC</i>	0.38	0.0420	2.23	Structural

<i>DDB2</i>	0.29	0.0429	2.17	DNA Repair
				Nucleotide excision repair
<i>MDM2</i>	0.51	0.0434	2.10	Pro-survival
<i>TOB1</i>	0.53	0.0434	2.09	Pro-arrest
<i>BLOC1S2</i>	0.31	0.0454	1.97	lysosome-related organelles/Neurite formation
<i>GADD45A</i>	0.74	0.0454	1.97	Pro-arrest
<i>ZMAT3</i>	0.59	0.0454	1.96	Pro-arrest/-apoptotic

Table 6-6 A larger subset of p53 transcriptional targets are induced by a combination of 75nM RG7388 and 2.5µM GSK2830371. OR: Odds ratio; ROS: Reactive oxygen species. This table is a continuation of the table on the previous page.

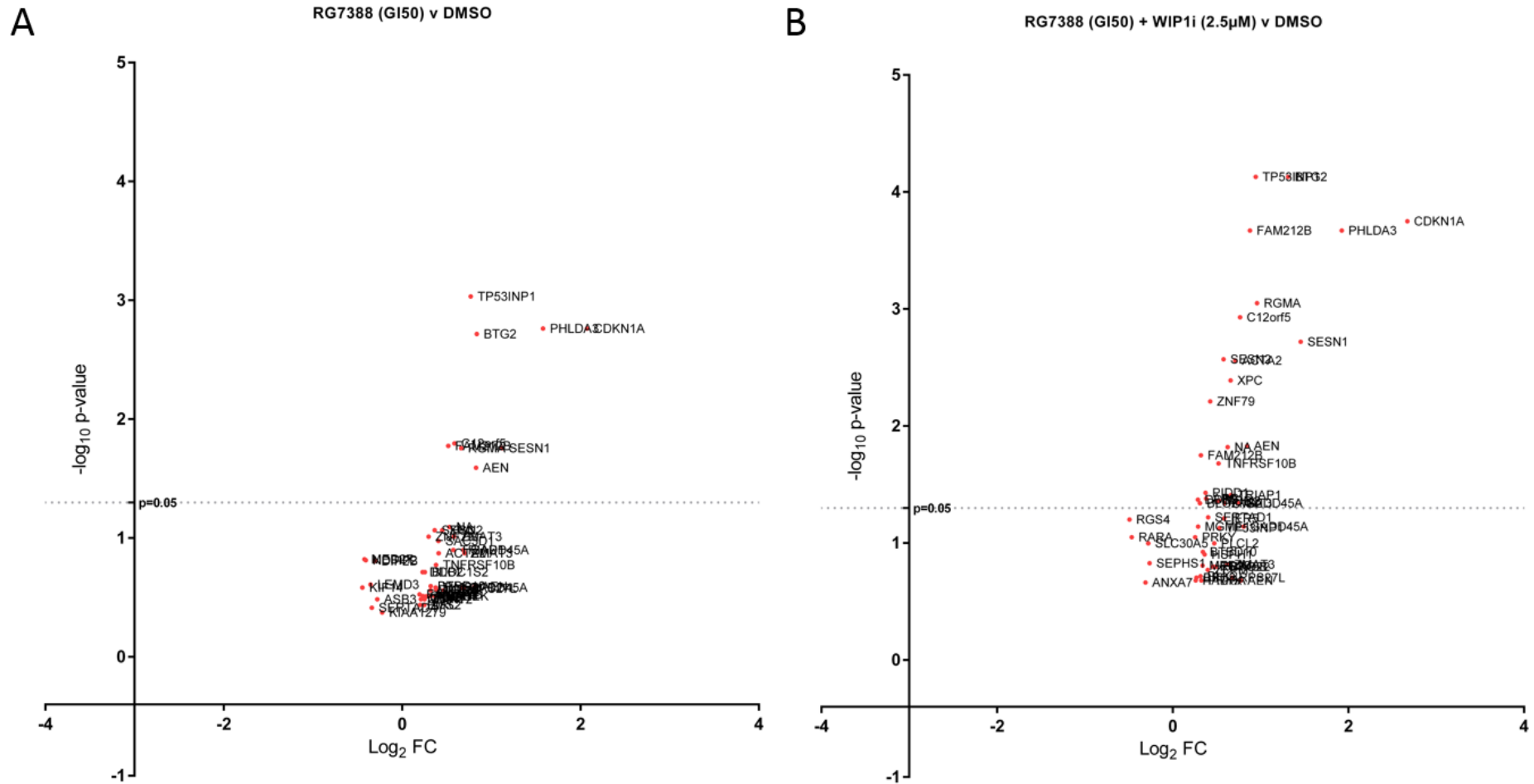


Figure 6-13 Volcano plot showing the top 50 differentially expressed genes between DMSO and the two treatment conditions. A larger subset of p53 target genes are differentially expressed in response to the combination of RG7388 and GSK2830371 at compared RG7388 single treatment at 4Hrs. Y-axis shows $-\log_{10}$ adjusted p-value (Benjamini-Hotchberg Corrected) and the x-axis shows \log_2 fold-change.

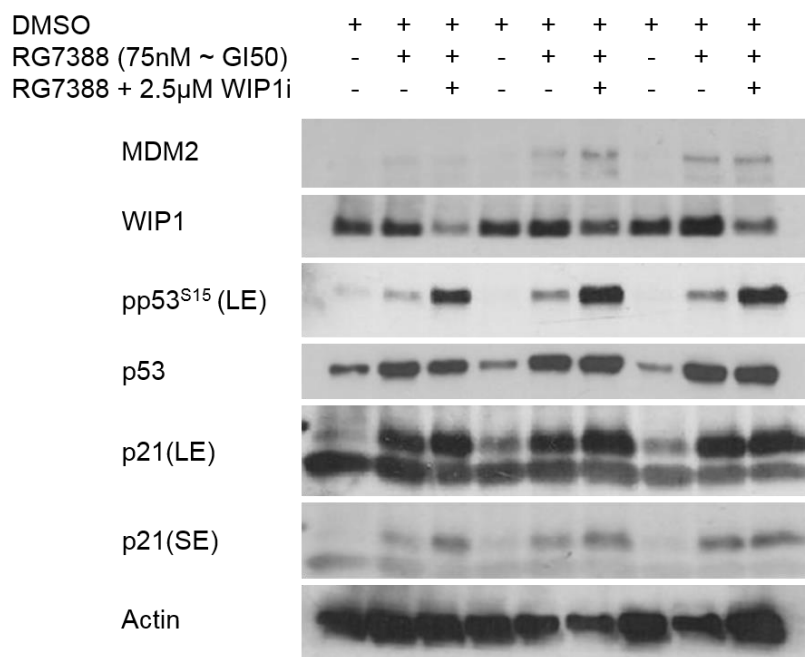


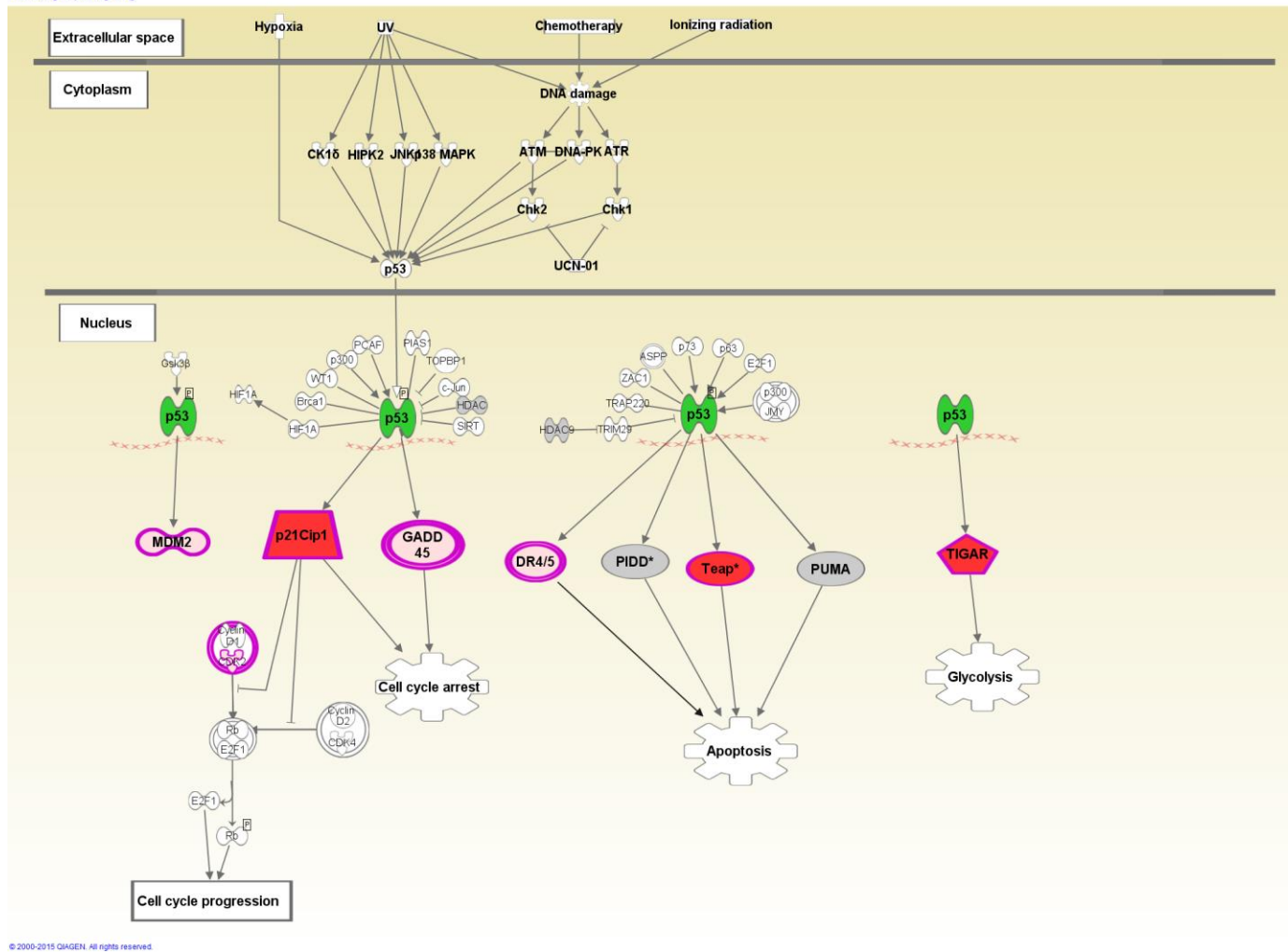
Figure 6-14 Immunoblot shows treatment with the combination of RG7388 and GSK2830371 compared to RG7388 alone results in an increase in p53^{Ser15} phosphorylation pp53^{Ser15} at 4Hrs which correlates with an increase in p53 transcriptional targets p21^{WAF1} and MDM2.

6.4.5 Pathway analysis of gene expression

Upon closer inspection genes just below the significance level, as ranked by raw p-value after correction for multiple testing, were mostly p53 transcriptional targets. This is unlikely to be coincidental given the total number of probes detected (~18000).

Benjamini-Hotchberg or Bonferroni methods used in correction for multiple testing in the context of microarray data for gene expression changes have been suggested to be too conservative. This is because the hypotheses tested are not wholly independent as the genes involved are generally altered in a mutually dependent groups by the same transcription factor (Perneger 1998, Bender and Lange 1999). Given our knowledge of the mechanism of action of MDM2 inhibitors and the p53 network and its transcriptional targets, we know that independence of all the tested variables is not a justifiable assumption. We wanted to assess whether other pathways are activated that are just below the statistical significance level after correction for multiple testing.

The number of statistically significant genes in both treatment conditions exceeded 1000 when p-values from paired t-tests were examined without correction for multiple testing if significance level (α) < 0.05. In order to detect biologically relevant changes, reduce the computational load and increase confidence levels, $\alpha < 0.001$ was used as the cut-off point prior to selection of genes for pathway analysis using Ingenuity Pathway Analysis (IPA) software package system. This analysis confirmed that most genes in the p-value range < 0.001, before correction for multiple testing, were involved in p53 signalling. This was the case with respect to both treatment conditions (RG7388 $p = 3.19 \times 10^{-9}$ and RG7388 + GSK2830371 $p = 7.78 \times 10^{-10}$). IPA calculates the p-values for pathway analysis as described in 6.3.5.5. Transcripts which are considered as canonical p53 targets are highlighted using IPA pathway designer (Figure 6-15 and Figure 6-16). Canonical p53 pro-apoptotic transcriptional targets PUMA and PIDD1 were induced only WIP1 was inhibited suggesting altered promoter selectivity in the presence of WIP1 inhibition. Although these results must be further investigated at mRNA and protein level at various time-points after treatment.



244

Figure 6-15 Canonical p53 transcriptional targets induced in response to treatment with 75nM RG7388 and their involvement in cellular processes ($p=3.19 \times 10^{-9}$). Nodes filled grey are not induced in response to RG7388 single treatment.

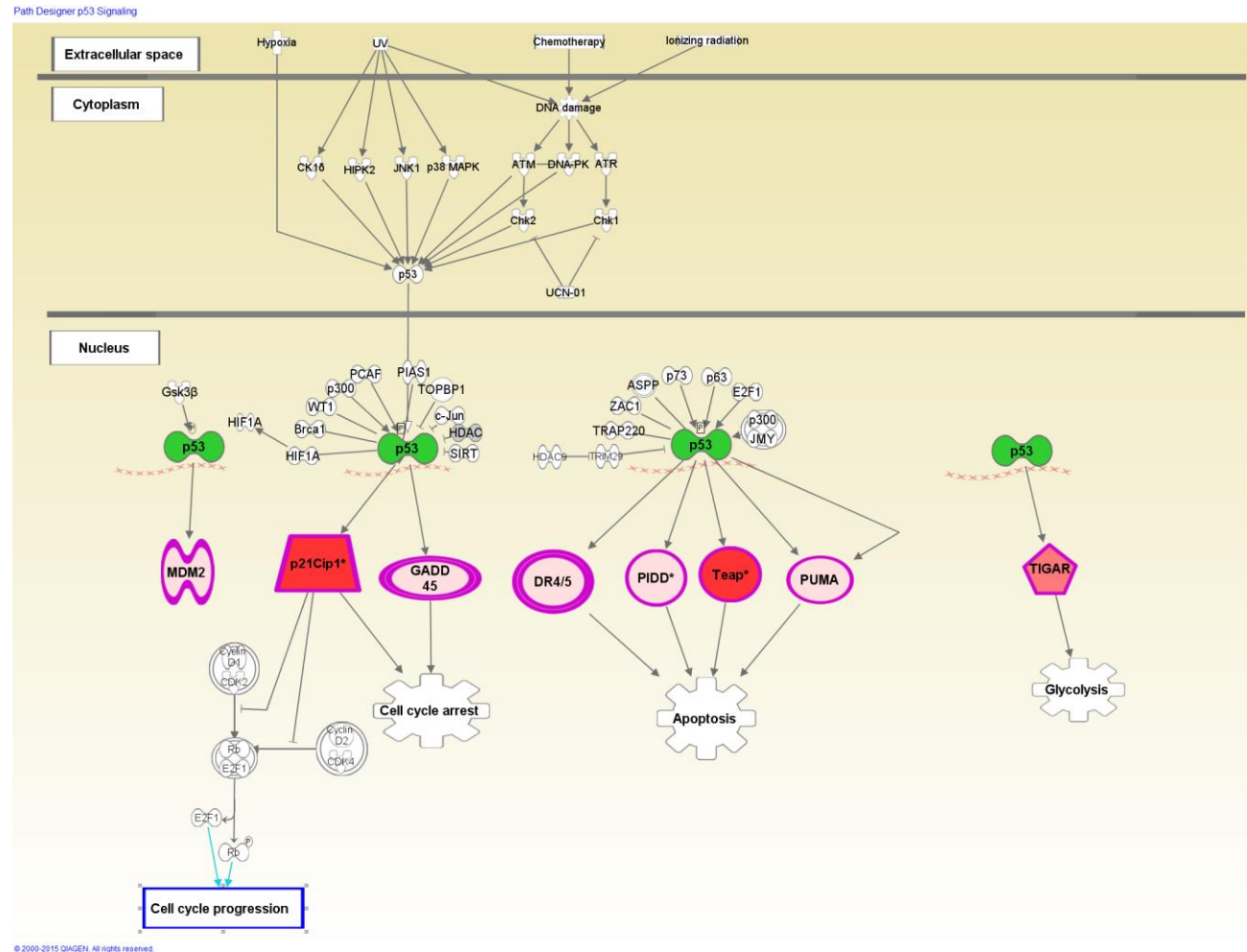


Figure 6-16 Canonical p53 transcriptional targets induced in response to treatment with 75nM RG7388 + 2.5 μ M GSK2830371 and their involvement in cellular processes as identified by IPA reference data set ($p=7.78 \times 10^{-10}$). PIDD1 and PUMA are induced in the presence of WIP1 inhibition.

6.4.5.1 qRT-PCR validation of the array data

Differentially expressed genes of interest among those listed in Table 6-6A & B which were implicated in important biological processes were selected for validation by qRT-PCR using cDNA generated from the same samples used for microarray analysis.

CDKN1A (p21^{WAF1}) and *BTG2* were among the genes validated which were involved in inhibition of cell cycle progression (Eldeiry, Tokino et al. 1993, Rouault, Falette et al. 1996). *TP53INP1* and *PHLDA3* also validated are pro-apoptotic p53 transcriptional target genes (Okamura, Arakawa et al. 2001, Kawase, Ohki et al. 2009). The increased basal expression of *XPC*, a gene involved in nucleotide excision repair, was also investigated as it is one member elevated in a gene expression signature associated with an increased sensitivity to MDM2 inhibitors RG7112 and RG7388 both pre-clinically and clinically in acute lymphoblastic leukaemia (ALL) (Zhong, Chen et al. 2015). *CDKN1A* and *BTG2* both showed increased fold-change in expression in response to single treatment with RG7388 and were elevated significantly when WIP1 inhibitor was additionally present (Figure 6-17). Consistent with an increase in apoptosis in response to the combination treatment compared to single MDM2 inhibitor in NGP cells there was a significant increase in the expression of *TP53INP1* in response to RG7388 which was also significantly elevated in the presence of GSK2830371 (WIP1i). Although the expression of *PHLDA3* was not significantly different between RG7388 single treatment and in the background of WIP1 inhibition there was a trend towards increased expression in the combination treatment as the p-value decreased by a decimal point. MDM2 was also differentially induced in the presence of the GSK2830371 compared to RG7388 alone. *XPC* expression was not differ in expression comparing the single treatment to combination treatment using qRT-PCR. These transcriptional changes likely contribute to the potentiation MDM2 inhibitors in NGP cells in the presence of GSK2830371 and are likely caused by an increase in p53^{Ser15} phosphorylation (Loughery, Cox et al. 2014).

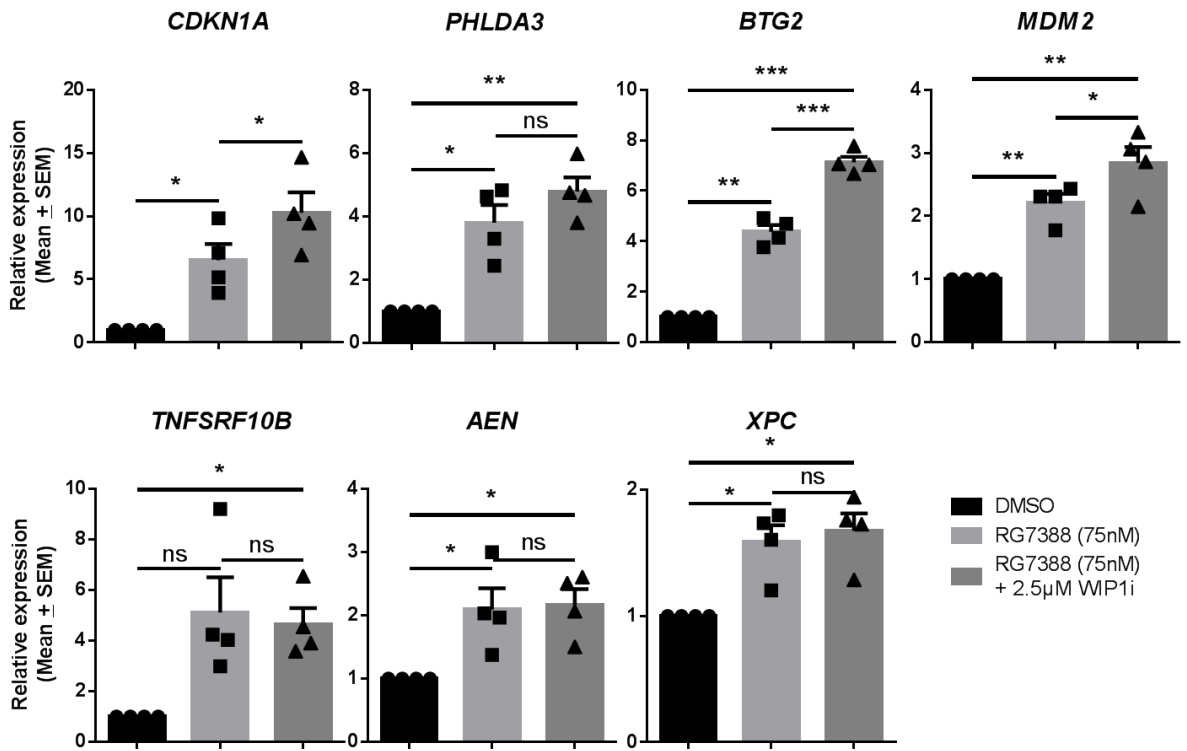


Figure 6-17 Quantitative real-time PCR carried out to assess the validity of microarray data. Data represent mean \pm standard error of mean (SEM) relative quantities of four independent repeats where *GAPDH* was used as endogenous control and DMSO as the calibrator for each independent repeat with the formula $2^{-\Delta\Delta C_T}$. P-values calculated by paired t-test; *: $p < 0.05$; **: $p < 0.005$; ***: $p < 0.0005$

6.4.6 p53-dependent reporter gene expression was induced by Nutlin-3 but showed no further change with the addition of GSK2830371 (WIP1i)

The combination of MDM2 and WIP1 inhibition at mechanistically relevant doses was shown to increase p53^{Ser15} transcription in the absence of any DNA damaging agents. We sought to assess p53 transcriptional activity from a p53 consensus sequence regulated luciferase reporter system stably transfected in *TP53* wild-type and mutant glioblastoma cell lines following multiples of Nutlin-3 GI50 \pm 2.5 μ M GSK2830371. No reporter activity was observed in response to 2.5 μ M GSK2830371. However, there was dose-dependent increase in reporter activity 24Hrs following Nutlin-3 multiples of GI50 dose in the DD7 (*TP53* Wild-type) cells but not in DR4 cells (*TP53* Mutant). This reporter activity was not enhanced in the presence of the WIP1 inhibitor. The 24Hrs time-point was chosen because earlier time-points did not produce a Nutlin-3 dose-dependent reporter signal. We aimed to assess whether GSK2830371 can sensitise cells to Nutlin-3. SRB growth inhibition assays were carried out as described in Chapter 5 which showed that GSK2830371 modestly (1.7-Fold, p=0.005) potentiated the response of DD7 cells to Nutlin-3 in the presence of 2.5 μ M GSK2830371 (Figure 6-18). Interestingly, WIP1 inhibitor on its own resulted in growth inhibition in the *TP53* mutant DR4 cell lines. These findings overall suggest that p53 transcriptional activity may not be important for the potentiation of MDM2 inhibitors by GSK2830371 in these cell lines.

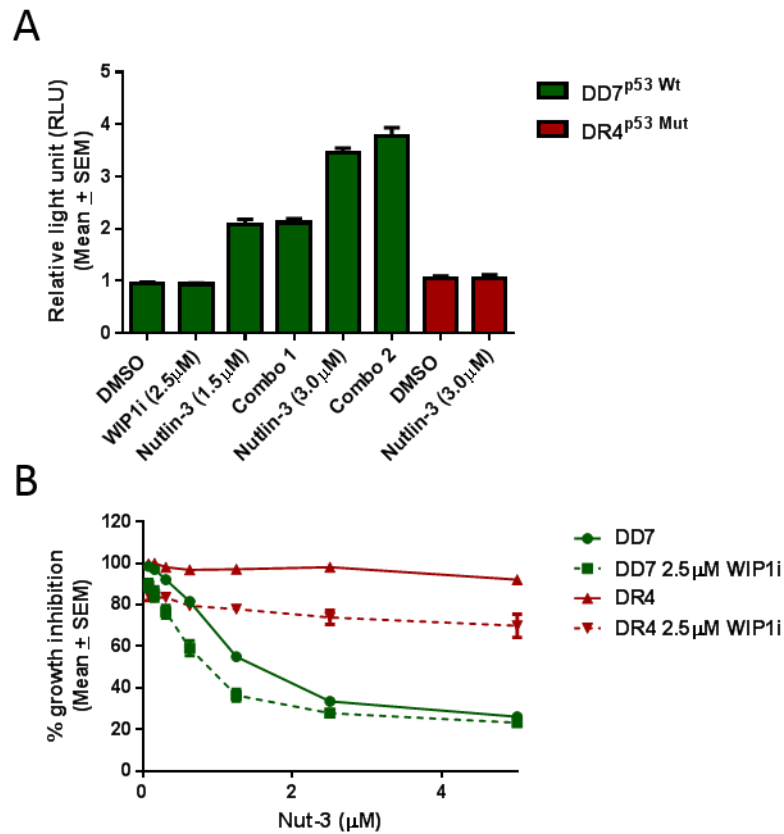


Figure 6-18 A) Firefly luciferase reporter enzyme activity 24Hrs following 1 × and 2 × Nutlin-3 DD7 GI50. B) SRB Growth inhibition of stably transfected glioblastoma cell lines in the presence and absence of 2.5 μM GSK2830371. Potentiation of the *TP53* wild-type cell lines is modest. Wt: Wild-type; Mut: Mutant

6.4.7 Mutations of p53^{Ser15} modulate the levels of p53 induced transcriptional targets

Previous reports in the literature have shown that p53^{Ser15} phosphorylation, while not necessary for the dissociation of p53 from MDM2, enhances transcription from p53-driven promoters (Dumaz and Meek 1999, Loughery, Cox et al. 2014). Residue Serine 15 was mutated to alanine (p53^{S15A}) to prevent phosphorylation at that site. Also separately we mutated this to aspartate (p53^{S15D}) known to mimic a phosphate group. We then ectopically expressed these mutants of p53 to assess their impact on p53 transcriptional activity compared to wild-type p53 overexpression. Site-directed mutagenesis was carried out on full-length wild-type p53 cDNA as described in 6.3.6 and Sanger sequencing data showed that the mutagenesis had been successful (Figure 6-19). Concentrations of plasmids were transfected in order to make the data more comparable to approximate physiological levels of p53 under these experimental conditions. Western blots (Figure 6-20) showed that p53^{S15A} or p53^{S15D} cannot be detected by a phospho-p53^{S15} (pp53^{Ser15}) antibody confirming that these mutants cannot be phosphorylated on that residue. Also interestingly consistent with previous findings, p53 transcriptional activity as measured by MDM2 and p21^{WAF1} expression, is subtly higher either when p53^{Ser15} can be phosphorylated or when the phosphorylation is mimicked by an aspartate residue (p53^{S15D}) (Figure 6-20). The observations are consistent with earlier findings that p53^{Ser15} plays a role in transcriptional activity from p53 regulated promoters (Loughery, Cox et al. 2014). Images obtained from cells transfected with these vectors show that there are more floating cells in wells transfected with wild-type p53 and p53^{S15D} compared to p53^{S15A} (Figure 6-21) which warrants further investigation into the expression of early and late apoptotic markers.

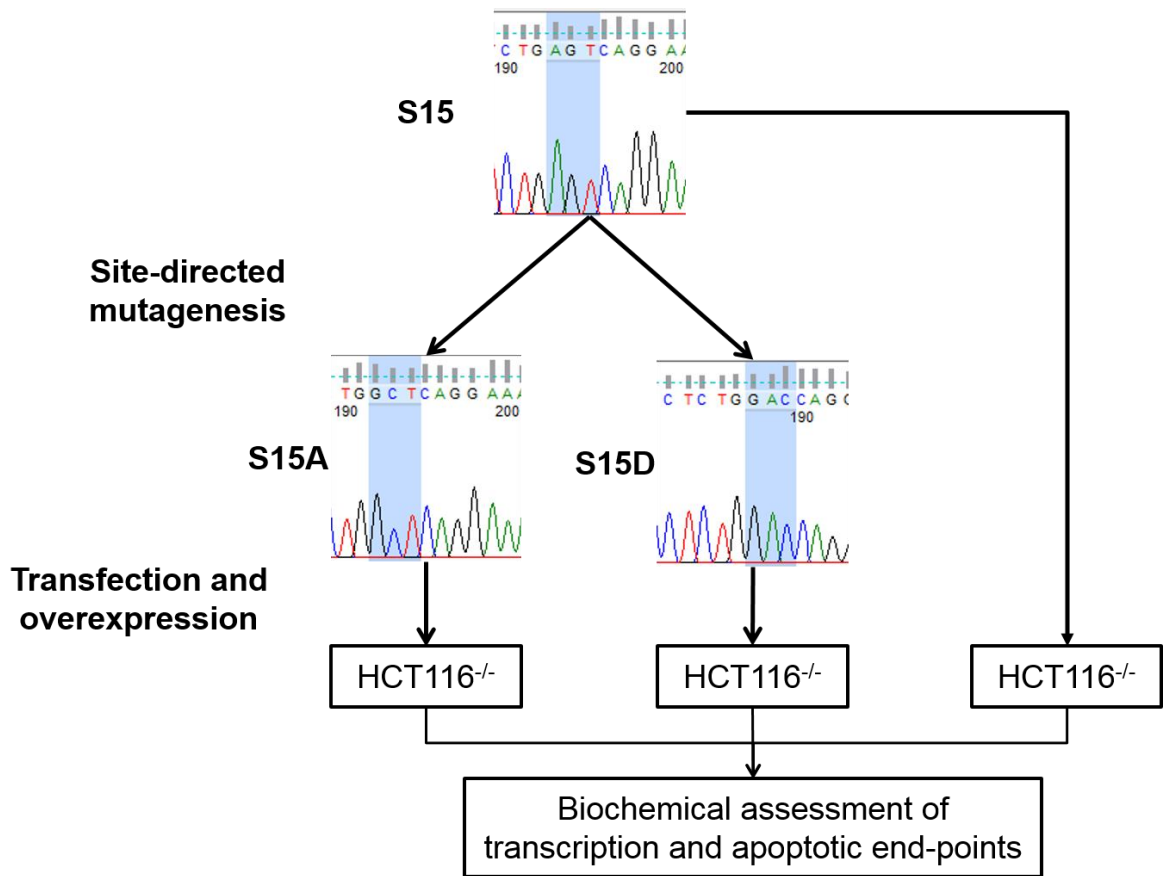


Figure 6-19 Chromatogram traces from the Sanger sequencing experiment before and after site-directed mutagenesis of full-length p53 plasmid.

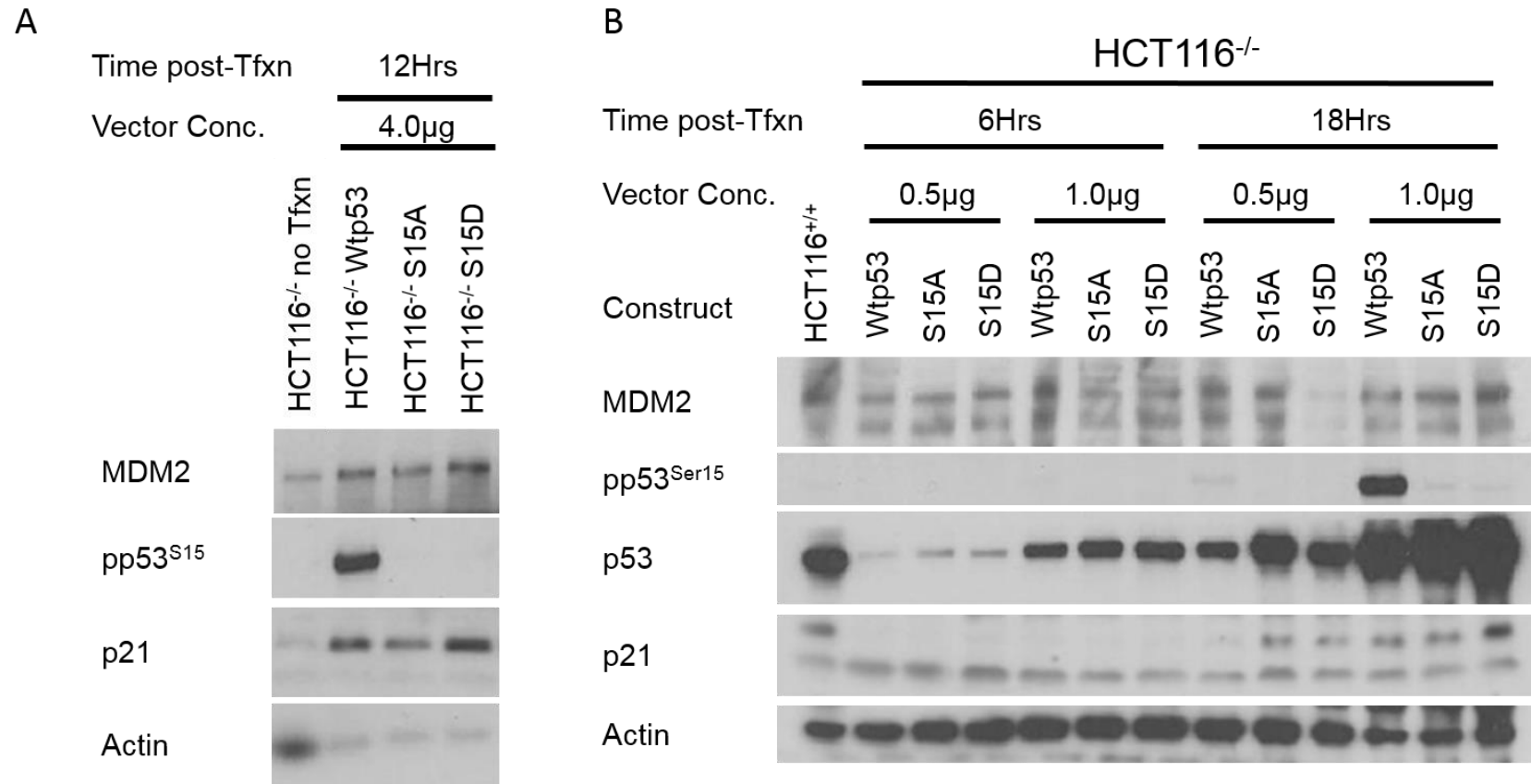


Figure 6-20 Phosphorylation of p53 influences expression of p53 transcriptional targets MDM2 and p21^{WAF1} at the protein level. A) Immunoblot showing TP53 Null HCT116 cells (HCT116^{-/-}) transfected with 4.0 μ g of either wild-type (Wtp53) or mutant p53 (p53^{S15A} or p53^{S15D}) expression plasmids 12Hrs before lysate extraction and western blotting. B) Immunoblot of HCT116^{-/-} cells transfected with lower amounts of p53 overexpressing plasmids with lysate collection at two different time-points. HCT116^{+/+} cells were used as a positive control in B. Tfxn: transfection; Conc.: Concentration

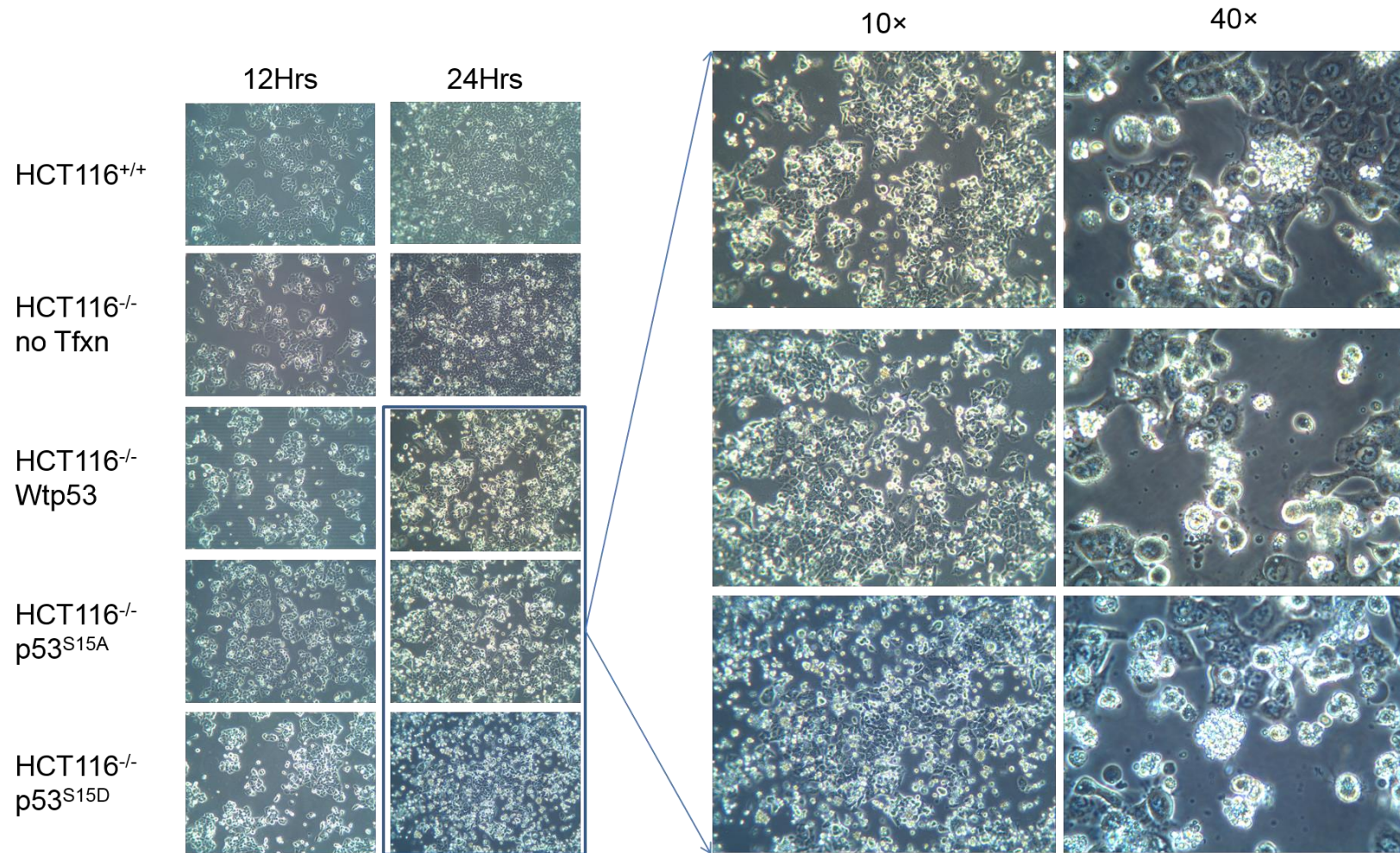


Figure 6-21 Apoptotic morphology of HCT116^{-/-} cells 24Hrs following overexpression of wild-type p53 (Wtp53) compared to p53^{S15A} or p53^{S15D}. Apoptotic/floating cells were more numerous in

6.5 Discussion

Activation of p53, in response to cellular stress, depends on a complex array of post-translational modifications (PTM's) that lead to the dissociation of p53 from MDM2, and both release and activate its transcriptional function. DNA damage induced p53 PTM's have been extensively investigated in contrast to those induced by MDM2 inhibitors. Phosphorylation of p53^{Ser15} following treatment with MDM2 inhibitors has been observed by various groups including ours. Our data show that pp53^{Ser15} accumulation is slow and proportional to p53 stabilisation following MDM2 inhibitors compared to its immediate and intense appearance after DNA damage with IR. These observations are consistent with an earlier model that MDM2 inhibitors result in exposure of p53^{Ser15} to the basal activity of kinases and phosphatases that target this residue. In the previous chapter we showed that WIP1 inhibition tilts this balance towards the kinases that target this residue and markedly increases MDM2 inhibitor induced pp53^{Ser15}. This was shown to correlate with potentiation of MDM2 inhibitors. In this evidence was presented to support the hypothesis that this potentiation is due to increased p53 transcriptional activity caused by increased p53^{Ser15} phosphorylation. This demonstrates that sensitivity to MDM2 inhibitors can be increased by pharmacologically modulating p53 transcriptional activity through influencing its post-translational modification.

6.5.1 Phosphorylation of p53^{Ser15} in the absence of DNA damage

Phosphorylation of p53^{Ser15} has also been used as a surrogate marker for DNA damage in the literature. However, this model presumes kinases that respond immediately following their activation by DNA damaging agents. Our observations suggest that while this model may hold true in response to the seemingly all or none activity of ATM kinase in phosphorylation of p53^{Ser15} after IR, it cannot explain the slow increase in pp53^{Ser15} following treatment with MDM2 inhibitors. Phosphorylation of p53^{Ser15} after MDM2 inhibitors is less intense more gradual and independent of MDM2 inhibitor class and cell type. Inhibition of ATM by KU55933 resulted in a marked reduction in p53^{Ser15} phosphorylation after IR in contrast to the relative lack of effect with DNA-PK inhibition (NU7441) or broad spectrum PI3K inhibition (Wortmannin). Inhibition of ATM or DNA-PK kinases alone did not influence pp53^{Ser15} following Nutlin-3, whereas their combination resulted in a notable reduction in Nutlin-3 mediated pp53^{Ser15}. Wortmannin also reduced p53^{Ser15} phosphorylation following Nutlin-3 treatment. The

above observation suggest that it is likely the basal activity of multiple kinases are involved in targeting this residue and their effect is only apparent when p53 is released from MDM2. Interestingly, in Chapter 5 we showed that single agent treatment with MDM2 or WIP1 inhibitors did not influence pp53^{Ser15} in contrast to their combination which resulted in a marked increase in pp53^{Ser15}. This showed that p53^{Ser15} phosphorylation status, after MDM2 inhibitor treatment is mostly down-regulated by WIP1 phosphatase and makes this a prime target for potentiating the effect of MDM2 inhibitors via its effect on p53 function and cell fate.

6.5.2 Increasing MDM2 inhibitor induced pp53^{Ser15} coincides with enhanced p53 transcriptional activity

Phosphorylation of p53^{Ser15} is considered a “nucleation event” which can initiate subsequent post-translational modifications important in modulation of p53 transcriptional function and its interaction with MDM2 (Sakaguchi, Saito et al. 2000, Meek and Anderson 2009). Phosphorylation of p53^{Ser15} after MDM2 inhibition was markedly increased in response to the selective WIP1 inhibitor GSK2830371 or siRNA mediated WIP1 knockdown. This pp53^{Ser15} increase concurred with increased sensitivity to MDM2 inhibitors only in p53 wild-type cell lines in which p53 is transcriptionally active. Protein levels of p53 transcriptional targets MDM2 and p21^{WAF1}, as measured by immunoblotting, were only slightly affected by the WIP1 inhibition. Array based differential gene expression analysis showed that more p53 transcriptional target genes were significantly upregulated in the presence of the selective WIP1 inhibitor GSK2830371 than with RG7388 alone. This correlation suggests that WIP1 inhibitor mediated potentiation of MDM2 inhibitors in NGP cells is caused by an increase in transcription from p53 regulated promoters. Interestingly, most genes that were differentially induced in the presence of the WIP1 inhibitor have been implicated in pro-apoptotic signalling. Validation by qRT-PCR confirmed that the expression of *CDKN1A*, *BTG2* and *MDM2* were increased in response to RG7388 and enhanced in the presence of GSK2830371. These were consistent with the subtle changes observed at the protein level in response to the combination of MDM2 and WIP1 inhibition in Chapter 5. Expression of other genes such as *TNFRSF10B*, *AEN* and *XPC* as measured by qRT-PCR were also increased in response to RG7388 ± GSK2830371. Although these genes showed a pattern towards enhanced transcriptional induction in the presence of GSK2830371 it would be difficult to assume biological relevance purely based on the changes detected by the qRT-PCR and the array at this

dose and time point alone. As it was noted in chapter 1 p53 transcriptional target genes have different kinetics of induction following p53 activation. This has been attributed to differences between p53 response elements at gene promoters and different efficiency of pre-initiation complex formation among target gene promoters (Espinosa, Verdun et al. 2003, Morachis, Murawsky et al. 2010). Therefore, interpretation of differential expression of p53 target genes detected by the array may require further mechanistic investigations following different doses and time-points of the combination treatment.

6.5.2.1 Induction of p53 targets and kinetics of PTM's

Modifications of other p53 residues important for p53 function such as acetylation of C-terminal residues K320 and K382 and phosphorylation of Ser9, Thr18 and Ser20 have also been reported to require p53^{Ser15} phosphorylation (Sakaguchi, Herrera et al. 1998, Sakaguchi, Saito et al. 2000, Saito, Goodarzi et al. 2002, Saito, Yamaguchi et al. 2003). These modifications may impact MDM2-p53 interaction or p53 transcriptional function at later time points than 4Hrs following p53 activation. There were many other p53 transcriptional targets that were just below the significance threshold p-value after correction for multiple testing. This was shown by pathway analysis for the top 50 differentially expressed genes (raw p-value <0.001) between both treatment conditions. The efficient induction of these genes may require special barcodes of p53 PTM's that occur in sequence to p53^{Ser15} and recruit other co-factors. Therefore analysis of gene expression following >4Hrs combination of MDM2 and WIP1 inhibitors may be informative about the role of pp53^{Ser15} in differential induction of these genes and in turn in cell fate determination. The dose of RG7388 used in this experiment was equivalent to the GI50 value for this compound in NGP cells, in which the greatest potentiation of MDM2 inhibitors was observed. Due to the differences between densities in the growth inhibition setting (~20%) and those used for RNA preparation (~50-60%) at the time of treatment however, a higher dose of MDM2 inhibitors may be better representative of any differential expression of p53 transcriptional targets.

6.5.2.2 Luciferase reporter gene expression in response to the combination of MDM2 and WIP1 inhibitors.

DD7 and DR4 cells stably transfected with p53 reporter gene construct were derived from DBTRG and T98G respectively, neither of which have been reported to show differences in WIP1 expression or *PPM1D* mutations. The growth inhibition of the *TP53* wild-type clone (DD7) to Nutlin-3 was potentiated in the presence of 2.5µM GSK2830371. The sensitivity of the *TP53* mutant clone did not change in the presence

of GSK2830371. Interestingly, 2.5 μ M GSK2830371 resulted in modest growth inhibition in the *TP53* mutant cell line which suggests a p53-independent mechanisms of action for this compound. However, this may be because both cell lines are grown under selection conditions which may make cells more sensitive to WIP1 inhibition through a p53 independent mechanism. This may result in p53-independent mechanisms of growth inhibition. Treatment with 1 \times and 2 \times Nutlin-3 GI50 doses resulted in a dose-dependent increase in luciferase activity in the *TP53* wild-type clone (DD7) and not the mutant (DR4). However the addition of 2.5 μ M GSK2830371 did not enhance this activity. This may suggest that the potentiation of the Nutlin-3 growth inhibitory response in DD7 cells does not rely on an increase in p53 transcriptional activity. Unfortunately because of time limitations pp53^{Ser15} following MDM2 and WIP1 inhibitor combination was not investigated in these cell lines to confirm the increased phosphorylation.

6.5.3 Transient expression of p53 containing mutations in p53^{Ser15}

Expression of wild-type p53 and its comparison with p53^{S15A} and p53^{S15D} variants generated by site-directed mutagenesis showed that the phosphorylation of this residue is important for transcriptional regulation from p53 driven promoters. The phospho-mimic aspartate residue on Ser15 consistently resulted in a notable increase in p53 transcriptional targets MDM2 and p21^{WAF1} when compared to non-phosphorylated alanine at the same residue. Interestingly all three p53 expression constructs resulted in apoptotic morphology 24Hrs following transfection. There appeared to be fewer cells with apoptotic morphology in response to p53^{S15A} overexpression as compared to p53 wild-type and p53^{S15D} overexpression. However this remains a qualitative impression at present and has not been quantified or biochemically assessed yet.

6.5.4 Summary

The overall evidence presented in Chapters 6 and 7 strongly supports the notion that phosphorylation of p53^{Ser15} is not only a reliable biomarker for on target activity of the combination treatment but it is also mechanistically important for p53 transcriptional activity. The evidence also supports the model of dynamic regulation of the phosphorylation status of p53^{Ser15} following MDM2 inhibitors. This model is summarised in (Figure 6-22). These findings provide a rationale for the combination of MDM2 and WIP1 inhibitors, particularly in *TP53* wild-type malignancies with increased *PPM1D* expression or gain-of-function. One such malignancy which is

mostly *TP53* wild-type at diagnosis and shows increased *PPM1D* mRNA expression in neuroblastoma (Saito-Ohara, Imoto et al. 2003, Carr-Wilkinson, O'Toole et al. 2010). WIP1 is considered a potential therapeutic target in neuroblastoma and increased expression of its mRNA is a marker of poor progression (Richter, Dayaram et al. 2015). In the following chapter *PPM1D* expression and its relationship to clinical and pathological information will be further investigated in neuroblastoma.

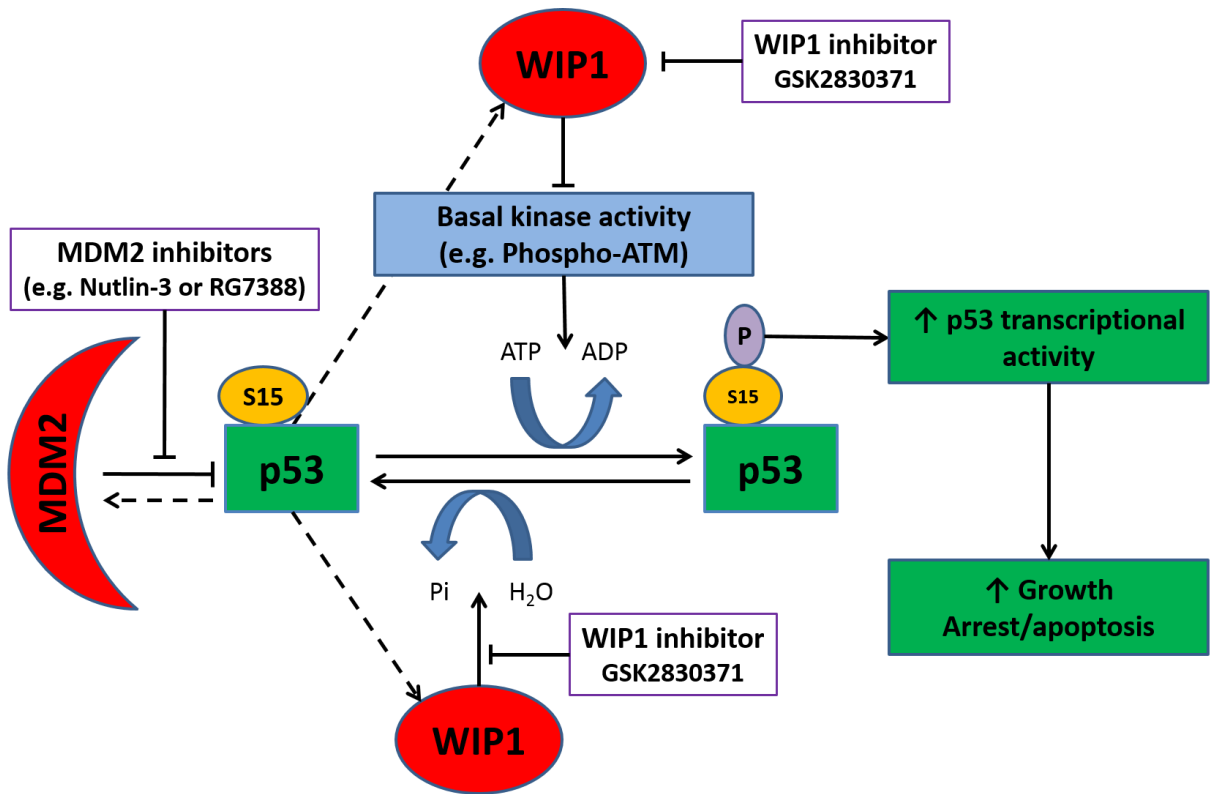


Figure 6-22 The working model explaining the underlying mechanism of regulation of p53^{Ser15} phosphorylation status and its contribution to potentiation of MDM2 inhibitors by the WIP1 inhibitor GSK2830371.

Chapter 7 The expression of *PPM1D* mRNA and WIP1 protein in neuroblastoma: relationship to pathology and survival

7.1 Introduction

In the previous chapters we showed that selective WIP1 inhibition results in potentiation of response to MDM2 inhibitors and related this to an increase in p53 transcriptional activity. This potentiation was most notable in *TP53* wild-type cell lines with increased WIP1 expression or gain-of-function mutations. Therefore, tumours with increased WIP1 expression or phosphatase activity would be ideal subgroups for use of WIP1 and MDM2 inhibitor combinations. Increased *PPM1D* mRNA expression has been reported to be associated with poor prognosis in neuroblastoma (Saito-Ohara, Imoto et al. 2003, Richter, Dayaram et al. 2015). However, the association between WIP1 protein expression and overall survival has not been investigated in this malignancy to date. In this chapter publically available online gene expression datasets are firstly investigated to assess the relative *PPM1D* mRNA expression in human malignancies and any correlation with overall survival, focusing on neuroblastoma. WIP1 immunohistochemical (IHC) staining is then investigated in an independent cohort of neuroblastoma tumour samples to analyse any correlation with clinical and pathological variables.

7.1.1 *PPM1D*/WIP1 expression as a marker of prognosis in human malignancies

Increased *PPM1D* mRNA expression was first reported to predict poorer survival in neuroblastoma (Saito-Ohara, Imoto et al. 2003). This was prompted by frequent gain of the distal region of chromosome 17q (17q21-17qter) which had been associated with poorer overall survival in neuroblastoma (Bown, Cotterill et al. 1999). Saito *et al.*, (2003) aimed to identify which gene(s) at this locus was the most likely target for the chromosomal gain. Comparative genomic hybridisation experiments showed that *PPM1D* lies within the minimal common region gained among 25 neuroblastoma cell lines (Saito-Ohara, Imoto et al. 2003). This region included 15 genes, among which 7, including *PPM1D*, showed an increase in mRNA expression due to regional copy number gain. Primary neuroblastoma samples were then investigated by qRT-PCR for any association between mRNA expression of these 7 genes and overall survival. Survival analysis (Log-rank tests) showed that above median *PPM1D* mRNA expression was associated with poorer overall survival in this malignancy (Saito-Ohara, Imoto et al. 2003). Interestingly, the prognostic significance was not independent of *MYCN*-amplification, which is established as the strongest cytogenetic marker of poor overall survival in neuroblastoma (Brodeur, Seeger et al. 1984, Seeger, Brodeur et al. 1985, Seeger, Wada et al. 1988). Another publication from the same group using similar

techniques showed that the 17q21-24 region, which includes *PPM1D*, is gained in clear cell ovarian carcinoma (Hirasawa, Saito-Ohara et al. 2003). This copy number gain also resulted in increased *PPM1D* mRNA expression and correlated with poorer overall survival in this malignancy. Interestingly, the mRNA expression of Amyloid Beta Precursor Protein (Cytoplasmic Tail) Binding Protein 2 (*APPBP2*) which is the first gene upstream of *PPM1D* was also shown to increase and correlate with poorer overall survival. Therefore, caution must be observed when interpreting genes affected in cytogenetic abnormalities as prognostic markers as it is difficult to distinguish driver genes from passenger genes. Driver genes are genes the products of which play a key mechanistic role in cancer development and progression and that are therefore more likely to be positively selected. Passenger genes however do not play a significant mechanistic role in cancer development; but are frequently positively selected along with key driver genes due to their close physical proximity.

Rauta *et al.*, (2006) showed that *PPM1D*-amplification was associated with an ERBB2 positive subgroup of breast cancers which confers a poorer prognosis. Although it was shown that *PPM1D*-amplification results in an increased mRNA expression, WIP1 protein level was not assessed (Rauta, Alarmo et al. 2006). Analysis of WIP1 protein expression in gastric carcinoma showed that approximately 75% of these tumours had intense IHC staining for WIP1 and that this correlated with tumour size; however no survival analysis was carried out (Fuku, Semba et al. 2007). In a more recent independent study investigating WIP1 expression in 800 gastric cancer samples however, high WIP1 IHC staining was correlated with various adverse clinical outcomes including poor overall survival (Ma, Zhang et al. 2014). Lung adenocarcinoma was the first malignancy in which WIP1 protein expression was linked to poorer clinical and pathological end-points, such as shorter survival after surgery, increased proliferation marker (Ki-67) and increased invasion to the pulmonary vein (Satoh, Maniwa et al. 2011). Interestingly, increased WIP1 expression also correlated to increased γ H2AX staining in these samples, which is contrary to the reported role of WIP1 in dephosphorylating γ H2AX (Cha, Lowe et al. 2010). This suggests that WIP1 may have been induced in response to DNA double strand breaks following genotoxic stress in these tumours.

Another study on glioma samples compared to healthy brain tissue showed that increased *PPM1D* mRNA expression correlated with increased WIP1 protein expression, as measured by western blotting and immunohistochemistry, (Liang, Guo et

al. 2012). Survival analysis then showed that increased WIP1 IHC staining correlated with poorer overall survival. The authors showed through immunofluorescence that WIP1 expression is both nuclear and cytoplasmic before attempting IHC staining. Interestingly, *PPM1D* activating truncating mutations, such as those in HCT116 and U2OS cells, are also frequent in brainstem gliomas (Zhang, Chen et al. 2014). In two studies carried out by the same group, WIP1 IHC staining was also shown to be a marker of poor prognosis in colorectal cancer and hepatocellular carcinoma (Li, Zhang et al. 2013, Li, Zhang et al. 2013). Elevated WIP1 IHC staining compared to healthy prostate tissue has also been correlated to poorer overall survival after radical prostatectomy (Peng, He et al. 2014). Most recently, WIP1 protein expression analysis by IHC staining is reported to be of prognostic significance in kidney carcinoma, non-small cell lung cancer and nasopharyngeal carcinoma (Sun, Wang et al. 2015, Sun, Zhang et al. 2015, Yang, Gao et al. 2015).

7.1.2 Summary

These findings strongly support the notion that *PPM1D* mRNA and WIP1 protein expression are of prognostic relevance in various malignancies. In keeping with the findings by Saito-Ohara *et al.*, (2003), data-mining was also used in a more recent study to show that increased *PPM1D* mRNA expression is a marker of poor prognosis in neuroblastoma (Richter, Dayaram et al. 2015). However, the prognostic significance of WIP1 protein expression in neuroblastoma tumours has not yet been investigated.

7.2 Hypothesis

- Elevated WIP1 immunohistochemical staining is an independent marker of poor prognosis in neuroblastoma

7.3 Specific materials and methods

7.3.1 Online resources

Large deposits of biomedical data collected by independent research groups are deposited on the World Wide Web and are publically available for mining and use in research. These databases include gene expression data on cell lines and tumour samples. Analysis of *PPM1D* mRNA expression in cell lines was carried out by mining the Broad Institute Database (Massachusetts Institute of Technology and Harvard). The R2 genetic analysis and visualisation platform of the Academic Medical Centre in

Amsterdam was then used to mine data across various malignancies. The R2: MegaSampler online tool was used for assessing *PPM1D* mRNA expression across 99 different tumour datasets from various malignancies. The highest *PPM1D* expressing dataset with publically available clinical and pathological data namely ‘Tumour Neuroblastoma public - Versteeg - 88 - MAS5.0 - u133p2’ was used for survival analysis. Kaplan Meier survival analysis and Log-rank test were performed with the categorisation cut-off set at median or varied using the scanner facility. The scanner will test all possible cut-off points and report the most significantly different expression cut-off statistics including a Bonferroni-corrected p-value to correct for multiple testing. The plots were also analysed according to *MYCN* amplified and non-amplified sub-categories.

7.3.2 Use immunocytochemistry to determine WIP1 antibody specificity

PPM1D-amplified MCF-7 cells were seeded and grown onto sterile glass slides and allowed to reach 50-60% confluence. Cells were then exposed to DMSO, 5 μ M Nutlin-3, 2.5 μ M GSK2830371 or their combination 4Hrs before being fixed and prepared for immunocytochemistry as explained in (2.12). Anti-WIP1 (F-10) antibody was diluted 1:200 in blocking reagent. Only blocking reagent was added to the no primary antibody control followed by the incubation with the secondary antibody. Exposure to 2.5 μ M GSK2830371 resulted in a marked reduction of WIP1 fluorescent signal (Alexa fluor 488 secondary (AF-488) secondary antibody) as expected from the ability of this drug to markedly degrade WIP1 protein (Figure 7-1). Also WIP1 signal was increased in response to Nutlin-3 and in its combination with GSK2830371 the reduction in WIP1 signal was reversed by Nutlin-3. Finally there was no WIP1 staining in the absence of the WIP1 primary antibody (Figure 7-2). The fluorescent signal was therefore attributable solely to WIP1 staining.

7.3.2.1 Confocal microscopy z-stack and WIP1 sub-cellular localisation

Confocal microscopy as described in materials and methods was used to assess WIP1 staining and localisation. A z-stack image capture was carried out with image capture from 20-50 slices from which a video of a series of images traversing through confocal planes of the cell were generated and a 3D image constructed (Please see electronic copies of PowerPoint slides accompanying this thesis for these images). It was observed that the fluorescence signal from the secondary antibody (AF-488) that detected F-10 was both nuclear and cytoplasmic regardless of *PPM1D* genetic status.

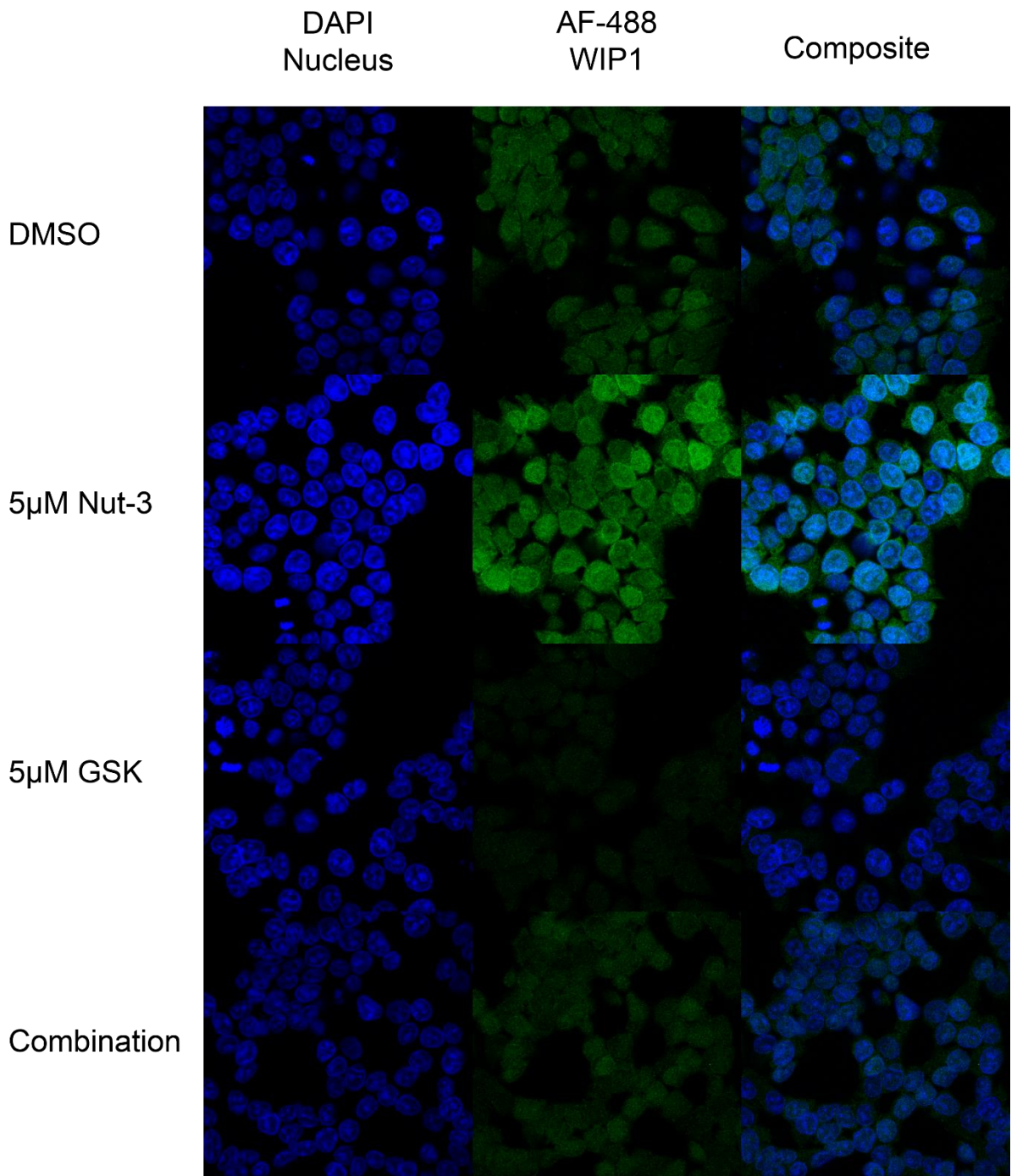


Figure 7-1 Confocal microscopy images of MCF-7 cells treated with DMSO, 5 μ M Nutlin-3, 2.5 μ M GSK2830371 or their combination for 4Hrs. GSK2830371 results in a dramatic reduction in both cytoplasmic and nuclear WIP1 signal intensity (AF-488 channel) which is restored modestly when it is combined with Nutlin-3. Nutlin-3 increases WIP1 signal intensity, most likely due to p53 dependent induction of WIP1.

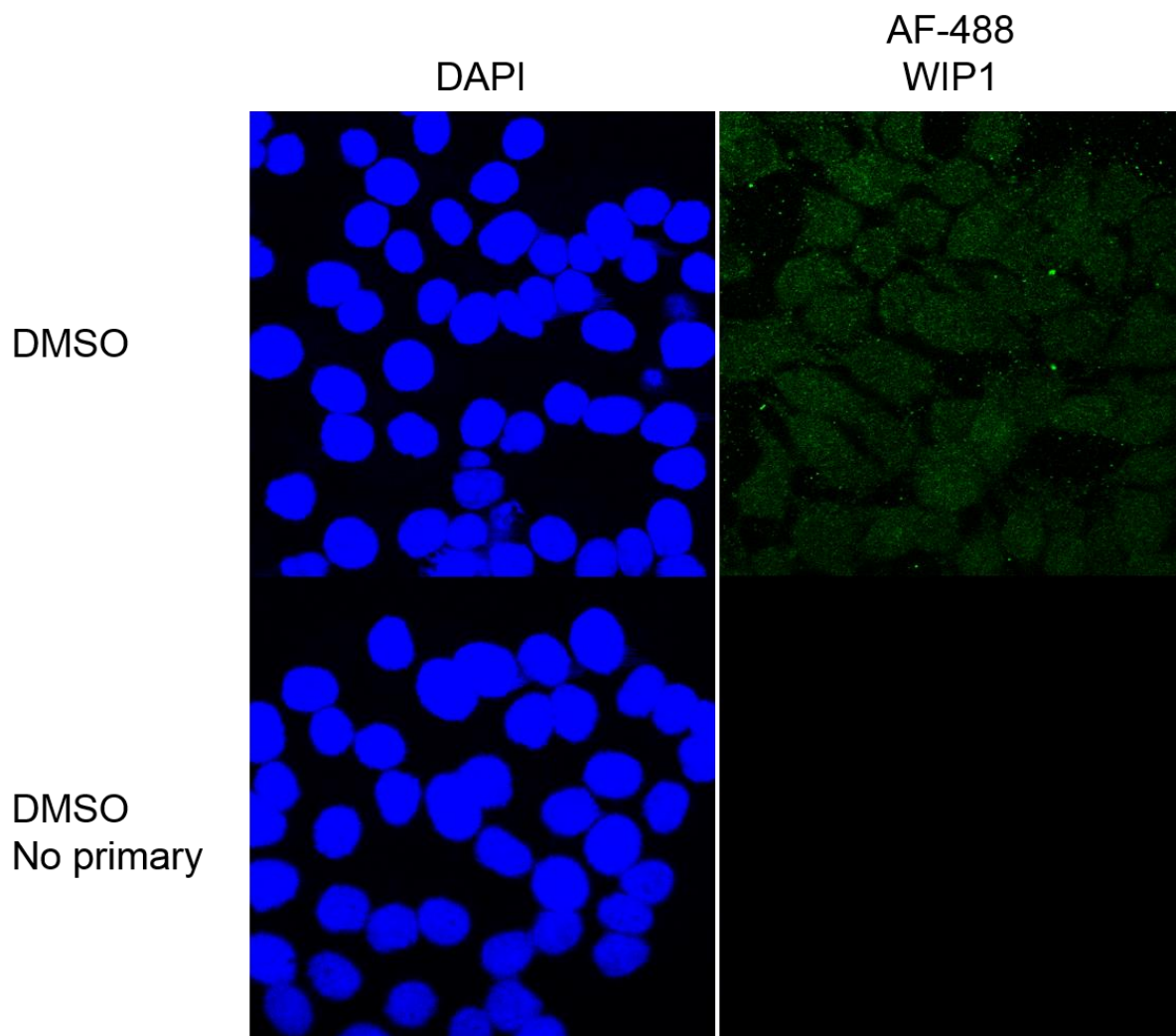


Figure 7-2 Gain on both DAPI and AF488 channels was increased to assess the no primary control. There was no WIP1 staining detected at high detector gain in the absence the WIP1 primary antibody showing that the secondary antibody does not bind to other non-specific antigens

7.3.3 Immunohistochemistry

Surgical resections or biopsies of tumour tissue can be examined by immunohistochemistry to explore the expression and subcellular localisation of antigens of interest with specific antibodies (Schacht and Kern 2015).

7.3.3.1 Sample preparation

The resected tissue region is fixed in 10% neutral buffered formalin, dehydrated through a series of ascending ethanol concentration (70%-100%), cleared in several changes of xylene and then infiltrated with paraffin wax. This tissue is embedded in paraffin wax blocks to prevent putrefaction. These are termed formalin fixed paraffin embedded (FFPE) blocks (Taylor and Burns 1974) and this procedure was carried out by Dr Jennifer Jackson. The blocks were then used for slide preparation.

7.3.3.2 Slide preparation from paraffin embedded formalin fixed blocks

Blocks were placed at -20°C for 20min and kept chilled on ice, covered with a thin layer of 70% ethanol in order to make sectioning easier. A microtome tissue sectioning device was then used to cut the paraffin block into 1µm slices which were then spread on the surface of 45°C water (just below wax paraffin melting temperature). A glass slide was then used to fish-out the tissue section and the wax paraffin was allowed to fully solidify onto the slide at room temperature.

7.3.3.3 Antigen retrieval

Although formalin fixing preserves the morphological features of the proteins it leads to the formation of methylene bridges between proteins which reduce antigenicity (Schacht and Kern 2015). Antigenicity is the ability of an antigen to be detected by an antibody raised against it through acquired immunity. Enzymes or heat can be used to unmask antigens in a process called antigen retrieval. Heat antigen retrieval was used. Therefore, Slides were dewaxed in xylene, hydrated through graded ethanol (100%-70% (v/v)) and rinsed in tap water before antigen retrieval by submerging them into Tris-EDTA buffer (Table 7-1) and heating them in a decloaker/pressure cooker. The temperature is raised slowly to 130°C and then kept there for 30sec after which it is dropped rapidly. The slides are then exposed to 3% (v/v) hydrogen peroxide for 10 min and rinsed in tap water. This leads to the unmasking of antigens before staining with the primary antibody.

7.3.3.4 Antibody application and visualisation

Anti-WIP1 F-10 was diluted in TBS/T as stated in figure legends. A hydrophobic

marker was used to draw around the tissue to prevent spillage of the diluted antibody solution. Slides were incubated with the antibody at room temperature for 60min then rinsed in TBST before using the X-cell-Plus horseradish peroxidase (HRP) detection kit (Menapath, #MP-XCPDAB-U100) to visualise primary antibody-antigen binding. A universal probe that detects mouse primary antibody fragment crystallisable (Fc) region is used to bind to the primary antibody (30min incubation) and excess probe is washed in TBST before the HRP-polymer is incubated with the sample (30min). HRP-polymer binds to the universal probe and by extension amplifies the signal from the primary antibody. Unbound polymer is washed off and 3, 3 diaminobenzidine (DAB) chromogen is applied to the samples for 10 min and rinsed in tap water. DAB precipitates a brown formazan stain in the presence of HRP. Slides were then washed with tap water (5min) and then counter stained in Gills No. 2 haematoxylin (Sigma, #: GHS216) for 5secs before being rinsed once in tap water and once in Scott's tap water (Table 7-1) for 30secs. Samples were then dehydrated through graded ethanol and cleared in xylene as before. Coverslips were then mounted using DPX mounting media (Thermo scientific) and left to dry overnight.

Buffer	Constituents and concentration
Tris-EDTA	Tris base (10mM) EDTA (1.3mM) Tween-20 0.05% (v/v) pH 9.0
Scotts tap-water	41.7mM Sodium hydrogen carbonate 0.17mM Magnesium sulphate A few crystals of Thymol

Table 7-1 Buffers ad their constituents

7.3.4 Neuroblastoma tissue microarrays

Tissue microarrays (TMA's) allow the simultaneous staining and analysis of many representative tumour core biopsies on one slide. Neuroblastoma TMA's were provided by Great Ormond's Street Hospital (In collaboration with Dr Ximena Montano). We were blinded to clinical and pathological data before assigning scores of WIP1 expression to each core. These samples included 71 anonymised core biopsies of neuroblastoma tumours with survival data, of which 67 had information on metastasis and *MYCN* cytogenetic status, 61 with information on stage (I-IV no IVs), 50 on chromosome 1p status, 39 on 17q status and 33 on 11q status.

7.3.5 WIP1 immunohistochemical staining and antibody optimisation

Because we only acquired one replicate of each neuroblastoma TMA, we could not justify the direct use of these samples in antibody optimisation. Therefore we had to optimise the conditions for IHC staining of WIP1 before attempting to stain these samples. For optimisation of WIP1 antibody we assessed the staining of the F-10 antibody in a two different samples before staining the neuroblastoma TMA's. 1) FFPE mouse NGP and N20R1 xenografts (kindly provided by Dr Lindi Chen). 2) TMA's of ovarian origin which were intended for use in an independent project (kindly provided by Mrs Maryam Zanjirband). We found optimal antibody dilution to be 1:500 as it resulted in differential staining between tumour and stroma in ovarian tissue (Figure 7-3 & Figure 7-4). The buffer chosen for antigen retrieval was Tris-EDTA.

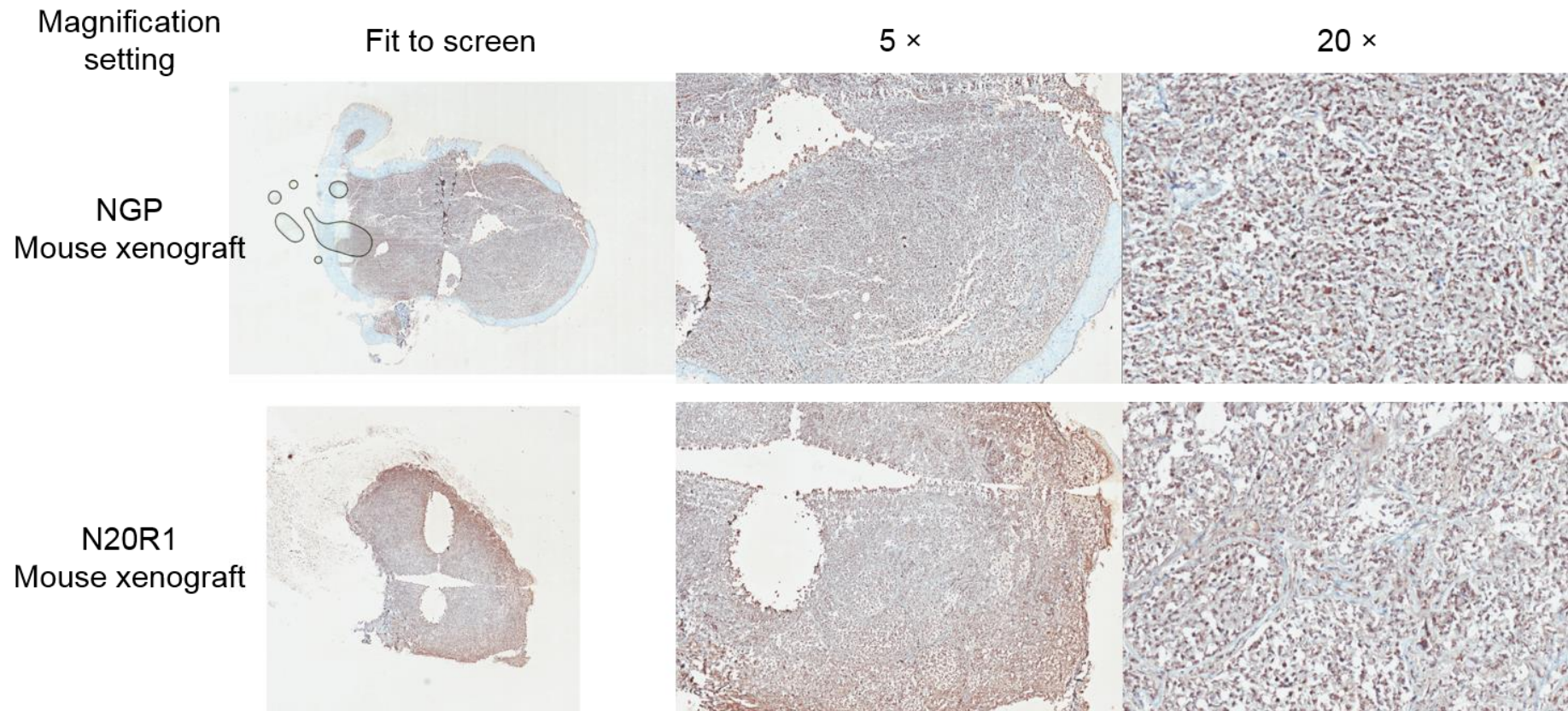


Figure 7-3 WIP1 IHC staining of xenografts arisen from NGP and N20R1 cell line pair. F-10 antibody dilution used here was 1:50 as recommended in the datasheet by the vendor.

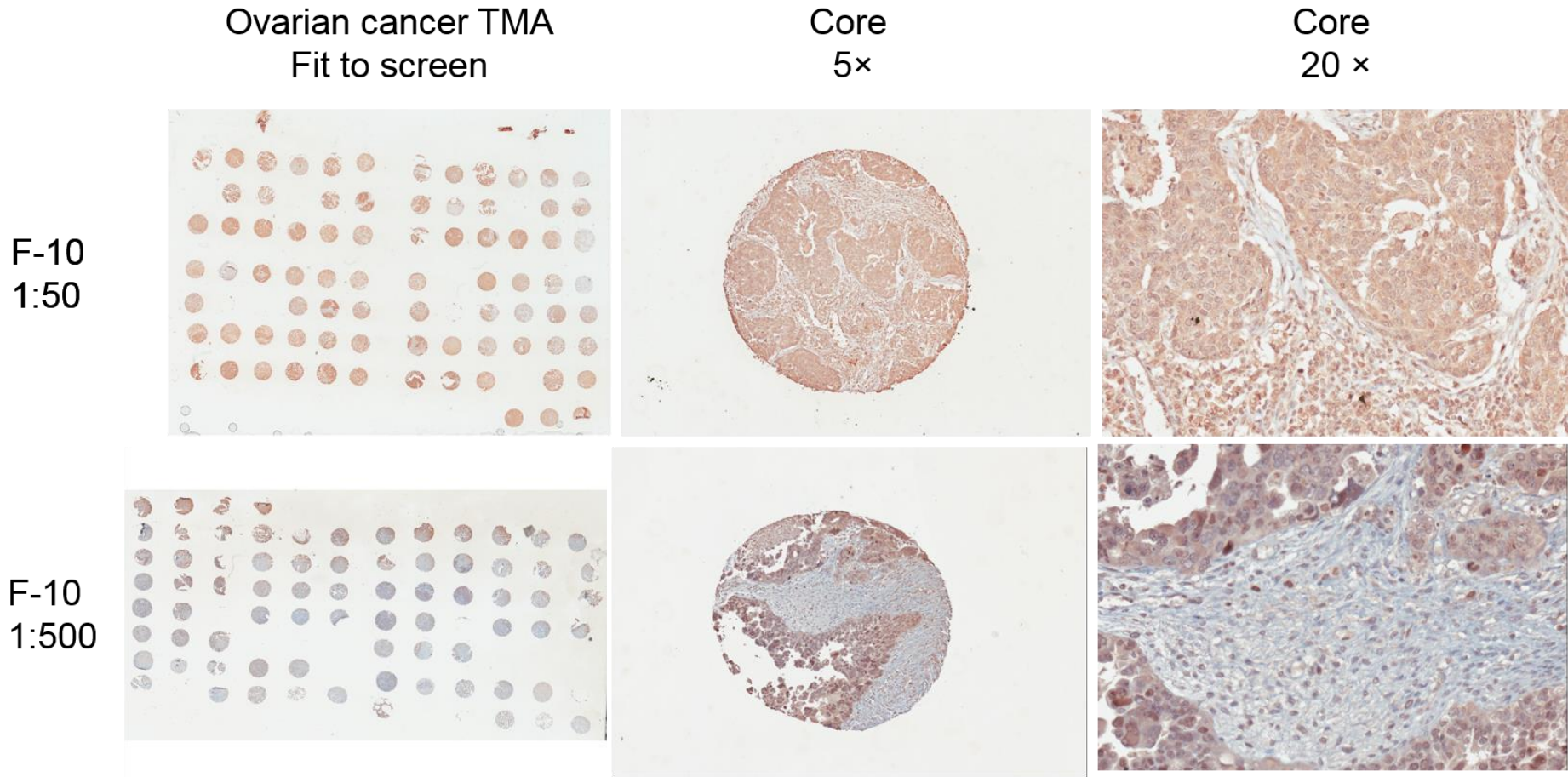


Figure 7-4 WIP1 IHC staining in ovarian TMA's at two different dilutions. 1:500 dilution is more specific at staining tumour tissue and nuclei compared to connective tissue.

7.3.5.1 Slide scanning and H-score calculation

Imaging of slides and scoring were carried out using an automated digital scanner Aperio ScanScope® CS (Aperio Technologies, Bristol, UK) and Spectrum™ image management software. Given that the core origins were not known and they were morphologically heterogeneous, an algorithm was used for calculating WIP1 nuclear stain intensity and proportion of staining in the field selected. Cytoplasmic staining was weak and therefore not used in scoring. The algorithm calculated the % of cells that showed no staining, weak staining, intermediate and strong staining. A modified H-score was used, which was the product of intensity (No staining = 0, weak = 1, intermediate = 2 and strong = 3) and percentage positive (1-14% = 1, 15-24% = 2, 25-39% = 3, 40-59% = 4, 60-79% = 5 and 80-100% = 6). There was a wide range of H-scores corresponding to WIP1 protein expression in different neuroblastoma cores on each array (Figure 7-5).

7.3.6 Statistical analysis

7.3.6.1 Receiver operating characteristic (ROC) curve

When using a continuous variable in a diagnostic/prognostic test the distribution of true positive (TP) and true negative (TN) cases for that measurement overlap (Figure 7-6A). The cut-off chosen for the continuous variable between normal and abnormal will determine the proportion of false positive (FP) and false negative (FN) diagnoses/prognoses. Receiver operating characteristic (ROC) curve analysis is used to determine optimal cut-off points for continuous variables intended for use in diagnostic tests. When a given cut-off is chosen the ratio of abnormal detected by the test to the total abnormal cases present is termed sensitivity. The ratio of normal cases detected by the test to total normal cases is termed specificity. A ROC curve can be generated by plotting the % Sensitivity against 1 - % Specificity at different cut-off points. An ideal diagnostic/prognostic cut-off for a continuous variable would have high specificity at low sensitivity and a large area under the curve as shown in Figure 7-6B. Although this could differ based on which is more important for that given endpoint and whether the cost: benefit ratio of choosing a cut-off with lower specificity or sensitivity is acceptable.

This approach was applied to WIP1 expression. WIP1 H-scores from our cohort were split into two groups of overall survival (Group 1: alive and Group 2: dead). ROC curve

analysis was then carried out in GraphPad Prism 6 software to assess which WIP1 H-score cut-off would result the most specificity while retaining optimal sensitivity.

7.3.6.2 The log-rank test and Kaplan Meier survival curves

The Log-rank test is a nonparametric hypothesis test used to compare the survival distributions of two groups (Bland and Altman 2004). The assumptions of this test are that 1) Missing data (censoring) are unrelated to prognosis, 2) Subjects have the same probability of survival regardless of their order and time of diagnosis 3) The time to event is accurate. Data were divided into two groups based on discrete or continuous variable of interest being investigated and their overall survival in months from diagnosis to death (endpoint). GraphPad prism 6 was then used to carry out a log-rank test and generate a Kaplan Meier plot to determine whether a given group had a poorer outcome. Hazard ratios which are a measure of the rate of death in each group based on the slopes of the survival curves were also derived.

7.3.6.3 Contingency tables and Fisher's exact test

To assess whether there was any correlation between other clinicopathological events and WIP1 H-score (High or low) we used contingency tables and Fisher's exact test.

7.3.6.4 Normality test

Normality tests were carried out using GraphPad Prism 6 software to assess how far the distribution of a given variable deviates from Gaussian distribution.

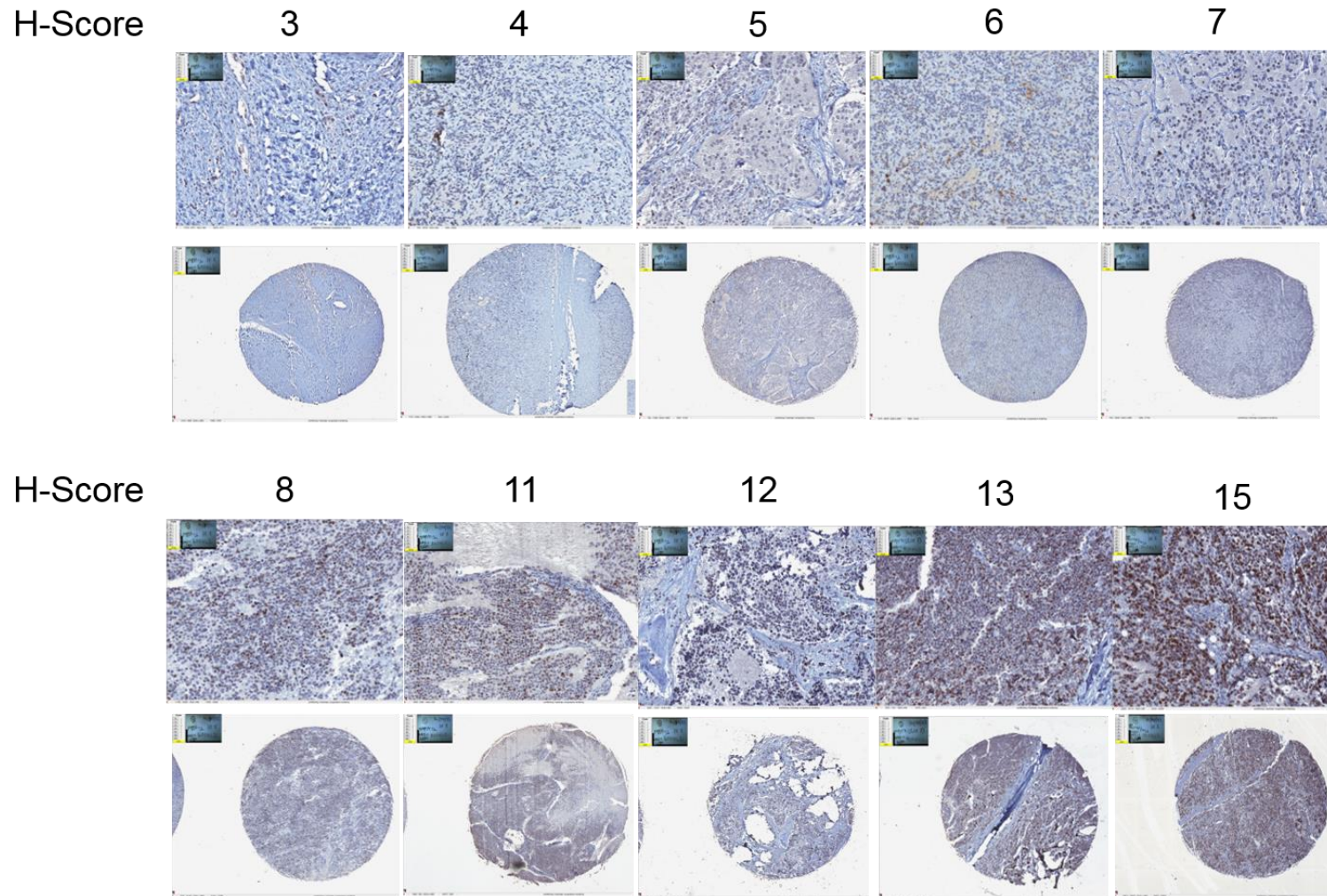


Figure 7-5 Range of WIP1 IHC staining and their corresponding H-scores.

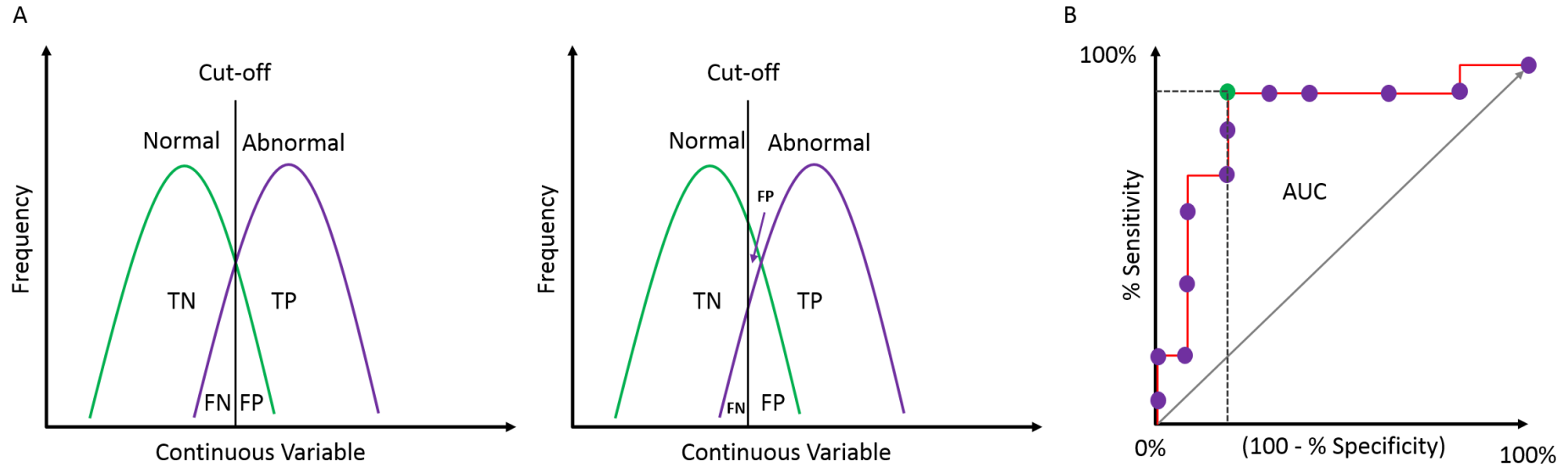


Figure 7-6 A) Overlapping distributions of hypothetical test results for a given continuous variable. B) Hypothetical representation of the ROC curve for an ideal test and the optimal cut off point (green point). TN: True Negative; TP: True Positive; FN: False Negative; FP: False Positive; AUC: Area Under the Curve.

7.4 Results

7.4.1 Data-mining shows that neuroblastoma cell lines have the highest average *PPM1D* mRNA expression

Publicly available Cancer Cell Line Encyclopaedia (CCLE) from the Broad Institute (MIT and Harvard) online cell line database was mined in order to compare *PPM1D* mRNA expression between cell lines of different tumour origin. The data showed that *PPM1D* copy number positively correlates with mRNA expression although the relationship is not close (Figure 7-7). Importantly cell lines of neuroblastoma and medulloblastoma origins had the highest average mRNA expression compared with other malignancies (Figure 7-8). The panel of cell lines includes *PPM1D*-amplified cell lines reported by Natrajan et al., (2009) including MCF-7 cells used for immunocytochemistry earlier (Figure 7-1). These findings are consistent with the reports in the literature of *PPM1D* gain and its higher expression in these malignancies (Saito-Ohara, Imoto et al. 2003, Castellino, De Bortoli et al. 2008, Richter, Dayaram et al. 2015). This is also consistent with the sensitivity of neuroblastoma cell lines to WIP1 inhibition by GSK2830371 (Richter, Dayaram et al. 2015).

7.4.2 Increased *PPM1D* mRNA expression in Neuroblastoma is a marker of poor prognosis

We assessed *PPM1D* mRNA expression across 99 different datasets derived from various malignancies on the R2: MegaSampler from the AMC. The only malignancy with relatively high *PPM1D* mRNA expression, for which clinicopathological data was publically available, was the Versteeg neuroblastoma database. We explored *PPM1D* mRNA expression in this dataset using the R2: Genomics Analysis and Visualisation Platform. The data show an 8-fold range of *PPM1D* mRNA expression in the 88 neuroblastoma tumour samples (Figure 7-9). Given that *MYCN* amplification is a well-established cytogenetic marker of poor prognosis in neuroblastoma used clinically for risk group treatment stratification (Brodeur, Seeger et al. 1984, Seeger, Brodeur et al. 1985, Seeger, Wada et al. 1988), we assessed the correlation between *MYCN* and *PPM1D* mRNA expression. The correlation between *MYCN* and *PPM1D* expression was weak ($R = 0.343$, $p = 0.001$) in this dataset (Figure 7-10). Using Kaplan Meier Scanner Pro we found that above median expression of *PPM1D* mRNA is significantly associated with poor prognosis ($p=0.02$) (Figure 7-11). A similar plot was independently published by Richter *et al.*, (2015) using the same online platform.

Although the authors had suggested that *PPM1D* mRNA correlated with survival ($p = 0.005$ before correction), the adjusted p -value reported was 0.364, which is not significant. Importantly, *MYCN*-amplification was not considered in their analysis. *PPM1D* mRNA expression was not of prognostic significance if *MYCN*-amplified (MNA) and non-amplified (MNnA) subgroups of tumours were analysed separately with the cut-off set at median expression ($p=0.091$ and $p=0.712$ respectively) (Figure 7-12A and B). If the cut-off was set to scan, as done by Richter *et al.*, 2015, then the *PPM1D* expression prognostic significance would also not be independent of *MYCN* status (MNnA, $p=0.06$ and MNA $p=0.712$, plots not shown). These findings suggest that when the threshold of *PPM1D* mRNA expression is set at median *PPM1D* is of prognostic relevance however, this is not independent of *MYCN*-amplification status. This is consistent with the findings of Saito-Ohara *et al.*, (2003) who had investigated *PPM1D* mRNA expression in an independent cohort of neuroblastoma tumour samples.

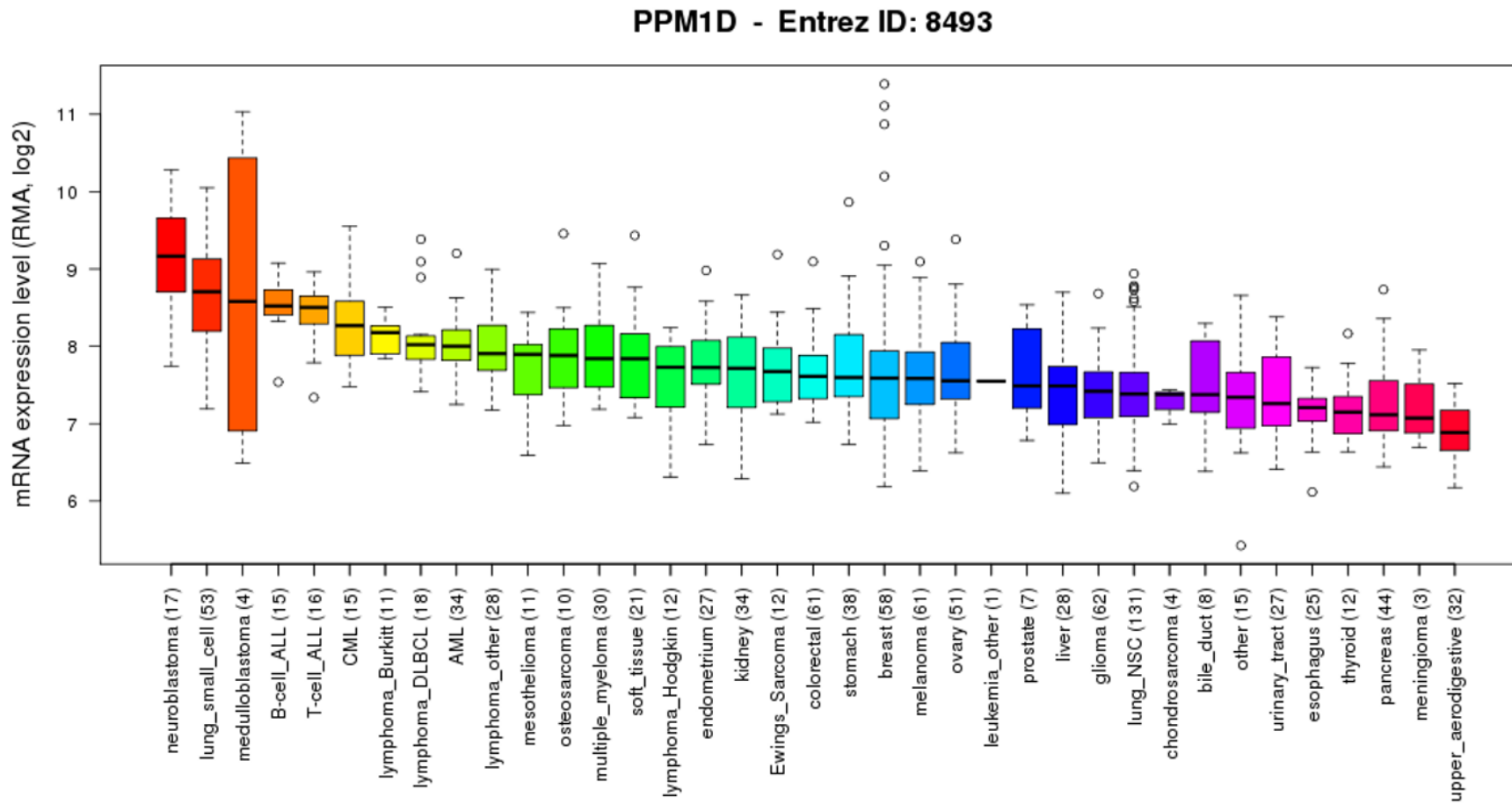


Figure 7-8 Box and whiskers plot mine from the Broad Institute database for *PPM1D* mRNA expression among cancer cell lines of different tissue origin.

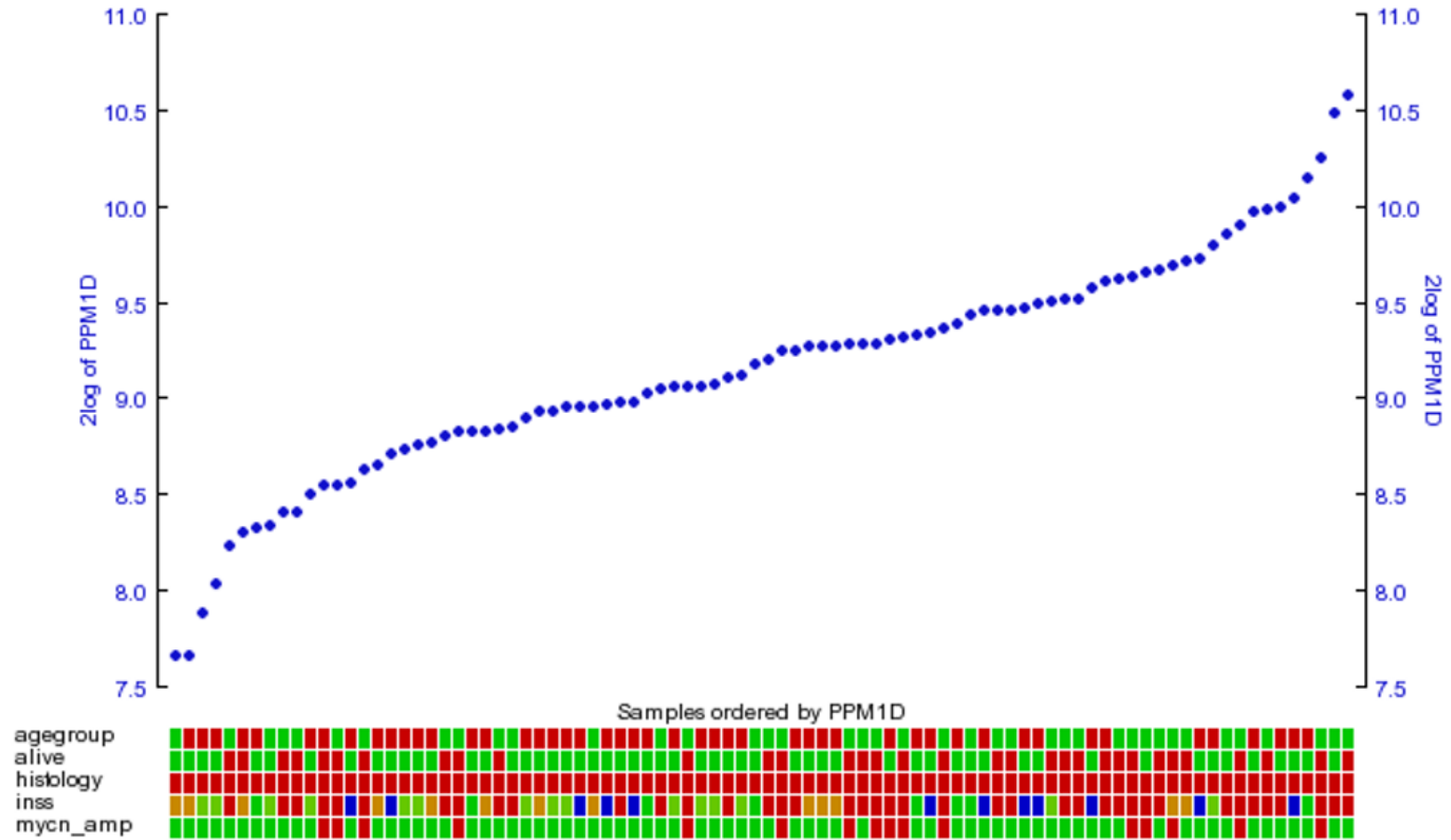


Figure 7-9 Range of *PPM1D* mRNA expression in neuroblastoma tumours. Age at diagnosis: Red \leq 18 months old, Green \geq 18 months old; Alive: Green = alive Red = dead; Histology: Red = Neuroblastoma; INSS stage: Green = stages 1 or 2, Amber = stage 3, Red = stage 4, Blue = stage 4s.

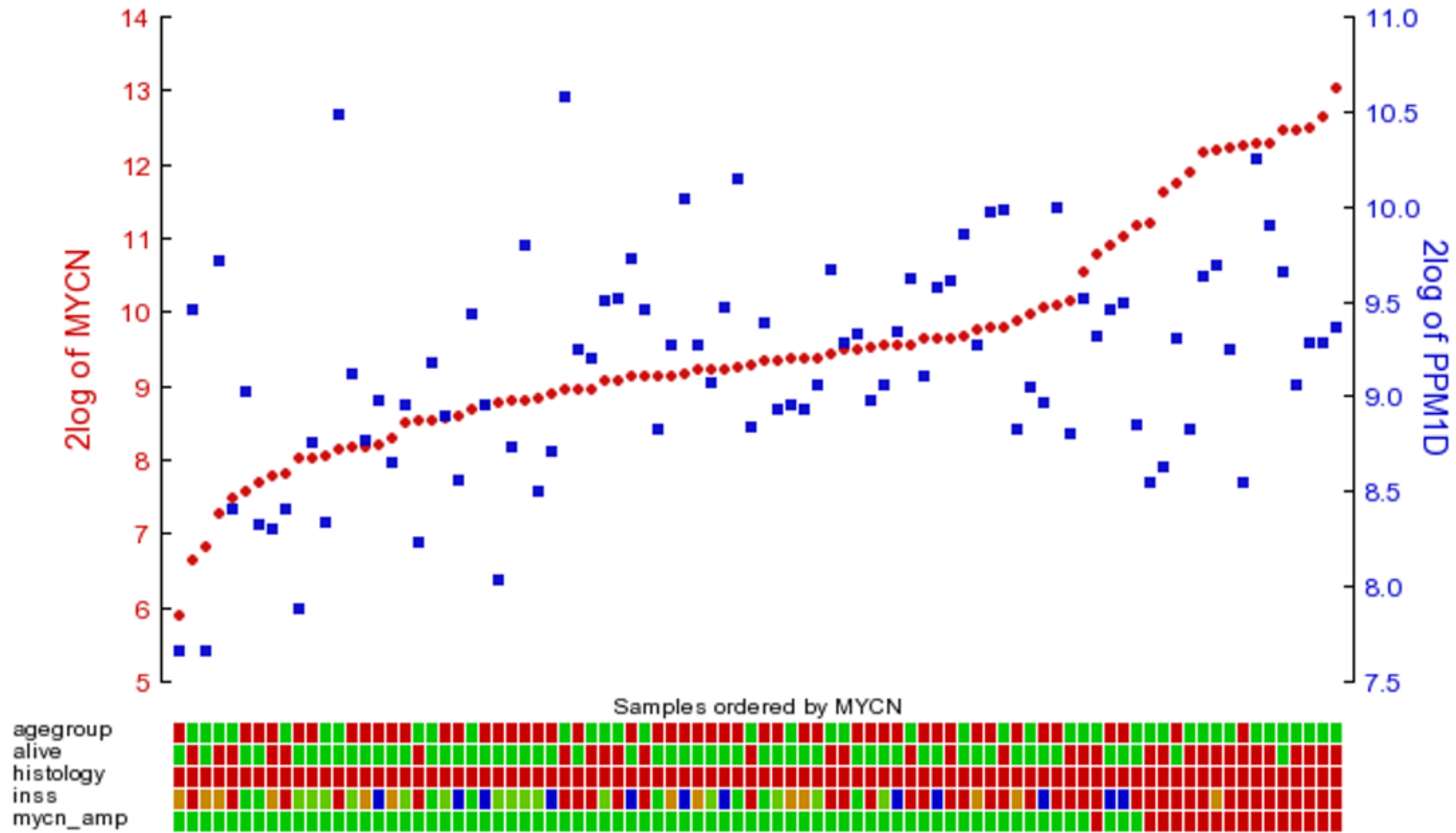


Figure 7-10 Correlation between *MYCN* and *PPM1D* expression. Age at diagnosis: Red ≤ 18 months old, Green ≥ 18 months old; Alive: Green = alive Red = dead; Histology: Red = Neuroblastoma; INSS stage: Green = stages 1 or 2, Amber = stage 3, Red = stage 4, Blue = stage 4s.

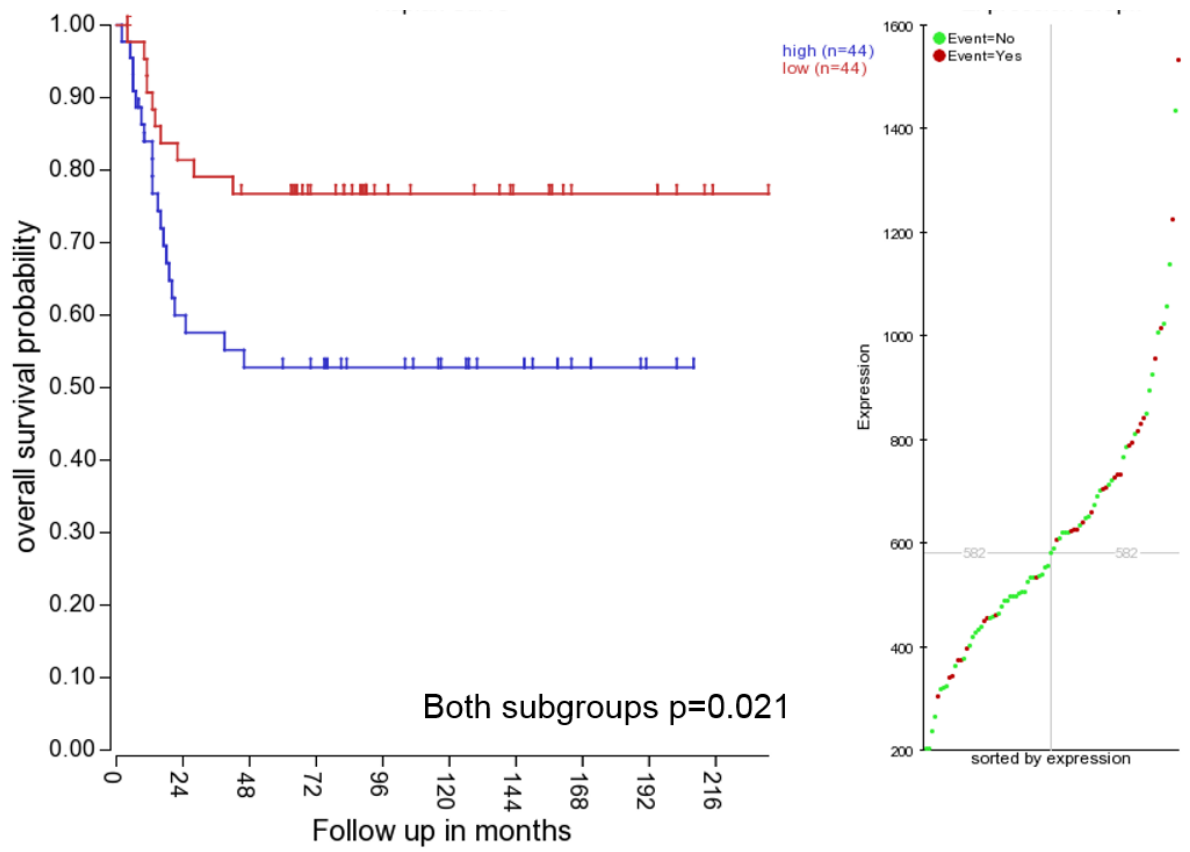


Figure 7-11 Above median *PPMID* mRNA expression is associated with poorer overall survival in the Versteeg neuroblastoma dataset.

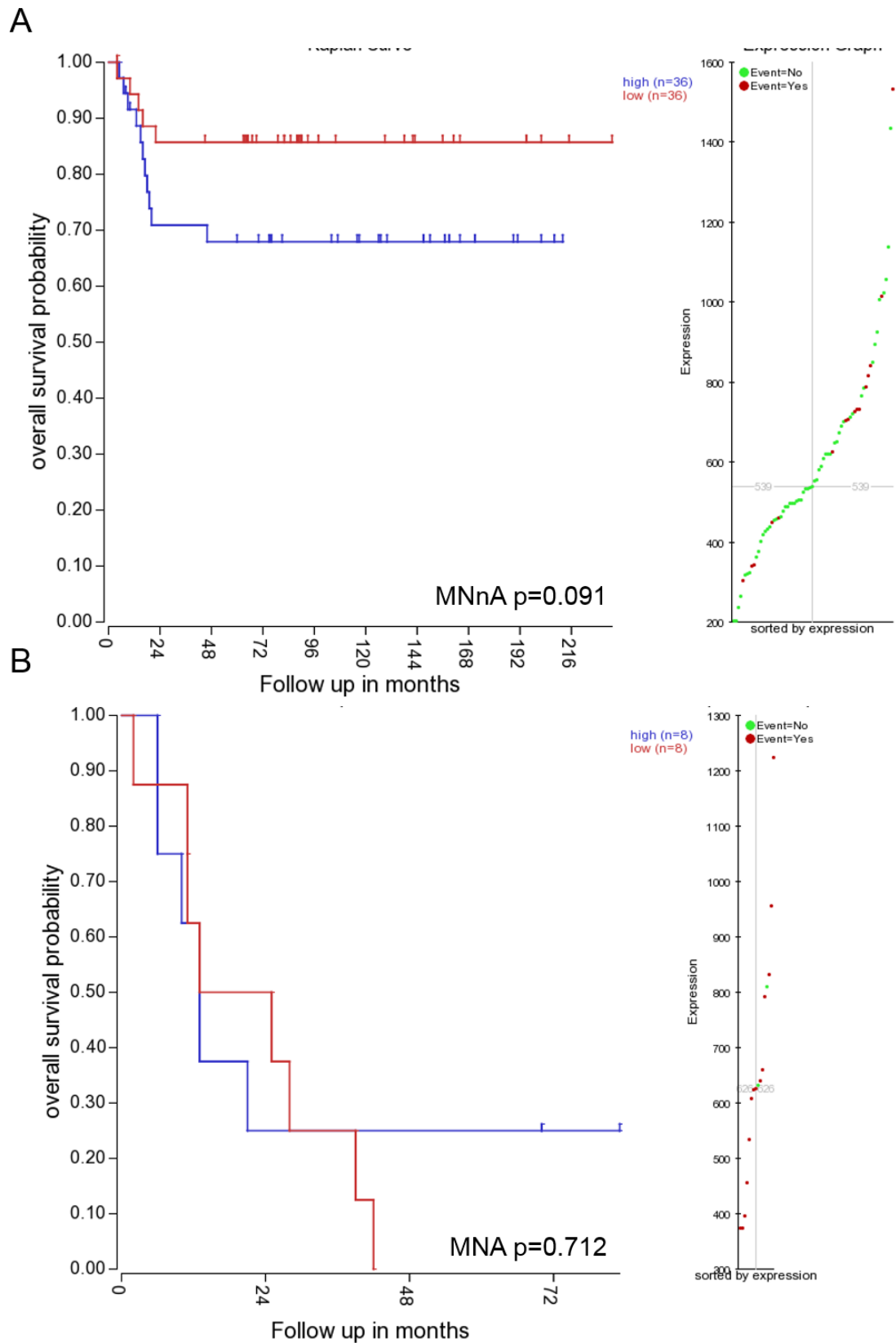


Figure 7-12 PPMID mRNA prognostic significance is not independent of MYCN amplification.

7.4.3 The relationship between WIP1 IHC staining and patient survival in a panel of neuroblastoma tumour samples

To assess whether the WIP1 protein expression is also of prognostic significance in neuroblastoma we assessed WIP1 IHC staining in a panel neuroblastoma tumour samples in the form of a series of TMA's. This was a cohort of 71 neuroblastoma core biopsies with provided survival data and different combinations of clinicopathological information (7.3.4). We first assessed the prognostic significance of established clinicopathological markers in neuroblastoma to examine the validity of the cohort and associated clinicopathological variables. In this cohort metastasis ($p = 0.0001$, Hazard ratio (HR) = 14.88) and advanced stage disease ($p = 0.003$), as determined by the International Neuroblastoma Staging System (INSS), both significantly correlated with poor overall survival (Figure 7-13A and B). Similarly, established cytogenetic prognostic biomarkers such as *MYCN* amplification ($p = 0.0001$, HR = 6) (Brodeur, Seeger et al. 1984, Seeger, Brodeur et al. 1985) or 11q deletion ($p = 0.005$, HR=5.3) correlated with poor overall survival in this cohort and dataset (Figure 7-14A and B). Other reportedly significant poor prognostic cytogenetic markers such as 1p deletion ($p = 0.3$) (Caron, vanSluis et al. 1996) and 17q gain ($p = 0.5$) (Bown, Cotterill et al. 1999) were not of prognostic significance in this cohort (Figure 7-15A and B). Given that *PPM1D* is reportedly the most commonly gained gene when 17q is gained in neuroblastoma cell lines (Saito-Ohara, Imoto et al. 2003) it was surprising to find that there is no difference between WIP1 H-score in tumours with and without 17q gain ($p = 0.239$) (Figure 7-15C). Although normality tests showed that the H-scores associated with 17q gain are not normally distributed which suggests that WIP1 protein expression/regulation is affected by 17q gain.

A ROC curve analysis showed that the median would be a reasonable cut-off point with optimal sensitivity and specificity (Figure 7-17A). The shape of the ROC curve suggested that WIP1 H-score is not a reliable prognostic marker. A log-rank test carried out on survival and WIP1 H-score in this cohort showed that high and low WIP1 protein expression defined by a median value cut-off was not significantly related to survival in our cohort of neuroblastoma patients (0.26) (Figure 7-17B). Further analysis of the established prognostic markers through contingency tables and Fisher's exact test showed that there was no difference in WIP1 H-score between clinicopathological sub-groups (Table 7-2).

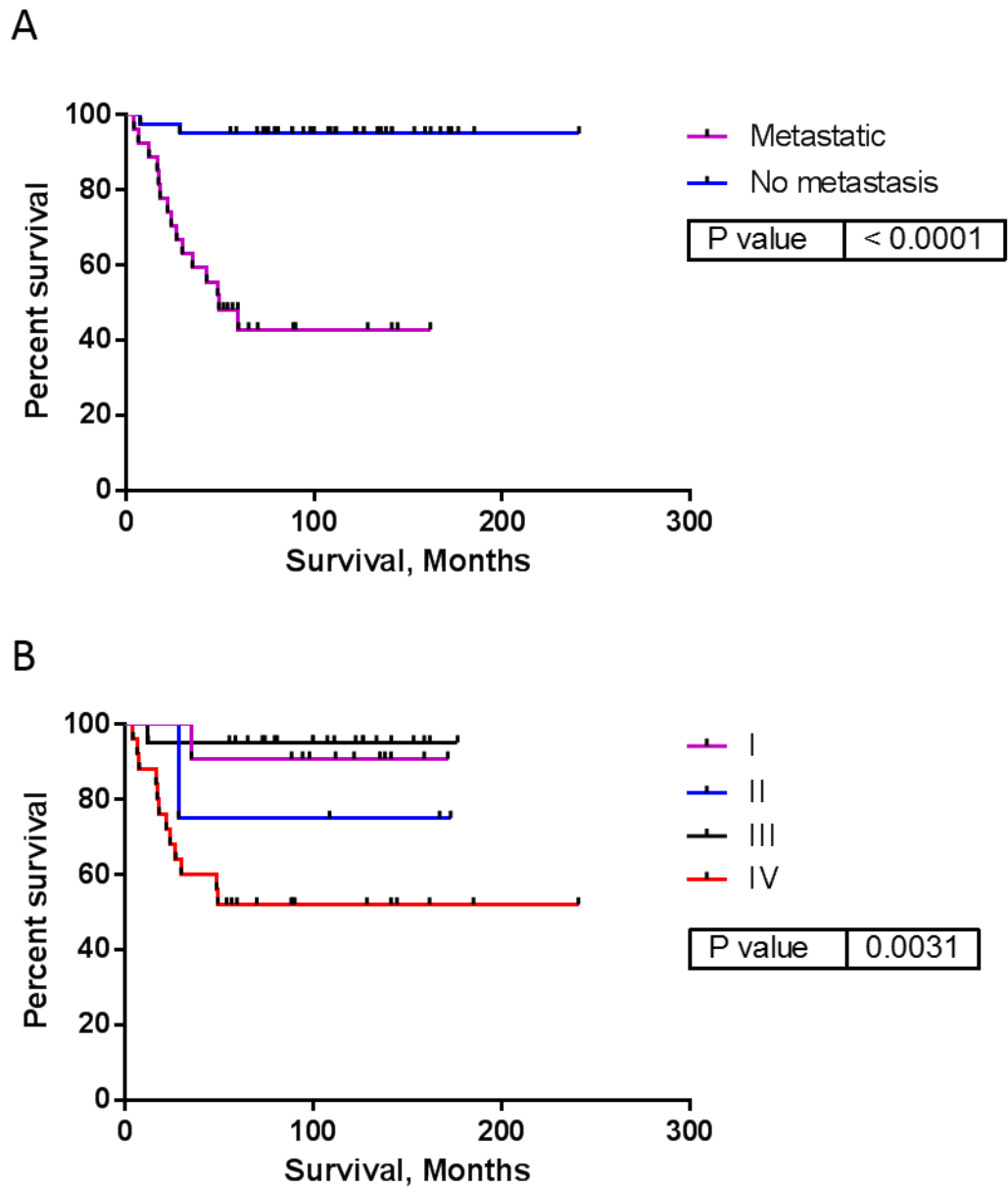


Figure 7-13 Metastasis and advanced INSS stage disease are significantly associated with of poor survival in our cohort of neuroblastoma patients.

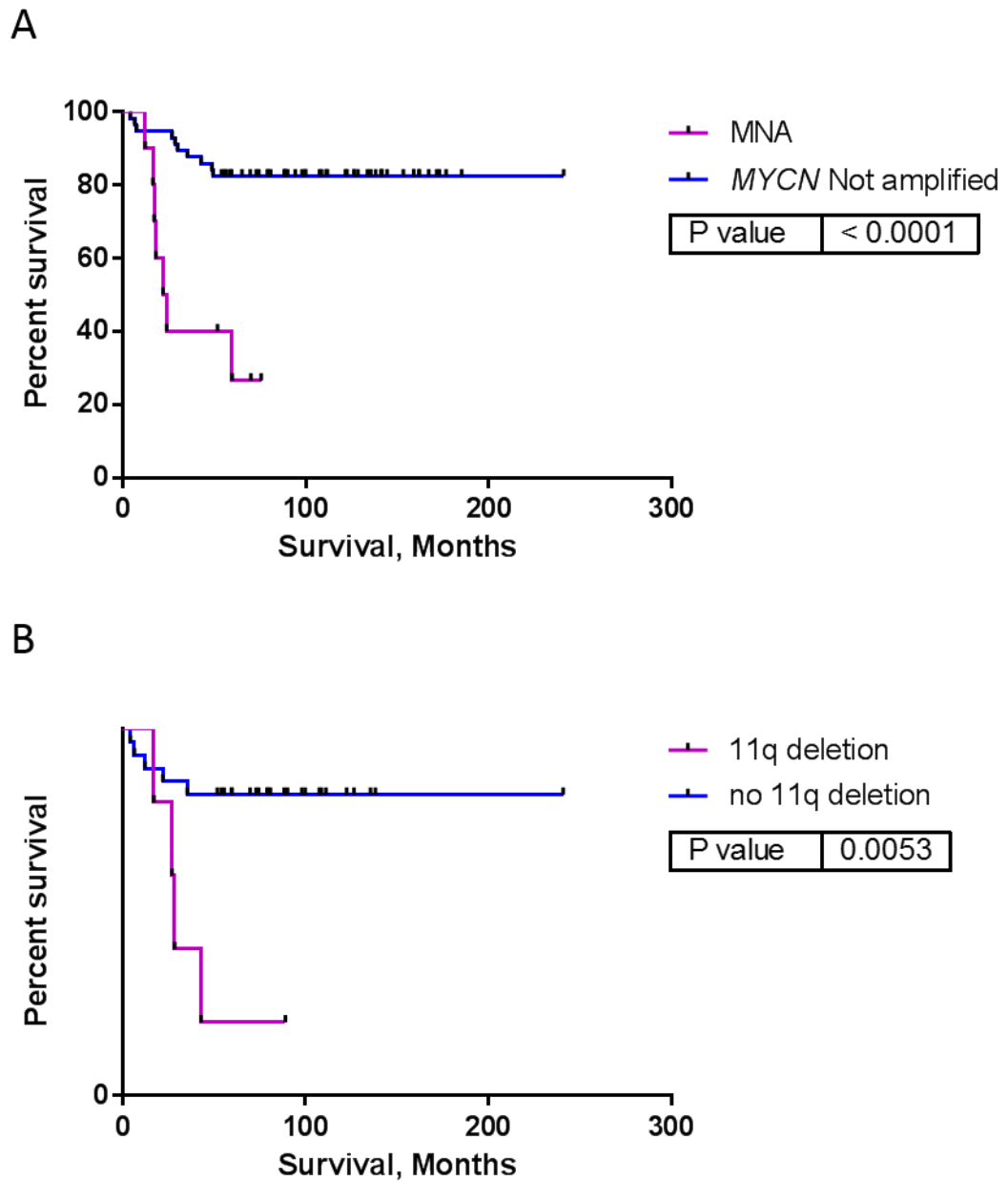


Figure 7-14 Tumour *MYCN*-amplification and 11q deletion are significantly associated with poor survival in our neuroblastoma patient cohort. Log-rank test and patient survival according to tumour *MYCN*-amplification (A) and 11q deletion status (B).

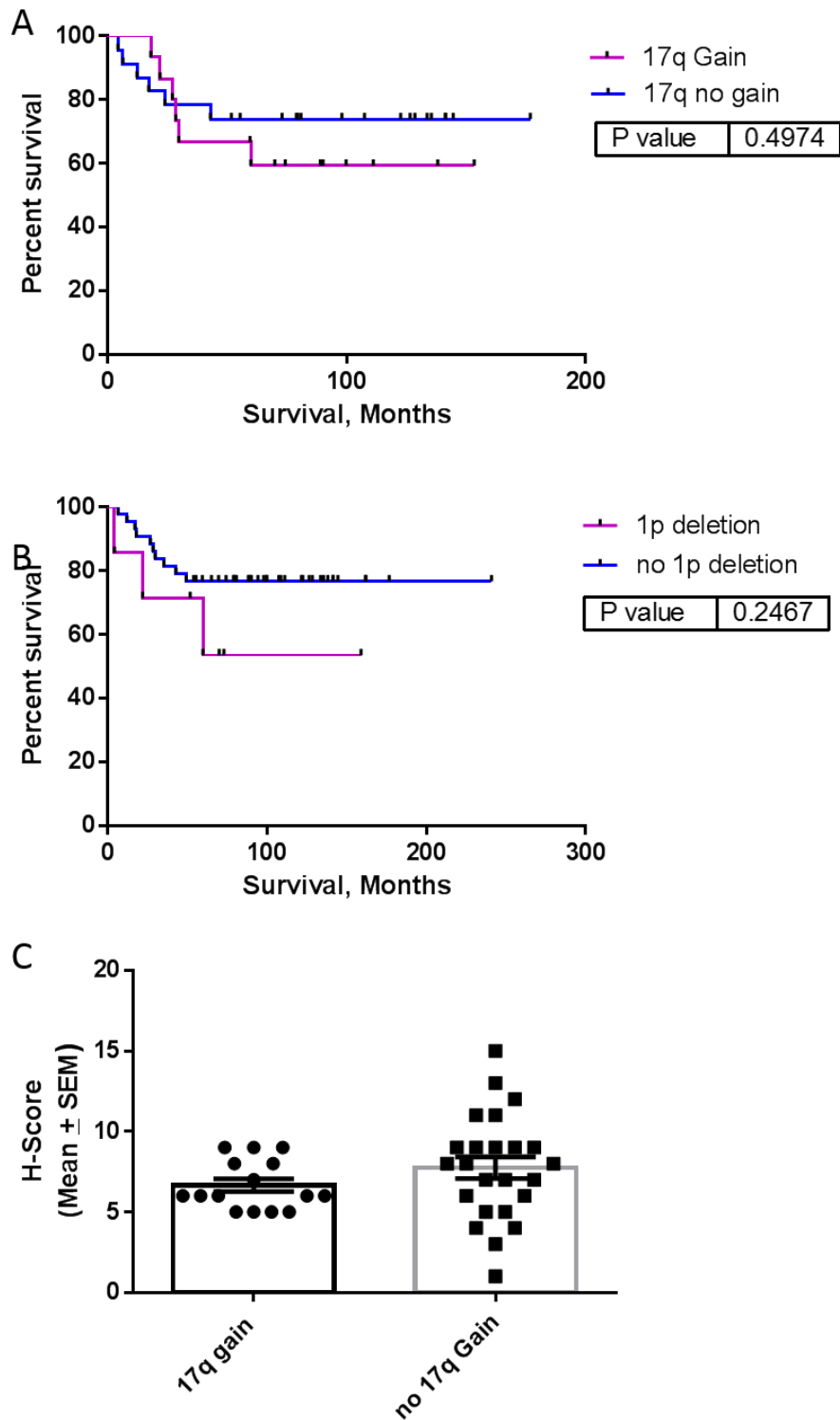


Figure 7-15 Tumour 17q gain and 1p deletion were not significantly predictive of overall survival in our neuroblastoma patient cohort. Log-rank test and patient survival according to tumour 17q gain (A) and 1p deletion status (B). C) There is no statistical difference between mean WIP1 H-score in tumours with and without 17q gain (Unpaired t-test $p = 0.239$).

	17q gain	no 17q Gain
D'Agostino & Pearson omnibus normality test		
K2	3.306	0.2313
P value	0.1915	0.8908
Passed normality test (alpha=0.05)?	Yes	Yes

	17q gain	no 17q Gain
Shapiro-Wilk normality test		
W	0.8434	0.9859
P value	0.0140	0.9756
Passed normality test (alpha=0.05)?	No	Yes

	17q gain	no 17q Gain
KS normality test		
KS distance	0.2671	0.1430
P value	0.0051	> 0.1000
Passed normality test (alpha=0.05)?	No	Yes

Figure 7-16 The three normality tests used to assess whether H-scores belonging to each subgroup of follow a Gaussian distribution. H-scores associated with the 17q gain subgroup are not normally distributed.

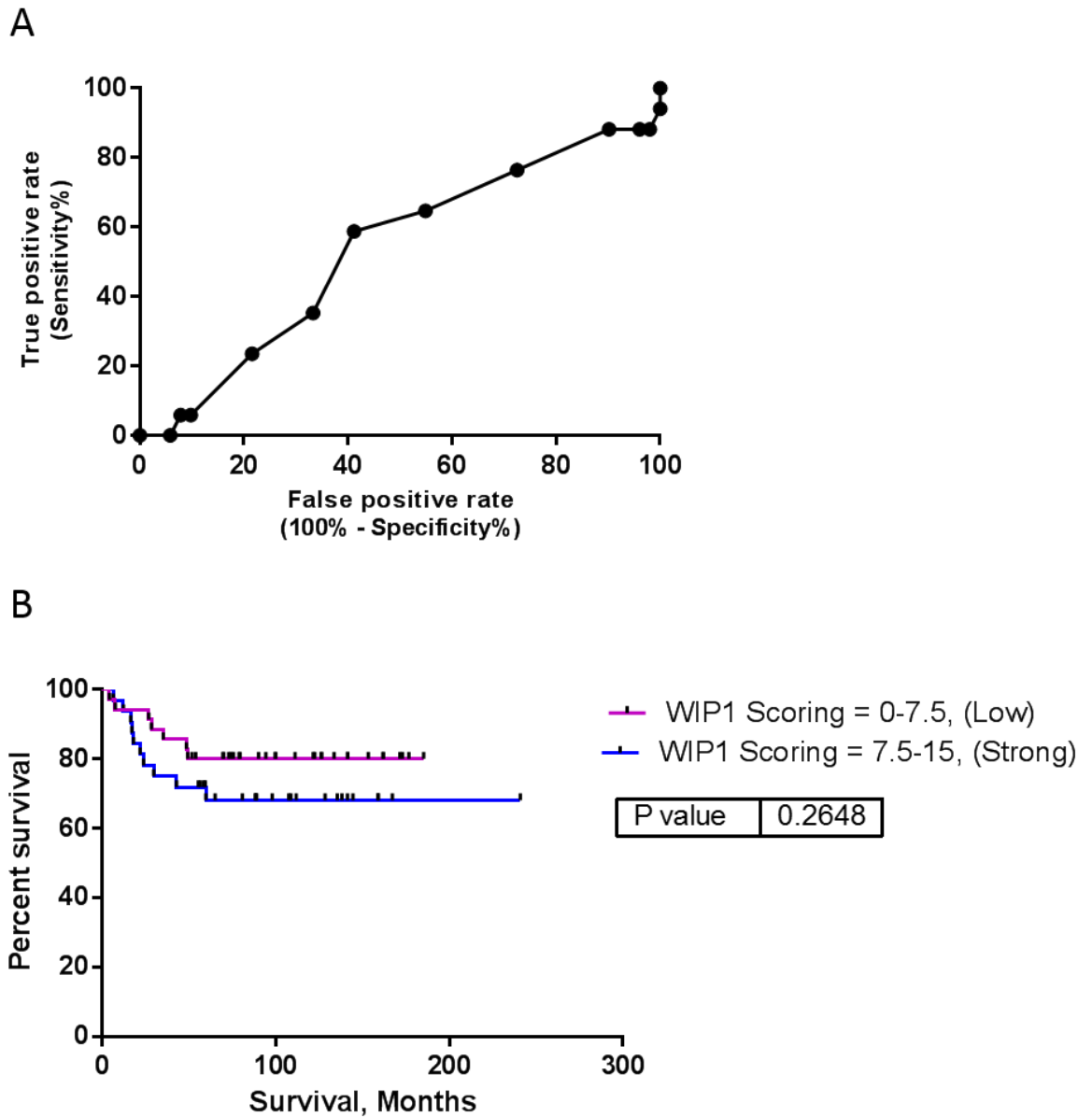


Figure 7-17 A) ROC curve of WIP1 H-scores as a prognostic test. B) Log-rank test and Kaplan Meier plot of WIP1 H-Scores ≤ 7.5 and H-scores ≥ 7.5 groups show that WIP1 protein expression was not significantly related to survival in our cohort of neuroblastoma patients.

		WIP1 Protein expression (H Score)		
Variables	n	H-Score < 7.5	H-Score > 7.5	p-value
Stage				
I-II	15	7	8	0.33
III-IV	46	28	18	
MYCN status				
MNA	10	6	4	0.88
MNnA	40	25	15	
11q status				
11q del	5	3	2	0.68
No 11q del	28	14	14	
17q status				
17q gain	15	10	5	0.16
No 17q gain	23	10	13	
1p status				
1p del	7	4	3	0.96
No 1p del	43	25	18	

Table 7-2 Contingency tables generated to assess any association between other prognostic markers and above and below median WIP1 H-score. The p-values in the last column were determined by Fisher's exact test.

7.5 Discussion

High *PPM1D* mRNA expression has been reported to be a marker of poor prognosis in neuroblastoma (Saito-Ohara, Imoto et al. 2003, Richter, Dayaram et al. 2015). Our data-mining shows that although above median value *PPM1D* expression is significantly associated with poor survival, when MNA and MNnA samples are assessed as separate groups, there is no significant correlation between elevated *PPM1D* mRNA and poorer overall survival. This suggests that the role of WIP1 phosphatase activity in neuroblastoma is likely subtle and could be influenced by MYCN function. This could also suggest that other genes gained on the distal end of the chromosome 17 may be more reliable markers of prognosis, in contrast to reports by Saito-Ohara *et al.*, (2003). However, in contrast to reports in the literature (Bown, Cotterill et al. 1999), the gain of 17q21-17qter was not a significant prognostic marker in our current cohort.

Liang *et al.*, (2012) had used immunofluorescence microscopy to show that WIP1

staining is both nuclear and cytoplasmic; however they had not tested the specificity of their antibody. During our antibody validation process we assessed specificity of the Anti-WIP1 antibody (F-10) by degrading WIP1 using GSK2830371 and then using immunofluorescence microscopy to assess whether the WIP1 signal had dropped. This showed that the antibody is specific for our target antigen and that WIP1 is both nuclear and cytoplasmic. The same antibody was then optimised for IHC staining of neuroblastoma core biopsies on a TMA, which showed that WIP1 IHC staining was not significantly related to overall survival and hence is unlikely to be a useful prognostic biomarker for neuroblastoma. The WIP1 H-score was not different in 17q21-17qter gain group of tumours or any other groups for which we had clinicopathological data. However, WIP1 H-score was shown to not be normally distributed in the 17q gain subgroup suggesting that this event results in tighter regulation of WIP1 protein expression. It would be of interest to investigate the 17q breakpoint and how it may impact regulation of WIP1 expression.

Chapter 8 General discussion

8.1 Mechanistically relevant dose range and scheduling of MDM2 inhibitors in pre-clinical evaluation

An overwhelming body of evidence in the literature and the data presented in this thesis have shown that the strongest determinant of response to MDM2 inhibitors is wild-type *TP53* genetic status. Indeed MDM2 inhibitor resistant sub-clones developed in our laboratory, through continuous exposure to an increment of Nutlin-3, and resistant sub-clones reported by others, all possess *TP53* inactivating mutations (Aziz, Shen et al. 2011, Michaelis, Rothweiler et al. 2011, Jones, Bjorklund et al. 2012). This suggests that *TP53*, but not *MDM2*, is under strong negative selection in a context where MDM2 inhibition is lethal. This is in stark contrast to the most common mechanism of acquired resistance observed in response to other targeted agents, such as tyrosine kinase inhibitors, which is mostly caused by the emergence of *de novo* mutations in genes that encode the target protein (point mutations in epidermal growth factor receptor in Gefitinib resistance) (Chen and Fu 2011). Notably, there have been no reports of *de novo* MDM2 mutations in MDM2 inhibitor resistant sub-clones to date. It could be argued that mutations in MDM2 that alter its hydrophobic binding pocket structure in a way that it can no longer accommodate an MDM2 inhibitor, would equally no longer house the p53 N-terminus and would be negatively selected in a p53-dependent manner. These observations reinforce the notion that MDM2 is the most important regulator of p53 stability and function and the primary mechanism through which MDM2 inhibition can result in cell cycle arrest and/or cell death is through activation of wild-type p53 signalling. Therefore, what distinguishes on-target from off-target activity of MDM2 inhibitors in cell lines, is likely the dose range that induces minimal to maximal p53-dependent growth inhibition or cell death. The upper limit of this dose range coincides with the lowest growth inhibitory or lethal dose of the same MDM2 inhibitor in a *TP53* mutant otherwise isogenic setting as shown in chapter 3 using the MDM2 inhibitor resistant clones. This could approximate the mechanistically relevant on-target dose range of MDM2 inhibitors in a given cell line. The importance of establishing this range must be considered when investigating whether MDM2 inhibitors cause direct DNA damage. The importance of timing discussed in Chapter 3 must also not be overlooked. The appearance of the DNA DSB marker, γ H2AX, detectable by immunofluorescent staining, 24 hours following a mechanistically relevant dose of Nutlin-3 (5 μ M) in *TP53* wild-type cell lines (See Chapter 3), may be attributed to DNA fragmentation during

apoptosis observed in NGP and SJSA-1 cells which was evident from significant increase in caspase-3/7 activity and significant loss of clonogenic survival (Rogakou, Nieves-Neira et al. 2000). The comparison of the rapid detection of γ H2AX immunofluorescent staining 30min following a dose of IR and the long delay in the case of Nutlin-3 supports this interpretation.

8.2 DNA repair enzymes as potential co-determinants of response to MDM2 inhibitors

Data presented in chapter 3 of this thesis focuses on the role of two members of the PI3KK family, ATM and DNA-PKcs, in determining or modulating the response to Nutlin-3. This investigation was prompted by a report suggesting that inhibition of ATM and Nutlin-3 results in synthetic lethality in *TP53* wild-type cell lines in culture (Sullivan, Padilla-Just et al. 2012). MDM2-p53 binding antagonists such as Nutlin-3 were optimised to activate wild-type p53 signalling through non-genotoxic inhibition of the p53-MDM2 protein-protein binding interaction (Vassilev, Vu et al. 2004). ATM kinase activity is associated with activation of p53 signalling by DNA damage, which meant that these results were counterintuitive (Canman, Lim et al. 1998, Appella and Anderson 2001). Given that Sullivan *et al.*, 2012 had used doses of Nutlin-3 (10 μ M, 20 μ M and 30 μ M) that had independently been reported to induce DNA DSBs (Verma, Rigatti et al. 2010, Valentine, Kumar et al. 2011, Rigatti, Verma et al. 2012), the synergy reported was suspected to be due to potentiation of the consequences of DSBs by MDM2 inhibitors rather than the intricate mechanism explained by the authors. It is well established that the inhibition of ATM kinase activity to potentiate the response of cells to DNA DSB inducing anticancer agents (Hickson, Zhao et al. 2004). Therefore, the potential for synergy between ATM and MDM2 inhibitors was tested at lower mechanistically relevant doses of Nutlin-3 that are related to the non-genotoxic activation of p53 by MDM2 inhibitors.

Combined inhibition of ATM (10 μ M KU55933) and Nutlin-3 doses <10 μ M did not enhance the Nutlin-3 sensitivity of *TP53* wild-type or mutant cells. However, *TP53* mutant cell were made slightly more sensitive to \geq 10 μ M doses of Nutlin-3 which would be consistent with the potentiation of cellular sensitivity to indirect DNA damage by ATM inhibition. Selective chemical inhibition of DNA-PKcs also did not result in increased sensitivity to Nutlin-3 over the dose range used. These findings suggested that ATM or DNA-PKcs alone do not determine sensitivity to MDM2 inhibitors as single

agents. However, the role of DNA-PKcs was pronounced in determining the response to combinations of Nutlin-3 and IR in a cell type dependent manner. IR protected SJSA-1 *TP53* wild-type osteosarcoma cells against Nutlin-3 regardless of DNA-PKcs inhibition. However, IR sensitised *TP53* wild-type NGP neuroblastoma cells, not their *TP53* mutant N20R1 daughter cell line, to Nutlin-3 and DNA-PKcs inhibition potentiated this effect significantly. Potentiation of IR by NU7441 in NGP *TP53* wild-type cells was then shown to be significantly enhanced by a non-cytotoxic dose of Nutlin-3 (0.2 μ M) in clonogenic assays. Whether or not the IR induced protection of SJSA-1 cells, against growth inhibition by Nutlin-3, would also translate to clonogenic survival was not investigated.

NGP cells are *MYCN*-amplified. It has been reported that *MYCN*-amplification, which is a frequently detected cytogenetic abnormality in advanced stage neuroblastoma and a marker of poor prognosis, impairs DNA DSB repair (Karlsson, Deb-Basu et al. 2003). This may be the underlying reason for the difference between the sensitivity of SJSA-1 cells and NGP cells to the combination treatments tested in the presence of IR. Indeed inhibition of PARP-1 using Rucaparib in NGP cell line pair resulted in growth inhibition in a p53-independent manner in contrast to the SJSA-1 cell line pair which were resistant to PARP-1 inhibition. Rucaparib potentiates cellular response to DSB inducing DNA damaging agents (Znojek, Willmore et al. 2014) which would be consistent with the consequences of defective DNA DSB repair in the *MYCN*-amplified NGP and N20R1 neuroblastoma cell line pair. A recent study also showed that increased *MYCN* expression increases cellular sensitivity to DNA-PKcs knockdown or its chemical inhibition by NU7441 (Zhou, Patel et al. 2014). Although our data did not show any notable difference between the sensitivity of SJSA-1 and NGP cells to NU7441 single agent treatment, it showed that inhibition of DNA-PKcs in NGP cells potentiated the cellular response to Nutlin-3 and IR whereas it did not impact on SJSA-1 sensitivity in response to the combination. Another possible explanation for difference in response between SJSA-1 and NGP cells may be that p53 induced G1 arrest is intact in SJSA-1 cells whereas it is defective in NGP cells (chapters 5), so SJSA-1 cells may be protected in response to DNA damage. It has been previously reported that *MYCN* amplification is associated with defects in p21^{WAF1} induction and IR induced G1 arrest in neuroblastoma cell lines including NGP cells (Tweddle, Malcolm et al. 2001). Further investigation into the role of *MYCN* expression in the observed potentiation of response to Nutlin-3 and IR are merited on these ground.

In the experiments described in chapter 3 of this thesis the cells were treated with a combination of Nutlin-3 \pm NU7441 for 4Hrs before exposure to IR, so that at the time of IR exposure p53 expression was maximal. Given the reported role of MDM2 in p53-independent inhibition of homologous recombination repair through its interaction with NBS1 (Bouska and Eischen 2009, Carrillo, Hicks et al. 2015), a component of the MRN complex, this schedule would have provided enough time for accumulation of MDM2 and its inhibition of DNA repair. Considering the results observed in NGP cells in isolation one would consider this hypothesis to hold true. However, their *TP53* mutant otherwise isogenic daughter cell line N20R1 was not made more sensitive by any of the combination treatments in the presence of Nutlin-3, which suggests that the increased sensitivity observed in NGP cells is p53-dependent. As the IR sensitivity of NGP and N20R1 cells was the same regardless of their *TP53* status the addition of a non-cytotoxic dose of Nutlin-3 further potentiated the effect of IR + NU7441 only in the *TP53* wild-type NGP parental cells. Also it could be expected that any p53-independent DNA repair inhibitory effects of Nutlin-3, which is reportedly mediated through MDM2 inhibition of NBS1, would be particularly pronounced in SJSA-1 cells which are MDM2 amplified and in which MDM2 induction following Nutlin-3 is very strong. However, in SJSA-1 DNA damage did not influence the sensitivity to Nutlin-3 even when DNA-PKcs was inhibited. Although this should be further investigated in clonogenic assays, based on the preliminary data presented in this thesis the impact of Nutlin-3 mediated p53 independent DNA repair inhibition does not seem to lead to a dramatic increase in sensitivity to IR in SJSA-1 cells. Also, if MDM2 inhibitors were to potentiate the response to DNA damage in a p53-independent manner then the Nutlin-3 mediated growth inhibition of both of the *TP53* mutant SN40R2 and N20R1 cells would have also been enhanced in the presence of IR. However, this was not the case.

These results are overall consistent with the non-genotoxic mechanism of action of Nutlin-3 as the chemical inhibition of key enzymes involved in homologous recombination repair (ATM), non-homologous end joining (DNA-PKcs) and base excision repair (PARP-1) could not influence sensitivity to the MDM2 inhibitor in the absence of additional DNA damage by IR. This also casts doubt over the reported p53-independent role of MDM2 inhibitors in inhibition of HRR. However, combination treatment with DNA-PKcs inhibition suggested that loss of DNA DSB repair integrity is important in determining the response to combination treatment of Nutlin-3 with IR. Finally, the efficacy of combination of Nutlin-3 with IR is context-dependent and

probably requires careful consideration of dosing and scheduling. More comprehensive pre-clinical investigation is required to avoid any potential antagonism in antitumour effects between the compounds.

8.3 WIP1 phosphatase activity as a determinant of cellular response to MDM2 inhibitors

Although *MDM2*-amplified or overexpressing *TP53* wild-type cell lines have been reported to be among the more sensitive to growth inhibition by MDM2 inhibitors (Saiki, Caenepeel et al. 2015, Zhong, Chen et al. 2015), many other *TP53* wild-type cell lines that do not share this genetic alteration are also sensitive to MDM2 inhibitors. For example, the Wellcome Trust Sanger Institute drug sensitivity data cited earlier, highlighted a number of other predictors of sensitivity to MDM2 inhibitors such as *MYCN*-amplification which has also been verified independently to increase sensitivity to MDM2 inhibitors in spite of wild-type *MDM2* genetic status (Gamble, Kees et al. 2012). The range of sensitivity to MDM2 inhibitors in *TP53* wild-type cell lines, and their limited anti-tumour efficacy in clinical trials, reflects a need for the identification other mechanisms that determine cell fate following the activation of p53 signalling. These mechanisms, some of which were introduced in chapter 1 (Section 1.16.6) are very complex and context-dependent; however combination treatments are already being considered, hence there is a need to investigate the mechanisms and optimise the use of MDM2 inhibitors. The ideal combination regimen would preferably rely on other non-genotoxic targeted agents that show tumour specific synthetic lethality with MDM2 inhibitors in order to increase tumour sensitivity and selectivity. Such agents may target proteins directly involved in regulation of p53 stability and/or function (such as MDMX (Graves, Thompson et al. 2012)) or parallel pathways, the inhibition of which results in increased sensitivity of cancer cells to MDM2 inhibitors (Such as PI3K or MAPK pathways (Saiki, Caenepeel et al. 2014)). Alternatively, these combinations may increase cellular sensitivity to other conventional DNA damaging anticancer agents as described above.

In chapters 4 and 5 of this thesis it was shown that knockdown or inhibition of the WIP1 phosphatase can potentiate the cellular growth inhibitory and apoptotic response to MDM2 inhibitors of *TP53* wild-type cells, particularly in those with increased *PPM1D* expression or gain-of-function. Transient knockdown of WIP1 resulted in sensitisation of the three *TP53* wild-type cell lines NGP, SJSA-1 and HCT116 cells to MDM2

inhibition. Interestingly, WIP1 knockdown also resulted in modest p53-dependent growth inhibition in the NGP cell line pair but not in the SJSA-1 or HCT116 cell line pairs. Monitoring the morphology of the cell lines in which WIP1 knockdown resulted in p53-independent growth inhibition suggested that transfection conditions may be causing additional stress that can potentially confound the findings. Large cytoplasmic vacuoles were observed under transfection conditions in HCT116 and SJSA-1 cell line pairs. Increased growth inhibition in *TP53* mutant SN40R2 and HCT116^{-/-} cell lines in the presence of WIP1 siRNA can be explained if these vacuoles are signs of autophagy as WIP1 knockdown may promote autophagic cell death involving inhibition of ATM (Le Guezennec, Brichkina et al. 2012). Further investigation of this mechanism was beyond the scope of this project. The NGP cell line pair, in which these morphological signs of stress were not observed, were used in the subsequent flow cytometry and clonogenic experiments combining Nutlin-3 and WIP1 siRNA knockdown. These experiments also showed that NGP *TP53* wild-type cells were significantly more sensitive to Nutlin-3 when WIP1 expression was knocked down.

The commercial availability of a highly selective allosteric WIP1 inhibitor, GSK2830371, allowed the investigation of the growth inhibitory efficacy of combining MDM2 and WIP1 inhibition (See chapter 5). Initially the sensitivity to WIP1 inhibitor as a single agent was tested showing that none of the four isogenically matched *TP53* wild-type and mutant pairs were sensitive to growth inhibition by GSK2830371 in the dose range used by the original authors, regardless of their *PPM1D* status. The efficacy of the compound was tested in parallel with a *PPM1D*-amplified *TP53* wild-type cell line, MCF-7, which had been reported to be sensitive to growth inhibition by GSK2830371. Single agent treatment with this compound in MCF-7 cells was confirmed to result in growth inhibition which was associated with degradation of WIP1 protein and its isoform in addition to p53 stabilisation and p21^{WAF1} induction. The GSK2830371 growth inhibitory curve for MCF-7 cells plateaued after reaching the GI50 dose for this compound in this cell line (2.5µM). This led to the assumption that there is a resistant sub-population that is likely unaffected by maximal WIP1 inhibition as the dose range covered (0.08-10µM). Since GSK2830371 has an *in vitro* IC50 of 6nM in cell-free assays, this compound is likely to be in excess at 2.5µM in culture.

Incidentally, 2.5µM GSK2830371 was the highest non-growth inhibitory dose in all of the other cell lines which meant that maximal inhibition of WIP1 does not impact the growth of these cell lines. However, because of the established role of WIP1 in

homeostatic regulation of p53 signalling it was pertinent to assess its role in determining the response to MDM2 inhibitors. 2.5µM GSK2830371 simultaneously combined with the relevant dose ranges of Nutlin-3 caused significant potentiation of the cellular growth inhibitory response in a p53-dependent manner. This was more pronounced in cell lines with either elevated *PPM1D* expression or gain-of-function mutations. Assessment of cell death endpoints showed that WIP1 inhibition by GSK2830371 resulted in significant and marked increase in either biochemical markers of cell death and loss of clonogenic survival. When 2.5µM GSK2830371 was combined with the more potent and selective clinical candidate MDM2 inhibitor, RG7388, pronounced potentiation of the response to the MDM2 inhibitor was also observed in *TP53* wild-type cell lines with elevated *PPM1D* expression or gain-of-function.

8.4 Phosphorylation of p53 and altered p53-dependent transcription in the potentiation of MDM2-p53 binding antagonists by WIP1 inhibition

The most interesting observation was that p53^{Ser15} phosphorylation (pp53^{Ser15}), which is a well-established substrate for WIP1, was only enhanced notably in response to the combination of WIP1 and MDM2 inhibition, whereas each compound alone did not impact its levels in cell line pairs that were unaffected by 2.5µM GSK2830371. It has been reported that increased Ser15 phosphorylation results in increased acetylation of p53 C-terminal residues, by p300, which are also ubiquitinated by MDM2. Therefore it was predicted that the increase in pp53^{Ser15} would result in reduced p53 degradation (Li, Luo et al. 2002). This would be consistent with the increased sensitivity in response to the combination treatment. However, it could also be said that an increase in pp53^{Ser15} may be proportional to an increase in total p53 and that the inhibition of WIP1 phosphatase activity has little to do with the increase in pp53^{Ser15} observed. The increase in pp53^{Ser15} in response to the combination however was not due to enhance p53 stabilisation in combination treatment, as the band intensity for total p53 in western blots was the same in MDM2 inhibitor treated cells in the presence and absence of WIP1 inhibition. This is consistent with the most recent *in vivo* data from knock-in mice that are with substitutions in the cluster of C-terminal lysins residues on p53 normally ubiquitinated by Mdm2. Substitution of K367, K369, K370, K378, K379, K383 and/or K384 residues to R, which cannot be ubiquitinated, resulted in no difference in p53 stability (Feng, Lin et al. 2005, Krummel, Lee et al. 2005). Furthermore addition of Nutlin resulted in stabilisation of p53 in these mice which suggests that MDM2 is still important for p53 proteasomal degradation in these mice. This suggests that other

MDM2 ubiquitinated p53 K residues may be important for p53 degradation. This is also consistent with a basal equilibrium between the phosphatases and kinases that target the p53^{Ser15} residue, which following p53-MDM2 decoupling by MDM2 inhibitors is tilted in favour of the basal activity of p53 activating kinases such as the PI3KKs. Given the importance of this post-translational modification in transcriptional transactivation of p53 it was hypothesised that the reason for potentiation observed may be due to the modulation or enhancement of p53 transcriptional activity promoting pro-apoptotic signalling. Global gene expression analysis was carried out in NGP cells, for which the most pronounced potentiation was observed, 4Hrs following treatment with 75nM RG7388 \pm 2.5 μ M GSK2830371, to assess which genes, if any, are differentially induced by p53 between the two treatments. The 75nM dose of RG7388 chosen was based on the GI50 for RG7388 in NGP SRB growth inhibition assays at which the greatest potentiation was observed. Protein levels of the canonical transcriptional targets of p53 are induced maximally at approximately 6-8Hrs following commencement of treatment with MDM2 inhibitors, which meant that altered p53-dependent transcriptional changes would be evident at 4Hrs if the p53-dependent induction of these proteins is at the transcriptional level. As hypothesised, the findings showed that the expression of p53 transcriptional target genes induced by RG7388 was enhanced when WIP1 was inhibited by GSK2830371. In addition to an increase in the transcript levels of genes induced by RG7388 alone, a larger subset of genes were significantly induced in response to the combination which was consistent with hypothesised enhanced p53 transcriptional activity. It is well understood that p53 transcriptional targets have different kinetics of induction following p53 activation in a context-dependent manner (see 1.16.6). Therefore, further investigation of the kinetics of these transcriptional target genes in response to the combination treatment and their biological significance may provide more distinct answers as to which mechanisms of cell death rather are activated in response to the combination treatment.

Interestingly, pathway analysis of all the genes that were differentially expressed in response to both treatment conditions identified activation of p53 signalling. This attests to the p53 mediated mechanism of action of MDM2 inhibitors regardless of WIP1 inhibition. These data are also consistent with the previous reports of *Trp53* knock-in transgenic mouse models in which S18A or S23A mutations were introduced in serine residues homologous to human Ser15 and Ser20. *Trp53*/p53 is still stabilised efficiently in response to IR in *Trp53*^{S18A} homozygous knock-in transgenic mice, which means that

the phosphorylation of this residue is dispensable for Trp53 dissociation from Mdm2 in mice following DNA damage. However, the induction of known Trp53 transcriptional targets 8Hrs following IR was different in Trp53^{S18A} homozygous transgenic mouse thymocytes compared to those derived from wild-type mice (Table 8-1). In spite of the differences between p53 activating stimulus (IR vs RG7388), species and tissue types, the pattern of differential expression of the human homologues of Trp53 transcriptional target genes, *CDKN1A* (p21^{WAF1}) and *MDM2*, bear similarities to the differential expression seen in the present study when comparing RG7388 ± 2.5µM GSK2830371. The Trp53^{S18A} mutation was reported to result in diminished mRNA expression from the *Cdkn1a* locus (p21^{Waf1}) whereas it did not impact significantly on *Mdm2* expression (Chao *et al.*, (2003)). In the presently reported study, the presence of GSK2830371 resulted in a marked increase in pp53^{Ser15} following RG7388 treatment, which then correlated with a 50% increase in *CDKN1A* (p21^{WAF1}) mRNA and a 7% increase in *MDM2* mRNA induction. This implies that the increased pp53^{Ser15} in combination treatment may be playing a role in promoter specific induction of p53 transcriptional target genes following non-genotoxic stabilisation of p53 by MDM2 inhibitors. However, further investigation of these subsets of genes at various time-points following the combination treatment regimens may be required for a more complete description of the time course of changes in the mRNA levels of the differentially expressed subset of genes. Furthermore, the preliminary findings in this thesis with the p53 overexpressing constructs with S15A and S15D mutations transfected into HCT116 p53 null cells are consistent with these findings and are supported by those reported by Loughery *et al.*, (2014), but require further validation..

Genes	Folds of induction in thymocytes after IR					
	Wild type Trp53			Trp53 ^{S18A}		
	Expt. 1	Expt. 2	Average	Expt. 1	Expt. 2	Average
p21	12	15	13.5	2.8	6	4.4
Mdm2	1.7	1.5	1.6	1.5	2.5	2
14-3-3σ	6.2	6	6.1	1.9	2.1	2
TNF-α	4.7	8	6.4	0.7	1.2	0.95
C/EBP	14	11.5	12.75	2.2	1.3	1.75
SNK	16	7.5	11.75	3.4	3.3	3.3
Calcyclin	18	14	16	0.5	0.8	0.7
Perp	8.5	4.5	6.5	3	1	2
Apaf1	4	2	3	3	3.5	3.25
Bax	4	4.5	4.25	5	6	5.5
BLK	1	2	1.5	2	4	3
Wig-1	6	4	5	6.5	8	7.25
Pig8	3.5	2.5	3	2.7	3.2	2.95

Table 8-1 Differential Trp53 target gene expression between Trp53 wild-type and Trp53^{S18A} knock-in transgenic mouse thymocytes, 8Hrs following 5Gy IR, show that Trp53 induced transcription of its canonical targets are diminished in a promoter specific manner when Trp53 Ser18 is mutated to Ala and cannot be phosphorylated. The cells highlighted in amber showed greater than 2-fold reduction in mRNA expression as measured by a murine Affymetrix array. The table is reproduced in modified form from Chao *et al.*, (2003).

The p53 regulated luciferase reporter assay used as a different endpoint for measuring the transcriptional transactivation activity of p53, showed a dose-dependent increase in reporter signal 24Hrs following treatment with Nutlin-3. This increase in response was not observed in the *TP53* mutant cell line stably transfected with the same reporter, suggesting that the Nutlin-3 mediated induction of this reporter is p53-dependent. Modest potentiation of growth inhibition (1.7-fold reduction in GI50) was observed in the *TP53* wild-type DD7 cells. However WIP1 inhibition by GSK2830371 did not enhance the Nutlin-3 mediated p53-dependent induction of the reporter in this context. This may indicate that the potentiation observed is due to transcriptional independent mechanisms of action. However, the reporter assay was not fully optimised as the dose dependent Nutlin-3 mediated reporter response could not be optimised at earlier time points because the signal was saturated at both doses used (Data not shown). Also the levels of p53^{Ser15} phosphorylation were not examined in response to the combination treatment in neither of the cell lines; therefore it cannot be assessed whether or not pp53^{Ser15} was enhanced in these cell lines in response to the combination treatment. Although these findings suggest that changes in the effect of WIP1 inhibitor on modulation of p53 mediated transcription may be context-dependent, further optimisation of this reporter system is necessary to increase the assay sensitivity for detection of modulations of p53 transcriptional activity.

As it was discussed in chapter 1, p53 transcriptional transactivation can be considered the key to p53 mediated cell fate determination between reversible cell cycle arrest, senescence and apoptosis. However, more recent studies have explored the potentially important role of other less well-characterised p53 transcriptional targets which are involved in metabolic processes. For example radiosensitive tissue or MEFs derived from transgenic knock-in mice homozygous for *Trp53*^{K117R, K161R, K162R}, which cannot be acetylated on those residues, do not undergo cell cycle arrest, senescence or apoptosis in response to IR because they cannot induce key p53 transcriptional targets involved in these processes (Li, Kon et al. 2012). Interestingly, the early onset tumour formation observed in *Trp53* null mice is not observed in these mice. The authors ascribe this to the fact that p53^{K117R, K161R, K162R} can still induce other transcriptional targets of p53 that are involved in metabolic processes. This is consistent with other findings showing efficient p53 mediated tumour suppression in transgenic mouse models that lack p21, Puma and Noxa (Valente, Gray et al. 2013). Therefore, investigating other p53 regulated mechanisms which are deemed important in tumour suppression, such as

metabolic control, may be of interest when investigating the combination treatment proposed in this thesis.

8.5 Assessing the role of WIP1 protein expression as a prognostic factor in neuroblastoma

Elevated *PPM1D* mRNA expression had been reported to be a potential marker of poor prognosis in neuroblastoma and WIP1 is reportedly a potential target for the treatment of *TP53* wild-type neuroblastoma (Saito-Ohara, Imoto et al. 2003, Richter, Dayaram et al. 2015). Richter *et al.*, (2015) analysed the sensitivity of a large panel of neuroblastoma cell lines to GSK2830371 and showed that only *TP53* wild-type cell lines responded to this compound, albeit with a wide range of sensitivity as measured by GI50 values. This is consistent with findings by Gilmartin *et al.*, (2014) showing that the response to GSK2830371 is p53-dependent. Overall these reports indicate that WIP1 phosphatase activity plays an important role in the negative regulation of p53 signalling in neuroblastoma and may confer a poorer overall survival when highly expressed. However, WIP1 protein levels have not been investigated in neuroblastoma to date. Our findings in chapter 7 show that although elevated *PPM1D* mRNA, as reported by others, may be a predictor of poorer outcome, WIP1 expression as measured by immunohistochemistry was not found to have prognostic significance in this study.

It is important to note that observations in chapter 7 do not nullify the potential usefulness of the WIP1 inhibitor (GSK2830371) in sensitising *TP53* wild-type neuroblastoma tumours to MDM2 inhibitors. The lack of prognostic relevance of WIP1 should not be misinterpreted as lack of mechanistic relevance in response to this combination regimen. The preclinical data presented in the previous chapters strongly support the notion that WIP1 inhibitors markedly potentiate MDM2 inhibitor response in the least GSK2830371 sensitive *TP53* wild-type neuroblastoma cell line with *PPM1D* copy number gain (Richter, Dayaram et al. 2015). However, there are other more subtle issues brought to attention in chapter 7 that must be considered before use of this combination regimen in a clinical setting. Cancer Cell Line Encyclopaedia (CCLE) and Amsterdam Medical Centre (AMC) data showed that cell lines or primary samples of haematological malignancies also had high *PPM1D* mRNA expression. Notably, Gilmartin *et al.*, (2014) reported that sensitivity to the selective WIP1 inhibitor, GSK2830371, was greatest in cell lines of the haematological lineage. This may mean that targeting WIP1 has the potential to cause toxicity to healthy cells of the

haematological lineage. This is not desirable for the combination treatment with WIP1 and MDM2 inhibitors as the dose limiting toxicities observed in MDM2 inhibitors are to tissues of haematological lineage and may be exacerbated in response to combination treatment. However, the sensitivity of healthy cells of haematological lineage in response to MDM2 and WIP1 inhibitors has not been investigated yet. This may be made possible by investigating the colony formation ability of healthy donor bone marrow cells in culture following single agent and combination treatments with WIP1 and MDM2 inhibitors.

8.6 MDM2 inhibitor resistant clones show the same sensitivity to IR

Although it is not the central line of inquiry in this thesis, it is very important to note that contrary to previous reports (Michaelis, Rothweiler et al. 2011, Jones, Bjorklund et al. 2012), MDM2 inhibitor resistant clones generated in our lab showed the exact same sensitivity to IR in clonogenic assays as their wild-type *TP53* parental cell line counterparts. This suggests that not all MDM2 inhibitor resistant *TP53* mutant sub-clones show cross-resistance to IR and perhaps other DNA damaging agents.

Interestingly, the drug sensitivity data on the Sanger database shows that the *TP53* genetic status is not a strong determinant of response for DNA damaging agents or other targeted agents (Figure 8-1). This suggests that *TP53* genetic status is not a universal determinant of response to IR. This is consistent with previous findings that suggest IR induced cell death is only dependent on *TP53* genetic status in certain radiation sensitive rapidly proliferating tissue (MacCallum et al., 1996) (Komarova et al., 1997). The importance of these observations must not be underestimated as they could have far reaching implications in devising first line cancer management strategies using MDM2 inhibitors in *TP53* wild-type tumours. The knowledge of radio- or chemo-sensitivity of MDM2 inhibitor resistant clone could be used in the following hypothetical clinical strategy to optimise the use of MDM2 inhibitors. An MDM2 inhibitor could induce apoptosis in a population of the *TP53* wild-type cells in the tumour within the first 24-48 hours, based on data from our work and other published pre-clinical data. Of course this will differ depending on tumour origin and the concentration achieved throughout the malignant tissue by oral or systemic administration. This process selects for *TP53* mutant cells in the tumour but it is very likely that it will also select for cells that have undergone p53-dependent reversible cell cycle arrest. The *TP53* mutant sub-population will still be sensitive to genotoxic agents and a lower dose can potentially be used to eliminate them. However, the scheduling must be considered carefully. If the genotoxic

agent was delivered concomitantly with the MDM2 inhibitor then the sub-population that had undergone reversible cell cycle arrest will be refractory to DNA damage. (Pawlik and Keyomarsi 2004). Therefore MDM2 inhibitors must be allowed to clear before the genotoxic agent is administered to eliminate the remaining MDM2 inhibitor insensitive *TP53* wild-type cells. Although, it must be noted that due to the range of sensitivity of *TP53* wild-type cell lines and tumours reported, optimal efficacy of MDM2 inhibitor single agent as first line treatment is highly unlikely for majority of solid tumours. However, a synergistic combination of MDM2 inhibitors with other non-genotoxic targeted agents (e.g. a WIP1 inhibitor) can potentially eliminate a larger proportion of the *TP53* wild-type cells within a tumour population. Furthermore, this may be achieved with considerably lower doses of both compounds avoiding toxicity caused by off-target or on-target activity. The non-genotoxic compounds can then be allowed to clear for the same reasons mentioned earlier and a round of less aggressive genotoxic treatment could be used to eliminate the combination treatment resistant subpopulation of cells remaining (Figure 8-2). There are many tumour types that are mostly *TP53* wild-type at diagnosis and many of them have interestingly been reported to also show *PPM1D* increased expression or gain-of function mutations. This approach could potentially provide an ideal model to optimise dosage in the aim to minimise both damage to healthy tissue and the likelihood of chemotherapy induced secondary cancers in malignancies that are *TP53* wild-type at diagnosis. However, this simplistic model does not take into account the multitude of other variables that influence tumour response to systemic treatment such as drug pharmacokinetics, tumour blood and oxygen supply and potential roles for the ancillary tumour components described by Hanhan and Weinberg (2000). These known and some yet to be discovered variables will determine the ultimate anti-tumour efficacy of MDM2 inhibitors or their combination with other targeted and/or DNA damaging anticancer agents.

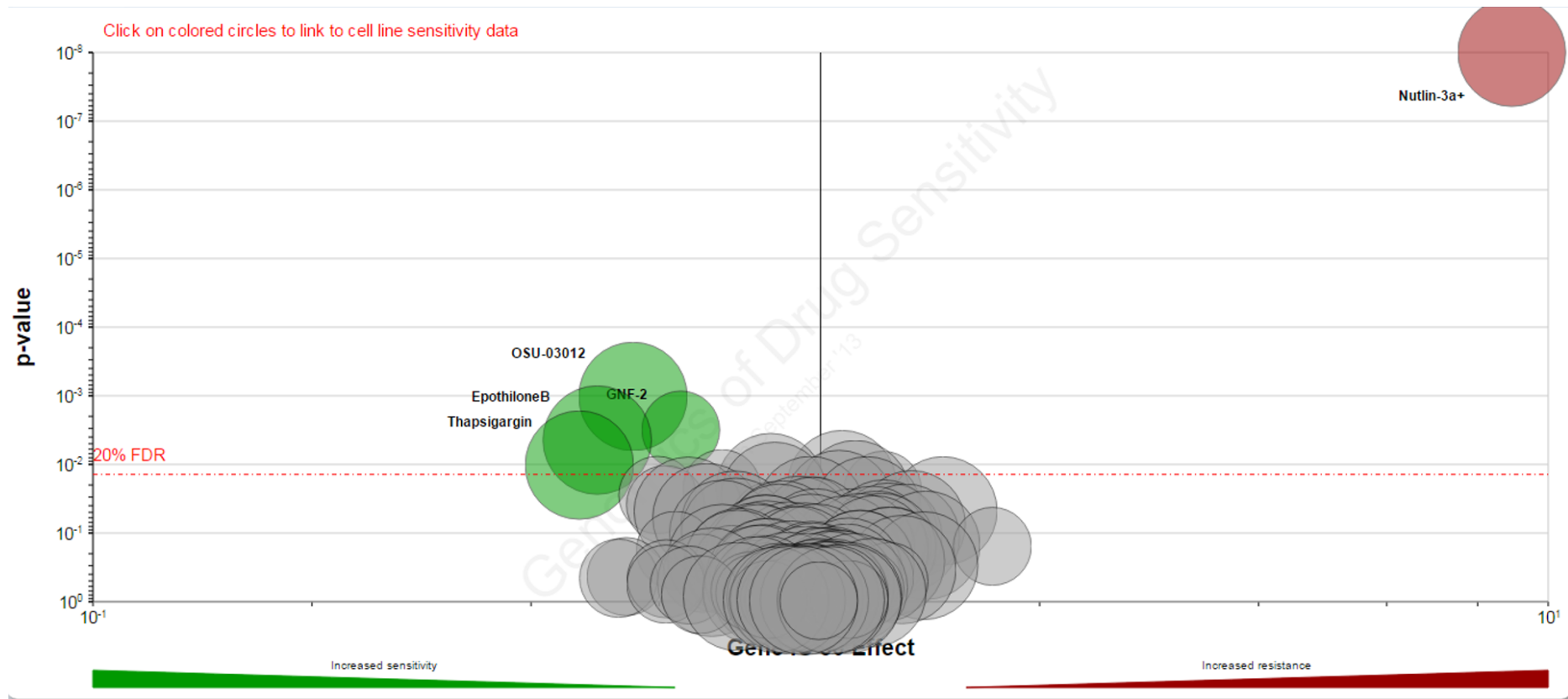


Figure 8-1 The volcano plot shows that the *TP53* genetic status is a far better determinant of response to Nutlin-3a (P-value = $1.26e^{-54}$) than it is for DNA damaging agents or other targeted agents. Y-axis: The p-value from multivariate ANOVA of drug gene interaction on an inverted log₁₀ scale. X-axis: Magnitude of the effect that genetic events have on the GI50 of the drug in cell lines. The size of the circle indicates the number of genetic events corresponding to the analysis for a given gene or a drug. Figure obtained from (<http://www.cancerrxgene.org/>).

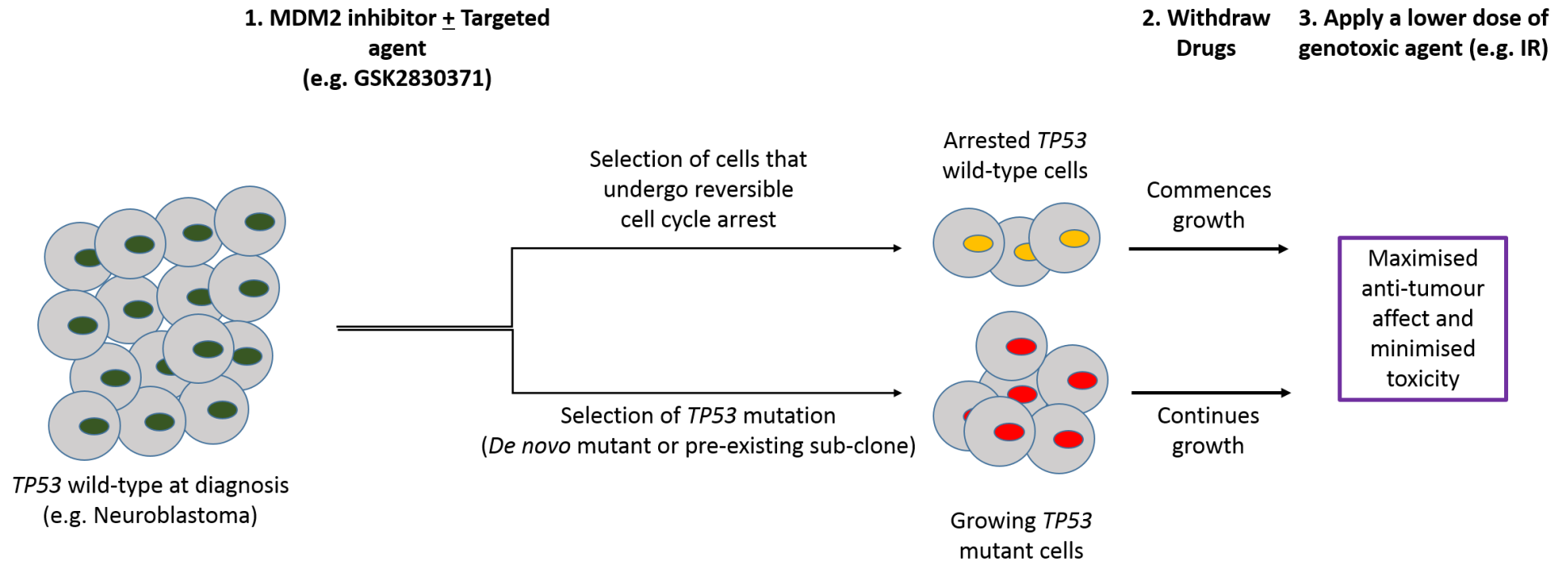


Figure 8-2 The diagram outlines the proposed ideal model for the use of MDM2 inhibitors in combination with other non-genotoxic and genotoxic agents. The main underlying assumption is that *TP53* mutant MDM2 inhibitor resistant cells remain sensitive to DNA damaging agents. See chapter 3 for data in support of this assumption. This strategy has the potential to reduce healthy tissue toxicities and the likelihood of secondary cancers.

8.7 Achieving the full potential of MDM2-p53 binding antagonists in anti-cancer therapy

Approximately 50% of human malignancies diagnosed overall are reported to have wild-type *TP53* genetic status however, it has been suggested that, in a proportion of these tumours, p53 signalling is inactivated through other means, such as the overexpression of MDM2 in sarcomas (Momand, Zambetti et al. 1992, Oliner, Kinzler et al. 1992, Momand, Jung et al. 1998, Kruse and Gu 2009). In spite of the many layers of post-translational regulation of p53 signalling making it very complex to predict cell fate following p53 activating treatment regimens, such modes of regulation can be exploited to harness the full p53 tumour suppressor potential in a more selective manner. MDM2-p53 binding antagonists have proven successful in stabilising and activating wild-type p53 signalling, albeit to varying degrees, pre-clinically and clinically. In anticipation/reaction to a wide range of sensitivity to MDM2 inhibitors in pre-clinical and clinical settings, determinants of sensitivity to MDM2 inhibitors have been investigated and the potential need for better tumour stratification and combination strategies are rapidly being explored (Saiki, Caenepeel et al. 2014, Saiki, Caenepeel et al. 2015, Zhong, Chen et al. 2015). These studies report to have identified candidate target pathways for efficacious combination treatments with MDM2 inhibitors, or to have deciphered optimal gene expression signatures which predict cell sensitivity to MDM2 inhibitors. Indeed these are positive steps toward overcoming the present challenges faced in clinical use of MDM2 inhibitors, such as limited anti-tumour efficacy and dose limiting haematological toxicities. In this thesis it has been shown that successful pre-clinical identification of such predictors of response to MDM2 inhibitors, or optimal combination regimens, depends on careful considerations of dosage, scheduling and translationally valid proposals of patient stratification. Furthermore one such strategy has been proposed with sufficient evidence to initiate *in vivo* preclinical studies combining MDM2 and WIP1 inhibition.

References

- Abarzua, P., J. E. LoSardo, M. L. Gubler, R. Spathis, Y. A. Lu, A. Felix and A. Neri (1996). "Restoration of the transcription activation function to mutant p53 in human cancer cells." *Oncogene* **13**(11): 2477-2482.
- Appella, E. and C. W. Anderson (2001). "Post-translational modifications and activation of p53 by genotoxic stresses." *European Journal of Biochemistry* **268**(10): 2764-2772.
- Armata, H. L., D. S. Garlick and H. K. Sluss (2007). "The Ataxia Telangiectasia–Mutated Target Site Ser18 Is Required for p53-Mediated Tumor Suppression." *Cancer Research* **67**(24): 11696-11703.
- Armstrong, J. F., M. H. Kaufman, D. J. Harrison and A. R. Clarke (1995). "HIGH-FREQUENCY DEVELOPMENTAL ABNORMALITIES IN P53-DEFICIENT MICE." *Current Biology* **5**(8): 931-936.
- Artandi, S. E. and L. D. Attardi (2005). "Pathways connecting telomeres and p53 in senescence, apoptosis, and cancer." *Biochemical and Biophysical Research Communications* **331**(3): 881-890.
- Aziz, M. H., H. Shen and C. G. Maki (2011). "Acquisition of p53 mutations in response to the non-genotoxic p53 activator Nutlin-3." *Oncogene* **30**(46): 4678-4686.
- Badciong, J. C. and A. L. Haas (2002). "MdmX is a RING finger ubiquitin ligase capable of synergistically enhancing Mdm2 ubiquitination." *Journal of Biological Chemistry* **277**(51): 49668-49675.
- Baker, S. J., E. R. Fearon, J. M. Nigro, S. R. Hamilton, A. C. Preisinger, J. M. Jessup, P. Vantuinen, D. H. Ledbetter, D. F. Barker, Y. Nakamura, R. White and B. Vogelstein (1989). "CHROMOSOME-17 DELETIONS AND P53 GENE-MUTATIONS IN COLORECTAL CARCINOMAS." *Science* **244**(4901): 217-221.
- Banin, S., L. Moyal, S. Y. Shieh, Y. Taya, C. W. Anderson, L. Chessa, N. I. Smorodinsky, C. Prives, Y. Reiss, Y. Shiloh and Y. Ziv (1998). "Enhanced Phosphorylation of p53 by ATM in Response to DNA Damage." *Science* **281**(5383): 1674-1677.
- Barak, Y., T. Juven, R. Haffner and M. Oren (1993). "mdm2 expression is induced by wild type p53 activity." *Embo j* **12**(2): 461-468.
- Barak, Y., T. Juven, R. Haffner and M. Oren (1993). "mdm2 expression is induced by wild type p53 activity." *The EMBO Journal* **12**(2): 461-468.
- Bargonetti, J., P. N. Friedman, S. E. Kern, B. Vogelstein and C. Prives (1991). "WILD-TYPE BUT NOT MUTANT P53 IMMUNOPURIFIED PROTEINS BIND TO SEQUENCES ADJACENT TO THE SV40 ORIGIN OF REPLICATION." *Cell* **65**(6): 1083-1091.
- Bargonetti, J., J. J. Manfredi, X. B. Chen, D. R. Marshak and C. Prives (1993). "A PROTEOLYTIC FRAGMENT FROM THE CENTRAL REGION OF P53 HAS MARKED SEQUENCE-SPECIFIC DNA-BINDING ACTIVITY WHEN GENERATED FROM WILD-TYPE BUT NOT FROM ONCOGENIC MUTANT P53-PROTEIN." *Genes & Development* **7**(12B): 2565-2574.
- Barretina, J., G. Caponigro, N. Stransky, K. Venkatesan, A. A. Margolin, S. Kim, C. J. Wilson, J. Lehar, G. V. Kryukov, D. Sonkin, A. Reddy, M. Liu, L. Murray, M. F. Berger, J. E. Monahan, P. Morais, J. Meltzer, A. Korejwa, J. Jane-Valbuena, F. A. Mapa, J. Thibault, E. Bric-Furlong, P. Raman, A. Shipway, I. H. Engels, J. Cheng, G. K. Yu, J. Yu, P. Aspesi, M. de Silva, K. Jagtap, M. D. Jones, L. Wang, C. Hatton, E. Palessandolo, S. Gupta, S. Mahan, C. Sougnez, R. C. Onofrio, T. Liefeld, L. MacConaill, W. Winckler, M. Reich, N. Li, J. P. Mesirov, S. B. Gabriel, G. Getz, K. Ardlie, V. Chan, V. E. Myer, B. L. Weber, J. Porter, M. Warmuth, P. Finan, J. L. Harris, M. Meyerson, T. R. Golub, M. P. Morrissey, W. R. Sellers, R. Schlegel and L. A. Garraway (2012). "The Cancer Cell Line Encyclopedia enables predictive modelling of

anticancer drug sensitivity." *Nature* **483**(7391): 603-307.

Bartek, J. and J. Lukas (2001). "Mammalian G1- and S-phase checkpoints in response to DNA damage." *Curr Opin Cell Biol* **13**(6): 738-747.

Bartel, F., H. Taubert and L. C. Harris (2002). "Alternative and aberrant splicing of MDM2 mRNA in human cancer." *Cancer Cell* **2**(1): 9-15.

Bates, S., A. C. Phillips, P. A. Clark, F. Stott, G. Peters, R. L. Ludwig and K. H. Vousden (1998). "p14ARF links the tumour suppressors RB and p53." *Nature* **395**(6698): 124-125.

Belyi, V. A., P. Ak, E. Markert, H. Wang, W. Hu, A. Puzio-Kuter and A. J. Levine (2010). "The Origins and Evolution of the p53 Family of Genes." *Cold Spring Harbor Perspectives in Biology* **2**(6): a001198.

Bender, R. and S. Lange (1999). "Multiple test procedures other than Bonferroni's deserve wider use." *BMJ : British Medical Journal* **318**(7183): 600-600.

Bergamaschi, D., Y. Samuels, A. Sullivan, M. Zvelebil, H. Breysens, A. Bisso, G. Del Sal, N. Syed, P. Smith, M. Gasco, T. Crook and X. Lu (2006). "iASPP preferentially binds p53 proline-rich region and modulates apoptotic function of codon 72-polymorphic p53." *Nat Genet* **38**(10): 1133-1141.

Bernal, F., M. Wade, M. Godes, T. N. Davis, D. G. Whitehead, A. L. Kung, G. M. Wahl and L. D. Walensky (2010). "A Stapled p53 Helix Overcomes HDMX-Mediated Suppression of p53." *Cancer Cell* **18**(5): 411-422.

Bertani, G. (1951). "Studies on lysogenesis. I. The mode of phage liberation by lysogenic *Escherichia coli*." *J Bacteriol* **62**(3): 293-300.

Bland, J. M. and D. G. Altman (2004). "The logrank test." *BMJ* **328**(7447): 1073.

Boddy, M. N., P. S. Freemont and K. L. Borden (1994). "The p53-associated protein MDM2 contains a newly characterized zinc-binding domain called the RING finger." *Trends Biochem Sci* **19**(5): 198-199.

Boesten, L. S., S. M. Zadelaar, S. De Clercq, S. Francoz, A. van Nieuwkoop, E. A. Biessen, F. Hofmann, S. Feil, R. Feil, A. G. Jochemsen, C. Zurcher, L. M. Havekes, B. J. van Vlijmen and J. C. Marine (2006). "Mdm2, but not Mdm4, protects terminally differentiated smooth muscle cells from p53-mediated caspase-3-independent cell death." *Cell Death Differ* **13**(12): 2089-2098.

Bond, G. L. and A. J. Levine (2007). "A single nucleotide polymorphism in the p53 pathway interacts with gender, environmental stresses and tumor genetics to influence cancer in humans." *Oncogene* **26**(9): 1317-1323.

Borges, H. L., C. Chao, Y. Xu, R. Linden and J. Y. J. Wang (2004). "Radiation-induced apoptosis in developing mouse retina exhibits dose-dependent requirement for ATM phosphorylation of p53." *Cell Death Differ* **11**(5): 494-502.

Böttger, A., V. Böttger, C. Garcia-Echeverria, P. Chène, H.-K. Hochkeppel, W. Sampson, K. Ang, S. F. Howard, S. M. Picksley and D. P. Lane (1997). "Molecular characterization of the hdm2-p53 interaction." *Journal of Molecular Biology* **269**(5): 744-756.

Bougeard, G., R. Sesboüé, S. Baert-Desurmont, S. Vasseur, C. Martin, J. Tinat, L. Brugières, A. Chompret, B. B.-d. Paillerets, D. Stoppa-Lyonnet, C. Bonaïti-Pellié and T. Frébourg (2008). "Molecular basis of the Li-Fraumeni syndrome: an update from the French LFS families." *Journal of Medical Genetics* **45**(8): 535-538.

Bourdon, J. C., V. DeguinChambon, J. C. Lelong, P. Dessen, P. May, B. Debuire and E. May (1997). "Further characterisation of the p53 responsive element - Identification of new candidate genes for trans-activation by p53." *Oncogene* **14**(1): 85-94.

Bouska, A. and C. M. Eischen (2009). "Mdm2 Affects Genome Stability Independent of p53." *Cancer Research* **69**(5): 1697-1701.

Bown, N., S. Cotterill, M. Lastowska, S. O'Neill, A. D. J. Pearson, D. Plantaz, M. Meddeb, G. Danglot, C. Brinkschmidt, H. Christiansen, G. Laureys and F. Speleman

(1999). "Gain of chromosome arm 17q and adverse outcome in patients with neuroblastoma." New England Journal of Medicine **340**(25): 1954-1961.

Brady, C. A., D. Jiang, S. S. Mello, T. M. Johnson, L. A. Jarvis, M. M. Kozak, D. K. Broz, S. Basak, E. J. Park, M. E. McLaughlin, A. N. Karnezis and L. D. Attardi (2011). "Distinct p53 Transcriptional Programs Dictate Acute DNA Damage Responses and Tumor Suppression." Cell **145**(4): 571-583.

Brodeur, G. M., R. C. Seeger, M. Schwab, H. E. Varmus and J. M. Bishop (1984). "Amplification of N-myc in untreated human neuroblastomas correlates with advanced disease stage." Science **224**(4653): 1121-1124.

Brown, E. J. and D. Baltimore (2000). "ATR disruption leads to chromosomal fragmentation and early embryonic lethality." Genes & Development **14**(4): 397-402.

Buesoramos, C. E., Y. Yang, E. Deleon, P. McCown, S. A. Stass and M. Albitar (1993). "THE HUMAN MDM-2 ONCOGENE IS OVEREXPRESSED IN LEUKEMIAS." Blood **82**(9): 2617-2623.

Bulavin, D. V., O. N. Demidov, S. Saito, P. Kauraniemi, C. Phillips, S. A. Amundson, C. Ambrosino, G. Sauter, A. R. Nebreda, C. W. Anderson, A. Kallioniemi, A. J. Fornace and E. Appella (2002). "Amplification of PPM1D in human tumors abrogates p53 tumor-suppressor activity." Nature Genetics **31**(2): 210-215.

Bulavin, D. V., C. Phillips, B. Nannenga, O. Timofeev, L. A. Donehower, C. W. Anderson, E. Appella and A. J. Fornace (2004). "Inactivation of the Wip1 phosphatase inhibits mammary tumorigenesis through p38 MAPK-mediated activation of the p16Ink4a-p19Arf pathway." Nat Genet **36**(4): 343-350.

Bulavin, D. V., S. Saito, M. C. Hollander, K. Sakaguchi, C. W. Anderson, E. Appella and A. J. Fornace (1999). "Phosphorylation of human p53 by p38 kinase coordinates N-terminal phosphorylation and apoptosis in response to UV radiation." The EMBO Journal **18**(23): 6845-6854.

Bumgarner, R. (2013). "Overview of DNA microarrays: types, applications, and their future." Curr Protoc Mol Biol **Chapter 22**: Unit 22.21.

Bunz, F., A. Dutriaux, C. Lengauer, T. Waldman, S. Zhou, J. P. Brown, J. M. Sedivy, K. W. Kinzler and B. Vogelstein (1998). "Requirement for p53 and p21 to Sustain G2 Arrest After DNA Damage." Science **282**(5393): 1497-1501.

Burnette, W. N. (1981). "“Western Blotting”: Electrophoretic transfer of proteins from sodium dodecyl sulfate-polyacrylamide gels to unmodified nitrocellulose and radiographic detection with antibody and radioiodinated protein A." Analytical Biochemistry **112**(2): 195-203.

Bush, K. (1988). "Beta-lactamase inhibitors from laboratory to clinic." Clinical Microbiology Reviews **1**(1): 109-123.

Buss, M. C., T. A. Read, M. J. Schniederjan, K. Gandhi and R. C. Castellino (2012). "HDM2 promotes WIP1-mediated medulloblastoma growth." Neuro-Oncology **14**(4): 440-458.

Cahilly-Snyder, L., T. Yang-Feng, U. Francke and D. L. George (1987). "Molecular analysis and chromosomal mapping of amplified genes isolated from a transformed mouse 3T3 cell line." Somat Cell Mol Genet **13**(3): 235-244.

Caldecott, K. W. (2008). "Single-strand break repair and genetic disease." Nat Rev Genet **9**(8): 619-631.

Call, K. M., T. Glaser, C. Y. Ito, A. J. Buckler, J. Pelletier, D. A. Haber, E. A. Rose, A. Kral, H. Yeger, W. H. Lewis, C. Jones and D. E. Housman (1990). "Isolation and characterization of a zinc finger polypeptide gene at the human chromosome 11 Wilms' tumor locus." Cell **60**(3): 509-520.

Campbell, R. M., B. D. Anderson, N. A. Brooks, H. B. Brooks, E. M. Chan, A. De Dios, R. Gilmour, J. R. Graff, E. Jambrina, M. Mader, D. McCann, S. Na, S. H. Parsons, S. E. Pratt, C. Shih, L. F. Stancato, J. J. Starling, C. Tate, J. A. Velasco, Y.

Wang and X. S. Ye (2014). "Characterization of LY2228820 Dimesylate, a Potent and Selective Inhibitor of p38 MAPK with Antitumor Activity." Molecular Cancer Therapeutics **13**(2): 364-374.

Candau, R., D. M. Scolnick, P. Darpino, C. Y. Ying, T. D. Halazonetis and S. L. Berger (1997). "Two tandem and independent sub-activation domains in the amino terminus of p53 require the adaptor complex for activity." Oncogene **15**(7): 807-816.

Canman, C. E., D.-S. Lim, K. A. Cimprich, Y. Taya, K. Tamai, K. Sakaguchi, E. Appella, M. B. Kastan and J. D. Siliciano (1998). "Activation of the ATM Kinase by Ionizing Radiation and Phosphorylation of p53." Science **281**(5383): 1677-1679.

Cao, C., E. T. Shinohara, T. K. Subhawong, L. Geng, K. W. Kim, J. M. Albert, D. E. Hallahan and B. Lu (2006). "Radiosensitization of lung cancer by nutlin, an inhibitor of murine double minute 2." Molecular Cancer Therapeutics **5**(2): 411-417.

Caron De Fromental, C. and T. Soussi (1992). "TP53 tumor suppressor gene: A model for investigating human mutagenesis." Genes Chromosomes and Cancer **4**(1): 1-15.

Caron, H., P. vanSluis, J. deKraker, J. Bokkerink, M. Egeler, G. Laureys, R. Slater, A. Westerveld, P. A. Voute and R. Versteeg (1996). "Allelic loss of chromosome 1p as a predictor of unfavorable outcome in patients with neuroblastoma." New England Journal of Medicine **334**(4): 225-230.

Carr-Wilkinson, J., K. O'Toole, K. M. Wood, C. C. Challen, A. G. Baker, J. R. Board, L. Evans, M. Cole, N.-K. V. Cheung, J. Boos, G. Köhler, I. Leuschner, A. D. J. Pearson, J. Lunec and D. A. Tweddle (2010). "High Frequency of p53/MDM2/p14ARF Pathway Abnormalities in Relapsed Neuroblastoma." Clinical Cancer Research **16**(4): 1108-1118.

Carrillo, A. M., M. Hicks, D. Khabele and C. M. Eischen (2015). "Pharmacologically Increasing Mdm2 Inhibits DNA Repair and Cooperates with Genotoxic Agents to Kill p53-Inactivated Ovarian Cancer Cells." Mol Cancer Res **13**(8): 1197-1205.

Carvajal, L. A. and J. J. Manfredi (2013). "Another fork in the road—life or death decisions by the tumour suppressor p53." EMBO reports **14**(5): 414-421.

Cary, R. B., S. R. Peterson, J. Wang, D. G. Bear, E. M. Bradbury and D. J. Chen (1997). "DNA looping by Ku and the DNA-dependent protein kinase." Proceedings of the National Academy of Sciences **94**(9): 4267-4272.

Castellino, R., M. De Bortoli, X. Lu, S.-H. Moon, T.-A. Nguyen, M. Shepard, P. Rao, L. Donehower and J. H. Kim (2008). "Medulloblastomas overexpress the p53-inactivating oncogene WIP1/PPM1D." Journal of Neuro-Oncology **86**(3): 245-256.

Celeste, A., O. Fernandez-Capetillo, M. J. Kruhlak, D. R. Pilch, D. W. Staudt, A. Lee, R. F. Bonner, W. M. Bonner and A. Nussenzweig (2003). "Histone H2AX phosphorylation is dispensable for the initial recognition of DNA breaks." Nature Cell Biology **5**(7): 675-U651.

Cha, H., J. M. Lowe, H. Li, J.-S. Lee, G. I. Belova, D. V. Bulavin and A. J. Fornace, Jr. (2010). "Wip1 Directly Dephosphorylates (Y)-H2AX and Attenuates the DNA Damage Response." Cancer Research **70**(10): 4112-4122.

Chaitanya, G., J. Alexander and P. Babu (2010). "PARP-1 cleavage fragments: signatures of cell-death proteases in neurodegeneration." Cell Communication and Signaling **8**(1): 1-11.

Chang, C., D. T. Simmons, M. A. Martin and P. T. Mora (1979). "Identification and partial characterization of new antigens from simian virus 40-transformed mouse cells." Journal of Virology **31**(2): 463-471.

Chang, C. J., D. J. Freeman and H. Wu (2004). "PTEN regulates Mdm2 expression through the P1 promoter." J Biol Chem **279**(28): 29841-29848.

Chao, C., M. Hergenbahn, M. D. Kaeser, Z. Wu, S. i. Saito, R. Iggo, M. Hollstein, E. Appella and Y. Xu (2003). "Cell Type- and Promoter-specific Roles of Ser18 Phosphorylation in Regulating p53 Responses." Journal of Biological Chemistry

278(42): 41028-41033.

Chao, C., D. Herr, J. Chun and Y. Xu (2006). "Ser18 and 23 phosphorylation is required for p53-dependent apoptosis and tumor suppression." The EMBO Journal **25**(11): 2615-2622.

Chao, C., S. Saito, J. Kang, C. W. Anderson, E. Appella and Y. Xu (2000). "p53 transcriptional activity is essential for p53-dependent apoptosis following DNA damage." Embo j **19**(18): 4967-4975.

Chehab, N. H., A. Malikzay, E. S. Stavridi and T. D. Halazonetis (1999).

"Phosphorylation of Ser-20 mediates stabilization of human p53 in response to DNA damage." Proceedings of the National Academy of Sciences **96**(24): 13777-13782.

Chen, B. P. C., D. W. Chan, J. Kobayashi, S. Burma, A. Asaithamby, K. Morotomi-Yano, E. Botvinick, J. Qin and D. J. Chen (2005). "Cell cycle dependence of DNA-dependent protein kinase phosphorylation in response to DNA double strand breaks." Journal of Biological Chemistry **280**(15): 14709-14715.

Chen, J., V. Marechal and A. J. Levine (1993). "Mapping of the p53 and mdm-2 interaction domains." Molecular and Cellular Biology **13**(7): 4107-4114.

Chen, J., X. Wu, J. Lin and A. J. Levine (1996). "mdm-2 inhibits the G1 arrest and apoptosis functions of the p53 tumor suppressor protein." Molecular and Cellular Biology **16**(5): 2445-2452.

Chen, J. D., J. Y. Lin and A. J. Levine (1995). "REGULATION OF TRANSCRIPTION FUNCTIONS OF THE P53 TUMOR-SUPPRESSOR BY THE MDM-2 ONCOGENE." Molecular Medicine **1**(2): 142-152.

Chen, L., S. Agrawal, W. Zhou, R. Zhang and J. Chen (1998). "Synergistic activation of p53 by inhibition of MDM2 expression and DNA damage." Proceedings of the National Academy of Sciences **95**(1): 195-200.

Chen, L., R. F. Rousseau, S. A. Middleton, G. L. Nichols, D. R. Newell, J. Lunec and D. A. Tweddle (2015). Pre-clinical evaluation of the MDM2-p53 antagonist RG7388 alone and in combination with chemotherapy in neuroblastoma.

Chen, X., L. J. Ko, L. Jayaraman and C. Prives (1996). "p53 levels, functional domains, and DNA damage determine the extent of the apoptotic response of tumor cells." Genes & Development **10**(19): 2438-2451.

Chen, Y.-f. and L.-w. Fu (2011). "Mechanisms of acquired resistance to tyrosine kinase inhibitors." Acta Pharmaceutica Sinica B **1**(4): 197-207.

Chene, P., J. Fuchs, J. Bohn, C. Garcia-Echeverria, P. Furet and D. Fabbro (2000). "A small synthetic peptide, which inhibits the p53-hdm2 interaction, stimulates the p53 pathway in tumour cell lines." Journal of Molecular Biology **299**(1): 245-253.

Cho, Y., S. Gorina, P. D. Jeffrey and N. P. Pavletich (1994). "Crystal structure of a p53 tumor suppressor-DNA complex: understanding tumorigenic mutations." Science **265**(5170): 346-355.

Choi, J., B. Nannenga, O. N. Demidov, D. V. Bulavin, A. Cooney, C. Brayton, Y. Zhang, I. N. Mbawuikie, A. Bradley, E. Appella and L. A. Donehower (2002). "Mice Deficient for the Wild-Type p53-Induced Phosphatase Gene (Wip1) Exhibit Defects in Reproductive Organs, Immune Function, and Cell Cycle Control." Molecular and Cellular Biology **22**(4): 1094-1105.

Choi, M., J. Shi, S. H. Jung, X. Chen and K.-H. Cho (2012). "Attractor Landscape Analysis Reveals Feedback Loops in the p53 Network That Control the Cellular Response to DNA Damage." Sci. Signal. **5**(251): ra83-.

Chou, T. C. (2010). "Drug Combination Studies and Their Synergy Quantification Using the Chou-Talalay Method." Cancer Research **70**(2): 440-446.

Chou, T. C. and P. Talalay (1984). "Quantitative analysis of dose-effect relationships: the combined effects of multiple drugs or enzyme inhibitors." Adv Enzyme Regul **22**: 27-55.

Chuman, Y., W. Kurihashi, Y. Mizukami, T. Nashimoto, H. Yagi and K. Sakaguchi (2009). "PPM1D430, a Novel Alternative Splicing Variant of the Human PPM1D, can Dephosphorylate p53 and Exhibits Specific Tissue Expression." Journal of Biochemistry **145**(1): 1-12.

Clarke, A. R., C. A. Purdie, D. J. Harrison, R. G. Morris, C. C. Bird, M. L. Hooper and A. H. Wyllie (1993). "Thymocyte apoptosis induced by p53-dependent and independent pathways." Nature **362**(6423): 849-852.

Clore, G. M., J. G. Omichinski, K. Sakaguchi, N. Zambrano, H. Sakamoto, E. Appella and A. M. Gronenborn (1994). "HIGH-RESOLUTION STRUCTURE OF THE OLIGOMERIZATION DOMAIN OF P53 BY MULTIDIMENSIONAL NMR." Science **265**(5170): 386-391.

Conradt, L., A. Henrich, M. Wirth, M. Reichert, M. Lesina, H. Algul, R. M. Schmid, O. H. Kramer, D. Saur and G. Schneider (2013). "Mdm2 inhibitors synergize with topoisomerase II inhibitors to induce p53-independent pancreatic cancer cell death." International Journal of Cancer **132**(10): 2248-2257.

Cordoncardo, C., E. Latres, M. Drobnjak, M. R. Oliva, D. Pollack, J. M. Woodruff, V. Marechal, J. D. Chen, M. F. Brennan and A. J. Levine (1994). "MOLECULAR ABNORMALITIES OF MDM2 AND P53 GENES IN ADULT SOFT-TISSUE SARCOMAS." Cancer Research **54**(3): 794-799.

Cortez, D., S. Guntuku, J. Qin and S. J. Elledge (2001). "ATR and ATRIP: Partners in Checkpoint Signaling." Science **294**(5547): 1713-1716.

Cosme-Blanco, W., M. F. Shen, A. J. F. Lazar, S. Pathak, G. Lozano, A. S. Multani and S. Chang (2007). "Telomere dysfunction suppresses spontaneous tumorigenesis in vivo by initiating p53-dependent cellular senescence." EMBO reports **8**(5): 497-503.

Crawford, L. V., D. C. Pim and R. D. Bulbrook (1982). "DETECTION OF ANTIBODIES AGAINST THE CELLULAR PROTEIN P53 IN SERA FROM PATIENTS WITH BREAST-CANCER." International Journal of Cancer **30**(4): 403-408.

Dang, C. V. and W. M. F. Lee (1989). "NUCLEAR AND NUCLEOLAR TARGETING SEQUENCES OF C-ERB-A, C-MYB, N-MYC, P53, HSP70, AND HIV TAT PROTEINS." Journal of Biological Chemistry **264**(30): 18019-18023.

Das, S., L. Raj, B. Zhao, Y. Kimura, A. Bernstein, S. A. Aaronson and S. W. Lee (2007). "Hzf determines cell survival upon genotoxic stress by modulating p53 transactivation." Cell **130**(4): 624-637.

Dashzeveg, N. and K. Yoshida (2015). "Cell death decision by p53 via control of the mitochondrial membrane." Cancer Letters **367**(2): 108-112.

De Leo, A. B., G. Jay, E. Appella, G. C. Dubois, L. W. Law and L. J. Old (1979). "Detection of a transformation-related antigen in chemically induced sarcomas and other transformed cells of the mouse." Proc Natl Acad Sci USA : **76**: 2420-2424.

de Oca Luna, R. M., D. S. Wagner and G. Lozano (1995). "Rescue of early embryonic lethality in mdm2-deficient mice by deletion of p53." Nature **378**(6553): 203-206.

de Rozières, S., R. Maya, M. Oren and G. Lozano (2000). "The loss of mdm2 induces p53 mediated apoptosis." Oncogene **19**(13): 1691-1697.

de Stanchina, E., M. E. McCurrach, F. Zindy, S. Y. Shieh, G. Ferbeyre, A. V. Samuelson, C. Prives, M. F. Roussel, C. J. Sherr and S. W. Lowe (1998). "E1A signaling to p53 involves the p19(ARF) tumor suppressor." Genes Dev **12**(15): 2434-2442.

DeFazio, L. G., R. M. Stansel, J. D. Griffith and G. Chu (2002). "Synapsis of DNA ends by DNA-dependent protein kinase." EMBO J. **21**(12): 3192–3200.

Demidenko, Z. N., L. G. Korotchikina, A. V. Gudkov and M. V. Blagosklonny (2010). "Paradoxical suppression of cellular senescence by p53." Proceedings of the National Academy of Sciences **107**(21): 9660-9664.

Deng, C. X., P. M. Zhang, J. W. Harper, S. J. Elledge and P. Leder (1995). "Mice lacking p21(CIP1/WAF1) undergo normal development, but are defective in G1 Checkpoint control." *Cell* **82**(4): 675-684.

Di Micco, R., M. Fumagalli, A. Cicalese, S. Piccinin, P. Gasparini, C. Luise, C. Schurra, M. Garre, P. Giovanni Nuciforo, A. Bensimon, R. Maestro, P. Giuseppe Pelicci and F. d'Adda di Fagagna (2006). "Oncogene-induced senescence is a DNA damage response triggered by DNA hyper-replication." *Nature* **444**(7119): 638-642.

Ding, Q., Z. Zhang, J.-J. Liu, N. Jiang, J. Zhang, T. M. Ross, X.-J. Chu, D. Bartkovitz, F. Podlaski, C. Janson, C. Tovar, Z. M. Filipovic, B. Higgins, K. Glenn, K. Packman, L. T. Vassilev and B. Graves (2013). "Discovery of RG7388, a Potent and Selective p53–MDM2 Inhibitor in Clinical Development." *Journal of Medicinal Chemistry* **56**(14): 5979-5983.

Dittmer, D., S. Pati, G. Zambetti, S. Chu, A. K. Teresky, M. Moore, C. Finlay and A. J. Levine (1993). "GAIN OF FUNCTION MUTATIONS IN P53." *Nature Genetics* **4**(1): 42-46.

Donehower, L. A. (2014). "Phosphatases reverse p53-mediated cell cycle checkpoints." *Proceedings of the National Academy of Sciences* **111**(20): 7172-7173.

Donehower, L. A. and A. Bradley (1993). "The tumore suppressor p53." *Biochimica et Biophysica Acta (BBA) - Reviews on Cancer* **1155**(2): 181-205.

Donehower, L. A., M. Harvey, B. L. Slagle, M. J. McArthur, C. A. Montgomery, J. S. Butel and A. Bradley (1992). "MICE DEFICIENT FOR P53 ARE DEVELOPMENTALLY NORMAL BUT SUSCEPTIBLE TO SPONTANEOUS TUMORS." *Nature* **356**(6366): 215-221.

Doyle, B., J. P. Morton, D. W. Delaney, R. A. Ridgway, J. A. Wilkins and O. J. Sansom (2010). "p53 mutation and loss have different effects on tumourigenesis in a novel mouse model of pleomorphic rhabdomyosarcoma." *The Journal of Pathology* **222**(2): 129-137.

Du, P., W. A. Kibbe and S. M. Lin (2008). "lumi: a pipeline for processing Illumina microarray." *Bioinformatics* **24**(13): 1547-1548.

Dudgeon, C., S. Shreeram, K. Tanoue, S. J. Mazur, A. Sayadi, R. C. Robinson, E. Appella and D. V. Bulavin (2013). "Genetic variants and mutations of PPM1D control the response to DNA damage." *Cell Cycle* **12**(16): 2656-2664.

Dumaz, N. and D. W. Meek (1999). "Serine15 phosphorylation stimulates p53 transactivation but does not directly influence interaction with HDM2." *The EMBO Journal* **18**(24): 7002-7010.

Duprez, L., E. Wirawan, T. V. Berghe and P. Vandenabeele (2009). "Major cell death pathways at a glance." *Microbes and Infection* **11**(13): 1050-1062.

Eck-Enriquez, K., T. L. Kiefer, L. L. Spriggs and S. M. Hill (2000). "Pathways through which a regimen of melatonin and retinoic acid induces apoptosis in MCF-7 human breast cancer cells." *Breast Cancer Res Treat* **61**(3): 229-239.

Elbashir, S. M., J. Harborth, W. Lendeckel, A. Yalcin, K. Weber and T. Tuschl (2001). "Duplexes of 21-nucleotide RNAs mediate RNA interference in cultured mammalian cells." *Nature* **411**(6836): 494-498.

Elbashir, S. M., J. Martinez, A. Patkaniowska, W. Lendeckel and T. Tuschl (2001). "Functional anatomy of siRNAs for mediating efficient RNAi in *Drosophila melanogaster* embryo lysate." *The EMBO Journal* **20**(23): 6877-6888.

Eldeiry, W. S., J. W. Harper, P. M. Oconnor, V. E. Velculescu, C. E. Canman, J. Jackman, J. A. Pietenpol, M. Burrell, D. E. Hill, Y. S. Wang, K. G. Wiman, W. E. Mercer, M. B. Kastan, K. W. Kohn, S. J. Elledge, K. W. Kinzler and B. Vogelstein (1994). "WAF1/CIP1 is induced in p53-mediated G(1) arrest and apoptosis." *Cancer Research* **54**(5): 1169-1174.

Eldeiry, W. S., S. E. Kern, J. A. Pietenpol, K. W. Kinzler and B. Vogelstein (1992).

"DEFINITION OF A CONSENSUS BINDING-SITE FOR P53." Nature Genetics **1**(1): 45-49.

Eldeiry, W. S., T. Tokino, V. E. Velculescu, D. B. Levy, R. Parsons, J. M. Trent, D. Lin, W. E. Mercer, K. W. Kinzler and B. Vogelstein (1993). "WAF1, A POTENTIAL MEDIATOR OF P53 TUMOR SUPPRESSION." Cell **75**(4): 817-825.

Eliyahu, D., A. Raz, P. Gruss, D. Givol and M. Oren (1984). "Participation of p53 cellular tumour antigen in transformation of normal embryonic cells." Nature **312**(5995): 646-649.

Espinosa, J. M. (2008). "Mechanisms of regulatory diversity within the p53 transcriptional network." Oncogene **27**(29): 4013-4023.

Espinosa, J. M., R. E. Verdun and B. M. Emerson (2003). "p53 functions through stress- and promoter-specific recruitment of transcription initiation components before and after DNA damage." Mol Cell **12**(4): 1015-1027.

Fakharzadeh, S. S., S. P. Trusko and D. L. George (1991). "TUMORIGENIC POTENTIAL ASSOCIATED WITH ENHANCED EXPRESSION OF A GENE THAT IS AMPLIFIED IN A MOUSE-TUMOR CELL-LINE." EMBO Journal **10**(6): 1565-1569.

Fang, S., J. P. Jensen, R. L. Ludwig, K. H. Vousden and A. M. Weissman (2000). "Mdm2 Is a RING Finger-dependent Ubiquitin Protein Ligase for Itself and p53." Journal of Biological Chemistry **275**(12): 8945-8951.

Farmer, G., J. Bargonetti, H. Zhu, P. Friedman, R. Prywes and C. Prives (1992). "WILD-TYPE P53 ACTIVATES TRANSCRIPTION INVITRO." Nature **358**(6381): 83-86.

Fearon, E. R. and B. Vogelstein (1990). "A genetic model for colorectal tumorigenesis." Cell **61**(5): 759-767.

Feng, L., M. Hollstein and Y. Xu (2006). "Ser46 Phosphorylation Regulates p53-Dependent Apoptosis and Replicative Senescence." Cell Cycle **5**(23): 2812-2819.

Feng, L., T. Lin, H. Uranishi, W. Gu and Y. Xu (2005). "Functional Analysis of the Roles of Posttranslational Modifications at the p53 C Terminus in Regulating p53 Stability and Activity." Molecular and Cellular Biology **25**(13): 5389-5395.

Ferreon, J. C., C. W. Lee, M. Arai, M. A. Martinez-Yamout, H. J. Dyson and P. E. Wright (2009). "Cooperative regulation of p53 by modulation of ternary complex formation with CBP/p300 and HDM2." Proceedings of the National Academy of Sciences **106**(16): 6591-6596.

Fields, S. and S. K. Jang (1990). "PRESENCE OF A POTENT TRANSCRIPTION ACTIVATING SEQUENCE IN THE P53 PROTEIN." Science **249**(4972): 1046-1049.

Finch, R. A., D. B. Donoviel, D. Potter, M. Shi, A. Fan, D. D. Freed, C.-y. Wang, B. P. Zambrowicz, R. Ramirez-Solis, A. T. Sands and N. Zhang (2002). "mdmx Is a Negative Regulator of p53 Activity in Vivo." Cancer Research **62**(11): 3221-3225.

Finlay, C. A., P. W. Hinds and A. J. Levine (1989). "THE P53 PROTO-ONCOGENE CAN ACT AS A SUPPRESSOR OF TRANSFORMATION." Cell **57**(7): 1083-1093.

Finlay, C. A., P. W. Hinds, T. H. Tan, D. Eliyahu, M. Oren and A. J. Levine (1988). "Activating mutations for transformation by p53 produce a gene product that forms an hsc70-p53 complex with an altered half-life." Molecular and Cellular Biology **8**(2): 531-539.

Fire, A., S. Xu, M. K. Montgomery, S. A. Kostas, S. E. Driver and C. C. Mello (1998). "Potent and specific genetic interference by double-stranded RNA in *Caenorhabditis elegans*." Nature **391**(6669): 806-811.

Fiscella, M., S. J. Ullrich, N. Zambrano, M. T. Shields, D. Lin, S. P. Lees-Miller, C. W. Anderson, W. E. Mercer and E. Appella (1993). "Mutation of the serine 15 phosphorylation site of human p53 reduces the ability of p53 to inhibit cell cycle progression." Oncogene **8**(6): 1519-1528.

Fiscella, M., H. L. Zhang, S. J. Fan, K. Sakaguchi, S. F. Shen, W. E. Mercer, G. F. VandeWoude, P. M. Oconnor and E. Appella (1997). "Wip1, a novel human protein phosphatase that is induced in response to ionizing radiation in a p53-dependent manner." Proceedings of the National Academy of Sciences of the United States of America **94**(12): 6048-6053.

Forbes, S. A., D. Beare, P. Gunasekaran, K. Leung, N. Bindal, H. Boutselakis, M. Ding, S. Bamford, C. Cole, S. Ward, C. Y. Kok, M. Jia, T. De, J. W. Teague, M. R. Stratton, U. McDermott and P. J. Campbell (2015). "COSMIC: exploring the world's knowledge of somatic mutations in human cancer." Nucleic Acids Research **43**(D1): D805-D811.

Fridman, J. S. and S. W. Lowe (2003). "Control of apoptosis by p53." Oncogene **22**(56): 9030-9040.

Fujimoto, H., N. Onishi, N. Kato, M. Takekawa, X. Z. Xu, A. Kosugi, T. Kondo, M. Imamura, I. Oishi, A. Yoda and Y. Minami (2005). "Regulation of the antioncogenic Chk2 kinase by the oncogenic Wip1 phosphatase." Cell Death Differ **13**(7): 1170-1180.

Fuku, T., S. Semba, H. Yutori and H. Yokozaki (2007). "Increased wild-type p53-induced phosphatase 1 (Wip1 or PPM1D) expression correlated with downregulation of checkpoint kinase 2 in human gastric carcinoma." Pathology International **57**(9): 566-571.

Funk, W. D., D. T. Pak, R. H. Karas, W. E. Wright and J. W. Shay (1992). "A TRANSCRIPTIONALLY ACTIVE DNA-BINDING SITE FOR HUMAN P53 PROTEIN COMPLEXES." Molecular and Cellular Biology **12**(6): 2866-2871.

Gamble, L. D., U. R. Kees, D. A. Tweddle and J. Lunec (2012). "MYCN sensitizes neuroblastoma to the MDM2-p53 antagonists Nutlin-3 and MI-63." Oncogene **31**(6): 752-763.

Gannon, Hugh S., Bruce A. Woda and Stephen N. Jones (2012). "ATM Phosphorylation of Mdm2 Ser394 Regulates the Amplitude and Duration of the DNA Damage Response in Mice." Cancer Cell **21**(5): 668-679.

Gannon, J. V., R. Greaves, R. Iggo and D. P. Lane (1990). "ACTIVATING MUTATIONS IN P53 PRODUCE A COMMON CONFORMATIONAL EFFECT - A MONOCLONAL-ANTIBODY SPECIFIC FOR THE MUTANT FORM." EMBO Journal **9**(5): 1595-1602.

Garber, J. E. and K. Offit (2005). "Hereditary cancer predisposition syndromes." J Clin Oncol **23**(2): 276-292.

Garnett, M. J., E. J. Edelman, S. J. Heidorn, C. D. Greenman, A. Dastur, K. W. Lau, P. Greninger, I. R. Thompson, X. Luo, J. Soares, Q. Liu, F. Iorio, D. Surdez, L. Chen, R. J. Milano, G. R. Bignell, A. T. Tam, H. Davies, J. A. Stevenson, S. Barthorpe, S. R. Lutz, F. Kogera, K. Lawrence, A. McLaren-Douglas, X. Mitropoulos, T. Mironenko, H. Thi, L. Richardson, W. Zhou, F. Jewitt, T. Zhang, P. O'Brien, J. L. Boisvert, S. Price, W. Hur, W. Yang, X. Deng, A. Butler, H. G. Choi, J. W. Chang, J. Baselga, I. Stamenkovic, J. A. Engelman, S. V. Sharma, O. Delattre, J. Saez-Rodriguez, N. S. Gray, J. Settleman, P. A. Futreal, D. A. Haber, M. R. Stratton, S. Ramaswamy, U. McDermott and C. H. Benes (2012). "Systematic identification of genomic markers of drug sensitivity in cancer cells." Nature **483**(7391): 570-575.

Gembarska, A., F. Luciani, C. Fedele, E. A. Russell, M. Dewaele, S. Villar, A. Zwolinska, S. Haupt, J. de Lange, D. Yip, J. Goydos, J. J. Haigh, Y. Haupt, L. Larue, A. Jochemsen, H. Shi, G. Moriceau, R. S. Lo, G. Ghanem, M. Shackleton, F. Bernal and J.-C. Marine (2012). "MDM4 is a key therapeutic target in cutaneous melanoma." Nat Med **18**(8): 1239-1247.

Gilmartin, A. G., T. H. Fajt, M. Richter, A. Groy, M. A. Seefeld, M. G. Darcy, X. Peng, K. Federowicz, J. Yang, S.-Y. Zhang, E. Minthorn, J.-P. Jaworski, M. Schaber, S. Martens, D. E. McNulty, R. H. Sinnamon, H. Zhang, R. B. Kirkpatrick, N. Nevins, G. Cui, B. Pietrak, E. Diaz, A. Jones, M. Brandt, B. Schwartz, D. A. Heerding and R.

Kumar (2014). "Allosteric Wip1 phosphatase inhibition through flap-subdomain interaction." Nat Chem Biol **10**(3): 181-187.

Ginsberg, D., F. Mechta, M. Yaniv and M. Oren (1991). "WILD-TYPE P53 CAN DOWN-MODULATE THE ACTIVITY OF VARIOUS PROMOTERS." Proceedings of the National Academy of Sciences of the United States of America **88**(22): 9979-9983.

Gobeil, S., C. C. Boucher, D. Nadeau and G. G. Poirier (2001). "Characterization of the necrotic cleavage of poly(ADP-ribose) polymerase (PARP-1): implication of lysosomal proteases." Cell Death Differ **8**(6): 588-594.

Gorina, S. and N. P. Pavletich (1996). "Structure of the p53 tumor suppressor bound to the ankyrin and SH3 domains of 53BP2." Science **274**(5289): 1001-1005.

Gottesman, M. M., T. Fojo and S. E. Bates (2002). "Multidrug resistance in cancer: role of ATP-dependent transporters." Nat Rev Cancer **2**(1): 48-58.

Gottlieb, T. M. and S. P. Jackson (1993). "The DNA-dependent protein kinase: requirement for DNA ends and association with Ku antigen." Cell **72**(1): 131-142.

Goarani, O. "Site Directed Mutagenesis with Stratagene Pfu Turbo." from <http://web.stanford.edu/group/goarani/cgi-bin/goaranilab/wp-content/uploads/2014/01/Site-Directed-Mutagenesis-with-Stratagene-Pfu-Turbo.pdf>.

Graves, B., T. Thompson, M. Xia, C. Janson, C. Lukacs, D. Deo, P. Di Lello, D. Fry, C. Garvie, K.-S. Huang, L. Gao, C. Tovar, A. Lovey, J. Wanner and L. T. Vassilev (2012). "Activation of the p53 pathway by small-molecule-induced MDM2 and MDMX dimerization." Proceedings of the National Academy of Sciences **109**(29): 11788-11793.

Greaves, M. and C. C. Maley (2012). "Clonal evolution in cancer." Nature **481**(7381): 306-313.

Grier, J. D., S. Xiong, A. C. Elizondo-Fraire, J. M. Parant and G. Lozano (2006). "Tissue-Specific Differences of p53 Inhibition by Mdm2 and Mdm4." Molecular and Cellular Biology **26**(1): 192-198.

Grunbaum, U., A. Meye, M. Bache, F. Bartel, P. Wurl, H. Schmidt, J. Dunst and H. Taubert (2001). "Transfection with mdm2-antisense or wtp53 results in radio sensitization and an increased apoptosis of a soft tissue sarcoma cell line." Anticancer Research **21**(3B): 2065-2071.

Hainaut, P. and M. Hollstein (2000). "p53 and human cancer: the first ten thousand mutations." Adv Cancer Res **77**: 81-137.

Hainaut, P. and J. Milner (1993). "REDOX MODULATION OF P53 CONFORMATION AND SEQUENCE-SPECIFIC DNA-BINDING IN-VITRO." Cancer Research **53**(19): 4469-4473.

Hainaut, P. and J. Milner (1993). "A STRUCTURAL ROLE FOR METAL-IONS IN THE WILD-TYPE CONFORMATION OF THE TUMOR SUPPRESSOR PROTEIN-P53." Cancer Research **53**(8): 1739-1742.

Haines, D. S., J. E. Landers, L. J. Engle and D. L. George (1994). "PHYSICAL AND FUNCTIONAL INTERACTION BETWEEN WILD-TYPE P53 AND MDM2 PROTEINS." Molecular and Cellular Biology **14**(2): 1171-1178.

Halazonetis, T. D. and A. N. Kandil (1993). "CONFORMATIONAL SHIFTS PROPAGATE FROM THE OLIGOMERIZATION DOMAIN OF P53 TO ITS TETRAMERIC DNA-BINDING DOMAIN AND RESTORE DNA-BINDING TO SELECT P53 MUTANTS." EMBO Journal **12**(13): 5057-5064.

Hanahan, D. and R. A. Weinberg (2000). "The Hallmarks of Cancer." Cell **100**(1): 57-70.

Hanahan, D. and Robert A. Weinberg (2011). "Hallmarks of Cancer: The Next Generation." Cell **144**(5): 646-674.

Haneda, M., E. Kojima, A. Nishikimi, T. Hasegawa, I. Nakashima and K. I. Isobe

(2004). "Protein phosphatase 1, but not protein phosphatase 2A, dephosphorylates DNA-damaging stress-induced phospho-serine 15 of p53." *FEBS Letters* **567**(2-3): 171-174.

Hannon, G. J. (2002). "RNA interference." *Nature* **418**(6894): 244-251.

Harper, J. W., G. R. Adami, N. Wei, K. Keyomarsi and S. J. Elledge (1993). "The p21 Cdk-interacting protein Cip1 is a potent inhibitor of G1 cyclin-dependent kinases." *Cell* **75**(4): 805-816.

Harris, H., O. J. Miller, G. Klein, P. Worst and T. Tachibana (1969). "Suppression of Malignancy by Cell Fusion." *Nature* **223**(5204): 363-368.

Harris, S. L. and A. J. Levine (2005). "The p53 pathway: positive and negative feedback loops." *Cell* **121**(7): 2899-2908.

Hartwell, L. H. and T. A. Weinert (1989). "Checkpoints: controls that ensure the order of cell cycle events." *Science* **246**(4930): 629-634.

Haupt, Y., R. Maya, A. Kazanietz and M. Oren (1997). "Mdm2 promotes the rapid degradation of p53." *Nature* **387**(6630): 296-299.

Hayashi, R., K. Tanoue, S. R. Durell, D. K. Chatterjee, L. M. M. Jenkins, D. H. Appella and E. Appella (2011). "Optimization of a Cyclic Peptide Inhibitor of Ser/Thr Phosphatase PPM1D (Wip1)." *Biochemistry* **50**(21): 4537-4549.

Helleday, T. (2011). "The underlying mechanism for the PARP and BRCA synthetic lethality: Clearing up the misunderstandings." *Molecular Oncology* **5**(4): 387-393.

Hermeking, H., C. Lengauer, K. Polyak, T. C. He, L. Zhang, S. Thiagalingam, K. W. Kinzler and B. Vogelstein (1997). "14-3-3 sigma is a p53-regulated inhibitor of G2/M progression." *Mol Cell* **1**(1): 3-11.

Hickson, I., Y. Zhao, C. J. Richardson, S. J. Green, N. M. B. Martin, A. I. Orr, P. M. Reaper, S. P. Jackson, N. J. Curtin and G. C. M. Smith (2004). "Identification and Characterization of a Novel and Specific Inhibitor of the Ataxia-Telangiectasia Mutated Kinase ATM." *Cancer Research* **64**(24): 9152-9159.

Hirasawa, A., F. Saito-Ohara, J. Inoue, D. Aoki, N. Susumu, T. Yokoyama, S. Nozawa, J. Inazawa and I. Imoto (2003). "Association of 17q21-q24 gain in ovarian clear cell adenocarcinomas with poor prognosis and identification of PPM1D and APPBP2 as likely amplification targets." *Clin Cancer Res* **9**(6): 1995-2004.

Hochegger, H., D. Dejsuphong, T. Fukushima, C. Morrison, E. Sonoda, V. Schreiber, G. Y. Zhao, A. Saberi, M. Masutani, N. Adachi, H. Koyama, G. de Murcia and S. Takeda (2006). "Parp-1 protects homologous recombination from interference by Ku and Ligase IV in vertebrate cells." *EMBO J* **25**(6): 1305-1314.

Hollstein, M., D. Sidransky, B. Vogelstein and C. C. Harris (1991). "p53 mutations in human cancers." *Science* **253**(5015): 49-53.

Honda, R., H. Tanaka and H. Yasuda (1997). "Oncoprotein MDM2 is a ubiquitin ligase E3 for tumor suppressor p53." *FEBS Letters* **420**(1): 25-27.

Honda, R. and H. Yasuda (2000). "Activity of MDM2, a ubiquitin Ligase, toward p53 or itself is dependent on the RING finger domain of the ligase." *Oncogene* **19**(11): 1473-1476.

Hu, B., D. M. Gilkes, B. Farooqi, S. M. Sebt and J. Chen (2006). "MDMX Overexpression Prevents p53 Activation by the MDM2 Inhibitor Nutlin." *Journal of Biological Chemistry* **281**(44): 33030-33035.

Huang, B., D. Deo, M. Xia and L. T. Vassilev (2009). "Pharmacologic p53 Activation Blocks Cell Cycle Progression but Fails to Induce Senescence in Epithelial Cancer Cells." *Molecular Cancer Research* **7**(9): 1497-1509.

Huang, L.-c., K. C. Clarkin and G. M. Wahl (1996). "p53-dependent Cell Cycle Arrests Are Preserved in DNA-activated Protein Kinase-deficient Mouse Fibroblasts." *Cancer Research* **56**(13): 2940-2944.

Hupp, T. R. and D. P. Lane (1994). "ALLOSTERIC ACTIVATION OF LATENT P53

TETRAMERS." Current Biology **4**(10): 865-875.

Hupp, T. R., A. Sparks and D. P. Lane (1995). "SMALL PEPTIDES ACTIVATE THE LATENT SEQUENCE-SPECIFIC DNA-BINDING FUNCTION OF P53." Cell **83**(2): 237-245.

Iancu-Rubin, C., G. Mosoyan, K. Glenn, R. E. Gordon, G. L. Nichols and R. Hoffman (2014). "Activation of p53 by the MDM2 inhibitor RG7112 impairs thrombopoiesis." Experimental Hematology **42**(2): 137-145.e135.

Iwabuchi, K., P. L. Bartel, B. Li, R. Marraccino and S. Fields (1994). "2 CELLULAR PROTEINS THAT BIND TO WILD-TYPE BUT NOT MUTANT P53." Proceedings of the National Academy of Sciences of the United States of America **91**(13): 6098-6102.

Iwabuchi, K., B. Li, H. F. Massa, B. J. Trask, T. Date and S. Fields (1998). "Stimulation of p53-mediated transcriptional activation by the p53-binding proteins, 53BP1 and 53BP2." Journal of Biological Chemistry **273**(40): 26061-26068.

Iwakuma, T. and G. Lozano (2003). "MDM2, An Introduction." Molecular Cancer Research **1**(14): 993-1000.

Iwakuma, T. and G. Lozano (2003). "MDM2, an introduction." Mol Cancer Res **1**(14): 993-1000.

Jänicke, R. U., M. L. Sprengart, M. R. Wati and A. G. Porter (1998). "Caspase-3 Is Required for DNA Fragmentation and Morphological Changes Associated with Apoptosis." Journal of Biological Chemistry **273**(16): 9357-9360.

Jeffrey, P. D., S. Gorina and N. P. Pavletich (1995). "Crystal structure of the tetramerization domain of the p53 tumor suppressor at 1.7 angstroms." Science **267**(5203): 1498-1502.

Jenkins, J. R., P. Chumakov, C. Addison, H. W. Sturzbecher and A. Wadevans (1988). "2 DISTINCT REGIONS OF THE MURINE-P53 PRIMARY AMINO-ACID SEQUENCE ARE IMPLICATED IN STABLE COMPLEX-FORMATION WITH SIMIAN VIRUS-40 T-ANTIGEN." Journal of Virology **62**(10): 3903-3906.

Jenkins, J. R., K. Rudge, P. Chumakov and G. A. Currie (1985). "The cellular oncogene p53 can be activated by mutagenesis." Nature **317**(6040): 816-818.

Jenkins, J. R., K. Rudge and G. A. Currie (1984). "CELLULAR IMMORTALIZATION BY A CDNA CLONE ENCODING THE TRANSFORMATION-ASSOCIATED PHOSPHOPROTEIN P53." Nature **312**(5995): 651-654.

Jenkins, L. M., S. R. Durell, S. J. Mazur and E. Appella (2012). "p53 N-terminal phosphorylation: a defining layer of complex regulation." Carcinogenesis **33**(8): 1441-1449.

Ji, Z., R. Kumar, M. Taylor, A. Rajadurai, A. Marzuka-Alcala, Y. E. Chen, C.-N. J. Njauw, K. Flaherty, G. Jonsson and H. Tsao (2013). "Vemurafenib Synergizes with Nutlin-3 to Deplete Survivin and Suppresses Melanoma Viability and Tumor Growth." Clinical Cancer Research **19**(16): 4383-4391.

Jiang, D., C. A. Brady, T. M. Johnson, E. Y. Lee, E. J. Park, M. P. Scott and L. D. Attardi (2011). "Full p53 transcriptional activation potential is dispensable for tumor suppression in diverse lineages." Proceedings of the National Academy of Sciences **108**(41): 17123-17128.

Jimenez, G. S., M. Nister, J. M. Stommel, M. Beeche, E. A. Barcarse, X. Q. Zhang, S. O'Gorman and G. M. Wahl (2000). "A transactivation-deficient mouse model provides insights into Trp53 regulation and function." Nat Genet **26**(1): 37-43.

Jin, X., E. Turcott, S. Englehardt, G. J. Mize and D. R. Morris (2003). "The two upstream open reading frames of oncogene mdm2 have different translational regulatory properties." J Biol Chem **278**(28): 25716-25721.

Johnson, T. M., E. M. Hammond, A. Giaccia and L. D. Attardi (2005). "The p53QS transactivation-deficient mutant shows stress-specific apoptotic activity and induces embryonic lethality." Nat Genet **37**(2): 145-152.

Jones, R. G., D. R. Plas, S. Kubek, M. Buzzai, J. Mu, Y. Xu, M. J. Birnbaum and C. B. Thompson (2005). "AMP-activated protein kinase induces a p53-dependent metabolic checkpoint." *Mol Cell* **18**(3): 283-293.

Jones, R. J., C. C. Bjorklund, V. Baladandayuthapani, D. J. Kuhn and R. Z. Orłowski (2012). "Drug resistance to inhibitors of the human double minute-2 E3 ligase is mediated by point mutations of p53, but can be overcome with the p53 targeting agent RITA." *Mol Cancer Ther* **11**(10): 2243-2253.

Jones, S. N., A. E. Roe, L. A. Donehower and A. Bradley (1995). "RESCUE OF EMBRYONIC LETHALITY IN MDM2-DEFICIENT MICE BY ABSENCE OF P53." *Nature* **378**(6553): 206-208.

Karlsson, A., D. Deb-Basu, A. Cherry, S. Turner, J. Ford and D. W. Felsher (2003). "Defective double-strand DNA break repair and chromosomal translocations by MYC overexpression." *Proceedings of the National Academy of Sciences* **100**(17): 9974-9979.

Kawase, T., R. Ohki, T. Shibata, S. Tsutsumi, N. Kamimura, J. Inazawa, T. Ohta, H. Ichikawa, H. Aburatani, F. Tashiro and Y. Taya (2009). "PH domain-only protein PHLDA3 is a p53-regulated repressor of Akt." *Cell* **136**(3): 535-550.

Kern, S. E., K. W. Kinzler, S. J. Baker, J. M. Nigro, V. Rotter, A. J. Levine, P. Friedman, C. Prives and B. Vogelstein (1991). "MUTANT P53 PROTEINS BIND DNA ABNORMALLY INVITRO." *Oncogene* **6**(1): 131-136.

Kern, S. E., J. A. Pietenpol, S. Thiagalingam, A. Seymour, K. W. Kinzler and B. Vogelstein (1992). "ONCOGENIC FORMS OF P53 INHIBIT P53-REGULATED GENE-EXPRESSION." *Science* **256**(5058): 827-830.

Kerr, J. F. R., A. H. Wyllie and A. R. Currie (1972). "Apoptosis: A Basic Biological Phenomenon with Wide-ranging Implications in Tissue Kinetics." *British Journal of Cancer* **26**(4): 239-257.

Khoo, K. H., C. S. Verma and D. P. Lane (2014). "Drugging the p53 pathway: understanding the route to clinical efficacy." *Nat Rev Drug Discov* **13**(3): 217-236.

Khoury, M. P. and J. C. Bourdon (2010). "The Isoforms of the p53 Protein." *Cold Spring Harbor Perspectives in Biology* **2**(3).

Kleiblova, P., I. A. Shaltiel, J. Benada, J. Ševčík, S. Pecháčková, P. Pohlreich, E. E. Voest, P. Dundr, J. Bartek, Z. Kleibl, R. H. Medema and L. Macurek (2013). "Gain-of-function mutations of PPM1D/Wip1 impair the p53-dependent G1 checkpoint." *The Journal of Cell Biology* **201**(4): 511-521.

Knudson, A. G. (1971). "Mutation and Cancer: Statistical Study of Retinoblastoma." *Proceedings of the National Academy of Sciences of the United States of America* **68**(4): 820-823.

Ko, L. J. and C. Prives (1996). "p53: Puzzle and paradigm." *Genes & Development* **10**(9): 1054-1072.

Kraiss, S., A. Quaiser, M. Oren and M. Montenarh (1988). "OLIGOMERIZATION OF ONCOPROTEIN-P53." *Journal of Virology* **62**(12): 4737-4744.

Kress, M., E. May, R. Cassingena and P. May (1979). "Simian virus 40-transformed cells express new species of proteins precipitable by anti-simian virus 40 tumor serum." *Journal of Virology* **31**(2): 472-483.

Krummel, K. A., C. J. Lee, F. Toledo and G. M. Wahl (2005). "The C-terminal lysines fine-tune P53 stress responses in a mouse model but are not required for stability control or transactivation." *Proceedings of the National Academy of Sciences of the United States of America* **102**(29): 10188-10193.

Kruse, J.-P. and W. Gu (2009). "Modes of p53 Regulation." *Cell* **137**(4): 609-622.

Kubbutat, M. H. G., S. N. Jones and K. H. Vousden (1997). "Regulation of p53 stability by Mdm2." *Nature* **387**(6630): 299-303.

Kuhn, K., S. C. Baker, E. Chudin, M. H. Lieu, S. Oeser, H. Bennett, P. Rigault, D.

Barker, T. K. McDaniel and M. S. Chee (2004). "A novel, high-performance random array platform for quantitative gene expression profiling." Genome Res **14**(11): 2347-2356.

Kussie, P. H., S. Gorina, V. Marechal, B. Elenbaas, J. Moreau, A. J. Levine and N. P. Pavletich (1996). "Structure of the MDM2 Oncoprotein Bound to the p53 Tumor Suppressor Transactivation Domain." Science **274**(5289): 948-953.

Lab, L. S. (2011). "Phase Contrast Microscope." from <http://www.leica-microsystems.com/science-lab/phase-contrast/>.

Ladanyi, M., C. Cha, R. Lewis, S. C. Jhanwar, A. G. Huvos and J. H. Healey (1993). "MDM2 GENE AMPLIFICATION IN METASTATIC OSTEOSARCOMA." Cancer Research **53**(1): 16-18.

Lambert, P. F., F. Kashanchi, M. F. Radonovich, R. Shiekhattar and J. N. Brady (1998). "Phosphorylation of p53 serine 15 increases interaction with CBP." J Biol Chem **273**(49): 33048-33053.

Lane, D. P. (1992). "p53, guardian of the genome." Nature **358**(6381): 15-16.

Lane, D. P. and L. V. Crawford (1979). "T antigen is bound to a host protein in SV40-transformed cells." Nature **278**(5701): 261-263.

Lang, G. A., T. Iwakuma, Y.-A. Suh, G. Liu, V. A. Rao, J. M. Parant, Y. A. Valentin-Vega, T. Terzian, L. C. Caldwell, L. C. Strong, A. K. El-Nagggar and G. Lozano (2004). "Gain of Function of a p53 Hot Spot Mutation in a Mouse Model of Li-Fraumeni Syndrome." Cell **119**(6): 861-872.

Laurie, N. A., S. L. Donovan, C.-S. Shih, J. Zhang, N. Mills, C. Fuller, A. Teunisse, S. Lam, Y. Ramos, A. Mohan, D. Johnson, M. Wilson, C. Rodriguez-Galindo, M. Quarto, S. Francoz, S. M. Mendrysa, R. Kiplin Guy, J.-C. Marine, A. G. Jochemsen and M. A. Dyer (2006). "Inactivation of the p53 pathway in retinoblastoma." Nature **444**(7115): 61-66.

Le Guezennec, X., A. Brichkina, Y.-F. Huang, E. Kostromina, W. Han and Dmitry V. Bulavin (2012). "Wip1-Dependent Regulation of Autophagy, Obesity, and Atherosclerosis." Cell Metabolism **16**(1): 68-80.

Leach, F. S., T. Tokino, P. Meltzer, M. Burrell, J. D. Oliner, S. Smith, D. E. Hill, D. Sidransky, K. W. Kinzler and B. Vogelstein (1993). "P53 MUTATION AND MDM2 AMPLIFICATION IN HUMAN SOFT-TISSUE SARCOMAS." Cancer Research **53**(10): 2231-2234.

Leahy, J. J. J., B. T. Golding, R. J. Griffin, I. R. Hardcastle, C. Richardson, L. Rigoreau and G. C. M. Smith (2004). "Identification of a highly potent and selective DNA-dependent protein kinase (DNA-PK) inhibitor (NU7441) by screening of chromenone libraries." Bioorganic & Medicinal Chemistry Letters **14**(24): 6083-6087.

Lechner, M. S., D. H. Mack, A. B. Finicle, T. Crook, K. H. Vousden and L. A. Laimins (1992). "HUMAN PAPILLOMAVIRUS E6 PROTEINS BIND P53 INVIVO AND ABROGATE P53-MEDIATED REPRESSION OF TRANSCRIPTION." EMBO Journal **11**(8): 3045-3052.

Lee, J.-H., H.-S. Kim, S.-J. Lee and K.-T. Kim (2007). "Stabilization and activation of p53 induced by Cdk5 contributes to neuronal cell death." Journal of Cell Science **120**(13): 2259-2271.

Lee, J. H. and T. T. Paull (2004). "Direct activation of the ATM protein kinase by the Mre11/Rad50/Nbs1 complex." Science **304**(5667): 93-96.

Lempiaainen, H. and T. D. Halazonetis (2009). "Emerging common themes in regulation of PIKKs and PI3Ks." Embo Journal **28**(20): 3067-3073.

Levine, A. J. (1997). "p53, the cellular gatekeeper for growth and division." Cell **88**(3): 323-331.

Levine, A. J., J. Momand and C. A. Finlay (1991). "THE P53 TUMOR SUPPRESSOR GENE." Nature **351**(6326): 453-456.

- Li, F. P. and J. F. Fraumeni, Jr. (1969). "Rhabdomyosarcoma in children: epidemiologic study and identification of a familial cancer syndrome." J Natl Cancer Inst **43**(6): 1365-1373.
- Li, F. P. and J. F. Fraumeni, Jr. (1969). "Soft-tissue sarcomas, breast cancer, and other neoplasms. A familial syndrome?" Ann Intern Med **71**(4): 747-752.
- Li, F. P., J. F. Fraumeni, J. J. Mulvihill, W. A. Blattner, M. G. Dreyfus, M. A. Tucker and R. W. Miller (1988). "A Cancer Family Syndrome in Twenty-four Kindreds." Cancer Research **48**(18): 5358-5362.
- Li, G. B., X. L. Zhang, L. Yuan, Q. Q. Jiao, D. J. Liu and J. Liu (2013). "Protein Phosphatase Magnesium-Dependent 1 delta (PPM1D) mRNA Expression Is a Prognosis Marker for Hepatocellular Carcinoma." Plos One **8**(3).
- Li, J., Y. Yang, Y. Peng, R. J. Austin, W. G. van Eyndhoven, K. C. Q. Nguyen, T. Gabriele, M. E. McCurrach, J. R. Marks, T. Hoey, S. W. Lowe and S. Powers (2002). "Oncogenic properties of PPM1D located within a breast cancer amplification epicenter at 17q23." Nat Genet **31**(2): 133-134.
- Li, M., C. L. Brooks, F. Wu-Baer, D. Chen, R. Baer and W. Gu (2003). "Mono- Versus Polyubiquitination: Differential Control of p53 Fate by Mdm2." Science **302**(5652): 1972-1975.
- Li, M., J. Luo, C. L. Brooks and W. Gu (2002). "Acetylation of p53 inhibits its ubiquitination by Mdm2." J Biol Chem **277**(52): 50607-50611.
- Li, T., N. Kon, L. Jiang, M. Tan, T. Ludwig, Y. Zhao, R. Baer and W. Gu (2012). "Tumor Suppression in the Absence of p53-Mediated Cell-Cycle Arrest, Apoptosis, and Senescence." Cell **149**(6): 1269-1283.
- Li, X. Q. and P. Coffino (1996). "High-risk human papillomavirus E6 protein has two distinct binding sites within p53, of which only one determines degradation." Journal of Virology **70**(7): 4509-4516.
- Li, Z.-T., L. Zhang, X.-Z. Gao, X.-H. Jiang and L.-Q. Sun (2013). "Expression and Significance of the Wip1 Proto-oncogene in Colorectal Cancer." Asian Pacific Journal of Cancer Prevention **14**(3): 1975-1979.
- Liang, C. H., E. K. Guo, S. K. Lu, S. Wang, C. S. Kang, L. Chang, L. Q. Liu, G. Y. Zhang, Z. D. Wu, Z. M. Zhao, S. C. Ma, L. Q. Wang and B. H. Jiao (2012). "Over-expression of Wild-type p53-induced phosphatase 1 confers poor prognosis of patients with gliomas." Brain Research **1444**: 65-75.
- Liang, H. and J. Lunec (2005). "Characterisation of a novel p53 down-regulated promoter in intron 3 of the human MDM2 oncogene." Gene **361**: 112-118.
- Lill, N. L., S. R. Grossman, D. Ginsberg, J. DeCaprio and D. M. Livingston (1997). "Binding and modulation of p53 by p300/CBP coactivators." Nature **387**(6635): 823-827.
- Lin, J., J. Chen, B. Elenbaas and A. J. Levine (1994). "Several hydrophobic amino acids in the p53 amino-terminal domain are required for transcriptional activation, binding to mdm-2 and the adenovirus 5 E1B 55-kD protein." Genes & Development **8**(10): 1235-1246.
- Lindqvist, A., M. de Bruijn, L. Macurek, A. Brás, A. Mensinga, W. Bruinsma, O. Voets, O. Kranenburg and R. H. Medema (2009). "Wip1 confers G2 checkpoint recovery competence by counteracting p53-dependent transcriptional repression." The EMBO Journal **28**(20): 3196-3206.
- Linzer, D. I. H. and A. J. Levine (1979). "Characterization of a 54K Dalton cellular SV40 tumor antigen present in SV40-transformed cells and uninfected embryonal carcinoma cells." Cell **17**(1): 43-52.
- Liu, D., L. Ou, G. D. Clemenson, C. Chao, M. E. Lutske, G. P. Zambetti, F. H. Gage and Y. Xu (2010). "Puma is required for p53-induced depletion of adult stem cells." Nat Cell Biol **12**(10): 993-998.

Liu, Q., S. Guntuku, X.-S. Cui, S. Matsuoka, D. Cortez, K. Tamai, G. Luo, S. Carattini-Rivera, F. DeMayo, A. Bradley, L. A. Donehower and S. J. Elledge (2000). "Chk1 is an essential kinase that is regulated by Atr and required for the G2/M DNA damage checkpoint." Genes & Development **14**(12): 1448-1459.

Lockhart, D. J. and E. A. Winzeler (2000). "Genomics, gene expression and DNA arrays." Nature **405**(6788): 827-836.

Lorenz, M. G. and W. Wackernagel (1994). "Bacterial gene transfer by natural genetic transformation in the environment." Microbiological Reviews **58**(3): 563-602.

Loughery, J., M. Cox, L. M. Smith and D. W. Meek (2014). "Critical role for p53-serine 15 phosphorylation in stimulating transactivation at p53-responsive promoters." Nucleic Acids Research **42**(12): 7666-7680.

Low, S. C., R. Shaimi, Y. Thandaithabany, J. K. Lim, A. L. Ahmad and A. Ismail (2013). "Electrophoretic interactions between nitrocellulose membranes and proteins: Biointerface analysis and protein adhesion properties." Colloids and Surfaces B: Biointerfaces **110**(0): 248-253.

Lowe, J., H. Cha, M.-O. Lee, S. J. Mazur, E. Appella and A. J. Fornace (2012). "Regulation of the Wip1 phosphatase and its effects on the stress response." Frontiers in bioscience : a journal and virtual library **17**: 1480-1498.

Lowe, S. W., H. E. Ruley, T. Jacks and D. E. Housman (1993). "p53-dependent apoptosis modulates the cytotoxicity of anticancer agents." Cell **74**(6): 957-967.

Lowe, S. W., E. M. Schmitt, S. W. Smith, B. A. Osborne and T. Jacks (1993). "p53 is required for radiation-induced apoptosis in mouse thymocytes." Nature **362**(6423): 847-849.

Lu, H. and A. J. Levine (1995). "Human TAFII31 protein is a transcriptional coactivator of the p53 protein." Proceedings of the National Academy of Sciences **92**(11): 5154-5158.

Lu, X., O. Ma, T.-A. Nguyen, S. N. Jones, M. Oren and L. A. Donehower (2007). "The Wip1 phosphatase acts as a gatekeeper in the p53-Mdm2 autoregulatory loop." Cancer Cell **12**(4): 342-354.

Lu, X., B. Nannenga and L. A. Donehower (2005). "PPM1D dephosphorylates Chk1 and p53 and abrogates cell cycle checkpoints." Genes & Development **19**(10): 1162-1174.

Lu, X., T.-A. Nguyen, S.-H. Moon, Y. Darlington, M. Sommer and L. Donehower (2008). "The type 2C phosphatase Wip1: An oncogenic regulator of tumor suppressor and DNA damage response pathways." Cancer and Metastasis Reviews **27**(2): 123-135.

Luna, R. M. D., D. S. Wagner and G. Lozano (1995). "RESCUE OF EARLY EMBRYONIC LETHALITY IN MDM2-DEFICIENT MICE BY DELETION OF P53." Nature **378**(6553): 203-206.

Lunghi, P., L. Mazzera, V. Rizzoli and A. Bonati (2007). "MDM2 antagonist Nutlin-3 activates p53 and enhances the apoptotic synergism between MEK inhibitor and arsenic trioxide (ATO) in AML cells." Haematologica-the Hematology Journal **92**: 51-52.

Ma, D., C. J. Zhang, Z. L. Chen and H. Yang (2014). "Prognostic value of PPM1D in 800 gastric cancer patients." Molecular Medicine Reports **10**(1): 191-194.

MacCallum, D. E., T. R. Hupp, C. A. Midgley, D. Stuart, S. J. Campbell, A. Harper, F. S. Walsh, E. G. Wright, A. Balmain, D. P. Lane and P. A. Hall (1996). "The p53 response to ionising radiation in adult and developing murine tissues." Oncogene **13**(12): 2575-2587.

Macleod, K. F., N. Sherry, G. Hannon, D. Beach, T. Tokino, K. Kinzler, B. Vogelstein and T. Jacks (1995). "P53-DEPENDENT AND INDEPENDENT EXPRESSION OF P21 DURING CELL-GROWTH, DIFFERENTIATION, AND DNA-DAMAGE." Genes & Development **9**(8): 935-944.

Macurek, L., J. Benada, E. Müllers, V. A. Halim, K. Krejčíková, K. Burdová, S.

Pecháčková, Z. Hodný, A. Lindqvist, R. H. Medema and J. Bartek (2013). "Downregulation of Wip1 phosphatase modulates the cellular threshold of DNA damage signaling in mitosis." Cell Cycle **12**(2): 251-262.

Mahaney, B. L., K. Meek and S. P. Lees-miller (2009). "Repair of ionizing radiation-induced DNA double-strand breaks by non-homologous end-joining." Biochem J **417**(3): 639-650.

Maki, C. G., J. M. Huibregtse and P. M. Howley (1996). "In vivo ubiquitination and proteasome-mediated degradation of p53." Cancer Research **56**(11): 2649-2654.

Malkin, D., F. P. Li, L. C. Strong, J. F. Fraumeni, C. E. Nelson, D. H. Kim, J. Kassel, M. A. Gryka, F. Z. Bischoff, M. A. Tainsky and a. et (1990). "Germ line p53 mutations in a familial syndrome of breast cancer, sarcomas, and other neoplasms." Science **250**(4985): 1233-1238.

Mandel, M. and A. Higa (1970). "Calcium-dependent bacteriophage DNA infection." Journal of Molecular Biology **53**(1): 159-162.

Marechal, V., B. Elenbaas, J. Piette, J. C. Nicolas and A. J. Levine (1994). "THE RIBOSOMAL L5 PROTEIN IS ASSOCIATED WITH MDM-2 AND MDM-2-P53 COMPLEXES." Molecular and Cellular Biology **14**(11): 7414-7420.

Marine, J.-C. W., M. A. Dyer and A. G. Jochemsen (2007). "MDMX: from bench to bedside." Journal of Cell Science **120**(3): 371-378.

Martín-Caballero, J., J. M. Flores, P. García-Palencia and M. Serrano (2001). "Tumor Susceptibility of p21Waf1/Cip1-deficient Mice." Cancer Research **61**(16): 6234-6238.

Martin, K., D. Trouche, C. Hagemeier, T. S. Sorensen, N. B. La Thangue and T. Kouzarides (1995). "Stimulation of E2F1/DP1 transcriptional activity by MDM2 oncoprotein." Nature **375**(6533): 691-694.

May, P. and E. May (1999). "Twenty years of p53 research: structural and functional aspects of the p53 protein." Oncogene **18**(53): 7621-7636.

Maya, R., M. Balass, S.-T. Kim, D. Shkedy, J.-F. M. Leal, O. Shifman, M. Moas, T. Buschmann, Z. e. Ronai, Y. Shiloh, M. B. Kastan, E. Katzir and M. Oren (2001). "ATM-dependent phosphorylation of Mdm2 on serine 395: role in p53 activation by DNA damage." Genes & Development **15**(9): 1067-1077.

Mayo, L. D., Y. R. Seo, M. W. Jackson, M. L. Smith, J. R. Guzman, C. K. Korgaonkar and D. B. Donner (2005). "Phosphorylation of Human p53 at Serine 46 Determines Promoter Selection and whether Apoptosis Is Attenuated or Amplified." Journal of Biological Chemistry **280**(28): 25953-25959.

McCabe, N., N. C. Turner, C. J. Lord, K. Kluzek, A. Bialkowska, S. Swift, S. Giavara, M. J. O'Connor, A. N. Tutt, M. Z. Zdzienicka, G. C. M. Smith and A. Ashworth (2006). "Deficiency in the repair of DNA damage by homologous recombination and sensitivity to poly(ADP-ribose) polymerase inhibition." Cancer Research **66**(16): 8109-8115.

McConnell, J. L. and B. E. Wadzinski (2009). "Targeting Protein Serine/Threonine Phosphatases for Drug Development." Molecular Pharmacology **75**(6): 1249-1261.

Meek, D. W. (1999). "Mechanisms of switching on p53: a role for covalent modification?" Oncogene **18**(53): 7666-7675.

Meek, D. W. (2004). "The p53 response to DNA damage." DNA Repair **3**(8-9): 1049-1056.

Meek, D. W. (2009). "Tumour suppression by p53: a role for the DNA damage response?" Nat Rev Cancer **9**(10): 714-723.

Meek, D. W. (2015). "Regulation of the p53 response and its relationship to cancer." Biochemical Journal **469**(3): 325-346.

Meek, D. W. and C. W. Anderson (2009). "Posttranslational Modification of p53: Cooperative Integrators of Function." Cold Spring Harbor Perspectives in Biology **1**(6).

Meek, D. W. and T. R. Hupp (2010). "The regulation of MDM2 by multisite phosphorylation—Opportunities for molecular-based intervention to target tumours?"

Seminars in Cancer Biology **20**(1): 19-28.

Melero, J., D. T. Stitt, W. F. Mangel and R. B. Carroll (1979). "Identification of new polypeptide species (48–55K) immunoprecipitable by antiserum to purified large T antigen and present in SV40-infected and -transformed cells." Virology **93**(2): 466-480.

Mercer, W. E., C. Avignolo and R. Baserga (1984). "Role of the p53 protein in cell proliferation as studied by microinjection of monoclonal antibodies." Molecular and Cellular Biology **4**(2): 276-281.

Mercer, W. E., D. Nelson, A. B. DeLeo, L. J. Old and R. Baserga (1982).

"Microinjection of monoclonal antibody to protein p53 inhibits serum-induced DNA synthesis in 3T3 cells." Proceedings of the National Academy of Sciences **79**(20): 6309-6312.

Michaelis, M., F. Rothweiler, S. Barth, J. Cinatl, M. van Rikxoort, N. Loschmann, Y. Voges, R. Breitling, A. von Deimling, F. Rodel, K. Weber, B. Fehse, E. Mack, T. Stiewe, H. W. Doerr, D. Speidel and J. Cinatl, Jr. (2011). "Adaptation of cancer cells from different entities to the MDM2 inhibitor nutlin-3 results in the emergence of p53-mutated multi-drug-resistant cancer cells." Cell Death Dis **2**: e243.

Michalovitz, D., O. Halevy and M. Oren (1991). "p53 mutations: gains or losses?" J Cell Biochem **45**(1): 22-29.

Midgley, C. A., B. Owens, C. V. Briscoe, D. B. Thomas, D. P. Lane and P. A. Hall (1995). "COUPLING BETWEEN GAMMA-IRRADIATION, P53 INDUCTION AND THE APOPTOTIC RESPONSE DEPENDS UPON CELL-TYPE IN-VIVO." Journal of Cell Science **108**: 1843-1848.

Milner, J. and F. McCormick (1980). "Lymphocyte stimulation: concanavalin A induces the expression of a 53K protein." Cell Biology International Reports **4**(7): 663-667.

Mirza, A., Q. Wu, L. Wang, T. McClanahan, W. R. Bishop, F. Gheys, W. Ding, B. Hutchins, T. Hockenberry, P. Kirschmeier, J. R. Greene and S. Liu (2003). "Global transcriptional program of p53 target genes during the process of apoptosis and cell cycle progression." Oncogene **22**(23): 3645-3654.

Momand, J., D. Jung, S. Wilczynski and J. Niland (1998). "The MDM2 gene amplification database." Nucleic Acids Research **26**(15): 3453-3459.

Momand, J., G. P. Zambetti, D. C. Olson, D. George and A. J. Levine (1992). "THE MDM-2 ONCOGENE PRODUCT FORMS A COMPLEX WITH THE P53 PROTEIN AND INHIBITS P53-MEDIATED TRANSACTIVATION." Cell **69**(7): 1237-1245.

Morachis, J. M., C. M. Murawsky and B. M. Emerson (2010). "Regulation of the p53 transcriptional response by structurally diverse core promoters." Genes & Development **24**(2): 135-147.

Morton, J. P., P. Timpson, S. A. Karim, R. A. Ridgway, D. Athineos, B. Doyle, N. B. Jamieson, K. A. Oien, A. M. Lowy, V. G. Brunton, M. C. Frame, T. R. J. Evans and O. J. Sansom (2010). "Mutant p53 drives metastasis and overcomes growth arrest/senescence in pancreatic cancer." Proceedings of the National Academy of Sciences **107**(1): 246-251.

Mowat, M., A. Cheng, N. Kimura, A. Bernstein and S. Benchimol (1985).

"Rearrangements of the cellular p53 gene in erythroleukaemic cells transformed by Friend virus." Nature **314**(6012): 633-636.

Muller, Patricia A. J. and Karen H. Vousden (2014). "Mutant p53 in Cancer: New Functions and Therapeutic Opportunities." Cancer Cell **25**(3): 304-317.

Murray-Zmijewski, F., D. P. Lane and J. C. Bourdon (2006). "p53/p63/p73 isoforms: an orchestra of isoforms to harmonise cell differentiation and response to stress." Cell Death Differ **13**(6): 962-972.

Murray-Zmijewski, F., E. A. Slee and X. Lu (2008). "A complex barcode underlies the heterogeneous response of p53 to stress." Nat Rev Mol Cell Biol **9**(9): 702-712.

Murray, A. (1994). "Cell cycle checkpoints." Curr Opin Cell Biol **6**(6): 872-876.

Nakamura, S., J. A. Roth and T. Mukhopadhyay (2000). "Multiple Lysine Mutations in the C-Terminal Domain of p53 Interfere with MDM2-Dependent Protein Degradation and Ubiquitination." *Molecular and Cellular Biology* **20**(24): 9391-9398.

Napoli, C., C. Lemieux and R. Jorgensen (1990). "Introduction of a Chimeric Chalcone Synthase Gene into Petunia Results in Reversible Co-Suppression of Homologous Genes in trans." *The Plant Cell* **2**(4): 279-289.

Nicol, C. J., M. L. Harrison, R. R. Laposa, I. L. Gimelshtein and P. G. Wells (1995). "A teratologic suppressor role for p53 in benzo[a]pyrene-treated transgenic p53-deficient mice." *Nat Genet* **10**(2): 181-187.

Nigro, J. M., S. J. Baker, A. C. Preisinger, J. M. Jessup, R. Hostetter, K. Cleary, S. H. Bigner, N. Davidson, S. Baylin, P. Devilee, T. Glover, F. S. Collins, A. Weston, R. Modali, C. C. Harris and B. Vogelstein (1989). "MUTATIONS IN THE P53 GENE OCCUR IN DIVERSE HUMAN-TUMOR TYPES." *Nature* **342**(6250): 705-708.

Nims, R. W., G. Sykes, K. Cottrill, P. Ikonomi and E. Elmore (2010). "Short tandem repeat profiling: part of an overall strategy for reducing the frequency of cell misidentification." *In Vitro Cellular & Developmental Biology. Animal* **46**(10): 811-819.

Norimura, T., S. Nomoto, M. Katsuki, Y. Gondo and S. Kondo (1996). "p53-dependent apoptosis suppresses radiation-induced teratogenesis." *Nature Medicine* **2**(5): 577-580.

Nowell, P. C. (1976). "The clonal evolution of tumor cell populations." *Science* **194**(4260): 23-28.

Nyberg, K. A., R. J. Michelson, C. W. Putnam and T. A. Weinert (2002). "Toward maintaining the genome: DNA damage and replication checkpoints." *Annu Rev Genet* **36**: 617-656.

O'Driscoll, M., V. L. Ruiz-Perez, C. G. Woods, P. A. Jeggo and J. A. Goodship (2003). "A splicing mutation affecting expression of ataxia-telangiectasia and Rad3-related protein (ATR) results in Seckel syndrome." *Nat Genet* **33**(4): 497-501.

Oberhammer, F., J. W. Wilson, C. Dive, I. D. Morris, J. A. Hickman, A. E. Wakeling, P. R. Walker and M. Sikorska (1993). "Apoptotic death in epithelial cells: cleavage of DNA to 300 and/or 50 kb fragments prior to or in the absence of internucleosomal fragmentation." *The EMBO Journal* **12**(9): 3679-3684.

Oda, K., H. Arakawa, T. Tanaka, K. Matsuda, C. Tanikawa, T. Mori, H. Nishimori, K. Tamai, T. Tokino, Y. Nakamura and Y. Taya (2000). "p53AIP1, a potential mediator of p53-dependent apoptosis, and its regulation by Ser-46-phosphorylated p53." *Cell* **102**(6): 849-862.

Okamura, S., H. Arakawa, T. Tanaka, H. Nakanishi, C. C. Ng, Y. Taya, M. Monden and Y. Nakamura (2001). "p53DINP1, a p53-Inducible Gene, Regulates p53-Dependent Apoptosis." *Molecular Cell* **8**(1): 85-94.

Okorokov, A. L., F. Ponchel and J. Milner (1997). "Induced N- and C-terminal cleavage of p53: a core fragment of p53, generated by interaction with damaged DNA, promotes cleavage of the N-terminus of full-length p53, whereas ssDNA induces C-terminal cleavage of p53." *EMBO Journal* **16**(19): 6008-6017.

Oliner, J. D., K. W. Kinzler, P. S. Meltzer, D. L. George and B. Vogelstein (1992). "Amplification of a gene encoding a p53-associated protein in human sarcomas." *Nature* **358**(6381): 80-83.

Oliner, J. D., J. A. Pietenpol, S. Thiagalingam, J. Gvuris, K. W. Kinzler and B. Vogelstein (1993). "ONCOPROTEIN MDM2 CONCEALS THE ACTIVATION DOMAIN OF TUMOR SUPPRESSOR-P53." *Nature* **362**(6423): 857-860.

Oliva-Trastoy, M., V. Berthonaud, A. Chevalier, C. Ducrot, M. C. Marsolier-Kergoat, C. Mann and F. Leteurtre (2007). "The Wip1 phosphatase (PPM1D) antagonizes activation of the Chk2 tumour suppressor kinase." *Oncogene* **26**(10): 1449-1458.

Olive, K. P., D. A. Tuveson, Z. C. Ruhe, B. Yin, N. A. Willis, R. T. Bronson, D.

Crowley and T. Jacks (2004). "Mutant p53 Gain of Function in Two Mouse Models of Li-Fraumeni Syndrome." *Cell* **119**(6): 847-860.

Olivier, M., M. Hollstein and P. Hainaut (2010). "TP53 mutations in human cancers: origins, consequences, and clinical use." *Cold Spring Harb Perspect Biol* **2**(1): a001008.

Olson, D. C., V. Marechal, J. Momand, J. Chen, C. Romocki and A. J. Levine (1993). "Identification and characterization of multiple mdm-2 proteins and mdm-2-p53 protein complexes." *Oncogene* **8**(9): 2353-2360.

Omerod, M. G. (2000). "Flow Cytometry: A Practical Approach (3rd edition)." http://flowbook.denovosoftware.com/Flow_Book/Chapter_6%3a_DNA_Analysis 2015.

Palmero, I., C. Pantoja and M. Serrano (1998). "p19ARF links the tumour suppressor p53 to Ras." *Nature* **395**(6698): 125-126.

Pant, V., S. Xiong, T. Iwakuma, A. Quintas-Cardama and G. Lozano (2011). "Heterodimerization of Mdm2 and Mdm4 is critical for regulating p53 activity during embryogenesis but dispensable for p53 and Mdm2 stability." *Proceedings of the National Academy of Sciences of the United States of America* **108**(29): 11995-12000.

Parada, L. F., H. Land, R. A. Weinberg, D. Wolf and V. Rotter (1984). "COOPERATION BETWEEN GENE ENCODING P53 TUMOR-ANTIGEN AND RAS IN CELLULAR-TRANSFORMATION." *Nature* **312**(5995): 649-651.

Parant, J., A. Chavez-Reyes, N. A. Little, W. Yan, V. Reinke, A. G. Jochemsen and G. Lozano (2001). "Rescue of embryonic lethality in Mdm4-null mice by loss of Trp53 suggests a nonoverlapping pathway with MDM2 to regulate p53." *Nat Genet* **29**(1): 92-95.

París, R., R. E. Henry, S. J. Stephens, M. McBryde and J. M. Espinosa (2008). "Multiple p53-independent gene silencing mechanisms define the cellular response to p53 activation." *Cell cycle (Georgetown, Tex.)* **7**(15): 2427-2433.

Parssinen, J., E. L. Alarmo, R. Karhu and A. Kallioniemi (2008). "PPM1D silencing by RNA interference inhibits proliferation and induces apoptosis in breast cancer cell lines with wild-type p53." *Cancer Genet Cytogenet* **182**(1): 33-39.

Pavletich, N. P., K. A. Chambers and C. O. Pabo (1993). "THE DNA-BINDING DOMAIN OF P53 CONTAINS THE 4 CONSERVED REGIONS AND THE MAJOR MUTATION HOT-SPOTS." *Genes & Development* **7**(12B): 2556-2564.

Pawlik, T. M. and K. Keyomarsi (2004). "Role of cell cycle in mediating sensitivity to radiotherapy." *International Journal of Radiation Oncology*Biophysics* **59**(4): 928-942.

Pazgier, M., M. Liu, G. Zou, W. Yuan, C. Li, C. Li, J. Li, J. Monbo, D. Zella, S. G. Tarasov and W. Lu (2009). "Structural basis for high-affinity peptide inhibition of p53 interactions with MDM2 and MDMX." *Proceedings of the National Academy of Sciences* **106**(12): 4665-4670.

Peng, T.-S., Y.-H. He, T. Nie, X.-D. Hu, H.-Y. Lu, J. Yi, Y.-F. Shuai and M. Luo (2014). "PPM1D is a prognostic marker and therapeutic target in colorectal cancer." *Experimental and Therapeutic Medicine* **8**(2): 430-434.

Perneger, T. V. (1998). *What's wrong with Bonferroni adjustments.*

Perry, M. E., J. Piette, J. A. Zawadzki, D. Harvey and A. J. Levine (1993). "The mdm-2 gene is induced in response to UV light in a p53-dependent manner." *Proc Natl Acad Sci U S A* **90**(24): 11623-11627.

Picksley, S. M., B. Vojtesek, A. Sparks and D. P. Lane (1994). "IMMUNOCHEMICAL ANALYSIS OF THE INTERACTION OF P53 WITH MDM2 - FINE MAPPING OF THE MDM2 BINDING-SITE ON P53 USING SYNTHETIC PEPTIDES." *Oncogene* **9**(9): 2523-2529.

Pierotti MA, Sozzi G and Croce CM. (2003). "Holland-Frei Cancer Medicine. 6th edition." *Discovery and identification of oncogenes.*, from <http://www.ncbi.nlm.nih.gov/books/NBK13714/>.

Polo, S. E. and S. P. Jackson (2011). "Dynamics of DNA damage response proteins at DNA breaks: a focus on protein modifications." Genes & Development **25**(5): 409-433.

Ponder, B. (1988). "CANCER - GENE LOSSES IN HUMAN-TUMORS." Nature **335**(6189): 400-402.

Popowicz, G. M., A. Czarna, U. Rothweiler, A. Szwagierczak, M. Krajewski, L. Weber and T. A. Holak (2007). "Molecular basis for the inhibition of p53 by Mdmx." Cell Cycle **6**(19): 2386-2392.

Prives, C. and P. A. Hall (1999). "The P53 pathway." Journal of Pathology **187**(1): 112-126.

Purvis, J. E., K. W. Karhohs, C. Mock, E. Batchelor, A. Loewer and G. Lahav (2012). "p53 Dynamics Control Cell Fate." Science **336**(6087): 1440-1444.

Quelle, D. E., F. Zindy, R. A. Ashmun and C. J. Sherr (1995). "Alternative reading frames of the INK4a tumor suppressor gene encode two unrelated proteins capable of inducing cell cycle arrest." Cell **83**(6): 993-1000.

Ragimov, N., A. Krauskopf, N. Navot, V. Rotter, M. Oren and Y. Aloni (1993). "WILD-TYPE BUT NOT MUTANT-P53 CAN REPRESS TRANSCRIPTION INITIATION INVITRO BY INTERFERING WITH THE BINDING OF BASAL TRANSCRIPTION FACTORS TO THE TATA MOTIF." Oncogene **8**(5): 1183-1193.

Rahman-Roblick, R., U. Johannes Roblick, U. Hellman, P. Conrotto, T. Liu, S. Becker, D. Hirschberg, H. Jörnvall, G. Auer and K. G. Wiman (2007). "p53 targets identified by protein expression profiling." Proceedings of the National Academy of Sciences **104**(13): 5401-5406.

Rainwater, R., D. Parks, M. E. Anderson, P. Tegtmeier and K. Mann (1995). "Role of cysteine residues in regulation of p53 function." Molecular and Cellular Biology **15**(7): 3892-3903.

Rana, T. M. (2007). "Illuminating the silence: understanding the structure and function of small RNAs." Nat Rev Mol Cell Biol **8**(1): 23-36.

Rathmell, W. K., W. K. Kaufmann, J. C. Hurt, L. L. Byrd and G. Chu (1997). "DNA-dependent Protein Kinase Is Not Required for Accumulation of p53 or Cell Cycle Arrest after DNA Damage." Cancer Research **57**(1): 68-74.

Rauta, J., E.-L. Alarmo, P. Kauraniemi, R. Karhu, T. Kuukasjärvi and A. Kallioniemi (2006). "The serine-threonine protein phosphatase PPM1D is frequently activated through amplification in aggressive primary breast tumours." Breast Cancer Research and Treatment **95**(3): 257-263.

Ray-Coquard, I., J.-Y. Blay, A. Italiano, A. Le Cesne, N. Penel, J. Zhi, F. Heil, R. Rueger, B. Graves, M. Ding, D. Geho, S. A. Middleton, L. T. Vassilev, G. L. Nichols and B. N. Bui (2012). "Effect of the MDM2 antagonist RG7112 on the P53 pathway in patients with MDM2-amplified, well-differentiated or dedifferentiated liposarcoma: an exploratory proof-of-mechanism study." The Lancet Oncology **13**(11): 1133-1140.

Raycroft, L., H. Wu and G. Lozano (1990). "TRANSCRIPTIONAL ACTIVATION BY WILD-TYPE BUT NOT TRANSFORMING MUTANTS OF THE P53 ANTIONCOGENE." Science **249**(4972): 1049-1051.

Rayter, S., R. Elliott, J. Travers, M. G. Rowlands, T. B. Richardson, K. Boxall, K. Jones, S. Linardopoulos, P. Workman, W. Aherne, C. J. Lord and A. Ashworth (2007). "A chemical inhibitor of PPM1D that selectively kills cells overexpressing PPM1D." Oncogene **27**(8): 1036-1044.

Reed, D., Y. Shen, A. A. Shelat, L. A. Arnold, A. M. Ferreira, F. Zhu, N. Mills, D. C. Smithson, C. A. Regni, D. Bashford, S. A. Cicero, B. A. Schulman, A. G. Jochemsen, R. K. Guy and M. A. Dyer (2010). "Identification and Characterization of the First Small Molecule Inhibitor of MDMX." Journal of Biological Chemistry **285**(14): 10786-10796.

Reed, J. C. (2000). "Mechanisms of Apoptosis." The American Journal of Pathology

157(5): 1415-1430.

Reed, M., B. Woelker, P. Wang, Y. Wang, M. E. Anderson and P. Tegtmeier (1995). "THE C-TERMINAL DOMAIN OF P53 RECOGNIZES DNA DAMAGED BY IONIZING-RADIATION." Proceedings of the National Academy of Sciences of the United States of America **92**(21): 9455-9459.

Reich, N. C. and A. J. Levine (1984). "GROWTH-REGULATION OF A CELLULAR TUMOR-ANTIGEN, P53, IN NONTRANSFORMED CELLS." Nature **308**(5955): 199-201.

Reich, N. C., M. Oren and A. J. Levine (1983). "2 DISTINCT MECHANISMS REGULATE THE LEVELS OF A CELLULAR TUMOR-ANTIGEN, P53." Molecular and Cellular Biology **3**(12): 2143-2150.

Reid, Y. and D. Storts. (2013). " Authentication of Human Cell Lines by STR DNA Profiling Analysis. ." from <http://www.ncbi.nlm.nih.gov/books/NBK144066/>.

Richter, M., T. Dayaram, A. G. Gilmartin, G. Ganji, S. K. Pemmasani, H. Van Der Key, J. M. Shohet, L. A. Donehower and R. Kumar (2015). "WIP1 Phosphatase as a Potential Therapeutic Target in Neuroblastoma." PLoS ONE **10**(2): e0115635.

Ries, S., C. Biederer, D. Woods, O. Shifman, S. Shirasawa, T. Sasazuki, M. McMahon, M. Oren and F. McCormick (2000). "Opposing effects of Ras on p53: transcriptional activation of mdm2 and induction of p19ARF." Cell **103**(2): 321-330.

Rigatti, M. J., R. Verma, G. S. Belinsky, D. W. Rosenberg and C. Giardina (2012). "Pharmacological inhibition of Mdm2 triggers growth arrest and promotes DNA breakage in mouse colon tumors and human colon cancer cells." Molecular Carcinogenesis **51**(5): 363-378.

Ritchie, M. E., B. Phipson, D. Wu, Y. Hu, C. W. Law, W. Shi and G. K. Smyth (2015). "limma powers differential expression analyses for RNA-sequencing and microarray studies." Nucleic Acids Research.

Rodriguez, M. S., J. M. P. Desterro, S. Lain, D. P. Lane and R. T. Hay (2000). "Multiple C-Terminal Lysine Residues Target p53 for Ubiquitin-Proteasome-Mediated Degradation." Molecular and Cellular Biology **20**(22): 8458-8467.

Rogakou, E. P., W. Nieves-Neira, C. Boon, Y. Pommier and W. M. Bonner (2000). "Initiation of DNA fragmentation during apoptosis induces phosphorylation of H2AX histone at serine 139." J Biol Chem **275**(13): 9390-9395.

Rogel, A., M. Popliker, C. G. Webb and M. Oren (1985). "P53 CELLULAR TUMOR-ANTIGEN - ANALYSIS OF MESSENGER-RNA LEVELS IN NORMAL ADULT TISSUES, EMBRYOS, AND TUMORS." Molecular and Cellular Biology **5**(10): 2851-2855.

Rosenthal, A. N., A. Ryan, R. M. Al-Jehani, A. Storey, C. A. Harwood and I. J. Jacobs (1998). "p53 codon 72 polymorphism and risk of cervical cancer in UK." Lancet **352**(9131): 871-872.

Rossi, M., O. N. Demidov, C. W. Anderson, E. Appella and S. J. Mazur (2008). "Induction of PPM1D following DNA-damaging treatments through a conserved p53 response element coincides with a shift in the use of transcription initiation sites." Nucleic Acids Res **36**(22): 7168-7180.

Roth, J., M. Dobbstein, D. A. Freedman, T. Shenk and A. J. Levine (1998). "Nucleocytoplasmic shuttling of the hdm2 oncoprotein regulates the levels of the p53 protein via a pathway used by the human immunodeficiency virus rev protein." EMBO Journal **17**(2): 554-564.

Rotter, V., D. Schwartz, E. Almon, N. Goldfinger, A. Kapon, A. Meshorer, L. A. Donehower and A. J. Levine (1993). "MICE WITH REDUCED LEVELS OF P53 PROTEIN EXHIBIT THE TESTICULAR GIANT-CELL DEGENERATIVE SYNDROME." Proceedings of the National Academy of Sciences of the United States of America **90**(19): 9075-9079.

Rotter, V., O. N. Witte, R. Coffman and D. Baltimore (1980). "ABELSON MURINE LEUKEMIA VIRUS-INDUCED TUMORS ELICIT ANTIBODIES AGAINST A HOST-CELL PROTEIN, P50." *Journal of Virology* **36**(2): 547-555.

Rouault, J. P., N. Falette, F. Guehenneux, C. Guillot, R. Rimokh, Q. Wang, C. Berthet, C. MoyretLalle, P. Savatier, B. Pain, P. Shaw, R. Berger, J. Samarut, J. P. Magaud, M. Ozturk, C. Samarut and A. Puisieux (1996). "Identification of BTG2, an antiproliferative p53-dependent component of the DNA damage cellular response pathway." *Nature Genetics* **14**(4): 482-486.

Ruark, E., K. Snape, P. Humburg, C. Loveday, I. Bajrami, R. Brough, D. N. Rodrigues, A. Renwick, S. Seal, E. Ramsay, S. D. V. Duarte, M. A. Rivas, M. Warren-Perry, A. Zachariou, A. Champion-Flora, S. Hanks, A. Murray, N. A. Pour, J. Douglas, L. Gregory, A. Rimmer, N. M. Walker, T.-P. Yang, J. W. Adlard, J. Barwell, J. Berg, A. F. Brady, C. Brewer, G. Brice, C. Chapman, J. Cook, R. Davidson, A. Donaldson, F. Douglas, D. Eccles, D. G. Evans, L. Greenhalgh, A. Henderson, L. Izatt, A. Kumar, F. Laloo, Z. Miedzybrodzka, P. J. Morrison, J. Paterson, M. Porteous, M. T. Rogers, S. Shanley, L. Walker, M. Gore, R. Houlston, M. A. Brown, M. J. Caufield, P. Deloukas, M. I. McCarthy, J. A. Todd, C. Turnbull, J. S. Reis-Filho, A. Ashworth, A. C. Antoniou, C. J. Lord, P. Donnelly and N. Rahman (2013). "Mosaic PPM1D mutations are associated with predisposition to breast and ovarian cancer." *Nature* **493**(7432): 406-410.

Rufini, A., P. Tucci, I. Celardo and G. Melino (2013). "Senescence and aging: the critical roles of p53." *Oncogene* **32**(43): 5129-5143.

Ruppert, J. M. and B. Stillman (1993). "ANALYSIS OF A PROTEIN-BINDING DOMAIN OF P53." *Molecular and Cellular Biology* **13**(6): 3811-3820.

Sabapathy, K. (2015). "The contrived mutant p53 oncogene – beyond loss of functions." *Frontiers in Oncology* **5**.

Sah, V. P., L. D. Attardi, G. J. Mulligan, B. O. Williams, R. T. Bronson and T. Jacks (1995). "A SUBSET OF P53-DEFICIENT EMBRYOS EXHIBIT EXENCEPHALY." *Nature Genetics* **10**(2): 175-180.

Saiki, A. Y., S. Caenepeel, E. Cosgrove, C. Su, M. Boedigheimer and J. D. Oliner (2015). "Identifying the determinants of response to MDM2 inhibition." *Oncotarget* **6**(10): 7701-7712.

Saiki, A. Y., S. Caenepeel, D. Yu, J. A. Lofgren, T. Osgood, R. Robertson, J. Canon, C. Su, A. Jones, X. Zhao, C. Deshpande, M. Payton, J. Ledell, P. E. Hughes and J. D. Oliner (2014). "MDM2 antagonists synergize broadly and robustly with compounds targeting fundamental oncogenic signaling pathways." *Oncotarget* **5**(8): 2030-2043.

Saiki, R. K., D. H. Gelfand, S. Stoffel, S. J. Scharf, R. Higuchi, G. T. Horn, K. B. Mullis and H. A. Erlich (1988). "Primer-directed enzymatic amplification of DNA with a thermostable DNA polymerase." *Science* **239**(4839): 487-491.

Saito-Ohara, F., I. Imoto, J. Inoue, H. Hosoi, A. Nakagawara, T. Sugimoto and J. Inazawa (2003). "PPM1D is a potential target for 17q gain in neuroblastoma." *Cancer Res* **63**(8): 1876-1883.

Saito, S., H. Yamaguchi, Y. Higashimoto, C. Chao, Y. Xu, A. J. Fornace, Jr., E. Appella and C. W. Anderson (2003). "Phosphorylation site interdependence of human p53 post-translational modifications in response to stress." *J Biol Chem* **278**(39): 37536-37544.

Saito, S., H. Yamaguchi, Y. Higashimoto, C. Chao, Y. Xu, A. J. Fornace Jr, E. Appella and C. W. Anderson (2003). "Phosphorylation site interdependence of human p53 post-translational modifications in response to stress." *Journal of Biological Chemistry* **278**(39): 37536-37544.

Saito, S. i., A. A. Goodarzi, Y. Higashimoto, Y. Noda, S. P. Lees-Miller, E. Appella and C. W. Anderson (2002). "ATM Mediates Phosphorylation at Multiple p53 Sites, Including Ser46, in Response to Ionizing Radiation." *Journal of Biological Chemistry*

277(15): 12491-12494.

Sakaguchi, K., J. E. Herrera, S. Saito, T. Miki, M. Bustin, A. Vassilev, C. W. Anderson and E. Appella (1998). "DNA damage activates p53 through a phosphorylation-acetylation cascade." Genes & Development **12**(18): 2831-2841.

Sakaguchi, K., S. i. Saito, Y. Higashimoto, S. Roy, C. W. Anderson and E. Appella (2000). "Damage-mediated Phosphorylation of Human p53 Threonine 18 through a Cascade Mediated by a Casein 1-like Kinase: EFFECT ON Mdm2 BINDING." Journal of Biological Chemistry **275**(13): 9278-9283.

Sakamuro, D., P. Sabbatini, E. White and G. C. Prendergast (1997). "The polyproline region of p53 is required to activate apoptosis but not growth arrest." Oncogene **15**(8): 887-898.

Samuels-Lev, Y., D. J. O'Connor, D. Bergamaschi, G. Trigiante, J.-K. Hsieh, S. Zhong, I. Campargue, L. Naumovski, T. Crook and X. Lu (2001). "ASPP Proteins Specifically Stimulate the Apoptotic Function of p53." Molecular Cell **8**(4): 781-794.

Sancar, A., L. A. Lindsey-Boltz, K. Unsal-Kacmaz and S. Linn (2004). "Molecular mechanisms of mammalian DNA repair and the DNA damage checkpoints." Annu Rev Biochem **73**: 39-85.

Sarkaria, J. N., R. S. Tibbetts, E. C. Busby, A. P. Kennedy, D. E. Hill and R. T. Abraham (1998). "Inhibition of Phosphoinositide 3-Kinase Related Kinases by the Radiosensitizing Agent Wortmannin." Cancer Research **58**(19): 4375-4382.

Satoh, N., Y. Maniwa, V. P. Bermudez, K. Nishimura, W. Nishio, M. Yoshimura, Y. Okita, C. Ohbayashi, J. Hurwitz and Y. Hayashi (2011). "Oncogenic phosphatase Wip1 is a novel prognostic marker for lung adenocarcinoma patient survival." Cancer Science **102**(5): 1101-1106.

Saucedo, L. J., C. D. Myers and M. E. Perry (1999). "Multiple murine double minute gene 2 (MDM2) proteins are induced by ultraviolet light." J Biol Chem **274**(12): 8161-8168.

Savitsky, K., A. Bar-Shira, S. Gilad, G. Rotman, Y. Ziv, L. Vanagaite, D. A. Tagle, S. Smith, T. Uziel, S. Sfez, M. Ashkenazi, I. Pecker, M. Frydman, R. Harnik, S. R.

Patanjali, A. Simmons, G. A. Clines, A. Sartiel, R. A. Gatti, L. Chessa, O. Sanal, M. F. Lavin, N. G. Jaspers, A. M. Taylor, C. F. Arlett, T. Miki, S. M. Weissman, M. Lovett, F. S. Collins and Y. Shiloh (1995). "A single ataxia telangiectasia gene with a product similar to PI-3 kinase." Science **268**(5218): 1749-1753.

Schacht, V. and J. S. Kern (2015). "Basics of Immunohistochemistry." J Invest Dermatol **135**(3): e30.

Scheffner, M., B. A. Werness, J. M. Huibregtse, A. J. Levine and P. M. Howley (1990). "THE E6 ONCOPROTEIN ENCODED BY HUMAN PAPILLOMAVIRUS TYPE-16 AND TYPE-18 PROMOTES THE DEGRADATION OF P53." Cell **63**(6): 1129-1136.

Schena, M., D. Shalon, R. W. Davis and P. O. Brown (1995). "QUANTITATIVE MONITORING OF GENE-EXPRESSION PATTERNS WITH A COMPLEMENTARY-DNA MICROARRAY." Science **270**(5235): 467-470.

Schroeder, A., O. Mueller, S. Stocker, R. Salowsky, M. Leiber, M. Gassmann, S. Lightfoot, W. Menzel, M. Granzow and T. Ragg (2006). "The RIN: an RNA integrity number for assigning integrity values to RNA measurements." BMC Molecular Biology **7**: 3-3.

Scolnick, D. M., N. H. Chehab, E. S. Stavridi, M. C. Lien, L. Caruso, E. Moran, S. L. Berger and T. D. Halazonetis (1997). "CREB-binding protein and p300/CBP-associated factor are transcriptional coactivators of the p53 tumor suppressor protein." Cancer Research **57**(17): 3693-3696.

Seeger, R. C., G. M. Brodeur, H. Sather, A. Dalton, S. E. Siegel, K. Y. Wong and D. Hammond (1985). "Association of multiple copies of the N-myc oncogene with rapid progression of neuroblastomas." N Engl J Med **313**(18): 1111-1116.

Seeger, R. C., R. Wada, G. M. Brodeur, T. J. Moss, R. L. Bjork, L. Sousa and D. J. Slamon (1988). "Expression of N-myc by neuroblastomas with one or multiple copies of the oncogene." Prog Clin Biol Res **271**: 41-49.

Sen, G. L. and H. M. Blau (2006). "A brief history of RNAi: the silence of the genes." The FASEB Journal **20**(9): 1293-1299.

Serrano, M., H. Lee, L. Chin, C. Cordon-Cardo, D. Beach and R. A. DePinho (1996). "Role of the INK4a locus in tumor suppression and cell mortality." Cell **85**(1): 27-37.

Serrano, M. A., Z. Li, M. Dangeti, P. R. Musich, S. Patrick, M. Roginskaya, B. Cartwright and Y. Zou (2012). "DNA-PK, ATM and ATR collaboratively regulate p53-RPA interaction to facilitate homologous recombination DNA repair." Oncogene.

Seto, E., A. Usheva, G. P. Zambetti, J. Momand, N. Horikoshi, R. Weinmann, A. J. Levine and T. Shenk (1992). "WILD-TYPE P53 BINDS TO THE TATA-BINDING PROTEIN AND REPRESSES TRANSCRIPTION." Proceedings of the National Academy of Sciences of the United States of America **89**(24): 12028-12032.

Shall, S. and G. de Murcia (2000). "Poly(ADP-ribose) polymerase-1: what have we learned from the deficient mouse model?" Mutation Research/DNA Repair **460**(1): 1-15.

Shaulian, E., A. Zauberman, D. Ginsberg and M. Oren (1992). "IDENTIFICATION OF A MINIMAL TRANSFORMING DOMAIN OF P53 - NEGATIVE DOMINANCE THROUGH ABROGATION OF SEQUENCE-SPECIFIC DNA-BINDING." Molecular and Cellular Biology **12**(12): 5581-5592.

Shaulsky, G., N. Goldfinger, A. Benzeev and V. Rotter (1990). "NUCLEAR ACCUMULATION OF P53 PROTEIN IS MEDIATED BY SEVERAL NUCLEAR-LOCALIZATION SIGNALS AND PLAYS A ROLE IN TUMORIGENESIS." Molecular and Cellular Biology **10**(12): 6565-6577.

Shaw, P., J. Freeman, R. Bovey and R. Iggo (1996). "Regulation of specific DNA binding by p53: Evidence for a role for O-glycosylation and charged residues at the carboxy-terminus." Oncogene **12**(4): 921-930.

Sherr, C. J. and J. M. Roberts (1995). "Inhibitors of mammalian G1 cyclin-dependent kinases." Genes Dev **9**(10): 1149-1163.

Shieh, S.-Y., M. Ikeda, Y. Taya and C. Prives (1997). "DNA Damage-Induced Phosphorylation of p53 Alleviates Inhibition by MDM2." Cell **91**(3): 325-334.

Shieh, S. Y., M. Ikeda, Y. Taya and C. Prives (1997). "DNA damage-induced phosphorylation of p53 alleviates inhibition by MDM2." Cell **91**(3): 325-334.

Shohat, O., M. Greenberg, D. Reisman, M. Oren and V. Rotter (1987). "Inhibition of cell growth mediated by plasmids encoding p53 anti-sense." Oncogene **1**(3): 277-283.

Shreeram, S., O. N. Demidov, W. K. Hee, H. Yamaguchi, N. Onishi, C. Kek, O. N. Timofeev, C. Dudgeon, A. J. Fornace, C. W. Anderson, Y. Minami, E. Appella and D. V. Bulavin "Wip1 Phosphatase Modulates ATM-Dependent Signaling Pathways." Molecular Cell **23**(5): 757-764.

Shvarts, A., W. T. Steegenga, N. Riteco, T. van Laar, P. Dekker, M. Bazuine, R. C. van Ham, W. van der Houven van Oordt, G. Hateboer, A. J. van der Eb and A. G. Jochemsen (1996). "MDMX: a novel p53-binding protein with some functional properties of MDM2." Embo j **15**(19): 5349-5357.

Siddiqui, W. A., A. Ahad and H. Ahsan (2015). "The mystery of BCL2 family: Bcl-2 proteins and apoptosis: an update." Archives of Toxicology **89**(3): 289-317.

Sigalas, I., A. H. Calvert, J. J. Anderson, D. E. Neal and J. Lunec (1996). "Alternatively spliced mdm2 transcripts with loss of p53 binding domain sequences: Transforming ability and frequent detection in human cancer." Nature Medicine **2**(8): 912-917.

Siu, L. L., A. Italiano, W. H. J. Miller, J. Y. Blay, J. A. Gietema, Y. J. Bang, L. R. Mileskin, H. W. Hirte, M. Reckner, B. Higgins, L. Jukofsky, S. Blotner, J. Zhi, S. Middleton, G. L. Nichols and L. C. Chen (2014). "Phase 1 dose escalation, food effect,

and biomarker study of RG7388, a more potent second-generation MDM2 antagonist, in patients (pts) with solid tumors." J. Clin Oncol., **32** (**Suppl.**) 2535.

Skehan, P., R. Storeng, D. Scudiero, A. Monks, J. McMahon, D. Vistica, J. T. Warren, H. Bokesch, S. Kenney and M. R. Boyd (1990). "New Colorimetric Cytotoxicity Assay for Anticancer-Drug Screening." Journal of the National Cancer Institute **82**(13): 1107-1112.

Slack, A., Z. Chen, R. Tonelli, M. Pule, L. Hunt, A. Pession and J. M. Shohet (2005). "The p53 regulatory gene MDM2 is a direct transcriptional target of MYCN in neuroblastoma." Proc Natl Acad Sci U S A **102**(3): 731-736.

Soussi, T. (1994). "The TP53 Website." from <http://p53.free.fr/>.

Soussi, T. and C. Beroud (2001). "Assessing TP53 status in human tumours to evaluate clinical outcome." Nature Reviews Cancer **1**(3): 233-240.

Soussi, T., C. C. Defromental, M. Mechali, P. May and M. Kress (1987). "CLONING AND CHARACTERIZATION OF A CDNA FROM XENOPUS-LAEVIS CODING FOR A PROTEIN HOMOLOGOUS TO HUMAN AND MURINE P53." Oncogene **1**(1): 71-78.

Soussi, T. and P. May (1996). "Structural Aspects of the p53 Protein in Relation to Gene Evolution: A Second Look." Journal of Molecular Biology **260**(5): 623-637.

Srivastava, S., Z. Zou, K. Pirollo, W. Blattner and E. H. Chang (1990). "Germ-line transmission of a mutated p53 gene in a cancer-prone family with Li-Fraumeni syndrome." Nature **348**(6303): 747-749.

Steinmeyer, K. and W. Deppert (1988). "DNA-BINDING PROPERTIES OF MURINE-P53." Oncogene **3**(5): 501-507.

Storey, A., M. Thomas, A. Kalita, C. Harwood, D. Gardiol, F. Mantovani, J. Breuer, I. M. Leigh, G. Matlashewski and L. Banks (1998). "Role of a p53 polymorphism in the development of human papillomavirus-associated cancer." Nature **393**(6682): 229-234.

Sullivan, K. D., N. Padilla-Just, R. E. Henry, C. C. Porter, J. Kim, J. J. Tentler, S. G. Eckhardt, A. C. Tan, J. DeGregori and J. M. Espinosa (2012). "ATM and MET kinases are synthetic lethal with non-genotoxic activation of p53." Nature chemical biology **8**(7): 646-654.

Sullivan, K. D., V. V. Palaniappan and J. M. Espinosa (2014). "ATM regulates cell fate choice upon p53 activation by modulating mitochondrial turnover and ROS levels." Cell Cycle **14**(1): 56-63.

Sun, G. G., Y. D. Wang, Q. Liu and W. N. Hu (2015). "Expression of Wip1 in Kidney Carcinoma and its Correlation with Tumor Metastasis and Clinical Significance." Pathology & Oncology Research **21**(1): 219-224.

Sun, G. G., J. Zhang, X. B. Ma, Y. D. Wang, Y. J. Cheng and W. N. Hu (2015). "Overexpression of Wild-Type p53-Induced Phosphatase 1 Confers Poor Prognosis of Patients with Nasopharyngeal Carcinoma." Pathology & Oncology Research **21**(2): 283-291.

Symonds, H., L. Krall, L. Remington, M. Saenz-Robles, S. Lowe, T. Jacks and T. Van Dyke (1994). "p53-dependent apoptosis suppresses tumor growth and progression in vivo." Cell **78**(4): 703-711.

Takahashi, T., M. M. Nau, I. Chiba, M. J. Birrer, R. K. Rosenberg, M. Vinocour, M. Levitt, H. Pass, A. F. Gazdar and J. D. Minna (1989). "p53: a frequent target for genetic abnormalities in lung cancer." Science **246**(4929): 491-494.

Takekawa, M., M. Adachi, A. Nakahata, I. Nakayama, F. Itoh, H. Tsukuda, Y. Taya and K. Imai (2000). "p53-inducible wip1 phosphatase mediates a negative feedback regulation of p38 MAPK-p53 signaling in response to UV radiation." Embo j **19**(23): 6517-6526.

Tan, D. S., M. B. Lambros, S. Rayter, R. Natrajan, R. Vatcheva, Q. Gao, C. Marchio, F. C. Geyer, K. Savage, S. Parry, K. Fenwick, N. Tamber, A. Mackay, T. Dexter, C.

Jameson, W. G. McCluggage, A. Williams, A. Graham, D. Faratian, M. El-Bahrawy, A. J. Paige, H. Gabra, M. E. Gore, M. Zvelebil, C. J. Lord, S. B. Kaye, A. Ashworth and J. S. Reis-Filho (2009). "PPM1D is a potential therapeutic target in ovarian clear cell carcinomas." Clin Cancer Res **15**(7): 2269-2280.

Tang, J., L. K. Qu, J. Zhang, W. Wang, J. S. Michaelson, Y. Y. Degenhardt, W. S. El-Deiry and X. Yang (2006). "Critical role for Daxx in regulating Mdm2." Nat Cell Biol **8**(8): 855-862.

Tanimura, S., S. Ohtsuka, K. Mitsui, K. Shirouzu, A. Yoshimura and M. Ohtsubo (1999). "MDM2 interacts with MDMX through their RING finger domains." Febs Letters **447**(1): 5-9.

Taylor, C. R. and J. Burns (1974). "The demonstration of plasma cells and other immunoglobulin-containing cells in formalin-fixed, paraffin-embedded tissues using peroxidase-labelled antibody." Journal of Clinical Pathology **27**(1): 14-20.

Teufel, D. P., M. Bycroft and A. R. Fersht (2009). "Regulation by phosphorylation of the relative affinities of the N-terminal transactivation domains of p53 for p300 domains and Mdm2." Oncogene **28**(20): 2112-2118.

Thut, C. J., J. L. Chen, R. Klemm and R. Tjian (1995). "p53 transcriptional activation mediated by coactivators TAFII40 and TAFII60." Science **267**(5194): 100-104.

Tortora, G., R. Caputo, V. Damiano, R. Bianco, J. D. Chen, S. Agrawal, A. R. Bianco and F. Ciardiello (2000). "A novel MDM2 anti-sense oligonucleotide has anti-tumor activity and potentiates cytotoxic drugs acting by different mechanisms in human colon cancer." International Journal of Cancer **88**(5): 804-809.

Tovar, C., J. Rosinski, Z. Filipovic, B. Higgins, K. Kolinsky, H. Hilton, X. Zhao, B. T. Vu, W. Qing, K. Packman, O. Myklebost, D. C. Heimbrook and L. T. Vassilev (2006). "Small-molecule MDM2 antagonists reveal aberrant p53 signaling in cancer: Implications for therapy." Proceedings of the National Academy of Sciences of the United States of America **103**(6): 1888-1893.

Towbin, H., T. Staehelin and J. Gordon (1979). "Electrophoretic transfer of proteins from polyacrylamide gels to nitrocellulose sheets: procedure and some applications." Proceedings of the National Academy of Sciences of the United States of America **76**(9): 4350-4354.

Truant, R., H. Xiao, C. J. Ingles and J. Greenblatt (1993). "DIRECT INTERACTION BETWEEN THE TRANSCRIPTIONAL ACTIVATION DOMAIN OF HUMAN P53 AND THE TATA BOX-BINDING PROTEIN." Journal of Biological Chemistry **268**(4): 2284-2287.

Tweddle, D. A., A. J. Malcolm, M. Cole, A. D. J. Pearson and J. Lunec (2001). "p53 Cellular Localization and Function in Neuroblastoma: Evidence for Defective G1 Arrest Despite WAF1 Induction in MYCN-Amplified Cells." The American Journal of Pathology **158**(6): 2067-2077.

Tweddle, D. A., A. D. J. Pearson, M. Haber, M. D. Norris, C. Xue, C. Flemming and J. Lunec (2003). "The p53 pathway and its inactivation in neuroblastoma." Cancer Letters **197**(1-2): 93-98.

Uchiyama, Y. (2001). "Autophagic cell death and its execution by lysosomal cathepsins." Arch Histol Cytol **64**(3): 233-246.

Unger, T., J. A. Mietz, M. Scheffner, C. L. Yee and P. M. Howley (1993). "FUNCTIONAL DOMAINS OF WILD-TYPE AND MUTANT P53 PROTEINS INVOLVED IN TRANSCRIPTIONAL REGULATION, TRANSDOMINANT INHIBITION, AND TRANSFORMATION SUPPRESSION." Molecular and Cellular Biology **13**(9): 5186-5194.

Valente, Liz J., Daniel H. D. Gray, Ewa M. Michalak, J. Pinon-Hofbauer, A. Egle, Clare L. Scott, A. Janic and A. Strasser (2013). "p53 Efficiently Suppresses Tumor Development in the Complete Absence of Its Cell-Cycle Inhibitory and Proapoptotic

Effectors p21, Puma, and Noxa." Cell Reports **3**(5): 1339-1345.

Valentine, J. M., S. Kumar and A. Moumen (2011). "A p53-independent role for the MDM2 antagonist Nutlin-3 in DNA damage response initiation." Bmc Cancer **11**.

van der Burg, M., H. Ijspeert, N. S. Verkaik, T. Turul, W. W. Wiegant, K. Morotomi-Yano, P. O. Mari, I. Tezcan, D. J. Chen, M. Z. Zdzienicka, J. J. van Dongen and D. C. van Gent (2009). "A DNA-PKcs mutation in a radiosensitive T-B- SCID patient inhibits Artemis activation and nonhomologous end-joining." J Clin Invest **119**(1): 91-98.

Van Maerken, T., A. Rihani, D. Dreidax, S. De Clercq, N. Yigit, J. C. Marine, F. Westermann, A. De Paepe, J. Vandesompele and F. Speleman (2011). "Functional analysis of the p53 pathway in neuroblastoma cells using the small-molecule MDM2 antagonist nutlin-3." Mol Cancer Ther **10**(6): 983-993.

Varmus, H. (1988). "Retroviruses." Science **240**(4858): 1427-1435.

Vassilev, L. T., B. T. Vu, B. Graves, D. Carvajal, F. Podlaski, Z. Filipovic, N. Kong, U. Kammlott, C. Lukacs, C. Klein, N. Fotouhi and E. A. Liu (2004). "In vivo activation of the p53 pathway by small-molecule antagonists of MDM2." Science **303**(5659): 844-848.

Venot, C., M. Maratrat, C. Dureuil, E. Conseiller, L. Bracco and L. Debussche (1998). "The requirement for the p53 proline-rich functional domain for mediation of apoptosis is correlated with specific PIG3 gene transactivation and with transcriptional repression." EMBO Journal **17**(16): 4668-4679.

Verma, R., M. J. Rigatti, G. S. Belinsky, C. A. Godman and C. Giardina (2010). "DNA damage response to the Mdm2 inhibitor Nutlin-3." Biochemical Pharmacology **79**(4): 565-574.

Vermeulen, K., D. R. Van Bockstaele and Z. N. Berneman (2003). "The cell cycle: a review of regulation, deregulation and therapeutic targets in cancer." Cell Proliferation **36**(3): 131-149.

Vivanco, I. (2014). "Targeting molecular addictions in cancer." Br J Cancer **111**(11): 2033-2038.

Vogelstein, B., E. R. Fearon, S. R. Hamilton, S. E. Kern, A. C. Preisinger, M. Leppert, A. M. M. Smits and J. L. Bos (1988). "Genetic Alterations during Colorectal-Tumor Development." New England Journal of Medicine **319**(9): 525-532.

Wade, M. and G. M. Wahl (2009). "Targeting Mdm2 and Mdmx in Cancer Therapy: Better Living through Medicinal Chemistry?" Molecular Cancer Research **7**(1): 1-11.

Wadgaonkar, R. and T. Collins (1999). "Murine double minute (MDM2) blocks p53-coactivator interaction, a new mechanism for inhibition of p53-dependent gene expression." Journal of Biological Chemistry **274**(20): 13760-13767.

Waga, S., R. Li and B. Stillman (1997). "p53-induced p21 controls DNA replication." Leukemia **11 Suppl 3**: 321-323.

Wagner, J., L. Ma, J. J. Rice, W. Hu, A. J. Levine and G. A. Stolovitzky (2005). "p53-Mdm2 loop controlled by a balance of its feedback strength and effective dampening using ATM and delayed feedback." Iee Proceedings Systems Biology **152**(3): 109-118.

Walker, K. K. and A. J. Levine (1996). "Identification of a novel p53 functional domain that is necessary for efficient growth suppression." Proceedings of the National Academy of Sciences of the United States of America **93**(26): 15335-15340.

Wang, H. Q., M. Zubrowski, E. Emerson, E. Pradhan, S. Jeay, M. Wiesmann, G. Caponigro, J. Wuerthner, R. Schlegel, Z. A. Cao, A. Huang and E. Halilovic (2014). "Abstract 5466: The Mdm2 inhibitor, NVP-CGM097, in combination with the BRAF inhibitor NVP-LGX818 elicits synergistic antitumor effects in melanoma." Cancer Research **74**(19 Supplement): 5466.

Wang, X. W., W. Vermeulen, J. D. Coursen, M. Gibson, S. E. Lupold, K. Forrester, G. W. Xu, L. Elmore, H. Yeh, J. H. J. Hoeijmakers and C. C. Harris (1996). "The XPB and XPD DNA helicases are components of the p53-mediated apoptosis pathway." Genes &

Development **10**(10): 1219-1232.

Wang, X. W., H. Yeh, L. Schaeffer, R. Roy, V. Moncollin, J. M. Egly, Z. Wang, E. C. Friedberg, M. K. Evans, B. G. Taffe, V. A. Bohr, G. Weeda, J. H. J. Hoeijmakers, K. Forrester and C. C. Harris (1995). "P53 modulation of BTF2-TFIIH associated nucleotide excision repair activity." Journal of Cellular Biochemistry Supplement **0**(21A): 281-281.

Wang, X. W., H. Yeh, L. Schaeffer, R. Roy, V. Moncollin, J. M. Egly, Z. Wang, E. C. Friedberg, M. K. Evans, B. G. Taffe, V. A. Bohr, G. Weeda, J. H. J. Hoeijmakers, K. Forrester and C. C. Harris (1995). "P53 MODULATION OF TFIIH-ASSOCIATED NUCLEOTIDE EXCISION-REPAIR ACTIVITY." Nature Genetics **10**(2): 188-195.

Wasylyk, C., R. Salvi, M. Argentini, C. Dureuil, I. Delumeau, J. Abecassis, L. Debussche and B. Wasylyk (1999). "p53 mediated death of cells overexpressing MDM2 by an inhibitor of MDM2 interaction with p53." Oncogene **18**(11): 1921-1934.

Watson, J. D. and F. H. Crick (1953). "The structure of DNA." Cold Spring Harbor symposia on quantitative biology **18**: 123-131.

Weinberg, R. L., D. B. Veprintsev, M. Bycroft and A. R. Fersht (2005). "Comparative binding of p53 to its promoter and DNA recognition elements." J Mol Biol **348**(3): 589-596.

Weisz, L., M. Oren and V. Rotter (2007). "Transcription regulation by mutant p53." Oncogene **26**(15): 2202-2211.

Wu, X. W., J. H. Bayle, D. Olson and A. J. Levine (1993). "THE P53 MDM-2 AUTOREGULATORY FEEDBACK LOOP." Genes & Development **7**(7A): 1126-1132.

Wu, Z., J. Earle, S. i. Saito, C. W. Anderson, E. Appella and Y. Xu (2002). "Mutation of Mouse p53 Ser23 and the Response to DNA Damage." Molecular and Cellular Biology **22**(8): 2441-2449.

Xiao, Z.-X., J. Chen, A. J. Levine, N. Modjtahedi, J. Xing, W. R. Sellers and D. M. Livingston (1995). "Interaction between the retinoblastoma protein and the oncoprotein MDM2." Nature **375**(6533): 694-698.

Xue, W., L. Zender, C. Miething, R. A. Dickins, E. Hernando, V. Krizhanovsky, C. Cordon-Cardo and S. W. Lowe (2007). "Senescence and tumour clearance is triggered by p53 restoration in murine liver carcinomas." Nature **445**(7128): 656-660.

Yagi, H., Y. Chuman, Y. Kozakai, T. Imagawa, Y. Takahashi, F. Yoshimura, K. Tanino and K. Sakaguchi (2012). "A small molecule inhibitor of p53-inducible protein phosphatase PPM1D." Bioorganic & Medicinal Chemistry Letters **22**(1): 729-732.

Yamaguchi, H., S. R. Durell, D. K. Chatterjee, C. W. Anderson and E. Appella (2007). "The Wip1 phosphatase PPM1D dephosphorylates SQ/TQ motifs in checkpoint substrates phosphorylated by PI3K-like kinases." Biochemistry **46**(44): 12594-12603.

Yamaguchi, H., S. R. Durell, H. Feng, Y. Bai, C. W. Anderson and E. Appella (2006). "Development of a substrate-based cyclic phosphopeptide inhibitor of protein phosphatase 2C delta, Wip1." Biochemistry **45**(44): 13193-13202.

Yang, H., X.-Y. Gao, P. Li and T.-S. Jiang (2015). "PPM1D overexpression predicts poor prognosis in non-small cell lung cancer." Tumor Biology **36**(3): 2179-2184.

Yannone, S. M., I. S. Khan, R.-Z. Zhou, T. Zhou, K. Valerie and L. F. Povirk (2008). "Coordinate 5' and 3' endonucleolytic trimming of terminally blocked blunt DNA double-strand break ends by Artemis nuclease and DNA-dependent protein kinase." Nucleic Acids Research **36**(10): 3354-3365.

Yoda, A., X. Z. Xu, N. Onishi, K. Toyoshima, H. Fujimoto, N. Kato, I. Oishi, T. Kondo and Y. Minami (2006). "Intrinsic kinase activity and SQ/TQ domain of Chk2 kinase as well as N-terminal domain of Wip1 phosphatase are required for regulation of Chk2 by Wip1." J Biol Chem **281**(34): 24847-24862.

Yu, J. and L. Zhang (2005). "The transcriptional targets of p53 in apoptosis control."

Biochem Biophys Res Commun **331**(3): 851-858.

Zauberman, A., D. Flusberg, Y. Haupt, Y. Barak and M. Oren (1995). "A functional p53-responsive intronic promoter is contained within the human mdm2 gene." Nucleic Acids Research **23**(14): 2584-2592.

Zerdoumi, Y., J. Aury-Landas, C. Bonaïti-Pellié, C. Derambure, R. Sesboüé, M. Renaux-Petel, T. Frebourg, G. Bougeard and J.-M. Flaman (2013). "Drastic Effect of Germline TP53 Missense Mutations in Li-Fraumeni Patients." Human Mutation **34**(3): 453-461.

Zhan, Q., M. J. Antinore, X. W. Wang, F. Carrier, M. L. Smith, C. C. Harris and A. J. Fornace, Jr. (1999). "Association with Cdc2 and inhibition of Cdc2/Cyclin B1 kinase activity by the p53-regulated protein Gadd45." Oncogene **18**(18): 2892-2900.

Zhang, C., Y. Chen, M. Wang, X. Chen, Y. Li, E. Song, X. Liu, S. Kim and H. Peng (2014). "PPM1D silencing by RNA interference inhibits the proliferation of lung cancer cells." World Journal of Surgical Oncology **12**(1): 258.

Zhang, L., L. H. Chen, H. Wan, R. Yang, Z. Wang, J. Feng, S. Yang, S. Jones, S. Wang, W. Zhou, H. Zhu, P. J. Killela, J. Zhang, Z. Wu, G. Li, S. Hao, Y. Wang, J. B. Webb, H. S. Friedman, A. H. Friedman, R. E. McLendon, Y. He, Z. J. Reitman, D. D. Bigner and H. Yan (2014). "Exome sequencing identifies somatic gain-of-function PPM1D mutations in brainstem gliomas." Nat Genet **46**(7): 726-730.

Zhang, R. and H. Wang (2003). "Antisense oligonucleotide inhibitors of MDM2 oncogene expression." Methods in molecular medicine **85**: 205-222.

Zhang, W., M. Konopleva, W. D. Schober, T. McQueen and M. Andreeff (2007). "MEK inhibitor AZD6244 induces cell growth arrest and synergizes nutlin-3a-mediated cell death by upregulating p53 and PUMA levels in acute myelogenous leukemia." Blood **110**(11): 201A-201A.

Zhang, X.-P., F. Liu, Z. Cheng and W. Wang (2009). "Cell fate decision mediated by p53 pulses." Proceedings of the National Academy of Sciences **106**(30): 12245-12250.

Zhang, X., L. Lin, H. Guo, J. Yang, S. N. Jones, A. Jochemsen and X. Lu (2009). "Phosphorylation and Degradation of MdmX Is Inhibited by Wip1 Phosphatase in the DNA Damage Response." Cancer Research **69**(20): 7960-7968.

Zhang, X., G. Wan, S. Mlotshwa, V. Vance, F. G. Berger, H. Chen and X. Lu (2010). "Oncogenic Wip1 Phosphatase Is Inhibited by miR-16 in the DNA Damage Signaling Pathway." Cancer Research **70**(18): 7176-7186.

Zhang, Y., H. Sun, G. He, A. Liu, F. Wang and L. Wang (2014). "WIP1 regulates the proliferation and invasion of nasopharyngeal carcinoma in vitro." Tumor Biology **35**(8): 7651-7657.

Zhao, R., K. Gish, M. Murphy, Y. Yin, D. Nottelman, W. H. Hoffman, E. Tom, D. H. Mack and A. J. Levine (2000). "Analysis of p53-regulated gene expression patterns using oligonucleotide arrays." Genes & Development **14**(8): 981-993.

Zhao, Y., A. Aguilar, D. Bernard and S. Wang (2015). "Small-Molecule Inhibitors of the MDM2-p53 Protein-Protein Interaction (MDM2 Inhibitors) in Clinical Trials for Cancer Treatment." Journal of Medicinal Chemistry **58**(3): 1038-1052.

Zhao, Y., L. Liu, W. Sun, J. Lu, D. McEachern, X. Li, S. Yu, D. Bernard, P. Ochsenbein, V. Ferey, J.-C. Carry, J. R. Deschamps, D. Sun and S. Wang (2013). "Diastereomeric Spirooxindoles as Highly Potent and Efficacious MDM2 Inhibitors." Journal of the American Chemical Society **135**(19): 7223-7234.

Zhao, Y., H. D. Thomas, M. A. Batey, I. G. Cowell, C. J. Richardson, R. J. Griffin, A. H. Calvert, D. R. Newell, G. C. M. Smith and N. J. Curtin (2006). "Preclinical evaluation of a potent novel DNA-dependent protein kinase inhibitor NU7441." Cancer Research **66**(10): 5354-5362.

Zheng, H., H. You, X. Z. Zhou, S. A. Murray, T. Uchida, G. Wulf, L. Gu, X. Tang, K. P. Lu and Z.-X. J. Xiao (2002). "The prolyl isomerase Pin1 is a regulator of p53 in

genotoxic response." Nature **419**(6909): 849-853.

Zhong, H., G. Chen, L. Jukofsky, D. Geho, S. W. Han, F. Birzele, S. Bader, L. Himmelein, J. Cai, Z. Albertyn, M. Rothe, L. Essioux, H. Burtscher, S. A. Middleton, R. Rueger, L.-C. Chen, M. Dangl, G. Nichols and W. E. Pierceall (2015). "MDM2 antagonist clinical response association with a gene expression signature in acute myeloid leukaemia." British Journal of Haematology: n/a-n/a.

Zhou, Z. X., M. Patel, N. Ng, M. H. Hsieh, A. P. Orth, J. R. Walker, S. Batalov, J. L. Harris and J. Liu (2014). "Identification of synthetic lethality of PRKDC in MYC-dependent human cancers by pooled shRNA screening." Bmc Cancer **14**.

Zindy, F., C. M. Eischen, D. H. Randle, T. Kamijo, J. L. Cleveland, C. J. Sherr and M. F. Roussel (1998). "Myc signaling via the ARF tumor suppressor regulates p53-dependent apoptosis and immortalization." Genes Dev **12**(15): 2424-2433.

Znojek, P., E. Willmore and N. J. Curtin (2014). "Preferential potentiation of topoisomerase I poison cytotoxicity by PARP inhibition in S phase." Br J Cancer **111**(7): 1319-1326.

Appendix I: Publications

Chemical Inhibition of Wild-Type p53-Induced Phosphatase 1 (WIP1/PPM1D) by GSK2830371 Potentiates the Sensitivity to MDM2 Inhibitors in a p53-Dependent Manner

Arman Esfandiari¹, Thomas A. Hawthorne¹, Sirintra Nakjang^{1,2}, and John Lunec¹

Abstract

Sensitivity to MDM2 inhibitors is widely different among responsive *TP53* wild-type cell lines and tumors. Understanding the determinants of MDM2 inhibitor sensitivity is pertinent for their optimal clinical application. Wild-type p53-inducible phosphatase-1 (WIP1) encoded by *PPM1D*, is activated, gained/amplified in a range of *TP53* wild-type malignancies, and is involved in p53 stress response homeostasis. We investigated cellular growth/proliferation of *TP53* wild-type and matched mutant/null cell line pairs, differing in *PPM1D* genetic status, in response to Nutlin-3/RG7388 ± a highly selective WIP1 inhibitor, GSK2830371. We also assessed the effects of GSK2830371 on MDM2 inhibitor-induced p53^{Ser15} phosphorylation, p53-mediated global transcriptional activity, and apoptosis. The investigated cell line pairs were relatively insensitive to single-agent GSK2830371. However, a non-growth-inhibitory dose of GSK2830371 markedly potentiated the response to

MDM2 inhibitors in *TP53* wild-type cell lines, most notably in those harboring *PPM1D*-activating mutations or copy number gain (up to 5.8-fold decrease in GI₅₀). Potentiation also correlated with significant increase in MDM2 inhibitor-induced cell death endpoints that were preceded by a marked increase in a WIP1 negatively regulated substrate, phosphorylated p53^{Ser15}, known to increase p53 transcriptional activity. Microarray-based gene expression analysis showed that the combination treatment increases the subset of early RG7388-induced p53 transcriptional target genes. These findings demonstrate that potent and selective WIP1 inhibition potentiates the response to MDM2 inhibitors in *TP53* wild-type cells, particularly those with *PPM1D* activation or gain, while highlighting the mechanistic importance of p53^{Ser15} and its potential use as a biomarker for response to this combination regimen. *Mol Cancer Ther*; 15(3); 379–91. ©2016 AACR.

Introduction

Mutational inactivation of the p53 tumor suppressor protein, encoded by the *TP53* gene, occurs in approximately 50% of malignancies overall (1, 2). Nongenotoxic activation of p53 in the remaining *TP53* wild-type malignancies has attracted attention as a therapeutic strategy (3–5). In unstressed cells, p53 is rapidly turned over by binding to one of its transcriptional target gene products, MDM2, which inhibits p53-mediated transcription, promotes p53 ubiquitin-mediated nuclear export and its proteasomal degradation (3). Cellular stress can activate effector molecules (e.g., DNA-PK, ATM, and ATR) that posttranslationally modify MDM2 and/or p53, leading to their dissociation followed by p53-mediated reversible cell-cycle arrest, senescence,

or programmed cell death (6). Proof-of-concept that pharmacologic inhibition of the MDM2-p53 interaction by small molecular weight MDM2 inhibitors can be successfully used for nongenotoxic activation of p53 has been established in preclinical and clinical settings with encouraging antitumor activity (4, 7). Although, it is firmly established that the most important determinant of response to MDM2 inhibitors is wild-type *TP53* genetic status (Supplementary Fig. S1A and ref. 8), multiple independent studies using various classes of MDM2 inhibitors, and drug sensitivity data generated by the Sanger Institute, have shown that there is a wide range of sensitivity to MDM2 inhibitors among *TP53* wild-type cell lines [Supplementary Fig. S1B (8–10)]. These highlight that the determinants of sensitivity to MDM2 inhibitors in a *TP53* wild-type background are poorly understood. The use of combination regimens and patient stratification strategies are therefore being investigated to optimize tumor-specific response in *TP53* wild-type malignancies (11–13).

Another strategy for nongenotoxic activation of p53 currently in preclinical development is inhibition of wild-type p53-inducible phosphatase-1 (WIP1/PPM1D), which is involved in homeostatic regulation of p53 function and stability following cellular stress (14–16). *PPM1D* is a bona fide oncogene that is activated, gained, or amplified mostly in *TP53* wild-type malignancies (17–19). Notably, *PPM1D* gain-of-function mutations (activation) and *TP53*-inactivating mutations are mutually exclusive in brainstem gliomas, consistent with the role of WIP1 (*PPM1D* gene product) in negative regulation of p53 (18). Following cellular

¹Northern Institute for Cancer Research, Newcastle University, Newcastle upon Tyne, United Kingdom. ²Bioinformatics Support Unit, Faculty of Medical Sciences, Newcastle University, Newcastle upon Tyne, United Kingdom.

Note: Supplementary data for this article are available at Molecular Cancer Therapeutics Online (<http://mct.aacrjournals.org/>).

Corresponding Author: John Lunec, Northern Institute for Cancer Research, Newcastle University, Paul O'Gorman Building, Framlington Place, Newcastle upon Tyne NE2 4HH, United Kingdom. Phone: 4401-9124-64420; Fax: 4401-9124-64301; E-mail: john.lunec@ncl.ac.uk

doi: 10.1158/1535-7163.MCT-15-0651

©2016 American Association for Cancer Research.

stress, p53 transcriptionally induces WIP1, which forms a negative automodulatory loop with the p53 network by dephosphorylating p53 and other signaling components involved in p53 posttranslational regulation (15). In spite of selectivity and bioavailability challenges associated with pharmacological targeting of phosphatases (20), recently a highly selective allosteric WIP1 inhibitor, GSK2830371, which targets the unique flap-subdomain on WIP1 was identified and characterized (16). Although, the response to GSK2830371 was contingent on wild-type *TP53*, some *TP53* wild-type cell lines did not respond in the dose range associated with on-target activity (16). In a subsequent publication that highlighted WIP1 as a potential target in neuroblastoma, GSK2830371 was shown to effectively inhibit the growth of *TP53* wild-type cell lines with *PPM1D* copy number gain. However, there was greater than 52-fold range in sensitivity, with NGP cells (*PPM1D* copy number gain) showing no response at all within the dose range tested (10 $\mu\text{mol/L}$ cutoff; ref. 21).

MDM2 blocks the p53 transactivation domain by interacting with three key p53 amino acids (Phe19, Tyr23, and Leu26) that are proximal to a WIP1 substrate, phosphorylated p53^{Ser15} (pp53^{Ser15}) (22, 23). Unlike the strong influence of p53^{Ser20} phosphorylation on binding to MDM2, the phosphorylation of p53^{Ser15} has been reported to either have no or a modest effect on binding of p53 to MDM2 (24, 25), it has nevertheless been shown to contribute to increased p53 proapoptotic transcriptional transactivation activity (25–27). After MDM2 inhibitor-mediated dissociation of p53 from MDM2, pp53^{Ser15} is generated by the basal unstimulated activity of effector kinases that normally phosphorylate p53^{Ser15} following genotoxic stress (26). This suggests that a dynamic equilibrium exists between kinases and phosphatases in regulating pp53^{Ser15} following MDM2 inhibitor-induced p53 stabilization, which can be tilted in favor of the p53-activating kinases by inhibiting WIP1. Therefore, in this study, we have investigated whether a selective WIP1 inhibitor GSK2830371 can potentiate the response to MDM2 inhibitors Nutlin-3 and RG7388 in a panel of cell line pairs differing in their *TP53* and *PPM1D* genetic status. Our findings show that a nongrowth-inhibitory dose of GSK2830371 can substantially increase sensitivity to MDM2 inhibitors in *TP53* wild-type cell lines, particularly in those with *PPM1D* copy number gain or gain-of-function mutation. Furthermore, global gene expression analysis showed that RG7388 in the presence of GSK2830371 induces additional early p53 transcriptional target genes involved in apoptosis in *TP53* wild-type cell lines that are not responsive to the WIP1 inhibitor alone. We propose that the combination of WIP1 and MDM2 inhibitors can selectively accentuate the sensitivity to MDM2 inhibitors in *TP53* wild-type tumors with increased WIP1 expression or activity, with elevated pp53^{Ser15} as a potential mechanistic biomarker for response to this combination.

Materials and Methods

Cell lines and growth conditions

All cell lines used were obtained from Northern Institute for Cancer Research cell line bank that only includes cell lines that have been authenticated using short tandem repeat DNA profiling (LGC Standards). Postauthentication passages were limited to 30 for experimental procedures (<6 months) before replacing with lower passage number stocks. Cell line pairs used and their *TP53* and *PPM1D* genetic status are described in Table 1. MCF-7 cells were used as a positive control for WIP1 protein expression and response to the WIP1 inhibitor GSK2830371. The S_N40R2 (SN40R2) and N_N20R1 (N20R1) cell lines were *TP53* mutant, otherwise isogenic, Nutlin-3-resistant clones derived from SJS-1 osteosarcoma and NGP neuroblastoma cells, respectively, and have been cited in preclinical studies of MDM2 inhibitors (28; see Table 1 for mutation details). U2OS-DN cells overexpress the R175H variant of p53 that is reported to have a dominant negative effect (29).

Growth inhibition assay

Cells were seeded in 96-well plates 24 hours before treatment. Cells were then fixed with Carnoy fixative and Sulforhodamine B assay was carried out as described in ref. 30. A spectrophotometer (Bio-Rad Model 680) was used for densitometry at 570 nm.

Immunoblotting

Western blotting was carried out as described in ref. 31. Antibodies used were MDM2 (Ab-1) 1:300 (Cat No.: OP46-100UG, Merck Millipore), MDMX (Cat No.: A300287A-2 Bethyl Laboratories), WIP1 (F-10) 1:200 (Cat No.: sc-376257, Santa Cruz Biotechnology), p53 1:500 (Cat No.: NCL-L-p53-DO7, Leica Microsystems Ltd.), phospho-p53^{Ser15} 1:1,000 (Cat No.: 9284 Cell Signaling Technology), p21^{WAF1} 1:100 (Cat No.: OP64, Calbiochem), BAX 1:1,000 (Cat No.: 2772S, Cell Signaling Technology), cleaved caspase-3 1:1,000 (Cat No.: 9664S, New England Biolabs Ltd.), and actin 1:3,000 (Cat No.: A4700, Sigma-Aldrich). Secondary goat anti-mouse/rabbit horseradish peroxidase-conjugated antibodies (Cat No.: P0447/P0448, Dako) were used at 1:1,000. All antibodies were diluted in 5% milk/1 \times TBS-tween (w/v). Proteins were visualized using enhanced chemiluminescence (GE Healthcare Life Sciences) and x-ray film (Fujifilm). Densitometry was carried out using ImageJ software.

Denaturing immunoprecipitation

Treated cells were lysed [50 mmol/L Tris, 150 mmol/L NaCl, 0.2 mmol/L Na₃VO₄, 1% NP40 v/v, 1 mmol/L phenylmethylsulfonyl fluoride, Roche cComplete protease inhibitor tablet, 1 mmol/L dithiothreitol (DTT), 2% SDS] then aliquots were conserved as input. Nondenaturing (no SDS) lysis buffer was used to dilute the

Table 1. *TP53* wild-type and mutant/null cell line pairs with different *PPM1D* genetic status

<i>TP53</i> wild-type parental cell lines	<i>TP53</i> -mutant/null daughter lines	Tumor of origin	<i>PPM1D</i> genetic alteration (citation)
SJS-1	SN40R2 (E285K)	Osteosarcoma	Wild-type (51)
HCT116 ^{+/+}	HCT116 ^{-/-} (Null)	Colorectal carcinoma	c.1344delT/Wt (L450X) gain-of-function (39)
U2OS	U2OS-DN (R175H)	Osteosarcoma	c.1372C>T/Wt (R458X) gain-of-function (39)
NGP	N20R1 (P152T and P98H)	Neuroblastoma	Copy number gain (21)
MCF-7	—	Breast adenocarcinoma	Amplified (38)

NOTE: *PPM1D* status of SJS-1 cells were obtained from sanger.ac.uk (51). *TP53*-mutant daughter cell lines of NGP and SJS-1 cell lines were derived as described in Materials and Methods.

Abbreviations: Mt, mutant; Wt, wild-type.

remainder of the lysates (<0.1% SDS). A total of 1 to 2 μ g of rabbit antiubiquitin antibody (Cat No.: FL-76, Santa Cruz Biotechnology) or rabbit IgG control (Cat No.: X0903, Dako) was added to each appropriate vessel and incubated overnight at 4°C. Sepharose beads (Cat No.: 17-0618-01, GE Healthcare) were then added and incubated for a further 4 hours at 4°C. Beads were washed first with 0.5 mol/L KCl then with 0.1 mol/L KCl, then treated as lysates in the immunoblotting protocol above.

Caspase-3/7 assay

A total of 2×10^4 cells/well ($\approx 60\%$ – 70% confluence) were seeded in white 96-well plates (CELLSTAR, Greiner Bio-One international) and treated after 24 hours. Caspase-3/7 enzymatic activities were quantified by adding a 1:1 ratio of CaspaseGlo 3/7 reagent (Promega) to growth media 30 minutes before measuring the luminescence signal using a FLUOstar Omega plate reader (BMG Labtech) and all values were expressed as a ratio of signal relative to solvent control.

Expression array

NGP cells were seeded at 6×10^5 cells per well of a 6-well plate and treated with either DMSO or 75 nmol/L of RG7388 ($\approx GI_{50}$) \pm 2.5 μ mol/L GSK2830371 for 4 hours before RNA extraction using RNeasy Plus Mini Kit (Qiagen). Concentration and quality of mRNA were determined using Agilent RNA 6000 nano kit on an Agilent 2100 Bioanalyzer (RNA integrity numbers > 9). RNA samples were sent to AROS Applied Biotechnology (Aarhus, Denmark) for gene expression analysis using Illumina Beadchip expression arrays (HumanHT-12v4.0). Array data processing, background correction, normalization, and quality control checks were performed using the R package "Lumi" (bioconductor.org). Probe intensity values were converted to variance stabilized data. Robust spline normalization was used as an array normalization method. Poor-quality probes (detection threshold < 0.01), and probes that are not detected at all in the remaining arrays were removed prior to downstream analysis. The remaining probe normalized intensity values (18,634) were used in the differential expression analysis. The data discussed in this article have been deposited in NCBI's Gene Expression Omnibus (GEO; ref. 32) and are accessible through GEO Series accession number GSE75197 (<https://www.ncbi.nlm.nih.gov/geo/query/acc.cgi?acc=GSE75197>).

RNA extraction and qRT-PCR

Complementary DNA was generated using the Promega Reverse Transcription System (A3500, Promega) as described by the manufacturer. qRT-PCR was carried out using SYBR green RT-PCR master mix (Life Technologies) as per the manufacturer's guidelines and the following primers (5'-3'): *CDKN1A* [forward (F)-TGTCGGTCAGAACCCATGC, reverse (R)-AAAGTCGAAGT-TCCATCGCTC], *TP53INP1* (F-TCTTGAGTGCTTGCGTGATACA, R-GGTGGGGTGATAAACCAGCTC), *BTG2* (F-CCTGTGGGTG-GACCCCTAT, R-GGCCTCTCTGACAAAGACG), *MDM2* (F-CAG-TAGCAGTGAATCTACAGGGA, R-CTGATCCAACCAATCACCT-GAAT) and *GAPDH* (F-CAATGACCCCTTCATTGACC, R-GATC-TCGCTCCTGGAAGAT)]. A total of 50 ng/ μ L of the cDNA samples per 10 μ L final reaction volume, with the standard cycling parameters (stage 1: 50°C for 2 minutes, stage 2: 95°C for 10 minutes, then 40 cycles of 95°C for 15 seconds, and 60°C for 1 minute), were set and carried out on an ABI 7900HT sequence detection system. Data were presented as mean \pm SEM relative quantities of

four independent repeats where *GAPDH* was used as endogenous control and DMSO used as the calibrator for each independent repeat with the formula $2^{-\Delta\Delta C_t}$. Analysis was carried out using SDS 2.2 software (Applied Biosystems).

Site-directed mutagenesis and p53 overexpression

The plasmid vector used in this study was pcDNA3.1 (+/-; Life Technologies, Cat No. V790-20 and V795-20) and full-length human *TP53* cDNA cloned into this backbone. The Gozani laboratory protocol for site-directed mutagenesis (33) was used to generate the p53^{Ser15} mutants. Primers used: p53^{S15A} (F-GTCC-AGCCCCCTCTGGCTCAGGAAACATTTTCA, R-TGAAAATGTT-TCTCTGAGCCAGAGGGGGCTCGAC) and p53^{S15D} (F-GTCGA-GCCCCCTCTGGACCAGGAAACATTTTCA, R-TGAAAATGTTTCTGCTCCAGAGGGGGCTCGAC). HCT116^{-/-} cells were transfected with Lipofectamine 2000 and plasmid DNA 12 hours before lysates were collected at different time intervals.

Flow cytometry

After treatment, floating and adhered cells were pooled and incubated in propidium iodide solution [150 μ mol/L propidium iodide (Calbiochem), 1.46 μ mol/L DNase free-RNase A (Sigma), 3.88 mmol/L sodium citrate (Sigma), and 0.3% Triton-X 100 (Sigma)] for 10 minutes at 25°C and then FACS was carried out using a FACSCalibur (BD Biosciences)]. CellQuest software was used to establish cell-cycle distribution and gated histograms.

Statistical analysis

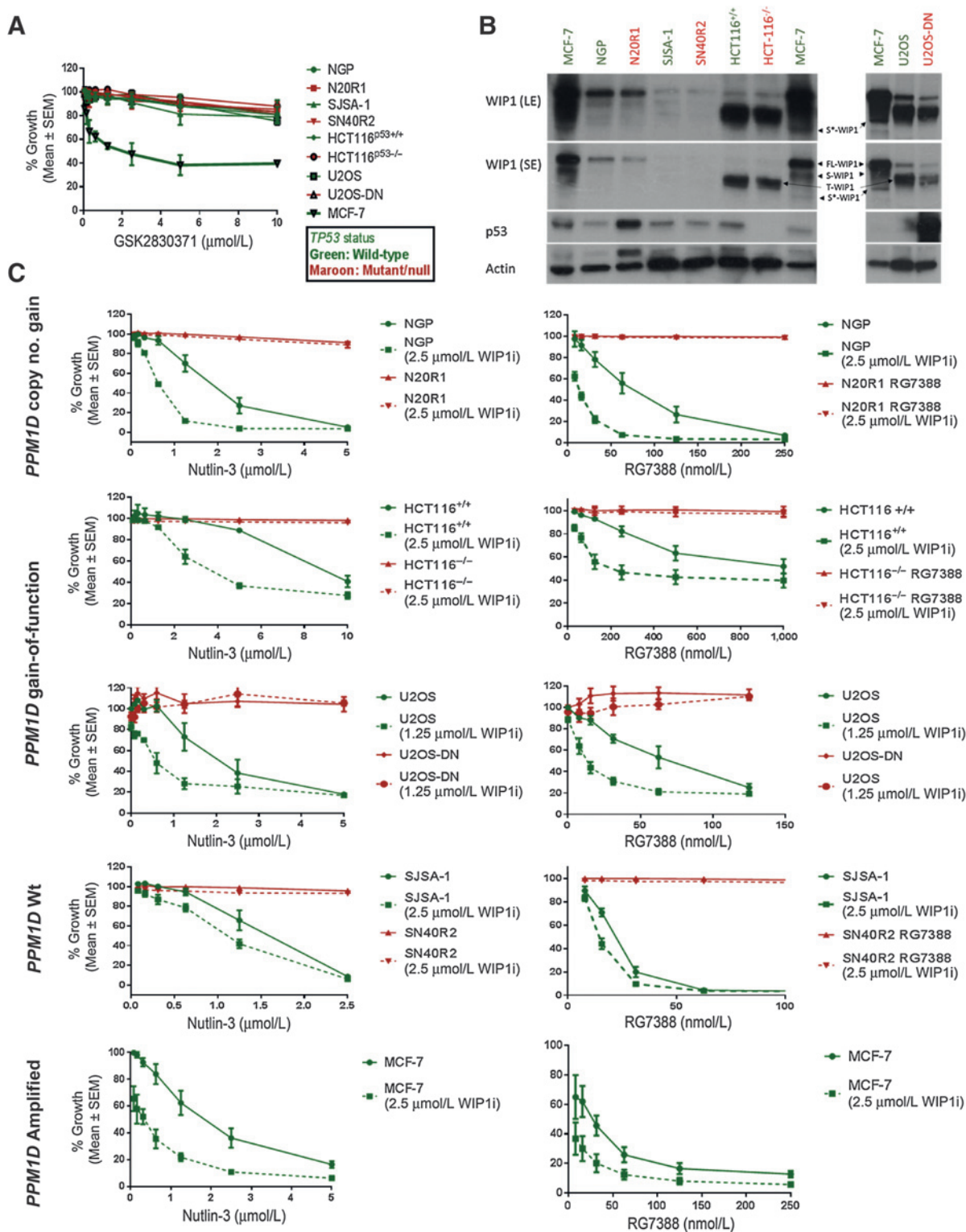
Statistical tests were carried out in GraphPad Prism 6 software and all *P* values represent two-tailed paired *t* tests of three or more independent repeats unless otherwise stated. For microarray differential expression analysis, R-statistical software was used. Microarray data was processed using R Bioconductor package *lumi* (34) Probes intensity values were transformed using variance stabilizing transformation implemented in the *lumi* package before data normalization. The robust spline normalization was used as a normalization method. Poor quality probes (detection threshold < 0.01), and probes that were not detected at all in the remaining arrays were removed. Differential expression analysis was performed using R Bioconductor package *limma* (35).

Results

GSK2830371 potentiates the response to MDM2 inhibitors Nutlin-3 and RG7388 in a p53-dependent manner

Growth inhibition assays were carried out on a panel of *TP53* wild-type and mutant/null cell line pairs differing in their *PPM1D* genetic status, to assess their sensitivity to the selective allosteric WIP1 inhibitor GSK2830371 and its ability in turn to sensitize cells to MDM2 inhibitors (Fig. 1A). GSK2830371-sensitive MCF-7 cells were used as a positive control for the growth-inhibitory activity and biochemical effect of this compound. GSK2830371 had a 50% growth inhibitory concentration (GI_{50}) of 2.65 μ mol/L \pm 0.54 (SEM) in MCF-7 cells. The growth inhibition curve for GSK2830371 plateauead in MCF-7 cells at doses 2.5 to 10 μ mol/L suggesting that a subpopulation of MCF-7 cells are resistant to growth inhibition and apoptosis in response to maximal WIP1 inhibition (Fig. 1A). All other cell line pairs were not sensitive to growth inhibition by GSK2830371 alone, with GI_{50} > 10 μ mol/L irrespective of their *PPM1D* or *TP53* genetic status (Fig. 1A). Basal expression of WIP1 across the panel of cell line pairs was

Esfandiari et al.

**Figure 1.**

A, the effect on growth of a panel of p53 wild-type (green) and mutant/null (maroon) cell line pairs with different *PPM1D* genetic status to 0.08–10 $\mu\text{mol/L}$ GSK2830371 exposure for 168 hours, using Sulforhodamine B growth inhibition assays. B, basal expression of WIP1 and p53 in cell lines (SE, short film exposure; LE, long exposure). C, the sensitivity of a panel of p53 Wt (green) and mutant/null (maroon) cell line pairs with different *PPM1D* genetic status to 0.08–10 $\mu\text{mol/L}$ Nutlin-3 and 0.008–1 $\mu\text{mol/L}$ RG7388 in 168 hours Sulforhodamine B growth inhibition assays in the presence and absence of the highest nongrowth inhibitory dose of GSK2830371 (2.5 $\mu\text{mol/L}$). The U2OS cell line pair was treated with MDM2 inhibitors \pm 1.25 $\mu\text{mol/L}$ GSK2830371. FL-WIP1, full-length WIP1; S-WIP1, WIP1 shorter isoform; S^{*}-WIP1, the shortest band detected by the F-10 antibody; T-WIP1, truncated WIP1 mutants; WIP1i, GSK2830371; WIP1 L450X in HCT116 cells or WIP1 R458X in U2OS cells.

assessed by immunoblotting with an antibody that detects WIP1 (FL-WIP1), its previously described shorter isoform (S-WIP1; ref. 36), and the two WIP1 gain-of-function mutant proteins in HCT116 and U2OS cell line pairs (Fig. 1B). Transient knock-down of WIP1 using four different anti-*PPM1D* siRNA constructs resulted in a reduction in the intensity of all the bands detected by the WIP1 antibody (F-10), which suggests that all of the bands detected in these conditions correspond to WIP1 (Supplementary Fig. S2A). This includes a further WIP1 isoform detected by F-10 (≈ 55 kDa), which is referred to here as S*-WIP1. *PPM1D*-amplified MCF-7 cells (37) showed the highest basal expression of WIP1 and its isoforms, consistent with their sensitivity to GSK2830371 single treatment (Fig. 1B; see ref. 38). NGP cells, with *PPM1D* copy number gain (21), and its otherwise isogenic *TP53*-mutant daughter cell line, N20R1, were insensitive to <10 $\mu\text{mol/L}$ GSK2830371 despite showing the second highest expression of full-length WIP1 after MCF-7 cells. The SJS-A1 and SN40R2 *TP53* wild-type and mutant pair, with wild-type *PPM1D*, showed the least WIP1 protein expression among all cell line pairs in the panel. Shorter bands corresponding to the previously reported truncated and activating WIP1-mutant proteins WIP1 L450X and WIP1 R458X were detected in lysates derived from HCT116 and U2OS cell line pairs, respectively (Fig. 1B; ref. 39).

Because of the role of WIP1 in homeostatic feedback regulation of the p53 network, we aimed to assess whether GSK2830371 (WIP1i) can potentiate the response to MDM2 inhibitors. Treatment with a combination of the highest nongrowth-inhibitory dose of GSK2830371 (2.5 $\mu\text{mol/L}$), potentiated the response to MDM2 inhibitors Nutlin-3 and RG7388 in a p53-dependent manner in cell lines that were not sensitive to growth inhibition by GSK2830371 alone (Fig. 1C). *TP53* wild-type parental cell lines HCT116^{+/+}, NGP, and SJS-A1 showed a 2.4-fold ($P = 0.007$), 2.1-fold ($P = 0.039$), and 1.3-fold ($P = 0.017$) decrease, respectively, in their Nutlin-3 GI₅₀ values in the presence of 2.5 $\mu\text{mol/L}$ GSK2830371. In contrast, Nutlin-3 GI₅₀ did not change for their *TP53* null/mutant matched pairs HCT116^{-/-}, N20R1, and SN40R2. However, pertinent to the widening of RG7388 therapeutic index in the clinic, the same dose of GSK2830371 resulted in a much greater potentiation of RG7388 in *TP53* wild-type cell lines with either *PPM1D* gain-of-function or copy number gain: NGP 5.8-fold ($P = 0.049$) and HCT116^{+/+} 4.8-fold ($P = 0.018$) compared with *PPM1D* wild-type SJS-A1 cells 1.4-fold ($P = 0.020$; Fig. 1C). U2OS *TP53* wild-type cells showed a similar trend toward potentiation of Nutlin-3 in combination with GSK2830371 at 1.25 $\mu\text{mol/L}$ as Nutlin-3 GI₅₀ was reduced by 3.2-fold ($P = 0.08$); however, the same dose of the WIP1 inhibitor resulted in a 5.3-fold ($P = 0.039$) decrease in RG7388 GI₅₀. None of the *TP53*-mutant daughter cell lines showed increased sensitivity to RG7388 in the presence of the WIP1 inhibitor. Interestingly, the combination of Nutlin-3 or RG7388 with 2.5 $\mu\text{mol/L}$ GSK2830371 also augmented the growth inhibitory effect in MCF-7 cells compared with each drug alone. Therefore, the most marked fold change in sensitivity to both MDM2 inhibitors was observed in *TP53* wild-type cell lines that have increased WIP1 expression or activity.

Inhibition of WIP1 catalytic activity by GSK2830371 is separable from its induction of ubiquitin-mediated WIP1 degradation

Treatment of MCF-7 cells with 2.5 $\mu\text{mol/L}$ GSK2830371 resulted in marked time-dependent degradation of both isoforms

of WIP1 over 8 hours, which correlated with p53 stabilization and pp53^{Ser15} consistent with previous reports by Gilmartin and colleagues, (Fig. 2A; ref. 16). Quantification of WIP1 signal intensity is presented in Supplementary Fig. S2B.

To test the effect of the GSK2830371 inhibitor on WIP1 phosphatase activity separate from degradation of WIP1, its effect on the phosphorylation of p53^{Ser15} 30 minutes following exposure of MCF7 cells to ionizing radiation was assessed. GSK2830371 was seen to inhibit pp53^{Ser15} dephosphorylation at a time point when the WIP1 protein expression had not yet been affected by this compound (compare pp53^{Ser15} on the last two tracks in Fig. 2B). These data show that inhibition of the catalytic activity of WIP1 by GSK2830371 is separable from its ubiquitin-mediated degradation.

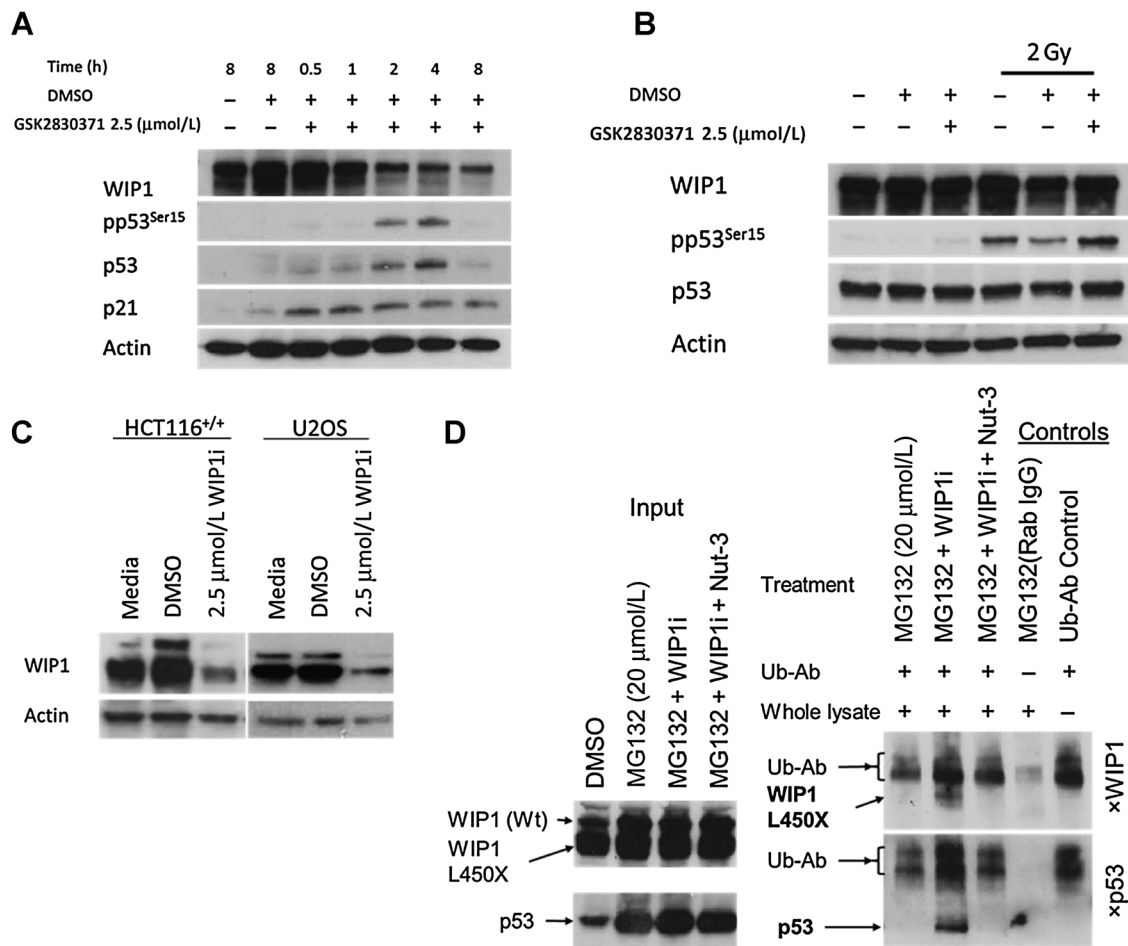
It was noteworthy that GSK2830371 also lead to the degradation of truncated WIP1 mutants within 4 hours (Fig. 2C). We carried out a denaturing immunoprecipitation experiment probing for all ubiquitinated species in HCT116^{+/+} cells treated with the proteasome inhibitor MG132 and either GSK2830371 alone or in combination with Nutlin-3, to assess whether wild-type WIP1 and WIP1 L450X are both degraded by ubiquitin-mediated processes (Fig. 2C). The anti-ubiquitin antibody (Ub-Ab) migrated to a similar molecular weight as full-length WIP1 and it was detected by the goat anti-mouse antibody (Fig. 2D, last lane Ub-Ab Control); therefore, the ubiquitination of full-length WIP1 could not be determined. However, ubiquitinated WIP1 L450X was observed to be increased by GSK2830371 (Fig. 2D). Interestingly, this ubiquitination event was also reduced in the presence of Nutlin-3. Increased ubiquitination of p53 in the presence of MG132 + GSK2830371 was reversed by Nutlin-3 as expected because inhibiting MDM2-p53 interaction prevents MDM2-mediated p53-ubiquitination.

GSK2830371 significantly increases MDM2 inhibitor-mediated apoptosis and reduces clonogenic cell survival in *TP53* wild-type cell lines

The combination of GSK2830371 and multiples of Nutlin-3 GI₅₀ dose resulted in a marked increase in caspase-3/7 activity in both NGP and SJS-A1 cells compared with treatment with either drug alone (Fig. 3A and B). For NGP cells, 24-hour treatment with 2.5 $\mu\text{mol/L}$ GSK2830371 did not lead to detectable caspase-3/7 activity, whereas Nutlin-3 at 0.5 \times and 1 \times GI₅₀ resulted in a dose-dependent increase in caspase-3/7 signal, which was significantly enhanced (≈ 4 -fold $P = 0.005$ and ≈ 3 -fold $P = 0.02$, respectively) in the presence of 2.5 $\mu\text{mol/L}$ GSK2830371 (Fig. 3A). No increased caspase-3/7 activity was observed in SJS-A1 cells after 24 hours of exposure to 2.5 $\mu\text{mol/L}$ GSK2830371 alone or Nutlin-3 \pm 2.5 $\mu\text{mol/L}$ GSK2830371 (data not shown). Similarly in both cell line pairs, 48 hours treatment with 2.5 $\mu\text{mol/L}$ GSK2830371 alone resulted in no increased caspase-3/7 activity, whereas its presence significantly increased response to Nutlin-3 (≈ 2.7 -fold $P = 0.01$ in NGP, ≈ 2 -fold $P = 0.04$ in SJS-A1) in a p53-dependent manner (Fig. 3B).

Caspase-3/7 activity could not be detected in HCT116^{+/+} and for up to 48 hours following treatment (data not shown), so continuous exposure cloning efficiency experiments were carried out as described in Fig. 3C (see caption) to assess clonogenic cell survival. There was no reduction in clonogenic efficiency in the presence of the GSK2830371 alone in comparison with untreated controls. Cloning efficiency of HCT116^{+/+} cells in the presence of

Esfandiari et al.

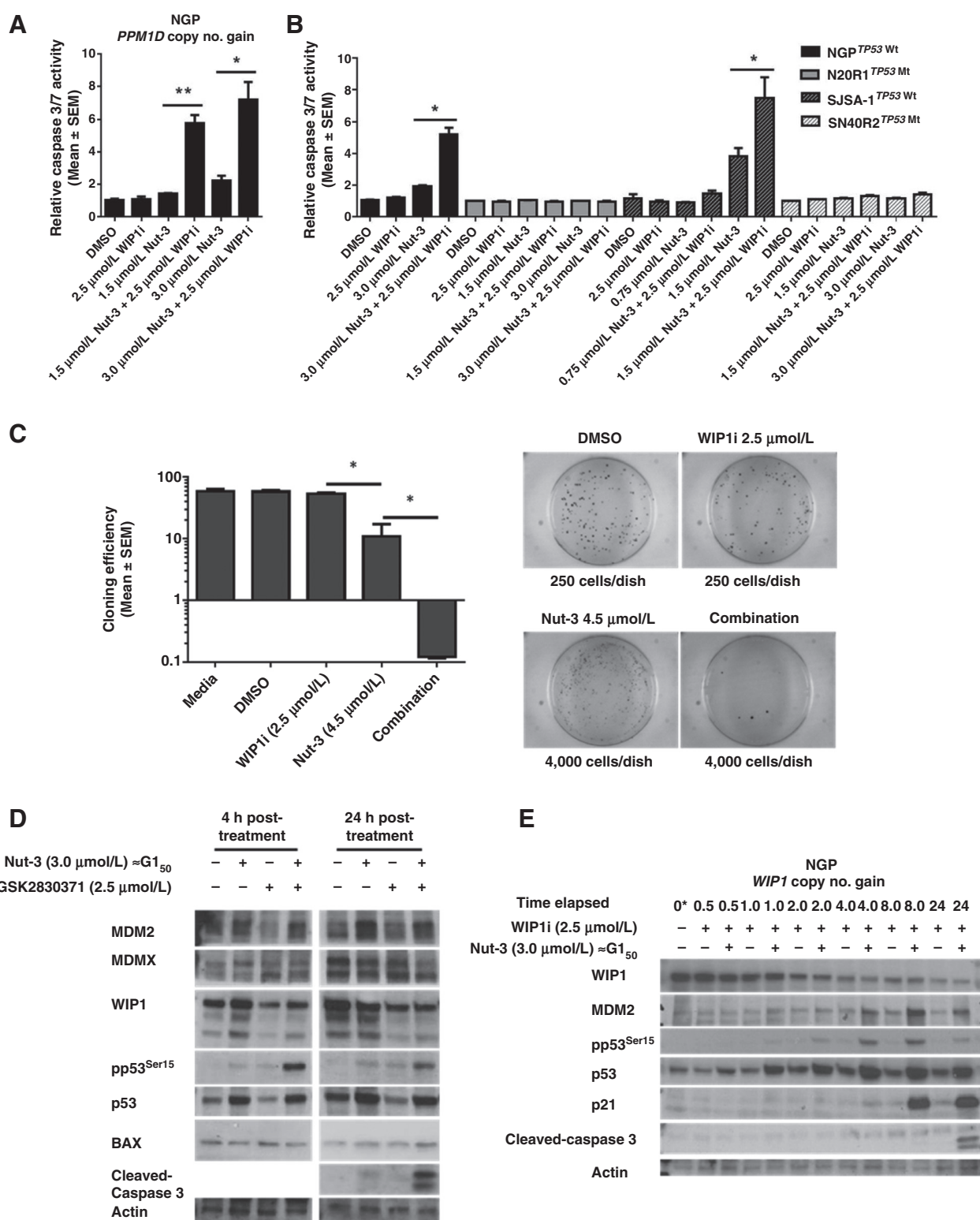
**Figure 2.**

A, GSK2830371 (2.5 μmol/L) treatment of MCF-7 cells over 8 hours shows WIP1 degradation over time, p53 stabilization, and Phospho-p53^{Ser15} (pp53^{Ser15}) accumulation. B, p53^{Ser15} phosphorylation in MCF-7 cells 30 minutes after 2 Gy ionizing radiation in the presence or absence of 2.5 μmol/L. GSK2830371 inhibits WIP1 catalytic activity independent of WIP1 protein levels. C, 4-hour treatment with 2.5 μmol/L GSK2830371 results in degradation of full-length and truncated WIP1 in HCT116^{+/+} and U2OS cells. D, lysates obtained from HCT116^{+/+} cells treated with 20 μmol/L proteasome inhibitor MG132 and 2.5 μmol/L GSK2830371 ± 3.0 μmol/L Nutlin-3 overnight underwent immunoprecipitation with anti-ubiquitin antibody (Ub-Ab) and the precipitates probed for WIP1 and p53 by western blot analysis. Input samples (left panel) are western blots of total lysate before IP for comparison with the IP results on the righthand panel. An aliquot of MG132-treated lysate was precipitated with rabbit IgG instead of Ub-Ab as a negative control. Ub-Ab, anti-ubiquitin antibody; WIP1i, GSK2830371; WIP1 (Wt), wild-type WIP1; WIP1 L450X, truncated WIP1.

0.5 × Nutlin-3 GI₅₀ significantly decreased ($P = 0.008$) when GSK2830371 was present at 2.5 μmol/L (Fig. 3C).

In NGP cells, pp53^{Ser15} was not affected by the GI₅₀ dose of Nutlin-3 or 2.5 μmol/L GSK2830371 alone, whereas in combination there was a marked increase in pp53^{Ser15} at 4 hours that persisted through to 24 hours and correlated with the detection of cleaved caspase-3 (Fig. 3D and E). GSK2830371 alone resulted in modest p53 stabilization in NGP cells, after 24-hour treatment, which did not result in detectable induction of p53 direct transcriptional targets p21^{WAF1} and MDM2 (Fig. 3E). Interestingly, monotreatment with the same dose of GSK2830371 in MCF-7 cells was sufficient for WIP1 degradation, p53 stabilization and increase pp53^{Ser15} in contrast to NGP cells (Fig. 2A vs. Fig. 3E). Consistently, WIP1 was also degraded in NGP cells in the presence of the WIP1 inhibitor (track 3 vs. track 1 in Fig. 3D) even when WIP1 was induced by Nutlin-3 (track 4 vs. track 2 in Fig. 3D). The lack of a p53 response of NGP cells to 2.5 μmol/L GSK2830371 may explain their insensitivity to GSK2830371

monotreatment compared with MCF-7 cells. Also, the addition of 2.5 μmol/L GSK283037 did not affect MDM2 induction by Nutlin-3 (Fig. 3D). This suggests that the reported role of WIP1 in downregulation of MDM2 (14) may be counterbalanced by the p53-dependent transcriptional induction of MDM2 in the presence of Nutlin-3. There was a reduction in MDMX expression 24 hours after combination treatment compared with Nutlin-3 treatment alone (Fig. 3D). Given that MDMX increased expression has been proposed to contribute to reduced sensitivity to MDM2 inhibitors (40), it is likely that the role of WIP1 in negative regulation of MDMX stability (41) may be a factor in its ability to potentiate MDM2 inhibitors in MDMX-overexpressing NGP cells. There was no change in the expression of the p53 proapoptotic transcriptional target BAX at 4 and 24 hours following combination treatment compared with Nutlin-3 or WIP1 inhibitor monotreatments (Fig. 3D). This suggests that BAX is likely not involved in potentiation of Nutlin-3 by the WIP1 inhibitors.

**Figure 3.**

A, dose-dependent increase in caspase 3/7 activity of NGP cells after 24 hours treatment with Nutlin-3 (Nut-3 $G1_{50} \approx 3.0 \mu\text{mol/L}$) alone or in combination with 2.5 $\mu\text{mol/L}$ GSK2830371. B, increase in caspase-3/7 activity in NGP and SJS-A-1 cells and their *TP53*-mutant daughter cell lines 48 hours after treatment with Nutlin-3 $\pm 2.5 \mu\text{mol/L}$ GSK2830371. C, reduction in clonogenic efficiency of HCT116^{+/+} cells following exposure to 0.5 $\times G1_{50}$ concentration of Nutlin-3 in the presence of 2.5 $\mu\text{mol/L}$ GSK2830371 compared with either inhibitor alone over 10 days. D, immunoblot of NGP cells showing Nutlin-3-dependent phosphorylation of p53 at Ser15 is markedly enhanced by GSK2830371 at 4- and 24-hour exposure and leads to increased caspase-3 cleavage at 48 hours. E, time-course of NGP response to 3.0 $\mu\text{mol/L}$ Nutlin-3 ($\approx G1_{50}$) $\pm 2.5 \mu\text{mol/L}$ GSK2830371 over 24 hours. WIP1i, GSK2830371; *, $P \leq 0.05$; **, $P \leq 0.005$.

GSK2830371 increases RG7388-induced p53-dependent transcription of growth inhibitory and proapoptotic genes

Phosphorylation of p53^{Ser15} has been reported to increase p53-mediated transcriptional transactivation but not to be necessary for dissociation of p53 from MDM2 in response to DNA damage (24, 26). Also, reports in the literature have suggested that p53 posttranslational modifications can behave as variable barcodes and induce transcription of alternate sets of p53 target genes that could lead to different cell fates after p53 activation (42). As the greatest potentiation of MDM2 inhibitors by GSK2830371 was observed in NGP cells (5.8-fold), we assessed whether the subset of early genes activated in response to RG7388 in this cell line differed in the presence of 2.5 $\mu\text{mol/L}$ GSK2830371, which produced a marked increase in p53^{Ser15}. Peak p53 transcriptional target expression (e.g., p21^{WAF1} and MDM2) as detected by western blotting is reached by 6 to 8 hours after treatment (Fig. 3E). Because later changes in transcription may be secondary effects and not directly p53-dependent, we assessed changes in global gene expression 4 hours following RG7388 ($\text{GI}_{50} \approx 75 \text{ nmol/L}$) \pm 2.5 $\mu\text{mol/L}$ GSK2830371 using the Illumina BeadChip expression array platform. A testament to the specificity of RG7388 in exclusively activating p53, 4 hours of exposure to a GI_{50} dose of RG7388 led to significantly increased mRNA expression of only 9 genes, all of which were known p53 transcriptional targets (Fig. 4A). The top 41 genes just below the statistical significance cut-off point ($P > 0.05$ after correction for multiple testing) were also mostly genes that are well established to be direct p53 transcriptional targets. Interestingly, in the presence of 2.5 $\mu\text{mol/L}$ GSK2830371, the subset of statistically significant RG7388-mediated transcriptional changes increased from 9 to 24 genes, indicating that inhibition of WIP1 results in a significant increase of additional p53-mediated transcriptional activity at this early time point (Fig. 4B; for a list of genes refer to Supplementary Tables S1A and S1B).

To validate the results of the array, we assessed the expression of the top three genes with the highest odds ratio difference between single and combination treatments [*CDKN1A* (p21^{WAF1}), *TP53INP1*, and *BTG2*] and one of the genes that was exclusively induced in the combination treatment (*MDM2*) by qRT-PCR using the same mRNA samples used in the expression array experiment (Fig. 4C). Consistent with the array data, all the genes tested showed significant increase in their mRNA expression in combination treatment compared with the RG7388 alone (Fig. 4C). *TP53INP1/P53DINP1* is a known proapoptotic p53 transcriptional target gene, the overexpression or induction of which following cellular stress has been associated with increased p53-mediated apoptosis (43). Among the 16 additional p53-regulated target genes induced exclusively in response to the combination treatment were TNF super family member 10B (*TNFRSF10B*) and p53-induced death domain protein 1 (*PIDD1*), two genes critical for extrinsic and intrinsic proapoptotic pathways, respectively (44–47). Interestingly, despite neither of the agents being genotoxic, one of the other genes that showed differential expression in response to the combination treatment was the DNA base excision repair gene xeroderma pigmentosum complementation group C (*XPC*), the increased basal expression of which has been reported to correlate with increased sensitivity to MDM2 inhibitors in a large panel of *TP53* wild-type cell lines and predict a better clinical response to RG7112 and RG7388 in acute myeloid leukaemia patients (13).

The increase in the subset of genes expressed correlated with a marked increase in the proportion of pp53^{Ser15} to total p53 in immunoblots of lysates prepared in parallel to the mRNA samples used in the expression array experiment (Fig. 4D and see Supplementary Fig. S3A). These data suggest that the underlying mechanism for the observed potentiation of MDM2 inhibitors in combination with WIP1 phosphatase inhibition may be contributed to by the increased p53^{Ser15} phosphorylation that enhances p53-dependent proapoptotic gene transcription.

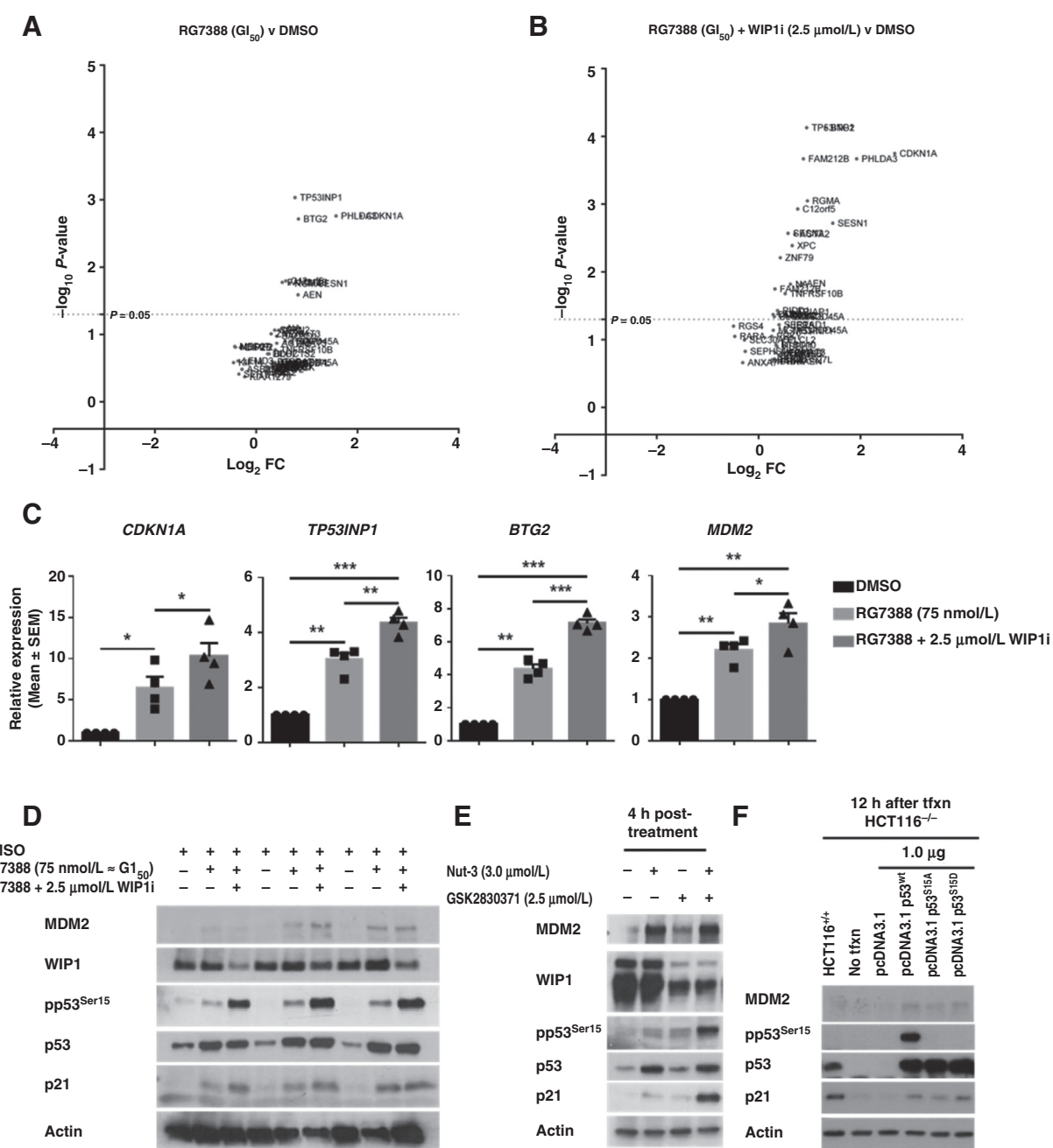
In line with this hypothesis, increased pp53^{Ser15} phosphorylation in HCT116^{+/+} following combination treatment resulted in an increase in the p21^{WAF1} product of the *CDKN1A* gene in comparison with monotherapy with either drug (Fig. 4E). To confirm earlier findings showing that phosphorylation of p53^{Ser15} increases p53-mediated transcription in HCT116 cells, we overexpressed wild-type (Wt) p53, mutant p53^{S15A}, or p53^{S15D} in HCT116^{-/-} cells and assessed p53-mediated expression of p21^{WAF1} protein encoded by the *CDKN1A* gene, which had showed the biggest fold change in expression on the array following the combination treatment in NGP cells. Consistent with previous findings (24, 26), Wt p53 and phospho-mimetic p53^{S15D} mutant constructs increased p53-mediated expression of p21^{WAF1} and MDM2 following transfection compared with the p53^{S15A} mutant, which could not be phosphorylated on that residue (Fig. 4F). See Supplementary Fig. S3B and S3C for repeat and densitometry data.

The effect of combined MDM2 and WIP1 inhibition on cell-cycle distribution

Given that WIP1 inhibition potentiated the growth inhibitory and apoptotic response of *TP53* wild-type cell lines to MDM2 inhibitors, and the highest fold increase in transcription was of the *CDKN1A* (p21^{WAF1}) cyclin-dependent kinase inhibitor gene, we investigated changes in cell-cycle distribution following this combination treatment. In all cell lines, 2.5 $\mu\text{mol/L}$ GSK2830371 alone did not significantly affect cell-cycle distribution throughout 72 hours of treatment (Fig. 5A and Supplementary Fig. S4). Changes in cell-cycle distribution after exposure to Nutlin-3 \pm 2.5 $\mu\text{mol/L}$ GSK2830371 were cell line-dependent. In SJS-A1 and NGP cell lines, 24 hours exposure to Nutlin-3 resulted in an increase in the proportion of cells in G₁–G₀ phases of the cell cycle. In SJS-A1 cells, this effect of Nutlin-3 remained unchanged in the following 48 hours treatment with Nutlin-3 \pm GSK2830371. However, in NGP cells, the relative proportion of cells in G₂–M and S-phase increased over the following 48 hours when Nutlin-3 and the WIP1 inhibitor were combined compared with Nutlin-3 alone. In HCT116^{+/+} cells, Nutlin-3 resulted in an increase in the proportion of cells in G₀–G₁ and G₂–M phases at 24 hours, which persisted to the 72 hours treatment time point (Fig. 5A), consistent with the increase in *CDKN1A* (p21^{WAF1}) expression in response to the combination treatment (Fig. 4E). Cell-cycle distribution was not affected in HCT116^{-/-} cells regardless of the treatment condition, suggesting that the changes in cell-cycle distribution observed in HCT116^{+/+} cells are p53-dependent (Fig. 5A).

Sub-G₁ changes

In response to the combination treatment compared with Nutlin-3 alone, the increase in sub-G₁ FACS signal after exposure to Nutlin-3 was significantly augmented in the presence of

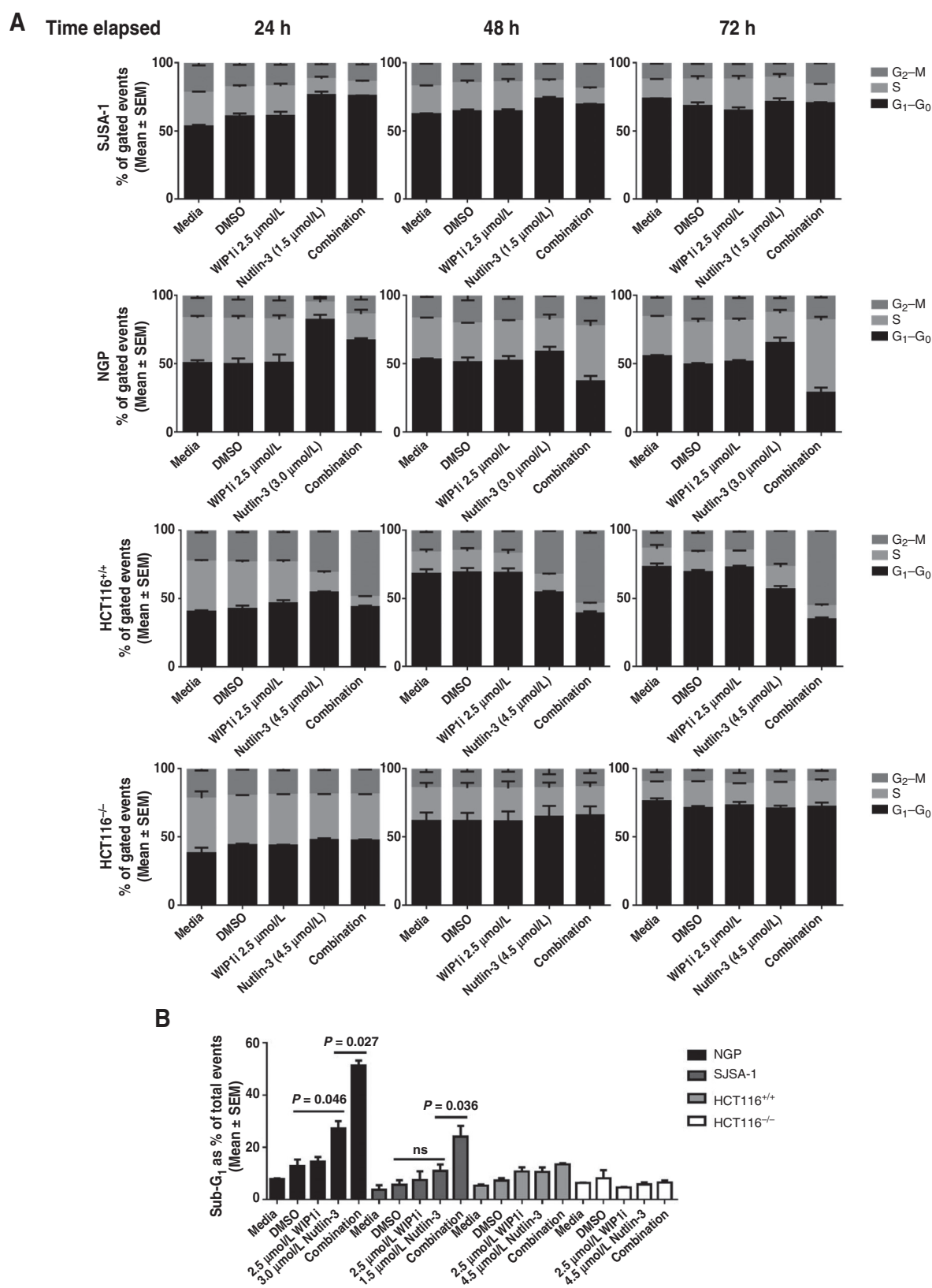
**Figure 4.**

A and B, volcano plots showing the significantly induced genes by RG7388 treatment of NGP cells for 4 hours in the presence or absence of 2.5 $\mu\text{mol/L}$ GSK2830371 [RG7388 vs. DMSO and RG7388 + WIP1 (2.5 $\mu\text{mol/L}$) vs. DMSO]. The results represent the mean of four independent biologic repeats. *y*-axis: $-\log_{10}$ of the *P* value adjusted for false discovery rate using the Benjamini–Hochberg procedure; *x*-axis Log_2 FC: log_2 fold change in normalized mRNA expression. For a list of genes induced, see Supplementary Table S1A and S1B. Microarray data have been deposited in the NCBI GEO databank (accession number: GSE75197). C, qRT-PCR validation of p53 target genes implicated in increased sensitivity to MDM2 inhibitors: *TNFRSF10B*, *AEN*, *XPC*, and *CDKN1A* using the same RNA samples as used for the microarray analysis. D, Western blot analysis for NGP cells showing changes in p53, pp53^{Ser15}, MDM2, WIP1, and p21^{WAF1} protein expression in response to 75 nmol/L RG7388 (G_{50}) \pm 2.5 $\mu\text{mol/L}$ GSK2830371. Lysates were obtained from samples treated in parallel to the microarray experiment and represent the first three independent repeats. E, Western blot analysis of HCT116^{+/+} cells 4 hours following treatment with the stated doses of Nutlin-3, GSK2830371 or their combination. F, Western blot analysis showing changes in pp53^{Ser15}, MDM2, and p21^{WAF1} detection 12 hours after ectopic expression of wild-type p53 (Wt), p53 mutants Ser15Ala (S15A), and Ser15Asp (S15D) in HCT116^{-/-} cells. WIP1i, GSK2830371; *, $P \leq 0.05$; **, $P \leq 0.005$; ***, $P \leq 0.0005$.

2.5 $\mu\text{mol/L}$ GSK2830371 (WIP1i) in both SJS-1 and NGP cell lines (Fig. 5B and Supplementary Fig. S4B). This is in keeping with the increased cleaved caspase-3/7 activity in NGP and SJS-1 cells

(Fig. 3A and B). Sub-G₁ signals were not significantly changed in HCT116^{+/+} cells throughout the 72 hours of Nutlin-3 \pm GSK2830371 treatment (Fig. 5B).

Esfandiari et al.

**Figure 5.**

A, time-course of cell-cycle distribution changes over 72 hours of treatment using FACS analysis. B, percent of sub-G₁ signals for NGP, SJS-A1, HCT116^{+/+}, and HCT116^{-/-} cells in response to the stated treatments at 72 hours. WIP11, GSK2830371.

Discussion

Although mutant *TP53* status is a dominant mechanism of resistance to MDM2-p53 binding antagonists, there is nevertheless a clinically relevant wide range of sensitivity to MDM2 inhibitors among *TP53* wild-type cancer cell lines. Importantly, this variation of response is not exclusive to one class of MDM2 inhibitors and is clearly seen in panels of cell lines with validated wild-type *TP53* status. Amgen has recently reported a wide range of sensitivity to their MDM2 inhibitor AMG283 among their carefully curated panel of *TP53* wild-type and functional cell lines showing a 500-fold GI_{50} difference between the least to most sensitive (8). These observations suggest that there are a diverse set of underlying genetic variables that determine cell fate following a dose of activated/stabilized p53. Here we have shown a non-growth-inhibitory dose of the selective orally bioavailable allosteric WIP1 phosphatase inhibitor, GSK2830371, can modulate the phosphorylation state of p53 and potentiate both the growth inhibitory and apoptotic response to MDM2 inhibitors in *TP53* wild-type cell lines, especially those with increased WIP1 expression or activity. MDM2 inhibitor potentiation was at its greatest when the cell line harbored either *PPM1D* copy number gain/elevated expression or gain-of-function truncating mutations, thus providing a rationale for specific combination treatment targeting of tumors with this genotype.

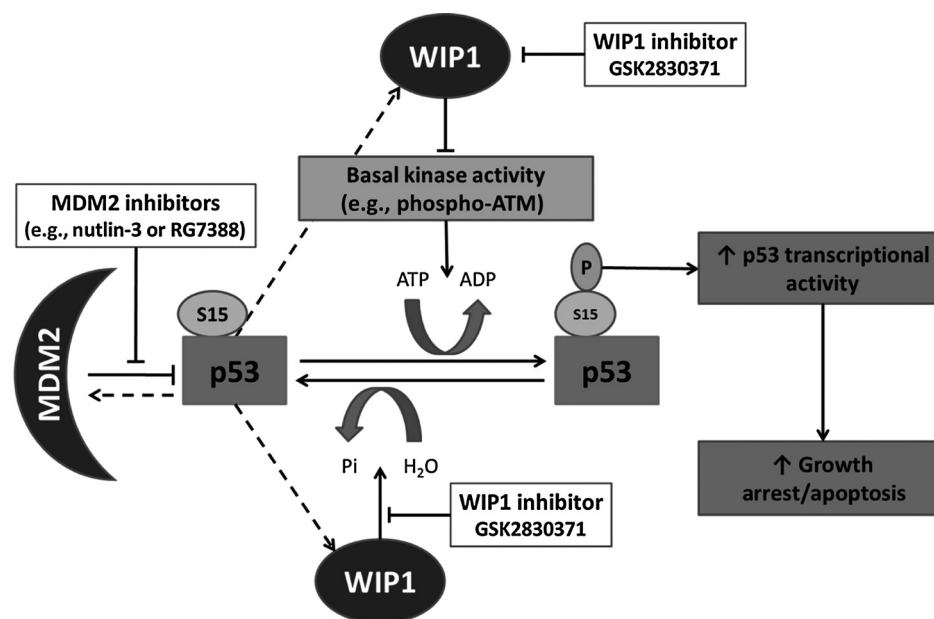
The argument in support of p53^{Ser15} phosphorylation increasing p53-mediated transcription (24, 26, 27) is compelling and consistent with our findings. In contrast to what was originally reported by Vassilev and colleagues, in 2004, phosphorylation of p53 following treatment with MDM2 inhibitors is observed; however, it is not as intense and immediate compared with p53^{Ser15} phosphorylation following DNA damaging agents of equivalent growth-inhibitory dose (7, 26). As shown by Loughery and colleagues, the basal activity of kinases involved in phosphorylation of p53^{Ser15} (e.g., ATM and ATR) in response to DNA damage are also likely responsible for, or contribute to, this posttranslational modification in response to MDM2 inhibitors

(26). Our findings have shown that, in the presence of a selective WIP1 inhibitor, the minimal phosphorylation of p53^{Ser15} in response to MDM2 inhibitors is markedly accentuated, which correlates with potentiation of apoptotic and growth-inhibitory response to MDM2 inhibitors in *TP53* wild-type cells, particularly in those with high WIP1 expression or activity. This was also associated with significantly increased transcript levels from an increased number of immediate p53 transcriptional target genes as compared with those induced by single-agent RG7388. Increased p53^{Ser15} phosphorylation in response to the combination treatment also resulted in increased p21^{WAF1} and MDM2 protein expression. Consistent with the reported role of p53^{Ser15} phosphorylation in increasing transcriptional activity of p53, we also confirmed that mutation of this residue influenced expression of p21^{WAF1} and MDM2 proteins. Thus, our current working model includes evidence for the role of enhanced p53 transcriptional activity in response to the combination of MDM2 inhibitors and GSK2830371 (Fig. 6). It is likely, however, that direct and/or indirect WIP1-mediated posttranslational modifications that effect the stability and function of stress response proteins and their cross-talk with the p53 network (as reviewed in ref. 15) may also contribute to MDM2 inhibitor potentiation in the presence of GSK2830371. Regardless of this, our data strongly suggest that increased pp53^{Ser15} can be considered a surrogate marker of p53 dissociation from MDM2 in response to single-agent GSK2830371 treatment or its combination with MDM2 inhibitors, as this modification coincides with p53 transcriptional activation that precedes the subsequent enhanced p53-mediated growth inhibitory or apoptotic response to each of these treatments.

Nutlin-3-mediated changes in cell-cycle distribution were all enhanced in the presence of a dose of GSK2830371 that on its own did not affect cell-cycle distribution. The observed increase in sub-G₁ FACS analysis signals with combination treatment of NGP cells is consistent with potentiation of apoptosis and growth inhibition in this cell line. Enhancement of Nutlin-3-mediated

Figure 6.

Proposed model for potentiation of cellular response to MDM2 inhibitors by the selective allosteric WIP1 inhibitor GSK2830371. After activation of p53 by MDM2 inhibitors, p53^{Ser15} is unmasked and therefore available as a substrate for the basal level activity of multiple kinases and phosphatases normally involved in posttranslational modification of this residue in response to cellular stress. In normal homeostatic control, phosphorylation of p53^{Ser15} is kept in check by an equilibrium between the kinase and phosphatase activities. Inhibition of WIP1 by GSK2830371 tilts this balance in favor of the activating kinases, which in turn increases p53 transcriptional activity and is enhanced in combination with MDM2 inhibitors. Dashed lines indicate direct p53 transcriptional upregulation of the corresponding genes for MDM2 and WIP1.



G₁:S and G₂:S ratios in the presence of GSK2830371 are also consistent with the increased *CDKN1A* (p21^{WAF1}) expression observed at both transcript and protein levels and its importance in negative regulation of cell-cycle progression (48, 49). Kleiblova and colleagues, (39) had previously shown that transient knock-down of truncated *PPM1D* increases G₁ checkpoint in response to ionizing radiation. Interestingly, in our current study, WIP1 inhibition and depletion by GSK2830371 in HCT116^{+/+} cells harboring a *PPM1D* L450X truncation mutation also resulted in an increase in p53-dependent G₁ arrest following p53 activation by Nutlin-3, whereas this did not occur in NGP and SJSA-1 cell lines that do not have *PPM1D* gain-of-function mutations. Lindqvist and colleagues (50) also reported that WIP1 knockdown ablates the competence of cellular p53-dependent G₂ checkpoint recovery following cellular stress, although the authors were not aware of the gain-of-function WIP1 R458X mutation in U2OS cells used in their study, as it had not yet been reported. These findings suggest that the increase in G₂:S ratio observed in HCT116^{+/+} cells treated with the combination of MDM2 inhibitors and GSK2830371 is likely due to inhibition of WIP1 L450X that would otherwise be negatively regulating p53 transcriptional activity in these cell lines. Of note, we have also shown that GSK2830371 increases the ubiquitin-mediated degradation of truncated WIP1 as postulated by Gilmartin and colleagues, (16). Interestingly, this increase in the ubiquitination of truncated WIP1 was reversed by inhibition of MDM2, which suggests that MDM2 is directly or indirectly involved in WIP1 ubiquitination following GSK2830371.

Wild-type *TP53* genetic status is the most important determinant of response to MDM2 inhibitors, while being necessary but not sufficient for growth inhibitory response to WIP1 inhibition by GSK2830371. Following their promising clinical outcomes so far, MDM2 inhibitors will be explored in combination with other anticancer agents to optimize their therapeutic potential. Combination regimens of these nongenotoxic agents could minimize DNA damage to healthy tissue that does not express altered forms of *PPM1D*. Here we have shown that specific pharmacologic

inhibition of WIP1 combined with MDM2 inhibitors is a promising therapeutic strategy in *TP53* wild-type tumors that show increased WIP1 function, and that pp53^{Ser15} and *PPM1D* genotype are important both mechanistically and as predictive biomarkers for response to this combination treatment.

Disclosure of Potential Conflicts of Interest

No potential conflicts of interest were disclosed.

Authors' Contributions

Conception and design: A. Esfandiari, J. Lunec

Development of methodology: A. Esfandiari, J. Lunec

Acquisition of data (provided animals, acquired and managed patients, provided facilities, etc.): A. Esfandiari, T.A. Hawthorne

Analysis and interpretation of data (e.g., statistical analysis, biostatistics, computational analysis): A. Esfandiari, T.A. Hawthorne, S. Nakjang, J. Lunec

Writing, review, and/or revision of the manuscript: A. Esfandiari, J. Lunec

Administrative, technical, or material support (i.e., reporting or organizing data, constructing databases): A. Esfandiari

Study supervision: J. Lunec

Acknowledgments

The authors thank Prof. Nicola J. Curtin for providing the U2OS cell line pair and also acknowledge Mrs. Mahsa Azizyan and Drs. Olivier Binda and Richard Heath for their provision of reagents and advice on experimental procedures. The encouragement and provision of RG7388 by Prof. Newell and the NICR Drug Discovery team are gratefully acknowledged.

Grant Support

This work was supported by the grants from Cancer Research UK (C240/A15751; to J. Lunec), Newcastle University and Northern Institute for Cancer Research (C0190R4011; to A. Esfandiari), and Newcastle University (C0190R4011; to S. Nakjang and T. Hawthorne).

The costs of publication of this article were defrayed in part by the payment of page charges. This article must therefore be hereby marked *advertisement* in accordance with 18 U.S.C. Section 1734 solely to indicate this fact.

Received August 6, 2015; revised December 8, 2015; accepted December 23, 2015; published OnlineFirst February 1, 2016.

References

- Levine AJ, Momand J, Finlay CA. The P53 tumor suppressor gene. *Nature* 1991;351:453–6.
- Levine AJ. p53, the cellular gatekeeper for growth and division. *Cell* 1997;88:323–31.
- Brown CJ, Lain S, Verma CS, Fersht AR, Lane DP. Awakening guardian angels: drugging the p53 pathway. *Nat Rev Cancer* 2009;9:862–73.
- Zhao Y, Aguilar A, Bernard D, Wang S. Small-molecule inhibitors of the MDM2–p53 protein–protein interaction (MDM2 Inhibitors) in clinical trials for cancer treatment. *J Med Chem* 2015;58:1038–52.
- Li Q, Lozano G. Molecular pathways: targeting Mdm2 and Mdm4 in cancer therapy. *Clin Cancer Res* 2013;19:34–41.
- Meek DW, Hupp TR. The regulation of MDM2 by multisite phosphorylation—Opportunities for molecular-based intervention to target tumours? *Semin Cancer Biol* 2010;20:19–28.
- Vassilev LT, Vu BT, Graves B, Carvajal D, Podlaski F, Filipovic Z, et al. *In vivo* activation of the p53 pathway by small-molecule antagonists of MDM2. *Science* 2004;303:844–8.
- Saiki AY, Caenepeel S, Cosgrove E, Su C, Boedigheimer M, Oliner JD. Identifying the determinants of response to MDM2 inhibition. *Oncotarget* 2015;6:7701–12.
- Garnett MJ, Edelman EJ, Heidorn SJ, Greenman CD, Dastur A, Lau KW, et al. Systematic identification of genomic markers of drug sensitivity in cancer cells. *Nature* 2012;483:570–5.
- Barretina J, Caponigro G, Stransky N, Venkatesan K, Margolin AA, Kim S, et al. The Cancer Cell Line Encyclopedia enables predictive modelling of anticancer drug sensitivity. *Nature* 2012;483:603–307.
- Jin Z, Shen J, He J, Hu C. Combination therapy with p53–MDM2 binding inhibitors for malignancies. *Med Chem Res* 2015;24:1369–79.
- Sullivan KD, Padilla-Just N, Henry RE, Porter CC, Kim J, Tentler JJ, et al. ATM and MET kinases are synthetic lethal with non-genotoxic activation of p53. *Nat Chem Biol* 2012;8:646–54.
- Zhong H, Chen G, Jukofsky L, Geho D, Han SW, Birzele F, et al. MDM2 antagonist clinical response association with a gene expression signature in acute myeloid leukaemia. *Br J Haematol* 2015;171:432–5.
- Lu X, Ma O, Nguyen T-A, Joness SN, Oren M, Donehower LA. The Wip1 phosphatase acts as a gatekeeper in the p53–Mdm2 autoregulatory loop. *Cancer Cell* 2007;12:342–54.
- Lowe J, Cha H, Lee M-O, Mazur SJ, Appella E, Fornace AJ. Regulation of the Wip1 phosphatase and its effects on the stress response. *Front Biosci* 2012;17:1480–98.
- Gilmartin AG, Faitg TH, Richter M, Groy A, Seefeld MA, Darcy MG, et al. Allosteric Wip1 phosphatase inhibition through flap-subdomain interaction. *Nat Chem Biol* 2014;10:181–7.
- Bulavin DV, Demidov ON, Saito S, Kauraniemi P, Phillips C, Amundson SA, et al. Amplification of *PPM1D* in human tumors abrogates p53 tumor-suppressor activity. *Nat Genet* 2002;31:210–5.

18. Zhang L, Chen LH, Wan H, Yang R, Wang Z, Feng J, et al. Exome sequencing identifies somatic gain-of-function PPM1D mutations in brainstem gliomas. *Nat Genet* 2014;46:726–30.
19. Ruark E, Snape K, Humburg P, Loveday C, Bajrami I, Brough R, et al. Mosaic PPM1D mutations are associated with predisposition to breast and ovarian cancer. *Nature* 2013;493:406–10.
20. Vintonyak VV, Antonchick AP, Rauh D, Waldmann H. The therapeutic potential of phosphatase inhibitors. *Curr Opin Chem Biol* 2009;13:272–83.
21. Richter M, Dayaram T, Gilmartin AG, Ganji G, Pemmasani SK, Van Der Key H, et al. WIP1 phosphatase as a potential therapeutic target in neuroblastoma. *PLoS One* 2015;10:e0115635.
22. Böttger A, Böttger V, Garcia-Echeverria C, Chène P, Hochkeppel H-K, Sampson W, et al. Molecular characterization of the hdm2-p53 interaction. *J Mol Biol* 1997;269:744–56.
23. Lu X, Nannenga B, Donehower LA. PPM1D dephosphorylates Chk1 and p53 and abrogates cell cycle checkpoints. *Genes Dev* 2005;19:1162–74.
24. Dumaz N, Meek DW. Serine15 phosphorylation stimulates p53 transactivation but does not directly influence interaction with HDM2. *EMBO J* 1999;18:7002–10.
25. Chehab NH, Malikzay A, Stavridi ES, Halazonetis TD. Phosphorylation of Ser-20 mediates stabilization of human p53 in response to DNA damage. *Proc Natl Acad Sci* 1999;96:13777–82.
26. Loughery J, Cox M, Smith LM, Meek DW. Critical role for p53-serine 15 phosphorylation in stimulating transactivation at p53-responsive promoters. *Nucleic Acids Res* 2014;42:7666–80.
27. Unger T, Sionov RV, Moallem E, Yee CL, Howley PM, Oren M, et al. Mutations in serines 15 and 20 of human p53 impair its apoptotic activity. *Oncogene* 1999;18:3205–12.
28. Chen L, Rousseau RF, Middleton SA, Nichols GL, Newell DR, Lunec J, et al. Pre-clinical evaluation of the MDM2-p53 antagonist RG7388 alone and in combination with chemotherapy in neuroblastoma. *Oncotarget* 2015;6:10207–21.
29. Allan LA, Fried M. p53-dependent apoptosis or growth arrest induced by different forms of radiation in U2OS cells: p21WAF1/CIP1 repression in UV induced apoptosis. *Oncogene* 1999;18:5403–12.
30. Skehan P, Storeng R, Scudiero D, Monks A, McMahon J, Vistica D, et al. New colorimetric cytotoxicity assay for anticancer-drug screening. *J Natl Cancer Inst* 1990;82:1107–12.
31. Chen L, Zhao Y, Halliday GC, Berry P, Rousseau RF, Middleton SA, et al. Structurally diverse MDM2-p53 antagonists act as modulators of MDR-1 function in neuroblastoma. *Br J Cancer* 2014;111:716–25.
32. Edgar R, Domrachev M, Lash AE. Gene Expression Omnibus: NCBI gene expression and hybridization array data repository. *Nucleic Acids Res* 2002;30:207–10.
33. Gozani O. Site Directed Mutagenesis with Stratagene Pfu Turbo. Available from: <http://web.stanford.edu/group/gozani/cgi-bin/gozanilab/wp-content/uploads/2014/01/Site-Directed-Mutagenesis-with-Stratagene-Pfu-Turbo.pdf>
34. Du P, Kibbe WA, Lin SM. lumi: a pipeline for processing Illumina microarray. *Bioinformatics* 2008;24:1547–8.
35. Ritchie ME, Phipson B, Wu D, Hu Y, Law CW, Shi W, et al. limma powers differential expression analyses for RNA-sequencing and microarray studies. *Nucleic Acids Res* 2015;43:e47.
36. Chuman Y, Kurihashi W, Mizukami Y, Nashimoto T, Yagi H, Sakaguchi K. PPM1D430, a novel alternative splicing variant of the human PPM1D, can dephosphorylate p53 and exhibits specific tissue expression. *J Biochem* 2009;145:1–12.
37. Castellino R, De Bortoli M, Lu X, Moon S-H, Nguyen T-A, Shepard M, et al. Medulloblastomas overexpress the p53-inactivating oncogene WIP1/PPM1D. *J Neurooncol* 2008;86:245–56.
38. Li J, Yang Y, Peng Y, Austin RJ, van Eynhoven WG, Nguyen KCQ, et al. Oncogenic properties of PPM1D located within a breast cancer amplification epicenter at 17q23. *Nat Genet* 2002;31:133–4.
39. Kleiblova P, Shaltiel IA, Benada J, Števcík J, Pecháčková S, Pohlreich P, et al. Gain-of-function mutations of PPM1D/Wip1 impair the p53-dependent G1 checkpoint. *J Cell Biol* 2013;201:511–21.
40. Marine J-CW, Dyer MA, Jochemsen AG. MDMX: from bench to bedside. *J Cell Sci* 2007;120:371–8.
41. Zhang X, Lin L, Guo H, Yang J, Jones SN, Jochemsen A, et al. Phosphorylation and degradation of MdmX is inhibited by Wip1 phosphatase in the DNA damage response. *Cancer Res* 2009;69:7960–8.
42. Murray-Zmijewski F, Slee EA, Lu X. A complex barcode underlies the heterogeneous response of p53 to stress. *Nat Rev Mol Cell Biol* 2008;9:702–12.
43. Okamura S, Arakawa H, Tanaka T, Nakanishi H, Ng CC, Taya Y, et al. p53DINP1, a p53-inducible gene, regulates p53-dependent apoptosis. *Mol Cell* 2001;8:85–94.
44. Wu GS, Burns TF, McDonald ER, Jiang W, Meng R, Krantz ID, et al. KILLER/DR5 is a DNA damage-inducible p53-regulated death receptor gene. *Nat Genet* 1997;17:141–3.
45. Ashkenazi A, Dixit VM. Death receptors: signaling and modulation. *Science* 1998;281:1305–8.
46. Lin YP, Ma WL, Benchimol S. Pidd, a new death-domain-containing protein, is induced by p53 and promotes apoptosis. *Nat Genet* 2000;26:122–5.
47. Tinel A, Tschopp J. The PIDDosome, a protein complex implicated in activation of caspase-2 in response to genotoxic stress. *Science* 2004;304:843–6.
48. Deng CX, Zhang PM, Harper JW, Elledge SJ, Leder P. Mice lacking p21 (CIP1/WAF1) undergo normal development, but are defective in G1 Checkpoint control. *Cell* 1995;82:675–84.
49. Eldeiry WS, Harper JW, Oconnor PM, Velculescu VE, Canman CE, Jackman J, et al. WAF1/CIP1 is induced in p53-mediated G(1) arrest and apoptosis. *Cancer Res* 1994;54:1169–74.
50. Lindqvist A, de Bruijn M, Macurek L, Brás A, Mensinga A, Bruinsma W, et al. Wip1 confers G2 checkpoint recovery competence by counteracting p53-dependent transcriptional repression. *EMBO J* 2009;28:3196–206.
51. Forbes SA, Beare D, Gunasekaran P, Leung K, Bindal N, Boutselakis H, et al. COSMIC: exploring the world's knowledge of somatic mutations in human cancer. *Nucleic Acids Res* 2015;43:D805–11.

Molecular Cancer Therapeutics

Chemical Inhibition of Wild-Type p53-Induced Phosphatase 1 (WIP1/PPM1D) by GSK2830371 Potentiates the Sensitivity to MDM2 Inhibitors in a p53-Dependent Manner

Arman Esfandiari, Thomas A. Hawthorne, Sirintra Nakjang, et al.

Mol Cancer Ther 2016;15:379-391. Published OnlineFirst February 1, 2016.

Updated version Access the most recent version of this article at:
doi:[10.1158/1535-7163.MCT-15-0651](https://doi.org/10.1158/1535-7163.MCT-15-0651)

Supplementary Material Access the most recent supplemental material at:
<http://mct.aacrjournals.org/content/suppl/2016/01/30/1535-7163.MCT-15-0651.DC1.html>

Cited articles This article cites 50 articles, 19 of which you can access for free at:
<http://mct.aacrjournals.org/content/15/3/379.full.html#ref-list-1>

E-mail alerts [Sign up to receive free email-alerts](#) related to this article or journal.

Reprints and Subscriptions To order reprints of this article or to subscribe to the journal, contact the AACR Publications Department at pubs@aacr.org.

Permissions To request permission to re-use all or part of this article, contact the AACR Publications Department at permissions@aacr.org.